Editors' Suggestion

FLAG review 2024

Y. Aoki,[1] T. Blum,[2,3] S. Collins,[4] L. Del Debbio,[5] M. Della Morte,[6] P. Dimopoulos,[7,8] X. Feng,[9,10,11,12] M. Golterman,[13] Steven Gottlieb,[14] R. Gupta,[15] G. Herdoíza,[16] P. Hernandez,[17] A. Jüttner,[18,19,20] T. Kaneko,[21,22] E. Lunghi,[14] S. Meinel,[23] C. Monahan,[24,25] A. Nicholson,[26] T. Onogi,[27] P. Petreczky,[28] A. Portelli,[1,5,20] A. Ramos,[17] S. R. Sharpe,[29] J. N. Simone,[30,31] S. Sint,[31] R. Sommer,[32,33] N. Tantalo,[34] R. Van de Water,[30] A. Vaquero,[35,36] U. Wenger,[37] and H. Wittig[38,39]

(Flavour Lattice Averaging Group (FLAG))

[1]*RIKEN Center for Computational Science, Kobe 650-0047, Japan*
[2]*Physics Department, University of Connecticut, Storrs, Connecticut 06269-3046, USA*
[3]*RIKEN BNL Research Center, Brookhaven National Laboratory, Upton, New York 11973, USA*
[4]*Institut für Theoretische Physik, Universität Regensburg, 93040 Regensburg, Germany*
[5]*Higgs Centre for Theoretical Physics, School of Physics and Astronomy, University of Edinburgh, Edinburgh EH9 3FD, United Kingdom*
[6]*IMADA, University of Southern Denmark, Campusvej 55, DK-5230 Odense M, Denmark*
[7]*Dipartimento di Scienze Matematiche, Fisiche e Informatiche, Università di Parma, 43124 Parma, Italy*
[8]*INFN, Gruppo Collegato di Parma, Parco Area delle Scienze 7/a (Campus), 43124 Parma, Italy*
[9]*School of Physics, Peking University, Beijing 100871, China*
[10]*Collaborative Innovation Center of Quantum Matter, Beijing 100871, China*
[11]*Center for High Energy Physics, Peking University, Beijing 100871, China*
[12]*State Key Laboratory of Nuclear Physics and Technology, Peking University, Beijing 100871, China*
[13]*Department of Physics and Astronomy, San Francisco State University, San Francisco, California 94132, USA*
[14]*Department of Physics, Indiana University, Bloomington, Indiana 47405, USA*
[15]*Los Alamos National Laboratory, Theoretical Division T-2, Los Alamos, New Mexico 87545, USA*
[16]*Instituto de Física Teórica UAM/CSIC and Departamento de Física Teórica, Universidad Autónoma de Madrid, Cantoblanco 28049 Madrid, Spain*
[17]*IFIC (CSIC-UVEG), Parc Científic de la Universitat de València, E-46980 Paterna, Spain*
[18]*School of Physics & Astronomy, University of Southampton, Southampton SO17 1BJ, United Kingdom*
[19]*STAG Research Center, University of Southampton, Highfield, Southampton SO17 1BJ, United Kingdom*
[20]*CERN, Theoretical Physics Department, Geneva, Switzerland*
[21]*High Energy Accelerator Research Organization (KEK), Ibaraki 305-0801, Japan*
[22]*Graduate Institute for Advanced Studies, SOKENDAI (The Graduate University for Advanced Studies), Ibaraki 305-0801, Japan*
[23]*Department of Physics, University of Arizona, Tucson, Arizona 85721, USA*
[24]*Department of Physics, The College of William & Mary, Williamsburg, Virginia 23187, USA*
[25]*Department of Physics, Colorado College, Colorado Springs, Colorado 80903, USA*
[26]*Department of Physics and Astronomy, University of North Carolina, Chapel Hill, North Carolina 27516-3255, USA*
[27]*Department of Physics, The University of Osaka, Toyonaka 560-0043, Japan*
[28]*Physics Department, Brookhaven National Laboratory, Upton, New York 11973, USA*
[29]*Physics Department, University of Washington, Seattle, Washington 98195-1560, USA*
[30]*Fermi National Accelerator Laboratory, Batavia, Illinois 60510 USA*
[31]*School of Mathematics & Hamilton Mathematics Institute, Trinity College Dublin, Dublin 2, Ireland*
[32]*Deutsches Elektronen-Synchrotron DESY, Platanenallee 6, 15738 Zeuthen, Germany*
[33]*Institut für Physik, Humboldt-Universität zu Berlin, Newtonstrasse 15, 12489 Berlin, Germany*
[34]*INFN, Sezione di Tor Vergata, c/o Dipartimento di Fisica, Università di Roma Tor Vergata, Via della Ricerca Scientifica 1, 00133 Rome, Italy*
[35]*Departamento de Física Teórica, Universidad de Zaragoza, Calle Pedro Cerbuna 12, 50009 Zaragoza, Spain*
[36]*Center for Astroparticles and High Energy Physics (CAPA), Calle Pedro Cerbuna 12, 50009 Zaragoza, Spain*
[37]*Albert Einstein Center for Fundamental Physics, Institut für Theoretische Physik, Universität Bern, Sidlerstrasse 5, 3012 Bern, Switzerland*
[38]*PRISMA Cluster of Excellence, Institut für Kernphysik and Helmholtz Institute Mainz, University of Mainz, 55099 Mainz, Germany*

[39]*Helmholtz Institute Mainz and GSI Helmholtz Center for Heavy Ion Research, 64291 Darmstadt, Germany*

(Received 11 February 2025; accepted 27 June 2025; published 30 January 2026)

We review lattice results related to pion, kaon, D-meson, B-meson, and nucleon physics with the aim of making them easily accessible to the nuclear and particle physics communities. More specifically, we report on the determination of the light-quark masses, the form factor $f_+(0)$ arising in the semileptonic $K \to \pi$ transition at zero momentum transfer, as well as the decay-constant ratio f_K/f_π and its consequences for the Cabibbo–Kobayashi–Maskawa (CKM) matrix elements V_{us} and V_{ud}. We review the determination of the B_K parameter of neutral kaon mixing as well as the additional four B parameters that arise in theories of physics beyond the Standard Model. For the heavy-quark sector, we provide results for m_c and m_b as well as those for the decay constants, form factors, and mixing parameters of charmed and bottom mesons and baryons. These are the heavy-quark quantities most relevant for the determination of CKM matrix elements and the global CKM unitarity-triangle fit. We review the status of lattice determinations of the strong coupling constant α_s. We review the determinations of nucleon charges from the matrix elements of both isovector and flavor-diagonal axial, scalar and tensor local quark bilinears, and momentum fraction, helicity moment and the transversity moment from one-link quark bilinears. We also review determinations of scale-setting quantities. Finally, in this review we have added a new section on the general definition of the low-energy limit of the Standard Model.

DOI: 10.1103/nfzp-p5dn

CONTENTS

I. INTRODUCTION 4
A. FLAG composition, guidelines and rules 6
B. Citation policy 8
C. General issues 9
II. QUALITY CRITERIA, AVERAGING AND ERROR ESTIMATION 12
A. Systematic errors and color code 12
1. Systematic effects and rating criteria 13
2. Data-driven criteria 14
3. Heavy-quark actions 15
4. Conventions for the figures 16
B. Averages and estimates 16
C. Averaging procedure and error analysis 17
1. Averaging—generic case 17
2. Nested averaging 18
III. GENERAL DEFINITION OF THE LOW-ENERGY LIMIT OF THE STANDARD MODEL 19
A. First-order isospin-breaking expansion 19
B. Edinburgh consensus 20
C. Comparison to other schemes 20
IV. QUARK MASSES 22
A. Masses of the light quarks 23
1. Lattice determination of m_s and m_{ud} 23
2. Lattice determinations of m_s/m_{ud} 27
3. Lattice determination of m_u and m_d 28
4. Estimates for R and Q 34
B. Charm-quark mass 34
1. $N_f = 2 + 1$ results 36
2. $N_f = 2 + 1 + 1$ results 36
3. Lattice determinations of the ratio m_c/m_s 37
C. Bottom-quark mass 39
1. $N_f = 2 + 1$ 39
2. $N_f = 2 + 1 + 1$ 39
V. LEPTONIC AND SEMILEPTONIC KAON AND PION DECAY AND $|V_{ud}|$ AND $|V_{us}|$ 42
A. Experimental information concerning $|V_{ud}|$, $|V_{us}|$, $f_+(0)$ and $f_{K^\pm}/f_{\pi^\pm}$ 42
B. Lattice results for $f_+(0)$ and $f_{K^\pm}/f_{\pi^\pm}$ 43
C. Direct determination of $f_+(0)$ and $f_{K^\pm}/f_{\pi^\pm}$ 46
1. Results for $f_+(0)$ 47
2. Results for $f_{K^\pm}/f_{\pi^\pm}$ 49
3. Extraction of $|V_{ud}|$ and $|V_{us}|$ 52
D. Tests of the Standard Model 52
E. Analysis within the Standard Model 53
F. Direct determination of $f_{K^\pm}$ and $f_{\pi^\pm}$ 54
VI. KAON MIXING 56
A. Indirect CP violation and ϵ_K in the SM 56
B. Lattice-QCD studies of the $K \to (\pi\pi)_I$ decay amplitudes, ξ_0, ξ_2 and ϵ'/ϵ 60
C. Lattice computation of B_K 63
D. Kaon BSM B-parameters 67
VII. CHARM-HADRON DECAY CONSTANTS AND FORM FACTORS 70
A. Leptonic decay constants f_D and f_{D_s} 71
B. Form factors for $D \to \pi\ell\nu$ and $D \to K\ell\nu$ semileptonic decays 74
C. Form factors for Λ_c and Ξ_c semileptonic decays 79
D. Form factors for charm semileptonic decays with heavy spectator quarks 79
E. Determinations of $|V_{cd}|$ and $|V_{cs}|$ and test of second-row CKM unitarity 80

Published by the American Physical Society under the terms of the Creative Commons Attribution 4.0 International license. Further distribution of this work must maintain attribution to the author(s) and the published article's title, journal citation, and DOI. Funded by SCOAP³.

VIII. BOTTOM-HADRON DECAYS AND MIXINGS 84
A. Leptonic decay constants f_B and f_{B_s} 85
B. Neutral B-meson mixing matrix elements 91
C. Semileptonic form factors for B decays to light flavors 95
1. Form factors for $B \to \pi\ell\nu$ 96
2. Form factors for $B \to \rho\ell\nu$ 99
3. Form factors for $B_s \to K\ell\nu$ 99
4. Form factors for rare and radiative B-semileptonic decays to light flavors 101
D. Semileptonic form factors for $B_{(s)} \to D_{(s)}\ell\nu$ and $B_{(s)} \to D^*_{(s)}\ell\nu$ 104
1. $B_{(s)} \to D_{(s)}$ decays 104
2. $B_{(s)} \to D^*_{(s)}$ decays 108
3. Lepton-flavor-universality ratios $R(D^{(*)})$ and $R(D_s^{(*)})$ 113
4. Fragmentation fraction ratio f_s/f_d 114
E. Semileptonic form factors for $B_c \to (\eta_c, J/\psi)\ell\nu$ decays 115
F. Semileptonic form factors for $\Lambda_b \to (p, \Lambda_c^{(*)})\ell\bar{\nu}$ decays 115
G. Semileptonic form factors for $\Lambda_b \to \Lambda^{(*)}\ell\ell$ 117
H. Determination of $|V_{ub}|$ 118
I. Determination of $|V_{cb}|$ 120
J. Determination of $|V_{ub}/V_{cb}|$ from Λ_b decays 125
K. Determination of $|V_{ub}/V_{cb}|$ from B_s decays 125
L. Summary: $|V_{ub}|$ and $|V_{cb}|$ 126
IX. THE STRONG COUPLING α_s 127
A. Introduction 127
1. Scheme and scale dependence of α_s and $\Lambda_{\rm QCD}$ 128
2. Overview of the review of α_s 130
3. Additions with respect to the FLAG 21 report 130
B. General issues 130
1. Discussion of criteria for computations entering the averages 130
2. Physical scale 133
3. Studies of truncation errors of perturbation theory 134
C. α_s from step-scaling methods 135
1. General considerations 135
2. Discussion of computations 137
D. The decoupling method 140
1. Discussion of computations 141
E. α_s from the potential at short distances 143
1. General considerations 143
2. Discussion of computations 143
F. α_s from the light-quark vacuum polarization in momentum/position space 148
1. General considerations 148
2. Definitions in position space 148
3. Discussion of computations 148
4. Vacuum polarization in position space 149
G. α_s from observables at the lattice spacing scale 150
1. General considerations 150
2. Continuum limit 151
3. Discussion of computations 151
H. α_s from heavy-quark current two-point functions 153
1. General considerations 153
2. Discussion of computations 155
I. Gradient flow schemes 158
1. General considerations 158
2. Discussion of computations 158
J. Summary 159
1. Ranges for $[r_0\Lambda_{\overline{\rm MS}}]^{(N_f)}$ and $\Lambda_{\overline{\rm MS}}^{(N_f)}$ 160
2. Our range for $\alpha_{\overline{\rm MS}}^{(5)}$ 162
3. Conclusions 166
X. NUCLEON MATRIX ELEMENTS 168
A. Isovector and flavor-diagonal charges of the nucleon 169
1. Technical aspects of the calculations of nucleon matrix elements 170
2. Controlling excited-state contamination 171
3. Renormalization and Symanzik improvement of local currents 174
4. Extrapolations in a, M_π and $M_\pi L$ 175
B. Quality criteria for nucleon matrix elements and averaging procedure 176
C. Isovector charges 177
1. Results for g_A^{u-d}, g_S^{u-d} and g_T^{u-d} 178
D. Flavor-diagonal charges 185
1. Results for $g_A^{u,d,s}$ and $g_T^{u,d,s}$ 186
2. Results for $g_S^{u,d,s}$ from direct and hybrid calculations of the matrix elements 189
3. Results for $g_S^{u,d,s}$ using the Feynman-Hellmann theorem 191
4. Summary of results for $g_S^{u,d,s}$ 193
E. Isovector second Mellin moments $\langle x\rangle_{u-d}$, $\langle x\rangle_{\Delta u-\Delta d}$ and $\langle x\rangle_{\delta u-\delta d}$ 196
1. Results for the isovector moments $\langle x\rangle_{u-d}$, $\langle x\rangle_{\Delta u-\Delta d}$ and $\langle x\rangle_{\delta u-\delta d}$ 196
XI. SCALE SETTING 199
A. Impact 199
B. Scale setting as part of hadronic renormalization schemes 200
1. Theory scales 201
2. Isospin breaking 202
C. Physical scales 202
1. The mass of the Ω baryon 202
2. Pion and kaon leptonic decay rates 202
3. Other physics scales 204
D. Theory scales 204
1. Potential scales 204
2. Gradient flow scales 204
3. Other theory scales 206
E. List of computations and results 206
1. Gradient-flow scales 206
2. Potential scales 208
3. Ratios of scales 211
F. Averages 211
1. Data-driven continuum-limit criterion 211
2. Gradient flow scale $\sqrt{t_0}$ 211
3. Gradient flow scale w_0 212

4. Gradient flow scale t_0/w_0 212
5. Potential scale r_0 212
6. Potential scale r_1 213
7. The scales M_{p4s} *and* f_{p4s} 214
8. Dimensionless ratios of scales 214
G. Observations and conclusions 214

ACKNOWLEDGMENTS 215
DATA AVAILABILITY 216
APPENDIX A:
LIST OF ACRONYMS 216

APPENDIX B
1. Inclusion of electromagnetic effects 217
2. Parametrizations of semileptonic form factors 218
a. The vector form factor for $B \to \pi\ell\nu$ 218
b. The scalar form factor for $B \to \pi\ell\nu$ 219
c. Extension to other form factors 220
d. Choice of form-factor basis for chiral-continuum extrapolations 220
3. Explicit parametrizations used in the form factor fits 221
a. $D \to K$ form factors 221
b. $B \to \pi$ form factors 221
c. $B_s \to K$ form factors 222
d. $B \to K$ form factors 222
e. $B \to D$ form factors 222
f. $B_s \to D_s$ form factors 222
g. $B \to D^*$ form factors 222
h. $B_s \to D_s^*$ form factors 222

APPENDIX C:
NOTES 222
1. Notes to Sec. IV on quark masses 222
2. Notes to Sec. V on $|V_{ud}|$ and $|V_{us}|$ 224
3. Notes to Sec. VI on kaon mixing 225
a. Kaon B-parameter B_K 225
b. Kaon BSM B-parameters 225
c. $K \to \pi\pi$ decay amplitudes 226
4. Notes to Sec. VII on D-meson decay constants and form factors 227
a. Form factors for semileptonic decays of charmed hadrons 229
5. Notes to Sec. VIII on B-meson decay constants, mixing parameters and form factors 231
a. $B_{(s)}$-meson decay constants 231
b. $B_{(s)}$-meson mixing matrix elements 234
c. Form factors entering determinations of $|V_{ub}|$ ($B \to \pi\ell\nu$, $B_s \to K\ell\nu$, $\Lambda_b \to p\ell\bar{\nu}$) 235
d. Form factors for rare decays of beauty hadrons 237
e. Form factors entering determinations of $|V_{cb}|$ ($B_{(s)} \to D_{(s)}^{(*)}\ell\nu$, $\Lambda_b \to \Lambda_c^{(*)}\ell\bar{\nu}$) and $R(D_{(s)})$ 239
6. Notes to Sec. IX on the strong coupling α_s 242
a. Renormalization scale and perturbative behavior 242
b. Continuum limit 242
7. Notes to Sec. X on nucleon matrix elements 243
8. Notes to Sec. XI on scale setting 254

I. INTRODUCTION

Flavor physics provides an important opportunity for exploring the limits of the Standard Model of particle physics and for constraining possible extensions that go beyond it. As the LHC and its experiments continue exploring the energy frontier, and as experiments such as Belle-II, BESIII, NA62 and KOTO-2 continue extending the precision and intensity frontiers, the importance of flavor physics will grow, both in terms of searches for signatures of new physics through precision measurements and in terms of attempts to construct the theoretical framework behind direct discoveries of new particles. Crucial to such searches for new physics is the ability to quantify strong-interaction effects. Large-scale numerical calculations of lattice QCD allow for the computation of these effects from first principles. The scope of the Flavour Lattice Averaging Group (FLAG) is to review the current status of lattice results for a variety of physical quantities that are important for flavor physics. Set up in November 2007, it comprises experts in lattice field theory, chiral perturbation theory, and Standard Model phenomenology. Our aim is to provide an answer to the frequently posed question "What is currently the best lattice value for a particular quantity?" in a way that is readily accessible to those who are not expert in lattice methods. This is generally not an easy question to answer; different collaborations use different lattice actions (discretizations of QCD) with a variety of lattice spacings and volumes, and with a range of masses for the u and d quarks. Not only are the systematic errors different, but also the methodology used to estimate these uncertainties varies between collaborations. In the present work, we summarize the main features of each of the calculations and provide a framework for judging and combining the different results. Sometimes, it is a single result that provides the "best" value; more often, it is a combination of results from different collaborations. Indeed, when consistency of values obtained using different formulations is found, this adds significantly to our confidence in the results.

The first five editions of the FLAG review were made public in 2010 [1], 2013 [2], 2016 [3], 2019 [4], and 2021 [5] (and will be referred to as FLAG 10, FLAG 13, FLAG 16, FLAG 19, and FLAG 21, respectively). The fifth edition reviewed results related to both light (u-, d- and s-quark), and heavy (c- and b-quark) flavors. The quantities related to pion and kaon physics were light-quark masses, the form factor $f_+(0)$ arising in semileptonic $K \to \pi$ transitions (evaluated at zero momentum transfer), the decay constants f_K and f_π, the B_K parameter from neutral kaon mixing, and the kaon mixing matrix elements of new operators that arise in theories of physics beyond the Standard Model. Their implications for the Cabibbo–Kobayashi–Maskawa (CKM) matrix elements V_{us} and V_{ud} were also discussed. Furthermore, results were reported for some of the low-energy constants of $\mathrm{SU}(2)_L \times \mathrm{SU}(2)_R$ and $\mathrm{SU}(3)_L \times \mathrm{SU}(3)_R$ chiral perturbation theory. The quantities related to D- and B-meson physics that were reviewed were the

masses of the charm and bottom quarks together with the decay constants, form factors, and mixing parameters of D and B mesons. These are the heavy-light quantities most relevant to the determination of CKM matrix elements and the global CKM unitarity-triangle fit. The current status of lattice results on the QCD coupling α_s was reviewed. Last but not least, we reviewed calculations of nucleon matrix elements of flavor nonsinglet and singlet bilinear operators, including the nucleon axial charge g_A and the nucleon sigma term. These results are relevant for constraining V_{ud}, for searches for new physics in neutron decays and other processes, and for dark matter searches.

In FLAG 21, we extended the scope of the review by adding a section on scale setting, Sec. XI. The motivation for adding this section was that uncertainties in the value of the lattice spacing a are a major source of error for the calculation of a wide range of quantities. Thus we felt that a systematic compilation of results, comparing the different approaches to setting the scale, and summarizing the present status, would be a useful resource for the lattice community. An additional update was the inclusion, in Sec. VI B, of a brief description of the status of lattice calculations of $K \to \pi\pi$ decay amplitudes. Although some aspects of these calculations were not yet at the stage to be included in our averages, they are approaching this stage, and we felt that, given their phenomenological relevance, a brief review was appropriate.

In the current review, we have omitted the section on low-energy constants in the chiral Lagrangian as progress in that area has slowed. FLAG will keep monitoring the situation and provide updates in future editions, should new results become available. On the other hand, we have added a new section on isospin breaking, Sec. III. For the most precisely determined quantities, isospin breaking—both from the up-down quark-mass difference and from quantum electrodynamics (QED)—must be included. An important issue here is that, in the context of a QED + QCD theory, the separation into QED and quantum chromodynamics (QCD) contributions to a given physical quantity is ambiguous. There are several ways of defining such a separation. The new section allows a more uniform treatment in the sections on quark masses (see Sec. IV) and scale setting (see Sec. XI). We stress, however, that the physical observable in QCD + QED is defined unambiguously. Any ambiguity only arises because we are trying to separate a well-defined, physical quantity into two unphysical parts that provide useful information for phenomenology.

Our main results are collected in Tables 1–5. As is clear from the tables, for most quantities there are results from ensembles with different values for N_f. In most cases, there is reasonable agreement among results with $N_f = 2, 2+1$, and $2+1+1$. As precision increases, we may some day be able to distinguish among the different values of N_f, in which case, presumably $2+1+1$ would be the most realistic. (If isospin violation is critical, then $1+1+1$ or $1+1+1+1$ might be desired.) At present, for some quantities the errors in the $N_f = 2+1$ results are smaller than those with $N_f = 2+1+1$ (e.g., for m_c), while for others the relative size of the errors is reversed. In most situations we expect the averages in this report for both $N_f = 2+1$ or $N_f = 2+1+1$ to provide a sufficiently accurate description of QCD. In situations where charm-sea-quark and/or isospin-breaking effects are expected to be subdominant systematic effects, both results can be used. We do not recommend using the $N_f = 2$ results, except for studies of the N_f-dependence of α_s, as these have an uncontrolled systematic error coming from quenching the strange quark.

Our plan is to continue providing FLAG updates, in the form of a peer reviewed paper, roughly on a triennial basis. This effort is supplemented by our more frequently updated website http://flag.itp.unibe.ch [6], where figures as well as pdf files for the individual sections can be downloaded. The papers reviewed in the present edition have appeared before the closing date 30 April 2024.[1]

This review is organized as follows. In the remainder of Sec. I, we summarize the composition and rules of FLAG and discuss general issues that arise in modern lattice calculations. In Sec. II, we explain our general methodology for evaluating the robustness of lattice results. We also describe the procedures followed for combining results from different collaborations in a single average or estimate (see Sec. II B for our definition of these terms). The rest of the paper consists of sections, each dedicated to a set of closely connected physical quantities, or, for the final section, to the determination of the lattice scale. Each of these sections is accompanied by an Appendix with explicatory notes.[2]

In previous editions, we have provided, in an appendix, a glossary summarizing some standard lattice terminology and describing the most commonly used lattice techniques and methodologies. Since no significant updates in this information have occurred recently, we have decided, in the interests of reducing the length of this review, to omit this glossary, and refer the reader to FLAG 19 for this information [4]. This appendix also contained, in previous versions, a tabulation of the actions used in the papers that were reviewed. Since this information is available in the discussions in the separate sections, and is time-consuming to collect from the sections, we have dropped these tables. In Appendix A, we have added a summary and explanations of acronyms introduced in the manuscript. Collaborations referred to by an acronym can be identified through the corresponding bibliographic reference. In Appendix B 1, we

[1]Working groups were given the option of including papers submitted to `arxiv.org` before the closing date but published after this date. This flexibility allows this review to be up-to-date at the time of submission. Two papers of this type were included, cf. footnote 9

[2]In order to keep the length of this review within reasonable bounds, we have dropped these notes for older data, since they can be found in previous FLAG reviews [1–5].

TABLE 1. Summary of the main results of this review concerning quark masses, light-meson decay constants, the kaon semileptonic form factor, and hadronic kaon-decay and kaon-mixing parameters. These are grouped in terms of N_f, the number of dynamical quark flavors in lattice simulations. Quark masses are given in the $\overline{\text{MS}}$ scheme at running scale $\mu = 2$ GeV or as indicated. BSM bag parameters $B_{2,3,4,5}$ are given in the $\overline{\text{MS}}$ scheme at scale $\mu = 3$ GeV. Further specifications of the quantities are given in the quoted sections. Results for $N_f = 2$ quark masses are unchanged since FLAG 16 [3], and are not included here. For each result, we list the references that enter the FLAG average or estimate, and we stress again the importance of quoting these original works when referring to FLAG results. From the entries in this column one can also read off the number of results that enter our averages for each quantity. We emphasize that these numbers only give a very rough indication of how thoroughly the quantity in question has been explored on the lattice and recommend consulting the detailed tables and figures in the relevant section for more significant information and for explanations on the source of the quoted errors.

Quantity	Sec.	$N_f = 2+1+1$	Ref.	$N_f = 2+1$	Ref.	$N_f = 2$	Ref.
m_{ud} [MeV]	IV A 1	3.427 (51)	[7–9]	3.387 (39)	[10–16]		
m_s [MeV]	IV A 1	93.46 (58)	[7–9,17,18]	92.4(1.0)	[11–15,19]		
m_s/m_{ud}	IV A 2	27.227 (81)	[7,8,20,21]	27.42 (12)	[12–14,19,22]		
m_u [MeV]	IV A 3	2.14 (8)	[9,23]	2.27 (9)	[24]		
m_d [MeV]	IV A 3	4.70 (5)	[9,23]	4.67 (9)	[24]		
m_u/m_d	IV A 3	0.465 (24)	[23,25]	0.485 (19)	[24]		
$\bar{m}_c(3\text{ GeV})$ [GeV]	IV B 2	0.989 (10)	[7–9,18,26,27]	0.991 (6)	[15,28–32]		
m_c/m_s	IV B 3	11.766 (30)	[7–9,18]	11.82 (16)	[29,33]		
$\bar{m}_b(\bar{m}_b)$ [GeV]	IV C	4.200 (14)	[9,34–37]	4.171 (20)	[15]		
$f_+(0)$	V C	0.9698 (17)	[38,39]	0.9677 (27)	[40,41]		
$f_{K^\pm}/f_{\pi^\pm}$	V C	1.1934 (19)	[20,42–45]	1.1916 (34)	[10,12,46–50]		
$f_{\pi^\pm}$ [MeV]	V F			130.2 (8)	[10,12,46,47]		
$f_{K^\pm}$ [MeV]	V F	155.7 (3)	[21,42,43,45]	155.7 (7)	[10,12,46,47]		
$\text{Re}(A_2)$ [GeV]	VI B			$1.50(4)(14) \times 10^{-8}$	[51]		
$\text{Im}(A_2)$ [GeV]	VI B			$-8.34(1.03) \times 10^{-13}$	[51]		
$\hat{B}_K$	VI C	0.717 (18) (16)	[52]	0.7533 (91)	[12,53–56]	0.727 (22) (12)	[57]
B_2	VI D	0.46 (1) (3)	[52]	0.488 (15)	[55,56,58]	0.47 (2) (1)	[57]
B_3	VI D	0.79 (6)	[52]	0.757 (27)	[55,56,58]	0.78 (4) (2)	[57]
B_4	VI D	0.78 (2) (4)	[52]	0.903 (14)	[55,56,58]	0.76 (2) (2)	[57]
B_5	VI D	0.49 (3) (3)	[52]	0.691 (14)	[55,56,58]	0.58 (2) (2)	[57]

provide a short review of how electromagnetic effects can be taken into account in lattice-QCD calculations. Appendix B 2 describes the parametrizations of semileptonic form factors that are used in Sec. VIII. A short appendix, Appendix B 3 provides all the details of the parameters used in the form factor fits in Secs. VII and VIII.

A. FLAG composition, guidelines and rules

FLAG strives to be representative of the lattice community, both in terms of the geographical location of its members and the lattice collaborations to which they belong. We aspire to provide the nuclear- and particle-physics communities with a single source of reliable information on lattice results.

In order to work reliably and efficiently, we have adopted a formal structure and a set of rules by which all FLAG members abide. The collaboration presently consists of an advisory board (AB), an editorial board (EB), and eight working groups (WG). The role of the advisory board is to provide oversight of the content, procedures, schedule and membership of FLAG, to help resolve disputes, to serve as a source of advice to the EB and to FLAG as a whole, and to provide a critical assessment of drafts. They also give their approval of the final version of the preprint before it is released. The editorial board coordinates the activities of FLAG, sets priorities and intermediate deadlines, organizes votes on FLAG procedures, writes the introductory sections, and takes care of the editorial work needed to integrate the sections written by the individual working groups into a uniform and coherent review. The working groups concentrate on writing the review of the physical quantities for which they are responsible, which is subsequently circulated to the whole collaboration for critical evaluation.

The current list of FLAG members and their working group assignments is

(i) Advisory board (AB): M. Golterman, P. Hernandez, T. Onogi, S.R. Sharpe, and R. Van de Water.

TABLE 2. Summary of the main results of this review concerning heavy-light mesons and the strong coupling constant. These are grouped in terms of N_f, the number of dynamical quark flavors in lattice simulations. The quantities listed are specified in the quoted sections. For each result, we list the references that enter the FLAG average or estimate, and we stress again the importance of quoting these original works when referring to FLAG results. From the entries in this column one can also read off the number of results that enter our averages for each quantity. We emphasize that these numbers only give a very rough indication of how thoroughly the quantity in question has been explored on the lattice and recommend consulting the detailed tables and figures in the relevant section for more significant information and for explanations on the source of the quoted errors.

Quantity	Sec.	$N_f = 2+1+1$	Ref.	$N_f = 2+1$	Ref.	$N_f = 2$	Ref.
f_D [MeV]	VII A	212.0 (7)	[20,43]	210.4(1.5)	[28,59–61]		
f_{D_s} [MeV]	VII A	249.9 (5)	[20,43]	247.7(1.2)	[28,29,60–62]		
$\frac{f_{D_s}}{f_D}$	VII A	1.1783 (16)	[20,43]	1.174 (7)	[28,59–61]		
$f_+^{D\to\pi}(0)$	VII B	0.6296 (50)	[63]	0.666 (29)	[64]		
$f_+^{D\to K}(0)$	VII B	0.7430 (27)	[63,65]	0.747 (19)	[66]		
f_B [MeV]	VIII A	190.0(1.3)	[20,36,67,68]	192.0(4.3)	[60,69–72]	188 (7)	[73,74]
f_{B_s} [MeV]	VIII A	230.3(1.3)	[20,36,67,68]	228.4(3.7)	[60,69–72]	225.3(6.6)	[73–75]
$\frac{f_{B_s}}{f_B}$	VIII A	1.209 (5)	[20,36,67,68]	1.201 (16)	[60,70–72,76]	1.206 (23)	[73,74]
$f_{B_d}\sqrt{\hat{B}_{b_d}}$ [MeV]	VIII B	210.6(5.5)	[77]	225 (9)	[71,78,79]	216 (10)	[73]
$f_{B_s}\sqrt{\hat{B}_{B_s}}$ [MeV]	VIII B	256.1(5.7)	[77]	274 (8)	[71,78,79]	262 (10)	[73]
$\hat{B}_{B_d}$	VIII B	1.222 (61)	[77]	1.30 (10)	[71,78,79]	1.30 (6)	[73]
$\hat{B}_{B_s}$	VIII B	1.232 (53)	[77]	1.35 (6)	[71,78,79]	1.32 (5)	[73]
ξ	VIII B	1.216 (16)	[77]	1.206 (17)	[71,79]	1.225 (31)	[73]
B_{B_s}/B_{B_d}	VIII B	1.008 (25)	[77]	1.032 (38)	[71,79]	1.007 (21)	[73]

Quantity	Sec.	$N_f = 2+1$ and $N_f = 2+1+1$	Ref.
$\alpha_{\overline{\rm MS}}^{(5)}(M_Z)$	IX J	0.1183 (7)	[15,18,80–87]
$\Lambda_{\overline{\rm MS}}^{(5)}$ [MeV]	IX J	213 (8)	[15,18,80–87]
$\Lambda_{\overline{\rm MS}}^{(4)}$ [MeV]	IX J	295 (10)	[15,18,80–87]
$\Lambda_{\overline{\rm MS}}^{(3)}$ [MeV]	IX J	338 (10)	[15,18,80–87]

(ii) Editorial board (EB): S. Gottlieb, A. Jüttner, and U. Wenger.
(iii) Working groups (coordinator listed first):
— Quark masses T. Blum, A. Portelli, and A. Ramos.
— V_{us}, V_{ud} T. Kaneko, J. N. Simone, and N. Tantalo.
— Kaon mixing P. Dimopoulos, X. Feng, and G. Herdoíza.
— $f_{B_{(s)}}$, $f_{D_{(s)}}$, B_B C. Monahan, Y. Aoki, and M. Della Morte.
— b and c semileptonic and radiative decays E. Lunghi, S. Meinel, and A. Vaquero.
— α_s S. Sint, L. Del Debbio, and P. Petreczky.
— Nucleon matrix elements R. Gupta, S. Collins, A. Nicholson, and H. Wittig.
— Scale setting R. Sommer, N. Tantalo, and U. Wenger.

The most important FLAG guidelines and rules are the following:

(i) the composition of the AB reflects the main geographical areas in which lattice collaborations are active, with members from America, Asia/Oceania, and Europe;
(ii) the mandate of regular members is not limited in time, but we expect that a certain turnover will occur naturally;
(iii) whenever a replacement becomes necessary this has to keep, and possibly improve, the balance in FLAG, so that different collaborations, from different geographical areas are represented;
(iv) in all working groups the members must belong to different lattice collaborations;
(v) a paper is in general not reviewed (nor color-coded, as described in the next section) by any of its authors;
(vi) lattice collaborations will be consulted on the color coding of their calculation;
(vii) there are also internal rules regulating our work, such as voting procedures.

TABLE 3. Summary of the main results of this review concerning nuclear matrix elements, grouped in terms of N_f, the number of dynamical quark flavors in lattice simulations. The quantities listed are specified in the quoted sections. For each result, we list the references that enter the FLAG average or estimate, and we stress again the importance of quoting these original works when referring to FLAG results. From the entries in this column one can also read off the number of results that enter our averages for each quantity. We emphasize that these numbers only give a very rough indication of how thoroughly the quantity in question has been explored on the lattice and recommend consulting the detailed tables and figures in the relevant section for more significant information and for explanations on the source of the quoted errors.

Quantity	Sec.	$N_f = 2+1+1$	Ref.	$N_f = 2+1$	Ref.
g_A^{u-d}	X C 1	1.263 (10)	[88–91]	1.265(20)	[92–96]
g_S^{u-d}	X C 1	1.085 (114)	[90]	1.083(69)	[93–97]
g_T^{u-d}	X C 1	0.981 (21)	[90,98]	0.993(15)	[93–96]
g_A^u	X D 1	0.777 (25) (30)	[99]	0.847(18)(32)	[92]
g_A^d	X D 1	−0.438(18)(30)	[99]	−0.407(16)(18)	[92]
g_A^s	X D 1	−0.053(8)	[99]	−0.035(6)(7)	[92]
g_T^u	X D 1	0.784 (28) (10)	[100]		
g_T^d	X D 1	−0.204(11)(10)	[100]		
g_T^s	X D 1	−0.0027(16)	[100]		
$\sigma_{\pi N}$ [MeV]	X D 4	60.9(6.5)	[26,101]	42.2(2.4)	[102–106]
σ_s [MeV]	X D 4	41.0(8.8)	[107]	44.9(6.4)	[102–108]
$\langle x \rangle_{u-d}$	X E 1	0.158 (32)	[98,109]	0.153(13)	[96,110,111]
$\langle x \rangle_{\Delta u - \Delta d}$	X E 1	0.213 (27)	[109]	0.200(13)	[96,110]
$\langle x \rangle_{\delta u - \delta d}$	X E 1	0.195 (25)	[98,109]	0.206(17)	[96,110]

TABLE 4. Summary of the main results of this review concerning setting of the lattice scale, grouped in terms of N_f, the number of dynamical quark flavors in lattice simulations. The quantities listed are specified in the quoted section. For each result, we list the references that enter the FLAG average or estimate, and we stress again the importance of quoting these original works when referring to FLAG results. From the entries in this column one can also read off the number of results that enter our averages for each quantity. We emphasize that these numbers only give a very rough indication of how thoroughly the quantity in question has been explored on the lattice and recommend consulting the detailed tables and figures in the relevant section for more significant information and for explanations on the source of the quoted errors.

Quantity	Sec.	$N_f = 1+1+1+1$	Ref.	$N_f = 2+1+1$	Ref.	$N_f = 2+1$	Ref.	$N_f > 2+1$	Ref.
$\sqrt{t_0}$ [fm]	XI F			0.14292 (104)	[42,45,112,113]	0.14474 (57)	[12,105,114,115]		
w_0 [fm]	XI F	0.17236 (70)	[116]	0.17256 (103)	[42,45,112,113]	0.17355 (92)	[12,115,117]	0.17250 (70)	[42,45,112,113,116]
t_0/w_0 [fm]	XI F			0.11969 (62)	[45]				
r_0 [fm]	XI F			0.4580 (73)	[8,118]	0.4701 (36)	[29,117,119–121]		
r_1 [fm]	XI F			0.3068 (37)	[42,118]	0.3127 (30)	[47,119–122]		
f_{4ps} [MeV]	XI F			153.98 (20)	[20]				
M_{4ps} [MeV]	XI F			433.12 (30)	[20]				

As for FLAG 21, for this review we sought the advice of external reviewers once a complete draft of the review was available. For each review section, we have asked one lattice expert (who could be a FLAG alumnus/alumna) and one nonlattice phenomenologist for a critical assessment.[3] This is similar to the procedure followed by the Particle Data Group in the creation of the Review of Particle Physics. The reviewers provide comments and feedback on scientific and stylistic matters. They are not anonymous, and enter into a discussion with the authors of the WG. Our aim with this additional step is to make sure that a wider array of viewpoints enter into the discussions, so as to make this review more useful for its intended audience.

B. Citation policy

We draw attention to this particularly important point. As stated above, our aim is to make lattice-QCD results easily accessible to those without lattice expertise, and we are well

[3]The one exception is the scale-setting section, where only a lattice expert has been asked to provide input.

TABLE 5. Summary of the main results of this review concerning z-parametrizations of lattice results for semileptonic meson-decay form factors and experimental data for differential decay rates (see Appendix B 2), grouped in terms of N_f, the number of dynamical quark flavors in lattice simulations. The entry in the column "fit" indicates whether the fit is to only lattice data ("lat") or combined to both lattice and experimental data ("lat + exp"). The references listed in the columns labeled "Table" lead to the tables that list the results for the z-parametrization coefficients and their correlations. For each result, we list the references that enter the FLAG average or estimate, and we stress again the importance of quoting these original works when referring to FLAG results. From the entries in this column one can also read off the number of results that enter our averages for each quantity. We emphasize that these numbers only give a very rough indication of how thoroughly the quantity in question has been explored on the lattice and recommend consulting the detailed tables and figures in the relevant section for more significant information and for explanations on the source of the quoted errors.

Decay	Form factor	Fit	Sec.	Fig.	Table $N_f = 2+1+1$	Ref.	Table $N_f = 2+1$	Ref.
$D \to K\ell\nu$	f_+, f_0	lat	VII B	18	30	[63,65,123]		
$D \to K\ell\nu$	f_+, f_0	lat + exp	VII E	19	32	[63,65,123]		
$B \to \pi\ell\nu$	f_+, f_0	lat	VIII C 1	25			38	[124–126]
$B_s \to K\ell\nu$	f_+, f_0	lat	VIII C 3	26			40	[127,128]
$B \to \pi\ell^-\ell^+$	f_T	lat	VIII C 4				42	[129]
$B \to K\ell^+\ell^-(\nu\bar{\nu})$	f_+, f_0, f_T	lat	VIII C 4	27			43	[130,131]
$B \to D\ell\nu$	f_+, f_0	lat	VIII D 1	28			45	[132,133]
$B_s \to D_s\ell\nu$	f_+, f_0	lat	VIII D 1		46	[134]		
$B \to D^*\ell\nu$	g, f, F_1, F_2	lat	VIII D 2	29	47	[135]	47	[136,137]
$B_s \to D_s^*\ell\nu$	g, f, F_1, F_2	lat	VIII D 2	30		[135]		
$B \to \pi\ell\nu$	f_+, f_0	lat + exp	VIII H	31			50	[124–126,138–141]
$B \to D\ell\nu$	f_+, f_0	lat + exp	VIII I	32			52	[132,133,142,143]
$B \to D^*\ell\nu$	g, f, F_1, F_2	lat + exp	VIII I	33, 34	53	[135,144–148]	53	[136,137,144–148]

aware that it is likely that some readers will only consult the present paper and not the original lattice literature. It is very important that this paper not be the only one cited when our results are quoted. We strongly suggest that readers also cite the original sources. In order to facilitate this, in Tables 1–5, besides summarizing the main results of the present review, we also cite the original references from which they have been obtained. In addition, for each figure we make a bibtex file available on our webpage [6] which contains the bibtex entries of all the calculations contributing to the FLAG average or estimate. The bibliography at the end of this paper should also make it easy to cite additional papers. Indeed, we hope that the bibliography will be one of the most widely used elements of the whole paper.

C. General issues

Several general issues concerning the present review are thoroughly discussed in Sec. I.1 of our initial 2010 paper [1], and we encourage the reader to consult the relevant pages. In the remainder of the present subsection, we focus on a few important points. Though the discussion has been duly updated, it is similar to that of the corresponding sections in the previous reviews [2–5].

The review aims to achieve two distinct goals: first, to provide a description of the relevant work done on the lattice; and, second, to draw conclusions on the basis of that work, summarizing the results obtained for the various quantities of physical interest.

The core of the information about the work done on the lattice is presented in the form of tables, which not only list the various results, but also describe the quality of the data that underlie them. We consider it important that this part of the review represents a generally accepted description of the work done. For this reason, we explicitly specify the quality requirements used and provide sufficient details in appendices so that the reader can verify the information given in the tables.[4]

On the other hand, the conclusions drawn on the basis of the available lattice results are the responsibility of FLAG alone. Preferring to err on the side of caution, in several cases we draw conclusions that are more conservative than those resulting from a plain weighted average of the available lattice results. This cautious approach is usually adopted when the average is dominated by a single lattice result, or when only one lattice result is available for a given quantity. In such cases, one does not have the same degree of confidence in results and errors as when there is agreement among several different calculations using different approaches. The reader should keep in mind that

[4]We also use terms like "quality criteria," "rating," "color coding," etc., when referring to the classification of results, as described in Sec. II.

the degree of confidence cannot be quantified, and it is not reflected in the quoted errors.

Each discretization has its merits, but also its shortcomings. For most topics covered in this review we have an increasingly broad database, and for most quantities lattice calculations based on totally different discretizations are now available. This is illustrated by the dense population of the tables and figures in most parts of this review. Those calculations that do satisfy our quality criteria indeed lead, in almost all cases, to consistent results, confirming universality within the accuracy reached. The consistency between independent lattice results, obtained with different discretizations, methods, and lattice parameters, is an important test of lattice QCD, and observing such consistency also provides further evidence that systematic errors are fully under control.

In the sections dealing with heavy quarks and with α_s, the situation is not the same. Since the b-quark mass can barely be resolved with current lattice spacings, most lattice methods for treating b quarks use effective field theory at some level. This introduces additional complications not present in the light-quark sector. An overview of the issues specific to heavy-quark quantities is given in the introduction of Sec. VIII. For B- and D-meson leptonic decay constants, there already exist a good number of different independent calculations that use different heavy-quark methods, but there are only a few independent calculations of semileptonic B, Λ_b, and D form factors and of $B-\bar{B}$ mixing parameters. For α_s, most lattice methods involve a range of scales that need to be resolved and controlling the systematic error over a large range of scales is more demanding. The issues specific to determinations of the strong coupling are summarized in Sec. IX.

Number of sea quarks in lattice calculations

Lattice-QCD calculations currently involve two, three or four flavors of dynamical quarks. Most calculations set the masses of the two lightest quarks to be equal, while the strange and charm quarks, if present, are heavier (and tuned to lie close to their respective physical values). Our notation for these calculations indicates which quarks are nondegenerate, e.g., $N_f = 2+1$ if $m_u = m_d < m_s$ and $N_f = 2+1+1$ if $m_u = m_d < m_s < m_c$. Calculations with $N_f = 2$, i.e., two degenerate dynamical flavors, often include strange valence quarks interacting with gluons, so that bound states with the quantum numbers of the kaons can be studied, albeit neglecting strange sea-quark contributions. The quenched approximation ($N_f = 0$), in which all sea-quark contributions are omitted, has uncontrolled systematic errors and is no longer used in modern lattice calculations with relevance to phenomenology. Lattice calculations with $N_f = 2$ also have an uncontrolled systematic error, although it is reasonable to expect it to be much smaller than for $N_f = 0$. Accordingly, we will review results obtained with $N_f = 2+1$ and $N_f = 2+1+1$, but omit earlier results with $N_f = 0$ and $N_f = 2$.[5] One notable exception concerns the QCD coupling constant α_s. Since this observable does not require valence light quarks, it is theoretically well defined also in the $N_f = 0$ theory, which is simply pure gluodynamics. The N_f-dependence of α_s, or more precisely of the related quantity $r_0\Lambda_{\overline{\rm MS}}$, is a theoretical issue of considerable interest; here r_0 is a quantity with the dimension of length that sets the physical scale, as discussed in Sec. XI. We stress, however, that only results with $N_f \geq 3$ are used to determine the physical value of α_s at a high scale.

Lattice actions, parameters, and scale setting

The remarkable progress in the precision of lattice calculations is due to improved algorithms, better computing resources, and, last but not least, conceptual developments. Examples of the latter are improved actions that reduce lattice artifacts and actions that preserve chiral symmetry to a very good approximation. A concise characterization of the various discretizations that underlie the results reported in the present review is given in Appendix A.1 of FLAG 19 [4].

Physical quantities are computed in lattice calculations in units of the lattice spacing so that they are dimensionless. For example, the pion decay constant that is obtained from a calculation is $f_\pi a$, where a is the spacing between two neighboring lattice sites. (All calculations with results quoted in this review use hypercubic lattices, i.e., with the same spacing in all four Euclidean directions.) To convert these results to physical units requires knowledge of the lattice spacing a at the fixed values of the bare QCD parameters (quark masses and gauge coupling) used in the calculation. This is achieved by requiring agreement between the lattice calculation and experimental measurement of a known quantity, which thus "sets the scale" of a given calculation. (See Sec. XI.)

Renormalization and scheme dependence

Several of the results covered by this review, such as quark masses, the gauge coupling, and B-parameters, are for quantities defined in a given renormalization scheme and at a specific renormalization scale. The schemes employed (e.g., regularization-independent MOM schemes) are often chosen because of their specific merits when combined with the lattice regularization. For a brief discussion of their properties, see Appendix A.3 of FLAG 19 [4]. The conversion of the results obtained in these so-called intermediate schemes to more familiar regularization schemes, such as the $\overline{\rm MS}$-scheme, is done with the aid of perturbation theory. It must be stressed that the renormalization scales accessible in calculations are limited, because of the presence of an ultraviolet (UV) cutoff of $\sim\pi/a$.

[5]It is left to the discretion of the WG to include $N_f = 2$ results in case they provide interesting additional information. We refer to previous editions of FLAG [6] for the discussion of omitted $N_f = 2$ results.

To safely match to $\overline{\text{MS}}$, a scheme defined in perturbation theory, renormalization group (RG) running to higher scales is performed, either perturbatively or nonperturbatively (the latter using finite-size scaling techniques).

Extrapolations

Because of limited computing resources, lattice calculations are often performed at unphysically heavy pion masses, although results at the physical point, where all quark masses take their physical values, have become increasingly common. Further, numerical calculations must be done at nonzero lattice spacing, and in a finite (four-dimensional) volume. In order to obtain physical results, lattice data are obtained at a sequence of pion masses and a sequence of lattice spacings, and then extrapolated to the physical pion mass and to the continuum limit. In principle, an extrapolation to infinite volume is also required. However, for most quantities discussed in this review, finite-volume effects are exponentially small in the linear extent of the lattice in units of the pion mass, and, in practice, one often verifies volume independence by comparing results obtained on a few different physical volumes, holding other parameters fixed. To control the associated systematic uncertainties, these extrapolations are guided by effective theories. For light-quark actions, the lattice-spacing dependence is described by Symanzik's effective theory [149,150]; for heavy quarks, this can be extended and/or supplemented by other effective theories such as heavy-quark effective theory (HQET). The pion-mass dependence can be parametrized with chiral perturbation theory (χPT), which takes into account the Nambu-Goldstone nature of the lowest excitations that occur in the presence of light quarks. Similarly, one can use heavy-light meson chiral perturbation theory (HMχPT) to extrapolate quantities involving mesons composed of one heavy (b or c) and one light quark. One can combine Symanzik's effective theory with χPT to simultaneously extrapolate to the physical pion mass and the continuum; in this case, the form of the effective theory depends on the discretization. See Appendix A. 4 of FLAG 19 [4] for a brief description of the different variants in use and some useful references. Finally, χPT can also be used to estimate the size of finite-volume effects measured in units of the inverse pion mass, thus providing information on the systematic error due to finite-volume effects in addition to that obtained by comparing calculations at different volumes.

Excited-state contamination

In all the hadronic matrix elements discussed in this review, the hadron in question is the lightest state with the chosen quantum numbers. This implies that it dominates the required correlation functions as their extent in Euclidean time is increased. Excited-state contributions are suppressed by $e^{-\Delta E \Delta\tau}$, where ΔE is the gap between the ground and excited states, and $\Delta\tau$ the relevant separation in Euclidean time. The size of ΔE depends on the hadron in question, and in general is a multiple of the pion mass. In practice, as discussed at length in Sec. X, the contamination of signals due to excited-state contributions is a much more challenging problem for baryons than for the other particles discussed here. This is in part due to the fact that the signal-to-noise ratio drops exponentially for baryons, which reduces the values of $\Delta\tau$ that can be used.

Critical slowing down

The lattice spacings reached in recent calculations go down to 0.05 fm or even smaller. In this regime, long autocorrelation times slow down the sampling of the configurations [151–160]. Many groups check for autocorrelations in a number of observables, including the topological charge, for which a rapid growth of the autocorrelation time is observed with decreasing lattice spacing. This is often referred to as topological freezing. A solution to the problem consists in using open boundary conditions in time [161], instead of the more common periodic or antiperiodic ones. A combination of open and periodic boundary conditions has recently been employed in a parallel tempering framework [162]. Other approaches have been proposed, e.g., based on a multiscale thermalization algorithm [163,164], or based on defining QCD on a nonorientable manifold [165], or using huge master fields [166,167]. Approaches using trivializing or normalizing flows [168] try to solve both the problem of topological freezing and critical slowing down by finding invertible maps from simple probability distributions for the lattice configurations, which can be efficiently sampled, to the target ones. Parametrizing these flows turns out to be difficult, but can be facilitated by using machine-learning tools [169–173]. So far, these attempts are restricted to simple field theories, low dimensions or, in four-dimensional SU(3) gauge theories, to very small and coarse systems [174]. Reference [175] uses machine learning to construct RG-improved gauge actions with highly suppressed lattice artifacts, such that efficient calculations on coarse lattices suffice to yield solid continuum limits. The problem of topological freezing and critical slowing down is also touched upon in Sec. IX B 1, where it is stressed that attention must be paid to this issue.

Few results reviewed here have been obtained with any of the above methods. It is usually *assumed* that the continuum limit can be reached by extrapolation from the existing calculations, and that potential systematic errors due to the long autocorrelation times have been adequately controlled. Partially or completely frozen topology would produce a mixture of different θ vacua, and the difference from the desired $\theta = 0$ result may be estimated in some cases using chiral perturbation theory, which gives predictions for the θ-dependence of the physical quantity of interest [176,177]. These ideas have been systematically and successfully tested in various models in [178,179], and a numerical test on MILC ensembles indicates that the topology dependence for some of the physical quantities

reviewed here is small, consistent with theoretical expectations [180].

Algorithms and numerical errors

Most of the modern lattice-QCD calculations use exact algorithms such as those of Refs. [181,182], which do not produce any systematic errors when exact arithmetic is available. In reality, one uses numerical calculations at double (or in some cases even single) precision, and some errors are unavoidable. More importantly, the inversion of the Dirac operator is carried out iteratively and it is truncated once some accuracy is reached, which is another source of potential systematic error. In most cases, these errors have been confirmed to be much less than the statistical errors. In the following, we assume that this source of error is negligible. Some of the most recent calculations use an inexact algorithm in order to speed up the computation, though it may produce systematic effects. Currently available tests indicate that errors from the use of inexact algorithms are under control [183].

II. QUALITY CRITERIA, AVERAGING AND ERROR ESTIMATION

The essential characteristics of our approach to the problem of rating and averaging lattice quantities have been outlined in our first publication [1]. Our aim is to help the reader assess the reliability of a particular lattice result without necessarily studying the original article in depth. This is a delicate issue, since the ratings may make things appear simpler than they are. Nevertheless, it safeguards against the possibility of using lattice results, and drawing physics conclusions from them, without a critical assessment of the quality of the various calculations. We believe that, despite the risks, it is important to provide some compact information about the quality of a calculation. We stress, however, the importance of the accompanying detailed discussion of the results presented in the various sections of the present review.

A. Systematic errors and color code

The major sources of systematic error are common to most lattice calculations. These include, as discussed in detail below, the chiral, continuum, and infinite-volume extrapolations. To each such source of error for which systematic improvement is possible we assign one of three colored symbols: green star, unfilled green circle (which replaced in Ref. [2] the amber disk used in the original FLAG review [1]) or red square. These correspond to the following ratings:

- ★ the parameter values and ranges used to generate the datasets allow for a satisfactory control of the systematic uncertainties;
- ○ the parameter values and ranges used to generate the datasets allow for a reasonable attempt at estimating systematic uncertainties, which however could be improved;
- ■ the parameter values and ranges used to generate the datasets are unlikely to allow for a reasonable control of systematic uncertainties.

The appearance of a red tag, even in a single source of systematic error of a given lattice result, disqualifies it from inclusion in the global average.

Note that in the first two editions [1,2], FLAG used the three symbols in order to rate the reliability of the systematic errors attributed to a given result by the paper's authors. Starting with FLAG 16 [3] the meaning of the symbols has changed slightly—they now rate the quality of a particular simulation, based on the values and range of the chosen parameters, and its aptness to obtain well-controlled systematic uncertainties. They do not rate the quality of the analysis performed by the authors of the publication. The latter question is deferred to the relevant sections of the present review, which contain detailed discussions of the results contributing (or not) to each FLAG average or estimate.

For most quantities the color-coding system refers to the following sources of systematic errors: (i) chiral extrapolation; (ii) continuum extrapolation; (iii) finite volume. As we will see below, renormalization is another source of systematic uncertainties in several quantities. This we also classify using the three colored symbols listed above, but now with a different rationale: they express how reliably these quantities are renormalized, from a field-theoretic point of view (namely, nonperturbatively, or with 2-loop or 1-loop perturbation theory).

Given the sophisticated status that the field has attained, several aspects, besides those rated by the colored symbols, need to be evaluated before one can conclude whether a particular analysis leads to results that should be included in an average or estimate. Some of these aspects are not so easily expressible in terms of an adjustable parameter such as the lattice spacing, the pion mass or the volume. As a result of such considerations, it sometimes occurs, albeit rarely, that a given result does not contribute to the FLAG average or estimate, despite not carrying any red tags. This happens, for instance, whenever aspects of the analysis appear to be incomplete (e.g., an incomplete error budget), so that the presence of inadequately controlled systematic effects cannot be excluded. This mostly refers to results with a statistical error only, or results in which the quoted error budget obviously fails to account for an important contribution.

Of course, any color coding has to be treated with caution; we emphasize that the criteria are subjective and evolving. Sometimes, a single source of systematic error dominates the systematic uncertainty and it is more important to reduce this uncertainty than to aim for green stars for other sources of error. In spite of these caveats,

we hope that our attempt to introduce quality measures for lattice simulations will prove to be a useful guide. In addition, we would like to stress that the agreement of lattice results obtained using different actions and procedures provides further validation.

1. Systematic effects and rating criteria

The precise criteria used in determining the color coding are unavoidably time-dependent; as lattice calculations become more accurate, the standards against which they are measured become tighter. For this reason FLAG reassesses criteria with each edition and as a result some of the quality criteria (the one on chiral extrapolation for instance) have been tightened up over time [1–4].

In the following, we present the rating criteria used in the current report. While these criteria apply to most quantities without modification, there are cases where they need to be amended or additional criteria need to be defined. For instance, the discussion of the strong coupling constant in Sec. IX requires tailored criteria for renormalization, perturbative behavior, and continuum extrapolation. Finally, in the section on nuclear matrix elements, Sec. X, the chiral extrapolation criterion is made slightly stronger, and a new criterion is adopted for excited-state contributions. In such cases, the modified criteria are discussed in the respective sections. Apart from only a few exceptions the following color code applies in the tables:

(i) Chiral extrapolation:

★ $M_{\pi,\mathrm{min}} < 200$ MeV, with three or more pion masses used in the extrapolation *or* two values of M_π with one lying within 10 MeV of 135 MeV (the physical neutral pion mass) and the other one below 200 MeV

○ 200 MeV $\leq M_{\pi,\mathrm{min}} \leq 400$ MeV, with three or more pion masses used in the extrapolation *or* two values of M_π with $M_{\pi,\mathrm{min}} < 200$ MeV *or* a single value of M_π, lying within 10 MeV of 135 MeV (the physical neutral pion mass)

■ otherwise

This criterion is unchanged from FLAG 19. In Sec. X the upper end of the range for $M_{\pi,\mathrm{min}}$ in the green circle criterion is lowered to 300 MeV, as in FLAG 19.

(ii) Continuum extrapolation:

★ at least three lattice spacings *and* at least two points below 0.1 fm *and* a range of lattice spacings satisfying $[a_{\mathrm{max}}/a_{\mathrm{min}}]^2 \geq 2$

○ at least two lattice spacings *and* at least one point below 0.1 fm *and* a range of lattice spacings satisfying $[a_{\mathrm{max}}/a_{\mathrm{min}}]^2 \geq 1.4$

■ otherwise

It is assumed that the lattice action is $\mathcal{O}(a)$-improved (i.e., the discretization errors vanish quadratically with the lattice spacing); otherwise this will be explicitly mentioned. For unimproved actions an additional lattice spacing is required. This condition is unchanged from FLAG 19.

(iii) Finite-volume effects:

The finite-volume color code used for a result is chosen to be the worst of the QCD and the QED codes, as described below. If only QCD is used the QED color code is ignored.

–For QCD:

★ $[M_{\pi,\mathrm{min}}/M_{\pi,\mathrm{fid}}]^2 \exp\{4 - M_{\pi,\mathrm{min}}[L(M_{\pi,\mathrm{min}})]_{\mathrm{max}}\} < 1$, *or* at least three volumes

○ $[M_{\pi,\mathrm{min}}/M_{\pi,\mathrm{fid}}]^2 \exp\{3 - M_{\pi,\mathrm{min}}[L(M_{\pi,\mathrm{min}})]_{\mathrm{max}}\} < 1$, *or* at least two volumes

■ otherwise

where we have introduced $[L(M_{\pi,\mathrm{min}})]_{\mathrm{max}}$, which is the maximum box size used in the simulations performed at the smallest pion mass $M_{\pi,\mathrm{min}}$, as well as a fiducial pion mass $M_{\pi,\mathrm{fid}}$, which we set to 200 MeV (the cutoff value for a green star in the chiral extrapolation). It is assumed here that calculations are in the p-regime of chiral perturbation theory, and that all volumes used exceed 2 fm. The rationale for this condition is as follows. Finite-volume effects contain the universal factor $\exp\{-M_\pi L\}$, and if this were the only contribution a criterion based on the values of $M_{\pi,\mathrm{min}}L$ would be appropriate. However, as pion masses decrease, one must also account for the weakening of the pion couplings. In particular, 1-loop chiral perturbation theory [184] reveals a behavior proportional to $M_\pi^2 \exp\{-M_\pi L\}$. Our condition includes this weakening of the coupling, and ensures, for example, that simulations with $M_{\pi,\mathrm{min}} = 135$ MeV and $M_{\pi,\mathrm{min}}L = 3.2$ are rated equivalently to those with $M_{\pi,\mathrm{min}} = 200$ MeV and $M_{\pi,\mathrm{min}}L = 4$.

–For QED (where applicable):

★ $1/([M_{\pi,\mathrm{min}}L(M_{\pi,\mathrm{min}})]_{\mathrm{max}})^{n_{\mathrm{min}}} < 0.02$, *or* at least four volumes

○ $1/([M_{\pi,\mathrm{min}}L(M_{\pi,\mathrm{min}})]_{\mathrm{max}})^{n_{\mathrm{min}}} < 0.04$, *or* at least three volumes

■ otherwise

Because of the infrared-singular structure of QED, electromagnetic finite-volume effects decay only like a power of the inverse spatial extent. In several cases like mass splittings [185,186] or leptonic decays [187], the leading corrections are known to be universal, i.e., independent of the structure of the involved hadrons. In such cases, the leading universal effects can be directly subtracted exactly from the lattice data. We denote n_{min} the smallest power of $\frac{1}{L}$ at which such a subtraction cannot be done. In the widely used finite-volume formulation QED$_L$, one always has $n_{\mathrm{min}} \leq 3$ due to the nonlocality of the theory [188]. The QED criteria are used here only in Sec. IV. Both QCD and QED criteria are unchanged from FLAG 19.

(iv) Isospin-breaking effects (where applicable):

★ all leading isospin-breaking effects are included in the lattice calculation

○ isospin-breaking effects are included using the electro-quenched approximation

■ otherwise

This criterion is used for quantities which are breaking isospin symmetry or which can be determined at the sub-percent accuracy where isospin-breaking effects, if not included, are expected to be the dominant source of uncertainty. In the current edition, this criterion is only used for the up- and down-quark masses, and related quantities (ϵ, Q^2 and R^2). The criteria for isospin-breaking effects are unchanged from FLAG 19.

(v) Renormalization (where applicable):

★ nonperturbative

○ 1-loop perturbation theory or higher with a reasonable estimate of truncation errors

■ otherwise

In Ref. [1], we assigned a red square to all results which were renormalized at 1-loop in perturbation theory. In FLAG 13 [2], we decided that this was too restrictive, since the error arising from renormalization constants, calculated in perturbation theory at 1-loop, is often estimated conservatively and reliably. These criteria have remained unchanged since then.

(vi) Renormalization group (RG) running (where applicable): For scale-dependent quantities, such as quark masses or B_K, it is essential that contact with continuum perturbation theory can be established. Various different methods are used for this purpose (cf. Appendix A.3 in FLAG 19 [4]): Regularization-independent momentum subtraction (RI/MOM), the Schrödinger functional, and direct comparison with (resummed) perturbation theory. Irrespective of the particular method used, the uncertainty associated with the choice of intermediate renormalization scales in the construction of physical observables must be brought under control. This is best achieved by performing comparisons between nonperturbative and perturbative running over a reasonably broad range of scales. These comparisons were initially only made in the Schrödinger functional approach, but are now also being performed in RI/MOM schemes. We mark the data for which information about nonperturbative-running checks is available and give some details, but do not attempt to translate this into a color code.

The pion mass plays an important role in the criteria relevant for chiral extrapolation and finite volume. For some of the regularizations used, however, it is not a trivial matter to identify this mass. In the case of twisted-mass fermions, discretization effects give rise to a mass difference between charged and neutral pions even when the up- and down-quark masses are equal: the charged pion is found to be the heavier of the two for twisted-mass Wilson fermions (cf. Ref. [189]). In early works, typically referring to $N_f = 2$ simulations (e.g., Refs. [189,190]), chiral extrapolations are based on chiral perturbation theory formulas which do not take these regularization effects into account. After the importance of accounting for isospin breaking when doing chiral fits was shown in Ref. [191], later works, typically referring to $N_f = 2 + 1 + 1$ simulations, have taken these effects into account [8]. We use $M_{\pi^\pm}$ for $M_{\pi,\mathrm{min}}$ in the chiral-extrapolation rating criterion. On the other hand, we identify $M_{\pi,\mathrm{min}}$ with the root mean square (RMS) of M_{π^+}, M_{π^-} and M_{π^0} in the finite-volume rating criterion.

In the case of staggered fermions, discretization effects give rise to several light states with the quantum numbers of the pion.[6] The mass splitting among these "taste" partners represents a discretization effect of $\mathcal{O}(a^2)$, which can be significant at large lattice spacings but shrinks as the spacing is reduced. In the discussion of the results obtained with staggered quarks given in the following sections, we assume that these artifacts are under control. We conservatively identify $M_{\pi,\mathrm{min}}$ with the root mean square (RMS) average of the masses of all the taste partners, both for chiral-extrapolation and finite-volume criteria.

In some of the simulations, the fermion formulations employed for the valence quarks are different from those used for the sea quarks. Even when the fermion formulations are the same, there are cases where the sea- and valence-quark masses differ. In such cases, we use the smaller of the valence-valence and valence-sea $M_{\pi_{\mathrm{min}}}$ values in the finite-volume criteria, since either of these channels may give the leading contribution depending on the quantity of interest at the 1-loop level of chiral perturbation theory. For the chiral-extrapolation criteria, on the other hand, we use the unitary point, where the sea- and valence-quark masses are the same, to define $M_{\pi_{\mathrm{min}}}$.

The strong coupling α_s is computed in lattice QCD with methods differing substantially from those used in the calculations of the other quantities discussed in this review. Therefore, we have established separate criteria for α_s results, which will be discussed in Sec. IX B 1.

In Sec. X on nuclear matrix elements, an additional criterion is used. This concerns the level of control over contamination from excited states, which is a more challenging issue for nucleons than for mesons. In response to an improved understanding of the impact of this contamination, the excited-state contamination criterion has been made more stringent compared to that in FLAG 19.

2. Data-driven criteria

For some time, the FLAG working groups have been considering using a data-driven criterion in assessing how

[6]We refer the interested reader to a number of reviews on the subject [192–196].

well the continuum limit is controlled. The quantity $\delta(a)$ is defined as

$$\delta(a) \equiv \frac{|Q(a) - Q(0)|}{\sigma_Q}, \tag{1}$$

were $Q(a)$ is the quantity under consideration with lattice spacing a, $Q(0)$ is the extrapolated continuum-limit value, and σ_Q is its error in the continuum limit. If $a_{\min}$ is the smallest lattice spacing used, there is concern if $\delta(a_{\min})$ is very large. That is, the results at the finest lattice spacing should not be too many standard deviations from the continuum limit in order for the extrapolation to be considered reliable.

The following is adopted for the current edition of the review: (1) Each working group attempts to determine $\delta(a_{\min})$ for each calculation that contributes to a FLAG average. However, it is not currently used as a criterion for inclusion in the averages. (2) The text of the report includes these values for calculations contributing to FLAG averages. (3) For the current edition of FLAG it is at the discretion of each working group to decide whether they wish to inflate the error of contributions to the average for calculations with large values of $\delta(a_{\min})$. If this is done, the inflation factor will be

$$s(\delta) = \max[1, 1 + 2(\delta - 3)/3]. \tag{2}$$

The inflation of the error is not displayed in tables or plots. It is only used to evaluate FLAG averages.

3. Heavy-quark actions

For the b quark, the discretization of the heavy-quark action follows a very different approach from that used for light flavors. There are several different methods for treating heavy quarks on the lattice, each with its own issues and considerations. Most of these methods use effective field theory (EFT) at some point in the computation, either via direct simulation of the EFT, or by using EFT as a tool to estimate the size of cutoff errors, or by using EFT to extrapolate from the simulated lattice quark masses up to the physical b-quark mass. Because of the use of an EFT, truncation errors must be considered together with discretization errors.

The charm quark lies at an intermediate point between the heavy and light quarks. In our earlier reviews, the calculations involving charm quarks often treated it using one of the approaches adopted for the b quark. Since FLAG 16 [3], however, most calculations simulate the charm quark using light-quark actions. This has become possible thanks to the increasing availability of dynamical gauge field ensembles with fine lattice spacings. But clearly, when charm quarks are treated relativistically, discretization errors are more severe than those of the corresponding light-quark quantities.

In order to address these complications, the heavy-quark section adds an additional, bipartite, treatment category to the rating system. The purpose of this criterion is to provide a guideline for the level of action and operator improvement needed in each approach to make reliable calculations possible, in principle.

A description of the different approaches to treating heavy quarks on the lattice can be found in Appendix A. 1. 3 of FLAG 19 [4]. For truncation errors we use HQET power counting throughout, since this review is focused on heavy-quark quantities involving B and D mesons rather than bottomonium or charmonium quantities. Here we describe the criteria for how each approach must be implemented in order to receive an acceptable rating (✓) for both the heavy-quark actions and the weak operators. Heavy-quark implementations without the level of improvement described below are rated not acceptable (■). The matching is evaluated together with renormalization, using the renormalization criteria described in Sec. II A 1. We emphasize that the heavy-quark implementations rated as acceptable and described below have been validated in a variety of ways, such as via phenomenological agreement with experimental measurements, consistency between independent lattice calculations, and numerical studies of truncation errors. These tests are summarized in Sec. VIII.

Relativistic heavy-quark actions

✓ at least tree-level $\mathcal{O}(a)$-improved action and weak operators

This is similar to the requirements for light-quark actions. All current implementations of relativistic heavy-quark actions satisfy this criterion.

NRQCD

✓ tree-level matched through $\mathcal{O}(1/m_h)$ and improved through $\mathcal{O}(a^2)$

The current implementations of NRQCD satisfy this criterion, and also include tree-level corrections of $\mathcal{O}(1/m_h^2)$ in the action.

HQET

✓ tree-level matched through $\mathcal{O}(1/m_h)$ with discretization errors starting at $\mathcal{O}(a^2)$

The current implementation of HQET by the ALPHA collaboration satisfies this criterion, since both action and weak operators are matched nonperturbatively through $\mathcal{O}(1/m_h)$. Calculations that exclusively use a static-limit action do not satisfy this criterion, since the static-limit action, by definition, does not include $1/m_h$ terms. We therefore include static computations in our final estimates only if truncation errors (in $1/m_h$) are discussed and included in the systematic uncertainties.

Light-quark actions for heavy quarks

✓ discretization errors starting at $\mathcal{O}(a^2)$ or higher

This applies to calculations that use the twisted-mass Wilson action, a nonperturbatively improved Wilson action, domain-wall fermions or the HISQ action for charm-quark quantities. It also applies to calculations that

use these light-quark actions in the charm region and above together with either the static limit or with an HQET-inspired extrapolation to obtain results at the physical b-quark mass. In these cases, the combined list of lattice spacings used for the datasets with $m_h > 0.5 m_{h,\mathrm{phys}}$ must satisfy the continuum-extrapolation criteria.

4. Conventions for the figures

For a coherent assessment of the present situation, the quality of the data plays a key role, but the color coding cannot be carried over to the figures. On the other hand, simply showing all data on equal footing might give the misleading impression that the overall consistency of the information available on the lattice is questionable. Therefore, in the figures we indicate the quality of the data in a rudimentary way, using the following symbols:

■ corresponds to results included in the average or estimate (i.e., results that contribute to the black square below);

□ corresponds to results that are not included in the average but pass all quality criteria;

◯ corresponds to all other results;

■ corresponds to FLAG averages or estimates; they are also highlighted by a gray vertical band.

The reason for not including a given result in the average is not always the same: the result may fail one of the quality criteria; the paper may be unpublished; it may be superseded by newer results; or it may not offer a complete error budget.

Symbols other than the ones above are used to distinguish results with specific properties and are always explained in the caption.[7]

Often, nonlattice data are also shown in the figures for comparison. For these we use the following symbols:

● corresponds to nonlattice results;

▲ corresponds to Particle Data Group (PDG) results.

B. Averages and estimates

FLAG results of a given quantity are denoted either as *averages* or as *estimates*. Here we clarify this distinction. To start with, both *averages* and *estimates* are based on results without any red tags in their color coding. For many observables there are enough independent lattice calculations of good quality, with all sources of error (not merely those related to the color-coded criteria), as analyzed in the original papers, appearing to be under control. In such cases, it makes sense to average these results and propose such an *average* as the best current lattice number. The averaging procedure applied to this data and the way the error is obtained is explained in detail in Sec. II C. In those cases where only a sole result passes our rating criteria (color coding), we refer to it as our FLAG *average*, provided it also displays adequate control of all other sources of systematic uncertainty.

On the other hand, there are some cases in which this procedure leads to a result that, in our opinion, does not cover all uncertainties. Systematic errors are by their nature often subjective and difficult to estimate, and may thus end up being underestimated in one or more results that receive green symbols for all explicitly tabulated criteria. Adopting a conservative policy, in these cases we opt for an *estimate* (or a range), which we consider as a fair assessment of the knowledge acquired on the lattice at present. This *estimate* is not obtained with a prescribed mathematical procedure, but reflects what we consider the best possible analysis of the available information. The hope is that this will encourage more detailed investigations by the lattice community.

There are two other important criteria that also play a role in this respect, but that cannot be color coded, because a systematic improvement is not possible. These are (i) the publication status, and (ii) the number of sea-quark flavors N_f. As far as the former criterion is concerned, we adopt the following policy: we average only results that have been published in peer-reviewed journals, i.e., they have been endorsed by referee(s). The only exception to this rule consists in straightforward updates of previously published results, typically presented in conference proceedings. Such updates, which supersede the corresponding results in the published papers, are included in the averages. Note that updates of earlier results rely, at least partially, on the same gauge-field-configuration ensembles. For this reason, we do not average updates with earlier results. Nevertheless, all results are listed in the tables,[8] and their publication status is identified by the following symbols:

(i) Publication status:
A published or plain update of published results.
P preprint.
C conference contribution.

In the present edition, the publication status on the 30th of April 2024 is relevant. If the paper appeared in print after that date, this is accounted for in the bibliography, but does not affect the averages.[9]

As noted above, in this review we present results from simulations with $N_f = 2$, $N_f = 2 + 1$ and $N_f = 2 + 1 + 1$ (except for $r_0\Lambda_{\overline{\mathrm{MS}}}$ where we also give the $N_f = 0$ result). We are not aware of an *a priori* way to quantitatively estimate the difference between results produced in simulations with a different number of dynamical quarks.

[7]For example, for quark-mass results we distinguish between perturbative and nonperturbative renormalization, and for heavy-flavor results we distinguish between those from leptonic and semileptonic decays.

[8]Whenever tables and figures turn out to be overcrowded, older, superseded results are omitted. However, all the most recent results from each collaboration are displayed.

[9]As noted above in footnote 1, two exceptions to this deadline were made, Refs. [56,197].

We therefore average results at fixed N_f separately; averages of calculations with different N_f are not provided.

To date, no significant differences between results with different values of N_f have been observed in the quantities listed in Tables 1–4. In particular, differences between results from simulations with $N_f = 2$ and $N_f = 2+1$ would reflect Zweig-rule violations related to strange-quark loops. Although not of direct phenomenological relevance, the size of such violations is an interesting theoretical issue *per se*, and one that can be quantitatively addressed only with lattice calculations. It remains to be seen whether the status presented here will change in the future, since this will require dedicated $N_f = 2$ and $N_f = 2+1$ calculations, which are not a priority of present lattice work.

The question of differences between results with $N_f = 2+1$ and $N_f = 2+1+1$ is more subtle. The dominant effect of including the charm sea quark is to shift the lattice scale, an effect that is accounted for by fixing this scale nonperturbatively using physical quantities. For most of the quantities discussed in this review, it is expected that residual effects are small in the continuum limit, suppressed by $\alpha_s(m_c)$ and powers of Λ^2/m_c^2. Here Λ is a hadronic scale that can only be roughly estimated and depends on the process under consideration. Note that the Λ^2/m_c^2 effects have been addressed in Refs. [198–202], and were found to be small for the quantities considered. Assuming that such effects are generically small, it might be reasonable to average the results from $N_f = 2+1$ and $N_f = 2+1+1$ simulations, although we do not do so here.

C. Averaging procedure and error analysis

In the present report, we repeatedly average results obtained by different collaborations, and estimate the error on the resulting averages. Here we provide details on how averages are obtained.

1. Averaging—generic case

We continue to follow the procedure of FLAG 13 and FLAG 16 [2,3] which we describe here in full detail.

One of the problems arising when forming averages is that not all of the datasets are independent. In particular, the same gauge-field configurations, produced with a given fermion discretization, are often used by different research teams with different valence-quark lattice actions, obtaining results that are not really independent. Our averaging procedure takes such correlations into account.

Consider a given measurable quantity Q, measured by M distinct, not necessarily uncorrelated, numerical experiments (simulations). The result of each of these measurement is expressed as

$$Q_i = x_i \pm \sigma_i^{(1)} \pm \sigma_i^{(2)} \pm \cdots \pm \sigma_i^{(E)}, \tag{3}$$

where x_i is the value obtained by the ith experiment ($i = 1, \ldots, M$) and $\sigma_i^{(\alpha)}$ (for $\alpha = 1, \ldots, E$) are the various errors. Typically $\sigma_i^{(1)}$ stands for the statistical error and $\sigma_i^{(\alpha)}$ ($\alpha \geq 2$) are the different systematic errors from various sources. For each individual result, we estimate the total error σ_i by adding statistical and systematic errors in quadrature

$$Q_i = x_i \pm \sigma_i,$$
$$\sigma_i \equiv \sqrt{\sum_{\alpha=1}^{E} [\sigma_i^{(\alpha)}]^2}. \tag{4}$$

With the weight factor of each total error estimated in standard fashion,

$$\omega_i = \frac{\sigma_i^{-2}}{\sum_{i=1}^{M} \sigma_i^{-2}}, \tag{5}$$

the central value of the average over all simulations is given by

$$x_{\text{av}} = \sum_{i=1}^{M} x_i \omega_i. \tag{6}$$

The above central value corresponds to a χ^2_{min}-weighted average, evaluated by adding statistical and systematic errors in quadrature. If the fit is not of good quality ($\chi^2_{\text{min}}/\text{dof} > 1$), the statistical and systematic error bars are stretched by a factor $S = \sqrt{\chi^2/\text{dof}}$.

Next, we examine error budgets for individual calculations and look for potentially correlated uncertainties. Specific problems encountered in connection with correlations between different datasets are described in the text that accompanies the averaging. If there is reason to believe that a source of error is correlated between two calculations, a 100% correlation is assumed. The covariance matrix C_{ij} for the set of correlated lattice results is estimated by a prescription due to Schmelling [203]. This consists in defining

$$\sigma_{i;j} = \sqrt{\sum\nolimits'_{\alpha} [\sigma_i^{(\alpha)}]^2}, \tag{7}$$

with $\sum'_\alpha$ running only over those errors of x_i that are correlated with the corresponding errors of the measurement x_j. This expresses the part of the uncertainty in x_i that is correlated with the uncertainty in x_j. If no such correlations are known to exist, then we take $\sigma_{i;j} = 0$. The diagonal and off-diagonal elements of the covariance matrix are then taken to be

$$C_{ii} = \sigma_i^2 \quad (i = 1, \ldots, M), \quad C_{ij} = \sigma_{i;j}\sigma_{j;i} \quad (i \neq j). \tag{8}$$

Finally, the error of the average is estimated by

$$\sigma_{\rm av}^2 = \sum_{i=1}^{M}\sum_{j=1}^{M}\omega_i\omega_j C_{ij}, \tag{9}$$

and the FLAG average is

$$Q_{\rm av} = x_{\rm av} \pm \sigma_{\rm av}. \tag{10}$$

2. Nested averaging

We have encountered one case where the correlations between results are more involved, and a nested averaging scheme is required. This concerns the B-meson bag parameters discussed in Sec. VIII B. In the following, we describe the details of the nested averaging scheme. This is an updated version of the section added in the web update of the FLAG 16 report.

The issue arises for a quantity Q that is given by a ratio, $Q = Y/Z$. In most simulations, both Y and Z are calculated, and the error in Q can be obtained in each simulation in the standard way. However, in other simulations only Y is calculated, with Z taken from a global average of some type. The issue to be addressed is that this average value $\bar{Z}$ has errors that are correlated with those in Q.

In the example that arises in Sec. VIII B, $Q = B_B$, $Y = B_B f_B^2$ and $Z = f_B^2$. In one of the simulations that contribute to the average, Z is replaced by $\bar{Z}$, the PDG average for f_B^2 [204] (obtained with an averaging procedure similar to that used by FLAG). This simulation is labeled with $i = 1$, so that

$$Q_1 = \frac{Y_1}{\bar{Z}}. \tag{11}$$

The other simulations have results labeled Q_j, with $j \geq 2$. In this set up, the issue is that $\bar{Z}$ is correlated with the Q_j, $j \geq 2$.[10]

We begin by decomposing the error in Q_1 in the same schematic form as above,

$$Q_1 = x_1 \pm \frac{\sigma_{Y_1}^{(1)}}{\bar{Z}} \pm \frac{\sigma_{Y_1}^{(2)}}{\bar{Z}} \pm \cdots \pm \frac{\sigma_{Y_1}^{(E)}}{\bar{Z}} \pm \frac{Y_1\sigma_{\bar{Z}}}{\bar{Z}^2}. \tag{12}$$

Here the last term represents the error propagating from that in $\bar{Z}$, while the others arise from errors in Y_1. For the remaining Q_j ($j \geq 2$) the decomposition is as in Eq. (3). The total error of Q_1 then reads

$$\sigma_1^2 = \left(\frac{\sigma_{Y_1}^{(1)}}{\bar{Z}}\right)^2 + \left(\frac{\sigma_{Y_1}^{(2)}}{\bar{Z}}\right)^2 + \cdots + \left(\frac{\sigma_{Y_1}^{(E)}}{\bar{Z}}\right)^2 + \left(\frac{Y_1}{\bar{Z}^2}\right)^2\sigma_{\bar{Z}}^2, \tag{13}$$

while that for the Q_j ($j \geq 2$) is

$$\sigma_j^2 = (\sigma_j^{(1)})^2 + (\sigma_j^{(2)})^2 + \cdots + (\sigma_j^{(E)})^2. \tag{14}$$

Correlations between Q_j and Q_k ($j, k \geq 2$) are taken care of by Schmelling's prescription, as explained above. What is new here is how the correlations between Q_1 and Q_j ($j \geq 2$) are taken into account.

To proceed, we recall from Eq. (9) that $\sigma_{\bar{Z}}$ is given by

$$\sigma_{\bar{Z}}^2 = \sum_{i',j'=1}^{M'} \omega[Z]_{i'}\omega[Z]_{j'}C[Z]_{i'j'}. \tag{15}$$

Here the indices i' and j' run over the M' simulations that contribute to $\bar{Z}$, which, in general, are different from those contributing to the results for Q. The weights $\omega[Z]$ and covariance matrix $C[Z]$ are given an explicit argument Z to emphasize that they refer to the calculation of this quantity and not to that of Q. $C[Z]$ is calculated using the Schmelling prescription [Eqs. (7)–(9)] in terms of the errors, $\sigma[Z]_{i'}^{(\alpha)}$, taking into account the correlations between the different calculations of Z.

We now generalize Schmelling's prescription for $\sigma_{i;j}$, Eq. (7), to that for $\sigma_{1;k}$ ($k \geq 2$), i.e., the part of the error in Q_1 that is correlated with Q_k. We take

$$\sigma_{1;k} = \sqrt{\frac{1}{\bar{Z}^2}{\sum_{(\alpha)\leftrightarrow k}}' [\sigma_{Y_1}^{(\alpha)}]^2 + \frac{Y_1^2}{\bar{Z}^4}\sum_{i',j'}^{M'}\omega[Z]_{i'}\omega[Z]_{j'}C[Z]_{i'j'\leftrightarrow k}}. \tag{16}$$

The first term under the square root sums those sources of error in Y_1 that are correlated with Q_k. Here we are using a more explicit notation from that in Eq. (7), with $(\alpha) \leftrightarrow k$ indicating that the sum is restricted to the values of α for which the error $\sigma_{Y_1}^{(\alpha)}$ is correlated with Q_k. The second term accounts for the correlations within $\bar{Z}$ with Q_k, and is the nested part of the present scheme. The new matrix $C[Z]_{i'j'\leftrightarrow k}$ is a restriction of the full covariance matrix $C[Z]$, and is defined as follows. Its diagonal elements are given by

$$C[Z]_{i'i'\leftrightarrow k} = (\sigma[Z]_{i'\leftrightarrow k})^2 \quad (i' = 1, \ldots, M'), \tag{17}$$

$$(\sigma[Z]_{i'\leftrightarrow k})^2 = {\sum_{(\alpha)\leftrightarrow k}}' (\sigma[Z]_{i'}^{(\alpha)})^2, \tag{18}$$

[10]There is also a small correlation between Y_1 and $\bar{Z}$, but we follow the original Ref. [79] and do not take this into account. Thus, the error in Q_1 is obtained by simple error propagation from those in Y_1 and $\bar{Z}$. Ignoring this correlation is conservative, because, as in the calculation of B_K, the correlations between $B_B f_B^2$ and f_B^2 tend to lead to a cancellation of errors. By ignoring this effect we are making a small overestimate of the error in Q_1.

where the summation $\sum'_{(\alpha)\leftrightarrow k}$ over (α) is restricted to those $\sigma[Z]^{(\alpha)}_{i'}$ that are correlated with Q_k. The off-diagonal elements are

$$C[Z]_{i'j'\leftrightarrow k} = \sigma[Z]_{i';j'\leftrightarrow k}\sigma[Z]_{j';i'\leftrightarrow k} \quad (i' \neq j'), \tag{19}$$

$$\sigma[Z]_{i';j'\leftrightarrow k} = \sqrt{\sum'_{(\alpha)\leftrightarrow j'k} (\sigma[Z]^{(\alpha)}_{i'})^2}, \tag{20}$$

where the summation $\sum'_{(\alpha)\leftrightarrow j'k}$ over (α) is restricted to $\sigma[Z]^{(\alpha)}_{i'}$ that are correlated with *both* $Z_{j'}$ and Q_k.

The last quantity that we need to define is $\sigma_{k;1}$.

$$\sigma_{k;1} = \sqrt{\sum'_{(\alpha)\leftrightarrow 1} [\sigma^{(\alpha)}_k]^2}, \tag{21}$$

where the summation $\sum'_{(\alpha)\leftrightarrow 1}$ is restricted to those $\sigma^{(\alpha)}_k$ that are correlated with one of the terms in Eq. (13).

In summary, we construct the covariance matrix C_{ij} using Eq. (8), as in the generic case, except the expressions for $\sigma_{1;k}$ and $\sigma_{k;1}$ are now given by Eqs. (16) and (21), respectively. All other $\sigma_{i;j}$ are given by the original Schmelling prescription, Eq. (7). In this way, we extend the philosophy of Schmelling's approach while accounting for the more involved correlations.

III. GENERAL DEFINITION OF THE LOW-ENERGY LIMIT OF THE STANDARD MODEL

Working group members: A. Portelli, A. Ramos, N. Tantalo

This section discusses the matching of quantum chromodynamics (QCD) and quantum electrodynamics (QED) to nature in order to obtain predictions for low-energy Standard Model observables. In particular, we discuss the prescription dependence, i.e., the dependence on which observables are matched, arising when one neglects electromagnetic interactions, an approximation made in numerous lattice and phenomenological calculations. These ambiguities need to be controlled when combining high-precision observables —typically with less than 1% of relative uncertainty—in that approximation. In order to facilitate that, we propose here a fixed prescription for the separation of QCD and QED contributions to any given hadronic observable. While this prescription is, in principle, arbitrary, one has to take care not to introduce artificially large QED contributions and to stay close to prescriptions used commonly in phenomenology. This prescription was discussed and agreed upon during an open workshop that took place at the Higgs Centre for Theoretical Physics, Edinburgh, in May 2023, and therefore is referred to as the "Edinburgh consensus."[11]

We note that since this consensus emerged only recently, the majority of results in this review are averaged neglecting potential discrepancies arising from the ambiguities. This is, on the one hand, an adequate procedure in the case of quantities with uncertainties larger than the size of expected QED corrections. On the other hand, it can be difficult to correct these ambiguities to a common prescription since it requires the knowledge of derivatives of observables in quark masses and couplings, rarely communicated in papers. We emphasize the present consensus in the hope that it will be widely adopted in upcoming high-precision Standard Model predictions, allowing future editions of this review to avoid uncertainties resulting from these ambiguities.

A. First-order isospin-breaking expansion

According to our present knowledge, hadronic physics is well described by the low-energy limit of the Standard Model, which is understood as energies well below the electroweak symmetry-breaking scale $\mathcal{S}_{\rm ESB} \approx 100$ GeV. In that limit, the Standard Model is an $\mathrm{SU}(3) \times \mathrm{U}(1)$ gauge theory defined by the QCD + QED Lagrangian, whose free parameters are the e-, μ-, and τ-lepton masses, the u-, d-, s-, c-, and b-quark masses, and the strong and electromagnetic coupling constants, respectively, g_s and e. In that context, isospin symmetry is defined by assuming that the up and down quarks are identical particles apart from their flavor. This symmetry is only approximate and it is broken by two effects: the small but different masses of the two quarks, and their different electric charges. The total effect is expected to be small, typically a $\mathcal{O}(1\%)$ perturbation of a hadronic energy or amplitude. Therefore, we consider only first-order perturbations in isospin-breaking effects, and we expect this approximation to be accurate at the level of $\mathcal{O}(10^{-4})$ relative precision.

The asymptotic states of QCD are hadrons not quarks, and hadron properties are the only unambiguous observables experimentally available. Similarly, the strong coupling constant is not directly accessible and can be substituted through dimensional transmutation by a dimensionful hadronic energy scale. Moreover, the running of the electromagnetic coupling constant is a higher-order correction beyond the order considered here. It can be fixed to its Thomson-limit value. Finally, nature can be reproduced (up to weak and gravitational effects) by fixing the bare parameters of the QCD + QED Lagrangian to reproduce the following inputs:

(1) the Thomson-limit constant $\alpha^\phi = \frac{e^2}{4\pi} = 7.2973525693(11) \times 10^{-3}$ [205],
(2) the experimentally observed lepton masses m^ϕ_ℓ,
(3) a choice of N_f known independent hadronic quantities M^ϕ, setting the quark masses,
(4) a single known dimensionful hadronic quantity $\mathcal{S}^\phi$, setting the QCD scale.

[11] https://indico.ph.ed.ac.uk/event/257/.

The vectors m_ℓ and M have three and N_f components, respectively, where N_f is the number of quark flavors in the calculation. In the present context, "known" is understood as experimentally known for measurable quantities, or theoretically predicted for more abstract quantities, which are not accessible experimentally, but are renormalized and gauge invariant and can be predicted by lattice gauge theory. If the dependency of a given observable $X(\alpha, m_\ell, M, \mathcal{S})$ on the above variables is known, then its physical value is predicted by

$$X^\phi = (\mathcal{S}^\phi)^{[X]} \tilde{X}(\alpha^\phi, m_\ell^\phi/\mathcal{S}^\phi, M^\phi/\mathcal{S}^\phi) \equiv X(\alpha^\phi, m_\ell^\phi, M^\phi, \mathcal{S}^\phi), \tag{22}$$

where $\tilde{X}$ is the dimensionless function describing X in units of the scale $\mathcal{S}$, and $[X]$ is the energy dimension of X. Here M and $\mathcal{S}$ are assumed, without loss of generality, to have an energy dimension of 1. Due to the renormalizability of QCD + QED, this prediction is unambiguous, i.e., changing the variables M^ϕ and $\mathcal{S}^\phi$ to other inputs with known physical values will lead to the same prediction for renormalized observables.[12]

In many instances, the precision required on hadronic observables is not as small as one percent, and isospin-breaking effects are potentially negligible. In those cases, it is generally considerably simpler to neglect the QED contributions, both for lattice and phenomenological calculations. Moreover, even for observables requiring isospin-breaking corrections to be computed, it can be phenomenologically relevant to separate an isospin-symmetric value and isospin-breaking corrections (e.g., specific parts of the HVP contribution to the muon $g-2$, decay constants in weak decays). However, since experimental measurements always contain isospin-breaking corrections, there are no experimental result available to define the list of inputs above for $\alpha = 0$, or in the isospin-symmetric limit. Still, one would like to define an expansion of the form

$$X^\phi = \bar{X} + X_\gamma + X_{\mathrm{SU}(2)}, \tag{23}$$

where $\bar{X}$ is the isospin-symmetric value of X, and X_γ and $X_{\mathrm{SU}(2)}$ are the first-order electromagnetic and strong isospin-breaking corrections, respectively. Only the sum of these three terms is unambiguous.[13] Defining a value for individual terms is prescription-dependent, and requires additional, in principle arbitrary, inputs. This issue has been discussed in reviews [206,207], and both the phenomenology [208–210] and lattice [24,25,116,211–221] literature. If quantities defined at $\alpha = 0$ are involved in the investigation of anomalies related to new physics searches, *the associated prescriptions must be matched across predictions*. In the next section, we propose a prescription agreed upon at the dedicated May 2023 workshop in Edinburgh.

B. Edinburgh consensus

The decomposition Eq. (23) can be unambiguously defined given two extra sets of inputs $(\hat{m}_\ell, \hat{M}, \hat{\mathcal{S}})$ and $(\bar{m}_\ell, \bar{M}, \bar{\mathcal{S}})$ specifying pure QCD and isospin-symmetric QCD, respectively (denoted QCD and isoQCD). It is understood that in QCD isospin symmetry can still be broken by the up-down quark-mass difference. The QCD and isoQCD values of an observable X can then be defined by

$$\hat{X} = X(0, \hat{m}_\ell, \hat{M}, \hat{\mathcal{S}}) \quad \text{and} \quad \bar{X} = X(0, \bar{m}_\ell, \bar{M}, \bar{\mathcal{S}}), \tag{24}$$

respectively. The variables $\bar{M}$, $\bar{\mathcal{S}}$ must have one dimension of linear dependency to reflect the exact isospin symmetry of this theory. This means that there are only N_f independent numbers. Finally, the corrections in Eq. (23) are then defined by

$$X_\gamma = X^\phi - \hat{X} \quad \text{and} \quad X_{\mathrm{SU}(2)} = \hat{X} - \bar{X}. \tag{25}$$

One should notice that these definitions already constitute in themselves a prescription, as QED has an isospin-symmetric component which is here assumed to be excluded from the component $\bar{X}$.

The proposed prescription defines lepton masses to always be equal to their experimental values (for which negligible experimental uncertainties are discarded), i.e., $\hat{m}_\ell = \bar{m}_\ell = m_\ell^\phi$, and is based on the mass variables $M = (M_{\pi^+}, M_{K^+}, M_{K^0}, M_{D_s^+}, M_{B_s^0})$ and the scale-setting quantity f_{π^+}, with the values given in Table 6.[14] We will now comment on the definition and applications of that prescription.

C. Comparison to other schemes

The hadronic quantities that define the proposed prescription, as well as their input values, have been chosen to balance between two main constraints, on the one hand numerical and on the other hand theoretical. Since any uncertainties on the theoretical inputs have to be propagated to the predictions, the numerical constraint requires choosing the matching observables among those that can be computed on the lattice with the highest accuracy. The theoretical constraint requires choosing a definition of

[12]Here "renormalizability" for QED is understood as perturbative renormalizability, which is sufficient in this context.

[13]Here "unambiguous" is used in a loose sense. Ambiguities of the order $\mathcal{O}(1/m_Z)$ and $\mathcal{O}(1/m_{N_f+1})$, as well as higher-order isospin-breaking corrections, remain and are considered to be irrelevant.

[14]For calculations with no active c and/or b quarks, the $M_{D_s^+}$ and/or $M_{B_s^0}$ components should be ignored.

QCD that leads to isospin-breaking corrections which are as close as possible to what has commonly been done in the past, in particular, in phenomenological calculations.

On the numerical side, all the chosen hadronic inputs can be extracted from the leading exponential behavior at large Euclidean times of two-point mesonic lattice correlators with high numerical precision. This constraint is the main reason behind the choice of f_{π^+} as the scale-setting observable. From the theoretical and phenomenological perspectives, this can be seen as an uncomfortable choice. Indeed, the physical quantity that is measured in experiments is the leptonic decay rate of the charged pion. In the full theory (QCD + QED) soft photons as well as non-factorizable virtual QED corrections have to be taken into account in the theoretical calculation in order to use the experimental values as an input, and previous knowledge of the CKM matrix element V_{ud} is required. From this perspective, for example, the choice of the Ω^--baryon mass used by several lattice collaborations might be more natural. However, the majority of lattice calculations are still performed in the $\alpha = 0$ limit, which makes f_{π^+} a more accessible choice than a baryonic quantity in most cases. It is crucial to note that our prescription defines QCD and isoQCD in the space of possible $\alpha = 0$ theories, but the choice of coordinates to define these points is arbitrary and can be changed using standard change-of-variable algebra, while keeping the prescription fixed. In particular, the scale setting variable can be changed, as we discuss now.

The prescription above can be implemented by using other inputs. This is possible because QCD is renormalizable. Indeed, one can start by defining QCD using our prescription to compute $\hat{X}$ and $\hat{M}_\Omega$, following the notation of the previous section, namely

$$\hat{X} = X(0, \hat{m}_\ell, \hat{M}, \hat{f}_{\pi^+}) \quad \text{and} \quad \hat{M}_\Omega = M_\Omega(0, \hat{m}_\ell, \hat{M}, \hat{f}_{\pi^+}), \tag{26}$$

where $\hat{M}$ and $\hat{f}_{\pi^+}$ are given by the "QCD" column in Table 6. Once this calculation has been done, the value of $\hat{M}_\Omega$ that has been obtained (assuming for the moment that the errors are negligible) can be substituted to $\hat{f}_{\pi^+}$ to redefine our prescription independently from the pion decay constant. In practice, though, it will not be possible to neglect the errors on $\hat{M}_\Omega$. This means that the equivalence between the two sets of coordinates, explicitly

$$\hat{X} = X(0, \hat{m}_\ell, \hat{M}, \hat{f}_{\pi^+}) = X(0, \hat{m}_\ell, \hat{M}, \hat{M}_\Omega), \tag{27}$$

can be established within the errors on $\hat{M}_\Omega$ that will have to be propagated on any prediction. In this respect, the choice of defining QCD by prescribing with no errors the values appearing in Table 6 puts the choice of $\hat{f}_{\pi^+}$ on a slightly different footing than $\hat{M}_\Omega$. The accuracy of this matching will directly depend on the accuracy of the dimensionless ratio $\hat{M}_\Omega/\hat{f}_{\pi^+}$. The whole discussion above can be reiterated identically for isoQCD, replacing hatted quantities ($\hat{X}$, …) with barred ones ($\bar{X}$, …). It is important to note that f_{π^+} is used only to define QCD and plays no role in defining the full QCD + QED theory. In particular, through a change of scale variable, like that discussed above, one does not need to know the QED correction to the π^+ leptonic decay rate to use our prescription, and one does not lose the ability to predict this rate for high-precision determinations of the $|V_{ud}|$ CKM matrix element.

TABLE 6. Edinburgh consensus for the definition of pure QCD and isospin-symmetric QCD. The rightmost table is redundant and provided for convenience.

	QCD	isoQCD
M_{π^+}	135.0 MeV	135.0 MeV
M_{K^+}	491.6 MeV	494.6 MeV
M_{K^0}	497.6 MeV	494.6 MeV
$M_{D_s^+}$	1967 MeV	1967 MeV
$M_{B_s^0}$	5367 MeV	5367 MeV
f_{π^+}	130.5 MeV	130.5 MeV

	QCD	isoQCD
M_{π^+}/f_{π^+}	1.034	1.034
M_{K^+}/f_{π^+}	3.767	3.790
M_{K^0}/f_{π^+}	3.813	3.790
$M_{D_s^+}/f_{\pi^+}$	15.07	15.07
$M_{B_s^0}/f_{\pi^+}$	41.13	41.13

Theoretical constraints are the main reason behind the particular choice of values prescribed in Table 6. Most isospin-breaking separation schemes used in the literature aim at keeping constant the value of a definition of the renormalized quark masses when sending α to zero between the physical QCD + QED theory and QCD. Such a class of constraints was implemented in various ways, for example by the RM123/RM123S collaboration by computing directly quark masses in the $\overline{\text{MS}}$ scheme at 2 GeV [212,217,222,223]. Another example comes from the BMW collaboration, which used in several calculations [24,116,211,221] a scheme defined by keeping fixed the squared masses of $\bar{q}q$-connected mesons when changing α. Although these schemes share similar aims, they are not equivalent and differ by the choice of renormalization scale and scheme, as well as the contribution from higher-order chiral corrections when using squared meson masses. However, at the level of precision of current lattice calculations, no significant discrepancies were observed between both approaches [217,220,221,224], and the numerical values of the pion and kaon masses in Table 6 are compatible with these determinations within the current level of precision. We also note that the mass

values prescribed here are compatible with those produced from phenomenological inputs in the first edition of FLAG [1], which predates the lattice references quoted above.

We end this chapter with a comment on Gasser-Rusetsky-Scimemi (GRS) type schemes [209]. These authors emphasized the importance of keeping track of the scheme dependence of the splitting in Eq. (23). They furthermore proposed to keep renormalized quark masses and the strong coupling at a particular matching scale μ_1 (and a chosen renormalization scheme) fixed as one turns off the electromagnetic coupling. In contrast to the perturbative models studied by GRS, such a scheme is hard to implement in QCD. Even on the lattice, uncertainties are introduced which are larger than the isospin-breaking corrections (see the sections on quark masses and α_s). The RM123S scheme [222] mentioned above is an electro-quenched GRS type scheme.[15] Since there are no electromagnetic contributions to α_s in the electro-quenched approximation, the generic difficulties of a GRS type scheme are circumvented.

IV. QUARK MASSES

Working group members: T. Blum, A. Portelli, A. Ramos

Quark masses are fundamental parameters of the Standard Model. An accurate determination of these parameters is important for both phenomenological and theoretical applications. The bottom- and charm-quark masses, for instance, are important sources of parametric uncertainties in several Higgs decay modes. The up-, down- and strange-quark masses govern the amount of explicit chiral symmetry breaking in QCD. From a theoretical point of view, the values of quark masses provide information about the flavor structure of physics beyond the Standard Model. The Review of Particle Physics of the Particle Data Group contains a review of quark masses [225], which covers light as well as heavy flavors. Here, we also consider light- and heavy-quark masses, but focus on lattice results and discuss them in more detail. We do not discuss the top quark, however, because it decays weakly before it can hadronize, and the nonperturbative QCD dynamics described by present day lattice calculations is not relevant. The lattice determination of light- (up, down, strange), charm- and bottom-quark masses is considered below in Secs. IV A, IV B, and IV C, respectively.

Quark masses cannot be measured directly in experiment because quarks cannot be isolated, as they are confined inside hadrons. From a theoretical point of view, in QCD with N_f flavors, a precise definition of quark masses requires one to choose a particular renormalization scheme. This renormalization procedure introduces a renormalization scale μ, and quark masses depend on this renormalization scale according to the renormalization group (RG) equations. In mass-independent renormalization schemes the RG equations read

$$\mu \frac{\mathrm{d}\bar{m}_i(\mu)}{\mathrm{d}\mu} = \bar{m}_i(\mu)\tau(\bar{g}), \tag{28}$$

where the function $\tau(\bar{g})$ is the anomalous dimension, which depends only on the value of the strong coupling $\alpha_s = \bar{g}^2/(4\pi)$. Note that in QCD $\tau(\bar{g})$ is the same for all quark flavors. The anomalous dimension is scheme dependent, but its perturbative expansion

$$\tau(\bar{g}) \overset{\bar{g}\to 0}{\sim} -\bar{g}^2(d_0 + d_1\bar{g}^2 + \ldots) \tag{29}$$

has a leading coefficient $d_0 = 8/(4\pi)^2$, which is scheme independent.[16] Equation (28), being a first order differential equation, can be solved exactly by using Eq. (29) as the boundary condition. The formal solution of the RG equation reads

$$M_i = \bar{m}_i(\mu)[2b_0\bar{g}^2(\mu)]^{-d_0/(2b_0)} \times \exp\left\{-\int_0^{\bar{g}(\mu)} \mathrm{d}x \left[\frac{\tau(x)}{\beta(x)} - \frac{d_0}{b_0 x}\right]\right\}, \tag{30}$$

where $b_0 = (11 - 2N_f/3)/(4\pi)^2$ is the universal leading perturbative coefficient in the expansion of the β-function

$$\beta(\bar{g}) \equiv \mu \frac{\mathrm{d}\bar{g}}{\mathrm{d}\mu} \overset{\bar{g}\to 0}{\sim} -\bar{g}^3(b_0 + b_1\bar{g}^2 + \ldots) \tag{31}$$

which governs the running of the strong coupling. The renormalization group invariant (RGI) quark masses M_i are formally integration constants of the RG Eq. (28). They are scale independent, and due to the universality of the coefficient d_0, they are also scheme independent. Moreover, they are nonperturbatively defined by Eq. (30). They only depend on the number of flavors N_f, making them a natural candidate to quote quark masses and compare determinations from different lattice collaborations. Nevertheless, it is customary in the phenomenology community to use the $\overline{\mathrm{MS}}$ scheme at a scale $\mu = 2$ GeV to compare different results for light quarks and the charm quark, and to use a scale equal to its own mass for the charm and bottom. In this review, we will quote final averages for both quantities.

Results for quark masses are always quoted in the four-flavor theory unless otherwise noted. $N_f = 2 + 1$ results have to be converted to the four-flavor theory. Fortunately, the charm quark is heavy $(\Lambda_{\mathrm{QCD}}/m_c)^2 < 1$, and this conversion can be performed in perturbation theory with negligible ($\sim$0.2%) perturbative uncertainties.

Nonperturbative corrections in this matching are more difficult to estimate. Lattice determinations do not show

[15]The electro-quenched approximation is defined by setting the electric charges of the sea quarks to zero.

[16]We follow the conventions of Gasser and Leutwyler [208].

any significant deviation between $N_f = 2+1$ and $N_f = 2+1+1$ calculations. For example, the difference in the final averages for the mass of the strange quark m_s between $N_f = 2+1$ and $N_f = 2+1+1$ determinations is about 1.3%, or about one standard deviation. Since these effects are suppressed by a factor of $1/N_c$, and a factor of the strong coupling at the scale of the charm mass, naive power counting arguments would suggest that the effects are ∼1%, in line with the above observation. On the other hand, numerical nonperturbative studies [198,200,226] have found this power counting argument to be an overestimate by one order of magnitude in the determination the Λ-parameter and other quantities.

We quote all final averages at 2 GeV in the $\overline{\text{MS}}$ scheme and also the RGI values (in the four-flavor theory). We use the exact RG Eq. (30). Note that to use this equation we need the value of the strong coupling in the $\overline{\text{MS}}$ scheme at a scale $\mu = 2$ GeV. All our results are obtained from the RG equation in the $\overline{\text{MS}}$ scheme and the 5-loop beta function together with the value of the Λ-parameter in the four-flavor theory $\Lambda^{(4)}_{\overline{\text{MS}}} = 295(10)$ MeV obtained in this review (see Sec. IX). We use the 5-loop mass anomalous dimension as well [227]. In the uncertainties of the RGI masses, we separate the contributions from the determination of the quark masses and the propagation of the uncertainty of $\Lambda^{(4)}_{\overline{\text{MS}}}$. These are identified with the subscripts m and Λ, respectively.

Conceptually, all lattice determinations of quark masses contain three basic ingredients:

(1) Tuning the lattice bare-quark masses to match the experimental values of some quantities. Pseudoscalar meson masses provide the most common choice, since they have a strong dependence on the values of quark masses.
(2) Renormalization of the bare-quark masses. Bare-quark masses determined with the above-mentioned criteria have to be renormalized. Many of the latest determinations use some nonperturbatively defined scheme. One can also use perturbation theory to connect directly the values of the bare-quark masses to the values in the $\overline{\text{MS}}$ scheme at 2 GeV. Experience shows that 1-loop calculations are unreliable for the renormalization of quark masses: usually at least two loops are required to have trustworthy results.
(3) If quark masses have been nonperturbatively renormalized, for example, to some MOM or SF scheme, the values in this scheme must be converted to the phenomenologically useful values in the $\overline{\text{MS}}$ scheme (or to the scheme/scale independent RGI masses). Either option requires the use of perturbation theory. The larger the energy scale of this matching with perturbation theory, the better, and many recent computations in MOM schemes do a nonperturbative running up to 3–4 GeV. Computations in the SF scheme allow us to perform this running nonperturbatively over large energy scales and match with perturbation theory directly at the electroweak scale ∼100 GeV.

Note that many lattice determinations of quark masses make use of perturbation theory at a scale of a few GeV.

We mention that lattice-QCD calculations of the b-quark mass have an additional complication which is not present in the case of the charm and light quarks. At the lattice spacings currently used in numerical calculations the direct treatment of the b quark with the fermionic actions commonly used for light quarks is very challenging. Only two determinations of the b-quark mass use this approach, reaching the physical b-quark mass region at two lattice spacings with $aM \sim 1$. There are a few widely used approaches to treat the b quark on the lattice, which have already been discussed in the FLAG 13 review (see Sec. 8 of Ref. [2]). Those relevant for the determination of the b-quark mass will be briefly described in Sec. IV C.

A. Masses of the light quarks

Light-quark masses are particularly difficult to determine because they are very small (for the up and down quarks) or small (for the strange quark) compared to typical hadronic scales. Thus, their impact on typical hadronic observables is minute, and it is difficult to isolate their contribution accurately.

Fortunately, the spontaneous breaking of $\text{SU}(3)_L \times \text{SU}(3)_R$ chiral symmetry provides observables which are particularly sensitive to the light-quark masses: the masses of the resulting Nambu-Goldstone bosons (NGB), i.e., pions, kaons, and eta. Indeed, the Gell-Mann-Oakes-Renner relation [228] predicts that the squared mass of a NGB is directly proportional to the sum of the masses of the quark and antiquark which compose it, up to higher-order mass corrections. Moreover, because these NGBs are light, and are composed of only two valence particles, their masses have a particularly clean statistical signal in lattice-QCD calculations. In addition, the experimental uncertainties on these meson masses are negligible. Thus, in lattice calculations, light-quark masses are typically obtained by renormalizing the input quark mass and tuning them to reproduce NGB masses, as described above.

1. Lattice determination of m_s and m_{ud}

We now turn to a review of the lattice calculations of the light-quark masses and begin with m_s, the isospin-averaged up- and down-quark mass m_{ud}, and their ratio. Most groups quote only m_{ud}, not the individual up- and down-quark masses. We then discuss the ratio m_u/m_d and the individual determinations of m_u and m_d.

Quark masses have been calculated on the lattice since the mid-nineties. However, early calculations were performed in the quenched approximation, leading to unquantifiable systematics. Thus, in the following, we only review

modern, unquenched calculations, which include the effects of light sea quarks.

Tables 7 and 8 list the results of $N_f = 2+1$ and $N_f = 2+1+1$ lattice calculations of m_s and m_{ud}. These results are given in the $\overline{\text{MS}}$ scheme at 2 GeV, which is standard nowadays, though some groups are starting to quote results at higher scales (e.g., Ref. [229]). The tables also show the color coding of the calculations leading to these results. As indicated earlier in this review, we treat calculations with different values of N_f separately.

$N_f = 2+1$ lattice calculations

We begin with $N_f = 2+1$ calculations (see FLAG 19 and earlier editions for two-flavor results). These and the corresponding results for m_{ud} and m_s are summarized in Table 7. Given the very high precision of a number of the results, with total errors on the order of 1%, it is important to consider the effects neglected in these calculations. Isospin-breaking and electromagnetic effects are small on m_{ud} and m_s, and have been approximately accounted for in the calculations that will be retained for our averages. We have already commented that the effect of the omission of the charm quark in the sea is expected to be small, below our current precision, and we do not add any additional uncertainty due to these effects in the final averages.

The only new computation since the previous FLAG edition is the determination of light-quark masses by the CLQCD collaboration (CLQCD 23 [10]). Using stout-smeared clover fermions, the ensembles reach the physical point and have three lattice spacings to perform the continuum extrapolation. These look under control, having in all cases $\delta(a_{\min}) < 2$ (see II A 2). Volumes are large, and these characteristics ensure that the rating is ★ in all criteria. Renormalization is performed nonperturbatively in two different setups (RI/MOM and SMOM), with the difference used as a systematic effect. This systematic effect, in fact, dominates their error budget.

The ALPHA collaboration [22] uses nonperturbatively $\mathcal{O}(a)$ improved Wilson fermions (a subset of the CLS ensembles [245]). The renormalization is performed nonperturbatively in the SF scheme from 200 MeV up to the electroweak scale ∼100 GeV [246]. This nonperturbative running over such large energy scales avoids any use of perturbation theory at low energy scales, but adds a cost in terms of uncertainty: the running alone propagates to ≈1% of the error in quark masses. This turns out to be one of the dominant pieces of uncertainty for the case of m_s. On the other hand, for the case of m_{ud}, the uncertainty is dominated by the chiral extrapolations. The ensembles used include four values of the lattice spacing below 0.09 fm, which qualifies for a ★ in the continuum extrapolation, and pion masses down to 200 MeV. This value lies just at the boundary of the ★ rating, but since the chiral extrapolation is a substantial source of systematic uncertainty, we opted to rate the work with a ○. In any case, this work enters in the average and their results show a reasonable agreement with the FLAG average. In all cases the data driven continuum limit criteria shows $\delta(a_{\min}) < 3$.

We now comment in some detail on previous works that also contribute to the averages.

RBC/UKQCD 14 [12] significantly improves on their RBC/UKQCD 12B [229] work by adding three new domain wall fermion ensembles to three used previously. Two of the new simulations are performed at essentially physical pion masses ($M_\pi \simeq 139$ MeV) on lattices of about 5.4 fm in size and with lattice spacings of 0.114 fm and 0.084 fm. It is complemented by a third simulation with $M_\pi \simeq 371$ MeV, $a \simeq 0.063$ fm and a rather small $L \simeq 2.0$ fm. Altogether, this gives them six simulations with six unitary ($m_{\text{sea}} = m_{\text{val}}$) M_π's in the range of 139 to 371 MeV, and effectively three lattice spacings from 0.063 to 0.114 fm. They perform a combined global continuum and chiral fit to all of their results for the π and K masses and decay constants, the Ω baryon mass and two Wilson-flow parameters. Quark masses in these fits are renormalized and run nonperturbatively in the RI-SMOM scheme. This is done by computing the relevant renormalization constant for a reference ensemble, and determining those for other simulations relative to it by adding appropriate parameters in the global fit. This calculation passes all of our selection criteria, with $\delta(a_{\min}) \approx 1$.

$N_f = 2+1$ MILC results for light-quark masses go back to 2004 [239,240]. They use rooted staggered fermions. By 2009 their simulations covered an impressive range of parameter space, with lattice spacings going down to 0.045 fm, and valence-pion masses down to approximately 180 MeV [19]. The most recent MILC $N_f = 2+1$ results, i.e., MILC 10A [16] and MILC 09A [19], feature large statistics and 2-loop renormalization. Since these datasets subsume those of their previous calculations, these latest results are the only ones that need to be kept in any world average.

The BMW 10A, 10B [13,14] calculation still satisfies our stricter selection criteria. They reach the physical up- and down-quark mass by *interpolation* instead of by extrapolation. Moreover, their calculation was performed at five lattice spacings ranging from 0.054 to 0.116 fm, with small extrapolations $\delta(a_{\min}) < 2$. The work uses full nonperturbative renormalization and running and in volumes of up to $(6\text{ fm})^3$, guaranteeing that the continuum limit, renormalization, and infinite-volume extrapolation are controlled. It does neglect, however, isospin-breaking effects, which are small on the scale of their error bars.

Finally, we come to another calculation which satisfies our selection criteria, HPQCD 10 [15]. It updates the staggered-fermions calculation of HPQCD 09A [33]. In those papers, the renormalized mass of the strange quark is obtained by combining the result of a precise calculation of the renormalized charm-quark mass m_c with the result of a calculation of the quark-mass ratio m_c/m_s. As described in Ref. [244] and in Sec. IV B, HPQCD determines m_c by

TABLE 7. $N_f = 2 + 1$ lattice results for the masses m_{ud} and m_s (MeV).

Collaboration	Ref.	Publication status	Chiral Extrapolation	Continuum extrapolation	Finite volume	Renormalization	Running	m_{ud}	m_s
CLQCD 23	[10]	A	★	★	★	★	[l]	3.60(11)(15)	98.8(2.9)(4.7)
ALPHA 19	[11]	A	○	★	★	★	[l]	3.54(12)(9)	95.7(2.5)(2.4)
Maezawa 16	[230]	A	■	★	★	★	[k]	...	92.0(1.7)
RBC/UKQCD 14B[a]	[12]	A	★	★	★	★	[k]	3.31(4)(4)	90.3(0.9)(1.0)
RBC/UKQCD 12 [a]	[229]	A	★	○	★	★	[k]	3.37(9)(7)(1)(2)	92.3(1.9)(0.9)(0.4)(0.8)
PACS-CS 12[b]	[231]	A	★	■	■	★	[i]	3.12(24)(8)	83.60(0.58)(2.23)
Laiho 11	[54]	C	○	★	★	○	...	3.31(7)(20)(17)	94.2(1.4)(3.2)(4.7)
BMW 10A, 10B[c]	[13,14]	A	★	★	★	★	[j]	3.469(47)(48)	95.5(1.1)(1.5)
PACS-CS 10	[232]	A	★	■	■	★	[i]	2.78(27)	86.7(2.3)
MILC 10A	[16]	C	○	★	★	○	...	3.19(4)(5)(16)	...
HPQCD 10[d]	[15]	A	○	★	★	...	...	3.39(6)	92.2(1.3)
RBC/UKQCD 10A	[119]	A	○	○	★	★	[h]	3.59(13)(14)(8)	96.2(1.6)(0.2)(2.1)
Blum 10[e]	[233]	A	○	■	○	★	...	3.44(12)(22)	97.6(2.9)(5.5)
PACS-CS 09	[234]	A	★	■	■	★	[i]	2.97(28)(3)	92.75(58)(95)
HPQCD 09A[f]	[33]	A	○	★	★	...	...	3.40(7)	92.4(1.5)
MILC 09A	[19]	C	○	★	★	○	...	3.25(1)(7)(16)(0)	89.0(0.2)(1.6)(4.5)(0.1)
MILC 09	[196]	A	○	★	★	○	...	3.2(0)(1)(2)(0)	88(0)(3)(4)(0)
PACS-CS 08	[235]	A	★	■	■	■	...	2.527(47)	72.72(78)
RBC/UKQCD 08	[236]	A	○	■	★	★	...	3.72(16)(33)(18)	107.3(4.4)(9.7)(4.9)
CP-PACS/JLQCD 07	[237]	A	■	★	★	■	...	$3.55(19)(^{+56}_{-20})$	$90.1(4.3)(^{+16.7}_{-4.3})$
HPQCD 05	[238]	A	○	○	○	○	...	3.2(0)(2)(2)(0)[g]	87(0)(4)(4)(0)[g]
MILC 04, HPQCD/ MILC/UKQCD 04	[239,240]	A	○	○	○	■	...	2.8(0)(1)(3)(0)	76(0)(3)(7)(0)

[a]The results are given in the $\overline{\text{MS}}$ scheme at 3 instead of 2 GeV. We run them down to 2 GeV using numerically integrated 4-loop running [241,242] with $N_f = 3$ and with the values of $\alpha_s(M_Z)$, m_b, and m_c taken from Ref. [243]. The running factor is 1.106. At three loops it is only 0.2% smaller, indicating that perturbative running uncertainties are small. We neglect them here.

[b]The calculation includes electromagnetic and $m_u \neq m_d$ effects through reweighting.

[c]The fermion action used is tree-level improved.

[d]m_s is obtained by combining m_c and HPQCD 09A's $m_c/m_s = 11.85(16)$ [33]. Finally, m_{ud} is determined from m_s with the MILC 09 result for m_s/m_{ud}. Since m_c/m_s is renormalization group invariant in QCD, the renormalization and running of the quark masses enter indirectly through that of m_c (see below).

[e]The calculation includes quenched electromagnetic effects.

[f]What is calculated is $m_c/m_s = 11.85(16)$. m_s is then obtained by combining this result with the determination $m_c(m_c) = 1.268(9)$ GeV from Ref. [244]. Finally, m_{ud} is determined from m_s with the MILC 09 result for m_s/m_{ud}.

[g]The bare numbers are those of MILC 04. The masses are simply rescaled, using the ratio of the 2-loop to 1-loop renormalization factors.

[h]The masses are renormalized nonperturbatively at a scale of 2 GeV in a couple of $N_f = 3$ RI-SMOM schemes. A careful study of perturbative matching uncertainties has been performed by comparing results in the two schemes in the region of 2 to 3 GeV [119].

[i]The masses are renormalized and run nonperturbatively up to a scale of 40 GeV in the $N_f = 3$ SF scheme. In this scheme, nonperturbative and NLO running for the quark masses are shown to agree well from 40 GeV all the way down to 3 GeV [232].

[j]The masses are renormalized and run nonperturbatively up to a scale of 4 GeV in the $N_f = 3$ RI-MOM scheme. In this scheme, nonperturbative and N^{3}LO running for the quark masses are shown to agree from 6 GeV down to 3 GeV to better than 1% [14].

[k]All required running is performed nonperturbatively.

[l]Running is performed nonperturbatively from 200 MeV to the electroweak scale ~100 GeV.

TABLE 8. $N_f = 2+1+1$ lattice results for the masses m_{ud} and m_s (MeV).

Collaboration	Ref.	Publication status	Chiral extrapolation	Continuum extrapolation	Finite volume	Renormalization	Running	m_{ud}	m_s
ETM 21A	[7]	A	★	★	★	★	···	$3.636(66)(^{+60}_{-57})$	$98.7(2.4)(^{+4.0}_{-3.2})$
HPQCD 18[a]	[17]	A	★	★	★	★	···		94.49(96)
FNAL/MILC/TUMQCD 18	[9]	A	★	★	★	★	···	3.404(14)(21)	92.52(40)(56)
HPQCD 14A[b]	[18]	A	★	★	★	···	···		93.7(8)
ETM 14[b]	[8]	A	○	★	★	★	···	3.70(13)(11)	99.6(3.6)(2.3)

[a]Bare-quark masses are renormalized nonperturbatively in the RI-SMOM scheme at scales $\mu \sim 2$–5 GeV for different lattice spacings and translated to the $\overline{\text{MS}}$ scheme. Perturbative running is then used to run all results to a reference scale $\mu = 3$ GeV.

[b]As explained in the text, m_s is obtained by combining the results $m_c(5\text{ GeV}; N_f = 4) = 0.8905(56)$ GeV and $(m_c/m_s)(N_f = 4) = 11.652(65)$, determined on the same dataset. A subsequent scale and scheme conversion, performed by the authors, leads to the value 93.6(8). In the table, we have converted this to $m_s(2\text{ GeV}; N_f = 4)$, which makes a very small change.

fitting Euclidean-time moments of the $\bar{c}c$ pseudoscalar density two-point functions, obtained numerically in lattice QCD, to fourth-order, continuum perturbative expressions. These moments are normalized and chosen so as to require no renormalization with staggered fermions. Since m_c/m_s requires no renormalization either, HPQCD's approach displaces the problem of lattice renormalization in the computation of m_s to one of computing continuum perturbative expressions for the moments. To calculate m_{ud} HPQCD 10 [15] use the MILC 09 determination of the quark-mass ratio m_s/m_{ud} [196].

HPQCD 09A [33] obtains $m_c/m_s = 11.85(16)$ [33] fully nonperturbatively, with a precision slightly larger than 1%. HPQCD 10's determination of the charm-quark mass, $m_c(m_c) = 1.268(6)$,[17] is even more precise, achieving an accuracy better than 0.5%.

This discussion leaves us with six results for our final average for m_s: CLQCD 23 [10], ALPHA 19 [22], MILC 09A [19], BMW 10A, 10B [13,14], HPQCD 10 [15] and RBC/UKQCD 14 [12]. Assuming that the result from HPQCD 10 is 100% correlated with that of MILC 09A, as it is based on a subset of the MILC 09A configurations, we find $m_s = 92.3(1.0)$ MeV with a $\chi^2/\text{dof} = 1.60$.

For the light-quark mass m_{ud}, the results satisfying our criteria are CLQCD 23, ALPHA 19, RBC/UKQCD 14B, BMW 10A, 10B, HPQCD 10, and MILC 10A. For the error, we include the same 100% correlation between statistical errors for the latter two as for the strange case, resulting in the following (at scale 2 GeV in the $\overline{\text{MS}}$ scheme, and $\chi^2/\text{dof} = 1.4$),

$$N_f = 2+1: \quad \begin{array}{ll} m_{ud} = 3.387(39)\text{ MeV} & \text{Refs. [11–16]}, \\ m_s = 92.4(1.0)\text{ MeV} & \text{Refs. [11–15, 19]}. \end{array} \tag{32}$$

And the RGI values

$$N_f = 2+1: \quad \begin{array}{ll} M_{ud}^{\text{RGI}} = 4.714(55)_m(46)_\Lambda\text{ MeV} & \text{Refs. [10–16]}, \\ M_s^{\text{RGI}} = 128.5(1.4)_m(1.2)_\Lambda\text{ MeV} & \text{Refs. [10–15, 19]}. \end{array} \tag{33}$$

$N_f = 2+1+1$ lattice calculations

Since the previous review a new computation of m_s, m_{ud} has appeared, ETM 21A [7]. Using twisted-mass fermions with an added clover term to suppress $\mathcal{O}(a^2)$ effects between the neutral and charged pions, this work represents a significant improvement over ETM 14 [8]. Renormalization is performed nonperturbatively in the RI-MOM scheme. Their ensembles comprise three lattice spacings (0.095, 0.082, and 0.069 fm), two volumes for the finest lattice spacings with pion masses reaching down to the physical point in the two finest lattices spacings

[17]To obtain this number, we have used the conversion from $\mu = 3$ GeV to m_c given in Ref. [244].

allowing a controlled chiral extrapolation. Their volumes are large, with $m_\pi L$ between four and five. These characteristics of their ensembles pass the most stringent FLAG criteria in all categories. This work extracts quark masses from two different quantities, one based on the meson spectrum and the other based on the baryon spectrum. Results obtained with these two methods agree within errors, but the size of the continuum extrapolation is much larger for the case of the extractions based on the meson spectrum. In particular, we estimate that $\delta(a_{\min}) = 4$–4.5 for the individual fits that enter the determination of $m_{\rm ud}, m_{\rm s}$ respectively. We note that while these values are somewhat large, the systematic errors that the authors estimate in the determinations of the light-quark masses are about the same size as the statistical fluctuations. This will reduce the stretching factors to a value close to one, and, therefore we do not apply any additional corrections for these cases. Nevertheless, we stress that some large continuum extrapolations are present in this work.

Determinations based on the baryon spectrum agree well with the FLAG average while the ones based on the meson sector are high in comparison (there is good agreement with their previous results, ETM 14 [8]). Related with the previous point, it is important to note that the determinations that involve large continuum extrapolations are the ones that show a larger tension.

There are three other works that enter in light-quark mass averages. Contributing both to the average of m_{ud} and m_s is FNAL/MILC/TUMQCD 18 [9]. They perform a determination of the strange-quark mass using masses of the heavy-strange mesons as input. In this case, some very large continuum extrapolations, with $\delta(a_{\min}) \approx 14$ enter in a global analysis, but for the determination of the light-quark masses, we believe that the influence of the data at heavier masses on the determination of the fit parameter that determines $m_{\rm s}$ is small. In the region $m_{\rm heavy} < 3$ GeV the extrapolations are much better under control, and in fact involve up to five lattice spacing. We conclude that the large value of $\delta(a_{\min})$ does not influence significantly the values of the light-quark masses. HPQCD 18 [17] and HPQCD 14A [18] contribute to the determination of m_{ud}, and both show $\delta(a_{\min}) < 3$ for most of their region of parameters.

The $N_f = 2+1+1$ results are summarized in Table 8. While the results of HPQCD 14A and HPQCD 18 agree well (using different methods), there are several tensions in the determination of m_s. The most significant discrepancy is between the results of the ETM collaboration and other results. But also the two very precise determinations of HPQCD 18 and FNAL/MILC/TUMQCD 18 show a tension. Note that the results of Ref. [18] are reported as $m_s(2\ \text{GeV}; N_f = 3)$ and those of Ref. [8] as $m_{ud(s)}(2\ \text{GeV}; N_f = 4)$. We convert the former to $N_f = 4$ and obtain $m_s(2\ \text{GeV}; N_f = 4) = 93.7(8)$ MeV. The average of ETM 21A, FNAL/MILC/TUMQCD 18, HPQCD 18, ETM 14 and HPQCD 14A is 93.46(58) MeV with $\chi^2/\text{dof} = 1.3$. For the light-quark mass, we average ETM 21A, ETM 14 and FNAL/MILC/TUMQCD 18 to obtain 3.427(51) with a $\chi^2/\text{dof} = 4.5$. We note these χ^2 values are large. For the case of the light-quark masses there is a clear tension between the ETM and FNAL/MILC/TUMQCD results. We also note that the $2+1$-flavor values are consistent with the four-flavor ones, so in all cases we have simply quoted averages according to FLAG rules, including stretching factors for the errors based on χ^2 values of our fits. Nevertheless it is worth pointing out that large continuum extrapolations are present in the $N_f = 2+1+1$ determination of quark masses. Global fits that aim at describing results obtained for a wide range of quark masses are involved in many analyses. At small quark masses many lattice spacing enter these determinations, but how the large quark mass region influences the precision obtained at small quark masses is something that deserves further investigation.

$$N_f = 2+1+1: \begin{array}{ll} m_{ud} = 3.427(51)\ \text{MeV} & \text{Refs. [7–9]}, \\ m_s = 93.46(58)\ \text{MeV} & \text{Refs. [7–9,17,18]} \end{array} \tag{34}$$

and the RGI values

$$N_f = 2+1+1: \begin{array}{ll} M_{ud}^{\rm RGI} = 4.768(71)_m(46)_\Lambda\ \text{MeV} & \text{Refs. [7–9]}, \\ M_s^{\rm RGI} = 130.0(0.8)_m(1.3)_\Lambda\ \text{MeV} & \text{Refs. [7–9,17,18]}. \end{array} \tag{35}$$

In Figs. 1 and 2 the lattice results listed in Tables 7 and 8 and the FLAG averages obtained at each value of N_f are presented and compared with various phenomenological results.

2. Lattice determinations of m_s/m_{ud}

The lattice results for m_s/m_{ud} are summarized in Table 9. In the ratio m_s/m_{ud}, one of the sources of systematic error—the uncertainties in the renormalization factors—drops out. This is especially important for the recent determination by the CLQCD collaboration, since their error budget for the individual quark masses was dominated by the systematic associated with the renormalization. Also, other systematic effects (like the effect of the scale setting) are reduced in these ratios. This might explain that despite the discrepancies that are present in the individual quark mass determinations, the ratios show an overall very good agreement.

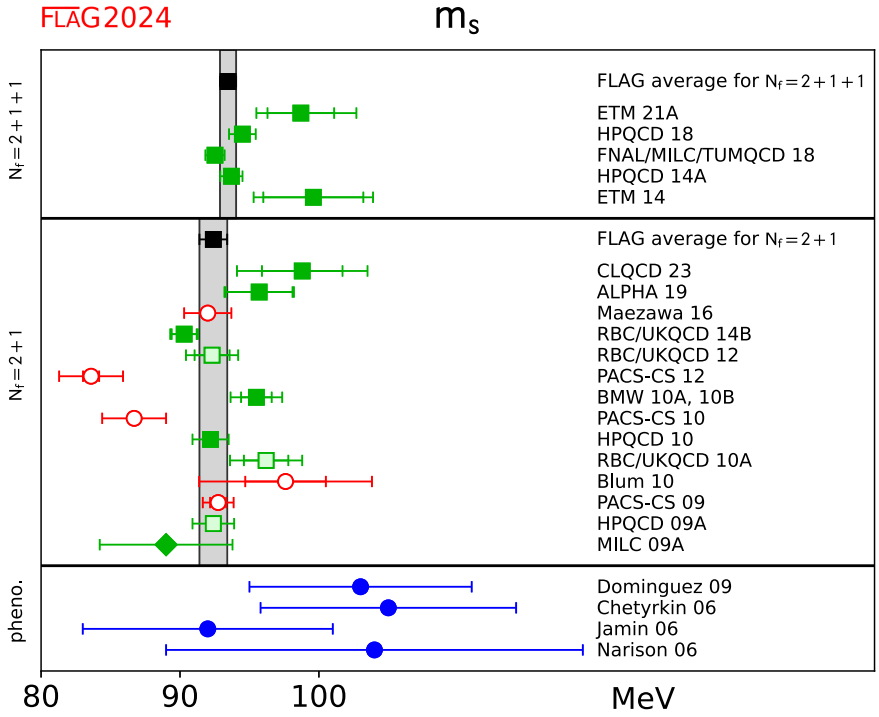


FIG. 1. $\overline{\text{MS}}$ mass of the strange quark (at 2 GeV scale) in MeV. The upper two panels show the lattice results listed in Tables 7 and 8, while the bottom panel collects sum rule results [247–251]. The diamond represents a result based on perturbative renormalization. The squares and open circles denote results based on nonperturbative renormalization. The black squares and the gray bands represent our averages (32) and (34). The significance of the colors is explained in Sec. II.

$N_f = 2+1$ lattice calculations

CLQCD 23 [10], discussed already, is the only new result for this section. The other works contributing to this average are ALPHA 19, RBC/UKQCD 14B, which replaces RBC/UKQCD 12 (see Sec. IV A 1), and the results of MILC 09A and BMW 10A, 10B.

The results show very good agreement with a $\chi^2/\text{dof} = 0.14$. The final uncertainty (≈0.5%) is smaller than the ones of the quark masses themselves. At this level of precision, the uncertainties in the electromagnetic and strong isospin-breaking corrections might not be completely negligible. Nevertheless, we decided not to add any uncertainty associated with this effect. The main reason is that most recent determinations try to estimate this uncertainty themselves and found an effect smaller than naive power counting estimates (see $N_f = 2+1+1$ section),

$$N_f = 2+1\text{:}\quad m_s/m_{ud} = 27.42(12)\quad \text{Refs. [12–14,19,22].} \tag{36}$$

$N_f = 2+1+1$ lattice calculations

For $N_f = 2+1+1$ there are four results, ETM 21 [7], MILC 17 [20], ETM 14 [8] and FNAL/MILC 14A [21], all of which satisfy our selection criteria.

All these works have been discussed in the previous FLAG edition [4], except the new result ETM 21A, that we have already examined. The fit has $\chi^2/\text{dof} \approx 1.7$, and the result shows reasonable agreement with the $N_f = 2+1$ result.

$$N_f = 2+1+1\text{:}\quad m_s/m_{ud} = 27.227(81)\quad \text{Refs. [7,8,20,21],} \tag{37}$$

which corresponds to an overall uncertainty equal to 0.4%. It is worth noting that Ref. [20] estimates the EM effects in this quantity to be ∼0.18% (or 0.049 which is less than the quoted error above).

All the lattice results listed in Table 9 as well as the FLAG averages for each value of N_f are reported in Fig. 3 and compared with χPT and sum rules.

3. Lattice determination of m_u and m_d

In this section, we review computations of the individual m_u and m_d quark masses, as well as the parameter ϵ related to the violations of Dashen's theorem

$$\epsilon = \frac{(\Delta M_K^2 - \Delta M_\pi^2)_\gamma}{\Delta M_\pi^2}, \tag{38}$$

where $\Delta M_\pi^2 = M_{\pi^+}^2 - M_{\pi^0}^2$ and $\Delta M_K^2 = M_{K^+}^2 - M_{K^0}^2$ are the pion and kaon squared mass splittings, respectively. The subscript γ, here and in the following, denotes corrections

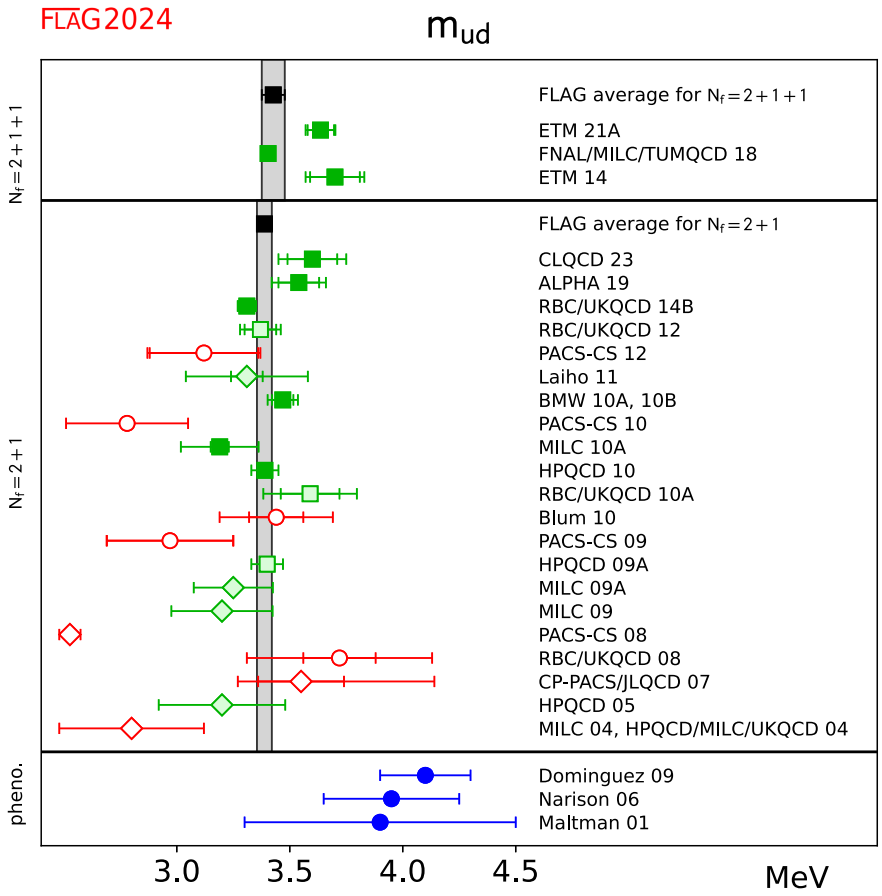


FIG. 2. Mean mass of the two lightest quarks, $m_{ud} = \frac{1}{2}(m_u + m_d)$. The bottom panel shows results based on sum rules [247,250,252] (for more details see Fig. 1).

that arise from electromagnetic effects only according to the prescription given in Sec. III. This parameter is often a crucial intermediate quantity in the extraction of the individual light-quark masses. Indeed, it can be shown using the G-parity symmetry of the pion triplet, that ΔM_π^2 does not receive $\mathcal{O}(m_u - m_d)$ isospin-breaking corrections. In other words

$$\Delta M_\pi^2 = (\Delta M_\pi^2)_\gamma \quad \text{and} \quad \epsilon = \frac{(\Delta M_K^2)_\gamma}{\Delta M_\pi^2} - 1, \tag{39}$$

at leading order in the isospin-breaking expansion. Once known, ϵ allows one to consistently subtract the electromagnetic part of the kaon-mass splitting to obtain the QCD part of the kaon mass splitting $(\Delta M_K^2)_{\mathrm{SU}(2)}$. In contrast with the pion, the kaon QCD splitting is sensitive to $m_u - m_d$ and, in particular, proportional to it at leading order in χPT. Therefore, the knowledge of ϵ allows for the determination of $m_u - m_d$ from a chiral fit to lattice-QCD data. Originally introduced in another form in [257], ϵ vanishes in the SU(3) chiral limit, a result known as Dashen's theorem. However, in the 1990s numerous phenomenological papers pointed out that ϵ might be an $\mathcal{O}(1)$ number, indicating a significant failure of SU(3) χPT in the description of electromagnetic effects on light-meson masses. However, the phenomenological determinations of ϵ feature some level of controversy, leading to the rather imprecise estimate $\epsilon = 0.7(5)$ given in the first edition of FLAG. Starting with the FLAG 19 edition of the review, we quote more precise averages for ϵ, directly obtained from lattice-QCD + QED simulations. We refer the reader to earlier editions of FLAG and to the review [214] for discussions of the phenomenological determinations of ϵ.

The quality criteria regarding finite-volume effects for calculations including QED are presented in Sec. II A 1. Due to the long-distance nature of the electromagnetic interaction, these effects are dominated by a power law in the lattice spatial size. The coefficients of this expansion depend on the chosen finite-volume formulation of QED. For $\mathrm{QED_L}$, these effects on the squared mass M^2 of a charged meson are given by [185,186,188]

$$\Delta_{\mathrm{FV}} M^2 = \alpha M^2 \left\{ \frac{c_1}{ML} + \frac{2c_1}{(ML)^2} + \mathcal{O}\left[\frac{1}{(ML)^3}\right] \right\}, \tag{40}$$

with $c_1 \simeq -2.83730$. It has been shown in [185] that the two first orders in this expansion are exactly known for hadrons, and are equal to the pointlike case. However, the

TABLE 9. Lattice results for the ratio m_s/m_{ud}.

Collaboration	Ref.	N_f	Publication status	Chiral extrapolation	Continuum extrapolation	Finite volume	m_s/m_{ud}
ETM 21A	[7]	$2+1+1$	A	★	★	★	$27.17(32)^{+56}_{-38}$
MILC 17[a]	[20]	$2+1+1$	A	★	★	★	$27.178(47)^{+86}_{-57}$
FNAL/MILC 14A	[21]	$2+1+1$	A	★	★	★	$27.35(5)^{+10}_{-7}$
ETM 14	[8]	$2+1+1$	A	○	★	○	26.66(32)(2)
CLQCD 23	[10]	$2+1$	A	★	★	★	27.47(30)(13)
ALPHA 19	[22]	$2+1$	A	○	★	★	27.0(1.0)(0.4)
RBC/UKQCD 14B	[12]	$2+1$	A	★	★	★	27.34(21)
RBC/UKQCD 12[b]	[229]	$2+1$	A	★	○	★	27.36(39)(31)(22)
PACS-CS 12[c]	[231]	$2+1$	A	★	■	■	26.8(2.0)
Laiho 11	[54]	$2+1$	C	○	★	★	28.4(0.5)(1.3)
BMW 10A, 10B[d]	[13,14]	$2+1$	A	★	★	★	27.53(20)(8)
RBC/UKQCD 10A	[119]	$2+1$	A	○	○	★	26.8(0.8)(1.1)
Blum 10[e]	[233]	$2+1$	A	○	■	○	28.31(0.29)(1.77)
PACS-CS 09	[234]	$2+1$	A	★	■	■	31.2(2.7)
MILC 09A	[19]	$2+1$	C	○	★	★	27.41(5)(22)(0)(4)
MILC 09	[196]	$2+1$	A	○	★	★	27.2(1)(3)(0)(0)
PACS-CS 08	[235]	$2+1$	A	★	■	■	28.8(4)
RBC/UKQCD 08	[236]	$2+1$	A	○	■	★	28.8(0.4)(1.6)
MILC 04, HPQCD/MILC/UKQCD 04	[239,240]	$2+1$	A	○	○	○	27.4(1)(4)(0)(1)

[a]The calculation includes electromagnetic effects.

[b]The errors are statistical, chiral and finite volume.

[c]The calculation includes electromagnetic and $m_u \neq m_d$ effects through reweighting.

[d]The fermion action used is tree-level improved.

[e]The calculation includes quenched electromagnetic effects.

$\mathcal{O}[1/(ML)^3]$ term and higher orders depend on the structure of the hadron. The universal corrections for QED_{TL} can also be found in [185]. In all this part, for all computations using such universal formulas, the QED finite-volume quality criterion has been applied with $n_{\min} = 3$, otherwise $n_{\min} = 1$ was used (see II A 1).

Since FLAG 21, one new result has been reported for nondegenerate light-quark masses, namely CLQCD 23 [10]. This result is based on a new set of $N_f = 2+1$ stout-smeared clover fermion simulations, including one ensemble at the physical light-quark mass. This calculation achieves a ★ rating in all criteria except the inclusion of isospin-breaking effects. Regarding the latter, $(\Delta M_K^2)^\gamma$ from RM123 17 [23] is used to estimate the QCD kaon-mass splitting required to constrain m_u and m_d. Because of the use of a result already averaged for $N_f = 2+1+1$ up- and down-quark masses, and in application of our quality criterion, we do not include CLQCD 23 in our average for m_u/m_d.

Regarding results already presented in previous FLAG editions, we start by reviewing predictions for the $N_f = 2+1$ sector. MILC 09A [19] uses the mass difference between K^0 and K^+, from which they subtract electromagnetic effects using Dashen's theorem with corrections, as discussed in the introduction of this section. The up and down sea quarks remain degenerate in their calculation, fixed to the value of m_{ud} obtained from M_{π^0}. To determine m_u/m_d, BMW 10A, 10B [13,14] follow a slightly different strategy. They obtain this ratio from their result for m_s/m_{ud} combined with a phenomenological determination of the isospin-breaking quark-mass ratio $Q = 22.3(8)$, from $\eta \to 3\pi$ decays [261] (the decay $\eta \to 3\pi$ is very sensitive to QCD isospin breaking, but fairly insensitive to QED isospin breaking). Instead of subtracting electromagnetic

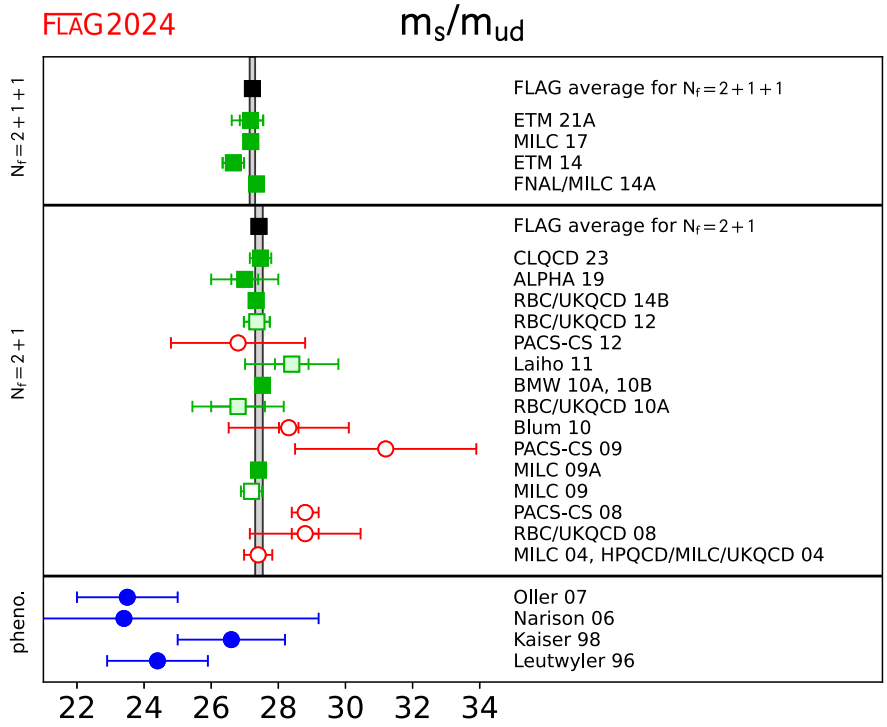


FIG. 3. Results for the ratio m_s/m_{ud}. The upper part shows the lattice results listed in Table 9 together with the FLAG averages for each value of N_f. The lower part shows results obtained from χPT and sum rules [250,253–256].

effects using phenomenology, RBC 07 [262] and Blum 10 [233] actually include a quenched electromagnetic field in their calculation. This means that their results include corrections to Dashen's theorem, albeit only in the presence of quenched electromagnetism. Since the up and down quarks in the sea are treated as degenerate, very small isospin corrections are neglected, as in MILC's calculation. PACS-CS 12 [231] takes the inclusion of isospin-breaking effects one step further. Using reweighting techniques, it also includes electromagnetic and $m_u - m_d$ effects in the sea. However, they do not correct for the large finite-volume effects coming from electromagnetism in their $M_\pi L \sim 2$ simulations, but provide rough estimates for their size, based on Ref. [263]. QCDSF/UKQCD 15 [259] uses QCD + QED dynamical simulations performed at the SU(3)-flavor-symmetric point, but at a single lattice spacing, so they do not enter our average. The smallest partially quenched ($m_{\rm sea} \neq m_{\rm val}$) pion mass is greater than 200 MeV, so our chiral-extrapolation criteria require a ○ rating. Concerning finite-volume effects, this work uses three spatial extents L of 1.6 fm, 2.2 fm, and 3.3 fm. QCDSF/UKQCD 15 claims that the volume dependence is not visible on the two largest volumes, leading them to assume that finite-size effects are under control. As a consequence of that, the final result for quark masses does not feature a finite-volume extrapolation or an estimation of the finite-volume uncertainty. However, in their work on the QED corrections to the hadron spectrum [259] based on the same ensembles, a volume study shows some level of compatibility with the $\mathrm{QED_L}$ finite-volume effects derived in [186]. We see two issues here. First, the analytical result quoted from [186] predicts large, $\mathcal{O}(10\%)$ finite-size effects from QED on the meson masses at the values of $M_\pi L$ considered in QCDSF/UKQCD 15, which is inconsistent with the statement made in the paper. Second, it is not known that the zero-mode regularization scheme used here has the same volume scaling as $\mathrm{QED_L}$. We therefore chose to assign the ■ rating for finite volume to QCDSF/UKQCD 15. BMW 16A [24] reuses the dataset produced from their determination of the light-baryon octet-mass splittings [211] using electro-quenched $\mathrm{QCD + QED_{TL}}$ smeared clover-fermion simulations. Finally, MILC 16 [258], which is a preliminary result for the value of ϵ published in MILC 18 [25], also provides a $N_f = 2+1$ computation of the ratio m_u/m_d.

We now describe the $N_f = 2+1+1$ calculations. ETM 14 [8] uses simulations in pure QCD, but determines $m_u - m_d$ from the slope $\partial M_K^2/\partial m_{ud}$ and the physical value for the QCD kaon-mass splitting taken from the phenomenological estimate in FLAG 13. In the $N_f = 2+1+1$ sector, MILC 18 [25] computed ϵ using $N_f = 2+1$ asqtad electro-quenched $\mathrm{QCD + QED_{TL}}$ simulations and extracted the ratio m_u/m_d from a new set of $N_f = 2+1+1$ HISQ QCD simulations. Although ϵ comes from $N_f = 2+1$ simulations, $(\Delta M_K^2)^{\mathrm{SU(2)}}$, which is about three times larger than $(\Delta M_K^2)^{\gamma}$, has been determined in the $N_f = 2+1+1$ theory. We therefore chose to classify this result

as a four-flavor one. This result is explicitly described by the authors as an update of MILC 17 [20]. In MILC 17 [20], m_u/m_d is determined as a side-product of a global analysis of heavy-meson decay constants, using a preliminary version of ϵ from MILC 18 [25]. In FNAL/MILC/TUMQCD 18 [9] the ratio m_u/m_d from MILC 17 [20] is used to determine the individual masses m_u and m_d from a new calculation of m_{ud}. The work RM123 17 [23] is the continuation of the $N_f = 2$ work named RM123 13 [212] in the previous edition of FLAG. This group now uses $N_f = 2+1+1$ ensembles from ETM 10 [264], however, still with a rather large minimum pion mass of 270 MeV, leading to the ○ rating for chiral extrapolations.

Lattice results for m_u, m_d and m_u/m_d are summarized in Table 10. The color coding is specified in detail in Sec. II A. Considering the important progress in the last years on including isospin-breaking effects in lattice simulations, we are now in a position where averages for m_u and m_d can be made without the need of phenomenological inputs. Therefore, lattice calculations of the individual quark masses using phenomenological inputs for isospin-breaking effects will be coded ■.

We begin with $N_f = 2+1$ (for $N_f = 2$ see the 2021 edition). The only result that qualifies to enter the FLAG average is BMW 16A [24],

$$N_f = 2+1: \quad \begin{array}{lll} m_u = 2.27(9)\ \text{MeV} & \text{Ref. [24]}, \\ m_d = 4.67(9)\ \text{MeV} & \text{Ref. [24]}, \\ m_u/m_d = 0.485(19) & \text{Ref. [24]}, \end{array} \tag{41}$$

with errors of roughly 4%, 2% and 4%, respectively. These numbers result in the following RGI averages

$$N_f = 2+1: \quad \begin{array}{lll} M_u^{\text{RGI}} = 3.15(12)_m(4)_\Lambda\ \text{MeV} & \text{Ref. [24]}, \\ M_d^{\text{RGI}} = 6.49(12)_m(7)_\Lambda\ \text{MeV} & \text{Ref. [24]}. \end{array} \tag{42}$$

Finally, for $N_f = 2+1+1$, RM123 17 [23] and FNAL/MILC/TUMQCD 18 [9] enter the average for the individual m_u and m_d masses, and RM123 17 [23] and MILC 18 [25] enter the average for the ratio m_u/m_d, giving

$$N_f = 2+1+1: \quad \begin{array}{lll} m_u = 2.14(8)\ \text{MeV} & \text{Refs. [9, 23]}, \\ m_d = 4.70(5)\ \text{MeV} & \text{Refs. [9, 23]}, \\ m_u/m_d = 0.465(24) & \text{Refs. [23, 25]}. \end{array} \tag{43}$$

with errors of roughly 4%, 1% and 5%, respectively. One can observe some marginal discrepancies between results coming from the MILC collaboration and RM123 17 [23]. More specifically, adding all sources of uncertainties in quadrature, one obtains a 1.7σ discrepancy between RM123 17 [23] and MILC 18 [25] for m_u/m_d, and a 2.2σ discrepancy between RM123 17 [23] and FNAL/MILC/TUMQCD 18 [9] for m_u. However, the values of m_d and ϵ are in very good agreement between the two groups. These discrepancies are presently too weak to constitute evidence for concern, and will be monitored as more lattice groups provide results for these quantities. The RGI averages for m_u and m_d are

$$N_f = 2+1+1: \quad \begin{array}{lll} M_u^{\text{RGI}} = 2.97(11)_m(3)_\Lambda\ \text{MeV} & \text{Refs. [9,23]}, \\ M_d^{\text{RGI}} = 6.53(7)_m(8)_\Lambda\ \text{MeV} & \text{Refs. [9,23]}. \end{array} \tag{44}$$

Every result for m_u and m_d used here to produce the FLAG averages relies on electro-quenched calculations, so there is some interest to comment on the size of quenching effects. Considering phenomenology and the lattice results presented here, it is reasonable for a rough estimate to use the value $(\Delta M_K^2)^\gamma \sim 2000\ \text{MeV}^2$ for the QED part of the kaon-mass splitting. Using the arguments presented in Sec. B 1, one can assume that the QED sea contribution represents $\mathcal{O}(10\%)$ of $(\Delta M_K^2)^\gamma$. Using SU(3) PQχPT + QED [265,266] gives a ∼5% effect. Keeping the more conservative 10% estimate and using the experimental value of the kaon-mass splitting, one finds that the QCD kaon-mass splitting $(\Delta M_K^2)^{\text{SU(2)}}$ suffers from a reduced 3% quenching uncertainty. Considering that this splitting is proportional to $m_u - m_d$ at leading order in SU(3) χPT, we can estimate that a similar error will propagate to the quark masses. So the individual up and down masses look mildly affected by QED quenching. However, one notices that ∼3% is the level of error in the new FLAG averages, and increasing significantly this accuracy will require using fully dynamical calculations.

In view of the fact that a *massless up quark* would solve the strong *CP* problem, many authors have considered this an attractive possibility, but the results presented above exclude this possibility: the value of m_u in Eq. (41) differs from zero by 26 standard deviations. We conclude that nature solves the strong *CP* problem differently.

Finally, we conclude this section by giving the FLAG averages for ϵ defined in Eq. (38). For $N_f = 2+1+1$, we average the results of RM123 17 [23] and MILC 18 [25] with the value of $(\Delta M_K^2)^\gamma$ from BMW 14 [185] combined with Eq. (39), giving

$$N_f = 2+1+1: \quad \epsilon = 0.79(6) \quad \text{Refs. [23, 25, 185]}. \tag{45}$$

Although BMW 14 [185] focuses on hadron masses and did not extract the light-quark masses, they are the only fully unquenched QCD + QED calculation to date that qualifies to enter a FLAG average. With the exception of renormalization, which is not discussed in the paper, that work has a ★ rating for every FLAG criterion considered for the m_u and m_d quark masses. For $N_f = 2+1$ we use the results from BMW 16A [24],

TABLE 10. Lattice results for m_u, m_d (MeV) and for the ratio m_u/m_d. The values refer to the $\overline{\text{MS}}$ scheme at scale 2 GeV. The top part of the table lists the results obtained with $N_f = 2+1+1$, while the lower part presents calculations with $N_f = 2+1$.

Collaboration	Ref.	Publication status	Chiral extrapolation	Continuum extrapolation	Finite volume	Isospin breaking	Renormalization	Running	m_u	m_d	m_u/m_d
MILC 18	[25]	A	★	★	★	○	★	···			$0.4529(48)(^{+150}_{-67})$
FNAL/MILC/TUMQCD 18[a]	[9]	A	★	★	★	○	★	···	2.118(17)(32)(12)(03)	4.690(30)(36)(26)(06)	
MILC 17[b]	[20]	A	★	★	★	○	★	···			$0.4556(55)(^{+114}_{-67})(13)$
RM123 17	[23]	A	○	★	★	○	★	[f]	2.50(15)(8)(2)	4.88(18)(8)(2)	0.513(18)(24)(6)
ETM 14	[8]	A	★	★	★	■	★	[f]	2.36(24)	5.03(26)	0.470(56)
CLQCD 23	[10]	A	★	★	★	■	★	[g]	2.45(22)(20)	4.74(11)(09)	0.519(51)(34)
BMW 16A	[24]	A	★	★	★	○	★	···	2.27(6)(5)(4)	4.67(6)(5)(4)	0.485(11)(8)(14)
MILC 16	[258]	C	○	★	★	○	★	···			$0.4582(38)(^{+12}_{-82})(1)(110)$
QCDSF/UKQCD 15	[259]	A	○	■	■	★	···	···			0.52(5)
PACS-CS 12	[231]	A	★	■	■	★	★	[e]	2.57(26)(7)	3.68(29)(10)	0.698(51)
Laiho 11	[54]	C	○	★	★	■	○	···	1.90(8)(21)(10)	4.73(9)(27)(24)	0.401(13)(45)
HPQCD 10[c]	[15]	A	○	★	★	■	★	···	2.01(14)	4.77(15)	
BMW 10A, 10B[d]	[13,14]	A	★	★	★	■	★	[f]	2.15(03)(10)	4.79(07)(12)	0.448(06)(29)
Blum 10	[233]	A	○	■	○	○	★	···	2.24(10)(34)	4.65(15)(32)	0.4818(96)(860)
MILC 09A	[19]	C	○	★	★	■	○	···	1.96(0)(6)(10)(12)	4.53(1)(8)(23)(12)	0.432(1)(9)(0)(39)
MILC 09	[196]	A	○	★	★	■	○	···	1.9(0)(1)(1)(1)	4.6(0)(2)(2)(1)	0.42(0)(1)(0)(4)
MILC 04, HPQCD/MILC/UKQCD 04	[239,240]	A	○	○	○	■	■	···	1.7(0)(1)(2)(2)	3.9(0)(1)(4)(2)	0.43(0)(1)(0)(8)

[a]FNAL/MILC/TUMQCD 18 uses ϵ from MILC 18 to produce the individual m_u and m_d masses.

[b]MILC 17 additionally quotes an optional 0.0032 uncertainty on m_u/m_d corresponding to QED and QCD separation scheme ambiguities. Because this variation is not *per se* an error on the determination of m_u/m_d, and because it is generally not included in other results, we choose to omit it here.

[c]Values obtained by combining the HPQCD 10 result for m_s with the MILC 09 results for m_s/m_{ud} and m_u/m_d.

[d]The fermion action used is tree-level improved.

[e]The masses are renormalized and run nonperturbatively up to a scale of 100 GeV in the $N_f = 2$ SF scheme. In this scheme, nonperturbative and NLO running for the quark masses are shown to agree well from 100 GeV all the way down to 2 GeV [260].

[f]The masses are renormalized and run nonperturbatively up to a scale of 4 GeV in the $N_f = 3$ RI-MOM scheme. In this scheme, nonperturbative and N^{3}LO running for the quark masses are shown to agree from 6 GeV down to 3 GeV to better than 1% [14].

[g]The masses are renormalized and run nonperturbatively in both the RI/MOM and SMOM schemes. The quoted quark-mass value is the RI/MOM one, with an assigned systematic error coming from the difference between the two schemes.

$$N_f = 2+1: \quad \epsilon = 0.73(17) \quad \text{Ref. [24]}. \tag{46}$$

It is important to notice that the ϵ uncertainties from BMW 16A and RM123 17 are dominated by estimates of the QED quenching effects. Indeed, in contrast with the quark masses, ϵ is expected to be rather sensitive to the sea-quark QED contributions. Using the arguments presented in Appendix B 1, if one conservatively assumes that the QED sea contributions represent $\mathcal{O}(10\%)$ of $(\Delta M_K^2)^\gamma$, then Eq. (39) implies that ϵ will have a quenching error of ∼0.15 for $(\Delta M_K^2)^\gamma \sim (45\ \text{MeV})^2$, representing a large ∼20% relative error. It is interesting to observe that such a discrepancy does not appear between BMW 14 and RM123 17, although the ∼10% accuracy of both results might not be sufficient to resolve these effects. On the other hand, in the context of SU(3) chiral perturbation theory, Bijnens and Danielsson [265] show that the QED quenching effects on ϵ do not depend on unknown LECs at NLO in the chiral expansion and are therefore computable at that order. In that approach, MILC 18 finds the effect at NLO to be only 5%. To conclude, although the controversy around the value of ϵ has been significantly reduced by lattice-QCD + QED determinations, computing this at few-percent accuracy requires simulations with charged sea quarks.

4. Estimates for R and Q

The quark-mass ratios

$$R \equiv \frac{m_s - m_{ud}}{m_d - m_u} \quad \text{and} \quad Q^2 \equiv \frac{m_s^2 - m_{ud}^2}{m_d^2 - m_u^2} \tag{47}$$

compare SU(3) breaking with isospin breaking. Both numbers only depend on the ratios m_s/m_{ud} and m_u/m_d,

$$R = \frac{1}{2}\left(\frac{m_s}{m_{ud}} - 1\right)\frac{1+\frac{m_u}{m_d}}{1-\frac{m_u}{m_d}} \quad \text{and} \quad Q^2 = \frac{1}{2}\left(\frac{m_s}{m_{ud}} + 1\right)R. \tag{48}$$

The quantity Q is of particular interest because of a low-energy theorem [267], which relates it to a ratio of meson masses,

$$Q_M^2 \equiv \frac{\hat{M}_K^2}{\hat{M}_\pi^2}\frac{\hat{M}_K^2 - \hat{M}_\pi^2}{\hat{M}_{K^0}^2 - \hat{M}_{K^+}^2}, \qquad \hat{M}_\pi^2 \equiv \frac{1}{2}(\hat{M}_{\pi^+}^2 + \hat{M}_{\pi^0}^2),$$
$$\hat{M}_K^2 \equiv \frac{1}{2}(\hat{M}_{K^+}^2 + \hat{M}_{K^0}^2). \tag{49}$$

(We remind the reader that the ˆ denotes a quantity evaluated in the $\alpha \to 0$ limit.) Chiral symmetry implies that the expansion of Q_M^2 in powers of the quark masses (i) starts with Q^2 and (ii) does not receive any contributions at NLO [267]

$$Q_M \overset{\text{NLO}}{=} Q. \tag{50}$$

TABLE 11. Our estimates for the average up-down-quark mass and the strange-quark mass in the $\overline{\text{MS}}$ scheme at running scale $\mu = 2$ GeV. Mass values are given in MeV. In the results presented here, the error is the one which we obtain by applying the averaging procedure of Sec. II C to the relevant lattice results.

N_f	m_{ud}	m_s	m_s/m_{ud}
$2+1+1$	3.410(43)	93.44(68)	27.23(10)
$2+1$	3.364(41)	92.03(88)	27.42(12)

TABLE 12. Our estimates for the masses of the two lightest quarks and related, strong isospin-breaking ratios. Again, the masses refer to the $\overline{\text{MS}}$ scheme at running scale $\mu = 2$ GeV. Mass values are given in MeV.

N_f	m_u	m_d	m_u/m_d	R	Q
$2+1+1$	2.14(8)	4.70(5)	0.465(24)	35.9(1.7)	22.5(0.5)
$2+1$	2.27(9)	4.67(9)	0.485(19)	38.1(1.5)	23.3(0.5)

For $N_f = 2+1$, we use Eqs. (36) and (41) and obtain

$$R = 38.1(1.5), \qquad Q = 23.3(0.5), \tag{51}$$

and for $N_f = 2+1+1$,

$$R = 35.9(1.7), \qquad Q = 22.5(0.5), \tag{52}$$

which are quite compatible (see the 2021 edition for the two flavor numbers which are also compatible with the above). It is interesting to note that the most recent phenomenological determination of R and Q from $\eta \to 3\pi$ decay [268] gives the values $R = 34.4(2.1)$ and $Q = 22.1(0.7)$, which are consistent with the averages presented here. The authors of Refs. [268,269] point out that this discrepancy is likely due to surprisingly large corrections to the approximation in Eq. (50) used in the phenomenological analysis.

Our final results for the masses m_u, m_d, m_{ud}, m_s and the mass ratios m_u/m_d, m_s/m_{ud}, R, Q are collected in Tables 11 and 12.

B. Charm-quark mass

In the following, we collect and discuss the lattice determinations of the $\overline{\text{MS}}$ charm-quark mass $\bar{m}_c$. Most of the results have been obtained by analyzing the lattice-QCD simulations of two-point heavy-light- or heavy-heavy-meson correlation functions, using as input the experimental values of the D, D_s, and charmonium mesons. Some groups use the moments method. The latter is based on the lattice calculation of the Euclidean time moments of pseudoscalar-pseudoscalar correlators for heavy-quark

TABLE 13. Lattice results for the $\overline{\text{MS}}$ charm-quark mass $\bar{m}_c(\bar{m}_c)$ and $\bar{m}_c(3\text{ GeV})$ in GeV, together with the color coding of the calculations used to obtain them.

Collaboration	Ref.	N_f	Publication status	Chiral extrapolation	Continuum extrapolation	Finite volume	Renormalization	$\bar{m}_c(\bar{m}_c)$	$\bar{m}_c(3\text{GeV})$
ETM 21A	[7]	$2+1+1$	P	★	★	★	★	$1.339(22)(^{+19}_{-10})(10)$[a]	$1.036(17)(^{+15}_{-8})$
HPQCD 20A	[27]	$2+1+1$	A	★	★	★	★	1.2719(78)	0.9841(51)
HPQCD 18	[17]	$2+1+1$	A	★	★	★	★	1.2757(84)	0.9896(61)
FNAL/MILC/ TUMQCD 18	[9]	$2+1+1$	A	★	★	★	···	1.273(4)(1)(10)	0.9837(43)(14)(33)(5)
HPQCD 14A	[18]	$2+1+1$	A	★	★	★	···	1.2715(95)	0.9851(63)
ETM 14A	[26]	$2+1+1$	A	○	★	○	★	1.3478(27)(195)	1.0557(22)(153)[b]
ETM 14	[8]	$2+1+1$	A	○	★	○	★	1.348(46)	1.058(35)[b]
ALPHA 23	[28]	$2+1$	A[c]	★	★	★	★	1.296(15)	1.006(9)
ALPHA 21	[32]	$2+1$	A[c]	★	★	★	★	1.296(19)	1.007(16)
Petreczky 19	[31]	$2+1$	A	★	★	★	★	1.265(10)	1.001(16)
Maezawa 16	[230]	$2+1$	A	■	★	★	★	1.267(12)	
JLQCD 16	[30]	$2+1$	A	○	★	★	···	1.2871(123)	1.0033(96)
χQCD 14	[29]	$2+1$	A	○	○	○	★	1.304(5)(20)	1.006(5)(22)
HPQCD 10	[15]	$2+1$	A	○	★	○	···	1.273(6)	0.986(6)
HPQCD 08B	[244]	$2+1$	A	○	★	○	···	1.268(9)	0.986(10)
PDG	[225]							1.27(2)	

[a]We applied the running factor 0.7739(60) for $\mu = 3$ GeV to $\bar{m}_c$. The errors are statistical, systematic, and the uncertainty in the running factor.

[b]A running factor equal to 0.900 between the scales $\mu = 2$ GeV and $\mu = 3$ GeV was applied by us.

[c]Published after the FLAG deadline.

currents followed by an OPE expansion dominated by perturbative QCD effects, which provides the determination of both the heavy-quark mass and the strong-coupling constant α_s.

The heavy-quark actions adopted by various lattice collaborations have been discussed in previous FLAG reviews [2–4], and their descriptions can be found in Sec. A.1.3 of FLAG 19 [4]. While the charm mass determined with the moments method does not need any lattice evaluation of the mass-renormalization constant Z_m, the extraction of $\bar{m}_c$ from two-point heavy-meson correlators does require the nonperturbative calculation of Z_m. The lattice scale at which Z_m is obtained is usually at least of the order 2–3 GeV, and therefore it is natural in this review to provide the values of $\bar{m}_c(\mu)$ at the renormalization scale $\mu = 3$ GeV. Since the choice of a renormalization scale equal to $\bar{m}_c$ is still commonly adopted (as by the PDG [225]), we have collected in Table 13 the lattice results for both $\bar{m}_c(\bar{m}_c)$ and $\bar{m}_c(3\text{ GeV})$, obtained for $N_f = 2+1$ and $2+1+1$. For $N_f = 2$, interested readers are referred to previous reviews [2,3].

When not directly available in the published work, we apply a conversion factor using perturbative QCD evolution at five loops to run down from $\mu = 3$ GeV to the scales $\mu = \bar{m}_c$ and 2 GeV of 0.7739(60) and 0.9026(23), respectively, where the error comes from the uncertainty in Λ_{QCD}. We use $\Lambda_{\text{QCD}} = 297(12)$ MeV for $N_f = 4$ (see Sec. IX). Perturbation theory uncertainties, estimated as the difference between results that use 4- and 5-loop running, are significantly smaller than the parametric uncertainty coming from Λ_{QCD}. For $\mu = \bar{m}_c$, the former is about about 2.5 times smaller.

In the next subsections, we review separately the results for $\bar{m}_c$ with three or four flavors of quarks in the sea.

1. $N_f = 2+1$ results

Since the last review [5], there is one new result: ALPHA 23 [28]. This work uses a subset of CLS ensembles, based on simulations of nonperturbatively $O(a)$-improved Wilson fermions. The difference with ALPHA 21 is that the valence sector uses both Wilson and twisted-mass discretizations instead of just Wilson. Renormalization is based on previous work by the ALPHA collaboration, and is performed nonperturbatively from 100 MeV to the electroweak scale. The subset of ensembles used have large volumes, four lattice spacings, and reach pion masses of 200 MeV, which guarantees entering in the average. Contrary to the extraction of light-quark masses in ALPHA 19, the chiral extrapolation does not dominate the error budget, and being less critical in this case we decide to give a ★ for the chiral extrapolation. The data-driven criteria quantity for the continuum extrapolation $\delta(a_{\min})$ (see II A 2) is smaller than 3 in all cases.

Petreczky 19 employs the HISQ action on ten ensembles with ten lattice spacings down to 0.025 fm, physical strange-quark mass, and two light-quark masses, the lightest corresponding to 161 MeV pions. Their study incorporates lattices with 11 different sizes, ranging from 1.6 to 5.4 fm. The masses are computed from moments of pseudoscalar quarkonium correlation functions, and $\overline{\text{MS}}$ masses are extracted with 4-loop continuum perturbation theory. Thus, that work easily rates green stars in all categories. Continuum extrapolations are challenging, but judging the data itself the values of $\delta(a_{\min})$ are not very large. It is just that the functional form of the data is complicated.

ALPHA 21 uses the $\mathcal{O}(a)$-improved Wilson-clover action with five lattice spacings from 0.087 to 0.039 fm, produced by the CLS collaboration. For each lattice spacing, several light sea-quark masses are used in a global chiral-continuum extrapolation (the lightest pion mass for one ensemble is 198 MeV). The authors also use nonperturbative renormalization and running through application of step-scaling and the Schrödinger functional scheme. Finite-volume effects are investigated at one lattice spacing and only for ∼400 MeV pions on the smallest two volumes where results are compatible within statistical errors. ALPHA 21 satisfies the FLAG criteria for green-star ratings in all of the categories listed in Table 13. The values of $\delta(a_{\min})$ are smaller than 3 in all continuum extrapolations. Descriptions of the other works in this section can be found in an earlier review [4].

According to our rules on the publication status, the FLAG average for the charm-quark mass at $N_f = 2+1$ is obtained by combining the results HPQCD 10, χQCD 14, JLQCD 16, Petreczky 19, ALPHA 21 and ALPHA 23,

$$N_f = 2+1: \quad \bar{m}_c(\bar{m}_c) = 1.278(6)\ \text{GeV} \quad \text{Refs. [15,28–32]}, \tag{53}$$

$$N_f = 2+1: \quad \bar{m}_c(3\,\text{GeV}) = 0.991(6)\ \text{GeV} \quad \text{Refs. [15,28–32]}, \tag{54}$$

This result corresponds to the following RGI average

$$M_c^{\text{RGI}} = 1.526(7)_m(21)_\Lambda\ \text{GeV} \quad \text{Refs. [15, 29–32]}. \tag{55}$$

2. $N_f = 2+1+1$ results

For a discussion of older results, see the previous FLAG reviews. Since FLAG 19 two groups have produced updated values with charm quarks in the sea.

HPQCD 20A [27] is an update of HPQCD 18, including a new finer ensemble ($a \approx 0.045$ fm) and EM corrections computed in the quenched approximation of QED for the first time. Besides these new items, the analysis is largely unchanged from HPQCD 18 except for an added α_s^3 correction to the SMOM-to-$\overline{\text{MS}}$ conversion factor and tuning the bare charm mass via the J/ψ mass rather than the η_c. Their new value in pure QCD is $\bar{m}_c(3\ \text{GeV}) = 0.9858(51)$ GeV which is quite consistent with HPQCD 18 and the FLAG 19 average. The effects of quenched QED in both the bare charm-quark mass and the renormalization constant are small. Both effects are precisely determined, and the overall effect shifts the mass down slightly to $\bar{m}_c(3\ \text{GeV}) = 0.9841(51)$ where the uncertainty due to QED is invisible in the final error. The shift from their pure QCD value due to quenched QED is about −0.2%.

ETM 21A [7] is a new work that follows a similar methodology as ETM 14, but with significant improvements. Notably, a clover-term is added to the twisted mass fermion action which suppresses $\mathcal{O}(a^2)$ effects between the neutral and charged pions. Additional improvements include new ensembles lying very close to the physical mass point, better control of nonperturbative renormalization systematics, and use of both meson and baryon correlation functions to determine the quark mass. They use the RI-MOM scheme for nonperturbative renormalization. The analysis comprises ten ensembles in total with three lattice spacings (0.095, 0.082, and 0.069 fm), two volumes for the finest lattice spacings and four for the other two, and pion masses down to 134 MeV for the finest ensemble. The values of $m_\pi L$ range mostly from almost four to greater than five. According to the FLAG criteria, green stars are earned in all categories. The authors find $m_c(3\ \text{GeV}) = 1.036(17)(^{+15}_{-8})$ GeV. In Table 13 we have applied a factor of 0.7739(60) to run from 3 GeV to $\bar{m}_c$. As in FLAG 19, the new value is consistent with ETM 14 and ETM 14A, but is still high compared to the FLAG average. The authors plan future improvements, including a finer lattice spacing for better control of the continuum limit and a new renormalization scheme, like RI-SMOM.

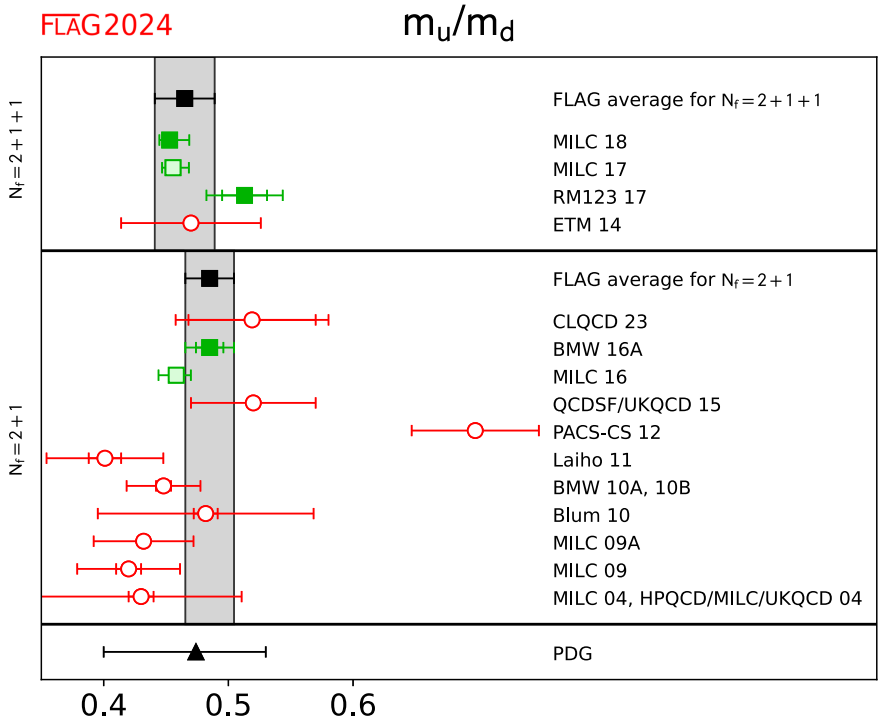


FIG. 4. Lattice results and FLAG averages at $N_f = 2+1$ and $2+1+1$ for the up-down-quark masses ratio m_u/m_d, together with the current PDG estimate.

Six results enter the FLAG average for $N_f = 2+1+1$ quark flavors: ETM 14, ETM 14A, HPQCD 14A, FNAL/MILC/TUMQCD 18, HPQCD 20A, and ETM 21A. We note that while the ETM determinations of $\bar{m}_c$ agree well with each other, they are incompatible with HPQCD 14A, FNAL/MILC/TUMQCD 18, and HPQCD 20A by several standard deviations. While the ETM 14 and ETM 14A use the same configurations, the analyses are quite different and independent, and ETM 21A is a new result on new ensembles with improved methodology. As mentioned earlier, m_{ud} and m_s values by ETM are also systematically high compared to their respective averages. Combining all six results yields yields

$$N_f = 2+1+1: \quad \bar{m}_c(\bar{m}_c) = 1.280(13)\ \text{GeV} \quad \text{Refs. [7–9, 18, 26, 27]}, \tag{56}$$

$$N_f = 2+1+1: \quad \bar{m}_c(3\ \text{GeV}) = 0.989(10)\ \text{GeV} \quad \text{Refs. [7–9, 18, 26, 27]}, \tag{57}$$

where the errors include large stretching factors $\sqrt{\chi^2/\text{dof}} \approx 2.0$ and 2.4, respectively. We have assumed 100% correlation for statistical errors between ETM 14 and ETM 14A results and the same for HPQCD 14A, HPQCD 20A, and FNAL/MILC/TUMQCD 18.

These are obviously poor χ^2 values, and the stretching factors are quite large. While it may be prudent in such a case to quote a range of values covering the central values of all results that pass the quality criteria, we believe in this case that would obscure rather than clarify the situation. From Fig. 5, we note that not only do ETM 21A, ETM 14A, and ETM 14 lie well above the other $2+1+1$ results, but also above all of the $2+1$ flavor results. A similar trend is apparent for the light-quark masses (see Figs. 1 and 2) while for mass ratios there is better agreement (Figs. 3, 4, and 6). The latter suggests there may be underestimated systematic uncertainties associated with scale setting and/or renormalization which have not been detected. Finally we note the ETM results are significantly higher than the PDG average. For these reasons, which admittedly are not entirely satisfactory, we continue to quote an average with a stretching factor as in previous reviews.

The RGI average reads as follows,

$$M_c^{\text{RGI}} = 1.528(15)_m(21)_\Lambda\ \text{GeV} \quad \text{Refs. [7–9, 18, 26, 27]}. \tag{58}$$

Figure 5 presents the values of $\bar{m}_c(\bar{m}_c)$ given in Table 13 along with the FLAG averages obtained for $2+1$ and $2+1+1$ flavors.

3. Lattice determinations of the ratio m_c/m_s

Because some of the results for quark masses given in this review are obtained via the quark-mass ratio m_c/m_s,

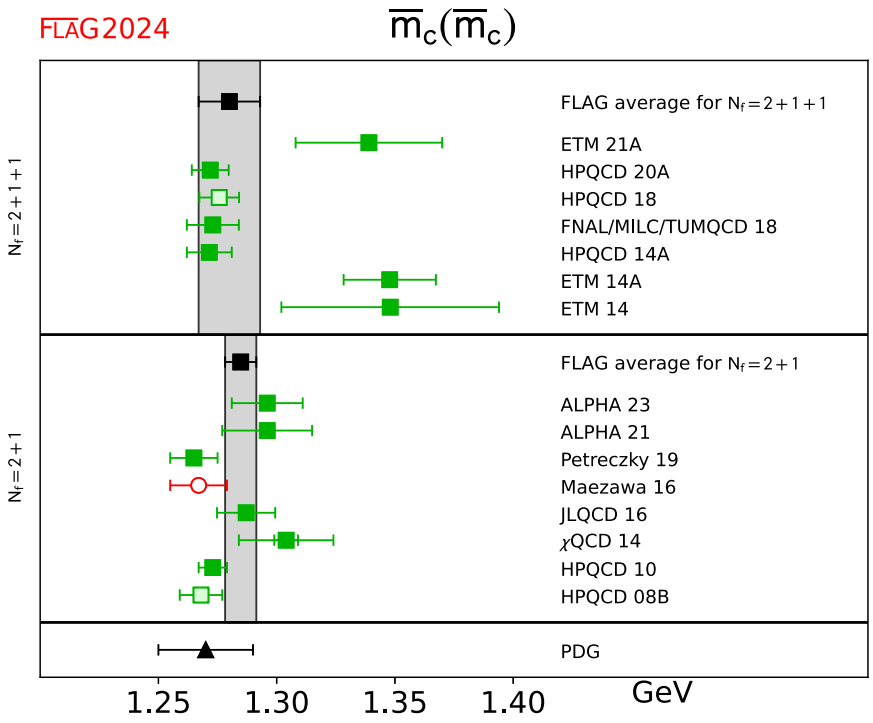


FIG. 5. The charm-quark mass for $2+1$ and $2+1+1$ flavors. For the latter a large stretching factor is used for the FLAG average due to poor χ^2 from our fit.

we review these lattice calculations, which are listed in Table 14, as well.

The $N_f = 2+1$ results from χQCD 14 and HPQCD 09A [33] are from the same calculations that were described for the charm-quark mass in the previous review. Maezawa 16 does not pass our chiral-limit test (see the previous review), though we note that it is quite consistent with the other values. Combining χQCD 14 and HPQCD 09A, we obtain the same result reported in FLAG 19,

$$N_f = 2+1: \quad m_c/m_s = 11.82(16) \quad \text{Refs. [29, 33]}, \tag{59}$$

with a $\chi^2/\text{dof} \simeq 0.85$.

TABLE 14. Lattice results for the quark-mass ratio m_c/m_s, together with the color coding of the calculations used to obtain them.

Collaboration	Ref.	N_f	Publication status	Chiral extrapolation	Continuum extrapolation	Finite volume	m_c/m_s
ETM 21A	[7]	$2+1+1$	P	★	★	★	$11.48(12)(^{+25}_{-19})$
FNAL/MILC/TUMQCD 18	[9]	$2+1+1$	A	★	★	★	11.784(11)(17)(00)(08)
HPQCD 14A	[18]	$2+1+1$	A	★	★	★	11.652(35)(55)
ETM 14	[8]	$2+1+1$	A	○	★	○	11.62(16)
Maezawa 16	[230]	$2+1$	A	■	★	★	11.877(91)
χQCD 14	[29]	$2+1$	A	○	○	○	11.1(8)
HPQCD 09A	[33]	$2+1$	A	○	★	★	11.85(16)

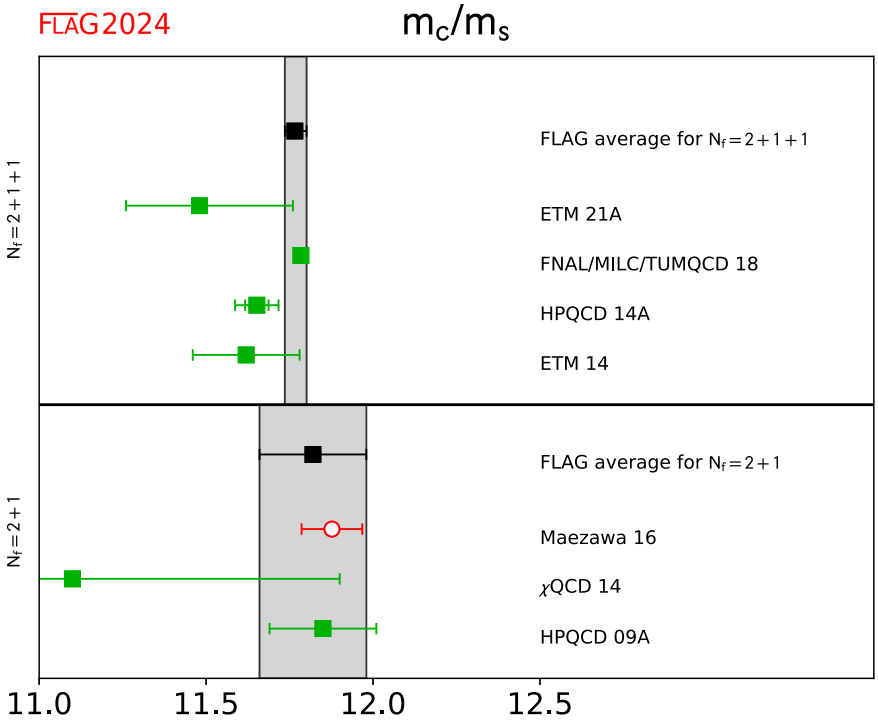


FIG. 6. Lattice results for the ratio m_c/m_s listed in Table 14 and the FLAG averages corresponding to $2+1$ and $2+1+1$ quark flavors. The latter average includes a stretching factor of 1.4 on the error due to a poor χ^2 from our fit.

Turning to $N_f = 2+1+1$, there is a new result from ETM 21A (see the previous section for details). The errors have actually increased compared to ETM 14, due to larger uncertainties in the baryon sector which enter their average with the meson sector. See the earlier reviews for a discussion of previous results.

We note that some tension exists between the HPQCD 14A and FNAL/MILC/TUMQCD results. Combining these with ETM 14 and ETM 21A yields

$$N_f = 2+1+1: \quad m_c/m_s = 11.766(30) \quad \text{Refs. [7–9,18]}, \tag{60}$$

where the error includes the stretching factor $\sqrt{\chi^2/\text{dof}} \simeq 1.4$. We have assumed a 100% correlation of statistical errors for FNAL/MILC/TUMQCD 18 and HPQCD 14A.

Results for m_c/m_s are shown in Fig. 6 together with the FLAG averages for $N_f = 2+1$ and $2+1+1$ flavors.

C. Bottom-quark mass

Now we review the lattice results for the $\overline{\text{MS}}$ bottom-quark mass $\bar{m}_b$. Related heavy-quark actions and observables have been discussed in previous FLAG reviews [2–4], and descriptions can be found in Sec. A.1.3 of FLAG 19 [4]. In Table 15, we collect results for $\bar{m}_b(\bar{m}_b)$ obtained with $N_f = 2+1$ and $2+1+1$ sea-quark flavors. Available results for the quark-mass ratio m_b/m_c are also reported. After discussing the new results, we evaluate the corresponding FLAG averages.

1. $N_f = 2+1$

There are no new results since the last review, so we simply quote the same average of HPQCD 10 and Petreczky 19 (both are reported for $N_f = 5$, so we simply quote the average for $N_f = 5$).

$$N_f = 2+1: \quad \bar{m}_b(\bar{m}_b) = 4.171(20)\ \text{GeV} \quad \text{Refs. [15,31]}. \tag{61}$$

The corresponding (four-flavor) RGI average is

$$N_f = 2+1: \quad M_b^{\text{RGI}} = 6.888(33)_m(45)_\Lambda\ \text{GeV} \quad \text{Refs. [15,31]}. \tag{62}$$

2. $N_f = 2+1+1$

HPQCD 21 [34] is an update of HPQCD 14A (and replaces it in our average. See FLAG 19 for details.), including EM corrections for the first time for the b-quark mass. Four flavors of HISQ quarks are used on MILC ensembles with lattice spacings from about 0.09 to 0.03 fm. Ensembles with physical- and unphysical-mass sea-quarks are used. Quenched QED is used to obtain the dominant

TABLE 15. Lattice results for the $\overline{\text{MS}}$ bottom-quark mass $\bar{m}_b(\bar{m}_b)$ in GeV, together with the systematic error ratings for each. Available results for the quark-mass ratio m_b/m_c are also reported.

Collaboration	Ref.	N_f	Publication status	Chiral extrapolation	Continuum extrapolation	Finite volume	Renormalization	Heavy-quark treatment	$\bar{m}_b(\bar{m}_b)$	m_b/m_c
HPQCD 21	[34]	$2+1+1$	A	★	○	★	⋯	✓	4.209(21)[a]	4.586(12)[b]
FNAL/MILC/TUM 18	[9]	$2+1+1$	A	★	○	★	⋯	✓	4.201(12)(1)(8)(1)	4.578(5)(6)(0)(1)
Gambino 17	[37]	$2+1+1$	A	○	★	○	★	✓	4.26(18)	
ETM 16B	[36]	$2+1+1$	A	○	★	○	★	✓	$4.26(3)(10)^+$	4.42(3)(8)
HPQCD 14B	[35]	$2+1+1$	A	★	★	★	★	✓	4.196(0)(23)[c]	
Petreczky19	[31]	$2+1$	A	★	★	★	★	✓	4.188(37)	4.586(43)
Maezawa 16	[230]	$2+1$	A	■	★	★	★	✓	4.184(89)	4.528(57)
HPQCD 13B	[270]	$2+1$	A	■	○	⋯	⋯	✓	4.166(43)	
HPQCD 10	[15]	$2+1$	A	★	★	★	⋯	✓	4.164(23)	4.51(4)
ETM 13B	[73]	2	A	○	★	○	★	✓	4.31(9)(8)	
ALPHA 13C	[271]	2	A	★	★	★	★	✓	4.21(11)	
ETM 11A	[272]	2	A	○	★	○	★	✓	4.29(14)	
PDG	[225]								$4.18^{+0.02}_{-0.03}$	

[a]We quote the four-flavor result. For $N_f = 5$, the value is 4.202(21).

[b]The ratio is quoted in the $\overline{\text{MS}}$ scheme for $\mu = 3$ GeV because of the different charges of the bottom and charm quarks.

[c]Only two pion points are used for chiral extrapolation.

$\mathcal{O}(\alpha)$ effect. The ratio of bottom- to charm-quark masses is computed in a completely nonperturbative formulation, and the b-quark mass is extracted using the value of $\bar{m}_c(3\text{ GeV})$ from HPQCD 20A. Since EM effects are included, the QED renormalization scale enters the ratio which is quoted for 3 GeV and $N_f = 4$. The total error on the new result is more than two times smaller than for HPQCD 14A, but is only slightly smaller compared to the NRQCD result reported in HPQCD 14B. The inclusion of QED shifts the ratio m_b/m_c up slightly from the pure QCD value by about one standard deviation, and the value of $\bar{m}_b(\bar{m}_b)$ is consistent, within errors, to the other pure QCD results entering our average. Therefore, we quote a single average. Cutoff effects are significant in that work, and are the dominant source of uncertainty in the ratio m_b/m_c. It is difficult to estimate the value of $\delta(a_{\min})$ from the data present in the publication, but the authors provided extra information about their analysis with the result that $\delta(a_{\min}) \approx 3$. Therefore, we do not inflate the errors of that computation. The work rates green stars for all FLAG criteria except for the continuum limit (see Table 15) where less than three ensembles at the physical b-quark mass were used in the $a \to 0$ extrapolation (in the previous FLAG review this was missed and is corrected here).

HPQCD 14B employs the NRQCD action [35] to treat the b quark. The b-quark mass is computed with the moments method, that is, from Euclidean-time moments of two-point, heavy-heavy-meson correlation functions (see also Sec. IX H for a description of the method). Due to the effective treatment of the heavy quark, continuum extrapolations are under control since five lattice spacings are employed, with the smallest about 0.09 fm, but the requirement that $am_b \ll 1$ is not relevant. Their final result is $\bar{m}_b(\mu = 4.18\text{ GeV}) = 4.207(26)$ GeV, where the error is from adding systematic uncertainties in quadrature only (statistical errors are smaller than 0.1% and ignored). The errors arise from renormalization, perturbation theory, lattice spacing, and NRQCD systematics. The finite-volume uncertainty is not estimated, but at the lowest pion mass they have $m_\pi L \simeq 4$, which leads to the tag ★. In this case, the continuum extrapolations seem mild, in part, thanks to the NRQCD action used to treat the b quark. The data-driven continuum-limit criterion $\delta(a_{\min}) < 3$, so no correction factor is necessary here.

The next four-flavor result (ETM 16B [36]) is from the ETM collaboration and updates their preliminary result appearing in a conference proceedings [273]. The calculation is performed on a set of ensembles generated with twisted-Wilson fermions with three lattice spacings in the range 0.06 to 0.09 fm and with pion masses in the range 210 to 440 MeV. The b-quark mass is determined from a ratio of heavy-light pseudoscalar meson masses designed to yield the quark pole mass in the static limit. The pole mass is related to the $\overline{\text{MS}}$ mass through perturbation theory at N^{3}LO. The key idea is that by taking ratios of ratios, the b-quark mass is accessible through fits to heavy-light(strange)-meson correlation functions computed on the lattice in the range $\sim$1–2 $\times$ m_c and the static limit, the latter being exactly 1. By simulating below $\bar{m}_b$, taking the continuum limit is easier. They find $\bar{m}_b(\bar{m}_b) = 4.26(3)(10)$ GeV, where the first error is statistical and the second systematic. The dominant errors come from setting the lattice scale and fit systematics.

Gambino *et al.* [37] use twisted-mass-fermion ensembles from the ETM collaboration and the ETM ratio method as in ETM 16B. Three values of the lattice spacing are used, ranging from 0.062 to 0.089 fm. Several volumes are also used. The light-quark masses produce pions with masses from 210 to 450 MeV. The main difference with ETM 16 is that the authors use the kinetic mass defined in the heavy-quark expansion (HQE) to extract the b-quark mass instead of the pole mass. They include an additional uncertainty stemming from the conversion between kinetic and $\overline{\text{MS}}$ schemes which leads to a somewhat larger total uncertainty compared to ETM 16B.

The final b-quark mass result is FNAL/MILC/TUM 18 [9]. The mass is extracted from the same fit and analysis done for the charm quark mass. Note that relativistic HISQ valence masses reach the physical b mass on the two finest lattice spacings ($a = 0.042$ fm, 0.03 fm) with physical and $0.2 \times m_s$ light-quark masses, respectively. In lattice units, the heavy valence masses correspond to $aM^{\text{RGI}} > 0.90$, making the continuum extrapolation challenging. The extrapolations have $\delta(a_{\text{min}}) \approx 14$ (taking into account only the statistical error of the continuum extrapolation, which is a 40% of their total error budget). According to our policy (II A 2) we increase the error for the average by a factor 3.5. Their results are also consistent with an analysis dropping the finest lattice spacing from the fit. Since the b-quark mass region is only reached with two lattice spacings, we rate this work with a green circle for the continuum extrapolation (the same as HPQCD 21). Note, however, that for other values of the quark masses they use up to five values of the lattice spacing (cf. their charm-quark mass determination) with small values of $\delta(a_{\text{min}})$ in the continuum extrapolation. In summary, we judge that these large scaling violations affect mainly the determination of the b-quark mass.

All of the above results enter our average. We note that here the ETM 16B result is consistent with the average and a stretching factor on the error is not used.

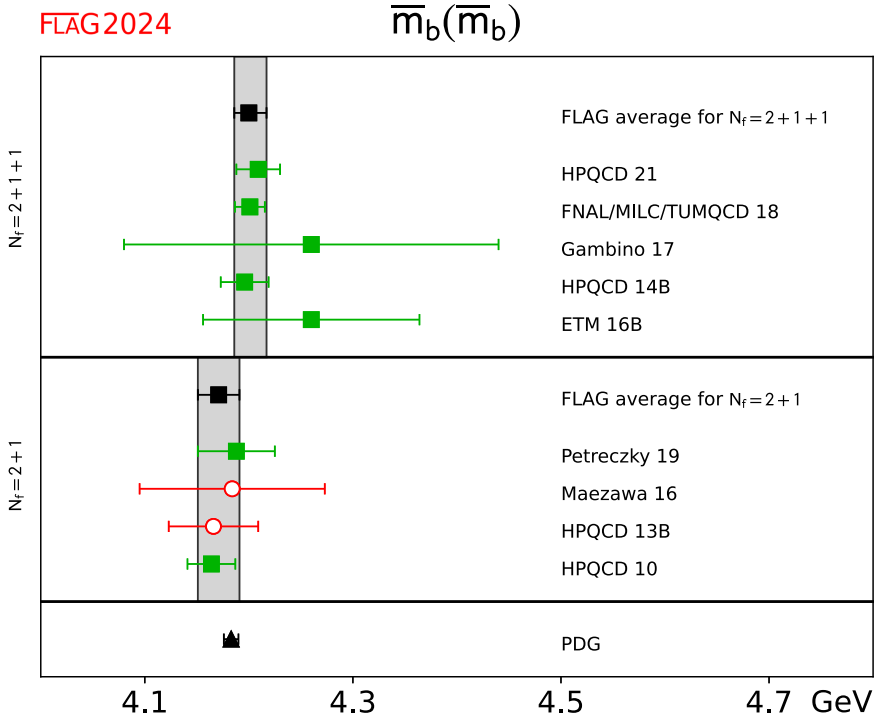


FIG. 7. The b-quark mass for $N_f = 2 + 1$ and $2 + 1 + 1$ flavors. The updated PDG value from Ref. [274] is reported for comparison.

$$N_f = 2+1+1: \quad \bar{m}_b(\bar{m}_b) = 4.200(14)\ \text{GeV} \quad \text{Refs. [9,34–37].} \tag{63}$$

We have included a 100% correlation on the statistical errors of ETM 16B and Gambino 17, since the same ensembles are used in both. While FNAL/MILC/TUM 18 and HPQCD 21 also use the same MILC HISQ ensembles, the statistical error in the HPQCD 21 analysis is negligible, so we do not include a correlation between them. The average has $\chi^2/\text{dof} = 0.02$.

The above translates to the RGI average

$$N_f = 2+1+1: \quad M_b^{\text{RGI}} = 6.938(23)_m(45)_\Lambda\ \text{GeV} \quad \text{Refs. [9,34–37].} \tag{64}$$

Results for $\bar{m}_b(\bar{m}_b)$ are shown in Fig. 7 together with the FLAG averages corresponding to $N_f = 2+1$ and $2+1+1$ quark flavors.

V. LEPTONIC AND SEMILEPTONIC KAON AND PION DECAY AND $|V_{ud}|$ AND $|V_{us}|$

Working group members: T. Kaneko, J. N. Simone, N. Tantalo

This section summarizes state-of-the-art lattice calculations of the leptonic kaon and pion decay constants, $f_K^{\pm}$ and $f_\pi^{\pm}$, and the kaon semileptonic-decay form factor $f_+(0)$, and provides an analysis in the framework of the Standard Model. With respect to the previous edition of the FLAG review [5], there has been a new study each for the decay constants and $f_+(0)$ for $N_f = 2+1$, and a new entry to the average of the ratio $f_{K^\pm}/f_{\pi^\pm}$ for $N_f = 2+1+1$.[18] As in Ref. [5], when combining lattice data with experimental results, we take into account the strong isospin correction, either obtained in lattice calculations or estimated by using chiral perturbation theory (χPT), both for $f_{K^\pm}$ and $f_{K^\pm}/f_{\pi^\pm}$.

A. Experimental information concerning $|V_{ud}|$, $|V_{us}|$, $f_+(0)$ and $f_{K^\pm}/f_{\pi^\pm}$

The following review relies on the fact that precision experimental data on kaon decays very accurately determine the product $|V_{us}|f_+(0)$ [275] and the ratio $|V_{us}/V_{ud}|f_{K^\pm}/f_{\pi^\pm}$ [205,275]

$$|V_{us}|f_+(0) = 0.21654(41), \qquad \left|\frac{V_{us}}{V_{ud}}\right|\frac{f_{K^\pm}}{f_{\pi^\pm}} = 0.27599(41). \tag{65}$$

Here, and in the following, $f_{K^\pm}$ and $f_{\pi^\pm}$ are the isospin-broken decay constants in QCD. We will refer to the decay constants in the isospin-symmetric limit as f_K and f_π (the latter at leading order in the mass difference $(m_u - m_d)$ coincides with $f_{\pi^\pm}$). The parameters $|V_{ud}|$ and $|V_{us}|$ are elements of the Cabibbo-Kobayashi-Maskawa matrix and $f_+(q^2)$ represents one of the form factors relevant for the semileptonic decay $K^0 \to \pi^-\ell\nu$, which depends on the momentum transfer q between the two mesons. What matters here is the value at $q^2 = 0$

$$f_+(0) \equiv f_+^{K^0\pi^-}(0) = f_0^{K^0\pi^-}(0) = q^\mu \langle \pi^-(p')|\bar{s}\gamma_\mu u|K^0(p)\rangle/(M_K^2 - M_\pi^2)|_{q^2\to 0}. \tag{66}$$

The pion and kaon decay constants are defined by[19]

$$\langle 0|\bar{d}\gamma_\mu\gamma_5 u|\pi^+(p)\rangle = ip_\mu f_{\pi^+}, \qquad \langle 0|\bar{s}\gamma_\mu\gamma_5 u|K^+(p)\rangle = ip_\mu f_{K^+}. \tag{67}$$

In this normalization, $f_{\pi^\pm} \simeq 130$ MeV, $f_{K^\pm} \simeq 155$ MeV.

In Eq. (65), the electromagnetic effects have already been subtracted in the experimental analysis using χPT [279–282]. In 2015, a new method [283] has been proposed by the RM123-SOTON collaboration for calculating the leptonic decay rates of hadrons including both QCD and QED on the lattice, and successfully applied to the case of the ratio of the leptonic decay rates of kaons and pions [217,223]. By employing the twisted-mass discretization, they simulate $N_f = 2+1+1$ QCD at three lattice spacings $a = 0.07$, 0.08, 0.09 fm with pion masses down to ≈220 MeV on multiple lattice volumes to directly examine finite-volume effects. The correction to the $K_{\mu 2}/\pi_{\mu 2}$ decay rate, including both electromagnetic and strong isospin-breaking effects, is found to be equal to $-1.26(14)\%$ [217] to be compared to the estimate $-1.12(21)\%$ based on χPT [204,282].[20] Using the experimental values of the $K_{\mu 2}$ and $\pi_{\mu 2}$ decay rates the result of Ref. [217] implies

$$\left|\frac{V_{us}}{V_{ud}}\right|\frac{f_K}{f_\pi} = 0.27683(29)_{\text{exp}}(20)_{\text{th}}[35], \tag{68}$$

[18] In this edition, we omit results for $N_f = 2$, because there has been no new entry after 2014. We refer to the 2016 edition [3] for the $N_f = 2$ results.

[19] The pion decay constant represents a QCD matrix element—in the full Standard Model, the one-pion state is not a meaningful notion: the correlation function of the charged axial current does not have a pole at $p^2 = M_{\pi^+}^2$, but a branch cut extending from $M_{\pi^+}^2$ to ∞. The analytic properties of the correlation function and the problems encountered in the determination of f_π are thoroughly discussed in Ref. [210]. The "experimental" value of f_π depends on the convention used when splitting the sum $\mathcal{L}_{\text{QCD}} + \mathcal{L}_{\text{QED}}$ into two parts. The lattice determinations of f_π do not yet reach the accuracy where this is of significance, but at the precision claimed by the Particle Data Group [243,276], the numerical value does depend on the convention used [209,210,277,278].

[20] See the discussion concerning the definition of QCD and of the isospin-breaking corrections in Sec. III.

where the last error in brackets is the sum in quadrature of the experimental and theoretical uncertainties, and the ratio of the decay constants is the one corresponding to isosymmetric QCD. A large part of the theoretical uncertainty comes from the statistical error and continuum and chiral extrapolation of lattice data, which can be systematically reduced by a more realistic simulation with high statistics.

An independent study of the electromagnetic effects is carried out by the RBC/UKQCD collaboration using the domain-wall discretization [220]. They simulate $N_f = 2+1$ QCD at a single lattice spacing $a = 0.11$ fm, a pion mass close to its physical value, and a lattice volume with $M_\pi L \sim 3.9$. Their result $-0.86(^{+41}_{-40})\%$ including the strong isospin corrections is consistent with the RM123-SOTON estimate. The larger uncertainty is due to the possibly large finite-volume effects, which are under active investigation in different lattice-QED prescriptions [284].

At present, the superallowed nuclear β transitions provide the most precise determination of $|V_{ud}|$. Its accuracy has been limited by hadronic uncertainties in the universal electroweak radiative correction Δ_R^V. A 2018 analysis in terms of a dispersion relation [285,286] found Δ_R^V larger than the previous estimate [287]. A more straightforward update [288] of Ref. [287] on the description of relevant hadronic contributions as well as a lattice and perturbative-QCD calculation [289] also reported larger Δ_R^V, which is consistent with the dispersive estimate within uncertainties. Together with conservative estimate of nuclear corrections [285,290–298], a recent reanalysis of twenty-three β decays obtained [205,299]

$$|V_{ud}| = 0.97373(31). \tag{69}$$

The matrix element $|V_{us}|$ can be determined from inclusive hadronic τ decays [300–303]. Both Gamiz *et al.* [304,305] and Maltman *et al.* [302,306,307] arrived at very similar values of $|V_{us}|$ by separating the inclusive decay $\tau \to X_{\{d,s\}}\nu_\tau$ into nonstrange ($X_d\nu_\tau$) and strange ($X_s\nu_\tau$) final states and evaluating the relevant spectral integral using the operator product expansion (OPE). However, $|V_{us}| = 0.2195(19)$ quoted by HFLAV 18 [308] differs from the result one obtains from the kaon decays by about three standard deviations (see Table 21 in Sec. V E). A new treatment of higher orders in the OPE obtained a slightly larger value of $|V_{us}| = 0.2219(22)$ with a different experimental input [309].

Reference [310] proposed a new method to determine $|V_{us}|$ without any recourse to the OPE by evaluating the spectral integral from lattice-QCD data of the hadronic vacuum polarization function through generalized dispersion relations. This led to an analysis [309] yielding $|V_{us}| = 0.2240(18)$, which is consistent with that from the kaon decays. However, this result mostly relies on the $\tau \to K\nu_\tau$ decay channel, which represents only ∼24% of the inclusive $\tau \to X_s\nu_\tau$ decay, due to their choice of the generalized dispersion relation [311].

The ETM collaboration carried out a first lattice calculation of the *fully* inclusive rate of the hadronic τ decays based on ideas to study inclusive processes on the lattice [312,313]. Their study of $\tau \to X_d\nu_\tau$ led to 0.4% determination of $|V_{ud}| = 0.9752(39)$, which is nicely consistent with Eq. (69) from nuclear β decay [314]. Their extension to the $\tau \to X_s\nu_\tau$ decay yields $|V_{us}| = 0.2189(19)$ and confirms the above tension with that from the kaon decays [315]. In Sec. V E of this review, we quote

$$|V_{us}| = 0.2184(21) \tag{70}$$

from HFLAV 22 [148] as $|V_{us}|$ from the inclusive hadronic τ decays.

The experimental results in Eq. (65) are for the semileptonic decay of a neutral kaon into a negatively charged pion and the charged pion and kaon leptonic decays, respectively, in QCD. In the case of the semileptonic decays the corrections for strong and electromagnetic isospin breaking in χPT at NLO have allowed for averaging the different experimentally measured isospin channels [316]. This is quite a convenient procedure as long as lattice-QCD calculations do not include strong or QED isospin-breaking effects. Several lattice results for f_K/f_π are quoted for QCD with (squared) pion and kaon masses of $M_\pi^2 = M_{\pi^0}^2$ and $M_K^2 = \frac{1}{2}(M_{K^\pm}^2 + M_{K^0}^2 - M_{\pi^\pm}^2 + M_{\pi^0}^2)$ for which the leading strong and electromagnetic isospin violations cancel. For these results, contact with experimental results is made by correcting leading isospin breaking guided either by χPT or by lattice calculations. We note, however, that the modern trend for the leptonic decays is to include strong and electromagnetic isospin breaking in the lattice calculations (e.g., Refs. [212–214,222,223,235,283,317,318]).

This trend is being extended to the semileptonic decays. Calculating the electromagnetic correction to the $K_{\ell 3}$ semileptonic decays on the lattice is more involved due to the photon exchange between $\pi^\pm$ and $\ell^\mp$ in the final state. A framework has been proposed [319], and its applicability to the kaon semileptonic decays has been discussed in Ref. [320]. References [321–323] pursue an effective field theory setup supplemented by nonperturbative lattice-QCD inputs to estimate the radiative corrections.

B. Lattice results for $f_+(0)$ and $f_{K^\pm}/f_{\pi^\pm}$

The traditional way of determining $|V_{us}|$ relies on using estimates for the value of $f_+(0)$, invoking the Ademollo-Gatto theorem [324]. This theorem states that the corrections to the SU(3) symmetric limit $f_+(0) = 1$ start at second order in SU(3) breaking, namely $\propto (m_s - m_{ud})^2$. Theoretical models are used to estimate higher-order corrections. Lattice methods have now reached the stage

TABLE 16. Color codes for the data on $f_+(0)$. In this and previous editions [4,5], old results with two red tags have been dropped.

Collaboration	Ref.	N_f	Publication status	Chiral extrapolation	Continuum extrapolation	Finite-volume errors	$f_+(0)$
FNAL/MILC 18	[39]	$2+1+1$	A	★	★	★	0.9696(15)(12)
ETM 16	[38]	$2+1+1$	A	○	★	○	0.9709(45)(9)
FNAL/MILC 13E	[341]	$2+1+1$	A	★	★	★	0.9704(24)(22)
PACS 22	[342]	$2+1$	A	○	■	★	$0.9615(10)(^{+47}_{-6})$
PACS 19	[343]	$2+1$	A	○	■	★	$0.9603(16)(^{+50}_{-48})$
JLQCD 17	[336]	$2+1$	A	○	■	○	$0.9636(36)(^{+57}_{-35})$
RBC/UKQCD 15A	[41]	$2+1$	A	★	○	○	0.9685(34)(14)
RBC/UKQCD 13	[344]	$2+1$	A	★	○	○	$0.9670(20)(^{+18}_{-46})$
FNAL/MILC 12I	[40]	$2+1$	A	○	○	★	0.9667(23)(33)
JLQCD 12	[345]	$2+1$	C	○	■	★	0.959(6)(5)
JLQCD 11	[346]	$2+1$	C	○	■	★	0.964(6)
RBC/UKQCD 10	[347]	$2+1$	A	○	■	★	$0.9599(34)(^{+31}_{-47})(14)$
RBC/UKQCD 07	[348]	$2+1$	A	○	■	★	0.9644(33)(34)(14)

where quantities like $f_+(0)$ or f_K/f_π can be determined to good accuracy. As a consequence, the uncertainties inherent in the theoretical estimates for the higher order effects in the value of $f_+(0)$ do not represent a limiting factor any more, and we shall, therefore, not invoke those estimates. Also, we will use the experimental results based on nuclear β decay and inclusive hadronic τ decay exclusively for comparison—the main aim of the present review is to assess the information gathered with lattice methods and to use it for testing the consistency of the SM and its potential to provide constraints for its extensions.

The database underlying the present review of the semileptonic form factor and the ratio of decay constants is listed in Tables 16, 17, and 18. The properties of the lattice data play a crucial role for the conclusions to be drawn from these results: ranges of a, M_π and LM_π to control continuum extrapolation, extrapolation in the quark masses, finite-size effects, etc. The key features of the various datasets are characterized by means of the color code specified in Sec. II A. More detailed information on individual computations are compiled in Appendix C 2, which in this edition is limited to new results and to those entering the FLAG averages. For other calculations the reader should refer to the Appendix B. 2 of Ref. [3].

The quantity $f_+(0)$ represents a matrix element of a strangeness-changing null-plane charge, $f_+(0) = \langle K|Q^{\bar{u}s}|\pi\rangle$ (see Ref. [325]). The vector charges obey the commutation relations of the Lie algebra of SU(3), in particular $[Q^{\bar{u}s}, Q^{\bar{s}u}] = Q^{\bar{u}u-\bar{s}s}$. This relation implies the sum rule $\sum_n |\langle K|Q^{\bar{u}s}|n\rangle|^2 - \sum_n |\langle K|Q^{\bar{s}u}|n\rangle|^2 = 1$. Since the contribution from the one-pion intermediate state to the first sum is given by $f_+(0)^2$, the relation amounts to an exact representation for this quantity [326]

$$f_+(0)^2 = 1 - \sum_{n\neq\pi} |\langle K|Q^{\bar{u}s}|n\rangle|^2 + \sum_n |\langle K|Q^{\bar{s}u}|n\rangle|^2. \quad (71)$$

While the first sum on the right extends over nonstrange intermediate states, the second runs over exotic states with strangeness ± 2 and is expected to be small compared to the first.

The expansion of $f_+(0)$ in SU(3) χPT in powers of m_u, m_d, and m_s starts with $f_+(0) = 1 + f_2 + f_4 + \cdots$ [327]. The NLO contribution f_2 is known, since it can be expressed in terms of M_π, M_K, M_η and f_π [325]. In the language of the sum rule (71), f_2 stems from nonstrange intermediate states with three mesons. Like all other nonexotic intermediate states, it lowers the value of $f_+(0)$: $f_2 = -0.023$ when using the experimental value of f_π as input. The corresponding expressions have also been derived in quenched or partially quenched (staggered) χPT [40,328]. At the same order in the SU(2) expansion [329], $f_+(0)$ is parametrized in terms of M_π and two *a priori* unknown parameters. The latter can be determined from the dependence of the lattice results on the masses of the quarks. For the SU(3) χPT formula for f_2, one may use

TABLE 17. Color codes for the data on the ratio of decay constants: f_K/f_π is the pure QCD isospin-symmetric ratio, while $f_{K^\pm}/f_{\pi^\pm}$ is in pure QCD including the isospin-breaking correction. In this and previous editions [4,5], old results with two red tags have been dropped.

Collaboration	Ref.	N_f	Publication status	Chiral extrapolation	Continuum extrapolation	Finite-volume errors	f_K/f_π	$f_{K^\pm}/f_{\pi^\pm}$
ETM 21	[45]	$2+1+1$	A	★	★	★	1.1995(44)(7)	1.1957(44)(7)
CalLat 20	[44]	$2+1+1$	A	★	★	★	1.1964(32)(30)	1.1942(32)(31)
FNAL/MILC 17	[20]	$2+1+1$	A	★	★	★	1.1980(12)$(^{+5}_{-15})$	1.1950(15)$(^{+6}_{-18})$
ETM 14E	[43]	$2+1+1$	A	○	★	○	1.188(11)(11)	1.184(12)(11)
FNAL/MILC 14A	[21]	$2+1+1$	A	★	★	★		1.1956(10)$(^{+26}_{-18})$
ETM 13F	[356]	$2+1+1$	C	○	★	○	1.193(13)(10)	1.183(14)(10)
HPQCD 13A	[42]	$2+1+1$	A	★	○	★	1.1948(15)(18)	1.1916(15)(16)
MILC 13A	[357]	$2+1+1$	A	★	★	★		1.1947(26)(37)
MILC 11	[358]	$2+1+1$	C	○	○	○		1.1872(42)$_{\text{stat.}}$[a]
ETM 10E	[359]	$2+1+1$	C	○	○	○	1.224(13)$_{\text{stat}}$	
CLQCD 23	[10]	$2+1$	A	★	★	★		1.1907(76)(17)
QCDSF/UKQCD 16	[50]	$2+1$	A	○	★	○	1.192(10)(13)	1.190(10)(13)
BMW 16	[49,360]	$2+1$	A	★	★	★	1.182(10)(26)	1.178(10)(26)
RBC/UKQCD 14B	[12]	$2+1$	A	★	★	★	1.1945(45)	
RBC/UKQCD 12	[229]	$2+1$	A	★	○	★	1.199(12)(14)	
Laiho 11	[54]	$2+1$	C	○	★	○		1.202(11)(9)(2)(5)[b]
MILC 10	[47]	$2+1$	C	○	★	★		1.197(2)$(^{+3}_{-7})$
JLQCD/TWQCD 10	[361]	$2+1$	C	○	■	★	1.230(19)	
RBC/UKQCD 10A	[119]	$2+1$	A	○	○	★	1.204(7)(25)	
BMW 10	[48]	$2+1$	A	★	★	★	1.192(7)(6)	
MILC 09A	[19]	$2+1$	C	○	★	★		1.198(2)$(^{+6}_{-8})$
MILC 09	[196]	$2+1$	A	○	★	★		1.197(3)$(^{+6}_{-13})$
Aubin 08	[362]	$2+1$	C	○	○	○		1.191(16)(17)
RBC/UKQCD 08	[236]	$2+1$	A	○	■	★	1.205(18)(62)	
HPQCD/UKQCD 07	[46]	$2+1$	A	○	○	○	1.189(2)(7)	
MILC 04	[239]	$2+1$	A	○	○	○		1.210(4)(13)

[a]Result with statistical error only from polynomial interpolation to the physical point.

[b]This work is the continuation of Aubin 08.

f_0, that is the decay constant in the chiral limit, instead of f_π. While this affects the result only at higher orders, it may make a significant numerical difference in calculations where the higher-order corrections are not explicitly accounted for. (Lattice results concerning the value of the ratio f_π/f_0 are reviewed in Sec. V.3 of the previous review [5].)

The lattice results shown in Fig. 8 indicate that the higher order contributions $\Delta f \equiv f_+(0) - 1 - f_2$ are negative and thus amplify the effect generated by f_2. This confirms the expectation that the exotic contributions are small. The entries in the lower part represent various model estimates for f_4. In Ref. [330], the symmetry-breaking effects are estimated in the framework of the quark model. The more

TABLE 18. Color codes for the lattice data on $f_{\pi^\pm}$ and $f_{K^\pm}$ together with information on the way the lattice spacing was converted to physical units and on whether or not an isospin-breaking correction has been applied to the quoted result (see Sec. V C). The numerical values are listed in MeV units. In this and previous editions [4,5], old results with two red tags have been dropped.

Collaboration	Ref.	N_f	Publication status	Chiral extrapolation	Continuum extrapolation	Finite-volume errors	Renormalization	Physical scale	Isospin breaking	$f_{\pi^\pm}$	$f_{K^\pm}$
ETM 21	[45]	$2+1+1$	A	★	★	★	na	f_π		⋯	155.92(62)(9)[a]
ETM 14E	[43]	$2+1+1$	A	○	★	○	na	f_π		⋯	154.4(1.5)(1.3)
FNAL/MILC 14A	[21]	$2+1+1$	A	★	★	★	na	f_π		⋯	$155.92(13)(^{+34}_{-23})$
HPQCD 13A	[42]	$2+1+1$	A	★	○	★	na	f_π		⋯	155.37(20)(27)
MILC 13A	[357]	$2+1+1$	A	★	○	★	na	f_π		⋯	155.80(34)(54)
ETM 10E	[359]	$2+1+1$	C	○	○	○	na	f_π	✓	⋯	159.6(2.0)
CLQCD 23	[10]	$2+1$	A	★	○	★	NPR	w_0		130.7(0.9)(2.1)	155.6(0.8)(2.7)
JLQCD 15C	[367]	$2+1$	C	○	★	★	NPR	t_0		$125.7(7.4)_{\text{stat}}$	
RBC/UKQCD 14B	[12]	$2+1$	A	★	★	★	NPR	m_Ω	✓	130.19(89)	155.18(89)
RBC/UKQCD 12	[229]	$2+1$	A	★	○	★	NPR	m_Ω	✓	127.1(2.7)(2.7)	152.1(3.0)(1.7)
Laiho 11	[54]	$2+1$	C	○	★	○	na	[b]		130.53(87)(2.10)	156.8(1.0)(1.7)
MILC 10	[47]	$2+1$	C	○	★	★	na	[b]		129.2(4)(1.4)	⋯
MILC 10	[47]	$2+1$	C	○	★	★	na	f_π		⋯	$156.1(4)(^{+6}_{-9})$
JLQCD/TWQCD 10	[361]	$2+1$	C	○	■	★	na	m_Ω	✓	$118.5(3.6)_{\text{stat}}$	$145.7(2.7)_{\text{stat}}$
RBC/UKQCD 10A	[119]	$2+1$	A	○	○	★	NPR	m_Ω	✓	124(2)(5)	148.8(2.0)(3.0)
MILC 09A	[19]	$2+1$	C	○	★	★	na	ΔM_Υ		128.0(0.3)(2.9)	153.8(0.3)(3.9)
MILC 09A	[19]	$2+1$	C	○	★	★	na	f_π		⋯	156.2(0.3)(1.1)
MILC 09	[196]	$2+1$	A	○	★	★	na	ΔM_Υ		$128.3(0.5)(^{+2.4}_{-3.5})$	$154.3(0.4)(^{+2.1}_{-3.4})$
MILC 09	[196]	$2+1$	A	○	★	★	na	f_π			$156.5(0.4)(^{+1.0}_{-2.7})$
Aubin 08	[362]	$2+1$	C	○	○	○	na	ΔM_Υ		129.1(1.9)(4.0)	153.9(1.7)(4.4)
RBC/UKQCD 08	[236]	$2+1$	A	○	■	★	NPR	m_Ω	✓	124.1(3.6)(6.9)	149.4(3.6)(6.3)
HPQCD/UKQCD 07	[46]	$2+1$	A	○	○	○	na	ΔM_Υ	✓	132(2)	156.7(0.7)(1.9)
MILC 04	[239]	$2+1$	A	○	○	○	na	ΔM_Υ		129.5(0.9)(3.5)	156.6(1.0)(3.6)

The label "na" indicates the lattice calculations that do not require the use of any renormalization constant for the axial current, while the label "NPR" signals the use of a renormalization constant calculated nonperturbatively.

[a]We evaluated from $f_{K^\pm}/f_{\pi^\pm}$ in Table 18 and their input to fix the scale $f_\pi = 130.4(2)$.

[b]The ratios of lattice spacings within the ensembles were determined using the quantity r_1. The conversion to physical units was made on the basis of Ref. [122], and we note that such a determination depends on the PDG value [276] of the pion decay constant.

recent calculations are more sophisticated, as they make use of the known explicit expression for the $K_{\ell 3}$ form factors to NNLO in χPT [331,332]. The corresponding formula for f_4 accounts for the chiral logarithms occurring at NNLO and is not subject to the ambiguity mentioned above.[21] The numerical result, however, depends on the model used to estimate the low-energy constants occurring in f_4 [332–335]. The figure indicates that the most recent numbers obtained in this way correspond to a positive or an almost vanishing rather than a negative value for Δf. We note that FNAL/MILC 12I [40], JLQCD 17 [336], FNAL/MILC 18 [39], and Ref. [337] have made an attempt at determining a combination of some of the low-energy constants appearing in f_4 from lattice data.

C. Direct determination of $f_+(0)$ and $f_{K^\pm}/f_{\pi^\pm}$

Many lattice results for the form factor $f_+(0)$ and for the ratio of decay constants, which we summarize here in Tables 16 and 18, respectively, have been computed in isospin-symmetric QCD. The reason for this unphysical parameter choice is that there are only a few simulations of isospin-breaking effects in lattice QCD, which is ultimately the cleanest way for predicting these effects [212–214,220,222,223,233,283,338–340]. In the meantime,

[21]Fortran programs for the numerical evaluation of the form factor representation in Ref. [332] are available on request from Johan Bijnens.

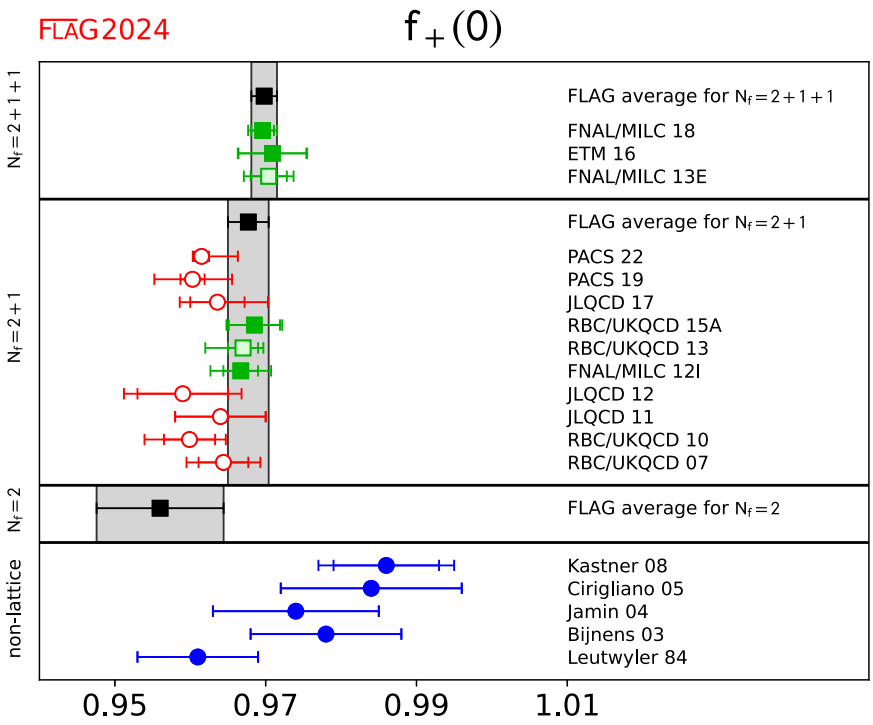


FIG. 8. Comparison of lattice results (squares and empty circles) for $f_+(0)$ with various model estimates based on χPT [330,332–335] (filled blue circles). The black squares and gray bands indicate our averages in Eqs. (72) and (73). The significance of the colors is explained in Sec. II.

one relies either on χPT [239,327] to estimate the correction to the isospin limit or one calculates the breaking at leading order in $(m_u - m_d)$ in the valence quark sector by extrapolating the lattice data for the charged kaons to the physical value of the $up(down)$-quark mass (the result for the pion decay constant is always extrapolated to the value of the average light-quark mass $\hat{m}$). This defines the prediction for $f_{K^\pm}/f_{\pi^\pm}$.

Since the majority of results that qualify for inclusion into the FLAG average include the strong isospin-breaking correction, we provide in Fig. 9 the overview of the world data of $f_{K^\pm}/f_{\pi^\pm}$. For all the results of Table 18 provided only in the isospin-symmetric limit we apply individually an isospin correction that will be described later on [see Eqs. (74) and (75)].

The plots in Figs. 8 and 9 illustrate our compilation of data for $f_+(0)$ and $f_{K^\pm}/f_{\pi^\pm}$. The lattice data for the latter quantity is largely consistent even when comparing simulations with different N_f. In the case of $f_+(0)$, a slight tendency to get higher values when increasing N_f seems to be visible, while it does not exceed one standard deviation. We now proceed to form the corresponding averages, separately for the data with $N_f = 2+1+1$ and $N_f = 2+1$ dynamical flavors, and in the following we will refer to these averages as the "direct" determinations.

1. Results for $f_+(0)$

For $f_+(0)$ there are currently two computational strategies: FNAL/MILC uses the Ward identity to relate the $K \to \pi$ form factor at zero momentum transfer to the matrix element $\langle \pi|S|K\rangle$ of the flavor-changing scalar current $S = \bar{s}u$. Peculiarities of the staggered fermion discretization used by FNAL/MILC (see Ref. [40]) makes this the favored choice. The other collaborations are instead computing the vector current matrix element $\langle \pi|\bar{s}\gamma_\mu u|K\rangle$. Apart from FNAL/MILC 13E, RBC/UKQCD 15A, FNAL/MILC 18, PACS 19 and 22, all simulations in Table 16 involve unphysically heavy quarks and, therefore, the lattice data needs to be extrapolated to the physical pion and kaon masses corresponding to the $K^0 \to \pi^-$ channel. We note also that the recent computations of $f_+(0)$ make use of the partially twisted boundary conditions to determine the form-factor results directly at the relevant kinematical point $q^2 = 0$ [349,350], avoiding in this way any uncertainty due to the momentum dependence of the vector and/or scalar form factors. The ETM collaboration uses partially twisted boundary conditions to compare the momentum dependence of the scalar and vector form factors with the one of the experimental data [38,351], while keeping at the same time the advantage of the high-precision determination of the scalar form factor at the kinematical end-point $q^2_{\rm max} = (M_K - M_\pi)^2$ [352,353] for the interpolation at $q^2 = 0$.

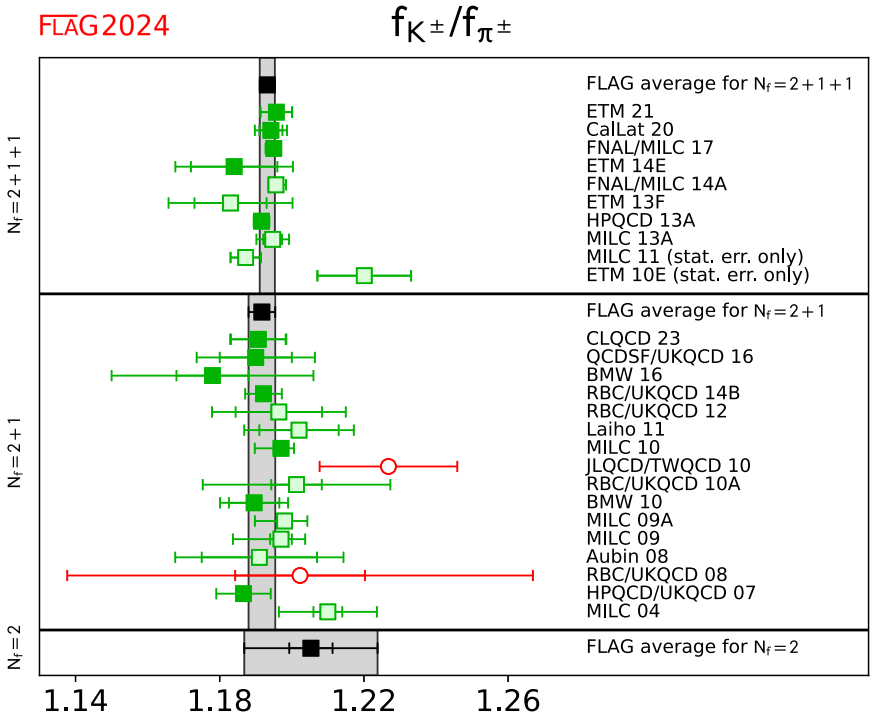


FIG. 9. Comparison of lattice results for $f_{K^\pm}/f_{\pi^\pm}$. This ratio is obtained in pure QCD including the isospin-breaking correction (see Sec. V C). The black squares and gray bands indicate our averages in Eqs. (76) and (77).

According to the color codes reported in Table 16 and to the FLAG rules of Sec. II B, the results FNAL/MILC 12I and RBC/UKQCD 15A with $N_f = 2+1$, and the results ETM 16 and FNAL/MILC 18 with $N_f = 2+1+1$ dynamical flavors of fermions, respectively, can enter the FLAG averages. Therefore, there is no new entry to form the averages in Eqs. (72) and (73) in this edition.

At $N_f = 2+1+1$ the result from the FNAL/MILC collaboration, $f_+(0) = 0.9704(24)(22)$ (FNAL/MILC 13E), is based on the use of the highly improved staggered quark (HISQ) action (for both valence and sea quarks), which has been tailored to reduce staggered taste-breaking effects, and includes simulations with three lattice spacings and physical light-quark masses. These features lead to uncertainties due to the chiral extrapolation and the discretization artifacts that are well below the statistical error. The remaining largest systematic uncertainty comes from finite-size effects, which have been investigated in Ref. [354] using one-loop χPT (with and without taste-violating effects). In Ref. [39], the FNAL/MILC collaboration presented a more precise determination of $f_+(0)$, $f_+(0) = 0.9696(15)(11)$ (FNAL/MILC 18). In this update, their analysis is extended to two smaller lattice spacings $a = 0.06$ and 0.042 fm. The physical light-quark mass is simulated at four lattice spacings. They also added a simulation at a small volume to study the finite-size effects. The improvement of the precision with respect to FNAL/MILC 13E is obtained mainly by an estimate of finite-size effects, which is claimed to be controlled at the level of ∼0.05% by comparing two analyses with and without the one-loop correction. The total uncertainty is reduced to ∼0.2%. An independent calculation of such high precision would be highly welcome to solidify the lattice prediction of $f_+(0)$, which currently suggests a tension with CKM unitarity with the updated value of $|V_{ud}|$ (see Sec. V D).

The result from the ETM collaboration, $f_+(0) = 0.9709(45)(9)$ (ETM 16), makes use of the twisted-mass discretization adopting three values of the lattice spacing in the range 0.06–0.09 fm and pion masses simulated in the range 210–450 MeV. The chiral and continuum extrapolations are performed in a combined fit together with the momentum dependence, using both a SU(2)-χPT inspired *Ansatz* (following Ref. [351]) and a modified z-expansion fit. The uncertainties coming from the chiral extrapolation, the continuum extrapolation and the finite-volume effects turn out to be well below the dominant statistical error, which includes also the error due to the fitting procedure. A set of synthetic data points, representing both the vector and the scalar semileptonic form factors at the physical point for several selected values of q^2, is provided together with the corresponding correlation matrix.

In ETM 16, a measure of the scaling violation $\delta(a)$ defined in Eq. (1) estimated from their continuum and chiral extrapolation decreases toward the chiral limit with the strange-quark mass kept fixed, because the SU(3)-breaking effects to be calculated on the lattice increases, and more

statistics are needed to keep the statistical accuracy toward this limit. At the physical point, $\delta(a)$ is consistent with zero in their region of the lattice spacing a. This is also the case for FNAL/MILC 18, where they demonstrated that $f_+(0)$ extrapolated to the physical point at each simulated value of a is consistent with the value extrapolated to the continuum limit within 2σ. We note that, in contrast to the heavy-meson semileptonic decays, relevant meson masses and momenta at zero momentum transfer are at most $\mathcal{O}(M_K)$, and hence well below the cutoff a^{-1}.

The PACS collaboration carried out a calculation (PACS 19) for $N_f = 2+1$ using the $\mathcal{O}(a)$-improved Wilson quark action by creating an ensemble with the physical light-quark mass on a large lattice volume of $(10.9\text{ fm})^4$ at a single spacing $a = 0.085$ fm [343]. Such a large lattice enables them to interpolate $f_+(q^2)$ to zero momentum transfer and study the momentum-transfer dependence of the form factors without using partially twisted boundary conditions. This was extended to a smaller lattice spacing $a = 0.063$ fm in PACS 22, which yields $f_+(0) = 0.9615(10)(^{+47}_{-6})$. However, their result does not enter the FLAG average, because they simulate only two lattice spacings using unimproved local and conserved vector currents. That setup is the source of the largest (and very asymmetric) error in their calculation. Further extension to an even smaller lattice spacing $a = 0.041$ fm has been reported in Ref. [355], where authors estimate the statistical error only, and refrain from quoting a numerical value of $f_+(0)$.

For $N_f = 2+1$, the two results eligible to enter the FLAG average are the one from RBC/UKQCD 15A, $f_+(0) = 0.9685(34)(14)$ [41], and the one from FNAL/MILC 12I, $f_+(0) = 0.9667(23)(33)$ [40]. These results, based on different fermion discretizations (staggered fermions in the case of FNAL/MILC and domain wall fermions in the case of RBC/UKQCD) are in nice agreement. Moreover, in the case of FNAL/MILC the form factor has been determined from the scalar current matrix element, while in the case of RBC/UKQCD it has been determined including also the matrix element of the vector current. To a certain extent, both simulations are expected to be affected by different systematic effects.

RBC/UKQCD 15A has analyzed results on ensembles with pion masses down to 140 MeV, mapping out the complete range from the SU(3)-symmetric limit to the physical point. No significant cutoff effects (results for two lattice spacings) were observed in the simulation results. Ensembles with unphysical light-quark masses are weighted to work as a guide for small corrections toward the physical point, reducing in this way the model dependence in the fitting *Ansatz*. The systematic uncertainty turns out to be dominated by finite-volume effects, for which an estimate based on effective theory arguments is provided.

The result FNAL/MILC 12I is from simulations reaching down to a lightest RMS pion mass of about 380 MeV (the lightest valence pion mass for one of their ensembles is about 260 MeV). Their combined chiral and continuum extrapolation (results for two lattice spacings) is based on NLO staggered χPT supplemented by the continuum NNLO expression [332] and a phenomenological parametrization of the breaking of the Ademollo-Gatto theorem at finite lattice spacing inherent in their approach. The p^4 low-energy constants entering the NNLO expression have been fixed in terms of external input [269].

Since there has been no new entry after the previous edition, the FLAG average for $f_+(0)$ remains unchanged. The $N_f = 2+1+1$ average is based on the FNAL/MILC 18 and ETM 16 (uncorrelated) results, the $N_f = 2+1$ average based on FNAL/MILC 12I and RBC/UKQCD 15A, which we consider uncorrelated

$$\text{direct, } N_f = 2+1+1\text{: } f_+(0) = 0.9698(17) \text{ Refs. [38,39]}, \tag{72}$$

$$\text{direct, } N_f = 2+1\text{: } f_+(0) = 0.9677(27) \text{ Refs. [40,41]}. \tag{73}$$

We stress that the results (72) and (73), corresponding to $N_f = 2+1+1$ and $N_f = 2+1$, respectively, include simulations with physical light-quark masses.

2. Results for $f_{K^\pm}/f_{\pi^\pm}$

In the case of the ratio of decay constants, the datasets that meet the criteria formulated in the introduction are HPQCD 13A [42], ETM 14E [43], FNAL/MILC 17 [20] (which updates FNAL/MILC 14A [21]), CalLat 20 [44] and ETM 21 [45] with $N_f = 2+1+1$, and HPQCD/UKQCD 07 [46], MILC 10 [47], BMW 10 [48], RBC/UKQCD 14B [12], BMW 16 [49,360], QCDSF/UKQCD 16 [50], and CLQCD 23 [10] with $N_f = 2+1$ dynamical flavors. Note that the new entry in this edition is ETM 21 for $N_f = 2+1+1$, which did not enter the previous FLAG average due to its publication status, and CLQCD 23 for $N_f = 2+1$.

CalLat 20 employs a mixed action setup with Möbius domain-wall valence quarks on gradient-flowed HISQ ensembles at four lattice spacings $a = 0.06$–0.15 fm. The valence pion mass reaches the physical point at three lattice spacings, and the smallest valence-sea and sea pion masses are below 200 MeV. Finite-volume corrections are studied on three lattice volumes at $a = 0.12$ fm and $M_\pi \sim 220$ MeV. The extrapolation to the continuum limit and the physical point is based on NNLO χPT [363]. A comprehensive study of systematic uncertainties is performed by exploring several options including the use of the mixed-action effective theory expression, and the

inclusion of N^{3}LO counterterms. They obtain $f_{K^\pm}/f_{\pi^\pm} = 1.1942(32)_{\rm stat}(12)_\chi(20)_{a^2}(1)_{\rm FV}(12)_M(7)_{\rm IB}$, where the errors are statistical, due to the extrapolation in pion and kaon masses, extrapolation in a^2, finite-size effects, choice of the fitting form and strong isospin-breaking corrections.

ETM 14E uses the twisted-mass discretization and provides a comprehensive study of the systematics by presenting results for three lattice spacings in the range 0.06–0.09 fm and for pion masses in the range 210–450 MeV. This makes it possible to constrain the chiral extrapolation, using both SU(2) [329] χPT and polynomial fits. The ETM collaboration includes the spread in the central values obtained from different *Ansätze* into the systematic errors. The final result of their analysis is $f_{K^\pm}/f_{\pi^\pm} = 1.184(12)_{\rm stat+fit}(3)_{\rm Chiral}(9)_{a^2}(1)_{Z_P}(3)_{\rm FV}(3)_{\rm IB}$ where the errors are (statistical + the error due to the fitting procedure), due to the chiral extrapolation, the continuum extrapolation, the mass-renormalization constant, the finite-volume and (strong) isospin-breaking effects.

In ETM 21 [45], the ETM collaboration presented an independent estimate of f_K/f_π in isosymmetric QCD with $2+1+1$ dynamical flavors of the twisted-mass quarks. Their new set of gauge ensembles reaches the physical pion mass. The quark action includes the Sheikoleslami-Wohlert term [364] for a better control of discretization effects. The finite-volume effects are examined by simulating three spatial volumes, and are corrected by SU(2) χPT formulas [184]. Their new estimate $f_K/f_\pi = 1.1995(44)_{\rm stat+fit}(7)_{\rm sys}$ is consistent with ETM 14E with the total uncertainty reduced by a factor of ∼3.5.

FNAL/MILC 17 has determined the ratio of the decay constants from a comprehensive set of HISQ ensembles with $N_f = 2+1+1$ dynamical flavors. They have generated 24 ensembles for six values of the lattice spacing (0.03–0.15 fm, scale set with f_{π^+}) and with both physical and unphysical values of the light sea-quark masses, controlling in this way the systematic uncertainties due to chiral and continuum extrapolations. With respect to FNAL/MILC 14A they have increased the statistics and added three ensembles at very fine lattice spacings, $a \simeq 0.03$ and 0.042 fm, including for the latter case also a simulation at the physical value of the light-quark mass. The final result of their analysis is $f_{K^\pm}/f_{\pi^\pm} = 1.1950(14)_{\rm stat}(^{+0}_{-17})_{a^2}(2)_{\rm FV}(3)_{f_\pi,{\rm PDG}}(3)_{\rm EM}(2)_{Q^2}$, where the errors are statistical, due to the continuum extrapolation, finite-volume, pion decay constant from PDG, electromagnetic effects and sampling of the topological charge distribution.[22]

HPQCD 13A has analyzed ensembles generated by MILC and therefore its study of $f_{K^\pm}/f_{\pi^\pm}$ is based on the same set of ensembles as FNAL/MILC 17 bar the ones at the finest lattice spacings (namely, only $a = 0.09$–0.15 fm, scale set with f_{π^+} and relative scale set with the Wilson flow [115,365]) supplemented by some simulation points with heavier quark masses. HPQCD employs a global fit based on continuum NLO SU(3) χPT for the decay constants supplemented by a model for higher-order terms including discretization and finite-volume effects (61 parameters for 39 data points supplemented by Bayesian priors). Their final result is $f_{K^\pm}/f_{\pi^\pm} = 1.1916(15)_{\rm stat}(12)_{a^2}(1)_{\rm FV}(10)$, where the errors are statistical, due to the continuum extrapolation, due to finite-volume effects and the last error contains the combined uncertainties from the chiral extrapolation, the scale-setting uncertainty, the experimental input in terms of f_{π^+} and from the uncertainty in m_u/m_d.

Because CalLat 20, FNAL/MILC 17 and HPQCD 13A partly share their gauge ensembles, we assume a 100% correlation among their statistical errors. A 100% correlation on the total systematic uncertainty is also assumed between FNAL/MILC 17 and HPQCD 13A with the HISQ valence quarks.

The discretization effects are not large, typically at the $\lesssim$1% level in HPQCD 13A, FNAL/MILC 17 and ETM21 in their simulation region of a. This does not necessarily mean that $\delta(a)$ in units of the uncertainty of the observable is small. HPQCD 13A observed that it also depends on the choice of the input to fix the lattice scale: $\delta(a)$ is consistent with zero with the relative scale setting using r_1 from the static potential and w_0 from the gradient flow, whereas $\delta(a) \lesssim 7$ with another flow scale $\sqrt{t_0}$.[23] It is not surprising that CalLat 20 observed larger scaling violation of $\lesssim$4%: while they partly share gauge ensembles with HPQCD 13A and FNAL/MILC 17, the Möbius domain-wall action without the tree-level $O(a^2)$ improvement is employed in their mixed action setup.

For $N_f = 2+1$, the CLQCD collaboration obtained a new result (CLQCD 23) by employing the tadpole-improved tree-level Symanzik gauge action and tadpole-improved tree-level clover quark action with one-step stout smearing for the gauge link. They simulate three values of the lattice spacing in a wide range $a = 0.05$–0.11 fm fixed from the gradient-flow scale w_0. The unitary light-quark mass reaches the physical point on the coarsest lattice. Two additional partially quenched masses satisfying $M_\pi L \geq 3.5$ are considered to calculate relevant two-point functions on each ensemble. Their results for f_K and f_π are renormalized nonperturbatively through the RI/MOM scheme. The chiral extrapolation is based on NLO partially quenched χPT for f_π and a polynomial form for f_K. Finite-volume effects are taken into account assuming $e^{-M_\pi L}$ dependence for data in two volumes on the two coarser lattices. They obtain $f_K^\pm/f_\pi^\pm = 1.1907(76)_{\rm stat+fit}(17)_{\rm sys}$, where the

[22]To form the average in Eq. (76), we have symmetrized the asymmetric systematic error and shifted the central value by half the difference as will be done throughout this section.

[23]We refer to Sec. XI for detailed discussions on the scale setting and choices of the input.

second error is taken from the difference with respect to a similar analysis using the RI/SMOM scheme, which shows larger discretization effects.

The results BMW 16 and QCDSF/UKQCD 16 are also eligible to enter the FLAG average. BMW 16 has analyzed the decay constants evaluated for 47 gauge ensembles generated using tree-level clover-improved fermions with two HEX-smearings and the tree-level Symanzik-improved gauge action. The ensembles correspond to five values of the lattice spacing (0.05–0.12 fm, scale set by Ω mass), to pion masses in the range 130–680 MeV and to values of the lattice size from 1.7 to 5.6 fm, obtaining a good control over the interpolation to the physical mass point and the extrapolation to the continuum and infinite volume limits.

QCDSF/UKQCD 16 has used the nonperturbatively $\mathcal{O}(a)$-improved clover action for the fermions (mildly stout-smeared) and the tree-level Symanzik action for the gluons. Four values of the lattice spacing (0.06–0.08 fm) have been simulated with pion masses down to ∼220 MeV and values of the lattice size in the range 2.0–2.8 fm. The decay constants are evaluated using an expansion around the symmetric SU(3) point $m_u = m_d = m_s = (m_u + m_d + m_s)^{\text{phys}}/3$.

Note, that for $N_f = 2 + 1$ MILC 10 and HPQCD/UKQCD 07 are based on staggered fermions, BMW 10, BMW 16, QCDSF/UKQCD 16 and CLQCD 23 have used improved Wilson fermions, and RBC/UKQCD 14B's result is based on the domain-wall formulation. In contrast to RBC/UKQCD 14B, BMW 16 and CLQCD 23, the other simulations are for unphysical values of the light-quark masses (corresponding to smallest pion masses in the range 220–260 MeV in the case of MILC 10, HPQCD/UKQCD 07, and QCDSF/UKQCD 16) and, therefore, slightly more sophisticated extrapolations needed to be controlled. Various *Ansätze* for the mass and cutoff dependence comprising SU(2) and SU(3) χPT or simply polynomials were used and compared in order to estimate the model dependence. While BMW 10, RBC/UKQCD 14B, QCDSF/UKQCD 16, and CLQCD 23 are entirely independent computations, subsets of the MILC gauge ensembles used by MILC 10 and HPQCD/UKQCD 07 are the same. MILC 10 is certainly based on a larger and more advanced set of gauge configurations than HPQCD/UKQCD 07. This allows them for a more reliable estimation of systematic effects. In this situation, we consider both statistical and systematic uncertainties to be correlated.

Before determining the average for $f_{K^\pm}/f_{\pi^\pm}$, which should be used for applications to Standard Model phenomenology, we apply the strong-isospin correction individually to all those results that have been published only in the isospin-symmetric limit, i.e., BMW 10, HPQCD/UKQCD 07 and RBC/UKQCD 14B at $N_f = 2 + 1$. To this end, as in the previous editions of the FLAG reviews [2–5], we make use of NLO SU(3) χPT [282,327], which predicts

$$\frac{f_{K^\pm}}{f_{\pi^\pm}} = \frac{f_K}{f_\pi}\sqrt{1 + \delta_{\text{SU}(2)}}, \tag{74}$$

where [282]

$$\delta_{\text{SU}(2)} \approx \sqrt{3}\epsilon_{\text{SU}(2)}\left[-\frac{4}{3}(f_K/f_\pi - 1) + \frac{2}{3(4\pi)^2 f_0^2}\left(M_K^2 - M_\pi^2 - M_\pi^2 \ln\frac{M_K^2}{M_\pi^2}\right)\right]. \tag{75}$$

We use as input $\epsilon_{\text{SU}(2)} = \sqrt{3}/(4R)$ with the FLAG result for R of Eq. (51), $F_0 = f_0/\sqrt{2} = 80(20)$ MeV, $M_\pi = 135$ MeV and $M_K = 495$ MeV (we decided to choose a conservative uncertainty on f_0 in order to reflect the magnitude of potential higher-order corrections). The results are reported in Table 19, where in the last column the last error is due to the isospin correction (the remaining errors are quoted in the same order as in the original data).

For $N_f = 2 + 1 + 1$, HPQCD [42], FNAL/MILC [20] and ETM [366] estimate a value for $\delta_{\text{SU}(2)}$ equal to −0.0054(14), −0.0052(9) and −0.0073(6), respectively. Note that the ETM result is obtained using the insertion of the isovector scalar current according to the expansion method of Ref. [222], while the HPQCD and FNAL/MILC results correspond to the difference between the values of the decay constant ratio extrapolated to the physical u-quark mass m_u and to the average $(m_u + m_d)/2$ light-quark mass.

To remain on the conservative side, we add a 100% error to the correction based on SU(3) χPT. For further analyses, we add (in quadrature) such an uncertainty to the systematic error (see Table 19).

Using the results of Table 19 for $N_f = 2 + 1$ we obtain

$$\text{direct,} \quad N_f = 2 + 1 + 1\text{:} \quad f_{K^\pm}/f_{\pi^\pm} = 1.1934(19) \quad \text{Refs. [20, 42–45]}, \tag{76}$$

$$\text{direct,} \quad N_f = 2 + 1\text{:} \quad f_{K^\pm}/f_{\pi^\pm} = 1.1916(34) \quad \text{Refs. [10, 12, 46–50]}, \tag{77}$$

for QCD with broken isospin.

TABLE 19. Values of the isospin-breaking correction $\delta_{\text{SU}(2)}$ applied to the lattice data for f_K/f_π, entering the FLAG average at $N_f = 2 + 1$, for obtaining the corrected charged ratio $f_{K^\pm}/f_{\pi^\pm}$. The last error in the last column is due to a 100% uncertainty assumed for $\delta_{\text{SU}(2)}$ from SU(3) χPT.

	f_K/f_π	$\delta_{\text{SU}(2)}$	$f_{K^\pm}/f_{\pi^\pm}$
HPQCD/UKQCD 07	1.189(2)(7)	−0.0038(6)	1.187(2)(7)(2)
BMW 10	1.192(7)(6)	−0.0039(6)	1.190(7)(6)(2)
RBC/UKQCD 14B	1.1945(45)	−0.0039(6)	1.1921(45)(24)

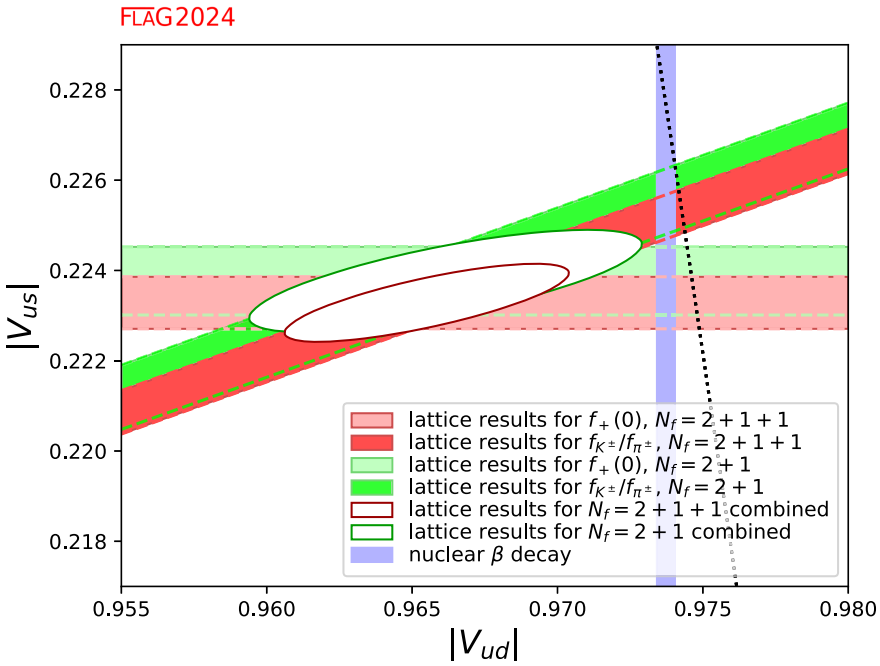


FIG. 10. The plot compares the information for $|V_{ud}|$, $|V_{us}|$ obtained using lattice QCD for $N_f = 2+1$ and $N_f = 2+1+1$ with $|V_{ud}|$ extracted from nuclear β transitions Eq. (69). The black dotted line indicates the correlation between $|V_{ud}|$ and $|V_{us}|$ that follows if the CKM-matrix is unitary.

The averages obtained for $f_+(0)$ and $f_{K^\pm}/f_{\pi^\pm}$ at $N_f = 2+1$ and $N_f = 2+1+1$ [see Eqs. (72), (73) and (76), (77)] exhibit a precision better than ∼0.3%. At such a level of precision, QED effects cannot be ignored, and a consistent lattice treatment of both QED and QCD effects in leptonic and semileptonic decays becomes mandatory.

3. Extraction of $|V_{ud}|$ and $|V_{us}|$

It is instructive to convert the averages for $f_+(0)$ and $f_{K^\pm}/f_{\pi^\pm}$ into a corresponding range for the CKM matrix elements $|V_{ud}|$ and $|V_{us}|$, using the relations in Eq. (65). Consider first the results for $N_f = 2+1+1$. The average for $f_+(0)$ in Eq. (72) is mapped into the interval $|V_{us}| = 0.22328(58)$, depicted as a horizontal red band in Fig. 10. That for $f_{K^\pm}/f_{\pi^\pm}$ in Eq. (76) is converted into $|V_{us}|/|V_{ud}| = 0.23126(50)$ using the result for $|V_{us}/V_{ud}|(f_{K^\pm}/f_{\pi^\pm})$ in Eq. (65), shown as a tilted red band. The red ellipse is the intersection of these two bands and represents the 68% likelihood contour, obtained by treating the above two results as independent measurements. Repeating the exercise for $N_f = 2+1$ leads to the green ellipse.[24] The vertical band shows $|V_{ud}|$ from nuclear β decay, Eq. (69). The PDG value (69) indicates a tension with both the $N_f = 2+1+1$ and $N_f = 2+1$ results from lattice QCD.

As we mentioned, the isospin corrections are becoming relevant for the extraction of the CKM elements at the current precision of lattice QCD inputs. We obtain $|V_{us}|/|V_{ud}| = 0.23131(45)$ by taking the average of f_K/f_π in isosymmetric QCD and combining it with the value for $|V_{us}|f_K/|V_{ud}|f_\pi$ in Eq. (68). This estimate plotted in Fig. 11 is consistent with that obtained from Eq. (65) using the isospin corrections from ChPT. Unlike the corrections from ChPT, the accuracy of the isospin corrections from lattice QCD can be readily improved by more realistic simulations and higher statistics, further sharpening the comparisons shown in the figure.

D. Tests of the Standard Model

In the Standard Model, the CKM matrix is unitary. In particular, the elements of the first row obey

$$|V_u|^2 \equiv |V_{ud}|^2 + |V_{us}|^2 + |V_{ub}|^2 = 1. \tag{78}$$

The tiny contribution from $|V_{ub}|$ is known much better than needed in the present context: $|V_{ub}| = 3.82(24) \times 10^{-3}$ [205].[25] In the following, we test the first row unitarity

[24]Note that the ellipses shown in Fig. 5 of both Ref. [1] and Ref. [2] correspond instead to the 39% likelihood contours. Note also that in Ref. [2] the likelihood was erroneously stated to be 68% rather than 39%.

[25]See also Sec. VIII H for our determination of $|V_{ub}|$.

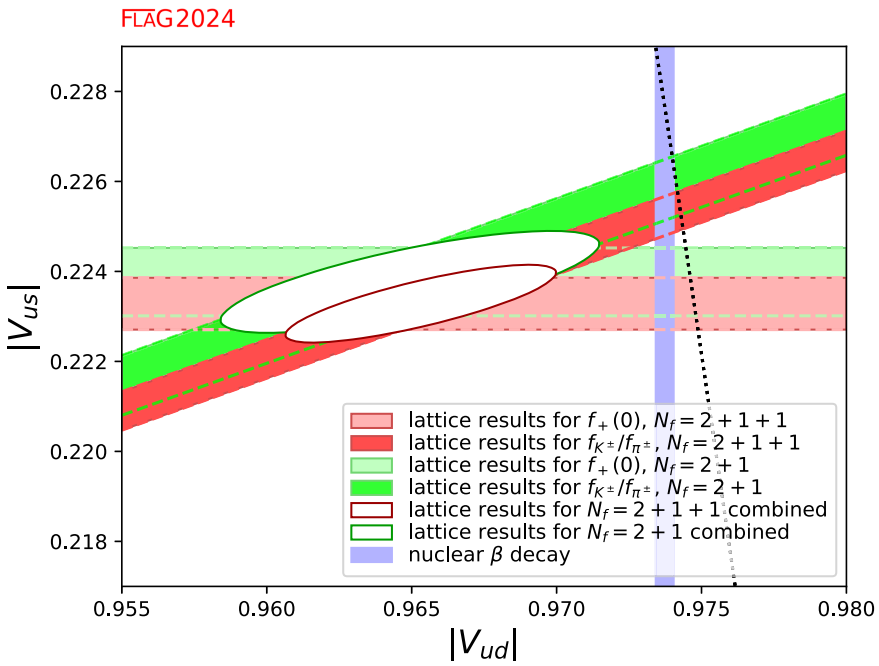


FIG. 11. Same as Fig. 10 but with $|V_{us}|/|V_{ud}|$ obtained using Eq. (68).

Eq. (78) by calculating $|V_u|^2$ and by analyzing the lattice data within the Standard Model.

In Fig. 10, the correlation between $|V_{ud}|$ and $|V_{us}|$ imposed by the unitarity of the CKM matrix is indicated by a dotted line (more precisely, in view of the uncertainty in $|V_{ub}|$, the correlation corresponds to a band of finite width, but the effect is too small to be seen here). The plot shows that there is a tension with unitarity in the data for $N_f = 2+1+1$: Numerically, the outcome for the sum of the squares of the first row of the CKM matrix reads $|V_u|^2 = 0.9820(65)$, which deviates from unity at the level of $\simeq 2.8$ standard deviations. Still, it is fair to say that at this level the Standard Model passes a nontrivial test on the kaon (semi)leptonic and pion leptonic decays.

The test sharpens considerably by combining the lattice results for $f_+(0)$ with the β decay value of $|V_{ud}|$: $f_+(0)$ for $N_f = 2+1+1$ in Eq. (72) and the PDG estimate of $|V_{ud}|$ in Eq. (69) lead to $|V_u|^2 = 0.99802(66)$, which also shows a $\simeq 3.0\sigma$ deviation with unitarity. On the other hand, unitarity is fulfilled (1.7σ) with $f_{K^\pm}/f_{\pi^\pm}$ and $|V_{ud}|$ (69) [$|V_u|^2 = 0.99888(67)$]. Note that the uncertainties on $|V_u|^2$ coming from the error of $|V_{ud}|$ is larger by a factor of about three than that from $|V_{us}|$.

The situation is similar for $N_f = 2+1$: with the lattice data alone one has $|V_u|^2 = 0.9835(89)$, which is consistent with unity at the level of $\simeq 1.8$ standard deviations. The lattice results for $f_+(0)$ in Eqs. (73) with the PDG value of $|V_{ud}|$ (69) lead to $|V_u|^2 = 0.99824(69)$, implying a $\simeq 2.5\sigma$ deviation from unitarity, whereas the deviation is reduced to 1.4σ with $f_{K^\pm}/f_{\pi^\pm}$ in Eq. (77) [$|V_u|^2 = 0.99903(72)$].

E. Analysis within the Standard Model

The Standard Model implies that the CKM matrix is unitary. The precise experimental constraints quoted in Eq. (65) and the unitarity condition Eq. (78) then reduce the four quantities $|V_{ud}|, |V_{us}|, f_+(0), f_{K^\pm}/f_{\pi^\pm}$ to a single unknown: any one of these determines the other three within narrow uncertainties.

Numerical results for $|V_{us}|$ and $|V_{ud}|$ are listed in Table 20, where we restrict ourselves to those determinations that enter the FLAG average in Sec. V C (the error in the experimental numbers used to convert the values of $f_+(0)$ and $f_{K^\pm}/f_{\pi^\pm}$ into values for $|V_{us}|$ is included in the statistical error). As Fig. 12 shows, the results obtained for $|V_{us}|$ and $|V_{ud}|$ from the data on $f_{K^\pm}/f_{\pi^\pm}$ (squares) are consistent with the determinations via $f_+(0)$ (triangles), while there is a tendency that $|V_{us}|$ ($|V_{ud}|$) from $f_+(0)$ is systematically smaller (larger) than that from $f_{K^\pm}/f_{\pi^\pm}$.

In order to calculate the average of $|V_{us}|$ for $N_f = 2+1+1$, we consider the data both for $f_+(0)$ and $f_{K^\pm}/f_{\pi^\pm}$, treating ETM 16 and ETM 14E on the one hand and FNAL/MILC 18, CalLat 20, FNAL/MILC 17, and HPQCD 13A on the other hand, as statistically correlated according to the prescription of Sec. II C. We obtain $|V_{us}| = 0.22483(61)$, where the error is stretched by a factor $\sqrt{\chi^2/\mathrm{dof}} \sim \sqrt{2.0}$. This result is indicated on the left-hand side of Fig. 12 by the narrow vertical band. In the case $N_f = 2+1$, we consider MILC 10, FNAL/MILC 12I and HPQCD/UKQCD 07 on the one hand, and RBC/UKQCD 14B and RBC/UKQCD 15A on the other hand, as mutually statistically correlated, since the analysis in the

TABLE 20. Values of $|V_{us}|$ and $|V_{ud}|$ obtained from the lattice determinations of either $f_+(0)$ or $f_{K^\pm}/f_{\pi^\pm}$ assuming CKM unitarity. The first number in brackets represents the statistical error including the experimental uncertainty, whereas the second is the systematic one.

Collaboration	Ref.	N_f	From	$\lvert V_{us}\rvert$	$\lvert V_{ud}\rvert$
FNAL/MILC 18	[39]	$2+1+1$	$f_+(0)$	0.22333(55)(28)	0.97474(13)(6)
ETM 16	[38]	$2+1+1$	$f_+(0)$	0.2230(11)(2)	0.97480(26)(5)
ETM 21	[45]	$2+1+1$	$f_{K^\pm}/f_{\pi^\pm}$	0.22490(85)(13)	0.97437(20)(3)
CalLat 20	[44]	$2+1+1$	$f_{K^\pm}/f_{\pi^\pm}$	0.22517(65)(56)	0.97431(15)(13)
FNAL/MILC 17	[20]	$2+1+1$	$f_{K^\pm}/f_{\pi^\pm}$	0.22513(42)(21)	0.97432(10)(5)
ETM 14E	[43]	$2+1+1$	$f_{K^\pm}/f_{\pi^\pm}$	0.2270(22)(20)	0.97388(51)(47)
HPQCD 13A	[42]	$2+1+1$	$f_{K^\pm}/f_{\pi^\pm}$	0.22564(42)(29)	0.97420(10)(7)
RBC/UKQCD 15A	[41]	$2+1$	$f_+(0)$	0.22358(89)(32)	0.97468(20)(7)
FNAL/MILC 12I	[40]	$2+1$	$f_+(0)$	0.22400(68)(76)	0.97458(16)(18)
CLQCD 23	[10]	$2+1$	$f_{K^\pm}/f_{\pi^\pm}$	0.2258(14)(3)	0.97417(33)(7)
QCDSF/UKQCD 16	[50]	$2+1$	$f_{K^\pm}/f_{\pi^\pm}$	0.2259(18)(23)	0.97414(42)(54)
BMW 16	[49,360]	$2+1$	$f_{K^\pm}/f_{\pi^\pm}$	0.2281(19)(48)	0.9736(4)(11)
RBC/UKQCD 14B	[12]	$2+1$	$f_{K^\pm}/f_{\pi^\pm}$	0.22555(87)(43)	0.97422(20)(10)
MILC 10	[47]	$2+1$	$f_{K^\pm}/f_{\pi^\pm}$	0.22503(48)(89)	0.97434(11)(21)
BMW 10	[48]	$2+1$	$f_{K^\pm}/f_{\pi^\pm}$	0.2259(13)(11)	0.97414(30)(26)
HPQCD/UKQCD 07	[46]	$2+1$	$f_{K^\pm}/f_{\pi^\pm}$	0.2265(5)(13)	0.97401(11)(31)

two cases starts from partially the same set of gauge ensembles. In this way, we arrive at $|V_{us}| = 0.22490(54)$ with $\chi^2/\mathrm{dof} \simeq 0.7$. The figure shows that the results obtained for the data with $N_f = 2+1$ and $N_f = 2+1+1$ are consistent with each other. However, the larger error for $N_f = 2+1+1$ due to the stretch factor $\sqrt{\chi^2/\mathrm{dof}}$ suggests a slight tension between the estimates from the semileptonic and leptonic decays.

We take the average of $|V_{ud}|$ similarly. Again, the result $|V_{ud}| = 0.97439(14)$ for $N_f = 2+1+1$ is perfectly consistent with the values $|V_{ud}| = 0.97436(12)$ obtained from the data with $N_f = 2+1$. These values are consistent with Eq. (69) from the superallowed nuclear transitions within 2σ.

TABLE 21. The upper half of the table shows the results for $|V_{us}|$ and $|V_{ud}|$ from the analysis of the kaon and pion decays within the Standard Model. For comparison, the lower half lists the values that follow if the lattice results are replaced by the experimental results on nuclear β decay and inclusive hadronic τ decay, respectively.

	Ref.	$\lvert V_{us}\rvert$	$\lvert V_{ud}\rvert$
$N_f = 2+1+1$		0.22483(61)	0.97439(14)
$N_f = 2+1$		0.22490(54)	0.97436(12)
nuclear β decay	[205]	0.2277(13)	0.97373(31)
inclusive τ decay	[148]	0.2184(21)	0.97585(47)

As mentioned in Sec. V A, the HFLAV value of $|V_{us}|$ from the inclusive hadronic τ decays differs from those obtained from the kaon decays by about three standard deviations. Assuming the first row unitarity defined in Eq. (78) leads to a larger value of $|V_{ud}|$ than those from the kaon and nuclear decays.

F. Direct determination of $f_{K^\pm}$ and $f_{\pi^\pm}$

It is useful for flavor-physics studies to provide not only the lattice average of $f_{K^\pm}/f_{\pi^\pm}$, but also the average of the decay constant $f_{K^\pm}$. The case of the decay constant $f_{\pi^\pm}$ is different, since the PDG value [276] of this quantity, based on the use of the value of $|V_{ud}|$ obtained from superallowed nuclear β decays [297], is often used for setting the scale in lattice QCD. However, the physical scale can be set in different ways, namely, by using as input the mass of the Ω baryon (m_Ω) or the Υ-meson spectrum (ΔM_Υ), which are less sensitive to the uncertainties of the chiral extrapolation in the light-quark mass with respect to $f_{\pi^\pm}$.[26] In such cases, the value of the decay constant $f_{\pi^\pm}$ becomes a direct prediction of the lattice-QCD simulations. Therefore, it is interesting to provide also the average of the decay constant $f_{\pi^\pm}$, obtained when the physical scale is set through another hadron observable, in order to check the consistency of different scale-setting procedures.

[26]See Sec. XI for detailed discussions.

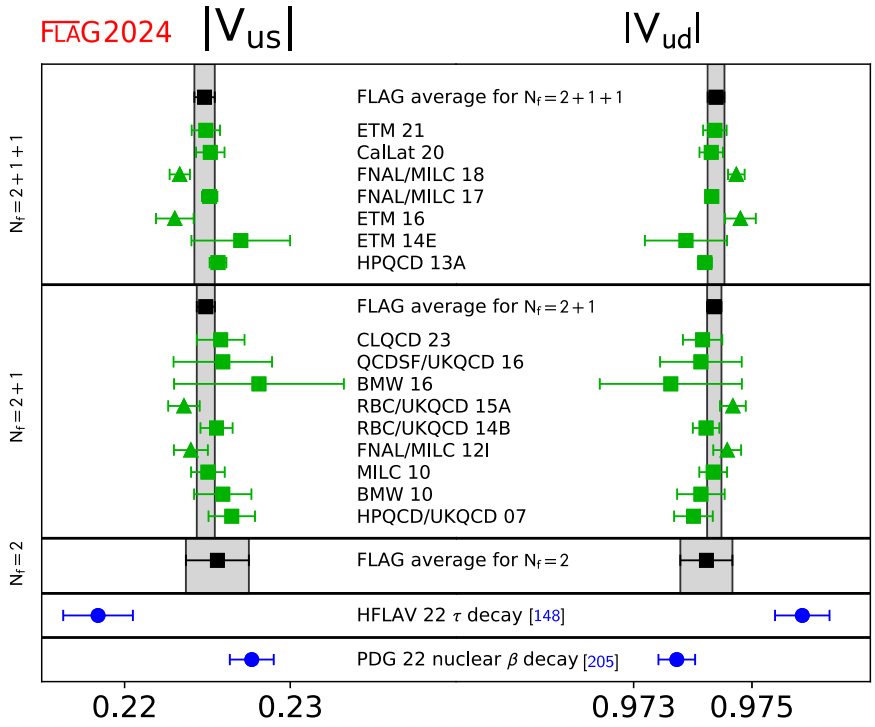


FIG. 12. Results for $|V_{us}|$ and $|V_{ud}|$ that follow from the lattice data for $f_+(0)$ (triangles) and $f_{K^\pm}/f_{\pi^\pm}$ (squares), on the basis of the assumption that the CKM matrix is unitary. The black square and the gray band represent the average for each value of N_f. For comparison, the figure also indicates the results obtained if the data on nuclear β decay and inclusive hadronic τ decay is analyzed within the Standard Model.

Our compilation of the values of $f_{\pi^\pm}$ and $f_{K^\pm}$ with the corresponding color code is presented in Table 18. The new entry in this edition is CLQCD 23 for $N_f = 2 + 1$.

In comparison to the case of $f_{K^\pm}/f_{\pi^\pm}$, we have added two columns indicating which quantity is used to set the physical scale and the possible use of a renormalization constant for the axial current. For several lattice formulations, the use of the nonsinglet axial-vector Ward identity allows us to avoid the use of any renormalization constant.

One can see that the determinations of $f_{\pi^\pm}$ and $f_{K^\pm}$ suffer from larger uncertainties than those of the ratio $f_{K^\pm}/f_{\pi^\pm}$, which is less sensitive to various systematic effects (including the uncertainty of a possible renormalization constant) and, moreover, is not exposed to the uncertainties of the procedure used to set the physical scale.

According to the FLAG rules, for $N_f = 2 + 1 + 1$ four datasets can form the average of $f_{K^\pm}$ only: ETM 21 [45], ETM 14E [43], FNAL/MILC 14A [21], and HPQCD 13A [42]. Following the same procedure already adopted in Sec. V C for the ratio of the decay constants, we assume 100% statistical and systematic correlation between FNAL/MILC 14A and HPQCD 13A. For $N_f = 2 + 1$ four datasets can form the average of $f_{\pi^\pm}$ and $f_{K^\pm}$: CLQCD 23 [10], RBC/UKQCD 14B [12] (update of RBC/UKQCD 12), HPQCD/UKQCD 07 [46], and MILC 10 [47], which is the latest update from the MILC program. We consider HPQCD/UKQCD 07 and MILC 10 as statistically and systematically correlated and use the prescription of Sec. II C to form an average.

Thus, our averages read

$$N_f = 2+1: \quad f_{\pi^\pm} = 130.2(0.8)\,\text{MeV} \quad \text{Refs. [10,12,46,47]}, \tag{79}$$

$$N_f = 2+1+1: \quad f_{K^\pm} = 155.7(0.3)\,\text{MeV} \quad \text{Refs. [21,42,43,45]}, \tag{80}$$

$$N_f = 2+1: \quad f_{K^\pm} = 155.7(0.7)\,\text{MeV} \quad \text{Refs. [10,12,46,47]}, \tag{81}$$

The lattice results of Table 18 and our averages in Eqs. (79)–(81) are reported in Fig. 13. Note that the FLAG average of $f_{K^\pm}$ for $N_f = 2 + 1 + 1$ is based on calculations in which $f_{\pi^\pm}$ is used to set the lattice scale, while the $N_f = 2 + 1$ average does not rely on that.

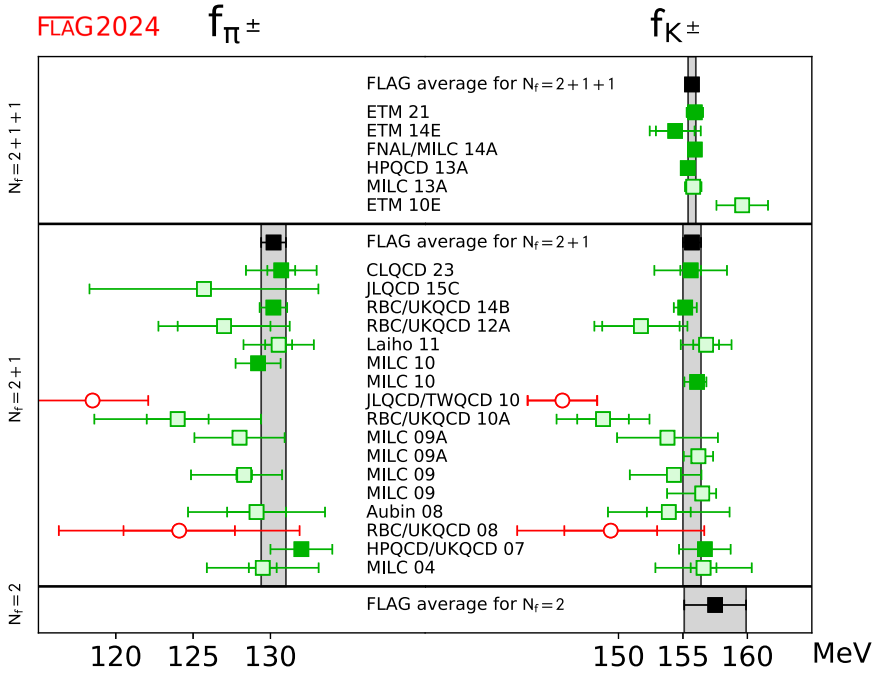


FIG. 13. Values of $f_{\pi^\pm}$ and $f_{K^\pm}$. The black squares and gray bands indicate our averages in Eqs. (79) and (81).

VI. KAON MIXING

Working group members: P. Dimopoulos, X. Feng, G. Herdoíza

The mixing of neutral pseudoscalar mesons plays an important role in the understanding of the physics of quark-flavor mixing and CP violation. In this section, we discuss $K^0 - \bar{K}^0$ oscillations, which probe the physics of indirect CP violation. Extensive reviews on this subject can be found in Refs. [368–373]. The main changes in this section with respect to the FLAG 21 edition [5] are as follows: A discussion on the ϵ_K calculation has been added in Sec. VI A. An updated discussion regarding new lattice determinations of the $K \to \pi\pi$ decay amplitudes and related quantities is provided in Sec. VI B. New FLAG averages for SM and BSM bag parameters are reported in Secs. VI C and VI D, which concern the kaon mixing within the Standard Model (SM) and Beyond the Standard Model (BSM), respectively.

A. Indirect CP violation and ϵ_K in the SM

Indirect CP violation arises in $K_L \to \pi\pi$ transitions through the decay of the CP $= +1$ component of K_L into two pions (which are also in a $CP = +1$ state). Its measure is defined as

$$\epsilon_K = \frac{\mathcal{A}[K_L \to (\pi\pi)_{I=0}]}{\mathcal{A}[K_S \to (\pi\pi)_{I=0}]}, \tag{82}$$

with the final state having total isospin zero. The parameter ϵ_K may also be expressed in terms of $K^0 - \bar{K}^0$ oscillations. In the Standard Model, ϵ_K is given by the following expression [372,374–377]

$$\epsilon_K = \exp(i\phi_\epsilon)\sin(\phi_\epsilon)\left[\frac{\mathrm{Im}(M_{12}^{\mathrm{SD}})}{\Delta M_K} + \frac{\mathrm{Im}(M_{12}^{\mathrm{LD}})}{\Delta M_K} + \frac{\mathrm{Im}(A_0)}{\mathrm{Re}(A_0)}\right], \tag{83}$$

where the various contributions can be related to: (i) short-distance (SD) physics given by $\Delta S = 2$ "box diagrams" involving $W^\pm$ bosons and u, c and t quarks; (ii) long-distance (LD) physics from light hadrons contributing to the imaginary part of the dispersive amplitude M_{12}, $\mathrm{Im}(M_{12}^{\mathrm{LD}})$, used in the two-component description of $K^0 - \bar{K}^0$ mixing; (iii) the imaginary part of the absorptive amplitude Γ_{12} from $K^0 - \bar{K}^0$ mixing which can be related to $\mathrm{Im}(A_0)/\mathrm{Re}(A_0)$, where A_0 is the $K \to (\pi\pi)_{I=0}$ decay amplitude, as $(\pi\pi)_{I=0}$ states provide the dominant contribution to the absorptive part of the integral in Γ_{12}. The various factors of this decomposition may vary according to phase conventions. In terms of the $\Delta S = 2$ effective Hamiltonian, $\mathcal{H}_{\mathrm{eff}}^{\Delta S=2}$, it is common to represent contribution (i) by

$$\mathrm{Im}(M_{12}^{\mathrm{SD}}) \equiv \frac{1}{2M_K}\mathrm{Im}[\langle \bar{K}^0|\mathcal{H}_{\mathrm{eff}}^{\Delta S=2}|K^0\rangle]. \tag{84}$$

The phase of ϵ_K is given by

$$\phi_\epsilon = \arctan\frac{\Delta M_K}{\Delta\Gamma_K/2}. \tag{85}$$

The quantities ΔM_K and $\Delta\Gamma_K$ are the mass and decay width differences between long- and short-lived neutral kaons. The experimentally known values of the above quantities are [274]

$$|\epsilon_K| = 2.228(11)\times 10^{-3}, \tag{86}$$

$$\phi_\epsilon = 43.52(5)^\circ, \tag{87}$$

$$\Delta M_K \equiv M_{K_L} - M_{K_S} = 3.484(6)\times 10^{-12}\ \text{MeV}, \tag{88}$$

$$\Delta\Gamma_K \equiv \Gamma_{K_S} - \Gamma_{K_L} = 7.3382(33)\times 10^{-12}\ \text{MeV}, \tag{89}$$

where the latter three measurements have been obtained by imposing CPT symmetry.

We will start by discussing the short-distance effects (i) since they provide the dominant contribution to ϵ_K. To lowest order in the electroweak theory, the contribution to $K^0-\bar{K}^0$ oscillations arises from the box diagrams, in which two W bosons and two "up-type" quarks (i.e., up, charm, top) are exchanged between the constituent down and strange quarks of the K mesons. The loop integration of the box diagrams can be performed exactly. In the limit of vanishing external momenta and external quark masses, the result can be identified with an effective four-fermion interaction, expressed in terms of the effective Hamiltonian

$$\mathcal{H}_{\text{eff}}^{\Delta S=2} = \frac{G_F^2 M_{\text{W}}^2}{16\pi^2}\mathcal{F}^0 Q^{\Delta S=2} + \text{H.c.}. \tag{90}$$

In this expression, G_F is the Fermi coupling, M_{W} the W-boson mass, and

$$Q^{\Delta S=2} = [\bar{s}\gamma_\mu(1-\gamma_5)d][\bar{s}\gamma_\mu(1-\gamma_5)d] \equiv O_{\text{VV+AA}} - O_{\text{VA+AV}}, \tag{91}$$

is a dimension-six, four-fermion operator. The subscripts V and A denote vector ($\bar{s}\gamma_\mu d$) and axial-vector ($\bar{s}\gamma_\mu\gamma_5 d$) bilinears, respectively. The function $\mathcal{F}^0$ is given by

$$\mathcal{F}^0 = \lambda_c^2 S_0(x_c) + \lambda_t^2 S_0(x_t) + 2\lambda_c\lambda_t S_0(x_c, x_t), \tag{92}$$

where $\lambda_a = V_{as}^* V_{ad}$, and $a = c,\ t$ denotes a flavor index. The quantities $S_0(x_c), S_0(x_t)$ and $S_0(x_c, x_t)$ with $x_c = m_c^2/M_{\text{W}}^2$, $x_t = m_t^2/M_{\text{W}}^2$ are the Inami-Lim functions [378], which express the basic electroweak loop contributions without QCD corrections. The contribution of the up quark, which is taken to be massless in this approach, has been taken into account by imposing the unitarity constraint $\lambda_u + \lambda_c + \lambda_t = 0$. By substituting $\lambda_c = -\lambda_u - \lambda_t$, one can rewrite $\mathcal{F}^0$ as [379,380]

$$\begin{aligned}\mathcal{F}^0 = {} & \lambda_u^2 S_0(x_c) + \lambda_t^2[S_0(x_t) + S_0(x_c) - 2S_0(x_c, x_t)] \\ & + 2\lambda_u\lambda_t[S_0(x_c) - S_0(x_c, x_t)].\end{aligned} \tag{93}$$

Equations (92) and (93) are denoted as "c-t unitarity" and "u-t unitarity," respectively. Since $\lambda_u^2 S_0(x_c)$ is real, it does not factor into ϵ_K, even when accounting for QCD corrections.

When strong interactions are included, $\Delta S = 2$ transitions can no longer be discussed at the quark level. Instead, the effective Hamiltonian must be considered between mesonic initial and final states. Since the strong coupling is large at typical hadronic scales, the resulting weak matrix element cannot be calculated in perturbation theory. The operator product expansion (OPE) does, however, factorize long- and short-distance effects. For energy scales below the charm threshold, the $K^0-\bar{K}^0$ transition amplitude of the effective Hamiltonian can be expressed in terms of the c-t unitarity framework as follows

$$\begin{aligned}\langle\bar{K}^0|\mathcal{H}_{\text{eff}}^{\Delta S=2}|K^0\rangle = {} & \frac{G_F^2 M_{\text{W}}^2}{16\pi^2}[\lambda_c^2 S_0(x_c)\eta_1 + \lambda_t^2 S_0(x_t)\eta_2 + 2\lambda_c\lambda_t S_0(x_c, x_t)\eta_3] \\ & \times\left(\frac{\bar{g}(\mu)^2}{4\pi}\right)^{-\gamma_0/(2\beta_0)}\exp\left\{\int_0^{\bar{g}(\mu)} dg\left(\frac{\gamma(g)}{\beta(g)} + \frac{\gamma_0}{\beta_0 g}\right)\right\}\langle\bar{K}^0|Q_{\text{R}}^{\Delta S=2}(\mu)|K^0\rangle + \text{H.c.},\end{aligned} \tag{94}$$

where $\bar{g}(\mu)$ and $Q_{\text{R}}^{\Delta S=2}(\mu)$ are the renormalized gauge coupling and the four-fermion operator in some renormalization scheme. The factors η_1, η_2 and η_3 depend on the renormalized coupling $\bar{g}$, evaluated at the various flavor thresholds m_t, m_b, m_c and M_{W}, as required by the OPE and renormalization-group (RG) running procedure that separate high- and low-energy contributions. Explicit expressions can be found in Ref. [371] and references therein, except that η_1 and η_3 have been calculated to NNLO in Refs. [381,382], respectively. We follow the same conventions for the RG equations as in Ref. [371]. Thus the Callan-Symanzik function and the anomalous dimension $\gamma(\bar{g})$ of $Q^{\Delta S=2}$ are defined by

$$\frac{d\bar{g}}{d\ln\mu} = \beta(\bar{g}), \qquad \frac{dQ_{\mathrm{R}}^{\Delta S=2}}{d\ln\mu} = -\gamma(\bar{g})Q_{\mathrm{R}}^{\Delta S=2}, \quad (95)$$

with perturbative expansions

$$\beta(g) = -\beta_0\frac{g^3}{(4\pi)^2} - \beta_1\frac{g^5}{(4\pi)^4} - \cdots,$$
$$\gamma(g) = \gamma_0\frac{g^2}{(4\pi)^2} + \gamma_1\frac{g^4}{(4\pi)^4} + \cdots. \quad (96)$$

We stress that β_0, β_1 and γ_0 are universal, i.e., scheme independent. As for $K^0 - \bar{K}^0$ mixing, this is usually considered in the naive dimensional regularization (NDR) scheme of $\overline{\mathrm{MS}}$, and below we specify the perturbative coefficient γ_1 in that scheme

$$\beta_0 = \left\{\frac{11}{3}N - \frac{2}{3}N_f\right\}, \quad \beta_1 = \left\{\frac{34}{3}N^2 - N_f\left(\frac{13}{3}N - \frac{1}{N}\right)\right\},$$
$$\gamma_0 = \frac{6(N-1)}{N}, \quad \gamma_1 = \frac{N-1}{2N}\left\{-21 + \frac{57}{N} - \frac{19}{3}N + \frac{4}{3}N_f\right\}. \quad (97)$$

Note that for QCD the above expressions must be evaluated for $N = 3$ colors, while N_f denotes the number of active quark flavors. As already stated, Eq. (94) is valid at scales below the charm threshold, after all heavier flavors have been integrated out, i.e., $N_f = 3$.

In Eq. (94), the terms proportional to η_1, η_2 and η_3, multiplied by the contributions containing $\bar{g}(\mu)^2$, correspond to the Wilson coefficient of the OPE, computed in perturbation theory. Its dependence on the renormalization scheme and scale μ is canceled by that of the weak matrix element $\langle\bar{K}^0|Q_{\mathrm{R}}^{\Delta S=2}(\mu)|K^0\rangle$. The latter corresponds to the long-distance effects of the effective Hamiltonian and must be computed nonperturbatively. For historical, as well as technical reasons, it is convenient to express it in terms of the B-parameter B_K, defined as

$$B_K(\mu) = \frac{\langle\bar{K}^0|Q_{\mathrm{R}}^{\Delta S=2}(\mu)|K^0\rangle}{\frac{8}{3}f_K^2M_K^2}. \quad (98)$$

The four-quark operator $Q^{\Delta S=2}(\mu)$ is renormalized at scale μ in some regularization scheme, for instance, NDR-$\overline{\mathrm{MS}}$. Assuming that $B_K(\mu)$ and the anomalous dimension $\gamma(g)$ are both known in that scheme, the renormalization group independent (RGI) B-parameter $\hat{B}_K$ is related to $B_K(\mu)$ by the exact formula

$$\hat{B}_K = \left(\frac{\bar{g}(\mu)^2}{4\pi}\right)^{-\gamma_0/(2\beta_0)}\exp\left\{\int_0^{\bar{g}(\mu)} dg\left(\frac{\gamma(g)}{\beta(g)} + \frac{\gamma_0}{\beta_0 g}\right)\right\}B_K(\mu). \quad (99)$$

At NLO in perturbation theory, the above reduces to

$$\hat{B}_K = \left(\frac{\bar{g}(\mu)^2}{4\pi}\right)^{-\gamma_0/(2\beta_0)}\left\{1 + \frac{\bar{g}(\mu)^2}{(4\pi)^2}\left[\frac{\beta_1\gamma_0 - \beta_0\gamma_1}{2\beta_0^2}\right]\right\}B_K(\mu). \quad (100)$$

To this order, this is the scale-independent product of all μ-dependent quantities in Eq. (94).

Lattice-QCD calculations provide results for $B_K(\mu)$. However, these results are usually obtained in intermediate schemes other than the continuum $\overline{\mathrm{MS}}$ scheme used to calculate the Wilson coefficients appearing in Eq. (94). Examples of intermediate schemes are the RI/MOM scheme [383] (also dubbed the "Rome-Southampton method") and the Schrödinger functional (SF) scheme [384]. These schemes permit the nonperturbative renormalization of the four-fermion operator to be conducted, using an auxiliary lattice simulation. This allows $B_K(\mu)$ to be calculated with percent-level accuracy, as described below.

In order to make contact with phenomenology, however, and in particular to use the results presented above, one must convert from the intermediate scheme to the $\overline{\mathrm{MS}}$ scheme or to the RGI quantity $\hat{B}_K$. This conversion relies on 1- or 2-loop perturbative matching calculations, the truncation errors in which are, for many calculations, the dominant source of error in $\hat{B}_K$ (see, for instance, Refs. [12,54–56,229,385]). While this scheme-conversion error is not, strictly speaking, an error of the lattice calculation itself, it must be included in results for the quantities of phenomenological interest, namely, $B_K(\overline{\mathrm{MS}}, 2\ \mathrm{GeV})$ and $\hat{B}_K$. Incidentally, we remark that this truncation error is estimated in different ways and that its relative contribution to the total error can considerably differ among the various lattice calculations. We note that this error can be minimized by matching between the intermediate scheme and $\overline{\mathrm{MS}}$ at as large a scale μ as possible (so that the coupling which determines the rate of convergence is minimized). The latest available calculations have pushed the matching μ up to the range 3–3.5 GeV. This is possible because of the use of nonperturbative RG running determined on the lattice [12,53,229]. The Schrödinger functional offers the possibility to run nonperturbatively to scales $\mu \sim M_{\mathrm{W}}$ where the truncation error can be safely neglected. However, so far this has been applied only for two flavors for B_K in Ref. [386] and for the case of the BSM bag parameters in Ref. [387], and in Ref. [388] for three flavors. (See more details in Sec. VI D.)

Perturbative truncation errors in Eq. (94) also affect the Wilson coefficients η_1, η_2 and η_3. It turns out that the largest uncertainty arises from the charm quark contribution $\eta_1 = 1.87(76)$ [381]. Although it is now calculated at NNLO, the series shows poor convergence. The net effect from the uncertainty on η_1 on the amplitude in Eq. (94) is larger than that of present lattice calculations of B_K. Exploiting an idea presented in Ref. [379], it has been shown in Ref. [380] that, by using the u-t instead of the usual c-t unitarity in the

ϵ_K computation, the perturbative uncertainties associated with residual short-distance quark contributions can be reduced. We will elaborate upon this point later.

Returning to Eq. (83), we note that an analytical estimate of the leading contribution from $\mathrm{Im}(M_{12}^{\mathrm{LD}})$ based on χPT, shows that it is approximately proportional to $\xi_0 \equiv \mathrm{Im}(A_0)/\mathrm{Re}(A_0)$ so that Eq. (83) can be written as follows [376,377]:

$$\epsilon_K = \exp(i\phi_\epsilon)\sin(\phi_\epsilon)\left[\frac{\mathrm{Im}(M_{12}^{\mathrm{SD}})}{\Delta M_K} + \rho\xi_0\right], \quad (101)$$

where the deviation of ρ from one parametrizes the long-distance effects in $\mathrm{Im}(M_{12})$.

The general formula presented in Eq. (101) for the parameter ϵ_K provides one of the most valuable inputs for tests of CKM unitarity. Moreover, it holds significant potential as a probe for new physics, provided that its precision can be enhanced. In the following, we will provide a general overview of the current status of the computation of $|\epsilon_K|$.

With a very good approximation the formula for $|\epsilon_K|$ can be written in the so-called Wolfenstein parametrization [389]. The determination of $|\epsilon_K|$ requires the knowledge of more than a dozen input quantities, which can be categorized into four groups. The first group includes six quantities ($G_F, \phi_\epsilon, M_{K^0}, \Delta M_K, M_W$ and m_t) whose values are known from experiment with high precision. The second group consists of several observables computed in lattice QCD, including the kaon decay constant f_K, the charm-quark mass $m_c(m_c)$, the neutral kaon mixing bag parameter B_K, and the ratio $\xi_0 = \mathrm{Im}(A_0)/\mathrm{Re}(A_0)$.[27] Moreover, the values of the CKM matrix elements $|V_{ud}|$, $|V_{us}|$ and $|V_{cb}|$ are required—see for instance Ref. [391]—which are based on lattice-QCD computations. It is worth recalling that the present FLAG report provides average values for these quantities, see Secs. V and VIII. The third group involves the short-distance interaction factors calculated in perturbation theory. In the c-t unitarity formula, these factors are η_1, η_2, and η_3, as mentioned earlier in this section and shown in Eq. (94). In the u-t unitarity case, there appear only two relevant factors (see Refs. [380,392]). Finally, the fourth group of inputs consists of the pair of CKM triangle variables $(\bar{\rho}, \bar{\eta})$ whose values are estimated from the unitarity triangle analysis. In particular, the angle-only fit (AoF) analysis used in Refs. [393–395] (see also Ref. [396]) prevents any correlation of $(\bar{\rho}, \bar{\eta})$ with the rest of the inputs used in the formula for $|\epsilon_K|$.

Among the various inputs, $|V_{cb}|$ introduces the dominant contribution on the uncertainty of $|\epsilon_K|$. This effect can be attributed to the presence of terms with $|V_{cb}|$ to the fourth and second power in the expression of $|\epsilon_K|$.

As discussed in Sec. VIII of this report, to which we refer for a comprehensive review, a longstanding discrepancy persists between the exclusive and inclusive determinations of $|V_{cb}|$. Exclusive determinations, which are primarily based on the differential decay rates of processes such as $B \to D^* \ell\nu$ and $B \to D\ell\nu$, rely on nonperturbative inputs from lattice QCD. In contrast, inclusive determinations employ the total semileptonic decay rate $B \to X_c \ell\nu$ and are analyzed within the framework of heavy quark effective theory and the operator product expansion. The application of these two types of theoretical approaches, in conjunction with distinct experimental inputs, yields the current sizeable tension between the exclusive and inclusive determinations of $|V_{cb}|$.

Another significant source of uncertainty, when the c-t unitarity formula for $|\epsilon_K|$ is employed, is related to the factor η_1 that is computed to NNLO in perturbation theory. For more information on the estimation of the systematic error due to perturbative truncation, see Refs. [381,394,397]. This source of uncertainty can be mitigated by adopting the u-t unitarity formula for $|\epsilon_K|$. In this case, it is found that the two relevant QCD perturbative factors are not subject to significant systematic uncertainties. Furthermore, this approach reduces the correlations between the individual perturbative contributions [380].

We close this discussion by mentioning that the use of the u-t unitarity formula leads to a total statistical error of about 8% in $|\epsilon_K|$. In this case, when analyzing the error budget, we see that nearly half of the total error comes from the propagation of the uncertainty from $|V_{cb}|$. Furthermore, the propagated error owing to the $\bar{\eta}$ error is the second most significant source of uncertainty in $|\epsilon_K|$. It is noteworthy that the propagated error from B_K is much smaller, accounting for only a few percent in the final error budget. It should also be noted that the relative uncertainties contributing to the error budget are rather sensitive to improvements in the precision of $|V_{cb}|$. The tension between the exclusive and inclusive determinations of $|V_{cb}|$ induces a corresponding difference in the predicted values of $|\epsilon_K|$ derived from these inputs. Recent detailed analyses of $|\epsilon_K|$, including the impact of different $|V_{cb}|$ determinations and the use of the c-t and u-t unitarity relations, can be found in Refs. [391,398,399]. It is also worth noting that ongoing advancements in lattice-QCD techniques may contribute in the future to reducing uncertainties in the inclusive determination of $|V_{cb}|$ [312,313,400–402]. The resolution of the longstanding discrepancy between the exclusive and inclusive determinations of $|V_{cb}|$ is highly desirable, as it would significantly enhance the precision of $|\epsilon_K|$ and its potential for probing new physics scenarios.[28]

[27]Furthermore, the long-distance effects owing to light hadrons can be estimated on the lattice as noted below in Sec. VI B, cf. Ref. [390]. However, the current accuracy of this calculation is not yet high enough to constrain the determination of $|\epsilon_K|$.

[28]Note that a more precise determination of $|\epsilon_K|$ will require taking into account the effect of short-distance power corrections from dim-8 operators to the $\Delta S = 2$ effective Hamiltonian. It is estimated that their effect leads to an increase of the central value by 1%, see Refs. [403,404].

In order to facilitate the subsequent discussions about the status of the lattice studies of $K \to \pi\pi$ and of the current estimates of $\xi_0 \equiv \mathrm{Im}(A_0)/\mathrm{Re}(A_0)$, we provide a brief account of the parameter ϵ' that describes direct CP-violation in the kaon sector. The definition of ϵ' is given by

$$\epsilon' \equiv \frac{1}{\sqrt{2}} \frac{\mathcal{A}[K_S \to (\pi\pi)_{I=2}]}{\mathcal{A}[K_S \to (\pi\pi)_{I=0}]} \left(\frac{\mathcal{A}[K_L \to (\pi\pi)_{I=2}]}{\mathcal{A}[K_S \to (\pi\pi)_{I=2}]} - \frac{\mathcal{A}[K_L \to (\pi\pi)_{I=0}]}{\mathcal{A}[K_S \to (\pi\pi)_{I=0}]} \right). \tag{102}$$

By selecting appropriate phase conventions for the mixing parameters between K^0 and $\bar{K}^0$ CP-eigenstates (see, e.g., Ref. [369] for further details), the expression of ϵ' can be expressed in terms of the real and imaginary parts of the isospin amplitudes as follows:

$$\epsilon' = \frac{i\omega e^{i(\delta_2 - \delta_0)}}{\sqrt{2}} [\xi_2 - \xi_0], \tag{103}$$

where $\omega \equiv \mathrm{Re}(A_2)/\mathrm{Re}(A_0)$, $\xi_2 \equiv \mathrm{Im}(A_2)/\mathrm{Re}(A_2)$, A_2 denotes the $\Delta I = 3/2$ $K \to \pi\pi$ decay amplitude, and δ_I denotes the strong scattering phase shifts in the corresponding, $I = 0, 2$, $K \to (\pi\pi)_I$ decays. Given that the phase $\phi'_\epsilon = \delta_2 - \delta_0 + \pi/2 \approx 42.3(1.5)°$ [274] is nearly equal to ϕ_ϵ in Eq. (87), the ratio of parameters characterizing the direct and indirect CP-violation in the kaon sector can be approximated in the following way,

$$\epsilon'/\epsilon \approx \mathrm{Re}(\epsilon'/\epsilon) = \frac{\omega}{\sqrt{2}|\epsilon_K|} [\xi_2 - \xi_0], \tag{104}$$

where on the left-hand side we have set $\epsilon \equiv \epsilon_K$. The experimentally measured value reads [274],

$$\mathrm{Re}(\epsilon'/\epsilon) = 16.6(2.3) \times 10^{-4}. \tag{105}$$

We remark that isospin breaking and electromagnetic effects (see Refs. [405,406], and the discussion in Ref. [370]) introduce additional correction terms into Eq. (104).

B. Lattice-QCD studies of the $K \to (\pi\pi)_I$ decay amplitudes, ξ_0, ξ_2 and ϵ'/ϵ

As a preamble to this section, it should be noted that the study of $K \to \pi\pi$ decay amplitudes requires the development of computational strategies that are at the forefront of lattice QCD techniques. These studies represent a significant advance in the study of kaon physics. However, at present, they have not yet reached the same level of maturity of most of the quantities analyzed in the FLAG report, where, for instance, independent results by various lattice collaborations are being compared and averaged. We will, therefore, review the current status of $K \to \pi\pi$ lattice computations, but we will provide a FLAG average only for the case of the decay amplitude A_2.

We start by reviewing the determination of the parameter $\xi_0 = \mathrm{Im}(A_0)/\mathrm{Re}(A_0)$. An estimate of ξ_0 has been obtained from a direct evaluation of the ratio of amplitudes $\mathrm{Im}(A_0)/\mathrm{Re}(A_0)$, where $\mathrm{Im}(A_0)$ is determined from a lattice-QCD computation by RBC/UKQCD 20 [407] employing $N_f = 2 + 1$ Möbius domain-wall fermions at a single value of the lattice spacing, while $\mathrm{Re}(A_0) \simeq |A_0|$ and the value $|A_0| = 3.320(2) \times 10^{-7}$ GeV are used based on the relevant experimental input [225] from the decay to two pions. This leads to a result for ξ_0 with a rather large relative error,

$$\xi_0 = -2.1(5) \times 10^{-4}. \tag{106}$$

Following a similar procedure, an estimate of ξ_0 was obtained through the use of a previous lattice QCD determination of $\mathrm{Im}(A_0)$ by RBC/UKQCD 15G [408]. We refer to Table 22 for further details about these

TABLE 22. Results for the real and imaginary parts of the $K \to \pi\pi$ decay amplitude A_0 from lattice-QCD computations with $N_f = 2 + 1$ dynamical flavors. Information about the renormalization, running and matching to the $\overline{\mathrm{MS}}$ scheme is indicated in the column "running/matching," with details given at the bottom of the table. We refer to the text for further details about the main differences between the lattice computations in Refs. [407,408].

Collaboration	Ref.	N_f	Publication status	Continuum extrapolation	Chiral extrapolation	Finite volume	Renormalization	Running/matching	$\mathrm{Re}(A_0)[10^{-7}\ \mathrm{GeV}]$	$\mathrm{Im}(A_0)[10^{-11}\ \mathrm{GeV}]$
RBC/UKQCD 23A	[415]	$2+1$	A	■	○	★	★	[a]	2.84(0.57)(0.87)	−8.7(1.2)(2.6)
RBC/UKQCD 20	[407]	$2+1$	A	■	○	○	★	[a]	2.99(0.32)(0.59)	−6.98(0.62)(1.44)
RBC/UKQCD 15G	[408]	$2+1$	A	■	○	○	★	[b]	4.66(1.00)(1.26)	−1.90(1.23)(1.08)

[a]Nonperturbative renormalization with the RI/SMOM scheme at a scale of 1.53 GeV and running to 4.0 GeV employing a nonperturbatively determined step-scaling function. Conversion to $\overline{\mathrm{MS}}$ at 1-loop order.

[b]Nonperturbative renormalization with the RI/SMOM scheme at a scale of 1.53 GeV. Conversion to $\overline{\mathrm{MS}}$ at 1-loop order at the same scale.

TABLE 23. Results for the real and the imaginary parts of the $K \to \pi\pi$ decay amplitude A_2 from lattice-QCD computations with $N_f = 2+1$ dynamical flavors. Information about the renormalization and matching to the $\overline{\text{MS}}$ scheme is indicated in the column "running/matching," with details given at the bottom of the table.

Collaboration	Ref.	N_f	Publication status	Continuum extrapolation	Chiral extrapolation	Finite volume	Renormalization	Running/matching	$\text{Re}(A_2)$ [10^{-8} GeV]	$\text{Im}(A_2)$ [10^{-13} GeV]
RBC/UKQCD 23A	[415]	$2+1$	A	■	○	★	★	[a]	1.74(0.15)(0.48)	−5.91(0.13)(1.75)
RBC/UKQCD 15F	[51]	$2+1$	A	○	○	★	★	[b]	1.50(0.04)(0.14)	−8.34(1.03)[c]

[a]Nonperturbative renormalization with the RI/SMOM scheme at a scale of 1.53 GeV and running to 4.0 GeV employing a nonperturbatively determined step-scaling function. Conversion to $\overline{\text{MS}}$ at 1-loop order.

[b]Nonperturbative renormalization with the RI/SMOM scheme at a scale of 3 GeV. Conversion to $\overline{\text{MS}}$ at 1-loop order.

[c]This value of $\text{Im}(A_2)$ is an update reported in Ref. [407] which is based on the lattice QCD computation in Ref. [51] but where a change in the value of the imaginary part of the ratio of CKM matrix elements $\tau = -V_{ts}^* V_{td}/V_{us}^* V_{ud}$ reported in Ref. [409] has been applied.

computations of $\text{Im}(A_0)$. The comparison of the estimates of ξ_0 based on lattice QCD input are collected in Table 24.

To determine the value of ξ_0, the expression in Eq. (104) together with the experimental values of $\text{Re}(\epsilon'/\epsilon)$, $|\epsilon_K|$ and ω can also be used. This approach has been pursued with the help of a lattice-QCD calculation of the ratio of amplitudes $\text{Im}(A_2)/\text{Re}(A_2)$ by RBC/UKQCD 15F [51] where the continuum-limit result is based on computations at two values of the lattice spacing employing $N_f = 2+1$ Möbius domain-wall fermions. Further details about the lattice computations of A_2 are collected in Table 23. In this case, we obtain $\xi_0 = -1.6(2) \times 10^{-4}$. The use of the updated value of $\text{Im}(A_2) = -8.34(1.03) \times 10^{-13}$ GeV from Ref. [407], in combination with the experimental value of $\text{Re}(A_2) = 1.479(4) \times 10^{-8}$ GeV, introduces a small change with respect to the above result.[29] The value for ξ_0 reads[30]

$$\xi_0 = -1.7(2) \times 10^{-4}. \tag{107}$$

A phenomenological estimate can also be obtained from the relationship of ξ_0 to $\text{Re}(\epsilon'/\epsilon)$, using the experimental value of the latter and further assumptions concerning the estimate of hadronic contributions. The corresponding value of ξ_0 reads [376,377]

$$\xi_0 = -6.0(1.5) \times 10^{-2} \times \sqrt{2}|\epsilon_K| = -1.9(5) \times 10^{-4}. \tag{108}$$

We note that the use of the experimental value for $\text{Re}(\epsilon'/\epsilon)$ is based on the assumption that it is free from new physics contributions. The value of ξ_0 can then be combined with a χPT-based estimate for the long-range contribution, $\rho = 0.6(3)$ [377]. Overall, the combination $\rho\xi_0$ appearing in Eq. (101) leads to a suppression of the SM prediction of $|\epsilon_K|$ by about 3(2)% relative to the experimental measurement of $|\epsilon_K|$ given in Eq. (86), regardless of whether the phenomenological estimate of ξ_0 [see Eq. (108)] or the most precise lattice result [see Eq. (106)] are used. The uncertainty in the suppression factor is dominated by the error on ρ. Although this is a small correction, we note that its contribution to the error of ϵ_K is larger than that arising from the value of B_K reported below.

The evolution of lattice-QCD methodologies has enabled recent ongoing efforts to calculate the long-distance contributions to ϵ_K [390,410] and the $K_L - K_S$ mass difference [379,411–414]. However, the results are not yet precise enough to improve the accuracy in the determination of the parameter ρ.

The lattice-QCD study of $K \to \pi\pi$ decays provides crucial input to the SM prediction of ϵ_K. During the last decade, the RBC/UKQCD collaboration has undertaken a series of lattice-QCD calculations of $K \to \pi\pi$ decay amplitudes [51,407,408,415]. In 2015, the first calculation of the $K \to (\pi\pi)_{I=0}$ decay amplitude A_0 was performed using physical kinematics on a $32^3 \times 64$ lattice with an inverse

[29]The update in $\text{Im}(A_2)$ is due to a change in the value of the imaginary part of the ratio of CKM matrix elements, $\tau = -V_{ts}^* V_{td}/V_{us}^* V_{ud}$, as given in Ref. [409]. The lattice-QCD input is therefore the one reported in Ref. [51].

[30]The current estimates for the corrections owing to isospin breaking and electromagnetic effects [406] imply a relative change on the theoretical value for ϵ'/ϵ by about −20% with respect to the determination based on Eq. (104). The size of these isospin breaking and electromagnetic corrections is related to the enhancement of the decay amplitudes between the $I = 0$ and the $I = 2$ channels. As a consequence, one obtains a similar reduction on ξ_0, leading to a value that is close to the result of Eq. (106).

lattice spacing of $a^{-1} = 1.3784(68)$ GeV [408,416]. The main features of the RBC/UKQCD 15G calculation included, fixing the $I = 0$ $\pi\pi$ energy very close to the kaon mass by imposing G-parity boundary conditions, a continuum-like operator mixing pattern through the use of a domain-wall fermion action with accurate chiral symmetry, and the construction of the complete set of correlation functions by computing seventy-five distinct diagrams. Results for the real and the imaginary parts of the decay amplitude A_0 from the RBC/UKQCD 15G computation are collected in Table 22, where the first error is statistical and the second is systematic.

The calculation in RBC/UKQCD 20 [407] using the same lattice setup has improved upon RBC/UKQCD 15G [408] in three important aspects: (i) an increase in statistics by a factor of 3.4; (ii) the inclusion of a scalar two-quark operator and the addition of another pion-pion operator to isolate the ground state, and (iii) the use of step scaling techniques to raise the renormalization scale from 1.53 GeV to 4.01 GeV. The updated determinations of the real and the imaginary parts of A_0 in Ref. [407] are shown in Table 22.

In addition to utilizing G-parity boundary conditions to address the challenges associated with extracting excited states for achieving the correct kinematics of $K \to \pi\pi$, the latest publications, RBC/UKQCD 23A [415] and RBC/UKQCD 23B [417], also investigate alternative approaches for overcoming this issue, namely employing variational methods and periodic boundary conditions. Two-pion scattering calculations are carried out for the isospin channels $I = 0$ and $I = 2$ on two gauge-field ensembles with physical pion masses and inverse lattice spacings of 1.023 and 1.378 GeV [417] employing domain-wall fermions. The results for scattering phase shifts in both $I = 0$ and $I = 2$ channels exhibit consistency with the Roy equation and chiral perturbation theory, although the statistical error for $I = 0$ remains relatively large. The computation of $K \to \pi\pi$ decay amplitudes and ϵ' is performed on a single ensemble with a physical pion mass and an inverse lattice spacing of 1.023 GeV [415]. The value obtained for $\mathrm{Re}(\epsilon'/\epsilon)$ is consistent with that of the previous 2020 calculation, albeit with 1.7 times larger uncertainty. Results from RBC/UKQCD 23A for the real and imaginary parts of A_0 and A_2 are reported in Tables 22 and 23, respectively.

As previously discussed, the determination of $\mathrm{Im}(A_0)$ from Ref. [407] has been used to obtain the value of the parameter ξ_0 in Eq. (106). A first-principles computation of $\mathrm{Re}(A_0)$ is essential to address the so-called $\Delta I = 1/2$ puzzle associated to the enhancement of $\Delta I = 1/2$ over $\Delta I = 3/2$ transitions owing, crucially, to long distance effects. Indeed, short-distance enhancements in the Wilson coefficients are not large enough to explain the $\Delta I = 1/2$ rule [418,419]. Lattice-QCD calculations do provide a method to study such a long-distance enhancement. The combination of the most precise result for A_0 in Table 22, Ref. [407], with the earlier lattice calculation of A_2 in Ref. [51] leads to the ratio, $\mathrm{Re}(A_0)/\mathrm{Re}(A_2) = 19.9(5.0)$, which agrees with the value $\mathrm{Re}(A_0)/\mathrm{Re}(A_2) = 22.45(6)$ that we obtain based solely on PDG 24 [274] experimental input. In Ref. [407], the lattice determination of relative size of direct CP violation was updated as follows,

$$\mathrm{Re}(\epsilon'/\epsilon) = 21.7(2.6)(6.2)(5.0) \times 10^{-4}, \qquad (109)$$

where the first two errors are statistical and systematic, respectively. The third error arises from having omitted the strong and electromagnetic isospin breaking effects. The value of $\mathrm{Re}(\epsilon'/\epsilon)$ in Eq. (109) uses the experimental values of $\mathrm{Re}(A_0)$ and $\mathrm{Re}(A_2)$. The lattice determination of $\mathrm{Re}(\epsilon'/\epsilon)$ is in good agreement with the experimental result in Eq. (105). However, while the result in Eq. (109) represents a significant step forward, it is important to keep in mind that the calculation of A_0 is currently based on a single value of the lattice spacing. It is expected that future work with additional values of the lattice spacing will contribute to improve the precision. For a description of the computation of the $\pi\pi$ scattering phase shifts entering in the determination of $\mathrm{Re}(\epsilon'/\epsilon)$ in Eq. (109), we refer to Ref. [420].

The complex amplitude A_2 has been determined by RBC/UKQCD 15F [51] employing $N_f = 2 + 1$ Möbius domain-wall fermions at two values of the lattice spacing, namely $a = 0.114$ fm and 0.083 fm, and performing simulations at the physical pion mass with $M_\pi L \approx 3.8$.

A compilation of lattice results for the real and imaginary parts of the $K \to \pi\pi$ decay amplitudes, A_0 and A_2, with $N_f = 2 + 1$ flavors of dynamical quarks is shown in Tables 22 and 23. In Appendix C 3 c, we collect the corresponding information about the lattice QCD simulations, including the values of some of the most relevant parameters.

The determination of the real and imaginary parts of A_2 by RBC/UKQCD 15F shown in Table 23 is free of red tags. We therefore quote the following FLAG averages:

$$N_f = 2 + 1: \quad \begin{matrix} \mathrm{Re}(A_2) = 1.50(0.04)(0.14) \times 10^{-8}\ \mathrm{GeV}, \\ \mathrm{Im}(A_2) = -8.34(1.03) \times 10^{-13}\ \mathrm{GeV}, \end{matrix} \quad \text{Ref. [51]}. \qquad (110)$$

TABLE 24. Results for the parameter $\xi_0 = \mathrm{Im}(A_0)/\mathrm{Re}(A_0)$ obtained through the combination of lattice-QCD determinations of $K \to \pi\pi$ decay amplitudes with $N_f = 2+1$ dynamical flavors and experimental inputs.

Collaboration	Ref.	N_f	ξ_0
RBC/UKQCD 23A[a]	[415]	$2+1$	$-2.63(37)(68) \times 10^{-4}$
RBC/UKQCD 20[b]	[407]	$2+1$	$-2.1(5) \times 10^{-4}$
RBC/UKQCD 15G[c]	[408]	$2+1$	$-0.6(5) \times 10^{-4}$
RBC/UKQCD 15F[d]	[51]	$2+1$	$-1.7(2) \times 10^{-4}$

[a]Estimate for ξ_0 has been provided by RBC/UKQCD (private communication with Masaaki Tomii.)

[b]Estimate for ξ_0 obtained from a direct evaluation of the ratio of amplitudes $\mathrm{Im}(A_0)/\mathrm{Re}(A_0)$ where $\mathrm{Im}(A_0)$ is determined from the lattice-QCD computation of Ref. [407] while for $\mathrm{Re}(A_0) \simeq |A_0|$ is taken from the experimental value for $|A_0|$.

[c]Estimate for ξ_0 obtained from a direct evaluation of the ratio of amplitudes $\mathrm{Im}(A_0)/\mathrm{Re}(A_0)$ where $\mathrm{Im}(A_0)$ is determined from the lattice-QCD computation of Ref. [408] while for $\mathrm{Re}(A_0) \simeq |A_0|$ is taken from the experimental value for $|A_0|$.

[d]Estimate for ξ_0 based on the use of Eq. (104). The new value of $\mathrm{Im}(A_2)$ reported in Ref. [407]—based on the lattice-QCD computation of Ref. [51] following an update of a nonlattice input—is used in combination with the experimental values for $\mathrm{Re}(A_2)$, $\mathrm{Re}(\epsilon'/\epsilon)$, $|\epsilon_K|$ and ω.

Results for the parameter ξ_0 are presented in Table 24. Except for the most recent calculation RBC/UKQCD 23A, which is based on the direct lattice calculation of the relevant quantities, we note that, for the other reported values of ξ_0, the total uncertainty depends on the specific way in which lattice and experimental inputs are selected.

Besides the RBC/UKQCD collaboration program [51,407,408,415,417] using domain-wall fermions, an approach based on improved Wilson fermions [421,422] has presented a determination of the $K \to \pi\pi$ decay amplitudes, A_0 and A_2, at unphysical quark masses. See Refs. [423–425] for an analysis of the scaling with the number of colors of $K \to \pi\pi$ decay amplitudes using lattice-QCD computations.

Proposals aiming at the inclusion of electromagnetism in lattice-QCD calculations of $K \to \pi\pi$ decays are being explored [426–428] in order to reduce the uncertainties associated with isospin breaking effects.

C. Lattice computation of B_K

Lattice calculations of B_K are affected by the same type of systematic effects discussed in the various sections of this review. However, the issue of renormalization merits special attention. The reason is that the multiplicative renormalizability of the relevant operator $Q^{\Delta S=2}$ is lost once the regularized QCD action ceases to be invariant under chiral transformations. As a result, the renormalization pattern of B_K depends on the specific choice of the fermionic discretization.

In the case of Wilson fermions, $Q^{\Delta S=2}$ mixes with four additional dimension-six operators, which belong to different representations of the chiral group, with mixing coefficients that are finite functions of the gauge coupling. This complicated renormalization pattern was identified as the main source of systematic error in earlier, mostly quenched calculations of B_K with Wilson quarks. It can be bypassed via the implementation of specifically designed methods, which are either based on Ward identities [429] or on a modification of the Wilson quark action, known as twisted-mass QCD [430–432].

An advantage of staggered fermions is the presence of a remnant $U(1)$ chiral symmetry. However, at nonvanishing lattice spacing, the symmetry among the extra unphysical degrees of freedom (tastes) is broken. As a result, mixing with other dimension-six operators cannot be avoided in the staggered formulation, which complicates the determination of the B-parameter. In general, taste conserving mixings are implemented directly in the lattice computation of the matrix element. The effects of the broken taste symmetry are usually treated through an effective field theory, staggered chiral perturbation theory (SχPT) [433,434], parametrizing the quark-mass and lattice-spacing dependences.

Fermionic lattice actions based on the Ginsparg-Wilson relation [435] are invariant under the chiral group, and hence four-quark operators such as $Q^{\Delta S=2}$ renormalize multiplicatively. However, depending on the particular formulation of Ginsparg-Wilson fermions, residual chiral symmetry breaking effects may be present in actual calculations. For instance, in the case of domain-wall fermions, the finiteness of the extra 5th dimension implies that the decoupling of modes with different chirality is not exact, which produces a residual nonzero quark mass m_{res} in the chiral limit. The mixing with dimension-six operators of different chirality is expected to be an $\mathcal{O}(m_{\mathrm{res}}^2)$ suppressed effect [436,437] that should be investigated on a case-by-case basis.

Before describing the results for B_K, we would like to reiterate a discussion presented in previous FLAG reports about an issue related to the computation of the kaon bag parameters through lattice-QCD simulations with $N_f = 2+1+1$ dynamical quarks. In practice, this only concerns the calculations of the kaon B-parameters including dynamical charm-quark effects in Ref. [52], that were examined in the FLAG 16 report. As described in Sec. VI A, the effective Hamiltonian in Eq. (90) depends solely on the operator $Q^{\Delta S=2}$ in Eq. (91)—which appears in the definition of B_K in Eq. (98)—at energy scales below the charm threshold where charm-quark contributions are absent. As a result, a computation of B_K based on $N_f = 2+1+1$ dynamical simulations will include an extra

sea-quark contribution from charm-quark loop effects for which there is at present no direct evaluation in the literature.

When the matrix element of $Q^{\Delta S=2}$ is evaluated in a theory that contains a dynamical charm quark, the resulting estimate for B_K must then be matched to the three-flavor theory that underlies the effective four-quark interaction.[31] In general, the matching of $2+1$-flavor QCD with the theory containing $2+1+1$ flavors of sea quarks is performed around the charm threshold. It is usually accomplished by requiring that the coupling and quark masses are equal in the two theories at a renormalization scale μ around m_c. In addition, B_K should be renormalized and run, in the four-flavor theory, to the value of μ at which the two theories are matched, as described in Sec. VI A. The corrections associated with this matching are of order $(E/m_c)^2$, where E is a typical energy in the process under study, since the subleading operators have dimension eight [438].

When the kaon-mixing amplitude is considered, the matching also involves the relation between the relevant box diagrams and the effective four-quark operator. In this case, corrections of order $(E/m_c)^2$ arise not only from the charm quarks in the sea, but also from the valence sector, since the charm quark propagates in the box diagrams. We note that the original derivation of the effective four-quark interaction is valid up to corrections of order $(E/m_c)^2$. The kaon-mixing amplitudes evaluated in the $N_f=2+1$ and $2+1+1$ theories are thus subject to corrections of the same order in E/m_c as the derivation of the conventional four-quark interaction.

Regarding perturbative QCD corrections at the scale of the charm-quark mass on the amplitude in Eq. (94), the uncertainty on η_1 and η_3 factors is of $\mathcal{O}(\alpha_s(m_c)^3)$ [381,382], while that on η_2 is of $\mathcal{O}(\alpha_s(m_c)^2)$ [439].[32] On the other hand, the corrections of order $(E/m_c)^2$ due to dynamical charm-quark effects in the matching of the amplitudes are further suppressed by powers of $\alpha_s(m_c)$ and by a factor of $1/N_c$, given that they arise from quark-loop diagrams. In order to make progress in resolving this so far uncontrolled systematic uncertainty, it is essential that any future calculation of B_K with $N_f=2+1+1$ flavors properly addresses the size of these residual dynamical charm effects in a quantitative way.

Another issue in this context is how the lattice scale and the physical values of the quark masses are determined in the $2+1$ and $2+1+1$ flavor theories. Here it is important to consider in which way the quantities used to fix the bare parameters are affected by a dynamical charm quark.

A recent study [226] using three degenerate light quarks, together with a charm quark, indicates that the deviations between the $N_f=3+1$ and the $N_f=3$ theories are considerably below the 1% level in dimensionless quantities constructed from ratios of gradient flow observables, such as t_0 and w_0, used for scale setting. This study extends the nonperturbative investigations with two heavy mass-degenerate quarks [198,200] which indicate that dynamical charm-quark effects in low-energy hadronic observables are considerably smaller than the expectation from a naive power counting in terms of $\alpha_s(m_c)$. For an additional discussion on this point, we refer to Ref. [52]. Given the hierarchy of scales between the charm-quark mass and that of B_K, we expect these errors to be modest. The ETM 15 $N_f=2+1+1$ B_K result does not include an estimate of this systematic uncertainty. A more quantitative understanding will be required as the statistical uncertainties in B_K will be reduced. Within this review we will not discuss this issue further. However, we wish to point out that the present discussion also applies to $N_f=2+1+1$ computations of the kaon BSM B-parameters discussed in Sec. VI D.

A compilation of results for B_K with $N_f=2+1+1$, $2+1$ and 2 flavors of dynamical quarks is shown in Tables 25 and 26, as well as Fig. 14. An overview of the quality of systematic error studies is represented by the color coded entries in Tables 25 and 26. The values of the most relevant lattice parameters and comparative tables on the various estimates of systematic errors have been collected in the corresponding Appendices of the previous FLAG editions [2–4].

Since the last FLAG report, one new result for B_K appeared in RBC/UKQCD 24 [56].[33] For the determination of B_K, the RBC/UKQCD Collaboration employs domain-wall fermions at three lattice spacings spanning the range $[0.07, 0.11]$ fm. For the two coarsest lattice spacings, simulations have been performed at the physical pion mass, whereas for the finest lattice spacing, a pion mass of about 230 MeV has been used. Residual chiral symmetry breaking effects induced by the finite extent of the 5th dimension in the domain-wall fermion formulation have been checked and found to contribute to the systematic uncertainty of the final estimate of B_K at the per-mille level. Finite-volume effects are found to be negligible. The renormalization constants of the lattice operators are

[31]We thank Martin Lüscher for an interesting discussion on this issue.

[32]The results of Ref. [380], based on the use of u-t unitarity for the two corresponding perturbative factors, also have an uncertainty of $\mathcal{O}(\alpha_s(m_c)^2)$ and $\mathcal{O}(\alpha_s(m_c)^3)$. The estimates for the missing higher-order contributions are, however, expected to be reduced with respect to the more traditional case where c-t unitarity is used; for a discussion on the $|\epsilon_K|$ computation in the u-t unitarity, see the relevant discussion in Sec. VI A.

[33]We also mention the report of an ongoing work [440] related to the calculation of B_K in which the relevant operators are defined in the framework of gradient flow. A small flow time expansion method was applied in order to compute, to 1-loop approximation, the finite matching coefficients between the gradient flow and the $\overline{\text{MS}}$ schemes for the operators entering the B_K computation.

TABLE 25. Results for the kaon B-parameter in QCD with $N_f = 2+1+1$ and $N_f = 2+1$, together with a summary of systematic errors. Information about nonperturbative running is indicated in the column "running," with details given at the bottom of the table.

Collaboration	Ref.	N_f	Publication status	Continuum extrapolation	Chiral extrapolation	Finite volume	Renormalization	Running	$B_K(\overline{\text{MS}}, 2\text{ GeV})$	$\hat{B}_K$
ETM 15	[52]	$2+1+1$	A	★	○	○	★	[b]	0.524(13)(12)	0.717(18)(16)[g]
RBC/UKQCD 24	[56]	$2+1$	A	★	★	★	★	[c]	0.540(2)(20)[h]	0.7436(25)(78)
RBC/UKQCD 16	[58]	$2+1$	A	○	○	○	★	[d]	0.543(9)(13)[i]	0.744(13)(18)[j]
SWME 15A	[55]	$2+1$	A	★	○	★	○[a]	⋯	0.537(4)(26)	0.735(5)(36)[k]
RBC/UKQCD 14B	[12]	$2+1$	A	★	★	★	★	[d]	0.5478(18)(110)[i]	0.7499(24)(150)
SWME 14	[385]	$2+1$	A	★	○	★	○[a]	⋯	0.5388(34)(266)	0.7379(47)(365)
SWME 13A	[441]	$2+1$	A	★	○	★	○[a]	⋯	0.537(7)(24)	0.735(10)(33)
SWME 13	[442]	$2+1$	C	★	○	★	○[a]	⋯	0.539(3)(25)	0.738(5)(34)
RBC/UKQCD 12A	[229]	$2+1$	A	○	★	○	★	[d]	0.554(8)(14)[i]	0.758(11)(19)
Laiho 11	[54]	$2+1$	C	★	○	○	★	⋯	0.5572(28)(150)	0.7628(38)(205)[k]
SWME 11A	[443]	$2+1$	A	★	○	○	○[a]	⋯	0.531(3)(27)	0.727(4)(38)
BMW 11	[53]	$2+1$	A	★	★	★	★	[e]	0.5644(59)(58)	0.7727(81)(84)
RBC/UKQCD 10B	[444]	$2+1$	A	○	○	★	★	[f]	0.549(5)(26)	0.749(7)(26)
SWME 10	[445]	$2+1$	A	★	○	○	○	⋯	0.529(9)(32)	0.724(12)(43)
Aubin 09	[446]	$2+1$	A	○	○	○	★	⋯	0.527(6)(21)	0.724(8)(29)

[a]The renormalization is performed using perturbation theory at 1-loop, with a conservative estimate of the uncertainty.

[b]B_K is renormalized nonperturbatively at scales $1/a \sim 2.2$–3.3 GeV in the $N_f = 4$ RI/MOM scheme using two different lattice momentum scale intervals, the first around $1/a$ while the second around 3.5 GeV. The impact of the two ways to the final result is taken into account in the error budget. Conversion to $\overline{\text{MS}}$ is at 1-loop order at 3 GeV.

[c]B_K is renormalized nonperturbatively at a scale of 2.0 GeV in two RI/SMOM schemes for $N_f = 3$, and then run to 3 GeV using a nonperturbatively determined step-scaling function. A direct computation at 3 GeV is also used to estimate systematic uncertainties related to discretization effects. Conversion to $\overline{\text{MS}}$ is at 1-loop order at 3 GeV.

[d]B_K is renormalized nonperturbatively at a scale of 1.4 GeV in two RI/SMOM schemes for $N_f = 3$, and then run to 3 GeV using a nonperturbatively determined step-scaling function. Conversion to $\overline{\text{MS}}$ is at 1-loop order at 3 GeV.

[e]B_K is renormalized and run nonperturbatively to a scale of 3.5 GeV in the RI/MOM scheme. At the same scale, conversion at 1-loop order to $\overline{\text{MS}}$ is applied. Nonperturbative and NLO perturbative running agrees down to scales of 1.8 GeV within statistical uncertainties of about 2%.

[f]B_K is renormalized nonperturbatively at a scale of 2 GeV in two RI/SMOM schemes for $N_f = 3$, and then run to 3 GeV using a nonperturbatively determined step-scaling function. Conversion to $\overline{\text{MS}}$ is at 1-loop order at 3 GeV.

[g]$B_K(\overline{\text{MS}}, 2\text{ GeV})$ and $\hat{B}_K$ are related using the conversion factor 1.369, i.e., the one obtained with $N_f = 2+1$.

[h]$B_K(\overline{\text{MS}}, 2\text{ GeV})$ value from a private communication with the authors. The first error is due to lattice statistical and systematic uncertainties; the second error is associated with the perturbative truncation uncertainty in matching to $\overline{\text{MS}}$ at a scale of 2 GeV.

[i]$B_K(\overline{\text{MS}}, 2\text{ GeV})$ is obtained from the estimate for $\hat{B}_K$ using the conversion factor 1.369.

[j]$\hat{B}_K$ is obtained from $B_K(\overline{\text{MS}}, 3\text{ GeV})$ using the conversion factor employed in Ref. [12].

[k]$\hat{B}_K$ is obtained from the estimate for $B_K(\overline{\text{MS}}, 2\text{ GeV})$ using the conversion factor 1.369.

determined nonperturbatively in two RI-SMOM schemes, namely $(\not{q}, \not{q})$ and (γ_μ, γ_μ), corresponding to two different choices of renormalization conditions (see Ref. [12]). The final values of the renormalization constants are obtained from the average over the results of the two schemes. The error from the (γ_μ, γ_μ) scheme is used to quote the uncertainty arising from the lattice computation. The renormalization constants in the RI-SMOM schemes are

TABLE 26. Results for the kaon B-parameter in QCD with $N_f = 2$, together with a summary of systematic errors. Information about nonperturbative running is indicated in the column "running," with details given at the bottom of the table.

Collaboration	Ref.	N_f	Publication status	Continuum extrapolation	Chiral extrapolation	Finite volume	Renormalization	Running	$B_K(\overline{\text{MS}}, 2\text{ GeV})$	$\hat{B}_K$
ETM 12D	[57]	2	A	★	○	○	★	[a]	0.531(16)(9)	0.727(22)(12)[c]
ETM 10A	[447]	2	A	★	○	○	★	[b]	0.533(18)(12)[c]	0.729(25)(17)

[a] B_K is renormalized nonperturbatively at scales $1/a \sim 2$–3.7 GeV in the $N_f = 2$ RI/MOM scheme. In this scheme, nonperturbative and NLO perturbative running are shown to agree from 4 GeV down to 2 GeV to better than 3% [447,448].

[b] B_K is renormalized nonperturbatively at scales $1/a \sim 2$–3 GeV in the $N_f = 2$ RI/MOM scheme. In this scheme, nonperturbative and NLO perturbative running are shown to agree from 4 GeV down to 2 GeV to better than 3% [447,448].

[c] $B_K(\overline{\text{MS}}, 2\text{ GeV})$ and $\hat{B}_K$ are related using the conversion factor 1.369, i.e., the one obtained with $N_f = 2 + 1$.

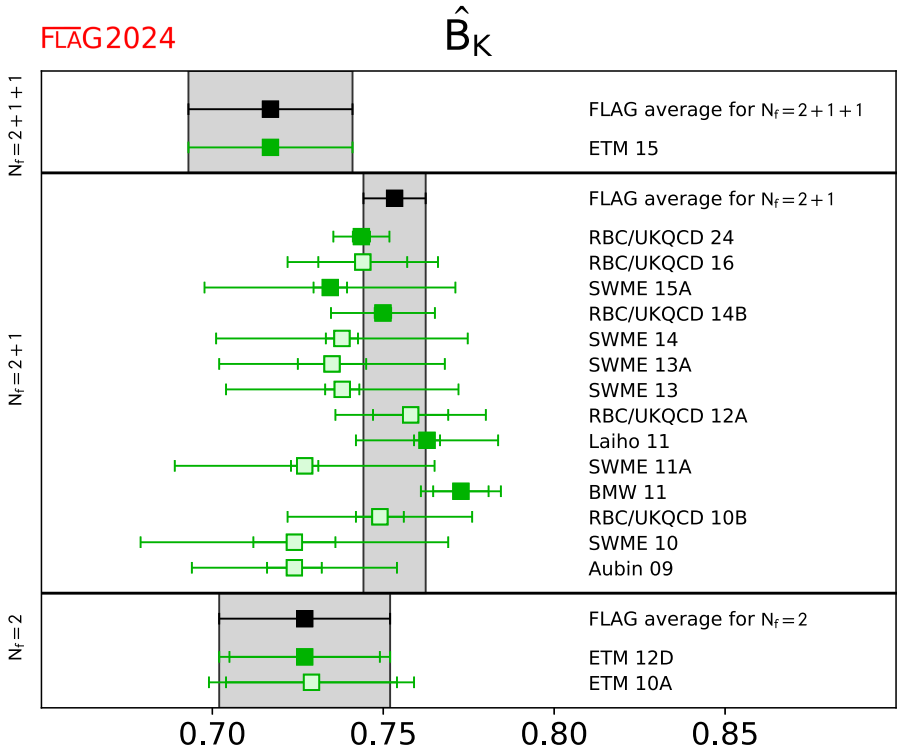


FIG. 14. Unquenched lattice results for the RGI B-parameter $\hat{B}_K$. The gray bands indicate our averages described in the text. For $N_f = 2 + 1 + 1$ and $N_f = 2$ the FLAG averages coincide with the results by ETM 15 and ETM 12D, respectively.

computed at the renormalization scale $\mu = 2$ GeV. A nonperturbative step-scaling procedure is used to run them to $\mu = 3$ GeV where the results are perturbatively matched to the $\overline{\text{MS}}$ scheme. The continuum and physical point result for B_K is obtained through a combined chiral and continuum extrapolation using NLO SU(2) chiral perturbation theory. The spread between the result obtained as described above and the result of a calculation performed directly at $\mu = 3$ GeV is taken as an estimate of the uncertainty due to discretization effects. The dominant error of the RBC/UKQCD 24 computation of B_K arises from the perturbative matching of the RI-SMOM schemes used in the lattice

computation to the $\overline{\text{MS}}$ scheme. This is estimated as half the difference of the results obtained from the use of the two intermediate RI-SMOM schemes in the matching. In this computation of B_K, a green star symbol is assigned to all FLAG quality criteria.

For a detailed description of previous B_K calculations we refer the reader to FLAG 16 [3].

We now give the FLAG averages for B_K for $N_f = 2+1+1, 2+1$, and 2 dynamical flavors.

We begin with the $N_f = 2+1$ global average, which is estimated by employing five different B_K results, namely BMW 11 [53], Laiho 11 [54], RBC/UKQCD 14B [12], SWME 15A [55], and RBC/UKQCD 24 [56]. Moreover, we recall that the expression of ϵ_K in terms of B_K is derived in the three-flavor theory (see Sec. VI A). Our procedure is first, we combine in quadrature the statistical and systematic errors of each individual result of the RGI B parameter $\hat{B}_{\text{K}}$. A weighted average is then obtained from the set of results. For the final error estimate, we take correlations between different collaborations into account. Specifically, we consider the statistical and finite-volume errors of SWME 15A and Laiho 11 to be correlated, since both groups use the asqtad ensembles generated by the MILC Collaboration. Laiho 11 and RBC/UKQCD 14B both use domain-wall quarks in the valence sector and employ similar procedures for the nonperturbative determination of matching factors. Hence, we treat their quoted renormalization and matching uncertainties as correlated. Moreover, we treat the results obtained by RBC/UKQCD 14B and RBC/UKQCD 24 as fully correlated because part of the sea ensembles in the two calculations are common.[34] In the calculation of the average, we incorporate the new FLAG data-driven criterion (see Sec. II A 2) concerning the extrapolation to the continuum limit which increases by approximately 3.7% the total error of the RBC/UKQCD 24 calculation. Following Schmelling's procedure [203] to construct the global covariance matrix of the results contributing to the average, we arrive at the following value, $\hat{B}_K = 0.7533(85)$. Since the fit implementing the weighted average has $\chi^2/\text{dof} = 1.142$, according to the general FLAG rule, we stretch the error by the square root of the reduced χ^2 value. This effect is mainly driven by the two most precise determinations of $\hat{B}_{\text{K}}$, corresponding to RBC/UKQCD 24 and BMW 11, which differ at the 2σ level. This procedure leads to the following result:

$$N_f = 2+1: \quad \hat{B}_K = 0.7533(91) \quad \text{Refs. [12, 53–56]}, \tag{111}$$

After applying the NLO conversion factors $\hat{B}_K/B_K^{\overline{\text{MS}}}(2\,\text{GeV}) = 1.369$ and $\hat{B}_K/B_K^{\overline{\text{MS}}}(3\ \text{GeV}) = 1.415$,[35] this becomes

$$N_f = 2+1: \begin{array}{l} B_K^{\overline{\text{MS}}}(2\,\text{GeV}) = 0.5503(66), \\ B_K^{\overline{\text{MS}}}(3\,\text{GeV}) = 0.5324(64), \ \text{Refs. [12,53–56]}. \end{array} \tag{112}$$

Improvements in lattice calculations in recent years have led to a considerable reduction in statistical errors. This has implied that some of the results contributing to the global average are nowadays statistically incompatible. Only by taking into account the contributions to systemic uncertainties, both from the lattice calculations themselves and, notably, from perturbative matching, can it be seen that the weighted average produces a value of $\mathcal{O}(1)$ for the reduced χ^2.

There is only a single result for $N_f = 2+1+1$, computed by the ETM collaboration [52]. Since it is free of red tags, it qualifies to the following average,

$$N_f = 2+1+1: \ \hat{B}_K = 0.717(18)(16), \ \text{Ref. [52]}. \tag{113}$$

Using the same conversion factors as in the three-flavor theory, this value translates into

$$N_f = 2+1+1: \begin{array}{l} B_K^{\overline{\text{MS}}}(2\,\text{GeV}) = 0.524(13)(12), \\ B_K^{\overline{\text{MS}}}(3\,\text{GeV}) = 0.507(13)(11), \ \text{Ref. [52]}. \end{array} \tag{114}$$

For $N_f = 2$ flavors the average is based on a single result, that of ETM 12D [57]

$$N_f = 2: \quad \hat{B}_K = 0.727(22)(12), \quad \text{Ref. [57]}, \tag{115}$$

which, using the same conversion factors as in the three-flavor theory, translates into

$$N_f = 2: \begin{array}{l} B_K^{\overline{\text{MS}}}(2\,\text{GeV}) = 0.531(16)(9), \\ B_K^{\overline{\text{MS}}}(3\,\text{GeV}) = 0.514(16)(8), \ \text{Ref. [57]}. \end{array} \tag{116}$$

D. Kaon BSM B-parameters

We now consider the matrix elements of operators that encode the effects of physics beyond the Standard Model (BSM) to the mixing of neutral kaons. In this theoretical

[34] However, due to partly different methodology in the analysis and the renormalization procedure the two computations are considered as separate, and for this reason they are both included in the global average.

[35] We refer to FLAG 19 [4] for a discussion of the procedure followed in estimating the conversion factors to $\overline{\text{MS}}$ at 2 GeV. In addition, for the computation of the conversion factor from RGI to the $\overline{\text{MS}}$ scheme at 3 GeV, which is new here, we have used the three-flavor Λ_{QCD} from FLAG 21 and the 4-loop formula for the β-function of the strong coupling constant. The propagation error owing to the error of Λ_{QCD} is found to be negligible compared to the total uncertainty of the B_K estimate.

TABLE 27. Results for the BSM B-parameters $B_2, \ldots, B_5$ in the $\overline{\text{MS}}$ scheme at a reference scale of 3 GeV. Information about nonperturbative running is indicated in the column "running," with details given at the bottom of the table.

Collaboration	Ref.	N_f	Publication status	Continuum extrapolation	Chiral extrapolation	Finite volume	Renormalization	Running	B_2	B_3	B_4	B_5
ETM 15	[52]	$2+1+1$	A	★	○	○	★	[b]	0.46(1)(3)	0.79(2)(5)	0.78(2)(4)	0.49(3)(3)
RBC/UKQCD 24	[56]	$2+1$	A	★	★	★	★	[c]	0.4794(25)(35)	0.746(13)(17)	0.897(02)(10)	0.6882(78)(94)
RBC/UKQCD 16	[58]	$2+1$	A	○	○	○	★	[c]	0.488(7)(17)	0.743(14)(65)	0.920(12)(16)	0.707(8)(44)
SWME 15A	[55]	$2+1$	A	★	○	★	○[a]	⋯	0.525(1)(23)	0.773(6)(35)	0.981(3)(62)	0.751(7)(68)
SWME 14C	[456]	$2+1$	C	★	○	★	○[a]	⋯	0.525(1)(23)	0.774(6)(64)	0.981(3)(61)	0.748(9)(79)
SWME 13A[e]	[441]	$2+1$	A	★	○	★	○[a]	⋯	0.549(3)(28)	0.790(30)	1.033(6)(46)	0.855(6)(43)
RBC/UKQCD 12E	[450]	$2+1$	A	■	○	★	★	[c]	0.43(1)(5)	0.75(2)(9)	0.69(1)(7)	0.47(1)(6)
ETM 12D	[57]	2	A	★	○	○	★	[d]	0.47(2)(1)	0.78(4)(2)	0.76(2)(2)	0.58(2)(2)

[a]The renormalization is performed using perturbation theory at 1-loop order, with a conservative estimate of the uncertainty.

[b]B_i are renormalized nonperturbatively at scales $1/a \sim 2.2$–3.3 GeV in the $N_f = 4$ RI/MOM scheme using two different lattice momentum scale intervals, with values around $1/a$ for the first and around 3.5 GeV for the second one. The impact of these two ways to the final result is taken into account in the error budget. Conversion to $\overline{\text{MS}}$ is at 1-loop order at 3 GeV.

[c]The B-parameters are renormalized nonperturbatively at a scale of 3 GeV.

[d]B_i are renormalized nonperturbatively at scales $1/a \sim 2$–3.7 GeV in the $N_f = 2$ RI/MOM scheme using two different lattice momentum scale intervals, with values around $1/a$ for the first and around 3 GeV for the second one.

[e]The computation of B_4 and B_5 has been revised in Refs. [55,456].

framework, both the SM and BSM contributions add up to reproduce the experimentally observed value of ϵ_K. As long as BSM contributions involve heavy particles with masses much larger than Λ_{QCD}, they will be short-distance dominated. The effective Hamiltonian for generic $\Delta S = 2$ processes including BSM contributions reads

$$\mathcal{H}^{\Delta S=2}_{\text{eff,BSM}} = \sum_{i=1}^{5} C_i(\mu) Q_i(\mu), \tag{117}$$

where Q_1 is the four-quark operator of Eq. (91) that gives rise to the SM contribution to ϵ_K. In the so-called SUSY basis introduced by Gabbiani *et al.* [449], the operators $Q_2, \ldots, Q_5$ are[36]

$$\begin{aligned} Q_2 &= (\bar{s}^a(1-\gamma_5)d^a)(\bar{s}^b(1-\gamma_5)d^b), \\ Q_3 &= (\bar{s}^a(1-\gamma_5)d^b)(\bar{s}^b(1-\gamma_5)d^a), \\ Q_4 &= (\bar{s}^a(1-\gamma_5)d^a)(\bar{s}^b(1+\gamma_5)d^b), \\ Q_5 &= (\bar{s}^a(1-\gamma_5)d^b)(\bar{s}^b(1+\gamma_5)d^a), \end{aligned} \tag{118}$$

where a and b are color indices. In analogy to the case of B_K, one then defines the B-parameters of $Q_2, \ldots, Q_5$ according to

$$B_i(\mu) = \frac{\langle \bar{K}^0 | Q_i(\mu) | K^0 \rangle}{N_i \langle \bar{K}^0 | \bar{s}\gamma_5 d | 0 \rangle \langle 0 | \bar{s}\gamma_5 d | K^0 \rangle}, \quad i = 2, \ldots, 5. \tag{119}$$

The factors $\{N_2, \ldots, N_5\}$ are given by $\{-5/3, 1/3, 2, 2/3\}$, and it is understood that $B_i(\mu)$ is specified in some renormalization scheme, such as $\overline{\text{MS}}$ or a variant of the regularization-independent momentum subtraction (RI-MOM) scheme.

The SUSY basis has been adopted in Refs. [52,56–58,450]. Alternatively, one can employ the chiral basis of Buras, Misiak and Urban [451]. The SWME collaboration prefers the latter since the anomalous dimension that enters the RG running has been calculated to 2-loop order in perturbation theory [451]. Results obtained in the chiral basis can be easily converted to the SUSY basis via

$$B_3^{\text{SUSY}} = \frac{1}{2}(5B_2^{\text{chiral}} - 3B_3^{\text{chiral}}). \tag{120}$$

The remaining B-parameters are the same in both bases. In the following, we adopt the SUSY basis and drop the superscript.

[36]Thanks to QCD parity invariance lattice computations for three more dimension-six operators, whose parity conserving parts coincide with the corresponding parity conserving contributions of the operators Q_1, Q_2 and Q_3, can be ignored.

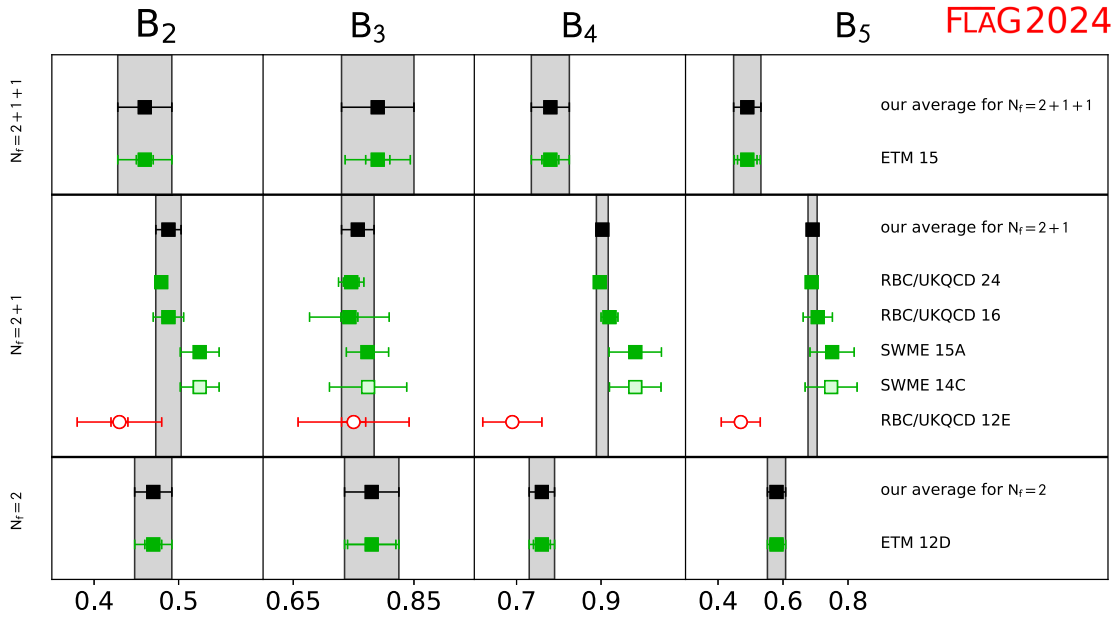


FIG. 15. Results for the BSM B-parameters defined in the $\overline{\text{MS}}$ scheme at a reference scale of 3 GeV (see Table 27).

Older quenched results for the BSM B-parameters can be found in Refs. [452–454]. For a nonlattice approach to get estimates for the BSM B-parameters see Ref. [455].

Estimates for $B_2, \ldots, B_5$ have been reported for QCD with $N_f = 2$ (ETM 12D [57]), $N_f = 2 + 1$ (RBC/UKQCD 12E [450], SWME 13A [441], SWME 14C [456], SWME 15A [55], RBC/UKQCD 16 [58,457], RBC/UKQCD 24 [56]) and $N_f = 2 + 1 + 1$ (ETM 15 [52]) flavors of dynamical quarks. Since the publication of FLAG 19 [4] a single new work Ref. [56] has appeared. The basic characteristics of this calculation have been reported in the B_K section, see Sec. VI C. As in the case of B_K, the dominant error for all the BSM B-parameters arises from the systematic uncertainty associated to the truncation error in the perturbative matching from the intermediate schemes to the $\overline{\text{MS}}$ scheme. This is estimated as half the difference of the results obtained from the matching to $\overline{\text{MS}}$ of the two intermediate schemes. The ratio of the BSM to SM matrix elements are also reported in Ref. [56].

All the available results are listed and compared in Table 27 and Fig. 15. In general, one finds that the BSM B-parameters computed by different collaborations do not show the same level of consistency as the SM kaon-mixing parameter B_K discussed previously. Control over the systematic uncertainties from chiral and continuum extrapolations as well as finite-volume effects in $B_2, \ldots, B_5$ is expected to be at a comparable level as that for B_K, as far as the results by ETM 12D, ETM 15, SWME 15A and RBC/UKQCD 16 are concerned, since the set of gauge ensembles employed in both kinds of computations is the same. However, the most recent results by RBC/UKQCD 24 with $N_f = 2 + 1$ flavors are, in general, much more precise than the older ones. Notice that the calculation by RBC/UKQCD 12E has been performed at a single value of the lattice spacing and a minimum pion mass of 290 MeV.

As reported in RBC/UKQCD 16 [58] and RBC/UKQCD 24 [56], the comparison of results obtained in the conventional RI-MOM and in two RI-SMOM schemes shows significant discrepancies for some of the BSM B-parameters. Tensions are observed for the cases of B_4 and B_5, where the discrepancies between results obtained with RI-MOM and RI-SMOM are at the level of 2.6σ and 4.5σ, respectively. The results of RBC/UKQCD 16 and RBC/UKQCD 24 lie closer to those of SWME 15A which rely on perturbative renormalization at 1-loop order. On the other hand, the results for B_2 and B_3 obtained by ETM 15, SWME 15A, RBC/UKQCD 16 and RBC/UKQCD 24 show a better level of compatibility.

The findings by RBC/UKQCD 16 [58], RBC/UKQCD 17A [457] and RBC/UKQCD 24 [56] highlight the importance of carefully assessing the systematic effects on the implementation of the Rome-Southampton method used for nonperturbative renormalization. In particular, the RI-MOM and RI-SMOM schemes differ in that the use of nonexceptional kinematics, in the RI-SMOM scheme, removes the need to subtract the pseudo-Goldstone boson pole contamination, as is required in the RI-MOM case. In addition, for each of the schemes a specific analysis of the truncation error in the perturbative matching to $\overline{\text{MS}}$ must be carried out.

A nonperturbative computation of the running of the four-fermion operators contributing to the $B_2, \ldots, B_5$ parameters has been carried out with two dynamical flavors using the Schrödinger functional renormalization scheme [387]. Renormalization matrices of the operator basis are used to build step-scaling functions governing the

continuum-limit running between hadronic and electroweak scales. A comparison to perturbative results using NLO (2-loop order) for the four-fermion operator anomalous dimensions indicates that, at scales of about 3 GeV, nonperturbative effects can induce a sizeable contribution to the running. Similar conclusions are obtained on the basis of preliminary results for the renormalization-group running of the complete basis of $\Delta F = 2$ four-fermion operators using $N_f = 3$ dynamical massless flavors in the Schrödinger setup [388].

A closer look at the calculations reported in ETM 15 [52], SWME 15A [55], RBC/UKQCD 16 [58], and RBC/UKQCD 24 [56] reveals that cutoff effects tend to be larger for the BSM B-parameters compared to those of B_K. In order to take into account this effect in the average analysis, we make use of the new FLAG data-driven criterion (see Sec. II A 2) concerning the extrapolation to the continuum limit. In summary, we report that in the average procedure, (a) for B_2 the total errors by RBC/UKQCD 24 and RBC/UKQCD 16 have been inflated by a factor 2.6 and by 22%, respectively; (b) for B_3 the total errors by ETM 15, RBC/UKQCD 16 and RBC/UKQCD 24 have been inflated by 11%, 45% and 52%, respectively; (c) for B_4 no error inflation is required; and (d) for B_5 the total errors by SWME 15A and RBC/UKQCD 16 have been inflated by 3% and 24%, respectively.

Finally we present our estimates for the BSM B-parameters, quoted in the $\overline{\text{MS}}$-scheme at scale 3 GeV. For $N_f = 2 + 1$ our estimate is given by the average of the results from SWME 15A, RBC/UKQCD 16, and RBC/UKQCD 24. In our analysis, the results in RBC/UKQCD 16 and RBC/UKQCD 24, though obtained through partially different analyses, are considered as fully correlated because some gauge ensembles are common in the two computations. We find $B_2 = 0.488(12)$ $(\chi^2/\text{dof} = 1.58)$; $B_3 = 0.757(27)$ $(\chi^2/\text{dof} = 0.17)$; $B_4 = 0.903(12)$ $(\chi^2/\text{dof} = 1.36)$; $B_5 = 0.691(14)$ $(\chi^2/\text{dof} = 0.43)$. Following the FLAG rule, for cases that have a value of the reduced χ^2 greater than unity, we use the square root of the latter to stretch the respective error. Hence our averages are

$$N_f = 2 + 1:$$
$$B_2 = 0.488(15), \quad B_3 = 0.757(27), \quad B_4 = 0.903(14),$$
$$B_5 = 0.691(14), \quad \text{Refs. [55, 56, 58]}. \tag{121}$$

For $N_f = 2 + 1 + 1$ and $N_f = 2$, our estimates coincide—with one exception—with the ones by ETM 15 and ETM 12D, respectively, since there is only one computation for each case. Only for the case of B_3 with $N_f = 2 + 1 + 1$, owing to the application of the $\delta(a_{\min})$ criterion the error of the average estimate is inflated by about 11% with respect to the ETM 15 reported value. Thus we quote

$$N_f = 2 + 1 + 1:$$
$$B_2 = 0.46(1)(3), \quad B_3 = 0.79(6), \quad B_4 = 0.78(2)(4),$$
$$B_5 = 0.49(3)(3), \quad \text{Ref. [52]}, \tag{122}$$

$$N_f = 2:$$
$$B_2 = 0.47(2)(1), \quad B_3 = 0.78(4)(2), \quad B_4 = 0.76(2)(2),$$
$$B_5 = 0.58(2)(2), \quad \text{Ref. [57]}. \tag{123}$$

Based on the above discussion about the effects of employing different intermediate momentum subtraction schemes in the nonperturbative renormalization of the operators, there is evidence that the discrepancy in the B_4 and B_5 results between $N_f = 2, 2 + 1 + 1$, and $N_f = 2 + 1$ calculations should not be directly attributed to an effect of the number of dynamical flavors. To clarify the present situation, it would be important to perform a direct comparison of results by the ETM collaboration obtained both with RI-MOM and RI-SMOM methods. A calculation based an on a different nonperturbative renormalization scheme, such as the Schrödinger functional, would provide valuable information to shed light on the current situation.

In closing, we encourage authors to provide the correlation matrix of the B_i parameters—as done in Ref. [56]—since this information is required in phenomenological studies of new physics scenarios.

VII. CHARM-HADRON DECAY CONSTANTS AND FORM FACTORS

Working group members: Y. Aoki, M. Della Morte, E. Lunghi, S. Meinel, C. Monahan, A. Vaquero

Leptonic and semileptonic decays of charmed D and D_s mesons or Λ_c and other charm baryons occur via charged W-boson exchange, and are sensitive probes of $c \to d$ and $c \to s$ quark flavor-changing transitions. Given experimental measurements of the branching fractions combined with sufficiently precise theoretical calculations of the hadronic matrix elements, they enable the determination of the CKM matrix elements $|V_{cd}|$ and $|V_{cs}|$ (within the Standard Model) and a precise test of the unitarity of the second row of the CKM matrix. Here, we summarize the status of lattice-QCD calculations of the charmed leptonic decay constants. Significant progress has been made in charm physics on the lattice in recent years, largely due to the availability of gauge configurations produced using highly improved lattice-fermion actions that enable treating the c quark with the same action as for the u, d, and s quarks.

This section updates the corresponding section in the last review (FLAG 21 [5]) for results that appeared before April 30, 2024. As in FLAG 19 [4] and FLAG 21 [5], we limit our review to results based on modern simulations with reasonably light pion masses (below approximately 500 MeV). This excludes results with two flavors in the sea,

even if they use light pion masses. $N_f = 2$ results can still be checked in previous FLAG editions.

For the heavy-meson decay constants and mixing parameters, estimates of the quantity $\delta(a_{\min})$ described in Sec. II A 2 are provided for all computations entering the final FLAG averages or ranges. For heavy-hadron semileptonic-decay form factors, implementing this data-driven continuum-limit criterion was found to be not feasible. The problem is that these quantities are functions of the momentum transfer in addition to the other lattice parameters, and many calculations are based on global fits whose reconstruction was not possible.

Following our review of lattice-QCD calculations of $D_{(s)}$-meson leptonic decay constants and charm-hadron semileptonic form factors, we then interpret our results within the context of the Standard Model. We combine our best-determined values of the hadronic matrix elements with the most recent experimentally measured branching fractions to obtain $|V_{cd(s)}|$ and test the unitarity of the second row of the CKM matrix.

A. Leptonic decay constants f_D and f_{D_s}

In the Standard Model, and up to electromagnetic corrections, the decay constant $f_{D_{(s)}}$ of a pseudoscalar D or D_s meson is related to the branching ratio for leptonic decays mediated by a W boson through the formula

$$\mathcal{B}(D_{(s)} \to \ell\nu_\ell) = \frac{G_F^2 |V_{cq}|^2 \tau_{D_{(s)}}}{8\pi} f_{D_{(s)}}^2 m_\ell^2 m_{D_{(s)}} \left(1 - \frac{m_\ell^2}{m_{D_{(s)}}^2}\right)^2, \tag{124}$$

where q is d or s and V_{cd} (V_{cs}) is the appropriate CKM matrix element for a D (D_s) meson. The branching fractions have been experimentally measured by CLEO, Belle, *BABAR* and BES with a precision around 2.5%–4.5% for both the D and the D_s-meson decay modes [274]. When combined with lattice results for the decay constants, they allow for determinations of $|V_{cs}|$ and $|V_{cd}|$.

The decay constants $f_{D_{(s)}}$ are defined through the matrix elements of the axial current

$$\langle 0|A_{cq}^\mu|D_q(p)\rangle = i f_{D_q} p_{D_q}^\mu, \tag{125}$$

with $q = d$, s and $A_{cq}^\mu = \bar{c}\gamma^\mu\gamma_5 q$. Such matrix elements can be extracted from Euclidean two-point functions computed on the lattice.

Results for $N_f = 2+1$ and $2+1+1$ dynamical flavors are summarized in Table 28 and Fig. 16. Since the publication of FLAG 21, a handful of results for f_D and f_{D_s} have appeared, as described below. We consider isospin-averaged quantities, although, in a few cases, results for f_{D^+} are quoted (see, for example, the FNAL/MILC 11,14A and 17 computations, where the strong-isospin-breaking effect given by the difference between f_D and f_{D^+} has been estimated to be around 0.5 MeV).

For the first time, we restrict the review here to results obtained using $N_f = 2+1$ and $2+1+1$ dynamical flavors. No new results with $N_f = 2$ appeared since 2019 and they have been presented in previous FLAG reviews.

Another novelty is the reinclusion of the quantity $\delta(a_{\min})$ described in the Introduction. Our working group introduced and applied this quantity in FLAG 13 [2], but it was not applied in following reviews. As computations have become increasingly precise and often dominated by systematic uncertainties, we believe that a closer scrutiny of the continuum extrapolations is needed since such extrapolations usually produce one of the largest systematic errors. Here, we provide (where possible) an estimate of $\delta(a_{\min})$ for all computations entering the final FLAG averages or ranges. Those estimates do not need to be very precise as the natural size of the error on $\delta(a_{\min})$ is $\mathcal{O}(1)$.

Two new results appeared with $N_f = 2+1$. In Ref. [28] (ALPHA 23) maximally twisted Wilson valence fermions (for light and heavy quarks) are implemented on a set of ensembles of configurations generated within the CLS initiative using $\mathcal{O}(a)$-improved Wilson fermions. As a consequence of the maximal twist, observables in the charm sector are free from $\mathcal{O}(am_c)$ discretization effects. In addition the decay constants $f_{D_{(s)}}$ are automatically normalized and do not require the computation of normalization factors. Four different lattice spacings have been used in the continuum extrapolation, ranging between 0.087 and 0.05 fm. Pion masses reach down to 200 MeV and volumes are such that $3.9 \le m_\pi L \le 6.4$. The uncertainties are dominated by statistics and the chiral-continuum fits. Judging from the plots in Ref. [28], the values for $\delta(a_{\min})$ are around 1 for f_D and around 3 for f_{D_s}.

A second new computation with $N_f = 2+1$ has been performed by the RQCD-ALPHA Collaboration [461] on a set of 49 gauge ensembles generated again within the CLS effort. For this reason statistical errors between ALPHA 23 and RQCD/ALPHA 24 will be treated as 100% correlated when performing averages. Notice, however, that since RQCD/ALPHA 24 was not yet published in a journal by the FLAG deadline, it is not being considered in the averages for this review. In RQCD/ALPHA 24 nonperturbatively $\mathcal{O}(a)$-improved Wilson fermions have been used both in the valence sector and the sea.[37] The simulations cover six different lattice spacings with 0.039 fm $\le a \le$ 0.098 fm, pion masses from 420 MeV down to 130 MeV and $m_\pi L$ ranging from 2.83 to 6.42. The largest volume at $m_\pi = 130$ MeV gives $m_\pi L = 4.05$. In the discussion of the final errors the uncertainty due to the scale setting is treated separately. That turns out to be the largest contribution to the total error for f_D and f_{D_s} (around 50%), while for the

[37]The coefficient $\bar{b}_A$ has been neglected because its nonperturbative value, computed in [465], turned out to be compatible with zero for the relevant range of gauge couplings.

TABLE 28. Decay constants of the D and D_s mesons (in MeV) and their ratio.

Collaboration	Ref.	N_f	Publication status	Continuum extrapolation	Chiral extrapolation	Finite volume	Renormalization/matching	Heavy-quark treatment	f_D	f_{D_s}	f_{D_s}/f_D
ETM 21B	[458]	$2+1+1$	C	★	★	★	★	✓	210.1 (2.4)	248.9 (2.0)	1.1838(115)
FNAL/MILC 17[c]	[20]	$2+1+1$	A	★	★	★	★	✓	212.1 (0.6)	249.9 (0.5)	1.1782(16)
FNAL/MILC 14A[b]	[21]	$2+1+1$	A	★	★	★	★	✓	$212.6(0.4)(^{+1.0}_{-1.2})$	$249.0(0.3)(^{+1.1}_{-1.5})$	$1.1745(10)(^{+29}_{-32})$
ETM 14E	[43]	$2+1+1$	A	★	○	○	★	✓	207.4 (3.8)	247.2 (4.1)	1.192(22)
ETM 13F	[356]	$2+1+1$	C	○	○	○	★	✓	202(8)	242(8)	1.199(25)
FNAL/MILC 13	[459]	$2+1+1$	C	★	★	★	★	✓	212.3 (0.3)(1.0)	248.7 (0.2)(1.0)	1.1714(10)(25)
FNAL/MILC 12B	[460]	$2+1+1$	C	★	★	★	★	✓	209.2 (3.0)(3.6)	246.4 (0.5)(3.6)	1.175(16)(11)
RQCD/ALPHA 24	[461]	$2+1$	P	★	★	★	★	✓	208.4 (0.7)(0.7)(1.1)	246.8 (0.6)(0.6)(1.0)	1.1842(21)(22)(19)
ALPHA 23	[28]	$2+1$	A	★	○	★	★	✓	211.3 (1.9)(0.6)	247.0 (1.9)(0.7)	1.177(15)(5)
χQCD 20A[f]	[462]	$2+1$	A	■	★	★	★	✓	213(5)	249(7)	1.16(3)
RBC/UKQCD 18A[d]	[76]	$2+1$	P	★	★	★	★	✓			$1.1740(51)(^{+68}_{-68})$
RBC/UKQCD 17	[61]	$2+1$	A	★	★	○	★	✓	$208.7(2.8)(^{+2.1}_{-1.8})$	$246.4(1.3)(^{+1.3}_{-1.9})$	$1.1667(77)(^{+57}_{-43})$
χQCD 14[e]	[29]	$2+1$	A	○	○	○	★	✓		254(2)(4)	
HPQCD 12A	[59]	$2+1$	A	○	○	○	★	✓	208.3(1.0)(3.3)	246.0(0.7)(3.5)	1.187(4)(12)
FNAL/MILC 11	[60]	$2+1$	A	○	○	○	○	✓	218.9(11.3)	260.1(10.8)	1.188(25)
PACS-CS 11	[463]	$2+1$	A	■	★	■	○	✓	226(6)(1)(5)	257(2)(1)(5)	1.14(3)
HPQCD 10A	[62]	$2+1$	A	★	○	★	★	✓	213(4)[a]	248.0(2.5)	
HPQCD/UKQCD 07	[46]	$2+1$	A	○	○	○	★	✓	207(4)	241(3)	1.164(11)
FNAL/MILC 05	[464]	$2+1$	A	○	○	■	○	✓	201(3)(17)	249(3)(16)	1.24(1)(7)

[a]This result is obtained by using the central value for f_{D_s}/f_D from HPQCD/UKQCD 07 and increasing the error to account for the effects from the change in the physical value of r_1.

[b]At $\beta = 5.8$, $m_{\pi,\mathrm{min}}L = 3.2$ but this lattice spacing is not used in the final cont./chiral extrapolations.

[c]Update of FNAL/MILC 14A. The ratio quoted is $f_{D_s}/f_{D^+} = 1.1749(16)$. In order to compare with results from other collaborations, we rescale the number by the ratio of central values for f_{D+} and f_D. We use the same rescaling in FNAL/MILC 14A. At the finest lattice spacing the finite-volume criterium would produce an empty green circle, however, as checked by the authors, results would not significantly change by excluding this ensemble, which instead sharpens the continuum limit extrapolation.

[d]Update of RBC/UKQCD 17.

[e]Two values of sea pion masses.

[f]Four valence pion masses between 208 MeV and 114 MeV have been used at one value of the sea pion mass of 139 MeV.

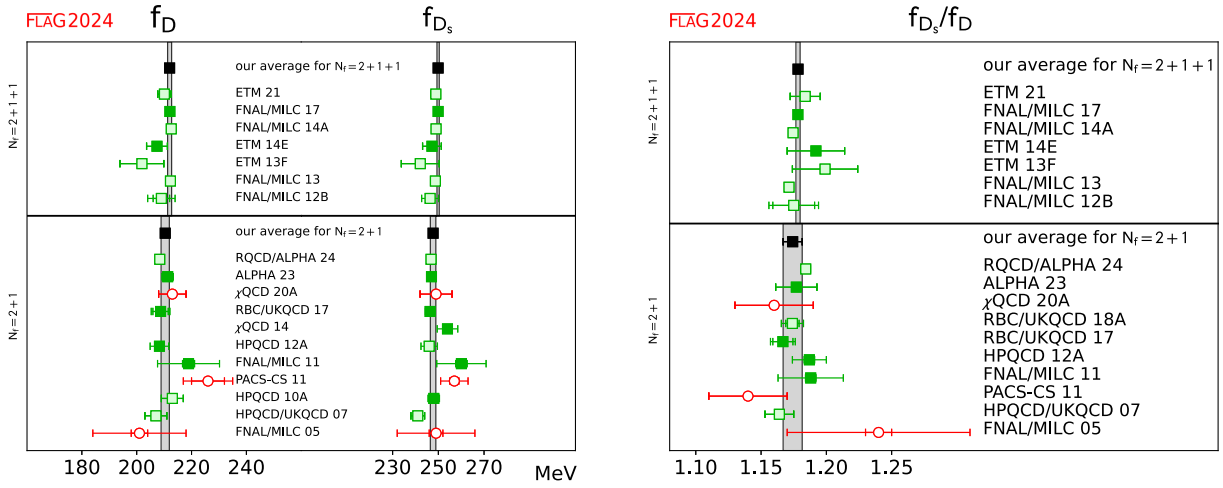


FIG. 16. Decay constants of the D and D_s mesons [values in Table 28 and Eqs. (126)–(131)]. As usual, full green squares are used in the averaging procedure, pale green squares have either been superseded by later determinations or are only published in proceedings or have not been published within the current deadline (April 30, 2024), while empty red circles do not satisfy the criteria. The black squares and gray bands indicate our averages.

ratio of decay constants statistical, systematic (chiral and continuum extrapolations) and scale-setting uncertainties are of about the same size. The quantity $\delta(a_{\min})$, as estimated from the figures in [461] is around 1.

The updated $N_f = 2+1$ FLAG averages read

$$N_f = 2+1: \quad f_D = 210.4(1.5)\ \text{MeV} \quad \text{Refs. [28,59–61]}, \tag{126}$$

$$N_f = 2+1: \quad f_{D_s} = 247.7(1.2)\ \text{MeV} \quad \text{Refs. [28,29,60–62]}, \tag{127}$$

$$N_f = 2+1: \qquad \frac{f_{D_s}}{f_D} = 1.174(0.007) \quad \text{Refs. [28,59–61]}. \tag{128}$$

Those come from the results in HPQCD 12A [59], FNAL/MILC 11 [60] as well as RBC/UKQCD 17 [61] and ALPHA 23 [28] concerning f_D while for f_{D_s} also the χQCD 14 [29] result contributes, and instead of the value in HPQCD 12A [59] the one in HPQCD 10A [62] is used. In addition, the statistical errors between the results of FNAL/MILC and HPQCD have been everywhere treated as 100% correlated since the two collaborations use overlapping sets of configurations. The same procedure had been used in the past reviews. Concerning the values of $\delta(a_{\min})$ for older computations entering those estimates, they are all smaller than 2 for the results before 2013, as discussed in the second FLAG review [2], where that was used as a necessary condition to enter the averages. For RBC/UKQCD 17 $\delta(a_{\min})$ is estimated to be around 1.5, while for χQCD 14 it is not possible to assess the value of $\delta(a_{\min})$ from the published figures and tables.

For $N_f = 2+1+1$ only a proceedings contribution to the 2021 Lattice Conference by the ETM Collaboration [458] appeared containing new results. This ETM 21B result extends ETM 14E [43] by including simulations closer to the physical point for light and heavy quarks. Twisted-mass fermions at maximal twist are used in the sea, in order to ensure automatic $\mathcal{O}(a)$ improvement. In the valence sector Osterwalder-Seiler fermions are adopted for the strange and charm quarks to avoid mixing effects at $\mathcal{O}(a^2)$. Three different lattice resolutions between 0.095 and 0.069 fm have been used with $m_\pi L$ at the lightest pion mass (134 MeV) being around 3.7. Also in this case the final errors are dominated by statistics and the chiral-continuum extrapolations. Although we do not provide an estimate of $\delta(a_{\min})$ for results that do not enter the final averages, ETM 21B makes an important observation in showing that the cutoff effects strongly depend on the intermediate scaling variable used. In the case of f_{D_s}, when using w_0, $\delta(a_{\min})$ would turn out to be very large, while when using the strange-charm meson mass cutoff effects are much reduced and $\delta(a_{\min})$ is around 1.

Our global averages coincide with those in FLAG 21, Ref. [5], namely

$$N_f = 2+1+1: \quad f_D = 212.0(0.7)\ \text{MeV} \quad \text{Refs. [20,43]}, \tag{129}$$

$$N_f = 2+1+1: \quad f_{D_s} = 249.9(0.5)\ \text{MeV} \quad \text{Ref. [130]}, \tag{130}$$

$$N_f = 2+1+1: \quad \frac{f_{D_s}}{f_D} = 1.1783(0.0016) \quad \text{Refs. [20,43]}, \tag{131}$$

where the error on the average of f_D has been rescaled by the factor $\sqrt{\chi^2/\text{dof}} = 1.22$. For the two computations entering the results above $\delta(a_{\min})$ is around 2 at most.

Concerning the inclusion of QED effects, significant progress has been made in the computation of form factors for radiative leptonic decays of D mesons.[38] We do not present results in detail here since they are not yet at the level to be reviewed according to the FLAG criteria, however, such processes are important for two reasons. In the region of soft-photon energies they are needed in order to compute the QED corrections to leptonic decays. In that case they have to be combined with the contributions stemming from virtual exchanges of photons between the meson and the charged lepton, in order to remove infrared divergent terms. For hard photons radiative leptonic decays become important probes of the internal structure of hadrons and therefore of physics beyond the Standard Model. The form factors appear in the decomposition of the hadronic matrix element

$$H_W^{\alpha r}(k,\mathbf{p}) = \epsilon_\mu^r(k) \int d^4y e^{iky} \mathrm{T}\langle 0|j_W^\alpha(0) j_{em}^\mu(y)|P(\mathbf{p})\rangle, \tag{132}$$

with $\epsilon_\mu^r(k)$ the polarization vector of the outgoing photon (with momentum k), $\mathbf{p}$ the momentum of the generic pseudoscalar meson P and j_W^α and j_{em}^μ the weak and electromagnetic currents, respectively. Such matrix elements can be extracted from suitable three-point correlation functions that can be computed on an Euclidean lattice. In Ref. [466] a set of numerical methods is explored with the main goals of keeping systematic effects due to contributions from unwanted states under control and of

[38]The accuracy of the estimates presented here is often below the percent level and a first-principles computation of isospin-breaking corrections is therefore very desirable. However, for the determination of the CKM matrix elements, the experimental accuracy on the branching ratios and hence on the products $|V_{cq}|^2 f^2_{D_{(q)}}$ varies between 2.2% and 5%, see Sec. VII E.

optimizing the signal. The study is performed on a single ensemble with $2+1$ flavors of domain wall fermions, $a \simeq 0.11$ fm and $m_\pi \simeq 340$ MeV.

In Ref. [467], which extends Ref. [468], the form factors for the decay $D_s \to \ell\nu_\ell\gamma$ have been computed on four different ensembles of $N_f = 2+1+1$ gauge configurations produced by the ETM Collaboration. Lattice spacings span the interval [0.056, 0.09] fm and quarks masses are close to their physical values. The full kinematical range, with a cut $E_\gamma \geq 10$ MeV, is covered by the results. The structure-dependent contribution is found to dominate the amplitude for $\ell = e$, as opposed to the cases with $\ell = \mu$ and τ. Since the point-like contribution is (helicity) suppressed by $(m_\ell/m_P)^2$, a nonperturbative computation of the form factors is of paramount importance for B mesons. An analysis of the noise-to-signal ratio for the three-point functions is presented following the Parisi-Lepage approach [469,470] and a strategy to mitigate the problem is discussed. That coincides with one of the methods studied, with different motivations, in Ref. [466].

B. Form factors for $D \to \pi\ell\nu$ and $D \to K\ell\nu$ semileptonic decays

The SM prediction for the differential decay rate of the semileptonic processes $D \to \pi\ell\nu$ and $D \to K\ell\nu$ can be written as

$$\frac{d\Gamma(D \to P\ell\nu)}{dq^2} = \frac{\eta_{\rm EW}^2 G_{\rm F}^2 |V_{cx}|^2}{24\pi^3} \frac{(q^2 - m_\ell^2)^2 \sqrt{E_P^2 - m_P^2}}{q^4 m_D^2} \times \left[\left(1 + \frac{m_\ell^2}{2q^2}\right) m_D^2 (E_P^2 - m_P^2) |f_+(q^2)|^2 + \frac{3m_\ell^2}{8q^2} (m_D^2 - m_P^2)^2 |f_0(q^2)|^2 \right] \tag{133}$$

where $x = d, s$ is the daughter light quark, $P = \pi, K$ is the daughter light-pseudoscalar meson, $\ell = e, \mu$ indicates the light charged lepton, E_P is the light-pseudoscalar meson energy in the rest frame of the decaying D, and $q = (p_D - p_P)$ is the momentum of the outgoing lepton pair. Here, we have included the short-distance electroweak correction factor [471], whose value at $\mu = m_D$ is $\eta_{\rm EW} = 1.009$ [123]. The vector and scalar form factors $f_+(q^2)$ and $f_0(q^2)$ parametrize the hadronic matrix element of the heavy-to-light quark flavor-changing vector current $V_\mu = \bar{x}\gamma_\mu c$,

$$\langle P|V_\mu|D\rangle = f_+(q^2)\left(p_{D\mu} + p_{P\mu} - \frac{m_D^2 - m_P^2}{q^2} q_\mu\right) + f_0(q^2) \frac{m_D^2 - m_P^2}{q^2} q_\mu, \tag{134}$$

and satisfy the kinematic constraint $f_+(0) = f_0(0)$. Because the contribution to the decay width from the scalar form factor is proportional to m_ℓ^2, within current precision standards it can be neglected for $\ell = e$, and Eq. (133) simplifies to

$$\frac{d\Gamma(D \to Pe\nu)}{dq^2} = \frac{\eta_{\rm EW}^2 G_{\rm F}^2}{24\pi^3} |\vec{p}_P|^3 |V_{cx}|^2 |f_+(q^2)|^2. \tag{135}$$

In models of new physics, decay rates may also receive contributions from matrix elements of other parity-even currents. In the case of the scalar density $(\bar{x}c)$, partial vector-current conservation allows one to write its matrix elements in terms of f_+ and f_0, while for tensor currents $T_{\mu\nu} = \bar{x}\sigma_{\mu\nu}c$ a new form factor has to be introduced, viz.,

$$\langle P|T^{\mu\nu}|D\rangle = \frac{2}{m_D + m_P} [p_P^\mu p_D^\nu - p_P^\nu p_D^\mu] f_T(q^2). \tag{136}$$

Recall that, unlike the Noether current V_μ, the operator $T_{\mu\nu}$ requires a scale-dependent renormalization.

Lattice-QCD computations of $f_{+,0}$ allow for comparisons to experiment to ascertain whether the SM provides the correct prediction for the q^2-dependence of $d\Gamma(D \to P\ell\nu)/dq^2$; and, subsequently, to determine the CKM matrix elements $|V_{cd}|$ and $|V_{cs}|$ from Eq. (133). The inclusion of f_T allows for analyses to constrain new physics. Currently, state-of-the-art experimental results by CLEO-c [472] and BESIII [473,474] provide data for the differential rates in the whole q^2 range, with a precision of order 2%–3% for the total branching fractions in both the electron and muon final channels.

Calculations of the $D \to \pi\ell\nu$ and $D \to K\ell\nu$ form factors typically use the same light-quark and charm-quark actions as those of the leptonic decay constants f_D and f_{D_s}. Therefore, many of the same issues arise; in particular, considerations about cutoff effects coming from the large charm-quark mass, or the normalization of weak currents, apply. Additional complications arise, however, due to the necessity of covering a sizeable range of values in q^2:

(i) Lattice kinematics impose restrictions on the values of the hadron momenta. Because lattice calculations are performed in a finite spatial volume, the pion or kaon three-momentum components can only take discrete values in units of $2\pi/L$ when periodic boundary conditions are used. For typical box sizes

in lattice D- and B-meson form-factor calculations at heavier-than-physical pion masses, $L \sim 2.5$–3 fm; thus, the smallest nonzero momentum in most of these analyses is $|\vec{p}_P| \sim 400$–500 MeV. On the other hand, the ranges relevant for the semileptonic decays are $0 \le |\vec{p}_\pi| \lesssim 940$ MeV and $0 \le |\vec{p}_K| \lesssim 1$ GeV, respectively. Thus, when using periodic boundary conditions, only a small number of allowed lattice momenta fall into this range. As a consequence, many studies have incorporated the use of nonperiodic "twisted" boundary conditions (tbc) [475,476] in the valence fields used for the computation of observables, which allows a continuous choice of momentum and hence finer resolution of the q^2-dependence [63,477–481]. Note that more recent calculations [65,123] include ensembles with physical pion masses and $L \approx 5.5$–5.75 fm, so the momentum unit when using periodic boundary conditions is correspondingly smaller, making the use of twisted boundary conditions less relevant.

(ii) Final-state pions and kaons can have energies $\gtrsim 1$ GeV, given the available kinematical range $0 \lesssim q^2 \le q^2_{\rm max} = (m_D - m_P)^2$. This makes the use of (heavy-meson) chiral perturbation theory to extrapolate to physical light-quark masses potentially problematic. This issue has become less relevant as modern calculations include ensembles with physical light-quark masses.

(iii) Accurate comparisons to experiment, including the determination of CKM parameters, requires good control of systematic uncertainties in the parametrization of the q^2-dependence of form factors. While this issue is far more important for semileptonic B decays, where it is harder to cover the kinematic range on the lattice, the increase in experimental precision requires accurate work in the charm sector as well. The parametrization of semileptonic form factors is discussed in detail in Appendix B 2.

The first published $N_f = 2 + 1$ lattice-QCD calculation of the $D \to \pi\ell\nu$ and $D \to K\ell\nu$ form factors came from the Fermilab Lattice, MILC, and HPQCD collaborations (FNAL/MILC 04) [482].[39] This work uses asqtad-improved staggered sea quarks and light (u, d, s) valence quarks and the Fermilab action for the charm quarks, with a single lattice spacing of $a \approx 0.12$ fm, and a minimum RMS-pion mass of ≈510 MeV, dictated by the presence of fairly large staggered taste splittings. The vector current is normalized using a mostly nonperturbative approach, such that the perturbative truncation error is expected to be negligible compared to other systematics. Results for the form factors are provided over the full kinematic range, rather than focusing just at $q^2 = 0$ as was customary in most previous work, and fitted to a Bečirević-Kaidalov *Ansatz* (calculations in the full kinematic range had already been done earlier in the quenched approximation [483,484]). The publication of Ref. [482] predated the precise measurements of the $D \to K\ell\nu$ decay width by the FOCUS [485] and Belle experiments [486], and showed good agreement with the experimental determination of the shape of $f_+^{D\to K}(q^2)$. Progress on extending this work was reported in [487]; efforts are aimed at reducing both the statistical and systematic errors in $f_+^{D\to\pi}(q^2)$ and $f_+^{D\to K}(q^2)$ by increasing the number of configurations analyzed, simulating with lighter pions, and adding lattice spacings as fine as $a \approx 0.045$ fm.

The most precise published calculations of the $D \to \pi\ell\nu$ and $D \to K\ell\nu$ form factors in $N_f = 2 + 1$ QCD are by the HPQCD collaboration (HPQCD 11 [64] and HPQCD 10B [66], respectively). They are also based on $N_f = 2 + 1$ asqtad-improved staggered MILC configurations, but use two lattice spacings $a \approx 0.09$ and 0.12 fm, and a HISQ action for the valence u, d, s, and c quarks. In these mixed-action calculations, the HISQ valence light-quark masses are tuned so that the ratio m_l/m_s is approximately the same as for the sea quarks; the minimum RMS sea-pion mass ≈390 MeV. Form factors are determined only at $q^2 = 0$, by using a Ward identity to relate matrix elements of vector currents to matrix elements of the absolutely normalized quantity $(m_c - m_x)\langle P|\bar{x}c|D\rangle$ (where $x = u,\ d,\ s$), and exploiting the kinematic identity $f_+(0) = f_0(0)$ to yield $f_+(q^2 = 0) = (m_c - m_x)\langle P|\bar{x}c|D\rangle/(m_D^2 - m_P^2)$. A modified z-expansion (cf. Appendix B 2) is employed to simultaneously extrapolate to the physical light-quark masses and the continuum and to interpolate to $q^2 = 0$, and allow the coefficients of the series expansion to vary with the light- and charm-quark masses. The form of the light-quark dependence is inspired by χPT, and includes logarithms of the form $m_\pi^2 \log(m_\pi^2)$ as well as polynomials in the valence-, sea-, and charm-quark masses. Polynomials in $E_{\pi(K)}$ are also included to parametrize momentum-dependent discretization errors. The number of terms is increased until the result for $f_+(0)$ stabilizes, such that the quoted fit error for $f_+(0)$ not only contains statistical uncertainties, but also reflects relevant systematics. The largest quoted uncertainties in these calculations are from statistics and charm-quark discretization errors.

The most recent $N_f = 2 + 1$ computation of D semileptonic form factors has been carried out by the JLQCD collaboration, and so far only published in conference proceedings; most recently in Ref. [488] (JLQCD 17B). They use their own Möbius domain-wall configurations at three values of the lattice spacing $a = 0.080, 0.055$, 0.044 fm, with several pion masses ranging from 226 to 501 MeV (though there is so far only one ensemble, with $m_\pi = 284$ MeV, at the finest lattice spacing). The vector

[39] Because only two of the authors of this work are members of HPQCD, and to distinguish it from other more recent works on the same topic by HPQCD, we hereafter refer to this work as "FNAL/MILC."

and scalar form factors are computed at four values of the momentum transfer for each ensemble. The computed form factors are observed to depend mildly on both the lattice spacing and the pion mass. The momentum dependence of the form factors is fitted to a BCL z-parametrization (see Appendix B 2) with a Blaschke factor that contains the measured value of the $D^*_{(s)}$ mass in the vector channel, and a trivial Blaschke factor in the scalar channel. The systematics of this latter fit is assessed by a BCL fit with the experimental value of the scalar resonance mass in the Blaschke factor. Continuum and chiral extrapolations are carried out through a linear fit in the squared lattice spacing and the squared pion and η_c masses. A global fit that uses hard-pion HMχPT to model the mass dependence is furthermore used for a comparison of the form factor shapes with experimental data.[40] Since the computation is only published in proceedings so far, it will not enter our $N_f = 2 + 1$ average.[41] Another $N_f = 2 + 1$ calculation of the $D \to \pi$, $D \to K$, and $D_s \to K$ form factors using domain-wall fermions is currently being carried out by the RBC/UKQCD collaboration, as reported in Ref. [490].

The first full computation of both the vector and scalar form factors in $N_f = 2 + 1 + 1$ QCD was achieved by the ETM collaboration [63] (ETM 17D). Furthermore, they have provided a separate determination of the tensor form factor, relevant for new-physics analyses [481] (ETM 18). Both works use the available $N_f = 2 + 1 + 1$ twisted-mass Wilson ensembles [264], totaling three lattice spacings down to $a \approx 0.06$ fm, and a minimum pion mass of 220 MeV. Matrix elements are extracted from suitable double ratios of correlation functions that avoid the need of nontrivial current normalizations. Only one source-sink separation per ensemble is used for the three-point functions, although the authors state that this separation was optimized to achieve a balance between excited-state contamination and statistical uncertainties. The use of twisted boundary conditions allows both for imposing several kinematical configurations, and considering arbitrary frames that include moving initial mesons. After interpolation to the physical strange- and charm-quark masses, the results for form factors are fitted to a modified z-expansion that takes into account both the light-quark mass dependence through hard-pion SU(2) χPT [491], and the lattice-spacing dependence. In the latter case, a detailed study of Lorentz-breaking effects due to the breaking of rotational invariance down to the hypercubic subgroup is performed, leading to a nontrivial momentum-dependent parametrization of cutoff effects. The z-parametrization (see Appendix B 2) itself includes a single-pole Blaschke factor (save for the scalar channel in $D \to K$, where the Blaschke factor is trivial), with pole masses treated as free parameters. The final quoted uncertainty on the form factors is about 5%–6% for $D \to \pi$, and 4% for $D \to K$. The dominant source of uncertainty is quoted as statistical + fitting procedure + input parameters—the latter referring to the values of quark masses, the lattice spacing (i.e., scale setting), and the LO SU(2) LECs.

The second $N_f = 2 + 1 + 1$ computation of f_+ and f_0 in the full kinematical range for the $D \to Kl\nu$ mode, performed by HPQCD, has been published in 2021—HPQCD 21A (Ref. [65]). This work uses MILC's HISQ ensembles at five values of the lattice spacing, and pion masses reaching to the physical point for the three coarsest values of a. Vector currents are normalized nonpertubatively by imposing that form factors satisfy Ward identities exactly at zero recoil. Results for the form factors are fitted to a modified z-expansion *Ansatz*, with all sub-threshold poles removed by using the experimental value of the mass shifted by a factor that matches the corresponding result at finite lattice spacing. The accuracy of the description of the q^2-dependence is crosschecked by comparing to a fit based on cubic splines. Finite-volume effects are expected to be small, and chiral-perturbation-theory-based estimates for them are included in the chiral fit. The impact of frozen topology at the finest lattice spacing is neglected (the size of this effect was later shown to be $\lesssim 0.03\%$ in a similar calculation [123]). The final uncertainty from the form factors in the determination of $|V_{cs}|$ quoted in HPQCD 21A is at the 0.5% level, and comparable to the rest of the uncertainty (due to the experimental error, as well as weak and electromagnetic corrections); in particular, the precision of the form factors is around seven times higher than that of the earlier $N_f = 2 + 1 + 1$ determination by ETM 17D. The work also provides an accurate prediction for the lepton-flavor-universality ratio between the muon and electron modes, where the uncertainty is overwhelmingly dominated by the electromagnetic corrections. An extension of the work of HPQCD 21A to heavier quark masses has also enabled the determination of the $B \to K$ form factors [492] (HPQCD 22), and provides the tensor form factors for both $B \to K$ and $D \to K$ in addition to the vector form factors.

In 2022, the FNAL/MILC collaboration completed another $N_f = 2 + 1 + 1$ computation of f_+ and f_0 in the full kinematic ranges for $D \to K\ell\nu$, $D \to \pi\ell\nu$, and $D_s \to Kl\nu$—FNAL/MILC 22 [123]. Like HPQCD 21A, this calculation uses the MILC HISQ ensembles and renormalization using the vector Ward identity. This calculation does not include the 0.15 fm ensembles that

[40]It is important to stress the finding in Ref. [489] that the factorization of chiral logs in hard-pion χPT breaks down, implying that it does not fulfill the expected requisites for a proper effective field theory. Its use to model the mass dependence of form factors can thus be questioned.

[41]The ensemble parameters quoted in Ref. [488] appear to show that the volumes employed at the lightest pion masses are insufficient to meet our criteria for finite-volume effects. There is, however, a typo in the table which results in a wrong assignment of lattice sizes, whereupon the criteria are indeed met. We thank T. Kaneko for correspondence on this issue.

TABLE 29. Summary of computations of charmed-meson semileptonic form factors. Note that HPQCD 20 (discussed in Sec. VII D) addresses the $B_c \to B_s$ and $B_c \to B_d$ transitions—hence the absence of quoted values for $f_+^{D\to\pi}(0)$ and $f_+^{D\to K}(0)$—while ETM 18 and HPQCD 22 provide computations of tensor form factors. The value for $f_+^{D\to K}(0)$ from HPQCD 22 [492] is obtained as a by-product of the $B \to K$ analysis and is not independent from HPQCD 21A [65]. FNAL/MILC 22 also provides results for the $D_s \to K$ form factors in addition to the $D \to K$ and $D \to \pi$ form factors [123].

Collaboration	Ref.	N_f	Publication status	Continuum extrapolation	Chiral extrapolation	Finite volume	Renormalization	Heavy-quark treatment	$f_+^{D\to\pi}(0)$	$f_+^{D\to K}(0)$
FNAL/MILC 22	[123]	$2+1+1$	A	★	★	★	★	✓	0.6300(51)	0.7452(31)
HPQCD 22	[492]	$2+1+1$	A	★	★	★	★	✓	n/a	0.7441(40)
HPQCD 21A	[65]	$2+1+1$	A	★	★	★	★	✓	n/a	0.7380(44)
HPQCD 20	[493]	$2+1+1$	A	★	○	★	★	✓	n/a	n/a
ETM 17D, 18	[63,481]	$2+1+1$	A	★	○	○	★	✓	0.612(35)	0.765(31)
JLQCD 17B	[488]	$2+1$	C	★	★	○	★	✓	$0.615(31)(^{+17}_{-16})(^{+28}_{-7})^{a}$	$0.698(29)(18)(^{+32}_{-12})^{a}$
HPQCD 11	[64]	$2+1$	A	○	○	○	★	✓	0.666(29)	
HPQCD 10B	[66]	$2+1$	A	○	○	○	★	✓		0.747(19)
FNAL/MILC 04	[482]	$2+1$	A	■	■	○	○	✓	0.64(3)(6)	0.73(3)(7)

[a]The first error is statistical, the second from the $q^2 \to 0$ extrapolation, the third from the chiral-continuum extrapolation.

were part of the HPQCD 21A analysis, and shares only one of the two 0.12 fm ensembles used in HPQCD 21A. Compared to HPQCD 21A, FNAL/MILC 22 reaches a finer lattice spacing at the physical pion mass, 0.057 fm, while the ensemble at the finest lattice spacing of 0.042 fm is common to both calculations. Overall, four of the seven ensembles are shared, but FNAL/MILC 22 uses more configurations and source positions on those ensembles. In FNAL/MILC 22, the chiral/continuum extrapolation is performed using rooted staggered heavy-meson chiral perturbation theory prior to a continuum BCL z expansion fit. This work also corrects the effects of the frozen topology at the finest lattice spacing using chiral perturbation theory; the correction is found to be $\lesssim 0.03\%$.

Table 29 contains our summary of the existing calculations of the charm-meson semileptonic form factors. Additional tables in Appendix C 4 a provide further details on the simulation parameters and comparisons of the error estimates. Recall that only calculations without red tags that are published in a refereed journal are included in the FLAG average. For $N_f = 2+1$, only HPQCD 10B,11 qualify, which provides our estimate for $f_+(q^2=0) = f_0(q^2=0)$. For $N_f = 2+1+1$, we quote as the FLAG estimate for $f_+^{D\to\pi}(0)$ the weighted average of the results by ETM 17D and FNAL/MILC 22, while for $f_+^{D\to K}(0)$ we quote the weighted average of the values published by ETM 17D, HPQCD 21A, and FNAL/MILC 22

$$N_f = 2+1: \quad \begin{aligned} f_+^{D\to\pi}(0) &= 0.666(29) \quad \text{Ref. [64]}, \\ f_+^{D\to K}(0) &= 0.747(19) \quad \text{Ref. [66]}, \end{aligned} \tag{137}$$

$$N_f = 2+1+1: \quad \begin{aligned} f_+^{D\to\pi}(0) &= 0.6296(50) \quad \text{Refs. [63,123]}, \\ f_+^{D\to K}(0) &= 0.7430(27) \quad \text{Refs. [63,65,123]}. \end{aligned} \tag{138}$$

In Fig. 17, we display the existing $N_f = 2$, $N_f = 2+1$, and $N_f = 2+1+1$ results for $f_+^{D\to\pi}(0)$ and $f_+^{D\to K}(0)$; the gray bands show our estimates of these quantities.

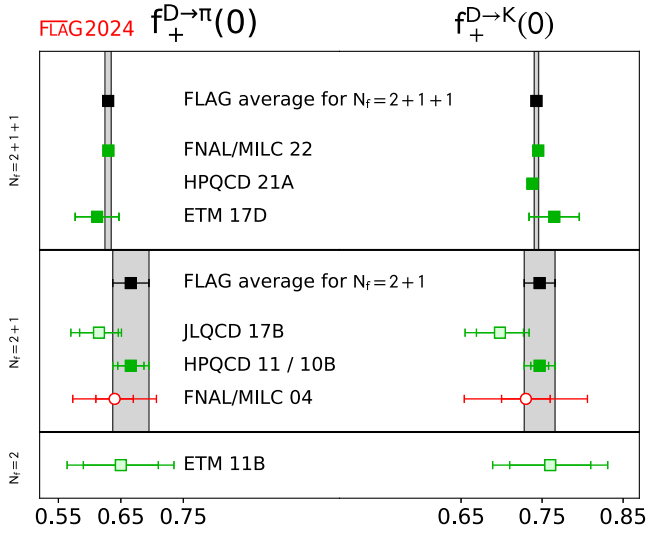


FIG. 17. $D \to \pi\ell\nu$ and $D \to K\ell\nu$ semileptonic form factors at $q^2 = 0$. The $N_f = 2+1$ HPQCD result for $f_+^{D\to\pi}(0)$ is from HPQCD 11, the one for $f_+^{D\to K}(0)$ represents HPQCD 10B (see Table 29).

TABLE 30. Coefficients for the $N^+ = 4, N^0 = 4$ z-expansion of the $N_f = 2+1+1$ FLAG average for the $D \to K$ form factors f_+ and f_0, and their correlation matrix. The inputs are from ETM 17D, HPQCD 21A, and FNAL/MILC 22. The form factors can be reconstructed using parametrization and inputs given in Appendix B 3 a.

$D \to K\ell\nu (N_f = 2+1+1)$								
	Values	Correlation matrix						
a_0^+	0.7953(53)	1.	−0.690759	−0.051101	−0.061092	0.501293	0.469810	0.132470
a_1^+	−1.0090(87)	−0.690759	1.	−0.231861	0.133663	0.004097	0.149657	0.137516
a_2^+	0.22(59)	−0.051101	−0.231861	1.	−0.113075	−0.095636	0.101738	0.238861
a_3^+	0.14(10)	−0.061092	0.133663	−0.113075	1.	−0.109883	0.116543	0.112918
a_0^0	0.7026(21)	0.501293	0.004097	−0.095636	−0.109883	1.	0.339786	−0.251322
a_1^0	0.773(39)	0.469810	0.149657	0.101738	0.116543	0.339786	1.	0.589149
a_2^0	0.54(40)	0.132470	0.137516	0.238861	0.112918	−0.251322	0.589149	1.

In the case of $N_f = 2+1+1$, we can also provide an analysis of the q^2-dependence of f_+ and f_0. FLAG 21 included a BCL fit to the ETM 17D and HPQCD 21 results for the $D \to K$ form factors; this fit had a relatively poor $\chi^2/\text{dof} = 9.17/3$ due to a tension between the results from the two collaborations at large q^2; for $D \to \pi$, only the ETM 17D results were available at that time. Now, the FNAL/MILC 22 calculation [123] provides new high-precision $N_f = 2+1+1$ results for both $D \to K$ and $D \to \pi$ (as well as $D_s \to K$). For $D \to K$, we update our previous BCL fit to include the FNAL/MILC 22 results. We consider the statistical correlations between the final HPQCD 21A and FNAL/MILC 22 results to be negligible, given that there is only partial overlap among the ensembles, the source positions for the correlation functions are different, and the analyses are performed with different fit methodologies. As in FLAG 21, we generate synthetic data from the parametrizations provided by the collaborations. The inputs to our fit from ETM 17D and HPQCD 21A are unchanged; for FNAL/MILC 22 we use four q^2 values because the parametrization used in that reference is of higher order. In both cases, this includes the kinematical endpoints $q^2 = 0$ and $q^2 = (m_D - m_K)^2$ of the semileptonic interval. We fit the resulting dataset to a BCL *Ansatz* [cf. Eqs. (B12) and (B13)]; the constraint $f_+(0) = f_0(0)$ is used to rewrite the highest-order coefficient $a^0_{N_0-1}$ in f_0 in terms of the other $N_+ + N_0 - 1$ coefficients. In both form factors, we include nontrivial Blaschke factors, with pole masses set to the experimental values of the D_s^* (for the vector channel) and D_{s0}^* (scalar channel) masses found in the PDG [225]. We take flavor averages of charged and neutral states for the D and K masses. Our external input is thus $m_D = 1.87265$ GeV, $m_K = 495.644$ MeV, $m_{D_s^*} = 2.1122$ GeV, and $m_{D_{s0}^*} = 2.317$ GeV. As a result of including the new FNAL/MILC 22 data points, we found it necessary to increase the order of the z expansion from $N_+ = N_0 = 3$ (as used in FLAG 21) to $N_+ = N_0 = 4$. The fit has $\chi^2/\text{dof} \approx 2.39$ (due to the tension between the ETM 17D results at high q^2 and the results from the other two collaborations, and due to a slight tension between the results from HPQCD 21A and FNAL/MILC 22 in f_0) and we have scaled the uncertainties of all parameters by a factor of $\sqrt{\chi^2/\text{dof}} \approx 1.55$. The results are quoted in full in Table 30 and illustrated in Fig. 18.

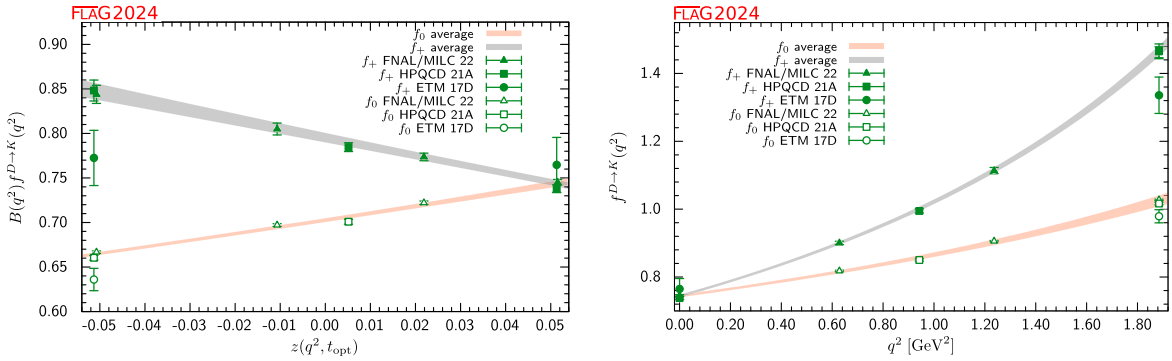


FIG. 18. The form factors $f_+(q^2)$ and $f_0(q^2)$ for $D \to K\ell\nu$ plotted versus z (left panel) and q^2 (right panel). In the left plot, we removed the Blaschke factors. See text for a discussion of the dataset. The gray and salmon bands display our preferred $N^+ = N^0 = 4$ BCL fit (seven parameters).

As can be seen in Fig. 19 of Ref. [123], for $D \to \pi$ there is a very large tension between the ETM 17D and FNAL/MILC 22 results at high q^2, in the same direction as the tension also seen for $D \to K$. In this case, the tension is so significant that attempting BCL fits to average the ETM 17D and FNAL/MILC 22 results gives values of χ^2/dof of order 100. We are concerned about possible excited-state contamination in ETM 17D, but the authors of ETM 17D stated that there is no evidence of an uncontrolled systematic effect; the tension remains unexplained. We therefore do not quote any results for the $D \to \pi$ form factors away from $q^2 = 0$.

C. Form factors for Λ_c and Ξ_c semileptonic decays

The motivation for studying charm-baryon semileptonic decays is two-fold. First, these decays allow for independent determinations of $|V_{cs}|$. Second, given that possible new-physics contributions to the $c \to s\ell\nu$ weak effective Hamiltonian are already constrained to be much smaller compared to $b \to u\ell\bar{\nu}$ and $b \to s\ell\ell$, charm-baryon semileptonic decays allow testing the lattice techniques for baryons that are also employed for bottom-baryon semileptonic decays (see Sec. VIII F) in a better-controlled environment.

The amplitudes of the decays $\Lambda_c \to \Lambda\ell\nu$ receive contributions from both the vector and the axial components of the current in the matrix element $\langle\Lambda|\bar{s}\gamma^\mu(\mathbf{1}-\gamma_5)c|\Lambda_c\rangle$, and can be parametrized in terms of six different form factors $f_+, f_0, f_\perp, g_+, g_0, g_\perp$—see, e.g., Ref. [494] for a complete description.

The computation in Meinel 16 [495] uses RBC/UKQCD $N_f = 2+1$ DWF ensembles, and treats the c quarks within the Columbia RHQ approach. Two values of the lattice spacing ($a \approx 0.11, 0.085$ fm) are considered, with the absolute scale set from the $\Upsilon(2S)$–$\Upsilon(1S)$ splitting. In one ensemble, the pion mass $m_\pi \approx 139$ MeV is at the physical point, while for other ensembles it ranges from 295 to 352 MeV. Results for the form factors are obtained from suitable three-point functions, and fitted to a modified z-expansion *Ansatz* that combines the q^2-dependence with the chiral and continuum extrapolations. The paper predicts for the total rates in the e and μ channels

$$\frac{\Gamma(\Lambda_c \to \Lambda e^+\nu_e)}{|V_{cs}|^2} = 0.2007(71)(74)\ \text{ps}^{-1},$$
$$\frac{\Gamma(\Lambda_c \to \Lambda \mu^+\nu_\mu)}{|V_{cs}|^2} = 0.1945(69)(72)\ \text{ps}^{-1}, \qquad (139)$$

where the uncertainties are statistical and systematic, respectively. In combination with the recent experimental determination of the total branching fractions by BESIII [496,497], it is possible to extract $|V_{cs}|$ as discussed in Sec. VII E below.

Lattice results are also available for the $\Lambda_c \to N$ form factors, where N is a neutron or proton [498]. This calculation uses the same lattice actions but a different set of ensembles with parameters matching those used in the 2015 calculation of the $\Lambda_b \to p$ form factors in Ref. [499] (cf. Sec. VIII F). Predictions are given for the rates of the $c \to d$ semileptonic decays $\Lambda_c \to n\ell^+\nu_\ell$; these modes have not yet been observed. Reference [498] also studies the phenomenology of the flavor-changing neutral-current decay $\Lambda_c \to p\mu^+\mu^-$. As is typical for rare charm decays to charged leptons, this mode is dominated by long-distance effects that have not yet been calculated on the lattice and whose description is model-dependent.

The authors of Zhang 21 [500] also performed a first lattice calculation of the $\Xi_c \to \Xi$ form factors and extracted $|V_{cs}|$, with still large uncertainties, from the recent Belle measurement of the $\Xi_c \to \Xi\ell^+\nu_\ell$ branching fractions [501]. This calculation uses only two ensembles with $2+1$ flavors of clover fermions, with lattice spacings of 0.108 and 0.080 fm and nearly identical pion masses of 290 and 300 MeV. The results are extrapolated to the continuum limit but are not extrapolated to the physical pion mass. No systematic uncertainty is estimated for the effect of the missing chiral extrapolation. A new calculation of the $\Xi_c \to \Xi$ form factors using domain-wall fermions is in progress [502].

The calculations discussed so far in this section all have $J^P = \frac{1}{2}^+$ baryons in the final state. A first lattice calculation of the form factors for a charm-baryon semileptonic decay to a $J^P = \frac{3}{2}^-$ baryon, $\Lambda_c \to \Lambda^*(1520)\ell^+\nu_\ell$, is also available: Meinel 21B [503]. The calculation was done using three RBC/UKQCD ensembles with $2+1$ flavors of domain-wall fermions, with $a \approx 0.11, 0.08$ fm and pion masses in the range from approximately 300 to 430 MeV. Chiral-continuum extrapolations linear in m_π^2 and a^2 were performed, with systematic uncertainties estimated using higher-order fits. Finite-volume effects and effects associated with the strong decays of the $\Lambda^*(1520)$ are not quantified. The calculation was done in the $\Lambda^*(1520)$ rest frame, where the cubic symmetry is sufficient to avoid mixing with unwanted lower-mass states.

A summary of the lattice calculations of charm-baryon semileptonic-decay form factors is given in Table 31.

D. Form factors for charm semileptonic decays with heavy spectator quarks

Two other decays mediated by the $c \to s\ell\nu$ and $c \to d\ell\nu$ transitions are $B_c \to B_s\ell\nu$ and $B_c \to B^0\ell\nu$, respectively. At present, there are no experimental results for these processes, but it may be possible to produce them at LHCb in the future. The HPQCD Collaboration has recently computed the form factors for both of these B_c decay modes with $N_f = 2+1+1$ [493]. The calculation uses six different MILC ensembles with HISQ light, strange, and

TABLE 31. Summary of computations of charmed-baryon semileptonic form factors. The rationale for the ■ rating of finite-volume effects in Meinel 21B (despite meeting the ○ criterion based on the minimum pion mass) is that the unstable nature of the final-state baryons was neglected in the analysis.

Process	Collaboration	Ref.	N_f	Publication status	Continuum extrapolation	Chiral extrapolation	Finite volume	Renormalization	Heavy-quark treatment
$\Lambda_c \to \Lambda^*(1520)\ell\nu$	Meinel 21B	[503]	$2+1$	A	○	○	■	○	✓
$\Xi_c \to \Xi\ell\nu$	Zhang 21	[500]	$2+1$	A	■	■	○	★	■
$\Lambda_c \to n\ell\nu$	Meinel 17	[498]	$2+1$	A	○	○	■	○	✓
$\Lambda_c \to \Lambda\ell\nu$	Meinel 16	[495]	$2+1$	A	○	★	★	○	✓

charm quarks, and employs the PCAC Ward identity to nonperturbatively renormalize the $c \to s$ and $c \to d$ currents. Data were generated for two different choices of the lattice action for the spectator b quark: lattice NRQCD on five of the six ensembles, and HISQ on three of the six ensembles (cf. Sec. VIII for a discussion of different lattice approaches used for the b quark). For the NRQCD calculation, two of the ensembles have a physical light-quark mass, and the lattice spacings are 0.15 fm, 0.12 fm, and 0.09 fm. The heavy-HISQ calculation is performed only at $m_l/m_s = 0.2$, and at lattice spacings of 0.12 fm, 0.09 fm, and 0.06 fm. The largest value of the heavy-HISQ mass used is 0.8 in lattice units on all three ensembles, which does not reach the physical b-quark mass even at the finest lattice spacing.

Form-factor fits are performed using z-expansions (see Appendix B 2) modified to include a dependence on the lattice spacing and quark masses, including an expansion in the inverse heavy quark mass in the case of the heavy-HISQ approach. The parameters t_+ are set to $(m_{B_c} + m_{B_{(s)}})^2$ even though the branch cuts start at $(m_D + m_K)^2$ or $(m_D + m_\pi)^2$, as also noted by the authors. The variable z is rescaled by a constant. The lowest charmed-meson poles are removed before the z-expansion, but this still leaves the branch cuts and higher poles below t_+. As a consequence of this structure, the good convergence properties of the z-expansion are not necessarily expected to apply. Fits are performed (i) using the NRQCD data only, (ii) using the HISQ data only, and (iii) using the NRQCD data, but with priors on the continuum-limit form-factor parameters equal to the results of the HISQ fit. The results from fits (i) and (ii) are mostly consistent, with the NRQCD fit having smaller uncertainties than the HISQ fit. Case (iii) then results in the smallest uncertainties and gives the predictions (for massless leptons)

$$\begin{aligned}
\frac{\Gamma(B_c \to B_s\ell^+\nu_\ell)}{|V_{cs}|^2} &= 1.738(55) \times 10^{-11}\ \text{MeV},\\
\frac{\Gamma(B_c \to B^0\ell^+\nu_\ell)}{|V_{cd}|^2} &= 2.29(12) \times 10^{-11}\ \text{MeV},\\
\frac{\Gamma(B_c \to B_s\ell^+\nu_\ell)|V_{cd}|^2}{\Gamma(B_c \to B^0\ell^+\nu_\ell)|V_{cs}|^2} &= 0.759(44).
\end{aligned} \tag{140}$$

We note that there is a discrepancy between the NRQCD and HISQ results in the case of $f_0(B_c \to B^0)$, and the uncertainty quoted for method (iii) does not cover this discrepancy. However, this form factor does not enter in the decay rate for massless leptons.

E. Determinations of $|V_{cd}|$ and $|V_{cs}|$ and test of second-row CKM unitarity

We now use the lattice-QCD results for the charm-hadron decays to determine the CKM matrix elements $|V_{cd}|$ and $|V_{cs}|$ in the Standard Model.

For the leptonic decays, we use the latest experimental averages from the Particle Data Group [274] (see Sec. 72.3.1)

$$\begin{aligned}
f_D|V_{cd}| &= 45.82(1.10)\ \text{MeV},\\
f_{D_s}|V_{cs}| &= 243.5(2.7)\ \text{MeV},
\end{aligned} \tag{141}$$

where the errors include those from nonlattice theory, e.g., estimates of radiative corrections to lifetimes [504]. Also, the values quoted by the Particle Data Group are obtained after applying the correction factor $\eta_{\text{EW}}^2 = 1.018$, due to universal short-distance electroweak contributions [471], to the branching ratios. Hadronic-structure-dependent electromagnetic corrections to the rate have not been computed on the lattice for the case of $D_{(s)}$ mesons, while they have been

calculated for pion and kaon decays [217,220]. The errors given above include a systematic uncertainty of 0.7% estimated as half the size of the applied radiative corrections.

By combining these with the averaged $N_f = 2+1$ and $2+1+1$ results for f_D and f_{D_s} in Eqs. (126)–(130), we obtain

$$N_f = 2+1+1: \begin{cases} |V_{cd}| = 0.2161(7)(52) \\ |V_{cs}| = 0.974(2)(11) \end{cases} \quad [D_{(s)} \to \ell\nu, \text{Refs. } [20,43]], \tag{142}$$

$$N_f = 2+1: \begin{cases} |V_{cd}| = 0.2178(16)(52) \\ |V_{cs}| = 0.983(5)(11) \end{cases} \quad [D_{(s)} \to \ell\nu, \text{Refs. } [28,29,59\text{–}62]], \tag{143}$$

where the errors shown are from the lattice calculation and experiment (plus nonlattice theory), respectively. For the $N_f = 2+1$ and the $N_f = 2+1+1$ determinations, the uncertainties from the lattice-QCD calculations of the decay constants are significantly smaller than the experimental uncertainties in the branching fractions.

For D-meson semileptonic decays, in the case of $N_f = 2+1$ there are no changes with respect to FLAG 21 other than the inclusion of the short-distance electroweak correction and a systematic uncertainty due to missing long-distance QED corrections; the only works entering the FLAG averages are HPQCD 10B/11 [64,66], which provide $f_+^{D\pi}(0)$ and $f_+^{DK}(0)$. We use these results in combination with the HFLAV averages for the combinations $f_+(0)\eta_{\rm EW}|V_{cx}|$ [308],

$$f_+^{D\pi}(0)\eta_{\rm EW}|V_{cd}| = 0.1426(18), \qquad f_+^{DK}(0)\eta_{\rm EW}|V_{cs}| = 0.7180(33), \tag{144}$$

and obtain

$$N_f = 2+1: \ |V_{cd}| = 0.2121(92)(29)(21) \quad [D \to \pi\ell\nu, \text{Ref. } [64]], \tag{145}$$

$$N_f = 2+1: \ |V_{cs}| = 0.958(25)(5)(10) \quad [D \to K\ell\nu, \text{Ref. } [66]], \tag{146}$$

where the uncertainties are lattice, experimental (plus nonlattice theory), and missing long-distance QED corrections (estimated to be 1%), respectively.

For $N_f = 2+1+1$, we update our BCL fit to the binned $D \to K\ell\nu$ differential decay rates by adding the FNAL/MILC 22 inputs for $f_+(q^2)$ and $f_0(q^2)$ at four q^2 values (the ETM 17D and HPQCD 21A inputs remain unchanged). The experimental datasets we include are unchanged with respect to FLAG 21 and are three different measurements of the $D^0 \to K^- e^+ \nu_e$ mode by *BABAR* (*BABAR* 07, Ref. [505]), CLEO-c (CLEO 09/0, Ref. [472]), and BESIII (BESIII 15, Ref. [506]); CLEO-c (CLEO 09/+, Ref. [472]) and BESIII measurements of the $D^+ \to \bar{K}^0 e^+ \nu_e$ mode (BESIII 17, Ref. [507]); and the recent first measurement of the $D^0 \to K^- \mu^+ \nu_\mu$ mode by BESIII, Ref. [508]. There is also a Belle dataset available in Ref. [509], but it provides results for parametrized form factors rather than partial widths, which implies that reverse modeling of the q^2-dependence of the form factor would be needed to add them to the fit, which involves an extra source of systematic uncertainty; it is, furthermore, the measurement with the largest error. Thus, we will drop it. The CLEO collaboration provides correlation matrices for the systematic uncertainties across the channels in their two measurements; the latter are, however, not available for BESIII, and, therefore, we will conservatively treat their systematics with a 100% correlation, following the same prescription as in the HFLAV review [308]. Since all lattice results have been obtained in the isospin limit, we average over the D^0 and D^+ electronic modes. The parametrization of the form factors we use here is the same as in the lattice-only fit discussed in Sec. VII B, and we again increase the order of the z expansion (with respect to FLAG 21) to $N^+ = N^0 = 4$. In contrast to FLAG 21, we now include the short-distance electroweak correction $\eta_{\rm EW}^2$ [471] in the calculation of the differential decay rate, using $\eta_{\rm EW} = 1.009$ [123]. The fit has $\chi^2/\text{dof} \approx 1.66$ and we have scaled all uncertainties by a factor of $\sqrt{\chi^2/\text{dof}} \approx 1.29$. The results for the z-expansion parameters and $|V_{cs}|$, as well as their correlation matrix, are given in Table 32, and a plot of the differential decay rates is shown in Fig. 19. For $D \to \pi l\nu$, we do not use the lattice results away from $q^2 = 0$ as discussed in Sec. VII B. To extract $|V_{cd}|$, we instead combine the average for $f_+^{D\pi}(0)$ from ETM 17D and FNAL/MILC 22 with the HFLAV result (144). Thus, we obtain

TABLE 32. Coefficients for the $N^+ = N^0 = 4$ z-expansion simultaneous fit of the $D \to K$ form factors f_+ and f_0 and $|V_{cs}|$ to the $D \to K\ell\nu$ differential decay rates and the ETM 17D, HPQCD 21A, and FNAL/MILC 22 lattice results. The form factors can be reconstructed using parametrization and inputs given in Appendix B 3 a.

$D \to K\ell\nu (N_f = 2+1+1)$									
	Values	Correlation matrix							
a_0^+	0.7896(38)	1.	−0.555568	−0.069722	−0.021610	0.587914	0.646372	0.247552	0.795354
a_1^+	−0.945(51)	−0.555568	1.	−0.303470	0.102546	−0.014576	0.043616	0.036587	−0.280176
a_2^+	0.29(49)	−0.069722	−0.303470	1.	−0.109799	−0.092179	0.107676	0.243102	−0.033821
a_3^+	0.257(84)	−0.021610	0.102546	−0.109799	1.	−0.112476	0.104107	0.101692	−0.003737
a_0^0	0.7029(18)	0.587914	−0.014576	−0.092179	−0.112476	1.	0.341851	−0.256955	0.554412
a_1^0	0.748(32)	0.646372	0.043616	0.107676	0.104107	0.341851	1.	0.578012	0.651080
a_2^0	0.11(33)	0.247552	0.036587	0.243102	0.101692	−0.256955	0.578012	1.	0.279081
$\|V_{cs}\|$	0.9592(50)	0.795354	−0.280176	−0.033821	−0.003737	0.554412	0.651080	0.279081	1.

$$N_f = 2+1+1\text{: } |V_{cd}| = 0.2245(33)(22) \quad [D \to \pi\ell\nu, \text{Refs. } [20,43]\,], \tag{147}$$

$$N_f = 2+1+1\text{: } |V_{cs}| = 0.9592(50)(96) \quad [D \to K\ell\nu, \text{Ref. } [66]\,], \tag{148}$$

where the two uncertainties correspond, respectively, to the combined lattice-QCD and experimental errors, and an estimate of the size of missing long-distance QED corrections, taken to be 1% following Ref. [123]. Note that FNAL/MILC 22 [123] also determined $|V_{cd}|$ from $D_s \to K\ell\nu$ using a BESIII measurement [510], with the result

$$N_f = 2+1+1\text{: } |V_{cd}| = 0.258(15)(03) \quad [D_s \to K\ell\nu, \text{Ref. } [123]\,], \tag{149}$$

where the large uncertainty is dominated by the experimental measurement.

For $\Lambda_c \to \Lambda\ell\nu$, there are new experimental results for the electronic and muonic branching fractions from BESIII, published in 2022 and 2023 [511,512]. In addition, the world average of the Λ_c lifetime has been updated in the 2024

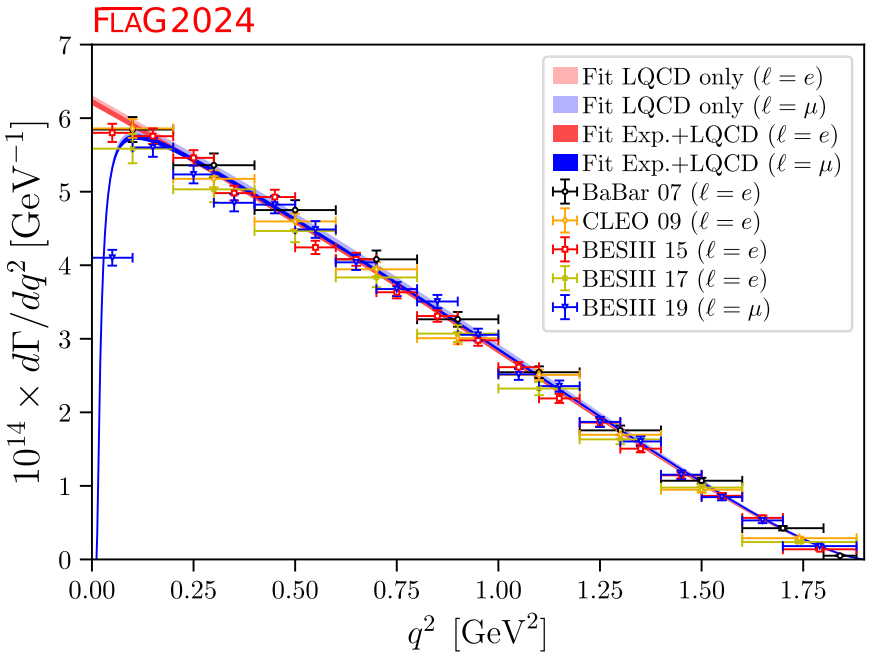


FIG. 19. Our fits to the $D \to K\ell\nu$ differential decay rates used to determine $|V_{cs}|$, with experimental inputs from Refs. [472,505–508] and lattice inputs from ETM17D [63], HPQCD 21A [65], and FNAL/MILC 22 [123].

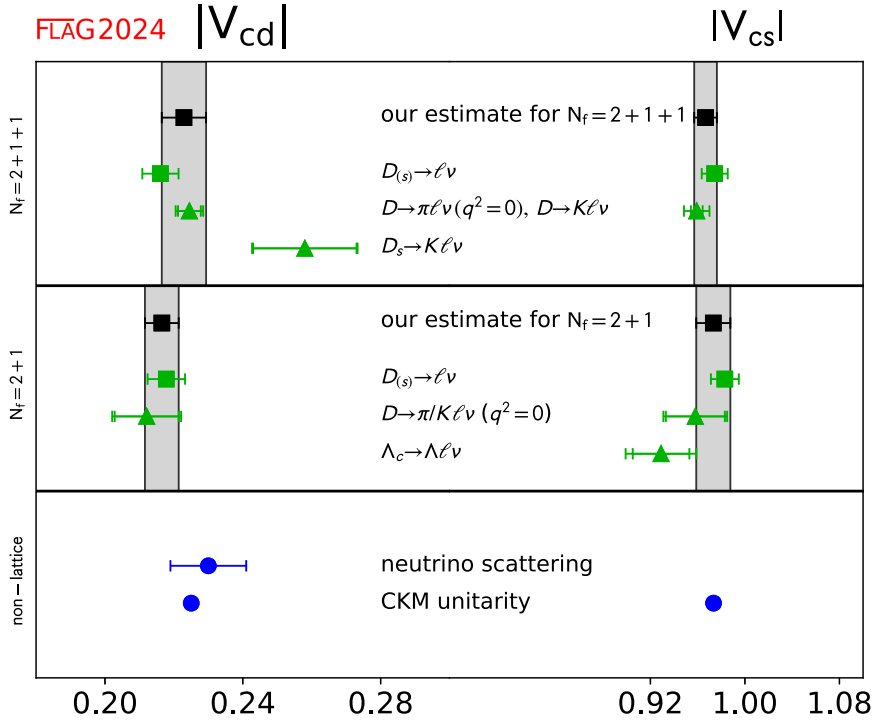


FIG. 20. Comparison of determinations of $|V_{cd}|$ and $|V_{cs}|$ obtained from lattice methods [Eqs. (142), (143), and (145)–(152)] with a nonlattice determination from neutrino scattering (for $|V_{cd}|$ only) [225] and with the Standard Model predictions from a global fit assuming CKM unitarity [396].

Review of Particle Physics to $\tau_{\Lambda_c} = (202.6 \pm 1.0) \times 10^{-15}$ s, following a new precise measurement by Belle II [513]. Using these results together with the lattice-QCD predictions of Meinel 16 for $\Gamma(\Lambda_c \to \Lambda \ell \nu)/|V_{cs}|^2$ [495], and including the factor of $\eta_{\rm EW}^2$ (not done in Ref. [495]), we obtain

$$N_f = 2+1\text{:}\ |V_{cs}| = 0.929(24)(16)(2)(9) \quad [\Lambda_c \to \Lambda \ell \nu, \text{Ref. } [492]\,], \tag{150}$$

where the uncertainties are from the lattice calculation, from the $\Lambda_c \to \Lambda \ell \nu$ branching fractions, from the Λ_c lifetime, and from the missing long-distance QED corrections, respectively.

In Fig. 20, we summarize the results for $|V_{cd}|$ and $|V_{cs}|$ from leptonic and semileptonic decays, and compare them to determinations from neutrino scattering (for $|V_{cd}|$ only) and global fits assuming CKM unitarity (see [225,396]). For both $|V_{cd}|$ and $|V_{cs}|$, the errors in the direct determinations from leptonic and semileptonic decays are approximately one order of magnitude larger than the indirect determination from CKM unitarity.

In order to provide final estimates, we average the available results from the different processes separately for each value of N_f and obtain

$$N_f = 2+1+1\text{:}\ \begin{cases} |V_{cd}| = 0.2229(64) \\ |V_{cs}| = 0.9667(96) \end{cases} \quad [\text{FLAG average, Refs. } [20, 43, 65, 123]\,], \tag{151}$$

$$N_f = 2+1\text{:}\ \begin{cases} |V_{cd}| = 0.2165(49) \\ |V_{cs}| = 0.973(14) \end{cases} \quad [\text{FLAG average, Refs. } [28, 29, 59\text{–}62, 64, 66, 492]\,], \tag{152}$$

where the errors include both theoretical and experimental uncertainties, and scale factors equal to $\sqrt{\chi^2/\text{dof}}$ of 1.88 and 1.26 have been included for $|V_{cd}|_{N_f=2+1+1}$ and $|V_{cs}|_{N_f=2+1}$, respectively. These averages also appear in Fig. 20, and are compatible with the values from the CKM global fit based on unitarity [396] within at most 1.5σ. The slight increases in the uncertainties of the $N_f = 2+1+1$ averages compared to FLAG 21 are due to the inclusion of QED systematic

uncertainties (treated as 100% correlated between the different processes) and the scale factors. The large scale factor for $|V_{cd}|_{N_f=2+1+1}$ is caused by the $D_s \to K\ell\nu$ result that has large uncertainty but also a considerably higher central value. Removing this result would change the average to $|V_{cd}|_{N_f=2+1+1} = 0.2214(44)$.

Using the lattice determinations of $|V_{cd}|$ and $|V_{cs}|$ in Eqs. (151), (152) and $|V_{cb}| \approx 0.04$, we can test the unitarity of the second row of the CKM matrix. We obtain

$$N_f = 2+1+1\text{: } |V_{cd}|^2 + |V_{cs}|^2 + |V_{cb}|^2 - 1 = -0.01(2) \quad \text{[FLAG average, Refs. [20, 43, 65, 123]]}, \tag{153}$$

$$N_f = 2+1\text{: } |V_{cd}|^2 + |V_{cs}|^2 + |V_{cb}|^2 - 1 = 0.00(3) \quad \text{[FLAG average, Refs. [28, 29, 59–62, 64, 66, 492]]}. \tag{154}$$

VIII. BOTTOM-HADRON DECAYS AND MIXINGS

Working group members: Y. Aoki, M. Della Morte, E. Lunghi, S. Meinel, C. Monahan, A. Vaquero

Exclusive (semi)leptonic decays and mixing processes of $B_{(s)}$ mesons play a crucial role in flavor physics. In particular, they contain important information for the investigation of the $b-d$ unitarity triangle in the Cabibbo-Kobayashi-Maskawa (CKM) matrix, and provide ideal probes of physics beyond the Standard Model. The charged-current decay channels $B^+ \to l^+\nu_l$ and $B^0 \to \pi^- l^+\nu_l$, where l^+ is a charged lepton with ν_l being the corresponding neutrino, are essential in extracting the CKM matrix element $|V_{ub}|$. Similarly, the B to $D^{(*)}$ semileptonic transitions can be used to determine $|V_{cb}|$. Flavor-changing neutral-current (FCNC) processes, such as $B \to K^{(*)}\ell^+\ell^-$ and $B_{d(s)} \to \ell^+\ell^-$, occur only beyond the tree level in weak interactions and are suppressed in the Standard Model. Therefore, these processes could be sensitive to new physics, since heavy particles can contribute to the loop diagrams. FCNC processes are also suitable channels for the extraction of the CKM matrix elements involving the top quark, which appears in loop contributions. The decays $B \to D^{(*)}\ell\nu$ and $B \to K^{(*)}\ell\ell$ can also be used to test lepton flavor universality by comparing results for $\ell = e$, μ and τ. In particular, anomalies have been seen in the ratios $R(D^{(*)}) = \mathcal{B}(B \to D^{(*)}\tau\nu)/\mathcal{B}(B \to D^{(*)}\ell\nu)_{\ell=e,\mu}$ and $R(K^{(*)}) = \mathcal{B}(B \to K^{(*)}\mu\mu)/\mathcal{B}(B \to K^{(*)}ee)$, although the latter are no longer statistically significant. In addition, the neutral $B_{d(s)}$-meson mixings are FCNC processes and are dominated by the 1-loop "box" diagrams containing the top quark and the W bosons. Thus, using the experimentally measured neutral $B^0_{d(s)}$-meson oscillation frequencies, $\Delta M_{d(s)}$, and the theoretical calculations for the relevant hadronic mixing matrix elements, one can obtain $|V_{td}|$ and $|V_{ts}|$ in the Standard Model.

At the Large Hadron Collider, decays of b quarks can also be probed with Λ_b and other bottom baryons, which can provide complementary constraints on physics beyond the Standard Model. The most important processes are the charged-current decays $\Lambda_b \to p\ell\bar{\nu}$ and $\Lambda_b \to \Lambda_c\ell\bar{\nu}$, and the neutral-current decay $\Lambda_b \to \Lambda\ell^+\ell^-$.

Accommodating the light quarks and the b quark simultaneously in lattice-QCD computations is a challenging endeavor. To incorporate the pion and the b hadrons with their physical masses, the simulations have to be performed using a lattice that is large enough in physical units to accommodate light pions without significant finite-volume effects, but, at the same time, fine enough to keep the heavy quark discretization errors under control. This usually results in a lattice size $\hat{L} = L/a \sim \mathcal{O}(10^2)$, where a is the lattice spacing and L is the physical (dimensionful) box size. The most ambitious calculations are now using such volumes; however, many ensembles are smaller. Therefore, in addition to employing chiral perturbation theory for the extrapolations in the light-quark mass, current lattice calculations for quantities involving b hadrons often make use of effective theories that allow one to expand in inverse powers of m_b. In this regard, two general approaches are widely adopted. On the one hand, effective field theories such as heavy-quark effective theory (HQET) and nonrelativistic QCD (NRQCD) can be directly implemented in numerical computations. On the other hand, a relativistic quark action can be improved *à la* Symanzik to suppress cutoff errors, and then reinterpreted in a manner that is suitable for heavy-quark physics calculations. This latter strategy is often referred to as the method of the relativistic heavy-quark action (RHQA). The utilization of such effective theories inevitably introduces systematic uncertainties that are not present in light-quark calculations. These uncertainties can arise from the truncation of the expansion in constructing the effective theories (as in HQET and NRQCD), or from more intricate cutoff effects (as in NRQCD and RHQA). They can also be introduced through more complicated renormalization procedures, which often lead to significant systematic

effects in matching the lattice operators to their continuum counterparts. For instance, due to the use of different actions for the heavy and the light quarks, it is more difficult to construct absolutely normalized bottom-light currents.

Complementary to the above "effective theory approaches," another popular method is to simulate the heavy and the light quarks using the same (typically Symanzik-improved) lattice action at several values of the heavy-quark mass m_h with $am_h < 1$ and $m_h < m_b$. This enables one to employ HQET-inspired relations to extrapolate the computed quantities to the physical b mass. When combined with results obtained in the static heavy-quark limit, this approach can be rendered into an interpolation, instead of extrapolation, in m_h. The discretization errors are the main source of the systematic effects in this method, and very small lattice spacings are needed to keep such errors under control.

In recent years, it has also been possible to perform lattice simulations at very fine lattice spacings and treat heavy quarks as fully relativistic fermions without resorting to effective field theories. Such simulations are, of course, very demanding in computing resources.

Because of the challenge described above, efforts to obtain reliable, accurate lattice-QCD results for the physics of the b quark have been enormous. These efforts include significant theoretical progress in formulating QCD with heavy quarks on the lattice. This aspect is briefly reviewed in Appendix A. 1. 3 of FLAG 19 [4].

In this section, we summarize the results of the B-meson leptonic decay constants, the neutral B-mixing parameters, and the semileptonic form factors of B mesons and Λ_b baryons, from lattice QCD. To focus on the calculations that have strong phenomenological impact, we limit the review to results based on modern simulations containing dynamical fermions with reasonably light pion masses (below approximately 500 MeV).

For heavy-meson decay constants and mixing parameters, estimates of the quantity $\delta(a_{\min})$ described in Sec. II A 2 are provided, where possible, for all computations entering the final FLAG averages or ranges. For heavy-hadron semileptonic-decay form factors, implementing this data-driven continuum-limit criterion was found to be not feasible. The problem is that these quantities are functions of the momentum transfer in addition to the other lattice parameters, and many calculations are based on global fits whose reconstruction was not possible.

Following our review of $B_{(s)}$-meson leptonic decay constants, the neutral B-meson mixing parameters, and semileptonic form factors, we then interpret our results within the context of the Standard Model. We combine our best-determined values of the hadronic matrix elements with the most recent experimentally measured branching fractions to obtain $|V_{ub}|$ and $|V_{cb}|$, and compare these results to those obtained from inclusive semileptonic B decays.

A. Leptonic decay constants f_B and f_{B_s}

The B- and B_s-meson decay constants are crucial inputs for extracting information from leptonic B decays. Charged B mesons can decay to a lepton-neutrino final state through the charged-current weak interaction. On the other hand, neutral $B_{d(s)}$ mesons can decay to a charged-lepton pair via a FCNC process.

In the Standard Model, the decay rate for $B^+_{(s)} \to \ell^+\nu_\ell$ is described by a formula identical to Eq. (124), with $D_{(s)}$ replaced by $B_{(s)}$, $f_{D_{(s)}}$ replaced by $f_{B_{(s)}}$, and the relevant CKM matrix element V_{cq} replaced by V_{bq},

$$\Gamma(B_{(s)} \to \ell\nu_\ell) = \frac{m_{B_{(s)}}}{8\pi} G_F^2 f^2_{B_{(s)}} |V_{bq}|^2 m_\ell^2 \left(1 - \frac{m_\ell^2}{m^2_{B_{(s)}}}\right)^2. \tag{155}$$

The only two-body charged-current B-meson decay that has been observed so far is $B^+ \to \tau^+\nu_\tau$, which has been measured by the Belle and *BABAR* collaborations [514,515]. Both collaborations have reported results with errors around 20%. These measurements can be used to extract $|V_{ub}|$ when combined with lattice-QCD predictions of the corresponding decay constant, but the experimental uncertainties currently preclude a precise determination.

Neutral $B_{d(s)}$-meson decays to a charged-lepton pair $B_{d(s)} \to \ell^+\ell^-$ is a FCNC process, and can only occur at 1-loop in the Standard Model. Hence these processes are expected to be rare, and are sensitive to physics beyond the Standard Model. The corresponding expression for the branching fraction has the form

$$B(B_q \to \ell^+\ell^-) = \tau_{B_q} \frac{G_F^2}{\pi} Y \left(\frac{\alpha_s}{4\pi \sin^2\Theta_W}\right)^2 \times m_{B_q} f^2_{B_q} |V^*_{tb} V_{tq}|^2 m_\ell^2 \sqrt{1 - 4\frac{m_\ell^2}{m^2_{B_q}}}, \tag{156}$$

where the light quark $q = s$ or d, τ_{B_q} is the mean meson lifetime, and the function Y includes NLO QCD and electroweak corrections that depend on the strong coupling α_s and the weak mixing angle Θ_W [378,516]. Evidence for the $B_s \to \mu^+\mu^-$ decay was first observed by the LHCb [517] and CMS collaborations, and a combined analysis was presented in 2014 in Ref. [518]. In 2020, the ATLAS [519], CMS [520] and LHCb [521] collaborations reported their measurements from a preliminary combined analysis as [522]

$$B(B \to \mu^+\mu^-) < 1.9 \times 10^{-10} \text{ at } 95\% \text{ CL},$$
$$B(B_s \to \mu^+\mu^-) = (2.69^{+0.37}_{-0.35}) \times 10^{-9}, \quad (157)$$

which are compatible with the Standard Model predictions within approximately 2 standard deviations [523]. More recently, updated observations have been reported by the LHCb collaboration [524] and the CMS collaboration [525], but these results do not improve on the precision of the combined analysis.[42] We note that the errors of these results are currently too large to enable a precise determination of $|V_{td}|$ and $|V_{ts}|$.

The related radiative leptonic decay, $B_s \to \mu^+\mu^-\gamma$, is another FCNC process that is sensitive to new physics and is expected to occur at a comparable rate to $B_s \to \mu^+\mu^-$. Recent searches for this decay by the LHCb collaboration found an upper limit of [524,527]

$$B(B_s \to \mu^+\mu^-\gamma) < 2.0 \times 10^{-9} \quad \text{at } 95\% \text{ CL}, \quad (158)$$

in the kinematic region $m_{\mu\mu} > 4.9$ GeV. The dominant hadronic contributions are parametrized by local form factors and by nonlocal resonance contributions, which have been estimated using light-cone sum rules [528], QCD-inspired models [529,530], and from models of the transition form factors based on lattice calculations of the D_s meson, assuming vector-meson dominance [531]. The first lattice calculation of the local form factors were reported in [532]. The form factors provide a reasonable estimate of the decay rate for large di-muon invariant mass, $q^2 > (4.15 \text{ GeV})^2$, where long-distance contributions are expected to be subdominant. Improved determinations of the branching fraction at lower di-muon invariant masses requires a systematic and quantitative treatment of the resonance region.

The rare leptonic $B^+ \to \ell^+\nu_\ell\gamma$ decay is proportional to $|V_{ub}|^2$ and has been constrained by the CLEO [533], *BABAR* [534], and Belle Collaborations [535,536]. The most stringent constraint, in the region $E_\gamma > 1$ GeV, is [536]

$$B(B^+ \to \ell^+\nu_\ell\gamma) < 3.0 \times 10^{-6} \quad \text{at } 90\% \text{ CL}. \quad (159)$$

This branching fraction can be expressed in terms of form factors that are yet to be directly determined on the lattice but have been modeled using QCD sum rules and dispersive approaches combined with an expansion in $\Lambda_{\rm QCD}/m_B$ and $\Lambda_{\rm QCD}/E_\gamma$ [537]. At leading order in this expansion, the branching fraction depends only on the light-cone distribution amplitude of the B meson. At present, this channel is primarily viewed as providing experimental constraints on the light-cone distribution amplitude. Direct calculations of this distribution amplitude from lattice QCD are now feasible with recent theoretical developments [538,539] and, in combination with experimental data, would provide a novel method for the determination of $|V_{ub}|^2$.

The decay constants f_{B_q} (with $q = u, d, s$) parametrize the matrix elements of the corresponding axial-vector currents $A^\mu_{bq} = \bar{b}\gamma^\mu\gamma^5 q$ analogously to the definition of f_{D_q} in Sec. VII A

$$\langle 0|A^\mu|B_q(p)\rangle = ip^\mu_{B_q} f_{B_q}. \quad (160)$$

For heavy-light mesons, it is convenient to define and analyze the quantity

$$\Phi_{B_q} \equiv f_{B_q}\sqrt{m_{B_q}}, \quad (161)$$

which approaches a constant (up to logarithmic corrections) in the $m_{B_q} \to \infty$ limit, because of heavy-quark symmetry. In the following discussion, we denote lattice data for Φ, and the corresponding decay constant f, obtained at a heavy-quark mass m_h and light valence-quark mass m_ℓ as $\Phi_{h\ell}$ and f_{hl}, to differentiate them from the corresponding quantities at the physical b and light-quark masses.

The SU(3)-breaking ratio f_{B_s}/f_B is of phenomenological interest, because many systematic effects can be partially reduced in lattice-QCD calculations of this ratio. The discretization errors, heavy-quark-mass tuning effects, and renormalization/matching errors may all be partially reduced.

This SU(3)-breaking ratio is, however, still sensitive to the chiral extrapolation. Provided the chiral extrapolation is under control, one can then adopt f_{B_s}/f_B as an input in extracting phenomenologically interesting quantities. In addition, it often happens to be easier to obtain lattice results for f_{B_s} with smaller errors than direct calculations of f_B. Therefore, one can combine the B_s-meson decay constant with the SU(3)-breaking ratio to calculate f_B. Such a strategy can lead to better precision in the computation of the B-meson decay constant, and has been adopted by the ETM [36,73] and the HPQCD collaborations [70]. An alternative strategy to the direct calculation of f_{B_s}, used in Ref. [75], is to obtain the B_s-meson decay constant by combining the D_s-meson decay constant with the ratio f_{B_s}/f_{D_s}.

It is clear that the decay constants for charged and neutral B mesons play different roles in flavor-physics phenomenology. Knowledge of the B^+-meson decay constant f_{B^+} is essential for extracting $|V_{ub}|$ from leptonic B^+ decays. The neutral B-meson decay constants f_{B^0} and f_{B_s} are inputs to searches for new physics in rare leptonic B^0 decays. In view of this, it is desirable to include isospin-breaking effects in lattice computations for these quantities

[42]The PDG quotes the branching fraction $B(B^0 \to \mu^+\mu^-) < 1.5 \times 10^{-10}$ at 90% CL [274]. Ref. [526] obtains $B(B^0 \to \mu^+\mu^-) = (0.56 \pm 70) \times 10^{-10}$ using a correlated global analysis.

TABLE 33. Decay constants of the B, B^+, B^0 and B_s mesons (in MeV). Here f_B stands for the mean value of f_{B^+} and f_{B^0}, extrapolated (or interpolated) in the mass of the light valence-quark to the physical value of m_{ud}.

Collaboration	Ref.	N_f	Publication status	Continuum extrapolation	Chiral extrapolation	Finite volume	Renormalization/matching	Heavy-quark treatment	f_{B^+}	f_{B^0}	f_B	f_{B_s}
Frezzotti 24	[532]	$2+1+1$	P	★	★	★	★	✓	⋯	⋯	⋯	224.5(5.0)
FNAL/MILC 17	[20]	$2+1+1$	A	★	★	★	★	✓	189.4(1.4)	190.5(1.3)	189.9(1.4)	230.7(1.2)
HPQCD 17A	[68]	$2+1+1$	A	○	★	★	○	✓	⋯	⋯	196(6)	236(7)
ETM 16B	[36]	$2+1+1$	A	★	○	○	○	✓	⋯	⋯	193(6)	229(5)
ETM 13E	[540]	$2+1+1$	C	★	○	○	○	✓	⋯	⋯	196(9)	235(9)
HPQCD 13	[67]	$2+1+1$	A	○	★	★	○	✓	184(4)	188(4)	186(4)	224(5)
RBC/UKQCD 14	[72]	$2+1$	A	○	○	○	○	✓	195.6(14.9)	199.5(12.6)	—	235.4(12.2)
RBC/UKQCD 14A	[71]	$2+1$	A	○	○	○	○	✓	⋯	⋯	219(31)	264(37)
RBC/UKQCD 13A	[541]	$2+1$	C	○	○	○	○	✓	⋯	⋯	$191(6)_{\text{stat}}$[a]	$233\,(5)_{\text{stat}}$[a]
HPQCD 12	[70]	$2+1$	A	○	○	○	○	✓	⋯	⋯	191(9)	228(10)
HPQCD 12	[70]	$2+1$	A	○	○	○	○	✓	⋯	⋯	189(4)[b]	⋯
HPQCD 11A	[69]	$2+1$	A	★	○	★	★	✓	⋯	⋯	⋯	225(4)[c]
FNAL/MILC 11	[60]	$2+1$	A	○	○	★	○	✓	197(9)	⋯	⋯	242(10)
HPQCD 09	[78]	$2+1$	A	○	○	○	○	✓	⋯	⋯	190(13)[d]	231(15)[d]
Balasubramamian 19[e]	[75]	2	A	★	★	★	○	✓	⋯	⋯	⋯	$215(10)(2)(^{+2}_{-5})$
ALPHA 14	[74]	2	A	★	★	★	★	✓	⋯	⋯	186(13)	224(14)
ALPHA 13	[542]	2	C	★	★	★	★	✓	⋯	⋯	187(12)(2)	224(13)
ETM 13B, 13C[f]	[73,543]	2	A	★	○	★	○	✓	⋯	⋯	189(8)	228(8)
ALPHA 12A	[544]	2	C	★	★	★	★	✓	⋯	⋯	193(9)(4)	219(12)
ETM 12B	[545]	2	C	★	○	★	○	✓	⋯	⋯	197(10)	234(6)
ALPHA 11	[546]	2	C	★	○	★	★	✓	⋯	⋯	174(11)(2)	⋯
ETM 11A	[272]	2	A	★	○	★	○	✓	⋯	⋯	195(12)	232(10)
ETM 09D	[547]	2	A	★	○	○	○	✓	⋯	⋯	194(16)	235(12)

[a]Statistical errors only.

[b]Obtained by combining f_{B_s} from HPQCD 11A with f_{B_s}/f_B calculated in this work.

[c]This result uses one ensemble per lattice spacing with light to strange sea-quark mass ratio $m_\ell/m_s \approx 0.2$.

[d]This result uses an old determination of $r_1 = 0.321(5)$ fm from Ref. [120] that has since been superseded.

[e]Obtained by combining f_{D_s}, updated in this work, with f_{B_s}/f_{D_s}, calculated in this work.

[f]Update of ETM 11A and 12B.

and to provide lattice results for both f_{B^+} and f_{B^0}. With the high precision of recent lattice calculations, isospin splittings for B-meson decay constants can be significant, and will play an important role in the foreseeable future.

A few collaborations have reported f_{B^+} and f_{B^0} separately by taking into account strong isospin effects in the valence sector, and estimated the corrections from electromagnetism [20,60,67,72]. The $N_f = 2+1+1$ strong isospin-breaking effect was computed in HPQCD 13 [67] (see Table 33 in this subsection). However, since only unitary points (with equal sea- and valence-quark masses) were considered in HPQCD 13 [67], this procedure only correctly accounts for the effect from the valence-quark masses, while introducing a spurious sea-quark contribution. The decay constants f_{B^+} and f_{B^0} are also separately reported in FNAL/MILC 17 [20] by taking into account the strong-isospin effect. The FNAL/MILC results were obtained by keeping the averaged light sea-quark mass fixed when varying the quark masses in their analysis procedure. Their finding indicates that the strong isospin-breaking effects, $f_{B^+} - f_B \sim 0.5$ MeV, could be smaller than those suggested by previous computations. One would have to take into account QED effects in the B-meson leptonic decay rates to properly use these results for extracting phenomenologically relevant information.[43]

[43]See Ref. [283] for a strategy that has been proposed to account for QED effects.

TABLE 34. Ratios of decay constants of the B and B_s mesons (for details see Table 33).

Collaboration	Ref.	N_f	Publication status	Continuum extrapolation	Chiral extrapolation	Finite volume	Renormalization/matching	Heavy-quark treatment	f_{B_s}/f_{B^+}	f_{B_s}/f_{B^0}	f_{B_s}/f_B
FNAL/MILC 17	[20]	$2+1+1$	A	★	★	★	★	✓	1.2180(49)	1.2109(41)	···
HPQCD 17A	[68]	$2+1+1$	A	○	★	★	○	✓	···	···	1.207(7)
ETM 16B	[36]	$2+1+1$	A	★	○	○	○	✓	···	···	1.184(25)
ETM 13E	[540]	$2+1+1$	C	★	○	○	○	✓	···	···	1.201(25)
HPQCD 13	[67]	$2+1+1$	A	○	★	★	○	✓	1.217(8)	1.194(7)	1.205(7)
QCDSF/UKQCD/CSSM 22	[548]	$2+1$	C	★	★	○	○	✓	···	···	$1.159(15)(^{+76}_{-71})$
RBC/UKQCD 18A	[76]	$2+1$	P	★	★	★	★	✓	···	···	$1.1949(60)(^{+95}_{-175})$
RBC/UKQCD 14	[72]	$2+1$	A	○	○	○	○	✓	1.223(71)	1.197(50)	···
RBC/UKQCD 14A	[71]	$2+1$	A	○	○	○	○	✓	···	···	1.193(48)
RBC/UKQCD 13A	[541]	$2+1$	C	○	○	○	○	✓	···	···	$1.20\,(2)_{\text{stat}}$[a]
HPQCD 12	[70]	$2+1$	A	○	○	○	○	✓	···	···	1.188(18)
FNAL/MILC 11	[60]	$2+1$	A	○	○	★	○	✓	1.229(26)	···	···
RBC/UKQCD 10C	[549]	$2+1$	A	■	■	■	○	✓	···	···	1.15(12)
HPQCD 09	[78]	$2+1$	A	○	○	○	○	✓	···	···	1.226(26)
ALPHA 14	[74]	2	A	★	★	★	★	✓	···	···	1.203(65)
ALPHA 13	[542]	2	C	★	★	★	★	✓	···	···	1.195(61)(20)
ETM 13B, 13C[b]	[73,543]	2	A	★	○	★	○	✓	···	···	1.206(24)
ALPHA 12A	[544]	2	C	★	★	★	★	✓	···	···	1.13(6)
ETM 12B	[545]	2	C	★	○	★	○	✓	···	···	1.19(5)
ETM 11A	[272]	2	A	○	○	★	○	✓	···	···	1.19(5)

[a]Statistical errors only.

[b]Update of ETM 11A and 12B.

Currently, errors on the experimental measurements of these decay rates are still very large. In this review, we will therefore concentrate on the isospin-averaged result f_B and the B_s-meson decay constant, as well as the SU(3)-breaking ratio f_{B_s}/f_B.

The status of lattice-QCD computations for B-meson decay constants and the SU(3)-breaking ratio, using gauge-field ensembles with light dynamical fermions, is summarized in Tables 33 and 34. Figures 21 and 22 contain the graphical presentation of the collected results and our averages. Most results in these tables and plots have been reviewed in detail in FLAG 19 [4] and in FLAG 21 [5]. Here, we describe the new results that have appeared since January 2021.

We also review the continuum-limit quantity, $\delta(a_{\min})$, described in Sec. II. We estimate, where possible, $\delta(a_{\min})$ for results entering the FLAG averages of f_B, f_{B_s}, and f_{B_s}/f_B, but we do not use $\delta(a_{\min})$ for averaging. We include estimates of $\delta(a_{\min})$ for those calculations that explicitly provide the relevant data in the manuscript.

As lattice calculations of leptonic decays have become statistically more precise, results are often dominated by systematic uncertainties. The continuum extrapolation is frequently the largest source of systematic uncertainty for lattice calculations of heavy quarks, for which the heavy-quark discretization can introduce effects of the $\mathcal{O}(am)^n$, and a more quantitative measure of discretization effects is a useful guide to the quality of the continuum extrapolation. For the lattice calculations of leptonic decay constants of bottom hadrons that appear in this review, the continuum-limit quantity should be interpreted with caution, because many final results are quoted from combined chiral-continuum extrapolations and, typically, more recent computations do not quote numerical values for the leptonic decay constants at the finest lattice spacings. Moreover, the finest ensembles may not be at, or close to, the physical pion mass. Thus, we generally quote our estimations of $\delta(a_{\min})$ to one significant figure because the natural size of the uncertainty on $\delta(a_{\min})$ is $\mathcal{O}(1)$.

There have been no new $N_f = 2$ calculations of f_B, f_{B_s}, or f_{B_s}/f_B. Therefore, our averages for these quantities stay

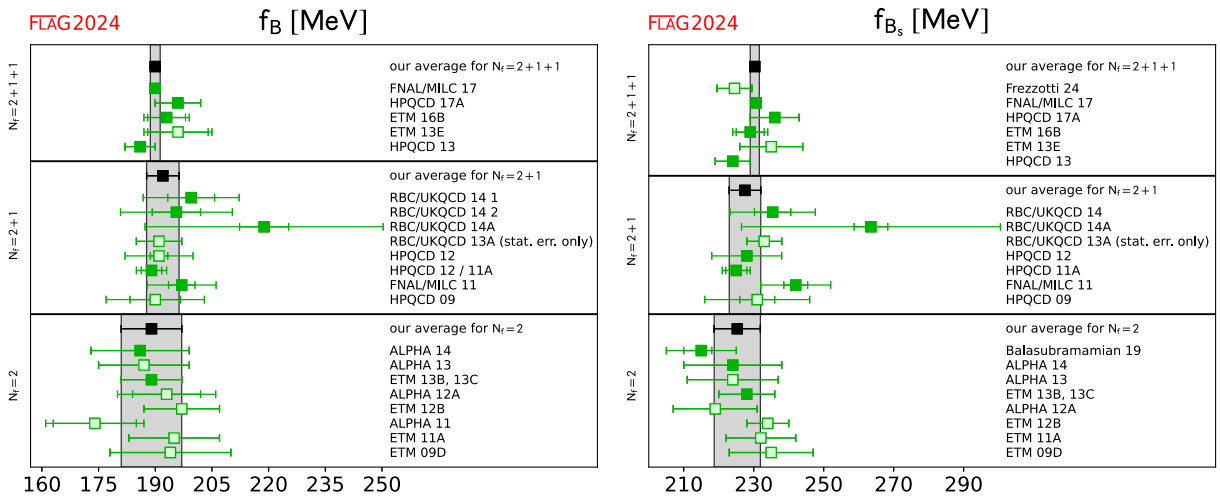


FIG. 21. Decay constants of the B and B_s mesons. The values are taken from Table 33 (the f_B entry for FNAL/MILC 11 represents f_{B^+}). The significance of the colors is explained in Sec. II. The black squares and gray bands indicate our averages in Eqs. (162), (165), (168), (163), (166) and (169).

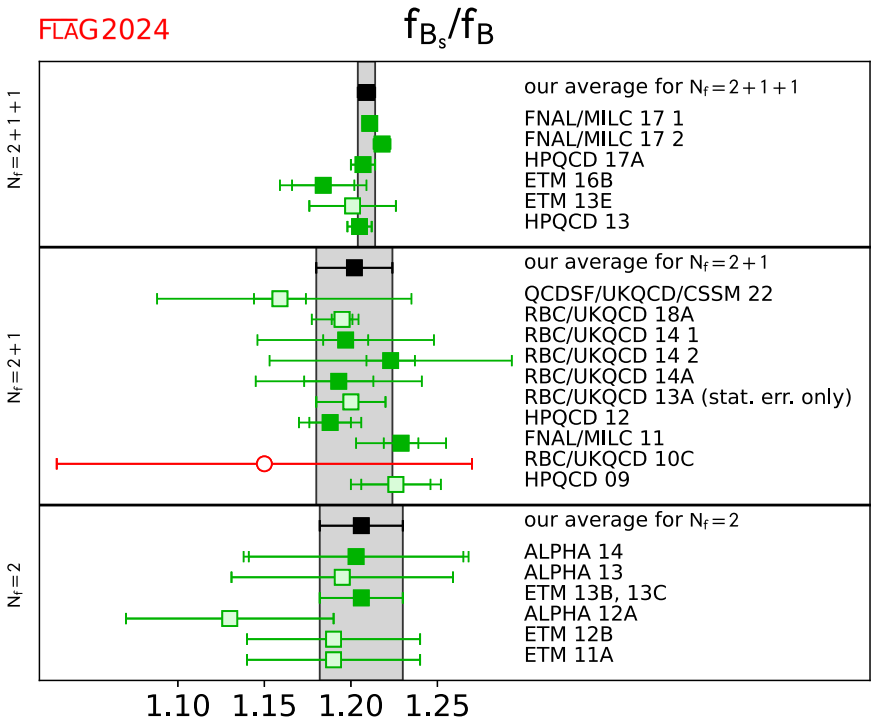


FIG. 22. Ratio of the decay constants of the B and B_s mesons. The values are taken from Table 34. Results labeled as FNAL/MILC 17 1 and FNAL/MILC 17 2 correspond to those for f_{B_s}/f_{B^0} and f_{B_s}/f_{B^+} reported in FNAL/MILC 17. The significance of the colors is explained in Sec. II. The black squares and gray bands indicate our averages in Eqs. (164), (167), and (170).

the same as those in FLAG 21 [5]. Our estimates for the continuum-limit quantity $\delta(a_{\min})$ are $\delta(a_{\min}) = 0.01$ for f_{B_s} in Ref. [73]. Data do not permit estimates of the continuum-limit quantity for f_B and f_{B_s}/f_B from Ref. [73], but discretization effects are generally small. From Ref. [74] we obtain $\delta(a_{\min}) = 0.6$ for f_B, $\delta(a_{\min}) = 0.3$ for f_{B_s}, and $\delta(a_{\min}) = 0.3$ for f_{B_s}/f_B. Finally, $\delta(a_{\min}) = 2.6$ for f_{B_s} in [75].

Our averages of the $N_f = 2$ results are

$$N_f = 2: \quad f_B = 188(7)\ \text{MeV} \qquad \text{Refs. [73, 74]}, \qquad (162)$$

$$N_f = 2: \quad f_{B_s} = 225.3(6.6)\ \text{MeV} \qquad \text{Refs. [73–75]}, \qquad (163)$$

$$N_f = 2: \quad \frac{f_{B_s}}{f_B} = 1.206(0.023) \qquad \text{Refs. [73, 74]}. \qquad (164)$$

Two new $N_f = 2 + 1$ calculations of f_{B_s}/f_B were presented in conference proceedings after the publication of FLAG 21 [5]. Only one of these calculations, Ref. [548], provides a preliminary quantitative result. In Table 34, this result is labeled QCDSF/UKQCD/CSSM 22 [548]. The second work, Ref. [550], is described in the text below, but not listed in Table 34.

In QCDSF/UKQCD/CSSM 22 [548] the QCDSF/UKQCD/CSSM collaboration presented the ratio of decay constants, f_{B_s}/f_B, using $N_f = 2 + 1$ dynamical ensembles generated using nonperturbatively $\mathcal{O}(a)$-improved clover-Wilson fermions. Four lattice spacings, of $a = 0.082, 0.074$, 0.068, and 0.059 fm, were used, with pion masses ranging from 155 to 468 MeV, and lattice sizes between 2.37 and 4.35 fm. The light-quark masses were tuned using the QCDSF procedure [551], for fixing the light- and strange-quark masses. Quark masses were chosen to keep the value of the SU(3) flavor-singlet mass, $\bar{m} = (2m_\ell + m_s)/3$, constant. Heavy quarks were simulated with a relativistic heavy-quark (RHQ) action, with bare-quark masses chosen to keep the SU(3) flavor-singlet mass, $X_B^2 = (2M_{B_\ell} + M_{B_s})/3$, constant. The bare parameters of the RHQ action were chosen to ensure that the masses and hyperfine splitting of the X_B and X_{B^*} mesons reproduce the properties of the physical, spin-averaged X_B and X_{B^*} [552].

The chiral extrapolation was performed using both linear and quadratic terms in $(M_\pi^2/M_X^2 - 1)$ and assuming that the SU(3) flavor breaking does not depend on the lattice spacing. The reported value for the ratio of decay constants assumes that the renormalization parameters for light- and strange-quark currents are approximately equal, but this is only true near the SU(3)-symmetric point. Effects of the order of 1%–2% are expected near the physical point and calculations of the relevant parameters on near-physical ensembles are underway. Tests of $\mathcal{O}(a^2)$ discretization effects indicate little dependence and the final results are quoted from the subset of ensembles with $m_\pi L > 4$ and assuming no dependence on a^2. Tests of heavy-quark mistuning effects indicate that the ratio of decay constants are minimally affected.

The RBC/UKQCD collaboration described ongoing efforts to calculate pseudoscalar and vector heavy-meson decay constants in Ref. [550], using $N_f = 2 + 1$ dynamical ensembles generated using domain wall fermions (DWF). Four lattice spacings, of $a = 0.11$, 0.083, 0.071, and 0.063 fm were used, with pion masses ranging from 267 to 433 MeV, and lattice sizes between 2.0 and 3.4 fm. Light and strange quarks were simulated with the Shamir DWF discretization and charm quarks were simulated with Möbius DWF action. These discretizations correspond to two different choices for the DWF kernel. The Möbius DWF are loosely equivalent to Shamir DWF at twice the extension in the fifth dimensions [12]. Ref. [550] presents a preliminary analysis with a two-step procedure. The first step corrects for strange-quark-mass mistunings and the second applies NLO SU(2) heavy-meson chiral perturbation theory to carry out a chiral-continuum extrapolation using various fit *Ansätze* to enable a full systematic error analysis. This analysis is ongoing at time of publication.

The results of Refs. [548,550] have not been published and therefore neither calculation is included in our average. Thus, our averages remain the same as in FLAG 21 [5],

$$N_f = 2 + 1: \quad f_B = 192.0(4.3)\ \text{MeV} \quad \text{Refs. [60, 69–72]}, \tag{165}$$

$$N_f = 2 + 1: \quad f_{B_s} = 228.4(3.7)\ \text{MeV} \quad \text{Refs. [60, 69–72]}, \tag{166}$$

$$N_f = 2 + 1: \quad \frac{f_{B_s}}{f_B} = 1.201(0.016) \quad \text{Refs. [60, 70–72, 76]}. \tag{167}$$

Our estimates for the continuum-limit quantity $\delta(a_{\min})$ for the results entering the FLAG averages for the $N_f = 2 + 1$ bottom-hadron leptonic decay constants, and their ratio, are $\delta(a_{\min}) = 5.6$ and $\delta(a_{\min}) = 7.4$ for f_{B_s} and f_B, respectively, in Ref. [60]; $\delta(a_{\min}) = 1.5$ for f_B in Ref. [69]; $\delta(a_{\min}) = 0.01$ and $\delta(a_{\min}) = 0.6$ for f_{B_s} and f_B, respectively, in Ref. [70]; $\delta(a_{\min}) = 1.9$ and $\delta(a_{\min}) = 2.3$ for f_{B_s} and f_B, respectively, in Ref. [71]; and $\delta(a_{\min}) = 1.7$ for f_{B_s} in Ref. [72]. For f_{B_s}/f_B we obtain approximately $\delta(a_{\min}) = 0.4$ for [60], approximately 2 for [70,71], 3 for [72], and around 0.5 for [76].

No new $N_f = 2 + 1 + 1$ calculations of f_B and f_{B_s}/f_B have appeared since FLAG 21. There has been one new calculation of $f_{B_{(s)}}$ in Ref. [532], labeled Frezzotti 24 in Table 33.

As part of the determination of the form factors for the radiative leptonic decay $B_s \to \mu^+\mu^-\gamma$, the decay constant f_{B_s} was determined in Ref. [532]. This work used ensembles with $N_f = 2 + 1 + 1$ clover-Wilson twisted-mass fermions at maximal twist. Four lattice spacings, ranging from 0.057 to 0.091 fm, were included and pion masses spanned a range from 137 to 175 MeV. The heavy-strange meson was simulated using clover-Wilson twisted-mass fermions at a range of heavy-strange masses, extrapolated up to the physical B_s mass. Reference [532] determined f_{H_s} from both two-point functions and the

spatial part of the axial hadronic tensor to better constrain the continuum limit because these determinations differ only by discretization effects. The results from both methods were simultaneously extrapolated to the continuum limit at fixed values of the heavy-strange meson mass M_{H_s}, with six different fit variations for each of the five values of M_{H_s}. The results of each fit were combined using the Akaike information criterion [553] and the corresponding continuum decay constants were then extrapolated to the physical B_s mass. The extrapolation in the heavy-strange mass was carried out using a fit form guided by HQET, with modifications to account for the anomalous dimension of the axial current in HQET and the matching between QCD and HQET.

Reference [532] has not been published at the time of publication of this review. Therefore, our averages for f_B, $f_{B_{(s)}}$ and f_{B_s}/f_B remain the same as in FLAG 21 [5],

$$N_f = 2+1+1: \quad f_B = 190.0(1.3)\ \text{MeV} \quad \text{Refs. [20, 36, 67, 68]}, \tag{168}$$

$$N_f = 2+1+1: \quad f_{B_s} = 230.3(1.3)\ \text{MeV} \quad \text{Refs. [20, 36, 67, 68]}, \tag{169}$$

$$N_f = 2+1+1: \quad \frac{f_{B_s}}{f_B} = 1.209(0.005) \quad \text{Refs. [20, 36, 67, 68]}. \tag{170}$$

The data reported in the calculations that appear in these averages do not permit estimates of $\delta(a_{\min})$.

The PDG presented averages for the $N_f = 2+1$ and $N_f = 2+1+1$ lattice-QCD determinations of the isospin-averaged f_B, f_{B_s} and f_{B_s}/f_B in 2024 [274]. The $N_f = 2+1$ and $N_f = 2+1+1$ lattice-computation results used in Ref. [274] are identical to those included in our current work, and the averages quoted in Ref. [274] are those determined in [4,5].

B. Neutral B-meson mixing matrix elements

Neutral B-meson mixing is induced in the Standard Model through 1-loop box diagrams to lowest order in the electroweak theory, similar to those for short-distance effects in neutral kaon mixing. The effective Hamiltonian is given by

$$\mathcal{H}_{\text{eff}}^{\Delta B=2,\text{SM}} = \frac{G_F^2 M_W^2}{16\pi^2}\left(\mathcal{F}_d^0 \mathcal{Q}_1^d + \mathcal{F}_s^0 \mathcal{Q}_1^s\right) + \text{H.c.}, \tag{171}$$

with

$$\mathcal{Q}_1^q = [\bar{b}\gamma^\mu(1-\gamma_5)q][\bar{b}\gamma_\mu(1-\gamma_5)q], \tag{172}$$

where $q = d$ or s. The short-distance function $\mathcal{F}_q^0$ in Eq. (171) is much simpler compared to the kaon mixing case due to the hierarchy in the CKM matrix elements. Here, only one term is relevant,

$$\mathcal{F}_q^0 = \lambda_{tq}^2 S_0(x_t) \tag{173}$$

where

$$\lambda_{tq} = V_{tq}^* V_{tb}, \tag{174}$$

and where $S_0(x_t)$ is an Inami-Lim function with $x_t = m_t^2/M_W^2$, which describes the basic electroweak loop contributions without QCD [378].

The transition amplitude for B_q^0 with $q = d$ or s can be written as

$$\begin{aligned}\langle \bar{B}_q^0 | \mathcal{H}_{\text{eff}}^{\Delta B=2} | B_q^0 \rangle = {} & \frac{G_F^2 M_W^2}{16\pi^2}[\lambda_{tq}^2 S_0(x_t)\eta_{2B}]\left(\frac{\bar{g}(\mu)^2}{4\pi}\right)^{-\gamma_0/(2\beta_0)} \\ & \times \exp\left\{\int_0^{\bar{g}(\mu)} dg \left(\frac{\gamma(g)}{\beta(g)} + \frac{\gamma_0}{\beta_0 g}\right)\right\} \\ & \times \langle \bar{B}_q^0 | Q_{\text{R}}^q(\mu) | B_q^0 \rangle + \text{H.c.},\end{aligned} \tag{175}$$

where $Q_{\text{R}}^q(\mu)$ is the renormalized four-fermion operator (usually in the NDR scheme of $\overline{\text{MS}}$). The running coupling $\bar{g}$, the β-function $\beta(g)$, and the anomalous dimension of the four-quark operator $\gamma(g)$ are defined in Eqs. (95) and (96). The product of μ-dependent terms on the second line of Eq. (175) is, of course, μ-independent (up to truncation errors arising from the use of perturbation theory). The explicit expression for the short-distance QCD correction factor η_{2B} (calculated to NLO) can be found in Ref. [371].

For historical reasons the B-meson-mixing matrix elements are often parametrized in terms of bag parameters defined as

$$B_{B_q}(\mu) = \frac{\langle \bar{B}_q^0 | Q_{\text{R}}^q(\mu) | B_q^0 \rangle}{\frac{8}{3} f_{B_q}^2 m_{B_q}^2}. \tag{176}$$

The renormalization-group-independent (RGI) B parameter $\hat{B}$ is defined as in the case of the kaon, and expressed to 2-loop order as

$$\hat{B}_{B_q} = \left(\frac{\bar{g}(\mu)^2}{4\pi}\right)^{-\gamma_0/(2\beta_0)} \left\{1 + \frac{\bar{g}(\mu)^2}{(4\pi)^2}\left[\frac{\beta_1\gamma_0 - \beta_0\gamma_1}{2\beta_0^2}\right]\right\} B_{B_q}(\mu), \tag{177}$$

with $\beta_0, \beta_1, \gamma_0$, and γ_1 defined in Eq. (97). Note, as Eq. (175) is evaluated above the bottom threshold ($m_b < \mu < m_t$), the active number of flavors here is $N_f = 5$.

Nonzero transition amplitudes result in a mass difference between the *CP* eigenstates of the neutral *B*-meson system. Writing the mass difference for a B_q^0 meson as Δm_q, its Standard Model prediction is

$$\Delta m_q = \frac{G_F^2 m_W^2 m_{B_q}}{6\pi^2} |\lambda_{tq}|^2 S_0(x_t) \eta_{2B} f_{B_q}^2 \hat{B}_{B_q}, \tag{178}$$

where λ_{tq} is defined in Eq. (174). Experimentally, the mass difference is determined from the oscillation frequency of the *CP* eigenstates. The frequencies are measured precisely with an error of less than a percent. Many different experiments have measured Δm_d, but the current average [225] is dominated by the LHC*b* experiment. For Δm_s the experimental average is again dominated by results from LHC*b* [225] and the precision reached is about one per mille. With these experimental results and lattice-QCD calculations of $f_{B_q}^2 \hat{B}_{B_q}$, λ_{tq} can be determined. In lattice-QCD calculations the flavor SU(3)-breaking ratio

$$\xi^2 = \frac{f_{B_s}^2 B_{B_s}}{f_{B_d}^2 B_{B_d}} \tag{179}$$

can be obtained more precisely than the individual B_q-mixing matrix elements because statistical and systematic errors cancel in part. From ξ^2, the ratio $|V_{td}/V_{ts}|$ can be determined and used to constrain the apex of the CKM triangle.

Neutral *B*-meson mixing, being loop-induced in the Standard Model, is also a sensitive probe of new physics. The most general $\Delta B = 2$ effective Hamiltonian that describes contributions to *B*-meson mixing in the Standard Model and beyond is given in terms of five local four-fermion operators

$$\mathcal{H}_{\text{eff,BSM}}^{\Delta B=2} = \sum_{q=d,s} \sum_{i=1}^{5} \mathcal{C}_i \mathcal{Q}_i^q, \tag{180}$$

where $\mathcal{Q}_1$ is defined in Eq. (172) and where

$$\begin{aligned}
\mathcal{Q}_2^q &= [\bar{b}(1-\gamma_5)q][\bar{b}(1-\gamma_5)q], \\
\mathcal{Q}_3^q &= [\bar{b}^\alpha(1-\gamma_5)q^\beta][\bar{b}^\beta(1-\gamma_5)q^\alpha], \\
\mathcal{Q}_4^q &= [\bar{b}(1-\gamma_5)q][\bar{b}(1+\gamma_5)q], \\
\mathcal{Q}_5^q &= [\bar{b}^\alpha(1-\gamma_5)q^\beta][\bar{b}^\beta(1+\gamma_5)q^\alpha],
\end{aligned} \tag{181}$$

with the superscripts α, β denoting color indices, which are shown only when they are contracted across the two bilinears. There are three other basis operators in the $\Delta B = 2$ effective Hamiltonian. When evaluated in QCD, however, they give identical matrix elements to the ones already listed due to parity invariance in QCD. The short-distance Wilson coefficients $\mathcal{C}_i$ depend on the underlying theory and can be calculated perturbatively. In the Standard Model only matrix elements of $\mathcal{Q}_1^q$ contribute to Δm_q, while all operators do, for example, for general SUSY extensions of the Standard Model [449]. The matrix elements or bag parameters for the non-SM operators are also useful to estimate the width difference $\Delta\Gamma_q$ between the *CP* eigenstates of the neutral *B* meson in the Standard Model, where combinations of matrix elements of $\mathcal{Q}_1^q$, $\mathcal{Q}_2^q$, and $\mathcal{Q}_3^q$ contribute to $\Delta\Gamma_q$ at $\mathcal{O}(1/m_b)$ [554,555].

In this section, we report on results from lattice-QCD calculations for the neutral *B*-meson mixing parameters $\hat{B}_{B_d}$, $\hat{B}_{B_s}$, $f_{B_d}\sqrt{\hat{B}_{B_d}}$, $f_{B_s}\sqrt{\hat{B}_{B_s}}$ and the SU(3)-breaking ratios B_{B_s}/B_{B_d} and ξ defined in Eqs. (176), (177), and (179). The results are summarized in Tables 35 and 36 and in Figs. 23 and 24. Additional details about the underlying simulations and systematic error estimates are given in Appendix C 5 b. Some collaborations do not provide the RGI quantities $\hat{B}_{B_q}$, but quote instead $B_B(\mu)^{\overline{\text{MS}},\text{NDR}}$. In such cases, we convert the results using Eq. (177) to the RGI quantities quoted in Table 35 with a brief description for each case. More detailed descriptions for these cases are provided in FLAG13 [2]. We do not provide the *B*-meson-matrix elements of the other operators $\mathcal{Q}_{2-5}$ in this report. They have been calculated in Ref. [73] for the $N_f = 2$ case, in Refs. [79,556] for $N_f = 2+1$, and in Ref. [77] for $N_f = 2+1+1$. A discussion is provided on the comparison of these results in a recent review [557].

Let us mention that our averages here have no updates from the previous review [5]. The new addition to this subsection is that we review a measure of continuum-limit quality $\delta(a_{\min})$ for each result that is included in the average. We used this quantity for the continuum-limit criterion for heavy-quark related quantities in FLAG 13 [2]. This time we only quote the value for information and we do not use it when calculating averages.

There are no new results for $N_f = 2$ reported after FLAG 16 [3]. In this category, one work (ETM 13B) [73] passes the quality criteria. A description of this work can be found in FLAG 13 [2] where it did not enter the average as it had not appeared in a journal. This is the only result available for $N_f = 2$, so we quote their values as our estimates

$$N_f = 2: \quad \begin{aligned} f_{B_d}\sqrt{\hat{B}_{b_d}} &= 216(10)\ \text{MeV}, \\ f_{B_s}\sqrt{\hat{B}_{B_s}} &= 262(10)\ \text{MeV} \quad \text{Ref. [73]}, \end{aligned} \tag{182}$$

TABLE 35. Neutral B- and B_s-meson mixing matrix elements (in MeV) and bag parameters.

Collaboration	Ref.	N_f	Publication status	Continuum extrapolation	Chiral extrapolation	Finite volume	Renormalization/matching	Heavy-quark treatment	$f_{\mathrm{B}_d}\sqrt{\hat{B}_{\mathrm{B}_d}}$	$f_{\mathrm{B}_s}\sqrt{\hat{B}_{\mathrm{B}_s}}$	$\hat{B}_{\mathrm{B}_d}$	$\hat{B}_{\mathrm{B}_s}$
HPQCD 19A	[77]	$2+1+1$	A	○	○	★	○	✓	210.6(5.5)	256.1(5.7)	1.222(61)	1.232(53)
FNAL/MILC 16	[79]	$2+1$	A	★	○	★	○	✓	227.7(9.5)	274.6(8.4)	1.38(12)(6)[a]	1.443(88)(48)[a]
RBC/UKQCD 14A	[71]	$2+1$	A	○	○	○	○	✓	240(15)(33)	290(09)(40)	1.17(11)(24)	1.22(06)(19)
FNAL/MILC 11A	[556]	$2+1$	C	★	○	★	○	✓	250(23)[b]	291(18)[b]	...	...
HPQCD 09	[78]	$2+1$	A	○	○[c]	○	○	✓	216(15)[d]	266(18)[d]	1.27(10)[d]	1.33(6)[d]
HPQCD 06A	[558]	$2+1$	A	■	■	★	○	✓	...	281(21)	...	1.17(17)
ETM 13B	[73]	2	A	★	○	○	★	✓	216(6)(8)	262(6)(8)	1.30(5)(3)	1.32(5)(2)
ETM 12A, 12B	[545,559]	2	C	★	○	○	★	✓	...	...	1.32(8)[e]	1.36(8)[e]

[a]PDG averages of decay constant f_{B^0} and f_{B_s} [204] are used to obtain these values.

[b]Reported $f_B^2 B$ at $\mu = m_b$ is converted to RGI by multiplying the 2-loop factor 1.517.

[c]While wrong-spin contributions are not included in the HMrSχPT fits, the effect is expected to be small for these quantities (see description in FLAG 13 [2]).

[d]This result uses an old determination of $r_1 = 0.321(5)$ fm from Ref. [120] that has since been superseded, which however has only a small effect in the total error budget (see description in FLAG 13 [2]).

[e]Reported B at $\mu = m_b = 4.35$ GeV is converted to RGI by multiplying the 2-loop factor 1.521.

TABLE 36. Results for SU(3)-breaking ratios of neutral B_d- and B_s-meson-mixing matrix elements and bag parameters.

Collaboration	Ref.	N_f	Publication status	Continuum extrapolation	Chiral extrapolation	Finite volume	Renormalization/matching	Heavy-quark treatment	ξ	$B_{\mathrm{B}_s}/B_{\mathrm{B}_d}$
HPQCD 19A	[77]	$2+1+1$	A	○	○	★	○	✓	1.216(16)	1.008(25)
RBC/UKQCD 18A	[76]	$2+1$	P	★	★	★	★	✓	$1.1939(67)(^{+95}_{-177})$	$0.9984(45)(^{+80}_{-63})$
FNAL/MILC 16	[79]	$2+1$	A	★	○	★	○	✓	1.206(18)	1.033(31)(26)[a]
RBC/UKQCD 14A	[71]	$2+1$	A	○	○	○	○	✓	1.208(41)(52)	1.028(60)(49)
FNAL/MILC 12	[560]	$2+1$	A	○	○	★	○	✓	1.268(63)	1.06(11)
RBC/UKQCD 10C	[549]	$2+1$	A	■	■	■	○	✓	1.13(12)	...
HPQCD 09	[78]	$2+1$	A	○	○[b]	○	○	✓	1.258(33)	1.05(7)
ETM 13B	[73]	2	A	★	○	○	★	✓	1.225(16)(14)(22)	1.007(15)(14)
ETM 12A, 12B	[545,559]	2	C	★	○	○	★	✓	1.21(6)	1.03(2)

[a]PDG average of the ratio of decay constants f_{B_s}/f_{B^0} [204] is used to obtain the value.

[b]Wrong-spin contributions are not included in the HMrSχPT fits. As the effect may not be negligible, these results are excluded from the average (see description in FLAG 13 [2]).

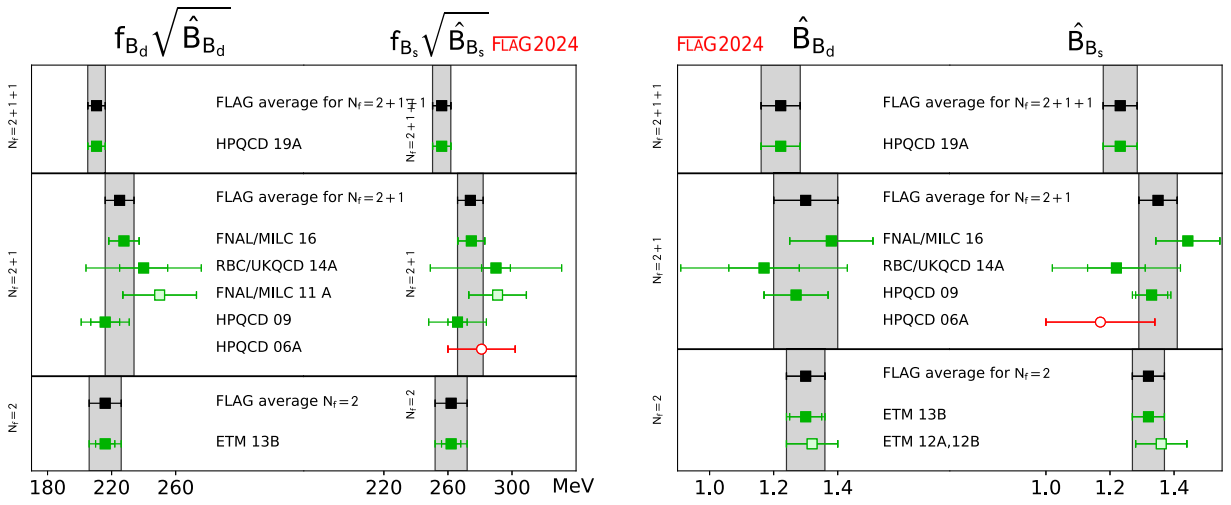


FIG. 23. Neutral B- and B_s-meson-mixing matrix elements and bag parameters [values in Table 35 and Eqs. (182), (185), (188), (183), (186), (189)].

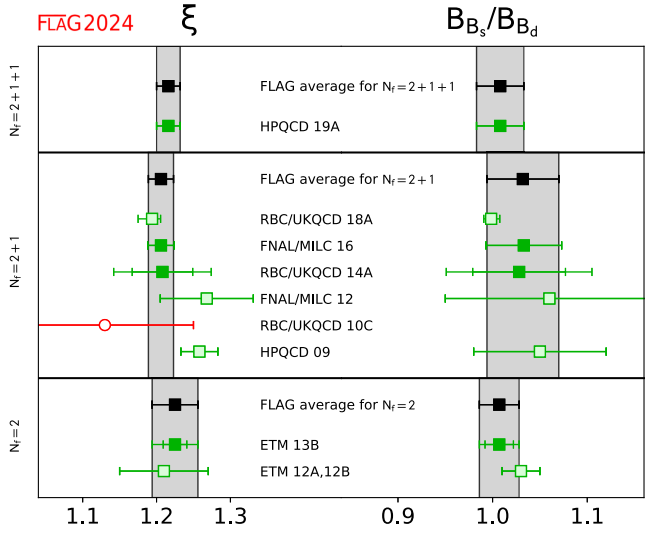


FIG. 24. The SU(3)-breaking quantities ξ and B_{B_s}/B_{B_d} [values in Table 36 and Eqs. (184), (187), (190)].

$$N_f=2:\quad \hat{B}_{B_d}=1.30(6),\quad \hat{B}_{B_s}=1.32(5)\quad \text{Ref. [73]},\quad (183)$$

$$\xi=1.225(31),\quad B_{B_s}/B_{B_d}=1.007(21)\quad \text{Ref. [73]}.\quad (184)$$

The continuum-limit measure, $\delta(a_{\min})$, cannot be estimated for the ETM 13B results for $\hat{B}_{B_d}$ because the relevant continuum-limit information is not provided. For the other quantities of ETM 13B, $\delta(a_{\min})\simeq 0.1$ ($\hat{B}_{B_d}$), 2 (ξ) and 0.7 (B_{B_s}/B_{B_d}).

For $N_f=2+1$ the results that enter our averages for $N_f=2+1$ are FNAL/MILC 16 [79], which had been included in the averages at FLAG 19 [4], RBC/UKQCD 14A [71], included in the averages at FLAG 16 [3], and HPQCD 09 [78] for which a description is available in FLAG 13 [2]. The work in RBC/UKQCD 18A [76] on the flavor SU(3)-breaking ratios, whose description can be found in FLAG 21 [5], has not been published yet and therefore do not enter into the averages. Thus, the averages for $N_f=2+1$ are unchanged

$N_f=2+1$:

$$f_{B_d}\sqrt{\hat{B}_{B_d}}=225(9)\ \text{MeV},$$

$$f_{B_s}\sqrt{\hat{B}_{B_s}}=274(8)\ \text{MeV}\quad \text{Refs. [71, 78, 79]},\quad (185)$$

$$\hat{B}_{B_d}=1.30(10),\quad \hat{B}_{B_s}=1.35(6)\quad \text{Refs. [71,78,79]},\quad (186)$$

$$\xi=1.206(17),\quad B_{B_s}/B_{B_d}=1.032(38)\quad \text{Refs. [71,79]}.\quad (187)$$

Here all the above equations have not been changed from FLAG 19. The averages were obtained using the nested averaging scheme described in Sec. II C 2, due to a nested correlation structure among the results. Details are discussed in the FLAG 19 report [4].

We estimate $\delta(a_{\min})\simeq 2$ for both $\hat{B}_{B_s}$ and $\hat{B}_{B_d}$ of FNAL/MILC 16. Data are not available in FNAL/MILC 16 to estimate $\delta(a_{\min})$ for the ratio of the bag parameters. Since the $f_{B_s}\sqrt{\hat{B}_{B_s}}$, $f_{B_d}\sqrt{\hat{B}_{B_d}}$ and ξ are quantities derived using PDG estimates of the decay constants and their ratio, we do not provide an estimate of $\delta(a_{\min})$ of these quantities. For RBC/UKQCD 14A, $\delta(a_{\min})\simeq 0.7$ ($f_{B_d}\sqrt{\hat{B}_{B_d}}$), 1.3 ($f_{B_s}\sqrt{\hat{B}_{B_s}}$), 0.3 ($\xi$), 0.3 ($\hat{B}_{B_d}$), 0.4 ($\hat{B}_{B_s}$) and 0 ($B_{B_s}/B_{B_d}$). For HPQCD 09, $\delta(a_{\min})\simeq 0.8$ ($f_{B_d}\sqrt{\hat{B}_{B_d}}$), 3

($f_{B_s}\sqrt{\hat{B}_{B_s}}$), 0.3 ($\xi$), at most 1 ($\hat{B}_{B_d}$), 0.8 ($\hat{B}_{B_s}$) and 1 ($B_{B_s}/B_{B_d}$).

We note that, for $N_f = 2+1$, there is an on-going study involving the JLQCD and RBC/UKQCD collaborations, with initial results reported in the Lattice 2021 proceedings [561]. These results utilize coarse lattices at the physical point from RBC/UKQCD along with very fine lattices from JLQCD (up to $a^{-1} = 4.5$ GeV) with unphysical pion masses, both using domain-wall fermions.

The only result available for $N_f = 2+1+1$ is HPQCD 19A [77], which uses MILC collaboration's HISQ ensembles and NRQCD for the b quark. A detailed description can be found in the previous review [5]. We quote their values as the FLAG estimates

$$N_f = 2+1+1:$$

$$f_{B_d}\sqrt{\hat{B}_{b_d}} = 210.6(5.5)\,\text{MeV},$$
$$f_{B_s}\sqrt{\hat{B}_{B_s}} = 256.1(5.7)\,\text{MeV} \quad \text{Ref. [77]}, \tag{188}$$

$$\hat{B}_{B_d} = 1.222(61), \quad \hat{B}_{B_s} = 1.232(53) \quad \text{Ref. [77]}, \tag{189}$$

$$\xi = 1.216(16), \quad B_{B_s}/B_{B_d} = 1.008(25) \quad \text{Ref. [77]}. \tag{190}$$

We estimate $\delta(a_{\min}) \simeq 0.1$ for $\hat{B}_{B_s}$, 1 for B_{B_s}/B_{B_d} and at most 1 for $\hat{B}_{B_d}$. The other quantities are derived ones using the estimates of decay constants in FNAL/MILC 17.

We note that the above results with the same N_f [e.g., those in Eqs. (188)–(190)] are all correlated with each other, due to the use of the same gauge-field ensembles for different quantities. The results are also correlated with the averages obtained in Sec. VIII A and shown in Eqs. (162)–(164) for $N_f = 2$, Eqs. (165)–(167) for $N_f = 2+1$ and Eqs. (168)–(170) for $N_f = 2+1+1$. This is because the calculations of B-meson decay constants and mixing quantities are performed on the same (or on similar) sets of ensembles, and results obtained by a given collaboration use the same actions and setups. These correlations must be considered when using our averages as inputs to unitarity triangle (UT) fits. For this reason, if one were for example to estimate $f_{B_s}\sqrt{\hat{B}_s}$ from the separate averages of f_{B_s} [Eq. (166)] and $\hat{B}_s$ [Eq. (186)] for $N_f = 2+1$, one would obtain a value about one standard deviation below the one quoted above in Eq. (185). While these two estimates lead to compatible results, giving us confidence that all uncertainties have been properly addressed, we do not recommend combining averages this way, as many correlations would have to be taken into account to properly assess the errors. We recommend instead using the numbers quoted above. In the future, as more independent calculations enter the averages, correlations between the lattice-QCD inputs to UT fits will become less significant.

C. Semileptonic form factors for B decays to light flavors

The Standard Model differential rate for the decay $B_{(s)} \to P\ell\nu$ involving a quark-level $b \to u$ transition is given, at leading order in the weak interaction, by a formula analogous to the one for D decays in Eq. (133), but with $D \to B_{(s)}$ and the relevant CKM matrix element $|V_{cq}| \to |V_{ub}|$:

$$\frac{d\Gamma(B_{(s)} \to P\ell\nu)}{dq^2} = \frac{G_F^2 |\eta_{\text{EW}}|^2 |V_{ub}|^2}{24\pi^3} \frac{(q^2 - m_\ell^2)^2 \sqrt{E_P^2 - m_P^2}}{q^4 m_{B_{(s)}}^2} \times \left[\left(1 + \frac{m_\ell^2}{2q^2}\right) m_{B_{(s)}}^2 (E_P^2 - m_P^2) |f_+(q^2)|^2 + \frac{3m_\ell^2}{8q^2} (m_{B_{(s)}}^2 - m_P^2)^2 |f_0(q^2)|^2 \right]. \tag{191}$$

Again, for $\ell = e, \mu$ the contribution from the scalar form factor f_0 can be neglected, and one has a similar expression to Eq. (135), which, in principle, allows for a direct extraction of $|V_{ub}|$ by matching theoretical predictions to experimental data. However, while for D (or K) decays the entire physical range $0 \le q^2 \le q^2_{\max}$ can be covered with moderate momenta accessible to lattice simulations, in $B \to \pi\ell\nu$ decays one has $q^2_{\max} \sim 26\ \text{GeV}^2$ and only part of the full kinematic range is reachable. As a consequence, obtaining $|V_{ub}|$ from $B \to \pi\ell\nu$ is more complicated than obtaining $|V_{cd(s)}|$ from semileptonic D-meson decays.

In practice, lattice computations are restricted to large values of the momentum transfer q^2 (see Sec. VII B) where statistical and momentum-dependent discretization errors can be controlled, which in existing calculations roughly cover the upper third of the kinematically allowed q^2 range.[44] Since, on the other hand, the decay rate is suppressed by phase space at large q^2, most of the semileptonic $B \to \pi$ events are observed in experiment at lower values of q^2, leading to more accurate experimental results for the binned differential rate in that region.[45] It is, therefore, a challenge to find a window of intermediate values of q^2 at which both the experimental and lattice results can be reliably evaluated.

State-of-the-art determinations of CKM matrix elements, say, $|V_{ub}|$, are obtained from joint fits to lattice and experimental results, keeping the relative normalization $|V_{ub}|^2$ as a free parameter. This requires, in particular, that

[44]The variance of hadron correlation functions at nonzero three-momentum is dominated at large Euclidean times by zero-momentum multiparticle states [562]; therefore the noise-to-signal grows more rapidly than for the vanishing three-momentum case.

[45]Upcoming data from Belle II are expected to significantly improve the precision of experimental results, in particular, for larger values of q^2.

both experimental and lattice data for the q^2-dependence be parametrized by fitting data to specific *Ansätze*, with the ultimate aim of minimizing the systematic uncertainties involved. This plays a key role in assessing the systematic uncertainties of CKM determinations, and will be discussed extensively in this section. A detailed discussion of the parametrization of form factors as a function of q^2 can be found in Appendix B 2.

1. Form factors for $B \to \pi \ell \nu$

The semileptonic decay process $B \to \pi \ell \nu$ enables the determination of the CKM matrix element $|V_{ub}|$ within the Standard Model via Eq. (191). Early results for $B \to \pi \ell \nu$ form factors came from the HPQCD [563] and FNAL/MILC [564] collaborations (HPQCD 06 and FNAL/MILC 08A).

Our 2016 review featured a significantly extended calculation of $B \to \pi \ell \nu$ from FNAL/MILC [124] (FNAL/MILC 15) and a new computation from RBC/UKQCD [125] (RBC/UKQCD 15). In 2022, the JLQCD collaboration published another new calculation using Möbius domain wall fermions—JLQCD 22 [126]. FNAL/MILC and RBC/UKQCD continue working on further new calculations of the $B \to \pi$ form factors and have reported on their progress at the annual Lattice conferences and the 2020 Asia-Pacific Symposium for lattice field theory. The results are preliminary or blinded, so not yet ready for inclusion in this review. FNAL/MILC is using $N_f = 2 + 1 + 1$ HISQ ensembles with $a \approx 0.15$, 0.12, 0.088 fm, 0.057 fm, with Goldstone-pion mass down to its physical value [565,566]. The RBC/UKQCD Collaborations have added a new Möbius-domain-wall-fermion ensemble with $a \approx 0.07$ fm and $m_\pi \approx 230$ MeV to their analysis [567]. In addition, HPQCD using MILC ensembles had published the first $N_f = 2 + 1 + 1$ results for the $B \to \pi \ell \nu$ scalar form factor, working at zero recoil ($q^2 = q^2_{\text{max}}$) and pion masses down to the physical value [568]; this adds to previous reports on ongoing work to upgrade their 2006 computation [569,570]. Since this latter result has no immediate impact on current $|V_{ub}|$ determinations, which come from the vector-form-factor-dominated decay channels into light leptons, we will from now on concentrate on the $N_f = 2 + 1$ determinations of the q^2-dependence of $B \to \pi$ form factors.

Both the HPQCD 06 and the FNAL/MILC 15 computations of $B \to \pi \ell \nu$ amplitudes use ensembles of gauge configurations with $N_f = 2 + 1$ flavors of rooted staggered quarks produced by the MILC collaboration; however, FNAL/MILC 15 makes a much more extensive use of the currently available ensembles, both in terms of lattice spacings and light-quark masses. HPQCD 06 has results at two values of the lattice spacing ($a \approx 0.12, 0.09$ fm), while FNAL/MILC 15 employs four values ($a \approx 0.12, 0.09, 0.06, 0.045$ fm). Lattice-discretization effects are estimated within heavy-meson rooted staggered chiral perturbation theory (HMrSχPT) in the FNAL/MILC 15 computation, while HPQCD 06 quotes the results at $a \approx 0.12$ fm as central values and uses the $a \approx 0.09$ fm results to quote an uncertainty. The relative scale is fixed in both cases through the quark-antiquark potential-derived ratio r_1/a. HPQCD 06 set the absolute scale through the Υ $2S$–$1S$ splitting, while FNAL/MILC 15 uses a combination of f_π and the same Υ splitting, as described in Ref. [60]. The spatial extent of the lattices employed by HPQCD 06 is $L \simeq 2.4$ fm, save for the lightest-mass point (at $a \approx 0.09$ fm) for which $L \simeq 2.9$ fm. FNAL/MILC 15, on the other hand, uses extents up to $L \simeq 5.8$ fm, in order to allow for light-pion masses while keeping finite-volume effects under control.

TABLE 37. Results for the $B \to \pi \ell \nu$ semileptonic form factor.

Collaboration	Ref.	N_f	Publication status	Continuum extrapolation	Chiral extrapolation	Finite volume	Renormalization	Heavy-quark treatment	z-parametrization
JLQCD 22	[126]	$2+1$	A	★	○	★	○	✓	BCL
FNAL/MILC 15	[124]	$2+1$	A	★	○	★	○	✓	BCL
RBC/UKQCD 15	[125]	$2+1$	A	○	○	○	○	✓	BCL
HPQCD 06	[563]	$2+1$	A	○	○	○	○	✓	n/a

Indeed, while in the HPQCD 06 work the lightest RMS pion mass is 400 MeV, the FNAL/MILC 15 work includes pions as light as 165 MeV—in both cases the bound $m_\pi L \gtrsim 3.8$ is kept. Other than the qualitatively different range of MILC ensembles used in the two computations, the main difference between HPQCD 06 and FNAL/MILC 15 lies in the treatment of heavy quarks. HPQCD 06 uses the NRQCD formalism, with a 1-loop matching of the relevant currents to the ones in the relativistic theory. FNAL/MILC 15 employs the clover action with the Fermilab interpretation, with a mostly nonperturbative renormalization of the relevant currents, within which the overall renormalization factor of the heavy-light current is written as a product of the square roots of the renormalization factors of the light-light and heavy-heavy temporal vector currents (which are determined nonperturbatively) and a residual factor that is computed using 1-loop perturbation theory. (See Table 37; full details about the computations are provided in tables in Appendix C 5 c.)

The RBC/UKQCD 15 computation is based on $N_f = 2 + 1$ DWF ensembles at two values of the lattice spacing ($a \approx 0.12, 0.09$ fm), and pion masses in a narrow interval ranging from slightly above 400 MeV to slightly below

300 MeV, keeping $m_\pi L \gtrsim 4$. The scale is set using the Ω^- baryon mass. Discretization effects coming from the light sector are estimated in the 1% ballpark using HMχPT supplemented with effective higher-order interactions to describe cutoff effects. The b quark is treated using the Columbia RHQ action, with a mostly nonperturbative renormalization of the relevant currents. Discretization effects coming from the heavy sector are estimated with power-counting arguments to be below 2%. The collaboration has also reported on progress toward an improved calculation that adds a third, finer lattice spacing [571].

The JLQCD 22 calculation is using Möbius domain wall fermions, including for the heavy quark, with $a \approx 0.08$, 0.055, and 0.044 fm and pion masses down to 230 MeV. The relative scales are set using the gradient-flow time $t_0^{1/2}/a$, with the absolute scale $t_0^{1/2}$ taken from Ref. [115]. All ensembles have $m_\pi L \gtrsim 4.0$. The bare heavy-quark masses satisfy $am_Q < 0.7$ and reach from the charm mass up to 2.44 times the charm mass. The form factors are extrapolated linearly in $1/m_Q$ to the bottom mass. For the lower range of the quark masses, the vector current is renormalized using a factor $Z_{V_{qq}}$ obtained from position-space current-current correlators. For heavier quark masses, $\sqrt{Z_{V_{QQ}} Z_{V_{qq}}}$ is used, where $Z_{V_{QQ}}$ is the renormalization factor of the flavor-conserving temporal vector current, determined using charge conservation. This corresponds to mostly nonperturbative renormalization with tree-level residual matching factors, but the residual matching factors are expected to be close to 1 and approach this value exactly in the continuum limit. We therefore assign a ○ rating for renormalization.

Given the large kinematical range available in the $B \to \pi$ transition, chiral extrapolations are an important source of systematic uncertainty: apart from the eventual need to reach physical pion masses in the extrapolation, the applicability of χPT is not guaranteed for large values of the pion energy E_π. Indeed, in all computations E_π reaches values in the 1 GeV ballpark, and chiral-extrapolation systematics is the dominant source of errors. FNAL/MILC uses SU(2) NLO HMrSχPT for the continuum-chiral extrapolation, supplemented by NNLO analytic terms and hard-pion χPT terms [491][46]; systematic uncertainties are estimated through an extensive study of the effects of varying the specific fit *Ansatz* and/or data range. RBC/UKQCD and JLQCD use SU(2) hard-pion HMχPT to perform their combined continuum-chiral extrapolations, and obtain estimates for systematic uncertainties by varying the *Ansätze* and ranges used in fits. HPQCD performs chiral extrapolations using HMrSχPT formulas, and estimates systematic uncertainties by comparing the result with the ones from fits to a linear behavior in the light-quark mass, continuum HMχPT, and partially quenched HMrSχPT formulas (including also data with different sea and valence light-quark masses).

FNAL/MILC 15, RBC/UKQCD 15, and JLQCD 22 describe the q^2-dependence of f_+ and f_0 by applying a BCL parametrization to the form factors extrapolated to the continuum limit, within the range of values of q^2 covered by data. (A discussion of the various parametrizations can be found in Appendix B 2.) RBC/UKQCD 15 and JLQCD 22 generate synthetic data for the form factors at some values of q^2 (evenly spaced in z) from the continuous function of q^2 obtained from the joint chiral-continuum extrapolation, which are then used as input for the fits. After having checked that the kinematical constraint $f_+(0) = f_0(0)$ is satisfied within errors by the extrapolation to $q^2 = 0$ of the results of separate fits, this constraint is imposed to improve fit quality. In the case of FNAL/MILC 15, rather than producing synthetic data a functional method is used to extract the z-parametrization directly from the fit functions employed in the continuum-chiral extrapolation. In the case of HPQCD 06, the parametrization of the q^2-dependence of form factors is somewhat intertwined with chiral extrapolations: a set of fiducial values $\{E_\pi^{(n)}\}$ is fixed for each value of the light-quark mass, and $f_{+,0}$ are interpolated to each of the $E_\pi^{(n)}$; chiral extrapolations are then performed at fixed E_π (i.e., m_π and q^2 are varied subject to $E_\pi =$ constant). The interpolation is performed using a Ball-Zwicky (BZ) *Ansatz* [572]. The q^2-dependence of the resulting form factors in the chiral limit is then described by means of a BZ *Ansatz*, which is cross-checked against Becirevic-Kaidalov (BK) [573], Richard Hill (RH) [574], and Boyd-Grinstein-Lebed (BGL) [575] parametrizations (see Appendix B 2), finding agreement within the quoted uncertainties. Unfortunately, the correlation matrix for the values of the form factors at different q^2 is not provided, which severely limits the possibilities of combining them with other computations into a global z-parametrization.

The different ways in which the current results are presented do not allow a straightforward averaging procedure. RBC/UKQCD 15 only provides synthetic values of f_+ and f_0 at a few values of q^2 as an illustration of their results, and FNAL/MILC 15 does not quote synthetic values at all. In both cases, full results for BCL z-parametrizations defined by Eq. (B12) are quoted. In the case of HPQCD 06, unfortunately, a fit to a BCL z-parametrization is not possible, as discussed above.

In order to combine these form factor calculations, we start from sets of synthetic data for several q^2 values. HPQCD 06, RBC/UKQCD 15, and JLQCD 22 directly provide this information; FNAL/MILC 15 present only fits to a BCL z-parametrization from which we can easily

[46]It is important to stress the finding in Ref. [489] that the factorization of chiral logs in hard-pion χPT breaks down, implying that it does not fulfill the expected requisites for a proper effective field theory. Its use to model the mass dependence of form factors can thus be questioned.

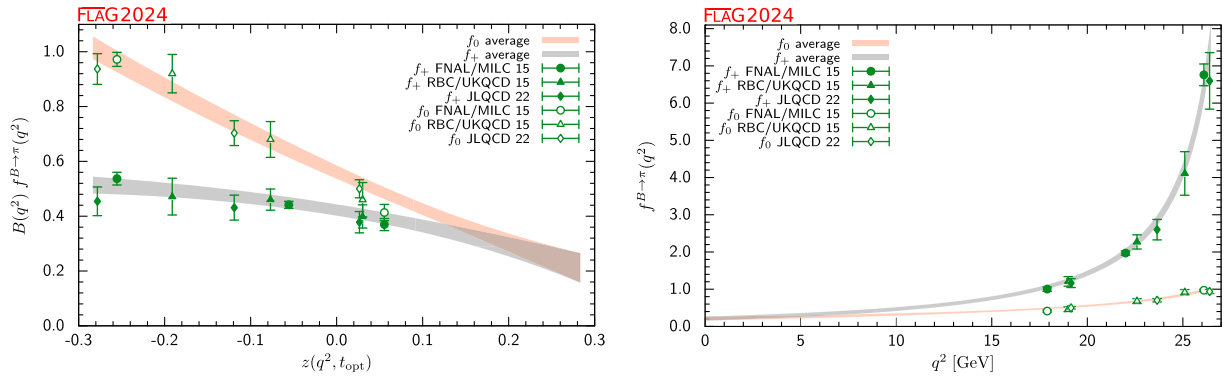


FIG. 25. The form factors $f_+(q^2)$ and $f_0(q^2)$ for $B \to \pi\ell\nu$ plotted versus z (left panel) and q^2 (right panel). In the left plot, we removed the Blaschke factors. See text for a discussion of the dataset. The gray and salmon bands display our preferred $N^+ = N^0 = 3$ BCL fit (five parameters).

generate an equivalent set of form factor values. It is important to note that in both the RBC/UKQCD 15 and JLQCD 22 synthetic data and the FNAL/MILC z-parametrization fits the kinematic constraint at $q^2 = 0$ is automatically included (in the FNAL/MILC 15 case the constraint is manifest in an exact degeneracy of the (a_n^+, a_n^0) covariance matrix). Due to these considerations, in our opinion, the most accurate procedure is to perform a simultaneous fit to all synthetic data for the vector and scalar form factors. Unfortunately, the absence of information on the correlation in the HPQCD 06 result between the vector and scalar form factors even at a single q^2 point makes it impossible to include consistently this calculation in the overall fit. In fact, the HPQCD 06 and FNAL/MILC 15 statistical uncertainties are highly correlated (because they are based on overlapping subsets of MILC $N_f = 2 + 1$ ensembles) and, without knowledge of the $f_+ - f_0$ correlation we are unable to construct the HPQCD 06-FNAL/MILC 15 off-diagonal entries of the overall covariance matrix.

In conclusion, we will present as our best result a combined vector and scalar form factor fit to the FNAL/MILC 15, RBC/UKQCD 15, and JLQCD 22 results that we treat as completely uncorrelated.

The resulting dataset is then fitted to the BCL parametrization in Eqs. (B12) and (B13). We assess the systematic uncertainty due to truncating the series expansion by considering fits to different orders in z. In Fig. 25 (left), we show $(1 - q^2/m_{B^*}^2) f_+(q^2)$ and $f_0(q^2)$ versus z; Fig. 25 (right) shows the full form factors versus q^2. The fit has $\chi^2/\text{dof} = 43.6/12$ with $N^+ = N^0 = 3$. The poor quality of the fit is caused by tensions between the results from the different collaborations; in particular in the slopes of f_0, which are very constrained due to strong correlations between data points. We have therefore rescaled the uncertainties of the z parameters by $\sqrt{\chi^2/\text{dof}} = 1.9$. We point out that tensions in the form factors, especially in f_0, might be an artifact associated with the basis of form factors employed to take the continuum limit, as explained in Appendix B 2. The outcome of the five-parameter $N^+ = N^0 = 3$ BCL fit to the FNAL/MILC 15, RBC/UKQCD 15, and JLQCD 22 calculations is shown in Table 38.

TABLE 38. Coefficients and correlation matrix for the $N^+ = N^0 = 3$ z-expansion fit of the $B \to \pi$ form factors f_+ and f_0. The coefficient a_2^0 is fixed by the $f_+(q^2 = 0) = f_0(q^2 = 0)$ constraint. The chi-square per degree of freedom is $\chi^2/\text{dof} = 43.6/12$ and the errors on the z-parameters have been rescaled by $\sqrt{\chi^2/\text{dof}} = 1.9$. The lattice calculations that enter this fit are taken from FNAL/MILC 15 [124], RBC/UKQCD 15 [125] and JLQCD 22 [126]. The parametrizations are defined in Eqs. (B12) and (B13). The form factors can be reconstructed using parametrization and inputs given in Appendix B 3 b.

$B \to \pi(N_f = 2 + 1)$						
	Central values	Correlation matrix				
a_0^+	0.423(21)	1	−0.00466	−0.0749	0.402	0.0920
a_1^+	−0.507 (93)	−0.00466	1	0.498	−0.0556	0.659
a_2^+	−0.75 (34)	−0.0749	0.498	1	−0.152	0.677
a_0^0	0.561(24)	0.402	−0.0556	−0.152	1	−0.548
a_1^0	−1.42 (11)	0.0920	0.659	0.677	−0.548	1

The fit shown in Table 38 can therefore be used as the averaged FLAG result for the lattice-computed form factor $f_+(q^2)$. The coefficient a_3^+ can be obtained from the values for a_0^+–a_2^+ using Eq. (B11). The coefficient a_2^0 can be obtained from all other coefficients imposing the $f_+(q^2 = 0) = f_0(q^2 = 0)$ constraint. We emphasize that future lattice-QCD calculations of semileptonic form factors should publish their full statistical and systematic correlation matrices to enable others to use the data. It is also preferable to present a set of synthetic form-factor data equivalent to the z-fit results, since this allows for an

independent analysis that avoids further assumptions about the compatibility of the procedures to arrive at a given z-parametrization.[47] It is also preferable to present covariance/correlation matrices with enough significant digits to calculate correctly all their eigenvalues.

2. Form factors for $B \to \rho \ell \nu$

Another process sensitive to $|V_{ub}|$ is $B \to \rho \ell \nu$, with experimental data available from *BABAR*, Belle, and Belle II [138,141,576]. Early lattice calculations of the $B \to \rho \ell \nu$ form factors were done in the quenched approximation and assumed the ρ resonance to be stable under the strong interaction [577,578]. A proper treatment of the ρ final state requires a calculation of the $B \to \pi\pi \ell \nu$ (P wave) form factors as a function of both q^2 and $\pi\pi$ invariant mass, followed by analytic continuation to the ρ resonance pole. On the lattice, this can be done using the Lellouch-Lüscher finite-volume method [579–589]. Early lattice results for the $B \to \pi\pi \ell \nu P$-wave vector form factor at $m_\pi \approx 320$ MeV were reported in Refs. [590,591].

3. Form factors for $B_s \to K \ell \nu$

Similar to $B \to \pi \ell \nu$, measurements of $B_s \to K \ell \nu$ decay rates enable determinations of the CKM matrix element $|V_{ub}|$ within the Standard Model via Eq. (191). From the lattice point of view, the two channels are very similar. As a matter of fact, $B_s \to K \ell \nu$ is actually somewhat simpler, in that the kaon mass region is easily accessed by all simulations making the systematic uncertainties related to chiral extrapolation smaller. Lattice calculations of the $B_s \to K$ form factors are available from HPQCD 14 [127], RBC/UKQCD [125,128] (RBC/UKQCD 15 and RBC/UKQCD 23), and FNAL/MILC 19 [592].

The HPQCD 14 computation uses ensembles of gauge configurations with $N_f = 2 + 1$ flavors of asqtad rooted staggered quarks produced by the MILC collaboration at two values of the lattice spacing ($a \approx 0.12, 0.09$ fm), for three and two different sea-pion masses, respectively, down to a value of 260 MeV. The b quark is treated within the NRQCD formalism, with a 1-loop matching of the relevant currents to the ones in the relativistic theory, omitting terms of $\mathcal{O}(\alpha_s \Lambda_{\rm QCD}/m_b)$. The HISQ action is used for the valence light and s quarks. The continuum-chiral extrapolation is combined with the description of the q^2-dependence of the form factors into a modified z-expansion (cf. Appendix B 2) that formally coincides in the continuum with the BCL *Ansatz*. The dependence of form factors on the pion energy and quark masses is fitted to a 1-loop *Ansatz* inspired by hard-pion χPT [491], that factorizes out the chiral logarithms describing soft physics.

[47]Note that generating synthetic data is a trivial task, but less so is choosing the number of required points and the q^2 values that lead to an optimal description of the form factors.

TABLE 39. Summary of lattice calculations of the $B_s \to K \ell \nu$ semileptonic form factors.

Collaboration	Ref.	N_f	Publication status	Continuum extrapolation	Chiral extrapolation	Finite volume	Renormalization	Heavy-quark treatment	z-parametrization
RBC/UKQCD 23[a]	[128]	$2+1$	A	★	○	★	○	✓	BGL[b]
FNAL/MILC 19	[592]	$2+1$	A	★	○	★	○	✓	BCL
RBC/UKQCD 15	[125]	$2+1$	A	○	○	○	○	✓	BCL
HPQCD 14	[127]	$2+1$	A	○	○	○	○	✓	BCL[c]

[a]Supersedes RBC/UKQCD 15.

[b]Generalized as discussed in Ref. [593].

[c]Results from modified z-expansion.

The FNAL/MILC computation (FNAL/MILC 19) coincides with HPQCD 14 in using ensembles of gauge configurations with $N_f = 2 + 1$ flavors of asqtad rooted staggered quarks produced by the MILC collaboration, but only one ensemble is shared, and a different valence regularization is employed; we will thus treat the two results as fully independent from the statistics point of view. FNAL/MILC 19 uses three values of the lattice spacing ($a \approx 0.12, 0.09, 0.06$ fm); only one value of the sea pion mass and the volume is available at the extreme values of the lattice spacing, while four different masses and volumes are considered at $a = 0.09$ fm. Heavy quarks are treated within the Fermilab approach. HMrSχPT expansion is used at next-to-leading order in SU(2) and leading order in $1/M_B$, including next-to-next-to-leading-order (NNLO) analytic and generic discretization terms, to perform continuum-chiral extrapolations. Hard kaons are assumed to decouple, i.e., their effect is reabsorbed in the SU(2) LECs. Continuum- and chiral-extrapolated values of the form factors are fitted to a z-parametrization imposing the kinematical constraint $f_+(0) = f_0(0)$. See Table 39 and the tables in Appendix C 5 c for full details.

The RBC/UKQCD 15 computation [125] had been published together with the $B \to \pi \ell \nu$ computation discussed in Sec. VIII C 1, all technical details being practically identical. The RBC/UKQCD 23 computation [128] (which considers $B_s \to K \ell \nu$ only) differs from RBC/UKQCD 15 by the addition of one new ensemble with a third, finer lattice spacing that also has a lower pion mass than the other ensembles, updated scale setting and updated tuning of m_s and of the RHQ parameters, and a change of the form-factor basis in which the chiral-continuum extrapolation is performed (previously: $f_\parallel$ and $f_\perp$, now: f_+ and f_0). RBC/UKQCD 23 [128] furthermore uses a new

TABLE 40. Coefficients and correlation matrix for the $N^+ = N^0 = 4$ z-expansion of the $B_s \to K$ form factors f_+ and f_0. The coefficient a_3^0 is fixed by the $f_+(q^2 = 0) = f_0(q^2 = 0)$ constraint. The chi-square per degree of freedom is $\chi^2/\mathrm{dof} = 3.82$ and the errors on the z-parameters have been rescaled by $\sqrt{\chi^2/\mathrm{dof}} = 1.95$. The form factors can be reconstructed using parametrization and inputs given in Appendix B 3 c.

$B_s \to K(N_f = 2+1)$								
	Central values	Correlation matrix						
a_0^+	0.370(21)	1	0.2781	−0.3169	−0.3576	0.6130	0.3421	0.2826
a_1^+	−0.68(10)	0.2781	1	0.3672	0.1117	0.4733	0.8487	0.8141
a_2^+	0.55(48)	−0.3169	0.3672	1	0.8195	0.3323	0.6614	0.6838
a_3^+	2.11(83)	−0.3576	0.1117	0.8195	1	0.2350	0.4482	0.4877
a_0^0	0.234(10)	0.6130	0.4733	0.3323	0.2350	1	0.6544	0.5189
a_1^0	0.135(86)	0.3421	0.8487	0.6614	0.4482	0.6544	1	0.9440
a_2^0	0.20(35)	0.2826	0.8141	0.6838	0.4877	0.5189	0.9440	1

method to perform extrapolations of the form factors to the full q^2 range with unitarity bounds, taking into account that the dispersive integral ranges only over an arc of the unit circle instead of the full circle [593,594]. However, we do not use these extrapolations in performing our average and instead use the synthetic data points provided in RBC/UKQCD 23 [128]. This allows users of our average to impose their own dispersive bounds in phenomenological applications if desired, since such bounds should be imposed only once.

In order to combine the results for the q^2-dependence of the form factors from the three collaborations, we will follow a similar approach to the one adopted above for $B \to \pi\ell\nu$, and produce synthetic data from the preferred fits quoted in the papers (or use the synthetic data provided in the paper), to obtain a dataset to which a joint fit can be performed. Note that the kinematic constraint at $q^2 = 0$ is included in all three cases; we will impose it in our fit as well, since the synthetic data will implicitly depend on that fitting choice. However, it is worth mentioning that the systematic uncertainty of the resulting extrapolated value $f_+(0) = f_0(0)$ can be fairly large, the main reason being the required long extrapolation from the high-q^2 region covered by lattice data. While we stress that the average far away from the high-q^2 region has to be used carefully, it is possible that increasing the number of z coefficients beyond what is sufficient for a good description of the lattice data and using unitarity constraints to control the size of additional terms, might yield fits with a more stable extrapolation at very low q^2. We plan to include said unitarity analysis into the next edition of the FLAG review. It is, however, important to emphasize that joint fits with experimental data, where the latter accurately map the low q^2 region, are expected to be safe.

Our fits employ a BCL *Ansatz* with $t_+ = (M_B + M_\pi)^2$ and $t_0 = t_+ - \sqrt{t_+(t_+ - t_-)}$, with $t_- = (M_{B_s} - M_K)^2$. Our pole factors will contain a single pole in both the vector and scalar channels, for which we take the mass values $M_{B^*} = 5.32465$ GeV and $M_{B^*(0^+)} = 5.68$ GeV.[48] The constraint $f_+(0) = f_0(0)$ is imposed by expressing the coefficient $b^0_{N^0-1}$ in terms of all others. The outcome of the seven-parameter $N^+ = N^0 = 4$ BCL fit, which we quote as our preferred result, is shown in Table 40. The fit has a chi-square per degree of freedom $\chi^2/\mathrm{dof} = 3.82$. Following the PDG recommendation, we rescale the whole covariance matrix by χ^2/dof: the errors on the z-parameters are increased by $\sqrt{\chi^2/\mathrm{dof}} = 1.95$ and the correlation matrix is unaffected. The parameters shown in Table 40 provide the averaged FLAG results for the lattice-computed form factors $f_+(q^2)$ and $f_0(q^2)$. The coefficient a_4^+ can be obtained from the values for a_0^+–a_3^+ using Eq. (B11). The fit is illustrated in Fig. 26.[49] As can be seen in Fig. 26, the large value of χ^2/dof is caused by a significant tension between the lattice results from the different collaborations for f_0. Compared to the FLAG 21 fit that used RBC/UKQCD 15, the tension has increased as the RBC/UKQCD results for f_0 have shifted upward. The tension indicates that the uncertainties have been underestimated in at least some of the calculations. One possible, at least partial, explanation was offered by the authors of RBC/UKQCD 23 [128], who found that the results for f_0 shift upward when

[48]These are the values used in the FNAL/MILC 19 determination, while HPQCD 14 and RBC/UKQCD 15 use $M_{B^*(0+)} = 5.6794(10)$ GeV and $M_{B^*(0+)} = 5.63$ GeV, respectively. They also employ different values of t_+ and t_0 than employed here, which again coincide with FNAL/MILC 19's choice.

[49]Note that in FLAG 19 [4] we had adopted the threshold $t_+ = (M_{B_s} + M_K)^2$ rather than $t_+ = (M_B + M_\pi)^2$. This change impacted the z-range which the physical q^2 interval maps onto. We also point out that, in the FLAG 19 version of Fig. 26, the three synthetic f_0 data points from HPQCD were plotted incorrectly, but this did not affect the fit.

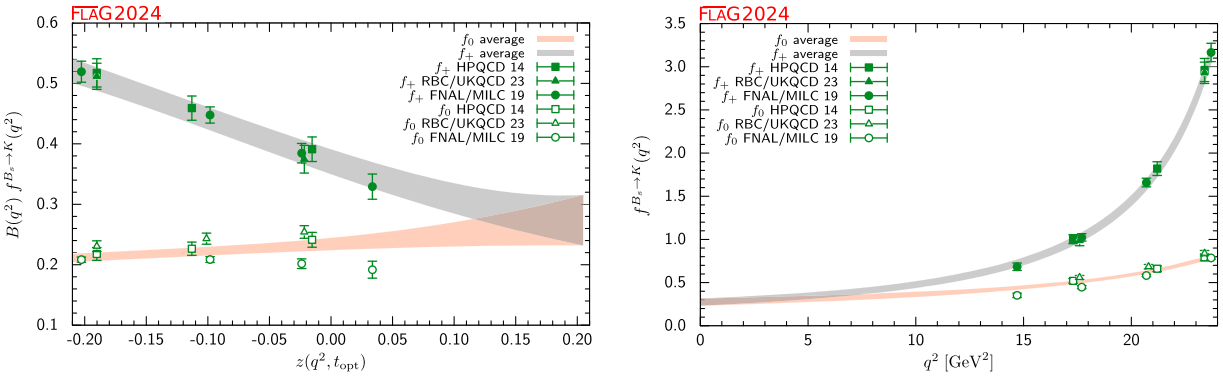


FIG. 26. The form factors $f_+(q^2)$ and $f_0(q^2)$ for $B_s \to K\ell\nu$ plotted versus z (left panel) and q^2 (right panel). In the left plot, we remove the Blaschke factors. See text for a discussion of the datasets. The gray and salmon bands display our preferred $N^+ = N^0 = 4$ BCL fit (seven parameters).

performing the chiral/continuum extrapolation directly for f_0 and f_+ rather than $f_\parallel$ and $f_\perp$ as was done in RBC/UKQCD 15 and FNAL/MILC 19. Using f_0 and f_+ is argued to be the better choice because these form factors have definite J^P quantum numbers for the bound states producing poles in q^2, and the chiral-continuum extrapolation fit functions include these poles. More details on the problems associated with taking the chiral/continuum extrapolation in the $f_\parallel$ and $f_\perp$ basis can be found in Appendix B 2.

A number of new calculations of the $B_s \to K$ form factors are underway. The JLQCD collaboration is using a fully relativistic approach with Möbius domain-wall fermions [595]. FNAL/MILC is pursuing two new calculations with HISQ light quarks, one of which uses Fermilab b quarks [596] and the other uses HISQ b quarks [597].

We will conclude by pointing out progress in the application of the npHQET method to the extraction of semileptonic form factors, reported for $B_s \to K$ transitions in Ref. [598], which extends the work of Ref. [599]. This is a methodological study based on CLS $N_f = 2$ ensembles at two different values of the lattice spacing and pion masses, and full $1/m_b$ corrections are incorporated within the npHQET framework. Emphasis is on the role of excited states in the extraction of the bare form factors, which are shown to pose an impediment to reaching precisions better than a few percent.

4. Form factors for rare and radiative B-semileptonic decays to light flavors

Lattice-QCD input is also available for some exclusive semileptonic decay channels involving neutral-current $b \to q$ transitions at the quark level, where $q = d,\ s$. Being forbidden at tree level in the SM, these processes allow for stringent tests of potential new physics; simple examples are $B \to K^*\gamma$, $B \to K^{(*)}\ell^+\ell^-$, or $B \to \pi\ell^+\ell^-$ where the B meson (and therefore the light meson in the final state) can be either neutral or charged.

The corresponding SM effective weak Hamiltonian is considerably more complicated than the one for the tree-level processes discussed above: after integrating out the top quark and the W boson, as many as ten dimension-six operators formed by the product of two hadronic currents or one hadronic and one leptonic current appear.[50] Three of the latter, coming from penguin and box diagrams, dominate at short distances and have matrix elements that, up to small QED corrections, are given entirely in terms of $B \to (\pi, K, K^*)$ form factors. The matrix elements of the remaining seven operators can be expressed, up to power corrections whose size is still unclear, in terms of form factors, decay constants and light-cone distribution amplitudes (for the π, K, K^* and B mesons) by employing OPE arguments (at large di-lepton invariant mass) [601,602] and results from QCD factorization (at small di-lepton invariant mass) [603]. In conclusion, the most important contributions to all of these decays are expected to come from matrix elements of current operators (vector, tensor, and axial-vector) between one-hadron states, which in turn can be parametrized in terms of a number of form factors (see Ref. [604] for a complete description).

In channels with pseudoscalar mesons in the final state, the level of sophistication of lattice calculations is similar to the $B \to \pi$ case. Early calculations of the vector, scalar, and tensor form factors for $B \to K\ell^+\ell^-$ by HPQCD 13E [130] and FNAL/MILC 15D [131] were performed with $N_f = 2 + 1$ flavors and EFT-based heavy-quark actions. FNAL/MILC 15E also determined the form factors for $B \to \pi\ell^+\ell^-$ [129]. Recently, HPQCD completed a new calculation of the $B \to K$ form factors with $N_f = 2 + 1 + 1$ flavors and HISQ b quarks (HPQCD 22) [492]. In the

[50]See, e.g., Ref. [600] and references therein.

TABLE 41. Summary of lattice calculations of the $B \to K$ semileptonic form factors.

Collaboration	Ref.	N_f	Publication status	Continuum extrapolation	Chiral extrapolation	Finite volume	Renormalization	Heavy-quark treatment	z-parametrization
HPQCD 22	[492]	$2+1+1$	A	★	★	★	★	✓	BCL
FNAL/MILC 15D	[131]	$2+1$	A	★	○	★	○	✓	BCL
HPQCD 13E	[130]	$2+1$	A	○	○	○	○	✓	BCL

following, we present an average of the two $N_f = 2+1$ calculations and a comparison with HPQCD's new $N_f = 2+1+1$ results. Details of the calculations are provided in Table 41 and in Appendix C 5 d.

The $N_f = 2+1$ calculations both employ MILC asqtad ensembles. HPQCD 13E [605] and FNAL/MILC 15D [606] have also companion papers in which they calculate the Standard Model predictions for the differential branching fractions and other observables and compare to experiment. The HPQCD computation employs NRQCD b quarks and HISQ valence light quarks, and parametrizes the form factors over the full kinematic range using a model-independent z-expansion as in Appendix B 2, including the covariance matrix of the fit coefficients. In the case of the (separate) FNAL/MILC computations, both of them use Fermilab b quarks and asqtad light quarks, and a BCL z-parametrization of the form factors.

FNAL/MILC 15E [129] includes results for the tensor form factor for $B \to \pi \ell^+ \ell^-$ not included in previous publications on the vector and scalar form factors (FNAL/MILC 15) [124]. Nineteen ensembles from four lattice spacings are used to control continuum and chiral extrapolations. The results for $N_z = 4$ z-expansion of the tensor form factor and its correlations with the expansions for the vector and scalar form factors presented in Table II of Ref. [129], which we consider the FLAG estimate, are shown in Table 42. Partial decay widths for decay into light leptons or $\tau^+\tau^-$ are presented as a function of q^2. The former is compared with results from LHCb [607], while the latter is a prediction.

The averaging of the HPQCD 13E and FNAL/MILC 15D $N_f = 2+1$ results for the $B \to K$ form factors is similar to our treatment of the $B \to \pi$ and $B_s \to K$ form factors. In this case, even though the statistical uncertainties are partially correlated because of some overlap between the adopted sets of MILC ensembles, we choose to treat the two calculations as independent. The reason is that, in $B \to K$, statistical uncertainties are subdominant and

TABLE 42. Coefficients and correlation matrix for the $N^T = 4$ z-expansion of the $B \to \pi$ form factor f_T. Results taken from Table II of Ref. [129].

$B \to \pi (N_f = 2+1)$					
	Central values	Correlation matrix			
a_0^T	0.393(17)	1.000	0.400	0.204	0.166
a_1^T	−0.65(23)	0.400	1.000	0.862	0.806
a_2^T	−0.6(1.5)	0.204	0.862	1.000	0.989
a_3^T	0.1(2.8)	0.166	0.806	0.989	1.000

cannot be easily extracted from the results presented by HPQCD 13E and FNAL/MILC 15D. Both collaborations provide only the outcome of a simultaneous z-fit to the vector, scalar and tensor form factors, that we use to generate appropriate synthetic data. We then impose the kinematic constraint $f_+(q^2 = 0) = f_0(q^2 = 0)$ and fit to a $(N^+ = N^0 = N^T = 3)$ BCL parametrization. The functional forms of the form factors that we use are identical to those adopted in Ref. [606].[51] The results of the fit are presented in Table 43. The fit is illustrated in Fig. 27. Note that the average for the f_T form factor appears to prefer the FNAL/MILC 15D synthetic data. This happens because we perform a correlated fit of the three form factors simultaneously (both FNAL/MILC 15D and HPQCD 13E present covariance matrices that include correlations between all form factors). We checked that the average for the f_T form factor, obtained neglecting correlations with f_0 and f_+, is a little lower and lies in between the two datasets. There is still a noticeable tension between the FNAL/MILC 15D and HPQCD 13E data for the tensor form factor; indeed, a stand-alone fit to these data results in $\chi^2_{\rm red} = 7.2/3 = 2.4$, while a similar stand-alone joint fit to f_+ and f_0 has $\chi^2_{\rm red} = 9.2/7 = 1.3$. Finally, the global fit that is shown in the figure has $\chi^2_{\rm red} = 18.6/10 = 1.86$.

The new $N_f = 2+1+1$ HPQCD 22 calculation of the $B \to K$ form factors [492] uses the HISQ action for all quarks including the b quark, which allows the determination of the vector- and axial-vector-current renormalization factors using Ward identities. The tensor current is renormalized using RI-SMOM [609]. The calculation is performed for multiple lighter-than-physical values of the heavy-quark mass and six different lattice spacings down to 0.044 fm; at the finest lattice spacing, the heavy-light pseudoscalar mass reaches approximately $0.94 M_{B,\rm phys}$. Three of the eight ensembles used have an approximately

[51]Note in particular that not much is known about the subthreshold poles for the scalar form factor. FNAL/MILC 15D includes one pole at the B^*_{s0} mass as taken from the calculation in Ref. [608].

TABLE 43. Coefficients and correlation matrix for the $N^+ = N^0 = N^T = 3$ z-expansion of the $B \to K$ form factors f_+, f_0 and f_T for $N_f = 2+1$. The coefficient a_2^0 is fixed by the $f_+(q^2=0) = f_0(q^2=0)$ constraint. The chi-square per degree of freedom is $\chi^2/\text{dof} = 1.86$ and the errors on the z-parameters have been rescaled by $\sqrt{\chi^2/\text{dof}} = 1.36$. The form factors can be reconstructed using parametrization and inputs given in Appendix B 3 d.

$B \to K(N_f = 2+1)$									
	Central values	Correlation matrix							
a_0^+	0.471(14)	1	0.513	0.128	0.773	0.594	0.613	0.267	0.118
a_1^+	−0.74 (16)	0.513	1	0.668	0.795	0.966	0.212	0.396	0.263
a_2^+	0.32(71)	0.128	0.668	1	0.632	0.768	−0.104	0.0440	0.187
a_0^0	0.301(10)	0.773	0.795	0.632	1	0.864	0.393	0.244	0.200
a_1^0	0.40(15)	0.594	0.966	0.768	0.864	1	0.235	0.333	0.253
a_0^T	0.455(21)	0.613	0.212	−0.104	0.393	0.235	1	0.711	0.608
a_1^T	−1.00 (31)	0.267	0.396	0.0440	0.244	0.333	0.711	1	0.903
a_2^T	−0.9 (1.3)	0.118	0.263	0.187	0.200	0.253	0.608	0.903	1

physical pion mass. The form factors in the physical limit are extracted from a modified BCL z-expansion fit with terms incorporating dependence on the heavy-quark mass, light and strange-quark masses, lattice spacing, and cover the entire q^2 range. The paper [492] includes supplemental files with the form-factor parameters and a Python code that can be used to reconstruct the form factors. The form factors are shown in Fig. 27 with the dark-shaded bands and are seen to be consistent with our average of the older $N_f = 2+1$ results. The $N_f = 2+1+1$ form factors are substantially more precise at low q^2 and somewhat less precise at high q^2. Standard Model predictions $B \to K\ell^+\ell^-$ and $B \to K\nu\bar{\nu}$ using these form factors are presented in a separate paper [610].

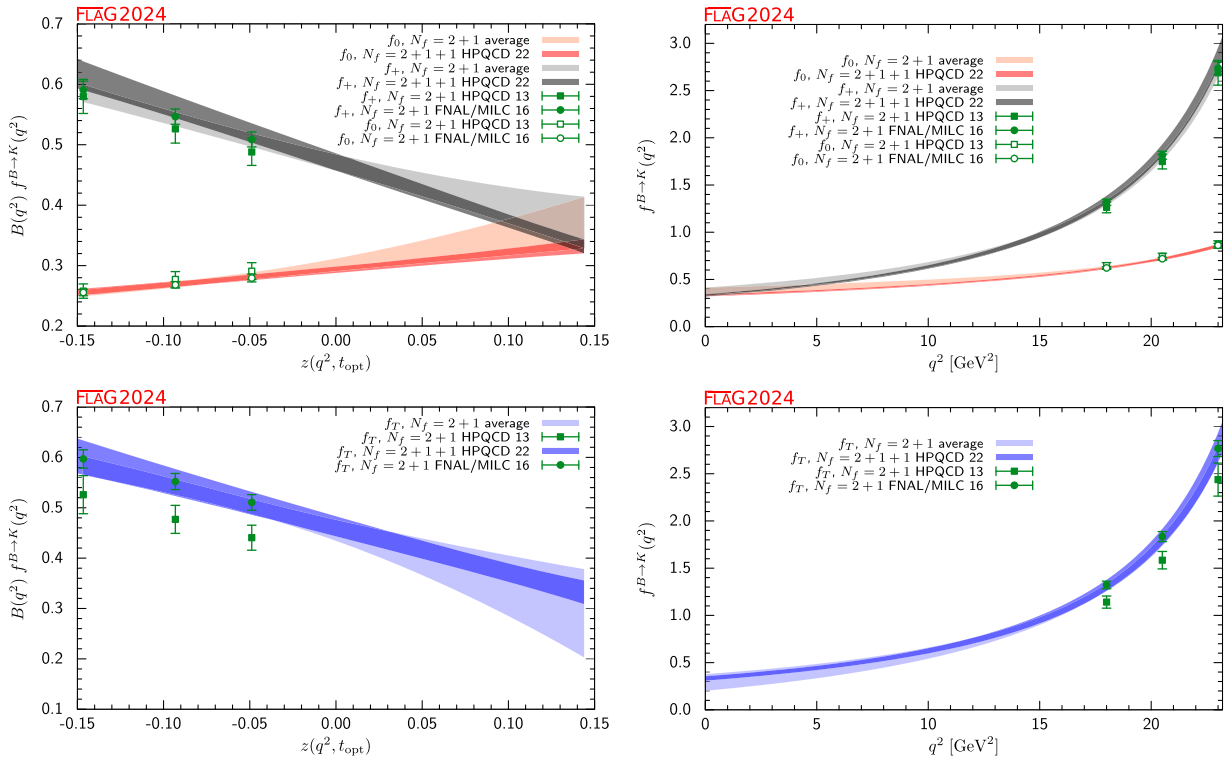


FIG. 27. The $B \to K$ form factors $f_+(q^2)$, $f_0(q^2)$ and $f_T(q^2)$ plotted versus z (left panels) and q^2 (right panels). In the plots as a function of z, we remove the Blaschke factors. See text for a discussion of the datasets. The light-shaded gray, salmon and blue bands display our preferred $N^+ = N^0 = N^T = 3$ BCL fit (eight parameters) to the $N_f = 2+1$ lattice results. The dark-shaded gray, salmon and blue bands display the $N_f = 2+1+1$ HPQCD 22 results [492].

Lattice computations of form factors in channels with a vector meson in the final state face extra challenges with respect to the case of a pseudoscalar meson: the state is unstable, and the extraction of the relevant matrix element from correlation functions is significantly more complicated; χPT cannot be used as a guide to extrapolate results at unphysically heavy pion masses to the chiral limit. While field-theory procedures to take resonance effects into account are available [579–589], they have not yet been implemented in the available computations of $B \to K^*$ and similar form factors, which therefore suffer from uncontrolled systematic errors (however, new calculations using these procedures are underway [591]).[52]

As a consequence of the complexity of the problem, the level of maturity of these computations is significantly below the one present for pseudoscalar form factors. Therefore, we only provide a short guide to the existing results. Horgan *et al.* have obtained the seven form factors governing $B \to K^* \ell^+ \ell^-$ (as well as those for $B_s \to \phi \ell^+ \ell^-$ and for the charged-current decay $B_s \to K^* \ell \nu$) in Ref. [611] using NRQCD b quarks and asqtad staggered light quarks. In this work, they use a modified z-expansion to simultaneously extrapolate to the physical light-quark masses and fit the q^2-dependence. As discussed above, the unstable nature of the vector mesons was not taken into account. Horgan *et al.* use their form-factor results to calculate the differential branching fractions and angular distributions and discuss the implications for phenomenology in a companion paper [612]. An update of the form factor fits that enforces endpoint relations and also provides the full correlation matrices can be found in Ref. [613]. Finally, preliminary results on $B \to K^* \ell^+ \ell^-$ and $B_s \to \phi \ell^+ \ell^-$ by RBC/UKQCD have been reported in Refs. [614–616].

D. Semileptonic form factors for $B_{(s)} \to D_{(s)} \ell \nu$ and $B_{(s)} \to D^*_{(s)} \ell \nu$

The semileptonic processes $B_{(s)} \to D_{(s)} \ell \nu$ and $B_{(s)} \to D^*_{(s)} \ell \nu$ have been studied extensively by experimentalists and theorists over the years. They allow for the determination of the CKM matrix element $|V_{cb}|$, an extremely important parameter of the Standard Model. The matrix element V_{cb} appears in many quantities that serve as inputs to CKM unitarity-triangle analyses and reducing its uncertainties is of paramount importance. For example, when ϵ_K, the measure of indirect CP violation in the neutral kaon system, is written in terms of the parameters ρ and η that specify the apex of the unitarity triangle, a factor of $|V_{cb}|^4$ multiplies the dominant term. As a result, the errors coming from $|V_{cb}|$ (and not those from B_K) are now the dominant uncertainty in the Standard Model (SM) prediction for this quantity.

[52]In cases such as $B \to D^*$ transitions, that will be discussed below, this is much less of a practical problem due to the very narrow nature of the resonance.

1. $B_{(s)} \to D_{(s)}$ decays

The decay rate for $B \to D \ell \nu$ can be parametrized in terms of vector and scalar form factors in the same way as, e.g., $B \to \pi \ell \nu$ (see Sec. VIII C). The quantities directly studied are the form factors $h_\pm$ defined by

$$\frac{\langle D(p_D)|i\bar{c}\gamma_\mu b|B(p_B)\rangle}{\sqrt{m_D m_B}} = h_+(w)(v_B + v_D)_\mu + h_-(w)(v_B - v_D)_\mu, \tag{192}$$

which are related to the standard vector and scalar form factors by

$$f_+(q^2) = \frac{1+r}{2\sqrt{r}}\left[h_+(w) - \frac{1-r}{1+r}h_-(w)\right] \equiv \frac{1+r}{2\sqrt{r}}\mathcal{G}(q^2), \tag{193}$$

$$f_0(q^2) = \sqrt{r}\left[\frac{1+w}{1+r}h_+(w) + \frac{1-w}{1-r}h_-(w)\right], \tag{194}$$

where $r = m_D/m_B$, $q^2 = (p_B - p_D)^2$, $v_A^\mu = p_A^\mu/m_A (A = D, B)$ are the four-velocities of the heavy mesons and $w = v_B \cdot v_D = (m_B^2 + m_D^2 - q^2)/(2m_B m_D)$.

The differential decay rate can then be written as

$$\frac{d\Gamma_{B^- \to D^0 \ell^- \bar{\nu}}}{dw} = \frac{G_F^2 m_D^3}{48\pi^3}(m_B + m_D)^2 (w^2-1)^{3/2} |\eta_{\rm EW}|^2 |V_{cb}|^2 |\mathcal{G}(w)|^2, \tag{195}$$

where $\eta_{\rm EW} = 1.0066$ is the 1-loop electroweak correction [471]. This formula does not include terms that are proportional to the lepton mass squared, which can be neglected for $\ell = e, \mu$.

Until recently, most unquenched lattice calculations for $B \to D \ell \nu$ decays focused on the form factor at zero recoil $\mathcal{G}^{B\to D}(1)$, which can then be combined with experimental input to extract $|V_{cb}|$. The main reasons for concentrating on the zero-recoil point are that (i) the decay rate then depends on a single form factor, and (ii) there are no $\mathcal{O}(\Lambda_{\rm QCD}/m_Q)$ contributions due to Luke's theorem [617]. Since HQET sets $\lim_{m_Q \to \infty} \mathcal{G}^{B\to D}(1) = 1$ [618–620], high precision calculations of $\mathcal{G}^{B\to D}(1)$ are possible [621–623]. The application of these HQET developments to lattice calculations leads to a better control of the systematic errors, especially at zero recoil [624,625]. In particular, the zero-recoil form factor can be computed via a double ratio in which most of the current renormalization cancels and heavy-quark discretization errors are suppressed by an additional power of $\Lambda_{\rm QCD}/m_Q$ [626].

Early computations of the form factors for $B \to D \ell \nu$ decays include $N_f = 2 + 1$ results by FNAL/MILC 04A

TABLE 44. Lattice results for mesonic processes involving $b \to c$ transitions. The form factor $\mathcal{G}$ is defined in Eqs. (192), (193), the form factor $\mathcal{F}$ is defined in Eqs. (202), (212), and the ratios R are defined in Eq. (221). Note that the results for $\mathcal{F}^{B\to D^*}(1)$, $\mathcal{F}^{B_s\to D_s^*}(1)$, $R(D^*)$ and $R(D_s^*)$ have been obtained using the results of the BGL fits described in the text and do not necessarily coincide with the results presented by the individual collaborations.

Collaboration	Ref.	N_f	Publication status	Continuum extrapolation	Chiral extrapolation	Finite volume	Renormalization	Heavy-quark treatment	$w=1$ form factor/ratio	
HPQCD 15, HPQCD 17	[133,627]	$2+1$	A	○	○	○	○	✓	$\mathcal{G}^{B\to D}(1)$	1.035(40)
FNAL/MILC 15C	[132]	$2+1$	A	★	○	★	○	✓	$\mathcal{G}^{B\to D}(1)$	1.054(4)(8)
HPQCD 19	[134]	$2+1+1$	A	★	★	○[a]	★	✓	$\mathcal{G}^{B_s\to D_s}(1)$	1.071(37)
HPQCD 15, HPQCD 17	[133,627]	$2+1$	A	○	○	○	○	✓	$\mathcal{G}^{B_s\to D_s}(1)$	1.068(40)
FNAL/MILC 21	[136]	$2+1$	A	★	○	★	○	✓	$\mathcal{F}^{B\to D^*}(1)$	0.909(17)
JLQCD 23	[137]	$2+1$	A	★	○	★	○	✓	$\mathcal{F}^{B\to D^*}(1)$	0.887(14)
HPQCD 23	[135]	$2+1+1$	A	★	★	★	★	✓	$\mathcal{F}^{B\to D^*}(1)$	0.903(14)
HPQCD 23	[135]	$2+1+1$	A	★	★	★	★	✓	$\mathcal{F}^{B_s\to D_s^*}(1)$	0.8970(92)
HPQCD 15, HPQCD 17	[133,627]	$2+1$	A	○	○	○	○	✓	$\mathcal{G}^{B_s\to D_s}(1)$	1.068(40)
HPQCD 20B	[628]	$2+1+1$	A	★	○	★	★	✓	n/a	n/a
HPQCD 15, HPQCD 17	[133,627]	$2+1$	A	○	○	○	○	✓	$R(D)$	0.300(8)
FNAL/MILC 15C	[132]	$2+1$	A	★	○	★	○	✓	$R(D)$	0.299(11)
FNAL/MILC 21	[136]	$2+1$	A	★	○	★	○	✓	$R(D^*)$	0.265(13)
JLQCD 23	[137]	$2+1$	A	★	○	★	○	✓	$R(D^*)$	0.252(22)
HPQCD 23	[135]	$2+1+1$	A	★	★	★	★	✓	$R(D^*)$	0.273(15)
HPQCD 23	[135]	$2+1+1$	A	★	★	★	★	✓	$R(D_s^*)$	0.266(9)

[a]The rationale for assigning a ○ rating is discussed in the text.

and FNAL/MILC 13B [629,630] for $\mathcal{G}^{B\to D}(1)$ and the $N_f = 2$ study by Atoui *et al.* [631], that in addition to providing $\mathcal{G}^{B\to D}(1)$ explored the $w > 1$ region. This latter work also provided the first results for $B_s \to D_s \ell\nu$ amplitudes, again including information about the momentum-transfer dependence. In 2014 and 2015, full results for $B \to D\ell\nu$ at $w \geq 1$ were published by FNAL/MILC 15C [132] and HPQCD 15 [133]. These works also provided full results for the scalar form factor, allowing analysis of the decay with a final-state τ. In FLAG 19 [4], we included new results for $B_s \to D_s \ell\nu$ form factors over the full kinematic range for $N_f = 2+1$ from HPQCD (HPQCD 17 [627] and Ref. [632]). Recently, HPQCD published new calculations of the $B_s \to D_s$ form factors in the full kinematic range [134] (HPQCD 19), now using MILC's HISQ $N_f = 2+1+1$ ensembles and using the HISQ action also for the b quark, reaching up to $m_b = 4m_c$ (unrenormalized mass) in their finest ensemble.[53] This calculation has recently been used by LHCb to determine $|V_{cb}|$ [633,634], as discussed further in Sec. VIII I.

In the discussion below, we mainly concentrate on the latest generation of results, which allows for an extraction of $|V_{cb}|$ that incorporates information about the q^2-dependence of the decay rate (cf. Sec. VIII I).

We will first discuss the $N_f = 2+1$ computations of $B \to D\ell\nu$ by FNAL/MILC 15C and HPQCD 15, both based on MILC asqtad ensembles. Full details about all the

[53]The ratio showed here is the ratio between the bare masses, which are inputs of the lattice action. The ratio between the renormalized masses of the quarks is usually very different from the ratio of bare masses. In order to tune the bare heavy-quark masses so they result in physical values of the renormalized quark masses, one normally tries to find out the value of the bare mass that results in a heavy meson with the right physical mass.

computations are provided in Table 44 and in the tables in Appendix C 5 e.

The FNAL/MILC 15C study [132] employs ensembles at four values of the lattice spacing ranging between approximately 0.045 fm and 0.12 fm, and several values of the light-quark mass corresponding to pions with RMS masses ranging between 260 MeV and 670 MeV (with just one ensemble with $M_\pi^{\mathrm{RMS}} \simeq 330$ MeV at the finest lattice spacing). The b and c quarks are treated using the Fermilab approach.

The hadronic form factor relevant for experiment, $\mathcal{G}(w)$, is then obtained from the relation $\mathcal{G}(w)=\sqrt{4r}f_+(q^2)/(1+r)$. The form factors are obtained from double ratios of three-point functions in which the flavor-conserving current renormalization factors cancel. The remaining matching factor to the flavor-changing normalized current is estimated with 1-loop lattice perturbation theory. In order to obtain $h_\pm(w)$, a joint continuum-chiral fit is performed to an *Ansatz* that contains the light-quark mass and lattice-spacing dependence predicted by next-to-leading order HMrSχPT, and the leading dependence on m_c predicted by the heavy-quark expansion ($1/m_c^2$ for h_+ and $1/m_c$ for h_-). The w-dependence, which allows for an interpolation in w, is given by analytic terms up to $(1-w)^2$, as well as a contribution from the logarithm proportional to $g^2_{D^*D\pi}$. The total resulting systematic error, determined as a function of w and quoted at the representative point $w = 1.16$ as 1.2% for f_+ and 1.1% for f_0, dominates the final error budget for the form factors. After f_+ and f_0 have been determined as functions of w within the interval of values of q^2 covered by the computation, synthetic data points are generated to be subsequently fitted to a z-expansion of the BGL form, cf. Sec. VIII C, with pole factors set to unity. This in turn enables one to determine $|V_{cb}|$ from a joint fit of this z-expansion and experimental data. The value of the zero-recoil form factor resulting from the z-expansion is

$$\mathcal{G}^{B\to D}(1) = 1.054(4)_{\mathrm{stat}}(8)_{\mathrm{sys}}. \tag{196}$$

The HPQCD computations HPQCD 15 and HPQCD 17 [133,627] use ensembles at two values of the lattice spacing, $a = 0.09, 0.12$ fm, and two and three values of light-quark masses, respectively. The b quark is treated using NRQCD, while for the c quark the HISQ action is used. The form factors studied, extracted from suitable three-point functions, are

$$\begin{aligned}\langle D_{(s)}(p_{D_{(s)}})|V^0|B_{(s)}\rangle &= \sqrt{2M_{B_{(s)}}}f_\parallel^{(s)},\\ \langle D_{(s)}(p_{D_{(s)}})|V^k|B_{(s)}\rangle &= \sqrt{2M_{B_{(s)}}}p^k_{D_{(s)}}f_\perp^{(s)},\end{aligned} \tag{197}$$

where V_μ is the relevant vector current and the $B_{(s)}$ rest frame is chosen. The standard vector and scalar form factors are retrieved as

$$f_+^{(s)} = \frac{1}{\sqrt{2M_{B_{(s)}}}}[f_\parallel^{(s)} + (M_{B_{(s)}} - E_{D_{(s)}})f_\perp^{(s)}], \tag{198}$$

$$f_0^{(s)} = \frac{\sqrt{2M_{B_{(s)}}}}{M^2_{B_{(s)}} - M^2_{D_{(s)}}}[(M_{B_{(s)}} - E_{D_{(s)}})f_\parallel^{(s)} + (M^2_{B_{(s)}} - E^2_{D_{(s)}})f_\perp^{(s)}]. \tag{199}$$

The currents in the effective theory are matched at 1-loop to their continuum counterparts. Results for the form factors are then fitted to a modified BCL z-expansion *Ansatz* [575], that takes into account simultaneously the lattice spacing, light-quark masses, and q^2-dependence. For the mass dependence, NLO chiral logarithms are included, in the form obtained in hard-pion χPT (see footnote 40). As in the case of the FNAL/MILC 15C computation, once f_+ and f_0 have been determined as functions of q^2, $|V_{cb}|$ can be determined from a joint fit of this z-expansion and experimental data. The papers quote for the zero-recoil vector form factor the result

$$\mathcal{G}^{B\to D}(1) = 1.035(40) \quad \mathcal{G}^{B_s\to D_s}(1) = 1.068(40). \tag{200}$$

The HPQCD 15 and FNAL/MILC 15C results for $B \to D$ differ by less than half a standard deviation (assuming they are uncorrelated, which they are not as some of the ensembles are common) primarily because of lower precision of the former result. The dominant source of errors in the $|V_{cb}|$ determination by HPQCD 15 are discretization effects and the systematic uncertainty associated with the perturbative matching.

In order to combine the form-factor determination of HPQCD 15 and the one of FNAL/MILC 15C into a lattice average, we proceed in a similar way as with $B \to \pi\ell\nu$ and $B_s \to K\ell\nu$ above. FNAL/MILC 15C quotes synthetic values for each form factor at three values of w (or, alternatively, q^2) with a full correlation matrix, which we take directly as input. In the case of HPQCD 15, we use their preferred modified z-expansion parametrization to produce synthetic values of the form factors at five different values of q^2 (three for f_+ and two for f_0). This leaves us with a total of six (five) data points in the kinematical range $w \in [1.00, 1.11]$ for the form factor f_+ (f_0). As in the case of $B \to \pi\ell\nu$, we conservatively assume a 100% correlation of statistical uncertainties between HPQCD 15 and FNAL/MILC 15C. We then fit this dataset to a BCL *Ansatz*, using $t_+ = (M_{B^0} + M_{D^\pm})^2 \simeq 51.12\,\mathrm{GeV}^2$ and $t_0 = (M_{B^0} + M_{D^\pm})(\sqrt{M_{B^0}} - \sqrt{M_{D^\pm}})^2 \simeq 6.19\ \mathrm{GeV}^2$. In our fits, pole factors have been set to unity, i.e., we do not take into account the effect of sub-threshold poles, which is then implicitly absorbed into the series coefficients. The reason for this is our imperfect knowledge of the relevant resonance spectrum in this channel, which does not allow us to decide the precise number of poles needed.[54] This, in turn, implies that unitarity bounds do not rigorously apply, which has to be taken into account when interpreting the results (cf. Appendix B 2).

[54]As noted above, this is the same approach adopted by FNAL/MILC 15C in their fits to a BGL *Ansatz*. HPQCD 15, meanwhile, uses one single pole in the pole factors that enter their modified z-expansion, using their spectral studies to fix the value of the relevant resonance masses.

TABLE 45. Coefficients and correlation matrix for the $N^+ = N^0 = 3$ z-expansion of the $B \to D$ form factors f_+ and f_0. The chi-square per degree of freedom is $\chi^2/\text{dof} = 4.6/6 = 0.77$. The lattice calculations that enter this fit are taken from FNAL/MILC 15C [132] and HPQCD 15 [133]. The form factors can be reconstructed using parametrization and inputs given in Appendix B 3 e.

$B \to D(N_f = 2+1)$						
a_n^i	Central values	Correlation matrix				
a_0^+	0.896(10)	1	0.423	−0.231	0.958	0.596
a_1^+	−7.94 (20)	0.423	1	0.325	0.498	0.919
a_2^+	51.4(3.2)	−0.231	0.325	1	−0.146	0.317
a_0^0	0.7821(81)	0.958	0.498	−0.146	1	0.593
a_1^0	−3.28 (20)	0.596	0.919	0.317	0.593	1

With a procedure similar to what we adopted for the $B \to \pi$ and $B_s \to K$ cases, we impose the kinematic constraint at $q^2 = 0$ by expressing the $a^0_{N^0-1}$ coefficient in the z-expansion of f_0 in terms of all the other coefficients. As mentioned above, FNAL/MILC 15C provides synthetic data for f_+ and f_0 including correlations; HPQCD 15 presents the result of simultaneous z-fits to the two form factors including all correlations, thus enabling us to generate a complete set of synthetic data for f_+ and f_0. Since both calculations are based on MILC ensembles, we then reconstruct the off-diagonal HPQCD 15-FNAL/MILC 15C entries of the covariance matrix by conservatively assuming that statistical uncertainties are 100% correlated. The FNAL/MILC 15C (HPQCD 15) statistical error is 58% (31%) of the total error for every f_+ value, and 64% (49%) for every f_0 one. Using this information we can easily build the off-diagonal block of the overall covariance matrix (e.g., the covariance between $[f_+(q_1^2)]_{\text{FNAL}}$ and $[f_0(q_2^2)]_{\text{HPQCD}}$ is $(\delta[f_+(q_1^2)]_{\text{FNAL}} \times 0.58)(\delta[f_0(q_2^2)]_{\text{HPQCD}} \times 0.49)$, where δf is the total error).

For our central value, we choose an $N^+ = N^0 = 3$ BCL fit, shown in Table 45. The coefficient a_3^+ can be obtained from the values for a_0^+–a_2^+ using Eq. (B11). We find $\chi^2/\text{dof} = 4.6/6 = 0.77$. The fit, which is dominated by the FNAL/MILC 15C calculation, is illustrated in Fig. 28.

Let us finally discuss the most recent results for $B_s \to D_s$ form factors, obtained by the HPQCD collaboration using MILC's $N_f = 2+1+1$ ensembles in Ref. [134] (HPQCD 19). Three values of the lattice spacing are used, including a very fine ensemble at $a \simeq 0.044$ fm; the pion mass is kept fixed at around 300 MeV, and in addition at the coarser $a \simeq 0.09$ fm lattice an ensemble with the physical pion mass is included. The scalar current needs no renormalization because of the partial conservation of the vector current (PCVC) relation, while the vector current is nonperturbatively normalized by imposing a condition based on the PCVC relation at zero recoil. Heavy quarks are treated in a fully relativistic fashion through the use of the HISQ regularization, employing bare values of the quark mass up to $am_h = 0.8$ for the extrapolation to the physical b point.

Results for the form factors are fitted to a modified z-expansion *Ansatz*, based on a BCL *Ansatz* with a Blaschke factor containing one sub-threshold pole, tuned to reproduce the lattice-spacing and heavy-quark-mass-dependent mass of the corresponding resonance. The final error budget is equally dominated by statistics and the combined effect of the continuum and heavy quark mass extrapolations, which correspond to 1.1% and 1.2% uncertainties, respectively, for the scalar form factor at zero recoil. The total uncertainty of f_0 is thus below 2%, which remains true in the whole q^2 range. The uncertainty of f_+ is somewhat larger, starting at around 2% at $q^2 = 0$ and increasing up to around 3.5% at zero recoil.

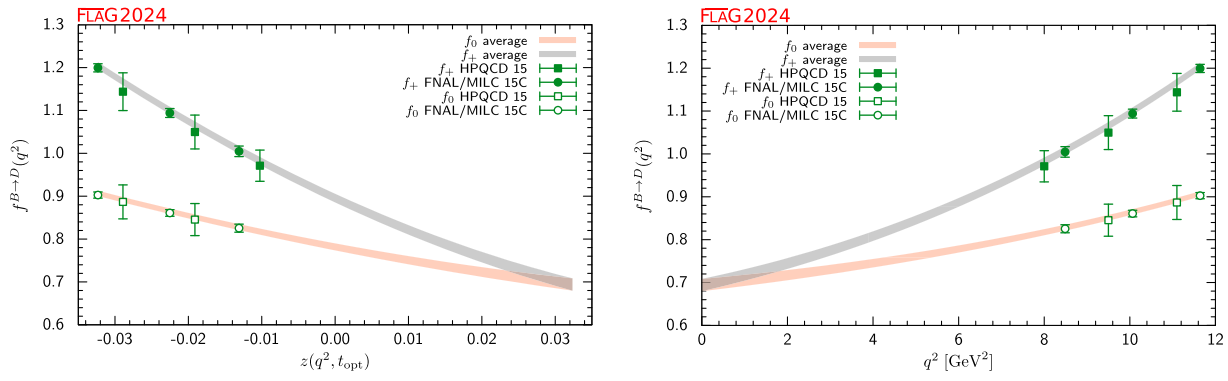


FIG. 28. The form factors $f_+(q^2)$ and $f_0(q^2)$ for $B \to D\ell\nu$ plotted versus z (left panel) and q^2 (right panel). See text for a discussion of the datasets. The gray and salmon bands display our preferred $N^+ = N^0 = 3$ BCL fit (five parameters).

TABLE 46. Coefficients and correlation matrix for the z-expansion of the $B_s \to D_s$ form factors f_+ and f_0. These results are a reproduction of Table VIII of Ref. [134] (HPQCD 19). The form factors can be reconstructed using parametrization and inputs given in Appendix B 3 f.

$B_s \to D_s (N_f = 2+1+1)$							
a_n^i	Central values	Correlation matrix					
a_0^0	0.666(12)	1	0.62004	0.03149	1	0.03973	0.00122
a_1^0	−0.26(25)	0.62004	1	0.36842	0.62004	0.12945	0.00002
a_2^0	−0.1(1.8)	0.03149	0.36842	1	0.03149	0.22854	−0.00168
a_0^+	0.666(12)	1	0.62004	0.03149	1	0.03973	0.00122
a_1^+	−3.24(45)	0.03973	0.12945	0.22854	0.03973	1	0.11086
a_2^+	−0.1(2.0)	0.00122	0.00002	−0.00168	0.00122	0.11086	1

One important matter of concern with this computation is the use of the $a \simeq 0.044$ fm ensemble with periodic boundary conditions, which suffers from severe topology freezing. Other than possible implications for statistical uncertainties, the lack of topology fluctuations are expected to significantly enhance finite-volume effects, which are no longer exponential in $m_\pi L$, but become power-like in the spatial volume. The authors neglect the impact of finite-volume effects in the computation, with a twofold argument: for the two coarser lattice spacings, the impact of pion-mass-related corrections on the heavy-meson states involved is presumably negligible; and, for the finest ensemble, the estimate of finite-volume effects on the D_s decay constant obtained in Ref. [180] turns out to be very small, a result which is presumed to extend to form factors. It is however unclear whether the latter argument would really hold, since the computation in Ref. [180] does show that the expected effect is heavily observable-dependent, reaching, e.g., more than 1% for f_D. We have, therefore, concluded that our standard criteria for finite-volume effects cannot be applied at the finest lattice spacing, and opted to assign ○ rating to them.

We thus proceed to quote the final result of HPQCD 19 as the FLAG estimate for the $N_f = 2+1+1$ $B_s \to D_s$ form factors. The preferred fit is a constrained BCL form with the imposition of the kinematical constraint $f_+(0) = f_0(0)$, carried through z^2 for f_0 and z^3 for f_+. Both form factors contain just one sub-threshold pole, to which the masses $M_{B_c^*} = 6.329\,\text{GeV}$ and $M_{B_{c0}} = 6.704\,\text{GeV}$, respectively, have been assigned. The fit parameters and covariance matrix, quoted in Table VIII of Ref. [134], are reproduced in Table 46.

There are ongoing efforts in these channels from several collaborations. The JLQCD collaboration is working on a $B \to D$ analysis at nonzero recoil using the domain-wall action for heavy and light quarks [635]. The FNAL/MILC collaborations are working on two parallel calculations of the form factors of the $B_{(s)} \to D_{(s)}$ channels sharing the same light-quark action, but with different heavy-quark actions [597].

2. $B_{(s)} \to D^*_{(s)}$ decays

The community has been focusing on the decays with final vector states, $B_{(s)} \to D^*_{(s)}$, because of increasing availability of high-quality experimental data. The decay rate for $B \to D^* \ell \nu$ involves a spin-1 hadron in the final-state whose vector and axial-vector current matrix elements require the introduction of four form factors

$$\frac{\langle D^*|V_\mu|B\rangle}{\sqrt{m_B m_{D^*}}} = h_V(w)\varepsilon_{\mu\nu\alpha\beta}\epsilon^{*\nu} v^\alpha_{D^*} v^\beta_B, \tag{201}$$

$$\frac{\langle D^*|A_\mu|B\rangle}{i\sqrt{m_B m_{D^*}}} = h_{A_1}(w)(1+w)\epsilon^{*\mu} - h_{A_2}(w)\epsilon^*\cdot v_B v_{B\mu} - h_{A_3}(w)\epsilon^*\cdot v_B v_{D^*\mu}. \tag{202}$$

where $w = v_B \cdot v_{D^{(*)}} = (m_B^2 + m_{D^*}^2 - q^2)/(2m_B m_{D^*})$. As has become customary, we further express the four form factors h_{V,A_1,A_2,A_3} in terms of the form factors g, f, F_1 and F_2 as follows (see, for instance, Eq. (31) of Ref. [135])

$$g = \frac{h_V}{m_B\sqrt{r}}, \tag{203}$$

$$f = m_B\sqrt{r}(1+w)h_{A_1}, \tag{204}$$

$$F_1 = m_B^2\sqrt{r}(1+w)[(w-r)h_{A_1} - (w-1)(rh_{A_2} + h_{A_3})], \tag{205}$$

$$F_2 = \frac{1}{\sqrt{r}}[(1+w)h_{A_1} + (rw-1)h_{A_2} + (r-w)h_{A_3}]. \tag{206}$$

One can then write the differential decay rate as [636,637]

$$\frac{d\Gamma_{\bar{B}\to D^*\ell\bar{\nu}}}{dw dc_v dc_l d\chi} = \frac{\eta_{\rm EW}^2 3 m_B m_{D^*}}{4(4\pi)^4}\sqrt{w^2-1}(1-2wr+r^2)G_F^2|V_{cb}|^2 \times [(1-c_l)^2 s_v^2 H_+^2 + (1+c_l)^2 s_v^2 H_-^2 + 4 s_l^2 c_v^2 H_0^2 - 2 s_l^2 s_v^2 \cos(2\chi) H_+ H_- - 4 s_l (1-c_l) s_v c_v \cos\chi H_+ H_0 + 4 s_l (1+c_l) s_v c_v \cos\chi H_- H_0], \tag{207}$$

where $c_v \equiv \cos\theta_v$, $s_v \equiv \sin\theta_v$, $c_l \equiv \cos\theta_l$, $s_l \equiv \sin\theta_l$. The angles θ_v, θ_l and χ parametrize the kinematics of the three-body final state (see, for instance, Fig. 3 of Ref. [144]). The helicity amplitudes $H_{\pm,0}$ have simple expressions in terms of the form factors g, f and F_1 (see, for instance, Eq. (13) of Ref. [144])

$$H_0 = \frac{F_1}{\sqrt{q^2}}, \tag{208}$$

$$H_\pm = f \mp m_B m_{D^*}\sqrt{w^2-1}\, g. \tag{209}$$

For the calculation of the ratio of the semileptonic rates in the τ and $\ell = e, \mu$ channels, it is necessary to consider the differential $d\Gamma/dw$ decay rate for nonzero lepton mass[55]

$$\frac{d\Gamma_{\bar{B}\to D^*\ell\bar{\nu}}}{dw} = |V_{cb}|^2 G_F^2 \eta_{\rm EW}^2 \frac{m_B^3}{48\pi^3} r^2 \sqrt{w^2-1}\left(1-\frac{m_l^2}{q^2}\right)^2 \times \left[\left(1+\frac{m_l^2}{2q^2}\right)\frac{q^2}{m_B^2}(H_+^2 + H_-^2 + m_B^2 H_0^2) + \frac{3}{2} r^2 \frac{m_B^2}{q^2} m_l^2 (w^2-1) F_2^2\right]. \tag{210}$$

In the limit of vanishing lepton mass, Eq. (210) reduces to

$$\frac{d\Gamma_{B^-\to D^{0*}\ell^-\bar{\nu}}}{dw} = \frac{G_F^2 m_{D^*}^3}{4\pi^3}(m_B - m_{D^*})^2 (w^2-1)^{1/2} |\eta_{\rm EW}|^2 |V_{cb}|^2 \chi(w) |\mathcal{F}(w)|^2. \tag{211}$$

The function $\chi(w)$ in Eq. (211) depends on the recoil w and the meson masses, and reduces to unity at zero recoil [600]. In particular, the normalization factor $\chi(w)$ [600] is defined in such a way that at zero recoil

$$\mathcal{F}(1) = h_{A_1}(1) = \frac{f(1)}{2\sqrt{m_B m_{D^*}}}. \tag{212}$$

Unquenched lattice calculations for $B \to D^*\ell\nu$ decays have focused on the form factors at zero recoil $\mathcal{F}^{B\to D^*}(1)$ until a few years ago (see, for instance, FNAL/MILC 08 [638], FNAL/MILC 14 [639], HPQCD 17B [640,641]); these can then be combined with experimental input to extract $|V_{cb}|$. The situation mirrors that of the channel $B \to D\ell\nu$: at the zero-recoil point a single form factor is enough to calculate the decay rate and Luke's theorem [617] guarantees the absence of $\mathcal{O}(\Lambda_{\rm QCD}/m_Q)$ corrections. By heavy-quark symmetry, $\lim_{m_Q\to\infty}\mathcal{F}^{B\to D^*}(1) = 1$ [618–620], since in that limit there is no distinction between heavy quarks. The calculation of higher-order corrections to this value has been systematically addressed in several publications [621–623,642], and also applied to lattice calculations [624,625]. On the lattice, the zero recoil form factor of this channel can also be computed via a double ratio, canceling most of the current renormalization and suppressing heavy-quark discretization errors by an additional power of $\Lambda_{\rm QCD}/m_Q$ [643]. The situation has dramatically improved recently, and now data away from the zero-recoil region is available from several sources. For that reason, we mainly concentrate on the latest generation of results in the discussion below, which allows for an extraction of $|V_{cb}|$ that incorporates information about the q^2-dependence of the decay rate (cf. Sec. VIII I).

Extraction of the form factors away from the zero-recoil point is quite challenging. The polarization of the D^* plays a key role in the correlation functions, as shown in Eq. (202). One can build the following double ratio

[55]This formula can be found, for instance, in Eq. (7) of Ref. [136]. Note that in Ref. [136] the normalizations of the helicity amplitudes $H_{\pm,0}$ differ from those adopted here.

$$\mathcal{R}_{A_1}(\mathbf{p}) = \frac{\langle D^*(\mathbf{p},\varepsilon_\perp)|\bar{c}\gamma_\perp\gamma_5 b|\bar{B}(\mathbf{0})\rangle\langle\bar{B}(\mathbf{0})|\bar{b}\gamma_\perp\gamma_5 c|D^*(\mathbf{p},\varepsilon_\perp)\rangle}{\langle D^*(\mathbf{0})|\bar{c}\gamma_4 c|D^*(\mathbf{0})\rangle\langle\bar{B}(\mathbf{0})|\bar{b}\gamma_4 b|\bar{B}(\mathbf{0})\rangle} \propto |h_{A_1}(w)|^2, \tag{213}$$

which is proportional to $|h_{A_1}(w)|^2$, as long as the D^* is transversally polarized (the spatial components of $\varepsilon_\perp$ are perpendicular to $\mathbf{p}$) and parallel to the axial current, which displays only spatial components ($\gamma_\perp$ is parallel to the spatial components of $\varepsilon_\perp$). At zero recoil, Eq. (213) greatly simplifies to give

$$\mathcal{R}_{A_1}(\mathbf{0}) = |h_{A_1}(1)|^2. \tag{214}$$

Hence, an alternative to directly computing Eq. (213) is to evaluate Eq. (214), and then compute the following ratio

$$\mathcal{Q}_{A_1} = \frac{\langle D^*(\mathbf{p},\varepsilon_\perp)|\bar{c}\gamma_\perp\gamma_5 b|\bar{B}(\mathbf{0})\rangle}{\langle D^*(\mathbf{0},\varepsilon)|\bar{c}\gamma_j\gamma_5 b|\bar{B}(\mathbf{0}))\rangle}, \tag{215}$$

which gives $h_{A_1}(w)/h_{A_1}(1)$ times extra factors that must be removed. Other form factors can be extracted by considering other polarizations and components of the axial current in Eq. (202), as well as the vector current. Normally, all the form factors are referenced to $h_{A_1}(w)$, therefore any systematics associated to the extraction of $h_{A_1}(w)$ are carried over to the remaining form factors.

Currently, there are two $N_f = 2+1$ calculations of the $B \to D^*\ell\nu$ form factors. One comes from the FNAL/MILC collaborations [136] (FNAL/MILC 21). It uses 15 MILC $N_f = 2+1$ ensembles generated with asqtad staggered quarks in the sea. The bottom and charm quarks are simulated using the clover action with the Fermilab interpretation, and they are tuned to their physical masses by using the D_s and the B_s mesons as references. This implies that the renormalization cannot be fully nonperturbative. The collaboration employs a clever scheme that computes ratios where the largest component of the renormalization factors cancels out, leaving a small component that is computed perturbatively. The MILC ensembles employed span five lattice spacings, ranging from $a \approx 0.15$ fm to $a \approx 0.045$ fm, and as many as five values of the light-quark masses per ensemble (though just one at the finest lattice spacing). Results are then extrapolated to the physical, continuum/chiral, limit employing staggered, heavy-light meson χPT.

The D^* meson is not a stable particle in QCD and decays predominantly into a D plus a pion. Nevertheless, heavy-light meson χPT can be applied to extrapolate lattice simulation results for the $B \to D^*\ell\nu$ form factor to the physical light-quark mass. The D^* width is quite narrow, 0.083(2) MeV for the $D^{*\pm}(2010)$ and less than 2.1 MeV for the $D^{*0}(2007)$ [274], making this system much more stable and long lived than the ρ or the K^* systems. Therefore it is appropriate to consider the D^* as a stable particle on the lattice, at the current level of precision. The fact that the $D^* - D$ mass difference is close to the pion mass leads to the well-known "cusp" in $\mathcal{R}_{A_1}$ just above the physical pion mass [643–645]. This cusp makes the chiral extrapolation sensitive to values used in the χPT formulas for the $D^*D\pi$ coupling $g_{D^*D\pi}$. In order to take this sensitivity into account, the FNAL/MILC collaboration includes this coupling in their fits as an input prior $g_{D^*D\pi} = 0.53 \pm 0.08$, but they do not analyze the impact of such a prior in the final result. By looking at their previous calculation at zero recoil [639] (FNAL/MILC 14), which used the same ensembles and statistics, we estimate a sub-percent increase in the total uncertainty for $h_{A_1}(1)$.

The final result presented in Ref. [136] (FNAL/MILC 21) is provided as synthetic data points for the four form factors in the HQET basis, $\{h_{A_1}, h_{A_2}, h_{A_3}, h_V\}$, at three different values of the recoil parameter, and a full covariance matrix. The result at zero recoil is

$$N_f = 2+1\text{: } \mathcal{F}^{B\to D^*}(1) = 0.909(17) \quad [\text{FNAL/MILC 21 [136]}] \tag{216}$$

making up a total error of 1.9%.The largest systematic uncertainty comes from discretization errors followed by effects of higher-order corrections in the chiral perturbation theory *Ansatz*.

The JLQCD collaboration has published the other $N_f = 2+1$ study of the $B \to D^*\ell\nu$ form factors away from the zero recoil point—JLQCD 23 [137]. Their calculation is based on nine $N_f = 2+1$ Möbius domain-wall ensembles, using the same action for the valence, heavy quarks b and c. The ensembles cover three different lattice spacings, starting from 0.080 fm down to 0.044 fm, and several pion masses ranging from ∼230 MeV to ∼500 MeV. The charm-quark mass is always physical, whereas the largest value of the bottom-quark mass reached is $\approx 3m_c$ (unrenormalized mass) in their finest ensemble. Each ensemble features at least 3 different values of the bottom-quark mass, but in the coarsest ensemble only $m_Q \approx 1.5m_c$ is reached. In terms of lattice units, the bottom-quark mass never exceeds $am_Q \lesssim 0.7$, and the final result does not significantly change if only data with $am_Q \lesssim 0.5$ (or equivalently $m_Q \lesssim 2.0m_c$) is employed. The three-point functions leading to the form factors are evaluated for four source-sink separations to properly control the excited-states contamination, and also the effects of possible topological freezing are carefully analyzed to rule out finite-volume effects. The renormalization scheme employed to renormalize the axial and vector currents is equivalent to a mostly nonperturbative renormalization scheme at tree level. However, the properties of the domain-wall action establish that $Z_A \approx Z_V$ at finite lattice spacing. Hence, we expect large cancellations of renormalization factors in ratios like Eq. (213). Also, discretization

errors in the coefficients are expected to behave better than $O(a)$ for the same reason.

Physical data is obtained after performing combined chiral-continuum and heavy-quark-mass extrapolations, which employs an approximate estimator for the covariance matrix, due to the low statistics of the input data and the large number of parameters involved (heavy- and light-quark masses, and lattice spacings). The *Ansatz* for the extrapolation is motivated by heavy-light meson χPT and HQET, and the collaboration uses the same value for the $D^*D\pi$ coupling $g_{D^*D\pi}$ as the FNAL/MILC collaboration, $g_{D^*D\pi} = 0.53 \pm 0.08$, but instead of including it as a prior in the fit, they estimate the systematics associated to the coupling by shifting the central value by $\pm\sigma$. The uncertainty arising from this choice is not provided, although it is explicitly stated that it is small.

The collaboration provides three synthetic data points per form factor in the BGL basis, $\{g, f, F_1, F_2\}$ as their final result of their extrapolation, along with a full covariance matrix. The result at zero recoil is not directly provided, but their BGL fit results in the following value,

$$N_f = 2+1: \mathcal{F}^{B\to D^*}(1) = 0.887(14) \quad [\text{JLQCD 23 [137]}]. \tag{217}$$

For $N_f = 2+1+1$ there is only one calculation away from the zero-recoil point, by the HPQCD collaboration [135]—HPQCD 23. They use five MILC HISQ ensembles and the HISQ action for both the light and the heavy quarks, reaching up to $m_b = 4m_c$ (unrenormalized mass) in their finest ensemble. The lattice spacings range from 0.090 fm down to 0.044 fm, and the pion masses are physical in two of the ensembles, whereas the rest use values $m_\pi \approx 320$ MeV. They calculate the form factors for three or four bare values of the heavy-quark mass, depending on the ensemble, topping at $am_Q \leq 0.8$. For the three-point functions, three different source-sink separations are evaluated, and the currents are renormalized nonperturbatively using the PCAC/PCVC relations and, for the tensor current, the RI-SMOM scheme [609]. The renormalization factors are interpolated for some correlators in one of the coarsest ensembles, and they are estimated for the finest ensemble with a physical pion mass, adding a conservative 1% error. As in previous analyses of HPQCD with a similar setup, the impact of fixing the topological charge in the finest ensembles is not discussed; nonetheless, it has been pointed out that the impact on the form factors of MILC ensembles with nonequilibrated topological charge is below 0.1% [123]. An important difference of this analysis from the $N_f = 2+1$ ones is the inclusion of twisted boundary conditions to reach larger values of the recoil parameter. As a result, HPQCD 23 offers data in the whole recoil range, as opposed to the other analyses, which are limited to the range $w \in [1.0, 1.2]$. The constraint between the form factors at maximum recoil then is naturally satisfied with great precision without any need to impose it. This feature also allows them to include higher powers of $(w-1)$ in the chiral-continuum extrapolation to model the recoil parameter dependence. Using BGL-inspired priors, the collaboration includes terms up to $(w-1)^{10}$, stemming from a z expansion up to z^4.

HPQCD 23 provides five synthetic data points per form factor, of which only three are completely independent, in the HQET basis, along with the full covariance matrix. The zero-recoil value of the decay amplitude is

$$N_f = 2+1+1: \mathcal{F}^{B\to D^*}(1) = 0.903(14) \quad [\text{FLAG average, HPQCD 23 [135]}], \tag{218}$$

in agreement with the value from FNAL/MILC 21, but with a slightly smaller total error, 1.6%. The largest systematic uncertainty comes from the treatment of the heavy quark.

We use synthetic data points provided by FNAL/MILC 21 [136] and JLQCD 23 [137] to fit the form factors g, f, F_1, and F_2 using a BGL parametrization. We adopt the same outer functions, poles, and z definition as in Sec. 5.1 of Ref. [136]. In particular, we impose the kinematic constraints at zero and maximal recoil (see Eqs. (72), (73) of Ref. [136]) by eliminating the coefficients $a_0^{F_1}$ and $a_0^{F_2}$. We also do not adopt priors for any of the coefficients and do not impose unitarity constraints. We found that a fit with $(N_g, N_f, N_{F_1}, N_{F_2}) = (2,3,3,2)$ provides an adequate description of the lattice data.[56] The results of the fits are presented in Table 47 and in Fig. 29. The two $N_f = 2+1$ calculations of FNAL/MILC 21 [136] and JLQCD 23 [137] are quite compatible and the combined fit yields $\chi^2_{\text{min}}/\text{dof} = 15.0/16$. In Fig. 29, we present also the $N_f = 2+1+1$ form factors obtained directly from results of the $N_f = 2+1+1$ HPQCD 23 [135] calculation in order to allow for a direct comparison between the $N_f = 2+1$ and $N_f = 2+1+1$ determinations. For completeness, we present the result for $\mathcal{F}^{B\to D^*}(1)$ as extracted from the fits in Table 47

$$N_f = 2+1: \mathcal{F}^{B\to D^*}(1) = 0.894(10) \quad [\text{FLAG average, Refs. [136, 137]}]. \tag{219}$$

Calculations in the $B_s \to D_s^*$ channel are relatively recent. The first calculations at zero recoil were done by the HPQCD collaboration in 2017 and 2019 [641,646] (HPQCD 17B and HPQCD 19B). In 2021, the same

[56]Adequate in the sense that the coefficients do not change much when adding more terms in the z expansion, but any extra coefficient becomes unphysically large with equally large errors. Hence, our choice is the maximum number of coefficients that can be reasonably determined with the given data without including extra information, like unitarity constraints.

TABLE 47. Coefficients and correlation matrix for the $(N_g, N_f, N_{F_1}, N_{F_2}) = (2,3,3,2)$ BGL fit to the $B \to D^*$ form factors g, f, F_1 and F_2 for $N_f = 2+1$. The form factors can be reconstructed using parametrization and inputs given in Appendix B 3 g.

$B \to D^*(N_f = 2+1)$									
Coeff	Central values	Correlation matrix							
a_0^g	0.03132(93)	1	0.1331	0.1786	0.03800	0.006578	0.06997	0.1061	0.03250
a_1^g	−0.057(26)	0.1331	1	0.001304	0.2425	0.1505	0.1342	0.1966	0.2331
a_0^f	0.01208(14)	0.1786	0.001304	1	−0.02370	0.09098	0.04710	0.1573	0.1161
a_1^f	0.0135(72)	0.03800	0.2425	−0.02370	1	−0.3968	0.6172	−0.01165	0.5136
a_2^f	−0.08(27)	0.006578	0.1505	0.09098	−0.3968	1	−0.2518	0.1880	−0.05661
$a_1^{F_1}$	−0.0032(18)	0.06997	0.1342	0.04710	0.6172	−0.2518	1	−0.1105	0.6653
$a_2^{F_1}$	−0.014(25)	0.1061	0.1966	0.1573	−0.01165	0.1880	−0.1105	1	0.5974
$a_1^{F_2}$	−0.188(44)	0.03250	0.2331	0.1161	0.5136	−0.05661	0.6653	0.5974	1

collaboration published the first study of the form factors of this channel at nonzero recoil [647] (HPQCD 21B), using four $N_f = 2+1+1$ MILC ensembles and the HISQ regularization for both sea and valence quarks, including the b quark. The lattice spacings range from 0.090 fm to 0.044 fm, and one of the coarsest ensembles features a physical pion mass, whereas the rest are generated with $m_\pi \approx 320$ MeV. Correlators are generated for each ensemble at three/four values of the bare-quark mass, never exceeding $am_Q \leq 0.8$, and the maximum heavy-quark mass simulated is $m_Q \approx 4m_c$ (nonrenormalized). Momentum is injected using twisted boundary conditions, which allows them to calculate the form factors directly at large values of the recoil parameter. This calculation was

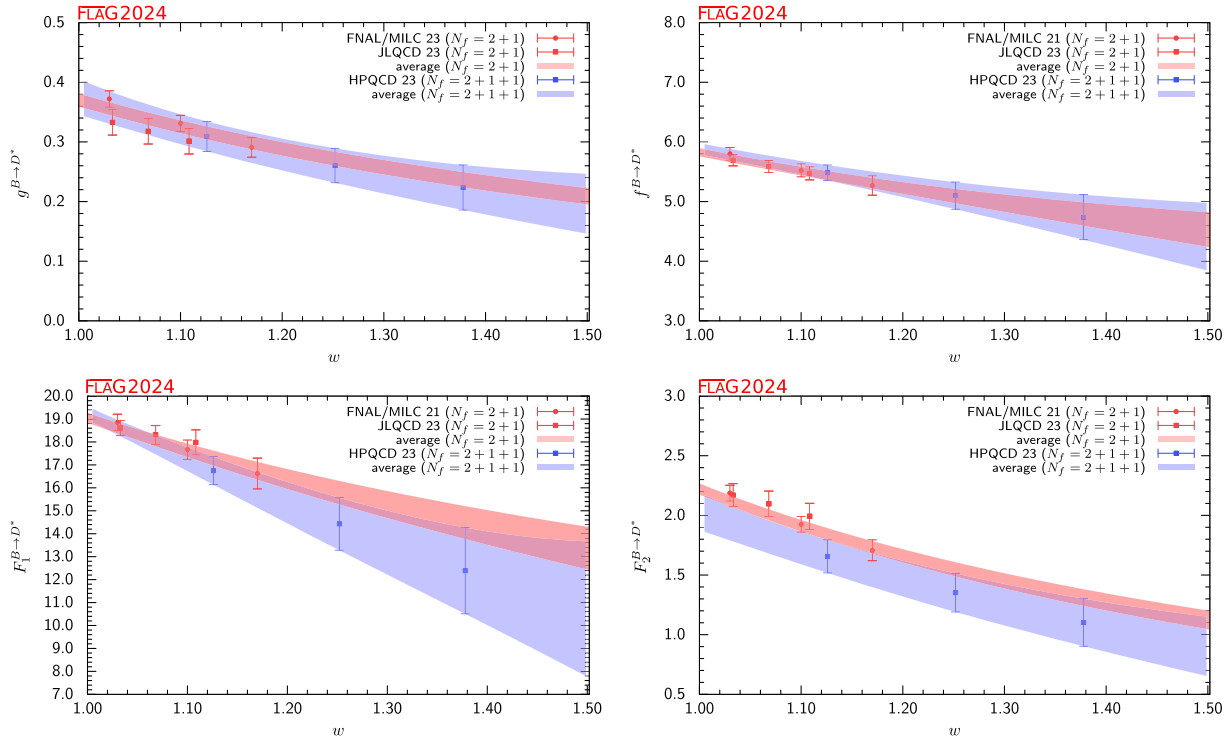


FIG. 29. The form factors g, f, F_1 and F_2 for $B \to D^* \ell\nu$ as a function of w. The red band displays our preferred $(N_g, N_f, N_{F_1}, N_{F_2}) = (2,3,3,2)$ BGL fit (eight parameters) to $N_f = 2+1$ lattice data. The constraints at zero and maximum recoil are imposed exactly. No use of unitarity constraints and priors has been made. The blue band is obtained using directly the $N_f = 2+1+1$ HPQCD 23 [135] results.

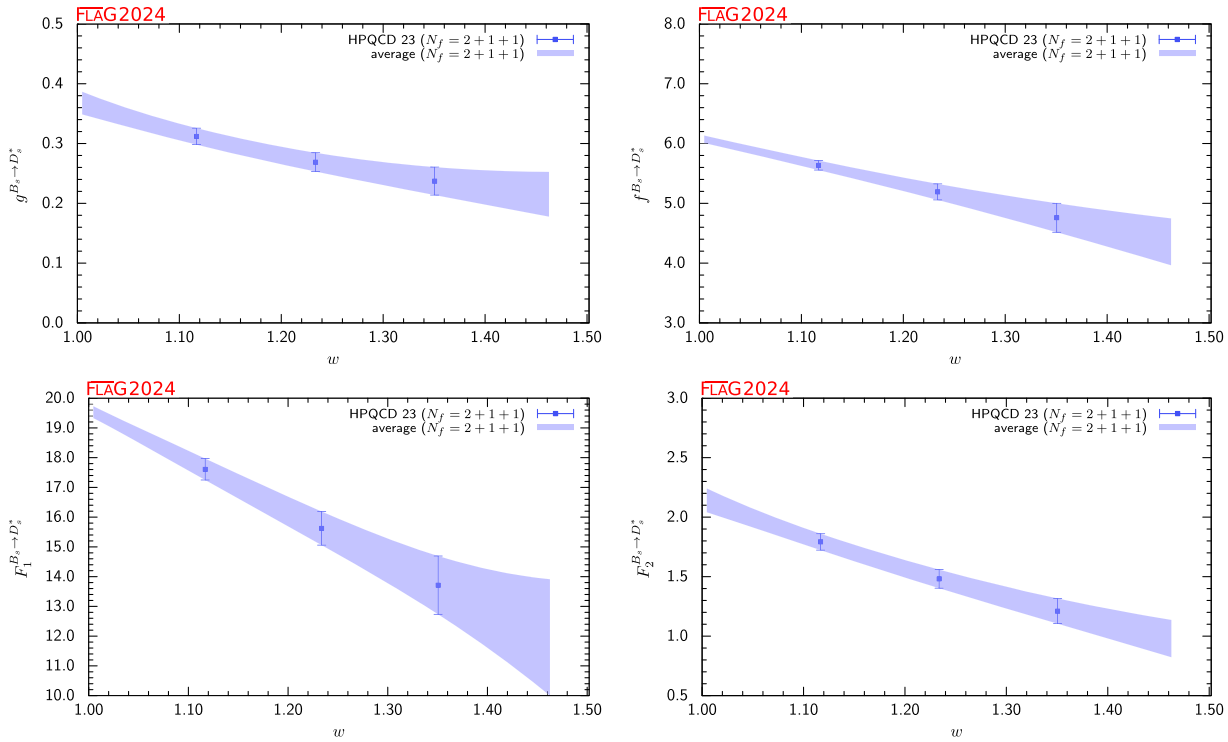


FIG. 30. The form factors g, f, F_1, and F_2 for $B_s \to D_s^* \ell\nu$ as a function of w. The blue band is obtained using directly the $N_f = 2+1+1$ HPQCD 23 [135] results.

recently superseded by a combined study of the $B_{(s)} \to D^*_{(s)}$ channels by HPQCD 23 [135], adding one more ensemble and increasing statistics. The details have already been outlined earlier in this section. Since there is only one available result (see Fig. 30), we set our $N_f = 2+1+1$ average to the HPQCD 23 value [135],

$$N_f = 2+1+1\text{: } \mathcal{F}^{B_s\to D_s^*}(1) = 0.8970(92) \quad \text{[FLAG average, Ref. [135]]}. \tag{220}$$

There are still ongoing efforts on both the $B \to D^*$ and the $B_s \to D_s^*$ channels, and we can expect improvements in the coming years. The FNAL/MILC collaborations are working in two different calculations in parallel for $B \to D^*$, mainly differing on the heavy-quark action: one calculation uses Fermilab heavy quarks, whereas the other uses the HISQ action for the c and the b quarks. Both calculations employ the HISQ action for the light sector [597]. The LANL-SWME collaboration is working on a different calculation, using MILC HISQ ensembles and the Oktay-Kronfeld action for the heavy sector [648].

3. Lepton-flavor-universality ratios $R(D^{(*)})$ and $R(D_s^{(*)})$

The availability of results for the scalar form factor f_0 for $B \to D\ell\nu$ amplitudes allows us to study interesting observables that involve the decay in the τ channel. One such quantity is the ratio

$$R\left(D^{(*)}_{(s)}\right) = \frac{\mathcal{B}\left(B \to D^{(*)}_{(s)}\tau\nu\right)}{\mathcal{B}\left(B \to D^{(*)}_{(s)}\ell\nu\right)} \quad \text{with} \quad \ell = e, \mu, \tag{221}$$

which, in the Standard Model, depends only on the form factors and hadron and lepton masses. Indeed, the recent availability of experimental results for $R(D)$ has made this quantity particularly relevant in the search for possible physics beyond the Standard Model. The most recent HFLAV average reads (see Ref. [148] and the Moriond 2024 update)

$$R(D)_{\text{exp}} = 0.342(26). \tag{222}$$

Using the FLAG average of the $B \to D$ form factors discussed above and presented in Table 45, we find $R(D)^{\text{FLAG}}_{\text{lat}} = 0.2938(38)$. The ratio $R(D)$ requires the integral of the branching ratios for $\ell = e$, μ, τ over the whole phase space. Since lattice simulations are sensitive mostly to relatively large q^2 values, lattice-only calculations of $R(D)$ rely on the extrapolation of the form factors to low q^2 and are especially sensitive to the choice of parametrization. In order to estimate this source of systematics, we repeated the fit using the parametrization adopted by HPQCD in Ref. [133]. The main difference with respect to our default paremeterization is the inclusion of Blaschke factors for the form factors f_+ and f_0 located at $M_+ = M_{B_c^*} = 6.330(9)$ GeV and $M_0 = 6.420(9)$ GeV~

$M_{B_{c0}}$[57]; additionally, the parameter t_0 is set to $(m_B - m_D)^2$. Using five coefficients ($a^+_{1,2,3}$ and $a^0_{1,2}$ with a^0_3 fixed by the $f_+(q^2=0)=f_0(q^2=0)$ condition) we find $R(D)^{\rm HPQCD}_{\rm lat} = 0.3009(38)$ which deviates from $R(D)^{\rm FLAG}_{\rm lat}$ by 1.4σ. To take this potential source of systematic uncertainty into account we rescale accordingly the uncertainty of our default fit and obtain

$$N_f = 2+1 : R(D)_{\rm lat} = 0.2938(54) \quad [\text{FLAG average, Refs. [132, 133]}]. \tag{223}$$

This result is about 1.5σ lower than the current experimental average [148] for this quantity. It has to be stressed that achieving this level of precision critically depends on the reliability with which the low-q^2 region is controlled by the parametrizations of the form factors.

HPQCD 17 also computes values for $R(D_s)$, the analog of $R(D)$ with both heavy-light mesons containing a strange quark. The earlier calculation using NRQCD b quarks gives

$$N_f = 2+1 : R(D_s)_{\rm lat} = 0.301(6) \quad [624]. \tag{224}$$

The newer calculation with HISQ b quarks, HPQCD 19, yields the somewhat more precise value

$$N_f = 2+1+1 : R(D_s)_{\rm lat} = 0.2987(46) \quad [134]. \tag{225}$$

A similar ratio $R(D^*)$ can be considered for $B \to D^*$ transitions. As a matter of fact, the experimental value of $R(D^*)$ is significantly more precise than the one of $R(D)$. The most recent HFLAV average reads (see Ref. [148] and the Moriond 2024 update)

$$R(D^*)_{\rm exp} = 0.287(12). \tag{226}$$

The recent developments in decays with vector products have yielded a variety of new lattice results for this LFU ratio. For $N_f = 2+1$ in the sea, the Fermilab lattice and MILC collaborations (FNAL/MILC 21) report the value

$$N_f = 2+1 : R(D^*)_{\rm lat} = 0.265(13) \quad [136], \tag{227}$$

which is around 1.5σ lower than the current experimental average [148].

The JLQCD collaboration has obtained the following value (JLQCD 23)

$$N_f = 2+1 : R(D^*)_{\rm lat} = 0.252(22) \quad [137]. \tag{228}$$

Their result is compatible with the FNAL/MILC 21 value, but it increases the tension with the experimental average up to 1.6σ, in spite of the larger error.

The HPQCD collaboration has also computed this ratio using $N_f = 2+1+1$ configurations, obtaining (HPQCD 23)

$$N_f = 2+1+1 : R(D^*)_{\rm lat} = 0.273(15) \quad [\text{FLAG average, [135]}], \tag{229}$$

which is closer to the current HFLAV average, but still lower by 1.3σ.

Using the results of the $N_f = 2+1$ (FNAL/MILC 21 and JLQCD 23) [136,137] fit summarized in Table 47, we calculate the following value for the ratio $R(D^*)$:

$$N_f = 2+1 : R(D^*)_{\rm lat} = 0.2582(51) \quad [\text{FLAG average, Refs. [136, 137]}]. \tag{230}$$

The HPQCD 23 analysis also covered the $B_s \to D_s^*$ channel, and for the first time a result for the $R(D_s^*)$ ratio is provided

$$N_f = 2+1+1 : R(D_s^*)_{\rm lat} = 0.266(9) \quad [\text{FLAG average, Ref. [135]}]. \tag{231}$$

4. Fragmentation fraction ratio f_s/f_d

Another area of immediate interest in searches for physics beyond the Standard Model is the measurement of $B_s \to \mu^+\mu^-$ decays, recently studied at the LHC. One of the inputs required by the LHCb analysis is the ratio of B_q meson ($q = d, s$) fragmentation fractions f_s/f_d, where f_q is the probability that a q quark hadronizes into a B_q. This ratio can be measured by writing it as a product of ratios that involve experimentally measurable quantities, cf. Refs. [649,650]. One of the factors is the ratio $f_0^{(s)}(M_\pi^2)/f_0^{(d)}(M_K^2)$ of scalar form factors for the corresponding semileptonic meson decay, which is where lattice input becomes useful.

A dedicated $N_f = 2+1$ study, FNAL/MILC 12C [651] addresses the ratios of scalar form factors $f_0^{(q)}(q^2)$,[58] and quotes

$$\begin{aligned} f_0^{(s)}(M_\pi^2)/f_0^{(d)}(M_K^2) &= 1.046(44)(15), \\ f_0^{(s)}(M_\pi^2)/f_0^{(d)}(M_\pi^2) &= 1.054(47)(17), \end{aligned} \tag{232}$$

where the first error is statistical and the second systematic. The more recent results from HPQCD 17 [627] are

[57]The value of $M_{B_{c0}}$ is not known from experiment and here we adopted the value used by HPQCD in Ref. [133].

[58]This work also provided a value for $R(D)$, now superseded by FNAL/MILC 15C [132].

$$f_0^{(s)}(M_\pi^2)/f_0^{(d)}(M_K^2) = 1.000(62),$$
$$f_0^{(s)}(M_\pi^2)/f_0^{(d)}(M_\pi^2) = 1.006(62). \quad (233)$$

Results from both groups lead to fragmentation fraction ratios f_s/f_d that are consistent with LHCb's measurements via other methods [650].

E. Semileptonic form factors for $B_c \to (\eta_c, J/\psi)\ell\nu$ decays

In a recent publication, HPQCD 20B [628] provided the first full determination of $B_c \to J/\psi$ form factors, extending earlier preliminary work that also covered $B_c \to \eta_c$, Refs. [652,653]. While the latter employed both NRQCD and HISQ actions for the valence b quark, and the HISQ action for the c quark, in HPQCD 20B the HISQ action is used throughout for all flavors. The setup is the same as for the $B_s \to D_s$ computation discussed above, HPQCD 19; we refer to the entries for the latter paper in summary tables for details. The flavor-singlet nature of the final state means that there are contributions to the relevant three-point functions from disconnected Wick contractions, which are not discussed in the paper.

Both the J/ψ and the η_c are unstable resonances, and the correct approach on the lattice would involve treating the J/ψ and the η_c as such. However, as in the case of the D^* meson, their widths are very narrow (93(2) keV for the J/ψ and 30.5(5) keV for the η_c). Hence, we can consider them as stable particles on the lattice.

In the J/ψ case, since the hadron in the final state has vector quantum numbers, the description of the hadronic amplitude requires four independent form factors, which in Ref. [628] have been chosen as

$$\langle J/\psi(p',\lambda)|\bar{c}\gamma^\mu b|B_c^-(p)\rangle = \frac{2iV(q^2)}{M_{B_c}+M_{J/\psi}}\varepsilon^{\mu\nu\rho\sigma}\epsilon_\nu^*(p',\lambda)p'_\rho p_\sigma,$$
$$\langle J/\psi(p',\lambda)|\bar{c}\gamma^\mu\gamma^5 b|B_c^-(p)\rangle = 2M_{J/\psi}A_0(q^2)\frac{\epsilon^*(p',\lambda)\cdot q}{q^2}q^\mu + (M_{B_c}+M_{J/\psi})A_1(q^2)\left[\epsilon^{*\mu}(p',\lambda) - \frac{\epsilon^*(p',\lambda)\cdot q}{q^2}q^\mu\right]$$
$$- A_2(q^2)\frac{\epsilon^*(p',\lambda)\cdot q}{M_{B_c}+M_{J/\psi}}\left[p^\mu + p'^\mu - \frac{M_{B_c}^2 - M_{J/\psi}^2}{q^2}q^\mu\right], \quad (234)$$

where ϵ_μ is the polarization vector of the J/ψ state. The computed form factors are fitted to a z-parametrization-inspired *Ansatz*, where coefficients are modified to model the lattice-spacing and the heavy- and light-mass dependences, for a total of 280 fit parameters. In the continuum and at physical kinematics only 16 parameters survive, as each form factor is parametrized by an expression of the form

$$F(q^2) = \frac{1}{P(q^2)}\sum_{n=0}^{3} a_n z^n, \quad (235)$$

where the pole factor is given by

$$P(q^2) = \prod_k z(q^2, M_k^2), \quad (236)$$

with $\{M_k\}$ a different set of pole energies below the BD^* threshold for each set of J^P quantum numbers, taken from a mixture of experimental results, lattice determinations, and model estimates. The values used (in GeV) are

$$0^-:\ 6.275, 6.872, 7.25;$$
$$1^-:\ 6.335, 6.926, 7.02, 7.28;$$
$$1^+:\ 6.745, 6.75, 7.15, 7.15. \quad (237)$$

The outcome of the fit, that we quote as a FLAG estimate, is

	a_0	a_1	a_2	a_3
V	0.1057(55)	−0.746(92)	0.10(98)	0.006(1.000)
$A0$	0.1006(37)	−0.731(72)	0.30(90)	−0.02(1.00)
$A1$	0.0553(19)	−0.266(40)	0.31(70)	0.11(99)
$A2$	0.0511(91)	−0.22(19)	−0.36(82)	−0.05(1.00)

The correlation matrix for the coefficients is provided in Tables XIX–XXVII of Ref. [628]. Using these form factors, the following Standard Model prediction for the lepton-flavor ratio $R(J/\psi)$ is obtained:

$$R(J/\psi)_{\text{lat}} = \frac{\Gamma(B_c^+ \to J/\psi\,\tau^+\nu_\tau)}{\Gamma(B_c^+ \to J/\psi\,\mu^+\nu_\mu)} = 0.2582(38),$$
$$N_f = 2+1+1 \quad [651]. \quad (238)$$

F. Semileptonic form factors for $\Lambda_b \to (p, \Lambda_c^{(*)})\ell\bar{\nu}$ decays

The $b \to c\ell\bar{\nu}$ and $b \to u\ell\bar{\nu}$ transitions can also be probed in decays of Λ_b baryons. With the LHCb experiment, the final state of $\Lambda_b \to p\mu\bar{\nu}$ is easier to identify than

that of $B \to \pi\mu\bar{\nu}$ [655], and the first determination of $|V_{ub}|/|V_{cb}|$ at the Large Hadron Collider was performed using a ratio of $\Lambda_b \to p\mu\bar{\nu}$ and $\Lambda_b \to \Lambda_c\mu\bar{\nu}$ decay rates [656] (cf. Sec. VIII J).

The amplitudes of the decays $\Lambda_b \to p\ell\bar{\nu}$ and $\Lambda_b \to \Lambda_c\ell\bar{\nu}$ receive contributions from both the vector and the axial-vector components of the current in the matrix elements $\langle p|\bar{u}\gamma^\mu(\mathbf{1}-\gamma_5)b|\Lambda_b\rangle$ and $\langle\Lambda_c|\bar{c}\gamma^\mu(\mathbf{1}-\gamma_5)b|\Lambda_b\rangle$. The matrix elements split into three form factors $f_+, f_0, f_\perp$ mediated by the vector component of the current, and another three form factors $g_+, g_0, g_\perp$ mediated by the axial-vector component—see, e.g., Ref. [494] for a complete description. Given the sensitivity to all Dirac structures, measurements of the baryonic decay rates also provides useful complementary constraints on right-handed couplings beyond the Standard Model [656].

To date, only one unquenched lattice-QCD computation of the $\Lambda_b \to p$ and $\Lambda_b \to \Lambda_c$ form factors with physical heavy-quark masses has been published: Detmold 15 [499]. This computation uses RBC/UKQCD $N_f = 2+1$ DWF ensembles, and treats the b and c quarks within the Columbia RHQ approach. The renormalization of the currents is carried out using a mostly nonperturbative method, with residual matching factors computed at one loop. Two values of the lattice spacing ($a \approx 0.11, 0.085$ fm) are considered, with the absolute scale set from the $\Upsilon(2S)$–$\Upsilon(1S)$ splitting. Sea-pion masses lie in a narrow interval ranging from slightly above 400 MeV to slightly below 300 MeV, keeping $m_\pi L \gtrsim 4$; however, lighter pion masses are considered in the valence DWF action for the u, d quarks. The lowest valence-valence pion mass is 227(3) MeV, which leads to a ■ rating of finite-volume effects. Results for the form factors are obtained from suitable three-point functions, and fitted to a modified z-expansion *Ansatz* that combines the q^2-dependence with the chiral and continuum extrapolations. The main results of the paper are the predictions (errors are statistical and systematic, respectively)

$$\zeta_{p\mu\bar{\nu}}(15\ \mathrm{GeV}^2) \equiv \frac{1}{|V_{ub}|^2}\int_{15\ \mathrm{GeV}^2}^{q^2_{\max}} \frac{\mathrm{d}\Gamma(\Lambda_b \to p\mu^-\bar{\nu}_\mu)}{\mathrm{d}q^2}\mathrm{d}q^2 = 12.31(76)(77)\ \mathrm{ps}^{-1}, \tag{239}$$

$$\zeta_{\Lambda_c\mu\bar{\nu}}(7\ \mathrm{GeV}^2) \equiv \frac{1}{|V_{cb}|^2}\int_{7\ \mathrm{GeV}^2}^{q^2_{\max}} \frac{\mathrm{d}\Gamma(\Lambda_b \to \Lambda_c\mu^-\bar{\nu}_\mu)}{\mathrm{d}q^2}\mathrm{d}q^2 = 8.37(16)(34)\ \mathrm{ps}^{-1}, \tag{240}$$

$$\frac{\zeta_{p\mu\bar{\nu}}(15\ \mathrm{GeV}^2)}{\zeta_{\Lambda_c\mu\bar{\nu}}(7\ \mathrm{GeV}^2)} = 1.471(95)(109), \tag{241}$$

which are the input for the LHCb analysis. Predictions for the total rates in all possible lepton channels, as well as for ratios similar to $R(D)$ (cf. Sec. VIII D) between the τ and light-lepton channels are also available, in particular,

$$R(\Lambda_c) = \frac{\Gamma(\Lambda_b \to \Lambda_c\,\tau^-\bar{\nu}_\tau)}{\Gamma(\Lambda_b \to \Lambda_c\,\mu^-\bar{\nu}_\mu)} = 0.3328(74)(70). \tag{242}$$

Datta 2017 [657] additionally includes results for the $\Lambda_b \to \Lambda_c$ tensor form factors h_+, $h_\perp$, $\tilde{h}_+$, $\tilde{h}_\perp$, based on the same lattice computation as Detmold 15 [499]. The main focus of Datta 2017 is the phenomenology of the $\Lambda_b \to \Lambda_c\tau\bar{\nu}_\tau$ decay and how it can be used to constrain contributions from beyond the Standard Model physics. Unlike in the case of the vector and axial-vector currents, the residual matching factors of the tensor currents are set to their tree-level value. While the matching systematic uncertainty is augmented to take this fact into account, the procedure implies that the tensor current retains an uncanceled logarithmic divergence at $\mathcal{O}(\alpha_s)$.

Progress with next-generation lattice calculations of the $\Lambda_b \to p$ and $\Lambda_b \to \Lambda_c$ form factors was reported in Ref. [658].

Recently, first lattice calculations have also been completed for Λ_b semileptonic decays to negative-parity baryons in the final state. Such calculations are substantially more challenging and have not yet reached the same level of precision. Meinel 21 [659], which was updated in Meinel 21B [503], considers the decays $\Lambda_b \to \Lambda_c^*(2595)\ell\bar{\nu}$ and $\Lambda_b \to \Lambda_c^*(2625)\ell\bar{\nu}$, where the $\Lambda_c^*(2595)$ and $\Lambda_c^*(2625)$ are the lightest charm baryons with isospin 0 and $J^P = \frac{1}{2}^-$ and $J^P = \frac{3}{2}^-$, respectively. These decay modes may eventually provide new opportunities to test lepton-flavor universality at the LHC, but are also very interesting from a theoretical point of view. The lattice results for the form factors may help tighten dispersive constraints in global analyses of $b \to c$ semileptonic decays [660], and may provide new insights into the internal structure of the negative-parity heavy baryons and their description in heavy-quark-effective-theory [661,662]. The $\Lambda_c^*(2595)$ and $\Lambda_c^*(2625)$ are very narrow resonances decaying through the strong interaction into $\Lambda_c\pi\pi$. The strong decays are neglected in Meinel 21 and Meinel 21B [503,659]. The calculation was performed using the same lattice actions as previously for $\Lambda_b \to \Lambda_c$, albeit with newly tuned RHQ parameters. Only three ensembles are used, with $a \approx 0.11, 0.08$ fm and pion masses in the range from approximately 300 to 430 MeV, with valence-quark masses equal to the sea-quark masses. Chiral-continuum extrapolations linear in m_π^2 and a^2 are performed, with systematic uncertainties estimated using higher-order fits. Finite-volume effects and effects associated with the strong decays of the Λ_c^*'s are not quantified. The calculation is done in the Λ_c^* rest frame, where the cubic symmetry is sufficient to avoid mixing with unwanted lower-mass states. As a consequence, the calculation is limited to a small kinematic region near the zero-recoil point $w = 1$. On each ensemble, lattice data were produced for two values of $w-1$ of approximately 0.01 and 0.03. The final results for the form factors are parametrized as linear functions of $w-1$ and

TABLE 48. Summary of computations of bottom-baryon semileptonic form factors (see also Refs. [665,671] for calculations with static b quarks). The rationale for the ■ rating of finite-volume effects in Meinel 20, Meinel 21, and Meinel 21B (despite meeting the ○ criterion based on the minimum pion mass) is that the unstable nature of the final-state baryons was neglected in the analysis.

Process	Collaboration	Ref.	N_f	Publication status	Continuum extrapolation	Chiral extrapolation	Finite volume	Renormalization	Heavy-quark treatment
$\Lambda_b \to \Lambda_c^*(2625)\ell^-\bar{\nu}_\ell$	Meinel 21B	[503]	$2+1$	A	○	○	■	○	✓
$\Lambda_b \to \Lambda_c^*(2595)\ell^-\bar{\nu}_\ell$	Meinel 21B	[503]	$2+1$	A	○	○	■	○	✓
$\Lambda_b \to \Lambda_c^*(2625)\ell^-\bar{\nu}_\ell$	Meinel 21	[659]	$2+1$	A	○	○	■	○	✓
$\Lambda_b \to \Lambda_c^*(2595)\ell^-\bar{\nu}_\ell$	Meinel 21	[659]	$2+1$	A	○	○	■	○	✓
$\Lambda_b \to \Lambda^*(1520)\ell^+\ell^-$	Meinel 21B	[503]	$2+1$	A	○	○	■	○	✓
$\Lambda_b \to \Lambda^*(1520)\ell^+\ell^-$	Meinel 20	[670]	$2+1$	A	○	○	■	○	✓
$\Lambda_b \to \Lambda\ell^+\ell^-$	Detmold 16	[666]	$2+1$	A	○	○	■	○	✓
$\Lambda_b \to p\ell^-\bar{\nu}_\ell$	Detmold 15	[499]	$2+1$	A	○	○	■	○	✓
$\Lambda_b \to \Lambda_c\ell^-\bar{\nu}_\ell$	Detmold 15, Datta 17	[499,657]	$2+1$	A	○	○	■	○	✓

can be found in Meinel 21B [503] and associated supplemental files.

G. Semileptonic form factors for $\Lambda_b \to \Lambda^{(*)}\ell\ell$

The decays $\Lambda_b \to \Lambda\ell^+\ell^-$ are mediated by the same underlying $b \to s\ell^+\ell^-$ FCNC transition as, for example, $B \to K\ell^+\ell^-$ and $B \to K^*\ell^+\ell^-$, and can therefore provide additional information on the hints for physics beyond the Standard Model seen in the meson decays. The Λ baryon in the final state decays through the weak interaction into $p\pi^-$ (or $n\pi^0$), leading to a wealth of angular observables even for unpolarized Λ_b. When including the effects of a nonzero Λ_b polarization, $\Lambda_b \to \Lambda(\to p\pi^-)\ell^+\ell^-$ decays are characterized by five angles leading to 34 angular observables [663], which have been measured by LHCb in the bin $q^2 \in [15, 20]$ GeV^2 [664]. Given that the Λ is stable under the strong interactions, the $\Lambda_b \to \Lambda$ form factors parametrizing the matrix elements of local $\bar{s}\Gamma b$ currents can be calculated on the lattice with high precision using standard methods. Of course, the process $\Lambda_b \to \Lambda\ell^+\ell^-$ also receives contributions from nonlocal matrix elements of four-quark and quark-gluon operators in the weak effective Hamiltonian combined with the electromagnetic current. As with the mesonic $b \to s\ell^+\ell^-$ decays, these contributions cannot easily be calculated on the lattice and one relies on other theoretical tools for them, including the local OPE at high q^2 and a light-cone OPE/QCD factorization at low q^2.

Following an early calculation with static b quarks [665], Detmold 16 [666] provides results for all ten relativistic $\Lambda_b \to \Lambda$ form factors parametrizing the matrix elements of the local vector, axial-vector and tensor $b \to s$ currents. The lattice setup is identical to that used in the 2015 calculation of the $\Lambda_b \to p$ form factors in Detmold 15 [499], and similar considerations as in the previous section thus apply. The lattice data cover the upper 60% of the q^2 range, and the form factors are extrapolated to the full q^2 range using BCL z-expansion fits. This extrapolation is done simultaneously with the chiral and continuum extrapolations. The caveat regarding the renormalization of the tensor currents also applies here. Progress with next-generation lattice calculations of the $\Lambda_b \to \Lambda$ form factors was reported in Ref. [658].

Reference [667] uses the lattice results for the $\Lambda_b \to \Lambda$ form factors together with the experimental results for $\Lambda_b \to \Lambda(\to p\pi^-)\mu^+\mu^-$ from LHCb [664,668] to perform fits of the $b \to s\mu^+\mu^-$ Wilson coefficients and of the Λ_b polarization parameter. Given the uncertainties (which are still dominated by experiment), the results for the Wilson coefficients are presently consistent both with the Standard Model values and with the deviations seen in global fits that include all mesonic decays [526,669].

As with the $b \to c$ semileptonic form factors, a first lattice calculation, Meinel 2020 [670] (updated in Meinel 21B [503]), was also completed for a $b \to s$ transition to a negative-parity baryon in the final state, in this case the $\Lambda^*(1520)$ with $J^P = \frac{3}{2}^-$ (no calculation has yet been

published for the strange $J^P = \frac{1}{2}^-$ final states, which would be the broader and even more challenging $\Lambda^*(1405)/\Lambda^*(1380)$ [225]). The $\Lambda^*(1520)$ decays primarily to $pK^-/n\bar{K}^0$, $\Sigma\pi$, and $\Lambda\pi\pi$ with a total width of 15.6 ± 1.0 MeV [225]. The analysis of the lattice data again neglects the strong decays and does not quantify finite-volume effects, and is again limited to a small kinematic region near $q^2_{\max}$. The results of Meinel 2020 are superseded by Meinel 21B [503], in which the fits to the lattice data were improved by including exact endpoint relations in the form-factor parametrizations.

H. Determination of $|V_{ub}|$

We now use the lattice-determined Standard Model transition amplitudes for leptonic (Sec. VIII A) and semileptonic (Sec. VIII C) B-meson decays to obtain exclusive determinations of the CKM matrix element $|V_{ub}|$. In this section, we describe the aspect of our work that involves experimental input for the relevant charged-current exclusive decay processes. The relevant formulas are Eqs. (155) and (191). Among leptonic channels the only input comes from $B \to \tau\nu_\tau$, since the rates for decays to e and μ have not yet been measured. In the semileptonic case, we only consider $B \to \pi\ell\nu$ transitions (experimentally measured for $\ell = e, \mu$).

We first investigate the determination of $|V_{ub}|$ through the $B \to \tau\nu_\tau$ transition. The experimental measurements of the branching fraction of this channel, $B(B^- \to \tau^-\bar{\nu})$, have not been updated since the publication of FLAG 16 [3]. The status of the experimental results for this branching fraction, summarized in Table 49, is unchanged from FLAG 16 [3]. Our corresponding values of $|V_{ub}|$ are unchanged from FLAG 19 [4].

It is obvious that all the measurements listed in Table 49 have significance smaller than 5σ, and the large uncertainties are dominated by statistical errors. These measurements lead to the averages of experimental measurements for $B(B^- \to \tau\bar{\nu})$ [514,515],

TABLE 49. Experimental measurements for $B(B^- \to \tau^-\bar{\nu})$. The first error on each result is statistical, while the second error is systematic.

Collaboration	Tagging method	$B(B^- \to \tau^-\bar{\nu}) \times 10^4$
Belle [672]	Hadronic	$0.72^{+0.27}_{-0.25} \pm 0.11$
Belle [515]	Semileptonic	$1.25 \pm 0.28 \pm 0.27$
BABAR [514]	Hadronic	$1.83^{+0.53}_{-0.49} \pm 0.24$
BABAR [673]	Semileptonic	$1.7 \pm 0.8 \pm 0.2$

$$B(B^- \to \tau\bar{\nu}) \times 10^4 = 0.91 \pm 0.22 \text{ from Belle}, \quad (243)$$

$$= 1.79 \pm 0.48 \text{ from } BABAR, \quad (244)$$

$$= 1.06 \pm 0.33 \text{ average}, \quad (245)$$

where, following our standard procedure, we perform a weighted average and rescale the uncertainty by the square root of the reduced chi-squared. Note that the Particle Data Group [274] did not inflate the uncertainty in the calculation of the averaged branching ratio.

Combining the results in Eqs. (243)–(245) with the experimental measurements of the mass of the τ-lepton and the B-meson lifetime and mass we get

$$|V_{ub}| f_B = 0.72 \pm 0.09 \text{ MeV from Belle}, \quad (246)$$

$$= 1.01 \pm 0.14 \text{ MeV from } BABAR, \quad (247)$$

$$= 0.77 \pm 0.12 \text{ MeV average}, \quad (248)$$

which can be used to extract $|V_{ub}|$ using the averages in Eqs. (162), (165) and (168), viz.,

$$|V_{ub}| = 3.83(14)(48) \times 10^{-3} \quad [B \to \tau\nu_\tau, \text{Belle}], \quad (249)$$

$$N_f = 2 : |V_{ub}| = 5.37(20)(74) \times 10^{-3} \quad [B \to \tau\nu_\tau, BABAR], \quad (250)$$

$$|V_{ub}| = 4.10(15)(64) \times 10^{-3} \quad [B \to \tau\nu_\tau, \text{average}], \quad (251)$$

$$|V_{ub}| = 3.75(8)(47) \times 10^{-3} \quad [B \to \tau\nu_\tau, \text{Belle}], \quad (252)$$

$$N_f = 2+1 : |V_{ub}| = 5.26(12)(73) \times 10^{-3} \quad [B \to \tau\nu_\tau, BABAR], \quad (253)$$

$$|V_{ub}| = 4.01(9)(63) \times 10^{-3} \quad [B \to \tau\nu_\tau, \text{average}], \quad (254)$$

$$|V_{ub}| = 3.79(3)(47) \times 10^{-3} \quad [B \to \tau\nu_\tau, \text{Belle}], \quad (255)$$

$$N_f = 2+1+1 : |V_{ub}| = 5.32(4)(74) \times 10^{-3} \quad [B \to \tau\nu_\tau, BABAR], \quad (256)$$

$$|V_{ub}| = 4.05(3)(64) \times 10^{-3} \quad [B \to \tau\nu_\tau, \text{average}], \quad (257)$$

TABLE 50. Value of $|V_{ub}|$, coefficients for the $N^+ = N^0 = N^T = 3$ z-expansion of the $B \to \pi$ form factors f_+ and f_0, and their correlation matrix. The chi-square per degree of freedom is $\chi^2/\text{dof} = 116.7/62 = 1.88$ and the errors on the fit parameters have been rescaled by $\sqrt{\chi^2/\text{dof}} = 1.37$. The lattice calculations that enter this fit are taken from FNAL/MILC 15 [124], RBC/UKQCD 15 [125] and JLQCD 22 [126]. The experimental inputs are taken from *BABAR* [138,139] and Belle [140,141]. The form factors can be reconstructed using parametrization and inputs given in Appendix B 3 b.

$B \to \pi\ell\nu (N_f = 2+1)$							
	Central values	Correlation matrix					
$\lvert V_{ub}\rvert \times 10^3$	3.61(16)	1	−0.812	−0.108	0.128	−0.326	−0.151
a_0^+	0.425(15)	−0.812	1	−0.188	−0.309	0.409	0.00926
a_1^+	−0.441 (39)	−0.108	−0.188	1	−0.498	−0.0343	0.150
a_2^+	−0.52 (13)	0.128	−0.309	−0.498	1	−0.190	0.128
a_0^0	0.560(17)	−0.326	0.409	−0.0343	−0.190	1	−0.772
a_1^0	−1.346 (53)	−0.151	0.00926	0.150	0.128	−0.772	1

where the first error comes from the uncertainty in f_B and the second comes from experiment. The experimental branching fractions do not yet meet the five-sigma discovery threshold and the relative uncertainties are significantly larger than the radiative electroweak corrections. Therefore, in line with the Particle Data Group [274] and in contrast to the $D_{(s)}$ decays, we do not include in these results the electroweak corrections.

Let us now turn our attention to semileptonic decays. The experimental value of $|V_{ub}|f_+(q^2)$ can be extracted from the measured branching fractions for $B^0 \to \pi^\pm \ell\nu$ or $B^\pm \to \pi^0 \ell\nu$ by applying Eq. (191).[59] We then determine $|V_{ub}|$ by performing fits to the constrained BCL z-parametrization of the form factor $f_+(q^2)$ given in Eq. (B12). This can be done in two ways: one option is to perform separate fits to lattice and experimental results, and extract the value of $|V_{ub}|$ from the ratio of the respective a_0 coefficients; a second option is to perform a simultaneous fit to lattice and experimental data, leaving their relative normalization $|V_{ub}|$ as a free parameter. We adopt the second strategy, because it combines the lattice and experimental input in a more efficient way, leading to a smaller uncertainty on $|V_{ub}|$.

The available state-of-the-art experimental input consists of five datasets: three untagged measurements by *BABAR* (6-bin [138] and 12-bin [139]) and Belle [140], all of which assume isospin symmetry and provide combined $B^0 \to \pi^-$ and $B^+ \to \pi^0$ data; and the two tagged Belle measurements of $\bar{B}^0 \to \pi^+$ (13-bin) and $B^- \to \pi^0$ (7-bin) [141]. Including all of them, along with the available information about cross-correlations, will allow us to obtain a meaningful final error estimate.[60] The lattice input dataset will be that discussed in Sec. VIII C.

We perform a constrained BCL fit of the vector and scalar form factors (this is necessary in order to take into account the $f_+(q^2=0) = f_0(q^2=0)$ constraint) together with the combined experimental datasets. We find that the error on $|V_{ub}|$ stabilizes for $N^+ = N^0 = 3$. The result of the combined fit is presented in Table 50. The fit has a chi-square per degree of freedom $\chi^2/\text{dof} = 116.7/62 = 1.88$. Following the PDG recommendation, we rescale the whole covariance matrix by χ^2/dof: the errors on the z-parameters are increased by $\sqrt{\chi^2/\text{dof}} = 1.37$ and the correlation matrix is unaffected. The value of $|V_{ub}|$ which we obtain is

$$N_f = 2+1: |V_{ub}| = (3.61 \pm 0.16) \times 10^{-3} \quad [B \to \pi\ell\nu, \text{FLAG average, Refs. [124–126,138–141]}]. \tag{258}$$

In Fig. 31, we show both the lattice and experimental data for $(1 - q^2/m_{B^*}^2) f_+(q^2)$ as a function of $z(q^2)$, together with our preferred fit; experimental data has been rescaled by the resulting value for $|V_{ub}|^2$. It is worth noting the good consistency between the form-factor shapes from lattice and experimental data. This can be quantified, e.g., by computing the ratio of the two leading coefficients in the constrained BCL parametrization: the fit to lattice form factors yields $a_1^+/a_0^+ = -1.20(23)$ (cf. the results presented in Sec. VIII C 1),

[59] Since $\ell = e, \mu$ the contribution from the scalar form factor in Eq. (191) is negligible.

[60] See, e.g., Sec. V. D of Ref. [124] for a detailed discussion.

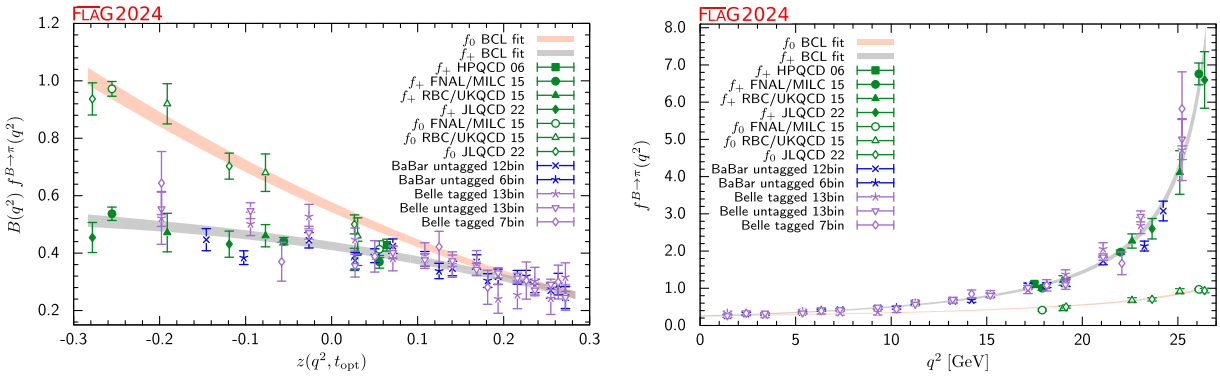


FIG. 31. Lattice and experimental data for $f_+^{B\to\pi}(q^2)$ and $f_0^{B\to\pi}(q^2)$ versus z (left panel) and q^2 (right panel). Experimental data has been rescaled by the value for $|V_{ub}|$ found from the joint fit. Green symbols denote lattice-QCD points included in the fit, while blue and indigo points show experimental data divided by the value of $|V_{ub}|$ obtained from the fit. The gray and orange bands display the preferred $N^+ = N^0 = 3$ BCL fit (five z-parameters and $|V_{ub}|$).

while the above lattice + experiment fit yields $a_1^+/a_0^+ = -1.039(94)$.

Finally we combine the $N_f = 2+1$ determinations of $|V_{ub}|$ from $B \to \tau\nu$ and $B \to \pi\ell\nu$ in Eqs. (254) and (259) and obtain

$$N_f = 2+1 : |V_{ub}| = (3.63 \pm 0.16) \times 10^{-3}$$
$$[B \to (\pi\ell\nu, \tau\nu), \text{FLAG average},$$
$$\text{Refs. } [60, 69\text{–}72, 124\text{–}126, 138\text{–}141, 511, 512]\,]. \tag{259}$$

Our results are summarized in Table 51 and will be displayed after our discussion of $|V_{cb}|$. In that figure we also show the PDG inclusive determination $|V_{ub}|_{\rm incl} = (4.13 \pm 0.12_{\rm exp} {}^{+0.13}_{-0.14\,\rm theo} \pm 0.18_{\Delta\rm model}) \times 10^{-3}$ [274] (the Δ model error has been added in Ref. [274] to account for the spread in results obtained using different theoretical models).

TABLE 51. Results for $|V_{ub}|$. The averages involving $B \to \pi\ell\nu$ and $B \to \tau\nu$ can be found in Eqs. (258), (254), (259) and (257); all uncertainties have been added in quadrature. The inclusive average is taken from PDG 24 [274]. The lattice calculations for the $B \to \pi$ form factors are taken from Refs. [124–126], for f_B at $N_f = 2+1$ from Refs. [60,69–72] and for f_B at $N_f = 2+1+1$ from Refs. [20,36,67,68].

	From	$\lvert V_{ub}\rvert \times 10^3$
FLAG average for $N_f = 2+1$	$B \to \pi\ell\nu$	3.61(16)
FLAG average for $N_f = 2+1$	$B \to \tau\nu$	4.01(64)
FLAG average for $N_f = 2+1$	$B \to (\pi\ell\nu, \tau\nu)$	3.63(16)
FLAG average for $N_f = 2+1+1$	$B \to \tau\nu$	4.05(64)
PDG 24	$B \to X_u\ell\nu$	4.13(26)

I. Determination of $|V_{cb}|$

We now combine the lattice-QCD results for the $B \to D^{(*)}$ form factors with all available experimental information on $B \to D^{(*)}\ell\nu(\ell = e, \mu)$ semileptonic decays to obtain determinations of the CKM matrix element $|V_{cb}|$ in the Standard Model.

For $B \to D$ we perform a joint fit to the available lattice data, i.e., the $N_f = 2+1$ FNAL/MILC 15C [132] and HPQCD 15 [133] calculations discussed in Sec. VIII D, and state-of-the-art experimental determinations. We combine the Belle measurement [143], which provides partial integrated decay rates in 10 bins in the recoil parameter w, with the 2010 *BABAR* dataset in Ref. [142], which quotes the value of $\mathcal{G}^{B\to D}(w)\eta_{\rm EW}|V_{cb}|$ for 10 values of w.[61] The fit is dominated by the more precise Belle data. Given this, and the fact that only partial correlations among systematic uncertainties are to be expected, we will treat both datasets as uncorrelated.[62] The formula for the differential $B \to D\ell\nu$ branching ratio is given in Eq. (195).

A constrained $(N^+ = N^0 = 3)$ BCL fit using the same *Ansatz* as for lattice-only data in Sec. VIII D yields our average

$$N_f = 2+1 : \ |V_{cb}| = 40.0(1.0) \times 10^{-3}$$
$$[B \to D\ell\nu, \text{FLAG average, Refs. } [132, 133, 142, 143]\,]. \tag{260}$$

The fit has a chi-square per degree of freedom $\chi^2/\text{dof} = 20.0/25 = 0.80$. The result of the full fit,

[61]We thank Marcello Rotondo for providing the 10 bins result of the *BABAR* analysis.

[62]We have checked that results using just one experimental dataset are compatible within 1σ. In the case of *BABAR*, we have taken into account the introduction of some EW corrections in the data.

TABLE 52. Value of $|V_{cb}|$, coefficients for the $N^+ = N^0$ z-expansion of the $B \to D$ form factors f_+ and f_0, and their correlation matrix. The coefficient a_2^0 is fixed by the $f_+(q^2 = 0) = f_0(q^2 = 0)$ constrain. The chi-square per degree of freedom is $\chi^2/\text{dof} = 20.0/25 = 0.80$. The lattice calculations that enter this fit are taken from FNAL/MILC 15C [132] and HPQCD 15 [133]. The experimental inputs are taken from *BABAR* [142] and Belle [143]. The form factors can be reconstructed using parametrization and inputs given in Appendix B 3 e.

$B \to D\ell\nu(N_f = 2+1)$							
	Central values	Correlation matrix					
$\lvert V_{cb}\rvert \times 10^3$	40.0(1.0)	1.00	−0.525	−0.339	0.0487	−0.521	−0.433
a_0^+	0.8946(94)	−0.525	1.00	0.303	−0.351	0.953	0.529
a_1^+	−8.03 (16)	−0.339	0.303	1.00	0.203	0.375	0.876
a_2^+	50.1(3.1)	0.0487	−0.351	0.203	1.00	−0.276	0.196
a_0^0	0.7804(75)	−0.521	0.953	0.375	−0.276	1.0	0.502
a_1^0	−3.38 (16)	−0.433	0.529	0.876	0.196	0.502	1.0

including the correlation matrix between $|V_{cb}|$ and the BCL coefficients is presented in Table 52 and illustrated in Fig. 32. In passing, we note that, if correlations between the FNAL/MILC and HPQCD calculations are neglected, the $|V_{cb}|$ central value rises to 40.3×10^{-3} in nice agreement with the results presented in Ref. [674].

Finally, using the fit results in Table 52, we extract a value for $R(D)$ which includes both lattice and experimental information

$$N_f = 2+1 : R(D)_{\text{lat+exp}} = 0.2955(32) \quad [\text{FLAG average, Refs. } [132,133,142,143]]. \tag{261}$$

Note that we do not need to rescale the uncertainty on $R(D)_{\text{lat+exp}}$ because, after the inclusion of experimental $B \to D\ell\nu(\ell = e, \mu)$ results, the shift in central value caused by using a different parametrization is negligible [see the discussion above Eq. (223)]. For $B \to D^*$, we perform a joint fit to all available lattice and experimental data. On the lattice side, we consider separately the two $N_f = 2+1$ calculations FNAL/MILC 21 [136] and JLQCD 23 [137] and the single $N_f = 2+1+1$ HPQCD 23 [135] calculation. On the experimental side, the situation is more complicated because we need to combine the following results.

(i) The Belle untagged measurement [144] of the differential $B^0 \to D^{*-}\ell^+\nu_\ell$ partial width.
(ii) The Belle tagged measurement [145] of the *normalized* differential $B \to D^*\ell\nu_\ell$ partial width (averaged over the B^- and $\bar{B}^0$ modes).
(iii) The Belle II tagged measurement [146] of the *normalized* differential $\bar{B}^0 \to D^{*+}\ell^-\bar{\nu}_\ell$ partial width.
(iv) The Belle II tagged branching ratio measurement $\text{BR}(\bar{B}^0 \to D^{*+}\ell^-\bar{\nu}_\ell) = (4.922 \pm 0.023 \pm 0.220)\%$ [146].
(v) A modified HFLAV world average for the branching ratio of $\bar{B}^0 \to D^{*+}\ell^-\bar{\nu}_\ell$ mode in which the contributions from the Belle untagged [144] (already included in the differential results we use) and Belle II tagged [147] (superseded by the Belle II tagged result [146] which we include separately)

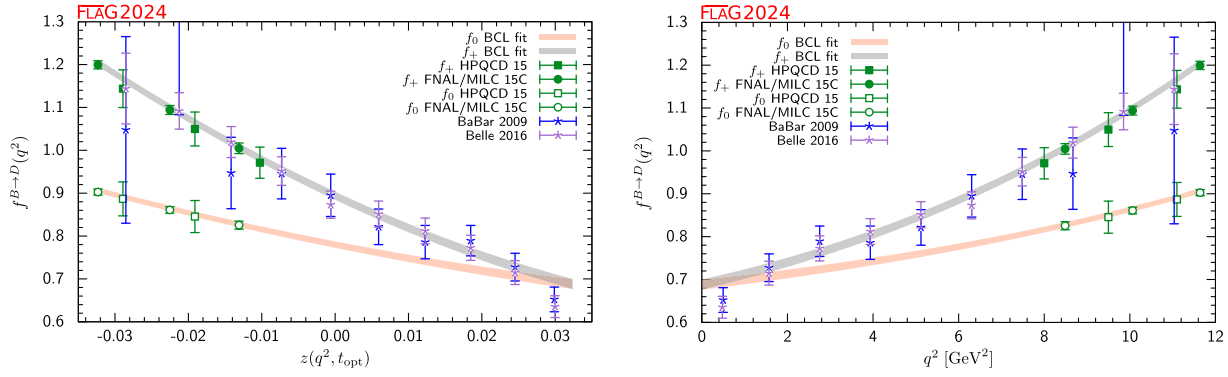


FIG. 32. Lattice and experimental data for $f_+^{B\to D}(q^2)$ and $f_0^{B\to D}(q^2)$ versus z (left panel) and q^2 (right panel). Green symbols denote lattice-QCD points included in the fit, while blue and indigo points show experimental data divided by the value of $|V_{cb}|$ obtained from the fit. The gray and orange bands display the preferred $N^+ = N^0 = 3$ BCL fit (five z-parameters and $|V_{cb}|$).

TABLE 53. $|V_{cb}|$, coefficients and correlation matrix for the $(N_g, N_f, N_{F_1}, N_{F_2}) = (2,3,3,2)$ BGL fit to the $B \to D^*$ form factors g, f, F_1 and F_2 for $N_f = 2+1$ and $N_f = 2+1+1$. The form factors can be reconstructed using parametrization and inputs given in Appendix B 3 g.

$B \to D^*(N_f = 2+1)$

Coeff	Central values	Correlation matrix								
$\|V_{cb}\| \times 10^3$	39.23(65)	1	−0.3552	−0.1269	−0.6672	−0.3260	0.2331	−0.2412	0.1118	−0.08658
a_0^g	0.03036(72)	−0.3552	1	−0.4976	0.3645	−0.0009317	−0.02169	0.1026	−0.02327	−0.09817
a_1^g	−0.083(21)	−0.1269	−0.4976	1	0.02961	0.1874	−0.2543	0.08161	−0.03930	0.1177
a_0^f	0.01213(15)	−0.6672	0.3645	0.02961	1	−0.08990	0.07897	−0.08767	0.07594	−0.09589
a_1^f	0.0234(64)	−0.3260	−0.0009317	0.1874	−0.08990	1	−0.8384	0.4660	−0.2491	0.3552
a_2^f	−0.59(16)	0.2331	−0.02169	−0.2543	0.07897	−0.8384	1	−0.2414	0.07961	−0.2880
$a_1^{F_1}$	0.00141(97)	−0.2412	0.1026	0.08161	−0.08767	0.4660	−0.2414	1	−0.9135	−0.06385
$a_2^{F_1}$	−0.005(17)	0.1118	−0.02327	−0.03930	0.07594	−0.2491	0.07961	−0.9135	1	0.2820
$a_1^{F_1}$	−0.093(17)	−0.08658	−0.09817	0.1177	−0.09589	0.3552	−0.2880	−0.06385	0.2820	1

$B \to D^*(N_f = 2+1+1)$

Coeff	Central values	Correlation matrix								
$\|V_{cb}\| \times 10^3$	39.44(89)	1	−0.1717	−0.06581	−0.7257	−0.4981	0.4426	−0.2473	0.08156	−0.2155
a_0^g	0.0311(21)	−0.1717	1	−0.9267	0.1121	−0.004683	0.1735	0.1230	−0.003372	0.07094
a_1^g	−0.125(75)	−0.06581	−0.9267	1	0.09615	0.1018	−0.2899	−0.03844	−0.03789	−0.03009
a_0^f	0.01207(21)	−0.7257	0.1121	0.09615	1	0.01430	−0.04137	−0.03342	0.02486	0.07847
a_1^f	0.023(12)	−0.4981	−0.004683	0.1018	0.01430	1	−0.9267	0.2522	0.03052	0.3601
a_2^f	−0.55(31)	0.4426	0.1735	−0.2899	−0.04137	−0.9267	1	−0.06981	−0.1655	−0.3503
$a_1^{F_1}$	0.0016(14)	−0.2473	0.1230	−0.03844	−0.03342	0.2522	−0.06981	1	−0.9270	−0.1678
$a_2^{F_1}$	−0.008(27)	0.08156	−0.003372	−0.03789	0.02486	0.03052	−0.1655	−0.9270	1	0.3148
$a_1^{F_1}$	−0.090(48)	−0.2155	0.07094	−0.03009	0.07847	0.3601	−0.3503	−0.1678	0.3148	1

measurements have been removed. Using the results from Table 69 of Ref. [148], we calculate $\mathrm{BR}(\bar{B}^0 \to D^{*+}\ell^-\bar{\nu}_\ell) = (5.12 \pm 0.19)\%$ where a PDG rescaling factor 1.36 has been applied.

(vi) The HFLAV world average $\mathrm{BR}(B^- \to D^{*0}\ell^-\bar{\nu}_\ell) = (5.58 \pm 0.07_{\mathrm{stat}} \pm 0.21_{\mathrm{syst}})\%$ [148] (which is not included in the Belle tagged shape-only measurement).

The theoretical predictions for the differential $B \to D^*\ell\nu$ rate binned over the variables w, $\cos\theta_v$, $\cos\theta_l$ and χ are obtained easily via direct integration of Eq. (210). One small subtlety is the inclusion of the so-called Coulomb factor $(1+\alpha\pi)$ for final states involving two charged particles, i.e., only for $\mathrm{BR}(\bar{B}^0 \to D^{*+}\ell^-\bar{\nu}_\ell)$. Regarding the fit methodology, we chose not to use any prior nor to impose unitarity constraints on the BGL coefficients. The Belle untagged analysis [144] presents the data in 10 bins of each kinematical variable; since the integral over the bins in each of the four distributions are identical, we remove the last bin in each of the three angular distributions. Moreover, we marginalize over N_{B^0}, the number of B^0 mesons in the data sample, thus properly correlating its impact over all the distributions and over the electron and muon modes.

The results of this global fit are presented in Table 53. The chi-square per degree of freedom of the two fits are $\chi^2/\mathrm{dof} = 216/160 = 1.35$ for $N_f = 2+1$ and $\chi^2/\mathrm{dof} = 200/148 = 1.35$ for $N_f = 2+1+1$ (the difference in the degrees of freedom is simply due to the presence of two sets of lattice synthetic data, each comprised of 12 points, for the $N_f = 2+1$ case). Note that we have rescaled all the errors by $\sqrt{\chi^2/\mathrm{dof}}$ following the standard PDG recipe. In particular, we find

$$N_f = 2+1\text{: } |V_{cb}| = 39.23(65) \times 10^{-3} \quad [B \to D^*\ell\nu, \text{FLAG average, Refs. [136, 137, 144–146, 148]}], \tag{262}$$

$$N_f = 2+1+1\text{: } |V_{cb}| = 39.44(89) \times 10^{-3} \quad [B \to D^*\ell\nu, \text{FLAG average, Refs. [135, 144–146, 148]}]. \tag{263}$$

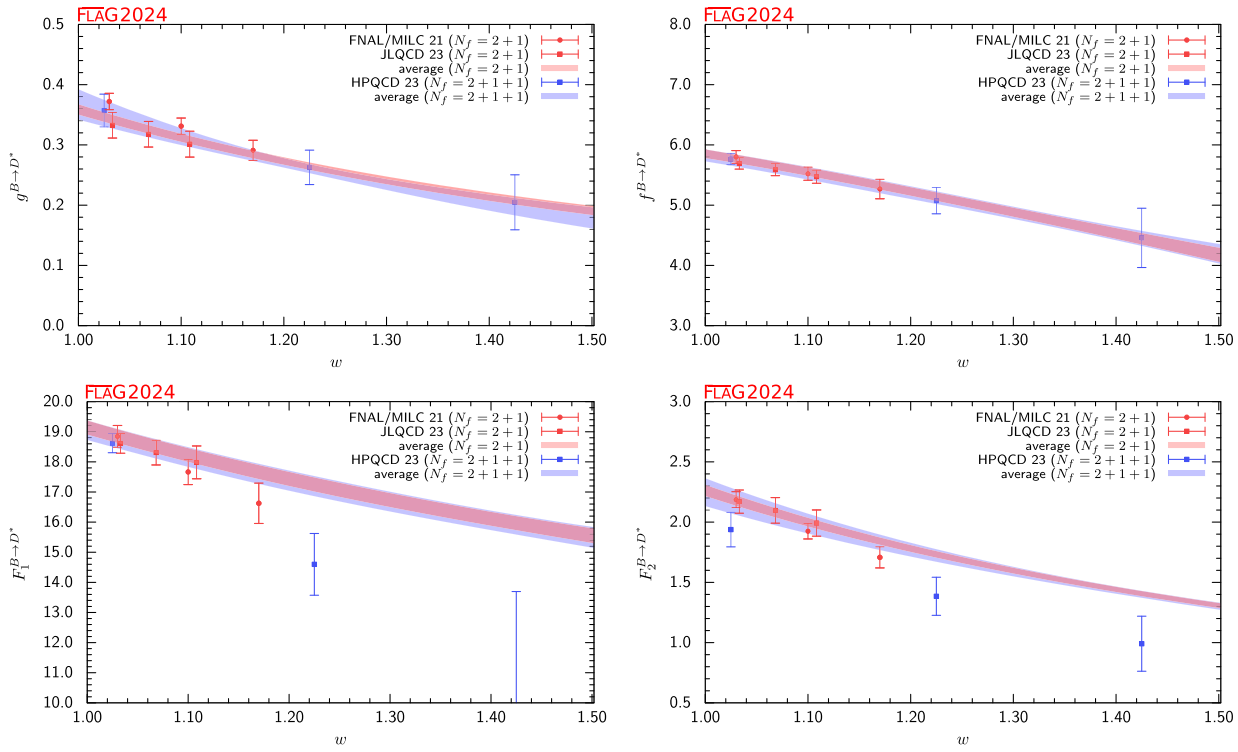


FIG. 33. The form factors $g(q^2)$, $f(q^2)$, $F_1(q^2)$, and $F_2(q^2)$ for $B \to D^* \ell \nu$ plotted as a function of w. The red (blue) band displays our preferred $(N_g, N_f, N_{F_1}, N_{F_2}) = (2,3,3,2)$ BGL fit (eight parameters) to experimental and $N_f = 2+1(2+1+1)$ lattice data. The constraints at zero and maximum recoil are imposed exactly. No use of unitarity constraints and priors has been made.

In Fig. 33, we show the form factors obtained from combining lattice and experimental results. In Fig. 34, we present a comparison of the four *normalized* differential distributions extracted from the experimental data, from the individual lattice results and from the combined lattice plus experiment fit.[63] The top (bottom) four panels correspond to $N_f = 2+1$ $(2+1+1)$. Direct inspection of these distributions shows quite a good agreement (as already evidenced by the relatively good chi-square per degree of freedom of the fits) albeit with some tensions in some of the shapes. In particular, the normalized distributions extracted from $N_f = 2+1$ and $N_f = 2+1+1$ results tend to deviate from the measured ones along similar patterns: deficit at large w, excess at large $\cos\theta_v$, flatter distribution in $\cos\theta_\ell$. The tensions in the $N_f = 2+1+1$ are only apparently more pronounced because of the larger lattice uncertainties.

Finally, using the fit results in Table 53, we extract a value for $R(D^*)$ which includes both lattice and experimental information

$$N_f = 2+1\text{: } R(D^*)_{\text{lat+exp}} = 0.2505(11) \quad [\text{FLAG average, Refs. [136, 137, 144–146, 148]}], \tag{264}$$

$$N_f = 2+1+1\text{: } R(D^*)_{\text{lat+exp}} = 0.2506(17) \quad [\text{FLAG average, Refs. [135, 144–146, 148]}]. \tag{265}$$

Before discussing the combination of the above $|V_{cb}|$ results, we note that the LHCb Collaboration recently reported the first determination of $|V_{cb}|$ at the Large Hadron Collider using $B_s \to D_s^- \mu^+ \nu_\mu$ and $B_s \to D_s^{*-} \mu^+ \nu_\mu$ decays [633,634]. The differential decay rates, in combination with the $N_f = 2+1+1$ HPQCD 19 [134] and HPQCD 19B [646] lattice results for $f_+^{B_s\to D_s}$ and $\mathcal{F}^{B_s\to D_s^*}(1)$, were analyzed using either the CLN or BGL form-factor parametrizations. The result for $|V_{cb}|$ from the BGL fit is [634]

$$N_f = 2+1+1\text{: } |V_{cb}| = (41.7 \pm 0.8 \pm 0.9 \pm 1.1) \times 10^{-3} \quad [B_s \to D_s^{(*)-} \mu^+ \nu_\mu, \text{LHCb}], \tag{266}$$

where the first two uncertainties are the statistical and systematic experimental uncertainties, and the third is due to the external inputs used, including the lattice inputs.

[63] For the Belle untagged case [144] we produce the normalized binned distributions by inverting the electron and muon response matrices and averaging over the leptons. Note that these distributions are presented for illustrative purpose only.

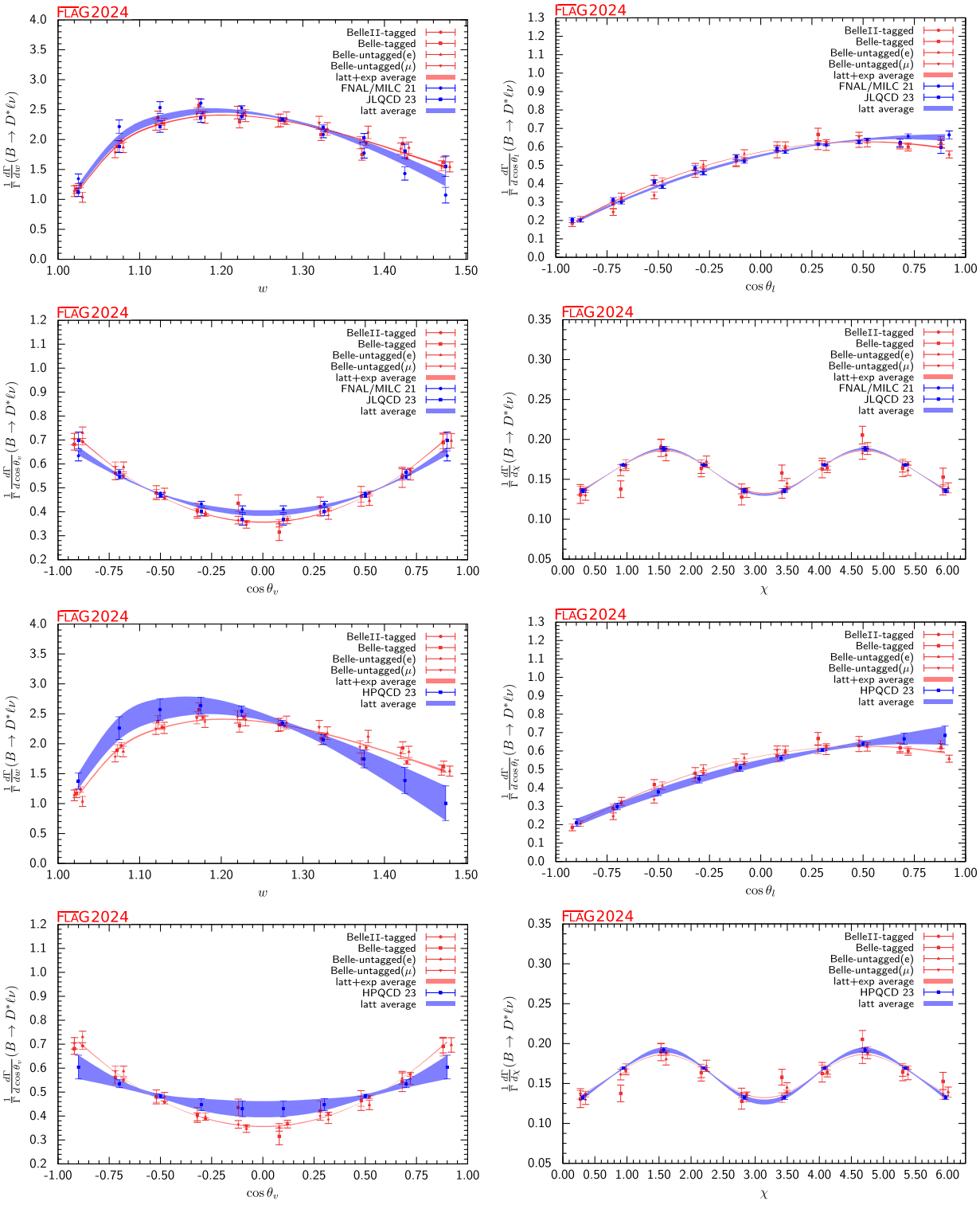


FIG. 34. Normalized differential decay rates with respect to the variables w, $\cos\theta_l$, $\cos\theta_v$ and χ. The red (blue) band displays our preferred $(N_g, N_f, N_{F_1}, N_{F_2}) = (2,3,3,2)$ BGL fit (eight parameters) obtained from lattice calculations with (without) the inclusion of experimental data. The constraints at zero and maximum recoil are imposed exactly. No use of unitarity constraints and priors has been made. The top and bottom four distributions are obtained using $N_f = 2+1$ and $N_f = 2+1+1$ lattice calculations, respectively.

The LHCb analysis used ratios to the reference decay modes $B^0 \to D^- \mu^+ \nu_\mu$ and $B^0 \to D^{*-} \mu^+ \nu_\mu$, whose branching fractions are used as input in the form of the Particle Data Group averages of measurements by other experiments [409]. The result (266) is therefore correlated with the determinations of $|V_{cb}|$ from $B \to D$ and $B \to D^*$

TABLE 54. Results for $|V_{cb}|$. The lattice calculations for the $B \to D$ form factors at $N_f = 2+1$ are taken from FNAL/MILC 15 [124], RBC/UKQCD 15 [125] and JLQCD 22 [126]; for the $B \to D^*$ form factors at $N_f = 2+1$ from FNAL/MILC 21 [136] and JLQCD 23 [137]; for the $B \to D^*$ form factors at $N_f = 2+1+1$ from HPQCD 23 [135]. The LHCb result using $B_s \to D_s^{(*)}\ell\nu$ decays [134,633,634,646], as well as the inclusive average obtained in the kinetic scheme from Ref. [675] are shown for comparison. In the LHCb result, the first two uncertainties are the statistical and systematic experimental uncertainties, and the third is due to the external inputs used, including the lattice inputs.

	From	$\lvert V_{cb}\rvert \times 10^3$
FLAG average for $N_f = 2+1$	$B \to D^*\ell\nu$	39.23(65)
FLAG average for $N_f = 2+1$	$B \to D\ell\nu$	40.0 1.0)
FLAG average for $N_f = 2+1$	$B \to (D, D^*)\ell\nu$	39.45(56)
FLAG average for $N_f = 2+1+1$	$B \to D^*\ell\nu$	39.44(89)
LHCb result for $N_f = 2+1+1$ (BGL)	$B_s \to D_s^{(*)}\ell\nu$	41.7(0.8)(0.9)(1.1)
Bordone et al.	$B \to X_c\ell\nu$	42.16(51)

semileptonic decays. Given the challenges involved in performing our own fit to the LHCb data, we do not, at present, include the LHCb results for $B_s \to D_s^- \mu^+ \nu_\mu$ and $B_s \to D_s^{*-}\mu^+\nu_\mu$ in our combination of $|V_{cb}|$.

We now proceed to combine the two $N_f = 2+1$ determinations of $|V_{cb}|$ from exclusive $B \to D$ and $B \to D^*$ semileptonic decays. To this end, we include an estimate of the correlation between the statistical lattice uncertainties on $|V_{cb}|^{N_f=2+1}_{B\to D}$ (FNAL/MILC and HPQCD) and $|V_{cb}|^{N_f=2+1}_{B\to D^*}$ (FNAL/MILC), because they are based on the same MILC configurations (albeit on different subsets). An estimate of this correlation is complicated due to the difficulty of disentangling lattice and experimental sources of uncertainties in a global BGL fit. Here we follow an approximate procedure which relies on estimating these correlations by looking at the $B \to D$ and $B \to D^*$ form factors at zero recoil, $\mathcal{G}^{B\to D}(1)$ and $\mathcal{F}^{B\to D^*}(1)$. The inclusion of these correlations has a very small impact on the average, thus providing an *a posteriori* justification for this approximate method. We obtain

$$\begin{aligned} N_f = 2+1\colon\ & |V_{cb}| = 39.45(56) \times 10^{-3} \\ & [B \to (D, D^*)\ell\nu, \text{FLAG average}, \\ & \text{Refs. } [132, 133, 136, 137, 142\text{–}146, 148]\,]. \end{aligned} \tag{267}$$

Our results are summarized in Table 54, which also shows the inclusive determination of $|V_{cb}| = 42.16(51) \times 10^{-3}$ [675] for comparison, and are illustrated in Fig. 35.[64]

J. Determination of $|V_{ub}/V_{cb}|$ from Λ_b decays

In 2015, the LHCb Collaboration reported a measurement of the ratio [656]

$$R_{\mathrm{BF}}(\Lambda_b) = \frac{\int_{15\ \mathrm{GeV}^2}^{q^2_{\max}} \frac{\mathrm{d}\mathcal{B}(\Lambda_b \to p\mu^-\bar{\nu}_\mu)}{\mathrm{d}q^2}\,\mathrm{d}q^2}{\int_{7\ \mathrm{GeV}^2}^{q^2_{\max}} \frac{\mathrm{d}\mathcal{B}(\Lambda_b \to \Lambda_c\mu^-\bar{\nu}_\mu)}{\mathrm{d}q^2}\,\mathrm{d}q^2}, \tag{268}$$

which, combined with the lattice QCD prediction from Ref. [499] (Detmold 15) discussed in Sec. VIII F yields a determination of $|V_{ub}/V_{cb}|$. The LHCb analysis uses the decay $\Lambda_c \to pK\pi$ to reconstruct the Λ_c and requires the branching fraction $\mathcal{B}(\Lambda_c \to pK\pi)$ of this decay as an external input. Using the latest world average of $\mathcal{B}(\Lambda_c \to pK\pi) = (6.28 \pm 0.32)\%$ [225] to update the LHCb measurement gives [308]

$$R_{\mathrm{BF}}(\Lambda_b) = (0.92 \pm 0.04 \pm 0.07) \times 10^{-2}, \tag{269}$$

and, combined with the lattice QCD prediction for $\frac{\zeta_{p\mu\bar{\nu}}(15\ \mathrm{GeV}^2)}{\zeta_{\Lambda_c\mu\bar{\nu}}(7\ \mathrm{GeV}^2)}$ discussed in Sec. VIII F,

$$|V_{ub}/V_{cb}| = 0.079 \pm 0.004_{\mathrm{lat}} \pm 0.004_{\mathrm{exp}}. \tag{270}$$

We remind the reader that the lattice calculation for the form factor ratio currently has a ■ rating; thus we will not use the result in Eq. (270) in the global $[V_{ub}, V_{cb}]$ fit.

K. Determination of $|V_{ub}/V_{cb}|$ from B_s decays

More recently, LHCb reported the measurements [676]

$$\begin{aligned} R_{\mathrm{BF}}(B_s, \mathrm{low}) &= \frac{\int_{q^2_{\min}=m^2_\mu}^{7\ \mathrm{GeV}^2} \frac{\mathrm{d}\mathcal{B}(B_s \to K^-\mu^+\nu_\mu)}{\mathrm{d}q^2}\,\mathrm{d}q^2}{\mathcal{B}(B_s \to D_s^-\mu^+\nu_\mu)} \\ &= (1.66 \pm 0.12) \times 10^{-3}, \end{aligned} \tag{271}$$

[64] This determination of $|V_{cb}|$ is also adopted by the PDG [274].

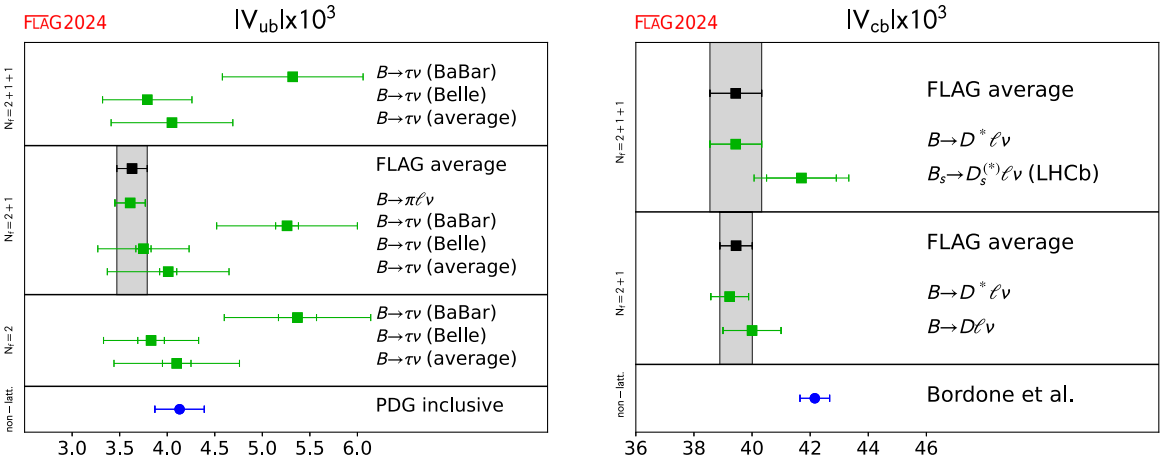


FIG. 35. Left: Summary of $|V_{ub}|$ determined using: (i) the B-meson leptonic decay branching fraction, $B(B^- \to \tau^- \bar{\nu})$, measured at the Belle and *BABAR* experiments, and our averages for f_B from lattice QCD; and (ii) the various measurements of the $B \to \pi \ell \nu$ decay rates by Belle and *BABAR*, and our averages for lattice determinations of the relevant vector form factor $f_+(q^2)$. The inclusive result is taken from PDG [274]. Right: Same for determinations of $|V_{cb}|$ using semileptonic decays. The inclusive result is taken from Ref. [675].

$$R_{\mathrm{BF}}(B_s, \mathrm{high}) = \frac{\int_{7\ \mathrm{GeV}^2}^{q^2_{\max}=(m_{B_s}-m_K)^2} \frac{\mathrm{d}\mathcal{B}(B_s \to K^- \mu^+ \nu_\mu)}{\mathrm{d}q^2} \mathrm{d}q^2}{\mathcal{B}(B_s \to D_s^- \mu^+ \nu_\mu)} = (3.25 \pm 0.28) \times 10^{-3}, \tag{272}$$

$$R_{\mathrm{BF}}(B_s, \mathrm{all}) = \frac{\mathcal{B}(B_s \to K^- \mu^+ \nu_\mu)}{\mathcal{B}(B_s \to D_s^- \mu^+ \nu_\mu)} = (4.89 \pm 0.33) \times 10^{-3}. \tag{273}$$

Using our average of the $B_s \to K$ form factors from lattice QCD as discussed in Sec. VIII C 3, we obtain the Standard Model predictions

$$\frac{1}{|V_{ub}|^2} \int_{q^2_{\min}=m_\mu^2}^{7\ \mathrm{GeV}^2} \frac{\mathrm{d}\Gamma(B_s \to K^- \mu^+ \nu_\mu)}{\mathrm{d}q^2} = (2.51 \pm 0.62)\ \mathrm{ps}^{-1}, \tag{274}$$

$$\frac{1}{|V_{ub}|^2} \int_{7\ \mathrm{GeV}^2}^{q^2_{\max}=(m_{B_s}-m_K)^2} \frac{\mathrm{d}\Gamma(B_s \to K^- \mu^+ \nu_\mu)}{\mathrm{d}q^2} = (4.02 \pm 0.51)\ \mathrm{ps}^{-1}, \tag{275}$$

$$\frac{1}{|V_{ub}|^2} \Gamma(B_s \to K^- \mu^+ \nu_\mu) = (6.5 \pm 1.1)\ \mathrm{ps}^{-1}. \tag{276}$$

For the denominator, we use the $B_s \to D_s$ form factors from Ref. [134] (HPQCD 19), which yields

$$\frac{1}{|V_{cb}|^2} \Gamma(B_s \to D_s^- \mu^+ \nu_\mu) = (9.15 \pm 0.37)\ \mathrm{ps}^{-1}. \tag{277}$$

Since the form factor shape is most reliably constrained by the lattice data only at high-q^2, the most reliable determination of the ratio $|V_{ub}/V_{cb}|$ is obtained by using LHCb measurements limited to the high-q^2 region. The result which we obtain and which is used in the combination presented in Sec. VIII L, reads

$$\frac{|V_{ub}|}{|V_{cb}|}(\mathrm{high}) = 0.0861 \pm 0.0057_{\mathrm{lat}} \pm 0.0038_{\mathrm{exp.}}. \tag{278}$$

For reference, the corresponding CKM ratio obtained at low-q^2 and in the whole q^2 regions are, $|V_{ub}|/|V_{cb}|(\mathrm{low}) = 0.0779 \pm 0.0098_{\mathrm{lat}} \pm 0.0028_{\mathrm{exp.}}$ and $|V_{ub}|/|V_{cb}|(\mathrm{all}) = 0.0828 \pm 0.0070_{\mathrm{lat}} \pm 0.0028_{\mathrm{exp.}}$, respectively.

L. Summary: $|V_{ub}|$ and $|V_{cb}|$

In Fig. 36, we present a summary of determinations of $|V_{ub}|$ and $|V_{cb}|$ from $B \to (\pi, D^{(*)})\ell\nu$, $B_s \to (K, D_s)\ell\nu$ (high q^2 only), $B \to \tau\nu$ and $\Lambda_b \to (p, \Lambda_c)\ell\nu$, as well as the results from inclusive $B \to X_{u,c}\ell\nu$ decays. Currently, the determinations of V_{cb} from $B \to D^*$ and $B \to D$ decays are quite compatible; however, a sizeable tension involving the extraction of V_{cb} from inclusive decays remains. Note that constraints on $|V_{ub}/V_{cb}|$ from baryon modes are displayed but, in view of the rating in Table 48, are not included in the global fit. As discussed in Sec. VIII I, experimental inputs used in the extraction of $|V_{cb}|$ from $B_s \to D_s^{(*)}\ell\nu$ decays [633,634] given in Eq. (266) are highly correlated with those entering the global $(|V_{ub}|, |V_{cb}|)$ fit described in this section. Given these correlations and the challenges in reproducing the LHCb analysis, for the time being we do not include the result Eq. (266) into the global fit.

In the global fit we include an estimate of the correlations between the $|V_{ub}|$ and $|V_{cb}|$ determinations from semileptonic B decays. We conservatively assume 100%

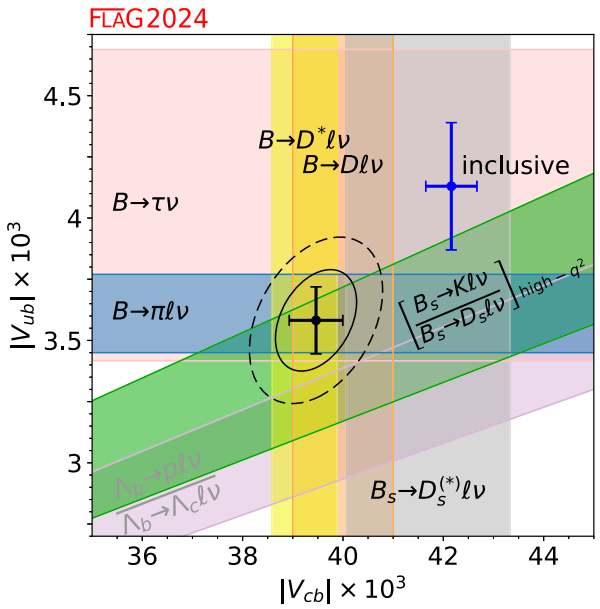


FIG. 36. Summary of $|V_{ub}|$ and $|V_{cb}|$ determinations. The black solid and dashed lines correspond to 68% and 95% confidence-level (C.L.) contours, respectively. The result of the global fit (which does not include $|V_{ub}/V_{cb}|$ from baryon modes nor $|V_{cb}|$ from $B_s \to D_s^{(*)}\ell\nu$) is $(|V_{cb}|, |V_{ub}|) = (39.46 \pm 0.53, 3.60 \pm 0.14) \times 10^{-3}$ with a p-value of 0.66. The lattice and experimental results that contribute to the various contours are the following. $B \to \pi\ell\nu$: lattice (FNAL/MILC 15 [124], RBC/UKQCD 15 [125], and JLQCD 22 [126]) and experiment (*BABAR* [138,139] and Belle [140,141]). $B \to D\ell\nu$: lattice (FNAL/MILC 15C [132] and HPQCD 15 [133]) and experiment (*BABAR* [142] and Belle [143]). $B \to D^*\ell\nu$: lattice (FNAL/MILC 21 [136], JLQCD 23 [137], HPQCD 23 [135]) and experiment (Belle [144,145], Belle II [146], HFLAV [148]). $B \to \tau\nu$: lattice ($N_f = 2+1+1$ determination of f_B in Eq. (168) [20,36,67,68]) and experiment (*BABAR* [515] and Belle [514]). $B_s \to K\ell\nu/B_s \to D_s\ell\nu$: lattice (HPQCD 14 [127], RBC/UKQCD 23 [128], FNAL/MILC 19 [592], HPQCD 19 [134]) and experiment (LHCb [676]). $\Lambda_b \to p\ell\nu/\Lambda_b \to \Lambda_c\ell\nu$: lattice (Detmold 15 [499]) and experiment (LHCb [656]). $B_s \to D_s^*\ell\nu/B_s \to D_s\ell\nu$: lattice (HPQCD 19 [134] and HPQCD 19B [646]) and experiment (LHCb [633,634]). The inclusive determinations are taken from Refs. [225,308,675] and read $(|V_{cb}|, |V_{ub}|)_{\text{incl}} = (42.16 \pm 0.51, 4.13 \pm 0.26) \times 10^{-3}$.

correlation between the statistical lattice uncertainties on (1) $|V_{ub}|$ (FNAL/MILC), $|V_{cb}|_{B\to D}$ (FNAL/MILC and HPQCD) and $|V_{cb}|_{B\to D^*}$ (FNAL/MILC) and (2) $|V_{ub}|$ (JLQCD) and $|V_{cb}|_{B\to D}$ (JLQCD). Due to the difficulty of disentangling statistical lattice uncertainties in the three BGL fits for $B \to (\pi, D, D^*)$, we follow the same approximate procedure described at the end of Sec. VIII I and estimate the correlations by looking at the zero-recoil form factors $f_+(0)$, $\mathcal{F}^{B\to D}(1)$ and $\mathcal{F}^{B\to D^*}(1)$. The results of the fit are

$$|V_{cb}| = 39.46(53) \times 10^{-3}, \tag{279}$$

$$|V_{ub}| = 3.60(14) \times 10^{-3}, \tag{280}$$

$$p\text{-value} = 0.66, \tag{281}$$

with a 0.36 correlation coefficient. For reference, the fit without the inclusion of any correlation between the various lattice calculations yield $|V_{cb}| = 39.50(51) \times 10^{-3}$, $|V_{ub}| = 3.60(13) \times 10^{-3}$ with a 0.09 correlation coefficient (the latter does not vanish because of the inclusion of $|V_{ub}/V_{cb}|$ from $B_s \to (K, D_s)\ell\nu$ decays).

The inclusive determinations read $|V_{cb}|_{\text{incl}} = (42.16 \pm 0.51) \times 10^{-3}$ [677] and $|V_{ub}|_{\text{incl}} = (4.13 \pm 0.12_{\text{exp}} {}^{+0.13}_{-0.14\,\text{theo}} \pm 0.18_{\Delta\text{model}}) \times 10^{-3}$ [274].

IX. THE STRONG COUPLING α_s

Working group members: L. Del Debbio, P. Petreczky, S. Sint

A. Introduction

The strong coupling $\alpha_s(\mu) = \bar{g}_s^2(\mu)/(4\pi)$ defined at scale μ, is the parameter that determines the strength of strong interactions in the Standard Model. It plays a key role in the understanding of QCD and in its application to collider physics, where it is ubiquitous in calculations of physical processes, e.g., at the LHC. For example, the parametric uncertainty from α_s is one of the dominant sources of uncertainty in the Standard Model predictions for the Higgs boson [678] and top quark cross sections, see, e.g., Ref. [679]. In order to fully exploit the experimental results that will be collected during the high-luminosity run of the LHC in the near future, it is mandatory to reduce the uncertainty on α_s below 1%. Similarly, high-accuracy determinations of this coupling will help in understanding the stability of the vacuum of the Standard Model and will yield one of the essential boundary conditions for completions of the Standard Model at high energies [680–687]. At this level of precision, it becomes imperative to have a robust understanding of systematic errors. Lattice simulations are ideally placed to play a central role in this quest. In the following we try to summarize the main features of the lattice approach in a way that we hope is understandable by nonexperts. For recent, complementary review articles, we refer the reader to Refs. [688,689].

In order to determine the running coupling at scale μ

$$\alpha_s(\mu) = \frac{\bar{g}_s^2(\mu)}{4\pi}, \tag{282}$$

we should first "measure" a short-distance quantity $\mathcal{Q}$ at scale μ either experimentally or by lattice calculations, and then match it to a perturbative expansion in terms of a running coupling, conventionally taken as $\alpha_{\overline{\text{MS}}}(\mu)$,

$$\mathcal{Q}(\mu) = c_1 \alpha_{\overline{\text{MS}}}(\mu) + c_2 \alpha_{\overline{\text{MS}}}^2(\mu) + \cdots. \tag{283}$$

We note that in some cases also a lowest-order constant term, c_0, may be present; in the following, we always assume that such a term has been subtracted on both sides and absorbed in a redefinition of $\mathcal{Q}(\mu)$. We distinguish between phenomenological and lattice determinations of α_s, the essential difference being the origin of the values of $\mathcal{Q}$ in Eq. (283). The basis of phenomenological determinations are experimentally measurable cross sections or decay widths from which $\mathcal{Q}$ is defined. These cross sections have to be sufficiently inclusive and at sufficiently high scales such that perturbation theory can be applied. Often hadronization corrections have to be used to connect the observed hadronic cross sections to the perturbative ones. Experimental data at high μ, where perturbation theory is progressively more precise, usually have increasing experimental errors, not least due to the very smallness of $\alpha_s(\mu)$. Hence, it is not easy to find processes that allow one to follow the μ-dependence of a single $\mathcal{Q}(\mu)$ over a range where $\alpha_s(\mu)$ changes significantly and precision is maintained. Note also that determinations of α_s from experimental data at hadron colliders necessarily require a simultaneous fit of the parton distribution functions (PDFs) [690], making the whole procedure more complicated and prone to systematic errors.

In contrast, in lattice gauge theory, one can design $\mathcal{Q}(\mu)$ Euclidean short-distance quantities that are not directly related to experimental observables. This allows us to follow the μ-dependence until the perturbative regime is reached and nonperturbative "corrections" are negligible. The only experimental input for lattice computations of α_s are the masses or decay constants of hadrons, which fixes the overall energy scale of the theory and the quark masses. Therefore, experimental errors are completely negligible and issues such as hadronization do not occur. We can construct many short-distance quantities that are easy to calculate nonperturbatively in lattice simulations with small statistical uncertainties. We can also simulate at parameter values that do not exist in nature (for example, with unphysical quark masses between bottom and charm) to help control systematic uncertainties. These features mean that precise results for α_s can be achieved with lattice-gauge-theory computations. Further, as in phenomenological determinations, the different methods available to determine α_s in lattice calculations with different associated systematic uncertainties enable valuable cross-checks. Practical limitations are discussed in the next section, but a simple one is worth mentioning here. Experimental results (and therefore the phenomenological determinations) of course have all quarks present, while in lattice gauge theories in practice only the lighter ones are included and one is then forced to use the matching at thresholds, as discussed in the following subsection.

It is important to keep in mind that the dominant source of uncertainty in most present day lattice-QCD calculations of α_s are from the truncation of continuum/lattice perturbation theory and from discretization errors. Perturbative truncation errors are of particular concern because they often cannot easily be estimated from studying the data itself. Perturbation theory provides an asymptotic series and the size of higher-order coefficients can sometimes turn out to be larger than suggested by naive expectations based on power counting from the behavior of lower-order terms. We note that perturbative truncation errors are also the dominant source of uncertainty in several of the phenomenological determinations of α_s.

The various phenomenological approaches to determining the running coupling constant, $\alpha^{(5)}_{\overline{\rm MS}}(M_Z)$ are summarized by the Particle Data Group [225]. The PDG review lists five categories of phenomenological results used to obtain the running coupling: using hadronic τ decays, hadronic final states of e^+e^- annihilation, deep inelastic lepton-nucleon scattering, electroweak precision data, and high-energy hadron-collider data. Excluding lattice results, the PDG, in their most recent update [274], quotes the weighted average as

$$\alpha^{(5)}_{\overline{\rm MS}}(M_Z) = 0.1175(10), \qquad \text{PDG 24 [274]} \tag{284}$$

compared to $\alpha^{(5)}_{\overline{\rm MS}}(M_Z) = 0.1176(11)$ of the older PDG 2020 [225]. For a general overview of the various phenomenological and lattice approaches see, e.g., Ref. [679]. The extraction of α_s from τ data, which is one of the most precise and thus has a large impact on the nonlattice average in Eq. (284), is especially sensitive to the treatment of higher-order perturbative terms as well as the treatment of nonperturbative effects. This is important to keep in mind when comparing our chosen range for $\alpha^{(5)}_{\overline{\rm MS}}(M_Z)$ from lattice determinations in Eq. (399) with the nonlattice average from the PDG.

1. Scheme and scale dependence of α_s and $\Lambda_{\rm QCD}$

Despite the fact that the notion of the QCD coupling is initially a perturbative concept, the associated Λ-parameter is nonperturbatively defined,

$$\Lambda \equiv \mu\varphi_s(\bar{g}_s(\mu)),$$
$$\varphi_s(\bar{g}_s) = (b_0\bar{g}_s^2)^{-b_1/(2b_0^2)} e^{-1/(2b_0\bar{g}_s^2)} \exp\left[-\int_0^{\bar{g}_s} dx \left(\frac{1}{\beta(x)} + \frac{1}{b_0 x^3} - \frac{b_1}{b_0^2 x}\right)\right], \tag{285}$$

provided that $\beta(\bar{g}_s) = \mu \frac{\partial \bar{g}_s(\mu)}{\partial \mu}$ is the full renormalization group function in the (mass-independent) scheme which defines $\bar{g}_s$. The first two coefficients, b_0 and b_1, in the perturbative expansion

$$\beta(x) \sim -b_0 x^3 - b_1 x^5 + \ldots, \tag{286}$$

are scheme-independent ("universal") and given by

$$b_0 = \frac{1}{(4\pi)^2}\left(11 - \frac{2}{3}N_f\right), \quad b_1 = \frac{1}{(4\pi)^4}\left(102 - \frac{38}{3}N_f\right). \tag{287}$$

In the $\overline{\text{MS}}$ scheme, the coefficients of the β-function have been calculated up to 5-loop order, i.e., b_2, b_3 and b_4 are known [241,691–694].

As a renormalization-group-invariant quantity, the Λ-parameter is μ-independent. However, it does depend on the renormalization scheme albeit in an exactly computable way: A perturbative change of the coupling from one mass-independent scheme S to another (taken here to be the $\overline{\text{MS}}$ scheme) takes the form

$$g^2_{\overline{\text{MS}}}(\mu) = g^2_{\text{S}}(\mu)(1 + c_g^{(1)} g^2_{\text{S}}(\mu) + \ldots), \tag{288}$$

where $c_g^{(i)}, i \geq 1$ are finite coefficients. Performing this change in the expression for the Λ-parameter at a large scale μ, so that higher-order terms can be neglected, one obtains the exact relation between the respective Λ-parameters of the two schemes,

$$\Lambda_{\overline{\text{MS}}} = \Lambda_{\text{S}} \exp\left[c_g^{(1)}/(2b_0)\right]. \tag{289}$$

Note that this exact relation allows us to nonperturbatively define $\Lambda_{\overline{\text{MS}}}$, by starting from any nonperturbatively defined scheme S for which $c_g^{(1)}$ is known. Given the high-order knowledge (5-loop by now) of $\beta_{\overline{\text{MS}}}$ then means that the errors in $\alpha_{\overline{\text{MS}}}(m_{\text{Z}})$ correspond almost completely with the errors of Λ_S. We will therefore mostly discuss them in that way. Starting from Eq. (285), we have to consider (i) the error of $\bar{g}^2_S(\mu)$ (denoted as $(\frac{\Delta\Lambda}{\Lambda})_{\Delta\alpha_S}$) and (ii) the truncation error in β_S (denoted as $(\frac{\Delta\Lambda}{\Lambda})_{\text{trunc}}$). Concerning (ii), note that knowledge of $c_g^{(n_1)}$ for the scheme S means that β_S is known to $n_1 + 1$ loop order; b_{n_1} is known. We thus see that in the region where perturbation theory can be applied, the following errors of Λ_S (or consequently $\Lambda_{\overline{\text{MS}}}$) have to be considered

$$\left(\frac{\Delta\Lambda}{\Lambda}\right)_{\Delta\alpha_S} = \frac{\Delta\alpha_S(\mu)}{8\pi b_0 \alpha_S^2(\mu)} \times [1 + \mathcal{O}(\alpha_S(\mu))], \tag{290}$$

$$\left(\frac{\Delta\Lambda}{\Lambda}\right)_{\text{trunc}} = k\alpha_S^{n_1}(\mu) + \mathcal{O}(\alpha_S^{n_1+1}(\mu)), \tag{291}$$

where the pre-factor k depends on b_{n_1+1} and in typical good schemes such as $\overline{\text{MS}}$ it is numerically of order one. Statistical and systematic errors such as discretization effects contribute to $\Delta\alpha_S(\mu)$. In the above we dropped a scheme subscript for the Λ-parameters because of Eq. (289).

By convention $\alpha_{\overline{\text{MS}}}$ is usually quoted at a scale $\mu = M_Z$ where the appropriate effective coupling is the one in the five-flavor theory: $\alpha^{(5)}_{\overline{\text{MS}}}(M_Z)$. In order to obtain it from a result with fewer flavors, one connects effective theories with different number of flavors as discussed by Bernreuther and Wetzel [695]. For example, one considers the $\overline{\text{MS}}$ scheme, matches the 3-flavor theory to the four-flavor theory at a scale given by the charm-quark mass [696–698], runs with the 5-loop β-function [241,691–694] of the four-flavor theory to a scale given by the b-quark mass, and there matches to the five-flavor theory, after which one runs up to $\mu = M_Z$ with the five-loop β-function. For the matching relation at a given quark threshold we use the mass $m_\star$ which satisfies $m_\star = \bar{m}^{(N_f)}_{\overline{\text{MS}}}(m_\star)$, where $\bar{m}$ is the running mass (analogous to the running coupling). Then

$$\bar{g}^2_{N_f-1}(m_\star) = \bar{g}^2_{N_f}(m_\star) \times \left[1 + 0 \times \bar{g}^2_{N_f}(m_\star) + \sum_{n\geq 2} t_n \bar{g}^{2n}_{N_f}(m_\star)\right] \tag{292}$$

with [696–699]

$$t_2 = \frac{1}{(4\pi^2)^2}\frac{11}{72}, \tag{293}$$

$$t_3 = \frac{1}{(4\pi^2)^3}\left[-\frac{82043}{27648}\zeta_3 + \frac{564731}{124416} - \frac{2633}{31104}(N_f - 1)\right], \tag{294}$$

$$t_4 = \frac{1}{(4\pi^2)^4}[5.170347 - 1.009932(N_f - 1) - 0.021978(N_f - 1)^2], \tag{295}$$

(where ζ_3 is the Riemann zeta-function) provides the matching at the thresholds in the $\overline{\text{MS}}$ scheme. Often the software packages RUNDEC [700,701] or the more recent one, REVOLVER [702], are used for quark-threshold matching and running in the $\overline{\text{MS}}$-scheme.

While t_2, t_3, t_4 are numerically small coefficients, the charm-threshold scale is also relatively low and so there are nonperturbative uncertainties in the matching procedure, which are difficult to estimate but which we assume here to be negligible. This is supported by nonperturbative tests [200], where perturbative decoupling relations in the $\overline{\text{MS}}$ scheme were shown to quantitatively describe decoupling at the few per mille level, down to the charm-quark region. Obviously there is no perturbative matching formula across the strange "threshold"; here matching is entirely nonperturbative. Model-dependent extrapolations of $\bar{g}^2_{N_f}$ from $N_f = 0$, 2 to $N_f = 3$ were done in the early days of lattice gauge theory. We will include these in our listings of results but not in our estimates, since such extrapolations are based on untestable assumptions.

2. Overview of the review of α_s

We begin by explaining lattice-specific difficulties in Sec. IX B 1 and the FLAG criteria designed to assess whether the associated systematic uncertainties can be controlled and estimated in a reasonable manner. These criteria remain unchanged since the FLAG 19 report, as there has still not been sufficiently broad progress to make them more stringent. However, in this report we have implemented a systematic scale variation to help assess systematic errors due to the truncation of the perturbative series. Scale variations are widely used in phenomenology and its application to lattice determinations has been advocated in Ref. [688]. We explain the procedure at the end of this introduction and, where possible, we will quote corresponding results.

We then discuss, in Secs. IX C,IX D,IX E,IX F,IX G, IX H,IX I, the various lattice approaches and results from calculations with $N_f = 0$, 2, $2 + 1$, and $2 + 1 + 1$ flavors. For lattice approaches with neither a new result nor a result passing all FLAG criteria, we refer to the discussion in previous FLAG reports. In particular, this regards determinations of α_s from QCD vertices and from the eigenvalue spectrum of the Dirac operator.

Since FLAG 21, the strategy of nonperturbative renormalization by decoupling, as introduced by the ALPHA collaboration in Ref. [703], produced a new result for α_s. It is important to realize that this method shifts the perspective on results for the Λ-parameter with unphysical flavor numbers, in particular for $N_f = 0$: Such results can be related to $N_f > 0$ results by a nonperturbative matching calculation. We therefore made an effort to review $N_f = 0$ results, some of which are now over 20 years old. In particular, we also included a new section on the gradient-flow (GF) coupling in infinite space-time volume, even though only results for $N_f = 0$ exist at the moment.

After the discussion of the various lattice methods, we proceed, in Sec. IX J, with the averages together with our best estimates for $\alpha^{(5)}_{\overline{\text{MS}}}$. These are currently determined from three- and four-flavor QCD simulations only, however, with the decoupling result also relying on the $N_f = 0$ Λ-parameter as input. Therefore, we discuss results for the $N_f = 0$ Λ-parameter in some detail, in addition to the physical cases with $N_f = 3$, 4 and 5, where the latter is derived from $N_f = 3$ and 4 results by the standard perturbative evolution across the bottom-quark threshold.

3. Additions with respect to the FLAG 21 report

Since the FLAG 21 report there were two new papers on $N_f = 3$:

Petreczky 20 [81] from heavy-quark current two-point functions (Sec. IX H).

ALPHA 22 [80] from the decoupling method (Sec. IX D).

In $N_f = 0$ QCD, there are a number of additional works:

Bribian 21 [704], from step-scaling with the twisted periodic gradient-flow coupling (Sec. IX C).

Hasenfratz 23 [705] and Wong 23 [706] from the GF scheme in infinite volume (Sec. IX I)

Chimirri 23 [707] from heavy-quark current two-point functions (Sec. IX H)

Brambilla 23 [197], from the force between static quarks (Sec. IX E)

B. General issues

1. Discussion of criteria for computations entering the averages

As in the PDG review, we only use calculations of α_s published in peer-reviewed journals, and that use NNLO or higher-order perturbative expansions, to obtain our final range in Sec. IX J. We also, however, introduce further criteria designed to assess the ability to control important systematics, which we describe here. Some of these criteria, e.g., that for the continuum extrapolation, are associated with lattice-specific systematics and have no continuum analogue. Other criteria, e.g., that for the renormalization scale, could in principle be applied to nonlattice determinations. Expecting that lattice calculations will continue to improve significantly in the near future, our goal in reviewing the state-of-the-art here is to be conservative and avoid prematurely choosing an overly small range.

In lattice calculations, we generally take $\mathcal{Q}$ to be some combination of physical amplitudes or Euclidean correlation functions which are free from UV and IR divergences and have a well-defined continuum limit. Examples include the force between static quarks and two-point functions of quark-bilinear currents.

In comparison to values of observables $\mathcal{Q}$ determined experimentally, those from lattice calculations require two more steps. The first step concerns obtaining the scale μ in physical units (GeV), given its value, $a\mu$, in lattice units. Ideally one compares the lattice result for some hadron mass $aM_{\rm had}$ with the known experimental result for $M_{\rm had}$ to determine a and thus μ in physical units. Alternatively, convenient intermediate scales such as $\sqrt{t_0}$, w_0, r_0, r_1, [115,365,708,709] can be used if their relation to an experimental dimensionful observable is established. For more details we refer to Sec. XI on scale setting in this FLAG report. The low-energy scale μ needs to be computed at the same lattice spacings (i.e., the same bare couplings) where $\mathcal{Q}$ is determined, at least as long as one does not use the step-scaling method (see below). This induces a practical difficulty given present computing resources. In the determination of the low-energy reference scale the volume needs to be large enough to avoid finite-size effects. On the other hand, in order for the perturbative expansion of Eq. (283) to be reliable, one has to reach sufficiently high values of μ, i.e., short enough distances. To avoid uncontrollable discretization effects the lattice spacing a has to be accordingly small. This means

$$L \gg \text{hadron size} \sim \Lambda_{\rm QCD}^{-1} \quad \text{and} \quad 1/a \gg \mu, \tag{296}$$

(where L is the box size) and therefore

$$L/a \ggg \mu/\Lambda_{\rm QCD}. \tag{297}$$

The currently available computer power, however, limits L/a, typically to $L/a = 32$–96. Unless one accepts compromises in controlling discretization errors or finite-size effects, this means one needs to set the scale μ according to

$$\mu \lll L/a \times \Lambda_{\rm QCD} \sim 10\text{–}30 \text{ GeV}. \tag{298}$$

(Here $\lll$ or $\ggg$ means at least one order of magnitude smaller or larger.) Therefore, μ can be 1–3 GeV at most. This raises the concern whether the asymptotic perturbative expansion truncated at 1-loop, 2-loop, or 3-loop in Eq. (283) is sufficiently accurate. There is a finite-size scaling method, usually called step-scaling method, which solves this problem by identifying $\mu = 1/L$ in the definition of $\mathcal{Q}(\mu)$, see Sec. IX C.

For the second step after setting the scale μ in physical units (GeV), one should compute $\mathcal{Q}$ on the lattice, $\mathcal{Q}_{\rm lat}(a,\mu)$ for several lattice spacings and take the continuum limit to obtain the left-hand side of Eq. (283) as

$$\mathcal{Q}(\mu) \equiv \lim_{a\to 0} \mathcal{Q}_{\rm lat}(a,\mu) \quad \text{with} \quad \mu \text{ fixed}. \tag{299}$$

This is necessary to remove the discretization error.

Here it is assumed that the quantity $\mathcal{Q}$ has a continuum limit, which is regularization-independent. The method discussed in Sec. IX G, which is based on the perturbative expansion of a lattice-regulated, divergent short-distance quantity $W_{\rm lat}(a)$ differs in this respect and must be treated separately.

In summary, a controlled determination of α_s needs to satisfy the following:

(1) The determination of α_s is based on a comparison of a short-distance quantity $\mathcal{Q}$ at scale μ with a well-defined continuum limit without UV and IR divergences to a perturbative expansion formula in Eq. (283).
(2) The scale μ is large enough so that the perturbative expansion in Eq. (283) is precise to the order at which it is truncated, i.e., it has good *asymptotic* convergence.
(3) If $\mathcal{Q}$ is defined by physical quantities in infinite volume, one needs to satisfy Eq. (297).
(4) Nonuniversal quantities, i.e., quantities that depend on the chosen lattice regularization and do not have a nontrivial continuum limit need a separate discussion, see Sec. IX G.

Conditions 2. and 3. give approximate lower and upper bounds for μ respectively. It is important to see whether there is a window to satisfy 2. and 3. at the same time. If it exists, it remains to examine whether a particular lattice calculation is done inside the window or not.

Obviously, an important issue for the reliability of a calculation is whether the scale μ that can be reached lies in a regime where perturbation theory can be applied with confidence. However, the value of μ does not provide an unambiguous criterion. For instance, the Schrödinger functional, or SF coupling (Sec. IX C) is conventionally taken at the scale $\mu = 1/L$, but one could also choose $\mu = 2/L$. Instead of μ we therefore define an effective $\alpha_{\rm eff}$. For schemes such as SF (see Sec. IX C) or qq (see Sec. IX E) this is directly the coupling of the scheme. For other schemes such as the vacuum polarization we use the perturbative expansion Eq. (283) for the observable $\mathcal{Q}$ to define

$$\alpha_{\rm eff} = \mathcal{Q}/c_1. \tag{300}$$

As mentioned earlier, if there is an α_s-independent term it should first be subtracted. Note that this is nothing but defining an effective, regularization-independent coupling, a physical renormalization scheme. For ease of notation, here and in what follows we denote by α_s the coupling $\alpha_{\overline{\rm MS}}(\mu)$ that appears in Eq. (283).

Let us now comment further on the use of the perturbative series. Since it is only an asymptotic expansion, the remainder $R_n(\mathcal{Q}) = \mathcal{Q} - \sum_{i\le n} c_i\alpha_s^i$ of a truncated perturbative expression $\mathcal{Q} \sim \sum_{i\le n} c_i\alpha_s^i$ cannot just be estimated as a perturbative error $k\alpha_s^{n+1}$. The error is nonperturbative. Often one speaks of "nonperturbative contributions," but nonperturbative and perturbative cannot be strictly

separated due to the asymptotic nature of the series (see, e.g., Ref. [710]).

Still, we do have some general ideas concerning the size of nonperturbative effects. The known ones such as instantons or renormalons decay for large μ like inverse powers of μ and are thus roughly of the form

$$\exp(-\gamma/\alpha_s), \tag{301}$$

with some positive constant γ. Thus we have, loosely speaking,

$$\mathcal{Q} = c_1\alpha_s + c_2\alpha_s^2 + \cdots + c_n\alpha_s^n + \mathcal{O}(\alpha_s^{n+1}) + \mathcal{O}(\exp(-\gamma/\alpha_s)). \tag{302}$$

For small α_s, the $\exp(-\gamma/\alpha_s)$ is negligible. Similarly the perturbative estimate for the magnitude of relative errors in Eq. (302) is small; as an illustration for $n = 3$ and $\alpha_s = 0.2$ the relative error is $\sim$0.8% (assuming coefficients $|c_{n+1}/c_1| \sim 1$).

For larger values of α_s nonperturbative effects can become significant in Eq. (302). An instructive example comes from the values obtained from τ decays, for which $\alpha_s \approx 0.3$. Here, different applications of perturbation theory (fixed order and contour improved) each look reasonably asymptotically convergent but the difference does not seem to decrease much with the order (see, e.g., the contribution by Pich to Ref. [711]; see, however, also the discussion in Refs. [712,713]). In addition, nonperturbative terms in the spectral function may be non-negligible even after the integration up to m_τ (see, e.g., Refs. [714,715]). All of this is because α_s is not really small.

Since the size of the nonperturbative effects is very hard to estimate one should try to avoid such regions of the coupling. In a fully controlled computation one would like to verify the perturbative behavior by changing α_s over a significant range instead of estimating the errors as $\sim\alpha_s^{n+1}$. Some computations try to take nonperturbative power corrections to the perturbative series into account by including such terms in a fit to the μ-dependence. We note that this is a delicate procedure, as a term like, e.g., $\alpha_s(\mu)^3$ is hard to distinguish from a $1/\mu^2$ term when the μ-range is restricted and statistical and systematic errors are present. We consider it safer to restrict the fit range to the region where the power corrections are negligible compared to the estimated perturbative error.

The above considerations lead us to the following special criteria for the determination of α_s:

(i) Renormalization scale

★ all data points relevant in the analysis have $\alpha_{\rm eff} < 0.2$

○ all data points have $\alpha_{\rm eff} < 0.4$ and at least one $\alpha_{\rm eff} \le 0.25$

■ otherwise

(ii) Perturbative behavior

★ verified over a range of a factor 4 change in $\alpha_{\rm eff}^{n_l}$ without power corrections or alternatively $\alpha_{\rm eff}^{n_l} \le \frac{1}{2}\Delta\alpha_{\rm eff}/(8\pi b_0\alpha_{\rm eff}^2)$ is reached

○ agreement with perturbation theory over a range of a factor $(3/2)^2$ in $\alpha_{\rm eff}^{n_l}$ possibly fitting with power corrections or alternatively $\alpha_{\rm eff}^{n_l} \le \Delta\alpha_{\rm eff}/(8\pi b_0\alpha_{\rm eff}^2)$ is reached

■ otherwise

Here $\Delta\alpha_{\rm eff}$ is the accuracy cited for the determination of $\alpha_{\rm eff}$ and n_l is the loop order to which the connection of $\alpha_{\rm eff}$ to the $\overline{\rm MS}$ scheme is known. Recall the discussion around Eqs. (290), (291); the β-function of $\alpha_{\rm eff}$ is then known to (n_l+1)-loop order.[65]

(iii) Continuum extrapolation

At a reference point of $\alpha_{\rm eff} = 0.3$ (or less) we require

★ three lattice spacings with $\mu a < 1/2$ and full $\mathcal{O}(a)$ improvement, or three lattice spacings with $\mu a \le 1/4$ and 2-loop $\mathcal{O}(a)$ improvement, or $\mu a \le 1/8$ and 1-loop $\mathcal{O}(a)$ improvement

○ three lattice spacings with $\mu a < 3/2$ reaching down to $\mu a = 1$ and full $\mathcal{O}(a)$ improvement, or three lattice spacings with $\mu a \le 1/4$ and 1-loop $\mathcal{O}(a)$ improvement

■ otherwise

In addition to the above criteria we have looked at scale variations as a general means to assess perturbative behavior (cf. subsection below). Continuum extrapolations are often not the primary concern in determinations of α_s. Where appropriate we will evaluate the new FLAG data-driven criterion, by which the distance of the data to the continuum-extrapolated value is measured in units of the quoted error. If the observable is $Q(a)$ with an extrapolated continuum value $Q(0) \pm \Delta Q$ we look at the size of

$$\delta_{\rm min} = \frac{|Q(0) - Q(a_{\rm min})|}{\Delta Q}. \tag{303}$$

Some scepticism is warranted if $\delta_{\rm min}$ exceeds 3 or so, although there may be cases where this can be justified. While we keep the core FLAG criteria unchanged, our general assessment will be informed by these measures.

We also need to specify what is meant by μ. Here are our choices

[65]Once one is in the perturbative region with $\alpha_{\rm eff}$, the error in extracting the Λ-parameter due to the truncation of perturbation theory scales like $\alpha_{\rm eff}^{n_l}$, as discussed around Eq. (291). In order to detect/control such corrections properly, one needs to change the correction term significantly; we require a factor of four for a ★ and a factor $(3/2)^2$ for a ○. An exception to the above is the situation where the correction terms are small anyway, i.e., $\alpha_{\rm eff}^{n_l} \approx (\Delta\Lambda/\Lambda)_{\rm trunc} < (\Delta\Lambda/\Lambda)_{\Delta\alpha} \approx \Delta\alpha_{\rm eff}/(8\pi b_0\alpha_{\rm eff}^2)$ is reached.

$$\begin{aligned}
\text{step scaling}&: \mu = 1/L,\\
\text{heavy quark-antiquark potential}&: \mu = 2/r,\\
\text{observables in position space}&: \mu = 1/|x|,\\
\text{observables in momentum space}&: \mu = q,\\
\text{moments of heavy-quark currents}&: \mu = 2\bar{m}_c,\\
\text{gradient-flow (GF) scheme in infinite volume}&: \mu = 1/\sqrt{8t},
\end{aligned} \tag{304}$$

where $|x|$ is the Euclidean norm of the four-vector x, q is the magnitude of the momentum, $\bar{m}_c$ is the heavy-quark mass (in the $\overline{\text{MS}}$ scheme with N_f quarks, including the heavy-quark flavor) and usually taken around the charm-quark mass. The parameter t denotes the gradient-flow time. We note again that the above criteria cannot be applied when regularization-dependent quantities $W_{\text{lat}}(a)$ are used instead of $\mathcal{Q}(\mu)$. These cases are specifically discussed in Sec. IX G.

In principle one should also account for electroweak radiative corrections. However, both in the determination of α_s at intermediate scales μ and in the running to high scales, we expect electroweak effects to be much smaller than the presently reached precision. Such effects are therefore not further discussed.

The attentive reader will have noticed that bounds such as $\mu a < 3/2$ or at least one value of $\alpha_{\text{eff}} \leq 0.25$ which we require for a ○ are not very stringent. There is a considerable difference between ○ and ★. We have chosen the above bounds, unchanged since FLAG 16, as not too many current computations would satisfy more stringent ones. Nevertheless, we believe that the ○ criteria already give reasonable bases for estimates of systematic errors. An exception may be Cali 20 [84], which is discussed in detail in Sec. IX F.

In anticipation of future changes of the criteria, we expect that we will be able to tighten our criteria for inclusion in the average, and that many more computations will reach the present ★ rating in one or more categories.

In addition to our explicit criteria, the following effects may influence the precision of results:

Topology sampling: In principle a good way to improve the quality of determinations of α_s is to push to very small lattice spacings thus enabling large μ. It is known that the sampling of field space becomes very difficult for the HMC algorithm when the lattice spacing is small and one has the standard periodic boundary conditions. In practice, for all known discretizations the topological charge slows down dramatically for $a \approx 0.05$ fm and smaller [117,153,156–160]. Open boundary conditions solve the problem [161] but are not frequently used. Since the effect of the freezing on short-distance observables is not known, we also do need to pay attention to this issue. Remarks are added in the text when appropriate.

Quark-mass effects: We assume that effects of the finite masses of the light quarks (including strange) are negligible in the effective coupling itself where large, perturbative, μ is considered.

Scale setting: The scale does not need to be very precise, since using the lowest-order β-function shows that a 3% error in the scale determination corresponds to a ∼0.5% error in $\alpha_s(M_Z)$. Since the errors of scale determinations are now typically at the 1–2 percent level or better, the corresponding error in $\alpha_s(M_Z)$ will remain subdominant for the foreseeable future.

Other limits/extrapolations: Besides the continuum limit and the infinite-volume extrapolation of hadronic observables, further limits may be required, depending on the method employed. An obvious case is the large-mass extrapolation in the decoupling method. While in this case, an effective theory can be deployed to derive plausible fit functions, this is less clear in other cases. An example is the infinite space-time volume extrapolation in the GF scheme, which is needed to make contact with the available perturbative calculations. One would expect the volume dependence to be quite different at low and high energies, and there may be a complicated intermediate regime. Systematic uncertainties are then much harder to quantify and our approach necessarily is on a case-by-case basis. Data-driven criteria like the new FLAG continuum-limit criterion are considered, however, these may fail if the data does not sufficiently overlap with the true (and possibly unknown) asymptotic regime.

2. Physical scale

Since FLAG 19, a new FLAG working group on scale setting has been established. We refer to Sec. XI for definitions and the current status. Note that the error from scale setting is sub-dominant for current α_s determinations.

A popular scale choice has been the intermediate r_0 scale, and its variant r_1, which both derive from the force between static quarks, see Eq. (335). One should bear in mind that their determination from physical observables also has to be taken into account. The phenomenological value of r_0 was originally determined as $r_0 \approx 0.49$ fm through potential models describing quarkonia [708]. Of course the quantity is precisely defined, independently of such model considerations. But a lattice computation with the correct sea-quark content is needed to determine a completely sharp value. When the quark content is not quite realistic, the value of r_0 may depend to some extent on which experimental input is used to determine (actually define) it.

The latest determinations from two-flavor QCD are $r_0 = 0.420(14)$–$0.450(14)$ fm by the ETM collaboration [190,716], using as input f_π and f_K and carrying out various continuum extrapolations. On the other hand, the ALPHA collaboration [717] determined $r_0 = 0.503(10)$ fm with input from f_K, and the QCDSF collaboration [718]

cites 0.501(10)(11) fm from the mass of the nucleon (no continuum limit). Recent determinations from three-flavor QCD are consistent with $r_1 = 0.313(3)$ fm and $r_0 = 0.472(5)$ fm [47,122,719]. Due to the uncertainty in these estimates, and as many results are based directly on r_0 to set the scale, we shall often give both the dimensionless number $r_0\Lambda_{\overline{\rm MS}}$, as well as $\Lambda_{\overline{\rm MS}}$. In the cases where no physical r_0 scale is given in the original papers or we convert to the r_0 scale, we use the value $r_0 = 0.472$ fm. In case $r_1\Lambda_{\overline{\rm MS}}$ is given in the publications, we use $r_0/r_1 = 1.508$ [719], to convert, which remains well consistent with the update [117] neglecting the error on this ratio. In some, mostly early, computations the string tension, $\sqrt{\sigma}$ was used. We convert to r_0 using $r_0^2\sigma = 1.65 - \pi/12$, which has been shown to be an excellent approximation in the relevant pure gauge theory [720,721].

The more recent gradient-flow scales t_0, w_0 are very attractive alternatives to r_0, as their determination is much simpler within a given simulation and most collaborations quote their values. The main downside are potentially large cutoff effects. We intend to transition from r_0 to t_0. In this report we start by reporting $N_f = 0$ results both with r_0 and with $\sqrt{8t_0}$, where we use as conversion factor the central value of $\sqrt{8t_0}/r_0 = 0.9435(97)$ from Dalla Brida 19 [703]. A general discussion of the various scales is given in the scale-setting section of this FLAG report, cf. Sec. XI.

3. Studies of truncation errors of perturbation theory

As discussed previously, we have to determine α_s in a region where the perturbative expansion for the β-function, Eq. (286) in the integral Eq. (285), is reliable. In principle this must be checked, and is difficult to achieve as we need to reach up to a sufficiently high scale. A recipe routinely used to estimate the size of truncation errors of the perturbative series is to study the dependence on the renormalization scale of an observable evaluated at a fixed order in the coupling, as the renormalization scale is varied around some optimal scale μ_*, from $\mu = \mu_*/2$ to $2\mu_*$. For examples, see Ref. [688].

Alternatively, or in addition, the renormalization scheme chosen can be varied, which investigates the perturbative conversion of the chosen scheme to the perturbatively defined $\overline{\rm MS}$ scheme and in particular fastest apparent convergence when the optimal scale is chosen so that the $\mathcal{O}(\alpha_s^2)$ coefficient vanishes.

The ALPHA collaboration in Ref. [722] and ALPHA 17 [723], within the SF approach defined a set of ν-schemes for which the 3-loop (scheme-dependent) coefficient of the β-function for $N_f = 2+1$ flavors was computed to be $b_2^\nu = -(0.064(27) + 1.259(1)\nu)/(4\pi)^3$. The standard SF scheme has $\nu = 0$. For comparison, $b_2^{\overline{\rm MS}} = 0.324/(4\pi)^3$. A range of scales from about 4 GeV to 128 GeV was investigated. It was found that while the procedure of varying the scale by a factor 2 up and down gave a correct estimate of the residual perturbative error for $\nu \approx 0\ldots0.3$, for negative values, e.g., $\nu = -0.5$, the estimated perturbative error is much too small to account for the mismatch in the Λ-parameter of $\approx 8\%$ at $\alpha_s = 0.15$. This mismatch, however, did, as expected, still scale with $\alpha_s^{n_l}$ with $n_l = 2$. In the schemes with negative ν, the coupling α_s has to be quite small for scale variations of a factor 2 to correctly signal the perturbative errors.

For a systematic study of renormalization-scale variations as a measure of perturbative truncation errors in various lattice determinations of α_s, we implement scale variations following the proposal in Ref. [688]. Scale variations are commonly used in phenomenology as a tool to investigate truncations errors. While they cannot give a precise estimate of the truncation errors, they provide a simple, quantitative test that can be uniformly applied to all observables. Furthermore, the implementation proposed in Ref. [688] does not rely on lattice data. The only inputs are the coefficients of the perturbative expansion of $\alpha_{\rm eff}$, so that, in principle, an estimate of the truncation errors can be done *before* embarking in a numerical simulation. Here we shall summarize briefly the methodology, provide the coefficients of the perturbative expansions for the observables of interest in this review, and compute the corresponding truncation errors.

Methodology. The use of scale variations for the determination of the missing higher-order uncertainties relies on a simple observation, namely that the scale μ that appears on the left-hand side of Eq. (283) does not need to match the scale at which the running coupling constant is computed on the right-hand side of the same equation. Equation (283) can be rewritten, with the same level of precision, as

$$\mathcal{Q}(\mu) = c_1\alpha_{\overline{\rm MS}}(\mu') + \sum_{k=2}^{n} c'_k(s)\alpha^k_{\overline{\rm MS}}(\mu') + \mathcal{O}(\alpha^{n+1}_{\overline{\rm MS}}(\mu')), \quad (s = \mu'/\mu). \tag{305}$$

The coefficients

$$c'_k(s) = \sum_{\ell=0}^{k-1} c'_{k,\ell}\log^\ell(s), \tag{306}$$

for $k \geq 2$, are determined from the coefficients c_k in Eq. (283) using the recursion

$$c'_{k,0} = c_k, \tag{307}$$

$$c'_{k,\ell} = \frac{2}{\ell}\sum_{j=1}^{k-1} j(4\pi)^{k-j} b_{k-j-1} c'_{j,\ell-1}, \tag{308}$$

where b_n are the coefficients of the beta function defined in Eq. (286). The dependence on s, and therefore on the scale

μ', is entirely due to the truncation of the perturbative expansion. Denoting the truncated series by

$$\mathcal{Q}^{(n)}(\mu,\mu') = c_1\alpha_{\overline{\rm MS}}(\mu') + \sum_{k=2}^{n} c'_k(s)\alpha^k_{\overline{\rm MS}}(\mu'), \qquad (309)$$

it is possible to show that the scale-variation procedure described below yields a sensible estimate of the truncation error

$$\delta_n = |\mathcal{Q}(\mu) - \mathcal{Q}^{(n)}(\mu,\mu')|, \qquad (310)$$

see, e.g., the discussion in Ref. [724]. Formally,

$$\mu'\frac{\partial}{\partial\mu'}\mathcal{Q}^{(n)}(\mu,\mu') \propto \alpha^{n+1}_{\overline{\rm MS}}(\mu'), \qquad (311)$$

showing that scale variations capture the correct size of the truncation error, at least parametrically.

Implementation. The implementation of the scale variations proceeds as follows.

(1) We assume a value for $\Lambda^{(3)}_{\overline{\rm MS}}$, e.g., the current best estimate in FLAG. Given this value, we compute the corresponding value of $\alpha_{\overline{\rm MS}}(s_{\rm ref}\mu)$ (at fixed $N_f = 3$) where μ is the scale associated to the observable $\mathcal{Q}$. Typical choices are $s_{\rm ref} = 1$ or $s_{\rm ref} = s^*$, the latter being the scale of fastest apparent convergence. Similarly, we also compute the value of $\alpha^{(5)}_{\overline{\rm MS}}(M_Z)$. All these values are computed using the running of the strong coupling, the value of $\Lambda^{(3)}_{\overline{\rm MS}}$ as the unique input, in addition to the $\overline{\rm MS}$ charm- and bottom-quark masses at their own scale, $\bar{m}^{(4)}_c(\bar{m}_c)$ and $\bar{m}^{(5)}_b(\bar{m}_b)$, respectively and m_Z.

(2) Using Eq. (309), we compute the value $\mathcal{Q}_{\rm ref}$ of the observable by imposing that it coincides with its truncated expansion,

$$\mathcal{Q}_{\rm ref} = \mathcal{Q}^{(n)}(\mu, s_{\rm ref}\mu), \qquad (312)$$

where $s_{\rm ref}\mu$ is the scale associated to the observable as shown explicitly in Eq. (283). By construction, using the value $\mathcal{Q}_{\rm ref}$, setting $s = s_{\rm ref}$, and solving Eq. (309), we recover for $\alpha_{\overline{\rm MS}}(s_{\rm ref}\mu)$ the value obtained in step 1. Hence, we interpret $\mathcal{Q}_{\rm ref}$ as the value of the observable that yields the value of $\alpha^{(5)}_{\overline{\rm MS}}(M_Z)$ in step 1, when performing the *usual* extraction of the strong coupling.

(3) We use Eq. (309) again, but this time set $s = s_{\rm ref}/2, 2s_{\rm ref}$, to extract $\alpha_{\overline{\rm MS}}(s\mu)$ by solving

$$\mathcal{Q}_{\rm ref} = \mathcal{Q}^{(n)}(\mu, s\mu). \qquad (313)$$

Because the expansion is truncated, the value obtained here for $\alpha_{\overline{\rm MS}}(s\mu)$ is different from the one obtained by running the coupling from the value of $\alpha_{\overline{\rm MS}}(s_{\rm ref}\mu)$ computed in step 2.

(4) Using $\alpha_{\overline{\rm MS}}(s\mu)$ as the initial condition, we run the strong coupling constant and compute $\alpha^{(5)}_{\overline{\rm MS}}(M_Z)$. The difference between this value and the value computed in step 1 is used as an estimate of the uncertainty due to the truncation of the perturbative expansion.

Typically scale variations are performed by multiplying and dividing the reference scale by a factor 2. For some determinations, where the perturbative matching is done at a few GeV, dividing the scale by a factor of 2 yields a low scale where perturbation theory is clearly no longer applicable and therefore the scale variation yields an artificially large error. In these cases, we consider only the variation obtained by multiplying the reference scale by a factor 2. To be more specific, we define the following quantities.

$\delta_{(4)}(s_{\rm ref})$: The renormalization scale $s_{\rm ref}\mu$ is multiplied and divided by a factor two. We quote a symmetric error by averaging the difference between the results obtained with the scales $s_{\rm ref}\mu$ and $2s_{\rm ref}\mu$, and the difference between the results obtained with scales $s_{\rm ref}/2\times\mu$ and $s_{\rm ref}\mu$. Note however that in some cases the error is markedly asymmetric. We will quote the differences as a percentage deviation from the reference value of $\alpha_s(m_Z)$.

$\delta_{(2)}(s_{\rm ref})$: The renormalization scale is multiplied by a factor two only. The error $\delta_{(2)}(s_{\rm ref})$ is simply the difference between the two results obtained with the two scales, again taken as a percentage deviation from the reference value of $\alpha_s(m_Z)$.

We also explore two common choices, namely $s_{\rm ref} = 1$ and $s_{\rm ref} = s^*$, the scale of fastest apparent convergence, i.e., the scale at which $c'_2(s^*) = 0$.

Perturbative coefficients. The coefficients of the perturbative expansion for the observables of interest in this review are summarized in Table 55. For each observable we report the number of coefficients that are available for the perturbative expansion, the scale at which the perturbative matching is done, the list of coefficients and the relevant references.

C. α_s from step-scaling methods

1. General considerations

The method of step-scaling functions avoids the scale problem, Eq. (296). It is in principle independent of the particular boundary conditions used and was first developed with periodic boundary conditions in a two-dimensional model [740].

The essential idea of the step-scaling strategy is to split the determination of the running coupling at large μ and of

TABLE 55. Summary of the coefficients of the perturbative expansion of the observables discussed in this review as a power series in $\alpha_{\overline{\rm MS}}$. We assume that the observables are normalized so that $c_1 = 1$ and we only quote the coefficients starting from c_2. The coefficients are computed for $N_f = 3$, unless the explicit dependence on the number of flavors is given. For each observable, we quote the number of coefficients that are known analytically and the scale of perturbative matching to the $\overline{\rm MS}$ scheme. Note that for the GF coupling there are two coefficients, reported as functions of N_f, over two separate lines.

Observable	n_l (loops)	μ [GeV]	Perturbative coefficients	References
Step-scaling	2	80	−1.37520970, 0.57120172	[725,726]
Potential	3	1.5	−0.0485502, 0.687447, 0.818808	[727–731]
		2.5	Same as line above, μ changed	
		5.0	Same as line above, μ changed	
Vacuum polarization	3	2.0	−1.4346, 0.16979, 3.21120	[732]
		4.0		[733]
		1.3		[84]
$-\log W_{11}$	2	4.4	−0.87811924, 4.20161085	[734,735]
$-\log W_{12}/u_0^6$		4.4	0.79128076, 3.18658638	
HQ r_4	2	m_c	−0.07762325, 0.07957445	[736–738]
HQ r_4		$2m_c$	Same as line above, μ changed	
HQ r_6		$2m_c$	0.77386542, −0.08560363	
HQ r_8		$2m_c$	1.08917060, 0.20034888	
GF coupling	2	$1/\sqrt{8t}$	$1.09778674 + 0.007555192\ N_f$	[365,739]
			$-0.98225 - 0.069913 N_f + 0.001872234 N_f^2$	

a hadronic scale into two lattice calculations and connect them by "step scaling". In the former part, we determine the running coupling constant in a finite-volume scheme in which the renormalization scale is set by the inverse lattice size $\mu = 1/L$. In this calculation, one takes a high renormalization scale while keeping the lattice spacing sufficiently small as

$$\mu \equiv 1/L \sim 10 \ldots 100\ \text{GeV}, \qquad a/L \ll 1. \tag{314}$$

In the latter part, one chooses a certain $\bar{g}^2_{\rm max} = \bar{g}^2(1/L_{\rm max})$, typically such that $L_{\rm max}$ is around 0.5–1 fm. With a common discretization, one then determines $L_{\rm max}/a$ and (in a large volume $L \geq 2$–3 fm) a hadronic scale such as a hadron mass, $\sqrt{t_0}/a$ or r_0/a at the same bare parameters. In this way one gets numbers for, e.g., $L_{\rm max}/r_0$ and by changing the lattice spacing a carries out a continuum-limit extrapolation of that ratio.

In order to connect $\bar{g}^2(1/L_{\rm max})$ to $\bar{g}^2(\mu)$ at high μ, one determines the change of the coupling in the continuum limit when the scale changes from L to L/s, where s is a scale factor, set to $s = 2$ in most applications. Then, starting from $L = L_{\rm max}$ one iteratively performs k steps to arrive at $\mu = s^k/L_{\rm max}$. This part of the strategy is called step scaling. Combining these results yields $\bar{g}^2(\mu)$ at $\mu = s^k(r_0/L_{\rm max})r_0^{-1}$, where r_0 stands for the particular chosen hadronic scale.

At present most applications in QCD use Schrödinger functional boundary conditions [384,741] and we discuss this below in a little more detail. (However, other boundary conditions are also possible, such as twisted periodic boundary conditions for the gauge fields and the discussion also applies to them.) An important reason is that these boundary conditions avoid zero modes for the quark fields and quartic modes [742] in the perturbative expansion in the gauge fields. Furthermore the corresponding renormalization scheme is well studied in perturbation theory [726,743,744] with the 3-loop β-function and 2-loop cutoff effects (for the standard Wilson regularization) known.

In order to have a perturbatively well-defined scheme, the SF scheme uses Dirichlet boundary conditions at time $t = 0$ and $t = T$. These break translation invariance and permit $\mathcal{O}(a)$ counter terms at the boundary through quantum corrections. Therefore, the leading discretization error is $\mathcal{O}(a)$. Improving the lattice action is achieved by adding counter terms at the boundaries whose coefficients are denoted as $c_t, \tilde{c}_t$. In practice, these coefficients are computed with 1-loop or 2-loop perturbative accuracy. A better precision in this step yields a better control over discretization errors, which is important, as can be seen, e.g., in Refs. [720,745].

Also computations with Dirichlet boundary conditions do in principle suffer from the insufficient change of topology in the HMC algorithm at small lattice spacing. However, in a small volume the weight of nonzero charge sectors in the path integral is exponentially suppressed [746] and in a Monte Carlo run of typical length very few configurations with nontrivial topology should appear.[66] Considering the issue quantitatively Ref. [747] finds a strong suppression below $L \approx 0.8$ fm. Therefore the lack of topology change of the HMC is not a serious issue for the high-energy regime in step-scaling studies. However, the matching to hadronic observables requires volumes where the problem cannot be ignored. Therefore, Ref. [748] includes a projection to zero topology into the *definition* of the coupling. A very interesting comparison of the step-scaling approach for a ($Q = 0$)-projected coupling and its unprojected version was recently carried out in Ref. [749], with $N_f = 0$ and twisted periodic boundary conditions for the gauge field. A new parallel-tempering approach to relate systems with different boundary conditions was used. The results validate the $Q = 0$ approach, in that step scaling in large volume (where contributions from $Q \neq 0$ configurations are sizeable) leads, within errors, to indistinguishable results, once the couplings are properly matched. We note also that a mix of Dirichlet and open boundary conditions is expected to remove the topology issue entirely [750] and may be considered in the future.

Apart from the boundary conditions, the very definition of the coupling needs to be chosen. We briefly discuss in turn, the two schemes used at present, namely, the Schrödinger functional (SF) and gradient flow (GF) schemes.

The SF scheme is the first one, which was used in step-scaling studies in gauge theories [384]. Inhomogeneous Dirichlet boundary conditions are imposed in time,

$$A_k(x)|_{x_0=0} = C_k, \qquad A_k(x)|_{x_0=L} = C'_k, \tag{315}$$

for $k = 1, 2, 3$. Periodic boundary conditions (up to a phase for the fermion fields) with period L are imposed in space. The matrices

$$LC_k = i\,\mathrm{diag}(\eta - \pi/3, -\eta/2, -\eta/2 + \pi/3),$$
$$LC'_k = i\,\mathrm{diag}(-(\eta + \pi), \eta/2 + \pi/3, \eta/2 + 2\pi/3),$$

just depend on the dimensionless parameter η. The coupling $\bar{g}_{\mathrm{SF}}$ is obtained from the η-derivative of the effective action,

$$\langle \partial_\eta S|_{\eta=0} \rangle = \frac{12\pi}{\bar{g}^2_{\mathrm{SF}}}. \tag{316}$$

For this scheme, the finite $c_g^{(i)}$, Eq. (288), are known for $i = 1, 2$ [726,744].

More recently, gradient-flow couplings have been used frequently because of their small statistical errors at large couplings (in contrast to $\bar{g}_{\mathrm{SF}}$, which has small statistical errors at small couplings). The gradient flow is introduced as follows [365,751]. Consider the flow gauge field $B_\mu(t, x)$ with the flow time t, which is a one-parameter deformation of the bare gauge field $A_\mu(x)$, where $B_\mu(t, x)$ is the solution to the gradient-flow equation

$$\partial_t B_\mu(t, x) = D_\nu G_{\nu\mu}(t, x),$$
$$G_{\mu\nu} = \partial_\mu B_\nu - \partial_\nu B_\mu + [B_\mu, B_\nu], \tag{317}$$

with initial condition $B_\mu(0, x) = A_\mu(x)$. The renormalized coupling is defined by [365]

$$\bar{g}^2_{\mathrm{GF}}(\mu) = \mathcal{N} t^2 \langle E(t, x) \rangle|_{\mu=1/\sqrt{8t}}, \tag{318}$$

with $\mathcal{N} = 16\pi^2/3 + \mathcal{O}((a/L)^2)$ and where $E(t, x)$ is the action density given by

$$E(t, x) = \frac{1}{4} G^a_{\mu\nu}(t, x) G^a_{\mu\nu}(t, x). \tag{319}$$

In a finite volume, one needs to specify additional conditions. In order not to introduce two independent scales one sets

$$\sqrt{8t} = cL, \tag{320}$$

for some fixed number c [752]. Schrödinger functional boundary conditions [753] or twisted periodic boundary conditions [704,754,755] have been employed. Matching of the GF coupling to the $\overline{\mathrm{MS}}$-scheme coupling is known to 1-loop for twisted boundary conditions with zero quark flavors and SU(3) group [755] and to 2-loop with SF boundary conditions with zero quark flavors [756]. The former is based on a MC evaluation at small couplings and the latter on numerical stochastic perturbation theory.[67]

2. Discussion of computations

In Table 56 we give results from various determinations of the Λ-parameter. For a clear assessment of the N_f-dependence, the last column also shows results that refer to a common hadronic scale, r_0. As discussed above, the renormalization scale can be chosen large enough such that $\alpha_s < 0.2$ and the perturbative behavior can be verified. Consequently only ★ is present for these criteria except for early work where the $n_l = 2$ loop correction to $\overline{\mathrm{MS}}$ was not yet known and we assigned a ■ concerning the renormalization scale. With dynamical fermions, results for the

[66] We simplify here and assume that the classical solution associated with the used boundary conditions has charge zero. In practice this is the case.

[67] For a variant of the twisted periodic finite volume scheme the 1-loop matching has been computed analytically [757].

TABLE 56. Results for the Λ-parameter from computations using step scaling of the SF-coupling. Entries without values for Λ computed the running and established perturbative behavior at large μ.

Collaboration	Ref.	N_f	Publication status	Renormalization scale	Perturbative behavior	Continuum extrapolation	Scale	$\Lambda_{\overline{\rm MS}}$ [MeV]	$r_0\Lambda_{\overline{\rm MS}}$
ALPHA 10A	[758]	4	A	★	★	★	only running of α_s in Fig. 4		
Perez 10	[759]	4	C	★	★	○	only step-scaling function in Fig. 4		
ALPHA 17	[85]	$2+1$	A	★	★	★	$\sqrt{8t_0} = 0.415$ fm	341(12)	0.816(29)
PACS-CS 09A	[86]	$2+1$	A	★	★	○	m_ρ	$371(13)(8)(^{+0}_{-27})$[a]	$0.888(30)(18)(^{+0}_{-65})$[b]
			A	★	★	○	m_ρ	345(59)[c]	0.824(141)[b]
ALPHA 12[d]	[717]	2	A	★	★	★	$f_{\rm K}$	310(20)	0.789(52)
ALPHA 04	[760]	2	A	■	★	★	$r_0 = 0.5$ fm[e]	245(16)(16)[e]	0.62(2)(2)[e]
ALPHA 01A	[761]	2	A	★	★	★	only running of α_s in Fig. 5		
Bribian 21	[704]	0	A	★	★	★	$r_0 = 0.5$ fm	249.4(8.0)	0.632(20)
Nada 20	[762]	0	A	★	★	★	consistency checks for [763], same gauge configurations		
Dalla Brida 19	[763]	0	A	★	★	★	$r_0 = 0.5$ fm	260.5(4.4)	0.660(11)
Ishikawa 17	[755]	0	A	★	★	★	r_0, $[\sqrt{\sigma}]$	$253(4)(^{+13}_{-2})$[b]	$0.606(9)(^{+31}_{-5})$[i]
CP-PACS 04[f]	[745]	0	A	★	★	○	only tables of $g^2_{\rm SF}$		
ALPHA 98[g]	[764]	0	A	★	★	○	$r_0 = 0.5$ fm	238(19)	0.602(48)
Lüscher 93	[743]	0	A	★	○	○	$r_0 = 0.5$ fm	233(23)	0.590(60)[h]

[a]Result with a constant (in a) continuum extrapolation of the combination $L_{\rm max}m_\rho$.

[b]In conversion from $\Lambda_{\overline{\rm MS}}$ to $r_0\Lambda_{\overline{\rm MS}}$ and vice versa, r_0 is taken to be 0.472 fm.

[c]Result with a linear continuum extrapolation in a of the combination $L_{\rm max}m_\rho$.

[d]Supersedes ALPHA 04.

[e]The $N_f = 2$ results were based on values for r_0/a which have later been found to be too small by [717]. The effect will be of the order of 10%–15%, presumably an increase in Λr_0. We have taken this into account by a ■ in the renormalization scale.

[f]This investigation was a precursor for PACS-CS 09A and confirmed two step-scaling functions as well as the scale setting of ALPHA 98.

[g]Uses data of Lüscher 93 and therefore supersedes it.

[h]Converted from $\alpha_{\overline{\rm MS}}(37r_0^{-1}) = 0.1108(25)$.

[i]Also $\Lambda_{\overline{\rm MS}}/\sqrt{\sigma} = 0.532(8)(^{+27}_{-5})$ is quoted.

step-scaling functions are always available for at least $a/L = \mu a = 1/4, 1/6, 1/8$. All calculations have a non-perturbatively $\mathcal{O}(a)$ improved action in the bulk. For the discussed boundary $\mathcal{O}(a)$ terms this is not so. In most recent calculations 2-loop $\mathcal{O}(a)$ improvement is employed together with at least three lattice spacings.[68] This means a ★ for the continuum extrapolation. In other computations only 1-loop c_t was available and we arrive at ○. We note that the discretization errors in the step-scaling functions of the SF coupling are usually found to be very small, at the percent level or below. However, the overall desired precision is very high as well, and the results in *CP-PACS 04* [745] show that discretization errors at the below percent level cannot be taken for granted. In particular with staggered fermions (unimproved except for boundary terms) few-percent effects are seen in Perez 10 [759].

In the work by PACS-CS 09A [86], the continuum extrapolation in the scale setting is performed using a

[68]With 2-loop $\mathcal{O}(a)$ improvement we here mean c_t including the g_0^4 term and $\tilde{c}_{\rm t}$ with the g_0^2 term. For gluonic observables such as the running coupling this is sufficient for cutoff effects being suppressed to $\mathcal{O}(g^6a)$.

constant function in a and with a linear function. Potentially the former leaves a considerable residual discretization error. We here use, as discussed with the collaboration, the continuum extrapolation linear in a, as given in the second line of PACS-CS 09A [86] results in Table 56. After perturbative conversion from a three-flavor result to five flavors (see Sec. IX B 1), they obtain

$$\alpha^{(5)}_{\overline{\rm MS}}(M_Z) = 0.118(3). \tag{321}$$

In Ref. [85], the ALPHA collaboration determined $\Lambda^{(3)}_{\overline{\rm MS}}$ combining step scaling in $\bar{g}^2_{\rm GF}$ in the lower-scale region $\mu_{\rm had} \le \mu \le \mu_0$, and step scaling in $\bar{g}^2_{\rm SF}$ for higher scales $\mu_0 \le \mu \le \mu_{\rm PT}$. Both schemes are defined with SF boundary conditions. For $\bar{g}^2_{\rm GF}$ a projection to the sector of zero topological charge is included, Eq. (319) is restricted to the magnetic components, and $c = 0.3$. The scales $\mu_{\rm had}$, μ_0, and $\mu_{\rm PT}$ are defined by $\bar{g}^2_{\rm GF}(\mu_{\rm had}) = 11.3$, $\bar{g}^2_{\rm SF}(\mu_0) = 2.012$, and $\mu_{\rm PT} = 16\mu_0$ which are roughly estimated as

$$1/L_{\rm max} \equiv \mu_{\rm had} \approx 0.2\,{\rm GeV}, \quad \mu_0 \approx 4\,{\rm GeV}, \quad \mu_{\rm PT} \approx 70\,{\rm GeV}. \tag{322}$$

Step scaling is carried out with an $\mathcal{O}(a)$-improved Wilson quark action [765] and Lüscher-Weisz gauge action [766] in the low-scale region and an $\mathcal{O}(a)$-improved Wilson quark action [767] and Wilson gauge action in the high-energy part. For the step scaling using steps of $L/a \to 2L/a$, three lattice sizes $L/a = 8$, 12, 16 were simulated for $\bar{g}^2_{\rm GF}$ and four lattice sizes $L/a = (4,)6$, 8, 12 for $\bar{g}^2_{\rm SF}$. The final results do not use the small lattices given in parenthesis. The parameter $\Lambda^{(3)}_{\overline{\rm MS}}$ is then obtained via

$$\Lambda^{(3)}_{\overline{\rm MS}} = \underbrace{\frac{\Lambda^{(3)}_{\overline{\rm MS}}}{\mu_{\rm PT}}}_{\text{perturbation theory}} \times \underbrace{\frac{\mu_{\rm PT}}{\mu_{\rm had}}}_{\text{step scaling}} \times \underbrace{\frac{\mu_{\rm had}}{f_{\pi K}}}_{\text{large volume simulation}} \times \underbrace{f_{\pi K}}_{\text{experimental data}}, \tag{323}$$

where the hadronic scale $f_{\pi K}$ is $f_{\pi K} = \frac{1}{3}(2f_K + f_\pi) = 147.6(5)$ MeV. The first factor on the right-hand side of Eq. (323) is obtained from $\alpha_{\rm SF}(\mu_{\rm PT})$ which is the output from SF step scaling using Eq. (285) with $\alpha_{\rm SF}(\mu_{\rm PT}) \approx 0.1$ and the 3-loop β-function and the exact conversion to the $\overline{\rm MS}$-scheme. The second factor is essentially obtained from step scaling in the GF scheme and the measurement of $\bar{g}^2_{\rm SF}(\mu_0)$ (except for the trivial scaling factor of 16 in the SF running). The third factor is obtained from a measurement of the hadronic quantity at large volume.

A large-volume simulation is done for three lattice spacings with sufficiently large volume and reasonable control over the chiral extrapolation so that the scale determination is precise enough. The step scaling results in both schemes satisfy renormalization criteria, perturbation theory criteria, and continuum-limit criteria just as previous studies using step scaling. So we assign green stars for these criteria.

The dependence of Λ, Eq. (285) with 3-loop β-function, on α_s and on the chosen scheme is discussed in [722]. This investigation provides a warning on estimating the truncation error of perturbative series. Details are explained in Sec. IX B 3.

The result for the Λ-parameter is $\Lambda^{(3)}_{\overline{\rm MS}} = 341(12)$ MeV, where the dominant error comes from the error of $\alpha_{\rm SF}(\mu_{\rm PT})$ after step scaling in the SF scheme. Using 4-loop matching at the charm and bottom thresholds and 5-loop running one finally obtains

$$\alpha^{(5)}_{\overline{\rm MS}}(M_Z) = 0.11852(84). \tag{324}$$

Several other results do not have a sufficient number of quark flavors or do not yet contain the conversion of the scale to physical units (ALPHA 10A [758], Perez 10 [759]). Thus no value for $\alpha^{(5)}_{\overline{\rm MS}}(M_Z)$ is quoted.

The computation of Ishikawa *et al.* [755] is based on the gradient-flow coupling with twisted boundary conditions [754] (TGF coupling) in the pure gauge theory. Again they use $c = 0.3$. Step scaling with a scale factor $s = 3/2$ is employed, covering a large range of couplings from $\alpha_s \approx 0.5$ to $\alpha_s \approx 0.1$ and taking the continuum limit through global fits to the step-scaling function on $L/a = 12$, 16, 18 lattices with between 6 and 8 parameters. Systematic errors due to variations of the fit functions are estimated. Two physical scales are considered: r_0/a is taken from [720] and σa^2 from [236,768]. As the ratio $\Lambda_{\rm TGF}/\Lambda_{\overline{\rm MS}}$ has not yet been computed analytically, Ref. [755] determines the 1-loop relation between $\bar{g}_{\rm SF}$ and $\bar{g}_{\rm TGF}$ from MC simulations performed in the weak coupling region and then uses the known $\Lambda_{\rm SF}/\Lambda_{\overline{\rm MS}}$. Systematic errors due to variations of the fit functions dominate the overall uncertainty.

Two extensive $N_f = 0$ step-scaling studies have been carried out in Dalla Brida 19 [763] and by Nada and Ramos [762]. They use different strategies for the running from mid to high energies, but use the same gauge configurations and share the running at low energies and matching to the hadronic scales. These results are therefore correlated. However, given the comparatively high value for $r_0\Lambda_{\overline{\rm MS}}$, it is reassuring that these conceptually different approaches yield perfectly compatible results within errors of similar size of around 1.5% for $\sqrt{8t_0}\Lambda_{\overline{\rm MS}} = 0.6227(98)$, or, alternatively $r_0\Lambda_{\overline{\rm MS}} = 0.660(11)$.

In Dalla Brida 19 [763] two GF-coupling definitions with SF-boundary conditions are considered, corresponding to (color-) magnetic and electric components of the action density respectively. The coupling definitions include the projection to $Q = 0$, as was also done in [85]. The flow-time parameter is set to $c = 0.3$, and both Zeuthen and Wilson flow are measured. Lattice sizes range from $L/a = 8$ to

$L/a = 48$, covering up to a factor of 3 in lattice spacings for the step-scaling function, where both L/a and $2L/a$ are needed. Lattice effects in the step-scaling function are visible but can be extrapolated using global fits with a^2 errors. Some remnant $\mathcal{O}(a)$ effects from the boundaries are expected, as their perturbative cancellation is incomplete. These $\mathcal{O}(a)$ contaminations are treated as a systematic error on the data, following [85], and are found to be subdominant. An intermediate reference scale $\mu_{\rm ref}$ is defined where $\alpha = 0.2$, and the scales above and below are analyzed separately. Again this is similar to [85], except that here GF-coupling data is available also at high energy scales. The GF β-functions are then obtained by fitting to the continuum extrapolated data for the step-scaling functions. In addition, a nonperturbative matching to the standard SF coupling is performed above $\mu_{\rm ref}$ for a range of couplings covering a factor of 2. The nonperturbative β-function for the SF scheme can thus be inferred from the GF β-function. It turns out that GF schemes are very slow to reach the perturbative regime. Particularly the Λ-parameter for the magnetic GF coupling shows a large slope in α^2, which is the parametric uncertainty with known 3-loop β-function. Also, convincing contact with the 3-loop β-function is barely seen down to $\alpha = 0.08$. This is likely to be related to the rather large 3-loop β-function coefficients, especially for the magnetic GF scheme [756]. In contrast, once the GF couplings are matched nonperturbatively to the SF scheme the contact to perturbative running can be safely made. It is also reassuring that in all cases the extrapolations (linear in α^2) to $\alpha = 0$ for the Λ-parameters agree very well, and the authors argue in favor of such extrapolations. Their data confirms that this procedure yields consistent results with the SF scheme for $\nu = 0$, where such an extrapolation is not required.

The low-energy regime between $\mu_{\rm ref}$ and a hadronic scale $\mu_{\rm had}$ is covered again using the nonperturbative step-scaling function and the derived β-function. Finally, contact between $\mu_{\rm had}$ and hadronic scales t_0 and r_0 is established using five lattice spacings covering a factor up to 2.7. The multitude of cross checks of both continuum limit and perturbative truncation errors make this a study which passes all current FLAG criteria by some margin. The comparatively high value for $r_0\Lambda_{\overline{\rm MS}}$ found in this study must therefore be taken very seriously.

In Nada 20 [762], Nada and Ramos provide further consistency checks of [763] for scales larger than $\mu_{\rm ref}$. The step-scaling function for $c = 0.2$ is constructed in two steps, by determining first the relation between couplings for $c = 0.2$ and $c = 0.4$ at the same L and then increasing L to $2L$ keeping the flow time fixed (in units of the lattice spacing), so that one arrives again at $c = 0.2$ on the $2L$ volume. The authors demonstrate that the direct construction of the step-scaling function for $c = 0.2$ would require much larger lattices in order to control the continuum limit at the same level of precision. The consistency with [763] for the Λ-parameter is therefore a highly nontrivial check on the systematic effects of the continuum extrapolations. The study obtains results for the Λ-parameter (again extrapolating to $\alpha = 0$) with a similar error as in [763] using the low-energy running and matching to the hadronic scale from that reference. For this reason and since gauge configurations are shared between both papers, these results are not independent of [763], so Dalla Brida 19 will be taken as representative for both works.

Since FLAG 21 a new step-scaling result with $N_f = 0$ has appeared in Bribian 21 [704]. It uses the gradient flow in a volume with twisted periodic boundary conditions for the gauge field. The volume has two shorter directions by a factor of 3; however, a reinterpretation as a symmetric physical volume is possible using internal degrees of freedom of the gauge field. This is a state-of-the-art step-scaling result, the main problem being the poor perturbative behavior of the gradient-flow coupling. Since the 3-loop β-function is not known, the parametric uncertainty in estimates of the Λ-parameter is of $\mathrm{O}(\alpha)$ and is quite large. The problem is bypassed by matching nonperturbatively to the SF scheme, which leads to stable estimates vs. α^2, and the result is $\sqrt{8\,t_0}\Lambda_{\overline{\rm MS}} = 0.603(17)$, or, in units of the Sommer scale, $r_0\Lambda_{\overline{\rm MS}} = 0.632(20)$. All FLAG criteria are passed with ★, and the data-driven criterion for the continuum limit is irrelevant in this case.

Scale variations. With a perturbative matching at $\mu \approx$ 80 GeV, we have computed the change in the determination of $\alpha_{\overline{\rm MS}}(M_Z)$ under scale variations as explained above. The systematic errors obtained from scale variations are

$$\delta^*_{(4)} = 0.1\%, \qquad \delta_{(2)} = 0.2\% \qquad \delta^*_{(2)} = 0.2\%. \quad (325)$$

Because the perturbative matching is performed at a high-energy scale, the systematic error obtained from scale variations is negligible.

D. The decoupling method

The ALPHA collaboration has proposed and pursued a new strategy to compute the Λ parameter in QCD with $N_f \geq 3$ flavors based on the simultaneous decoupling of $N_f \geq 3$ heavy quarks with RGI mass M [703]. We refer to [689] for a pedagogical introduction. Generically, for large quark mass M, a running coupling in a mass-dependent renormalization scheme

$$\bar{g}^2(\mu, M)^{(N_f)} = \bar{g}^2(\mu)^{(N_f=0)} + O(1/M^k) \quad (326)$$

can be represented by the corresponding $N_f = 0$ coupling, up to power corrections in $1/M$. The leading power is usually $k = 2$, however renormalization schemes in finite volume may have $k = 1$, depending on the set-up. For example, this is the case with standard SF or open boundary conditions in combination with a standard mass term. In practice such boundary contributions can be made numerically small by a careful choice of the scheme's parameters. In

principle, power corrections can be either $(\mu/M)^k$ or $(\Lambda/M)^k$. Fixing $\mu = \mu_{\rm dec}$, e.g., by prescribing a value for the mass-independent coupling, such that $\mu_{\rm dec}/\Lambda = \mathcal{O}(1)$ thus helps to reduce the need for very large M. Defining $\bar{g}^2(\mu_{\rm dec}, M) = u_M$ at fixed $\bar{g}^2(\mu_{\rm dec}, M = 0)$, Eq. (326) translates to a relation between Λ-parameters, which can be cast in the form,

$$\frac{\Lambda^{(N_f)}_{\overline{\rm MS}}}{\mu_{\rm dec}} P\left(\frac{M}{\mu_{\rm dec}}\frac{\mu_{\rm dec}}{\Lambda^{(N_f)}_{\overline{\rm MS}}}\right) = \frac{\Lambda^{(0)}_{\overline{\rm MS}}}{\Lambda^{(0)}_{s}} \varphi_s^{(N_f=0)}(\sqrt{u_{\rm M}}) + \mathcal{O}(M^{-k}), \tag{327}$$

with the function φ_s as defined in Eq. (285), for scheme s and $N_f = 0$. A crucial observation is that the function P, which gives the ratios of Λ-parameters $\Lambda^{(0)}_{\overline{\rm MS}}/\Lambda^{(N_f)}_{\overline{\rm MS}}$, can be evaluated perturbatively to a very good approximation [198,200]. Equation (326) also implies a relation between the couplings in mass-independent schemes, in the theories with N_f and zero flavors, respectively. In the $\overline{\rm MS}$ scheme this relation is analogous to Eq. (292),

$$\left[\bar{g}^{(N_f=0)}_{\overline{\rm MS}}(m_\star)\right]^2 = \left[\bar{g}^{(N_f)}_{\overline{\rm MS}}(m_\star)\right]^2 \times C\left(\bar{g}^{(N_f)}_{\overline{\rm MS}}(m_\star)\right), \tag{328}$$

where the evaluation of the coupling is done at the scale $m_\star = m^{(N_f)}_{\overline{\rm MS}}(\mu = m_\star)$. This removes the leading 1-loop correction of $\mathrm{O}(g^2)$ in the expansion of the function, $C(g) = 1 + c_2 g^4 + \mathrm{O}(g^6)$, which is known up to 4-loop order [696–699,769]. The mass scale $m_\star$ is in one-to-one correspondence with the RGI mass M, and $g^\star(y) = \bar{g}^{(N_f)}_{\overline{\rm MS}}(m_\star)$ can thus be considered a function of $y \equiv M^{(N_f)}/\Lambda^{(N_f)}_{\overline{\rm MS}}$. The function $P(y)$ can be evaluated perturbatively in the $\overline{\rm MS}$ scheme, as the ratio,

$$P(y) = \frac{\varphi^{(N_f=0)}_{\overline{\rm MS}}(g^\star(y)\sqrt{C(g^\star(y))})}{\varphi^{(N_f)}_{\overline{\rm MS}}(g^\star(y))}. \tag{329}$$

Note that perturbation theory is only required at the scale set by the heavy-quark mass, which works better the larger M can be chosen. Given the function $P(y)$, the left-hand side (lhs) of Eq. (327) can be inferred from a $N_f = 0$ computation of the right-hand side (rhs) in the scheme s, if the argument $\sqrt{u_M}$ of $\varphi^{(0)}_s$ is known (and the ratio $\Lambda_{\overline{\rm MS}}/\Lambda_s$ for the scheme s). The main challenge then consists in the computation of the mass-dependent coupling u_M for large masses.

1. Discussion of computations

To put the decoupling strategy to work, ALPHA 22 [80] uses $N_f = 3$, so that information from [85] can be used. Using the massless GF coupling in finite volume from this project, $\mu_{\rm dec}$ is defined through $\bar{g}^2_{\rm GF}(\mu_{\rm dec}) = 3.949$, and thus known in physical units, $\mu_{\rm dec} = 789(15)$ MeV. Imposing this condition for lattice sizes between $L/a = 12$ to $L/a = 48$, a corresponding sequence of β-values between 4.302 and 5.174 is obtained (the lattice action is the same as used by CLS, there for much coarser lattice spacings at $\beta \le 3.85$). Using the available information on nonperturbative mass renormalization [246], six values for the $\mathrm{O}(a)$-improved RGI quark masses are considered at each of these β-values, such that the ratios $z = M/\mu_{\rm dec}$ are close to 2, 4, 6, 8, 10, and 12. While great care is taken to implement nonperturbative $\mathrm{O}(a)$ improvement, there is only perturbative 1-loop information on $b_{\rm g}$, which parametrizes a mass-dependent rescaling of the bare coupling,

$$\tilde{g}_0^2 = g_0^2(1 + b_{\rm g}(g_0) a m_{\rm q}),$$
$$b_{\rm g}(g_0) = 0.012 \times N_f g_0^2 + \mathrm{O}(g_0^4).$$

Here, $m_{\rm q}$ denotes the subtracted bare quark mass, related to M by a renormalization factor of $O(1)$ at the relevant lattice spacings. Consistent $\mathrm{O}(a)$ improvement requires that $\tilde{\beta} = 6/\tilde{g}_0^2$ be kept fixed as the quark mass is varied. The authors of ALPHA 22 here assume a 100% uncertainty of the perturbative $b_{\rm g}$-estimate, which is treated as a systematic error (cf. below). At the chosen quark-mass parameters, the GF coupling with doubled time extent, $T = 2L$, is measured. This GFT coupling is used in order to minimize effects from the time boundaries, which introduce linear effects in $1/M$ in the decoupling relation, and also residual lattice effects linear in a. Both of these effects are monitored and found to be negligible. The continuum limit is then taken, either separately for each z-value, or using a global fit to all z-values $z > 2$, which turns out too small to be useful in the large-M limit (cf. Fig. 37). The lattice effects are fitted to $\mathrm{O}(a^2)$, including an $[\alpha_{\overline{\rm MS}}(1/a)]^{\hat{\Gamma}}$ term, as expected from Symanzik's effective theory with RG improvement [770–774]. The global fit uses the combined arguments from heavy-quark and Symanzik effective theories to separate the leading $(aM)^2$-effects with yet another logarithmic correction term. Cuts in the data are considered for $(aM)^2 < 0.25$ and $(aM)^2 < 0.16$. The continuum-extrapolated values include a systematic error due to the uncertainty in $b_{\rm g}$. The fits are repeated for different choices of $\hat{\Gamma}$ and $\hat{\Gamma}'$ in intervals constrained by the effective heavy-quark and Symanzik theories, and the variation is used as an estimate of systematic effects due to the possible presence of such non-power-like cutoff effects. The continuum extrapolated GFT coupling defines the starting point for the $N_f = 0$ running. Before the GF running can be used, a matching from the GFT to GF scheme is done to high precision in the $N_f = 0$ theory. The running in $N_f = 0$ is taken from Dalla Brida 19 [763] and the results are then inserted into the Eq. (327), for each of the available M-values. This defines "effective" Λ-parameters, equal to the asymptotic value up to $1/M^2$ effects. Taking the $z \to \infty$ limit (again allowing for a logarithmic correction with exponent Γ_m) then yields the final result, with the scale set using $\sqrt{t_0}$ from Ref. [114],

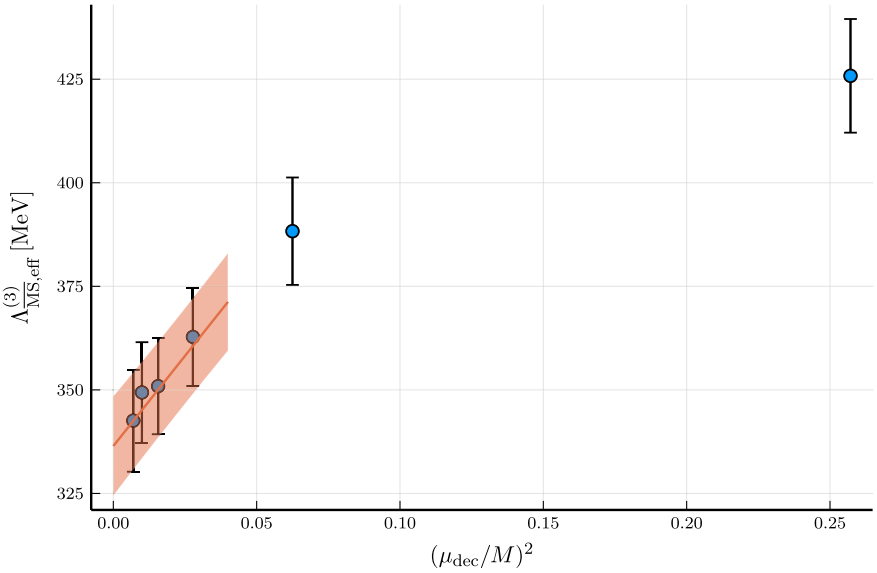


FIG. 37. The decoupling limit $M \to \infty$ in ALPHA 22, Ref. [80].

$$\Lambda^{(3)}_{\overline{\rm MS}} = 336(10)(6)_{b_g}(3)_{\Gamma_m}\ \text{MeV} = 336(12)\ \text{MeV} \quad (330)$$

which translates to $\alpha_s(m_Z) = 0.11823(84)$. Despite some common elements with ALPHA 17, the authors emphasize that the decoupling method is largely independent, with the overlap in squared error amounting to 28 percent. This is due to the fact that the error in ALPHA 17 is dominated by the $N_f = 3$ step-scaling procedure at *high* energy, and this part is completely replaced by the $N_f = 0$ result by Dalla Brida 19 [763]. ALPHA 22 also give the covariance matrix between both results which allows for combining both results with correlations taken into account.

The FLAG criteria are only indirectly applicable; decoupling relies on the step-scaling analysis with $N_f = 0$ in Dalla Brida 19 [763], which passes all FLAG criteria (cf. Sec. IX C). Except for the (well-established, cf. Refs. [198,200]) perturbative evaluation of the function $P(y)$, perturbation theory is only applied in the $N_f = 0$ theory at very high energy, which yields a ★ for perturbative behavior and renormalization scale. Using the FLAG criterion for continuum extrapolations (the constraint on values of $\alpha_{\rm eff}$ is not applicable here) the relevant scale is M, and the continuum extrapolations are based on data cut at $aM < 0.5$ or $aM < 0.4$, which leaves 3–4 values satisfying this cut even at the largest mass of O(10 GeV). A remaining uncertainty of O(aM) due to a perturbative estimate of b_g is treated as a systematic uncertainty, so that full O(a) improvement is expected to be realized within the errors. This is confirmed by—now available—nonperturbative data on b_g [775], and we use ★ for continuum extrapolations. With these errors the distance of the extrapolated result is less than one sigma away from the last data point, i.e., $\delta(\min) \approx 1$ for the data-driven criterion.

Final remark: The decoupling method offers scope for a further error reduction, by using the result for b_g and both, improved scale setting and improved $N_f = 0$ step-scaling results.

In Table 57 we list the result.

TABLE 57. Decoupling result.

Collaboration	Ref.	N_f	Publication status	Renormalization scale	Perturbative behavior	Continuum extrapolation	Scale	$\Lambda_{\overline{\rm MS}}$ [MeV]	$r_0\Lambda_{\overline{\rm MS}}$
ALPHA 22	[80]	$2+1$	A	★	★	★	$\sqrt{t_0}$ [114]	336(12)[a]	0.804(29)[a]

[a] $\alpha^{(5)}_{\overline{\rm MS}}(M_Z) = 0.11823(84)$; $r_0\Lambda_{\overline{\rm MS}}$ determined using $r_0 = 0.472$ fm

E. α_s from the potential at short distances

1. General considerations

The basic method was introduced in Ref. [776] and developed in Ref. [777]. The force or potential between an infinitely massive quark and antiquark pair defines an effective coupling constant via

$$F(r) = \frac{dV(r)}{dr} = C_F \frac{\alpha_{\rm qq}(r)}{r^2}. \tag{331}$$

The coupling can be evaluated nonperturbatively from the potential through a numerical differentiation, see below. In perturbation theory one also defines couplings in different schemes $\alpha_{\tilde{V}}$, α_V via

$$V(r) = -C_F \frac{\alpha_{\tilde{V}}(r)}{r}, \quad \text{or} \quad \tilde{V}(Q) = -C_F \frac{\alpha_V(Q)}{Q^2}, \tag{332}$$

where one fixes the unphysical constant in the potential by $\lim_{r\to\infty} V(r) = 0$, which is compatible with fixed-order perturbation theory. $\tilde{V}(Q)$ is the Fourier transform of $V(r)$. Nonperturbatively, the subtraction of a constant in the potential introduces an additional renormalization constant, the value of $V(r_{\rm ref})$ at some distance $r_{\rm ref}$. Perturbatively, it is believed to entail a renormalon ambiguity. In perturbation theory, the different definitions are all simply related to each other, and their perturbative expansions are known including the $\alpha_s^4, \alpha_s^4 \log \alpha_s$ and $\alpha_s^5 \log \alpha_s, \alpha_s^5 (\log \alpha_s)^2$ terms [727,729,730,778–784].

The potential $V(r)$ is determined from ratios of Wilson loops, $W(r,t)$, which behave as

$$\langle W(r,t)\rangle = |c_0|^2 e^{-V(r)t} + \sum_{n\neq 0} |c_n|^2 e^{-V_n(r)t}, \tag{333}$$

where t is taken as the temporal extension of the loop, r is the spatial one and V_n are excited-state potentials. To improve the overlap with the ground state, and to suppress the effects of excited states, t is taken large. Also various additional techniques are used, such as a variational basis of operators (spatial paths) to help in projecting out the ground state. Furthermore some lattice-discretization effects can be reduced by averaging over Wilson loops related by rotational symmetry in the continuum.

In order to reduce discretization errors it is of advantage to define the numerical derivative giving the force as

$$F(r_{\rm I}) = \frac{V(r) - V(r-a)}{a}, \tag{334}$$

where $r_{\rm I}$ is chosen so that at tree level the force is the continuum force. $F(r_{\rm I})$ is then a tree-level improved quantity and similarly the tree-level improved potential can be defined [785].

Lattice potential results are in position space, while perturbation theory is naturally computed in momentum space at large momentum. Usually, the Fourier transform of the perturbative expansion is then matched to lattice data.

Finally, as was noted in Sec. IX B 1, a determination of the force can also be used to determine the scales r_0, r_1, by defining them from the static force by

$$r_0^2 F(r_0) = 1.65, \qquad r_1^2 F(r_1) = 1. \tag{335}$$

2. Discussion of computations

In Table 58, we list results of determinations of $r_0\Lambda_{\overline{\rm MS}}$ (together with $\Lambda_{\overline{\rm MS}}$ using the scale determination of the authors).

The first determinations in the three-color Yang Mills theory are by UKQCD 92 [777] and Bali 92 [796] who used $\alpha_{\rm qq}$, Eq. (331), as explained above, but not in the tree-level improved form. Rather a phenomenologically determined lattice-artifact correction was subtracted from the lattice potentials. The comparison with perturbation theory was on a more qualitative level on the basis of a 2-loop β-function ($n_l = 1$) and a continuum extrapolation could not be performed as yet. A much more precise computation of $\alpha_{\rm qq}$ with continuum extrapolation was performed in Refs. [720,785]. Satisfactory agreement with perturbation theory was found [785] but the stability of the perturbative prediction was not considered sufficient to be able to extract a Λ parameter.

In Brambilla 10 [795] the same quenched lattice results of Ref. [785] were used and a fit was performed to the continuum potential, instead of the force. Perturbation theory to $n_l = 3$ loop was used including a resummation of terms $\alpha_s^3(\alpha_s \ln \alpha_s)^n$ and $\alpha_s^4(\alpha_s \ln \alpha_s)^n$. Close agreement with perturbation theory was found when a renormalon subtraction was performed. Note that the renormalon subtraction introduces a second scale into the perturbative formula which is absent when the force is considered.

Bazavov 14 [788] updates Bazavov 12 [789] and modifies this procedure somewhat. They consider the perturbative expansion for the force. They set $\mu = 1/r$ to eliminate logarithms and then integrate the force to obtain an expression for the potential. The resulting integration constant is fixed by requiring the perturbative potential to be equal to the nonperturbative one exactly at a reference distance $r_{\rm ref}$ and the two are then compared at other values of r. As a further check, the force is also used directly.

For the quenched calculation of Brambilla 10 [795] very small lattice spacings, $a \sim 0.025$ fm, were available from Ref. [785]. For ETM 11C [792], Bazavov 12 [789], Karbstein 14 [791] and Bazavov 14 [788] using dynamical fermions such small lattice spacings are not yet realized (Bazavov 14 reaches down to $a \sim 0.041$ fm).

TABLE 58. Short-distance potential results.

Collaboration	Ref.	N_f	Publication status	Renormalization scale	Perturbative behavior	Continuum extrapolation	Scale	$\Lambda_{\overline{\text{MS}}}$ [MeV]	$r_0\Lambda_{\overline{\text{MS}}}$
Ayala 20	[82]	$2+1$	A	○	★	○	$r_1 = 0.3106(17)$ fm[c]	338(13)	0.802(31)
TUMQCD 19	[83]	$2+1$	A	○	★	○	$r_1 = 0.3106(17)$ fm[c]	$314(^{+16}_{-8})$	$0.745(^{+38}_{-19})$
Takaura 18	[786,787]	$2+1$	A	■	○	○	$\sqrt{t_0} = 0.1465(25)$ fm[a]	$334(10)(^{+20}_{-18})$[b]	0.799(51)[l]
Bazavov 14	[788]	$2+1$	A	○	★	○	$r_1 = 0.3106(17)$ fm[c]	$315(^{+18}_{-12})$[d]	$0.746(^{+42}_{-27})$
Bazavov 12	[789]	$2+1$	A	○[f]	○	○[g]	$r_0 = 0.468$ fm	295(30)[h]	0.70(7)[i]
Karbstein 18	[790]	2	A	○	○	○	$r_0 = 0.420(14)$ fm[e]	302(16)	0.643(34)
Karbstein 14	[791]	2	A	○	○	○	$r_0 = 0.42$ fm	331(21)	0.692(31)
ETM 11C	[792]	2	A	○	○	○	$r_0 = 0.42$ fm	315(30)[j]	0.658(55)
Brambilla 23	[197]	0	A	○	○	★	$\sqrt{8t_0} = 0.9569(66)r_0$	$275(^{+9}_{-12})$[l]	$0.657(^{+23}_{-28})$
Husung 20	[793]	0	C	○	★	★	no quoted value for $\Lambda_{\overline{\text{MS}}}$		
Husung 17	[794]	0	C	○	★	★	$r_0 = 0.50$ fm	232(6)	0.590(16)
Brambilla 10	[795]	0	A	○	★	○[k]		266(13)[l]	$0.637(^{+32}_{-30})$[k]
UKQCD 92	[777]	0	A	★	○[m]	■	$\sqrt{\sigma} = 0.44$ GeV	256(20)	0.686(54)
Bali 92	[796]	0	A	★	○[m]	■	$\sqrt{\sigma} = 0.44$ GeV	247(10)	0.661(27)

[a]Scale determined from t_0 in Ref. [115].

[b]$\alpha^{(5)}_{\overline{\text{MS}}}(M_Z) = 0.1179(7)(^{+13}_{-12})$.

[c]Determination on lattices with $m_\pi L = 2.2 - 2.6$. Scale from r_1 [117] as determined from f_π in Ref. [47].

[d]$\alpha^{(3)}_{\overline{\text{MS}}}(1.5\text{ GeV}) = 0.336(^{+12}_{-8})$, $\alpha^{(5)}_{\overline{\text{MS}}}(M_Z) = 0.1166(^{+12}_{-8})$.

[e]Scale determined from f_π, see [190].

[f]Since values of α_{eff} within our designated range are used, we assign a ○ despite values of α_{eff} up to $\alpha_{\text{eff}} = 0.5$ being used.

[g]Since values of $2a/r$ within our designated range are used, we assign a ○ although only values of $2a/r \geq 1.14$ are used at $\alpha_{\text{eff}} = 0.3$.

[h]Using results from Ref. [719].

[i]$\alpha^{(3)}_{\overline{\text{MS}}}(1.5\text{ GeV}) = 0.326(19)$, $\alpha^{(5)}_{\overline{\text{MS}}}(M_Z) = 0.1156(^{+21}_{-22})$.

[j]Both potential and r_0/a are determined on a small ($L = 3.2r_0$) lattice.

[k]Uses lattice results of Ref. [720], some of which have very small lattice spacings where according to more recent investigations a bias due to the freezing of topology may be present.

[l]Our conversion using $r_0 = 0.472$ fm.

[m]We give a ○ because only a NLO formula is used and the error bars are very large; our criterion does not apply well to these very early calculations.

They all use the tree-level improved potential as described above. We note that the value of $\Lambda_{\overline{\text{MS}}}$ in physical units by ETM 11C [792] is based on a value of $r_0 = 0.42$ fm. This is at least 10% smaller than the large majority of other values of r_0. Also the values of r_0/a on the finest lattices in ETM 11C [792] and r_1/a for Bazavov 14 [788] come from rather small lattices with $m_\pi L \approx 2.4$, 2.2 respectively.

Instead of the procedure discussed previously, Karbstein 14 [791] reanalyzes the data of ETM 11C [792] by first estimating the Fourier transform $\tilde{V}(p)$ of $V(r)$ and then fitting the perturbative expansion of $\tilde{V}(p)$ in terms of $\alpha_{\overline{\text{MS}}}(p)$. Of course, the Fourier transform requires some modeling of the r-dependence of $V(r)$ at short and at large distances. The authors fit a linearly rising potential at large distances together with string-like corrections of order r^{-n}

and define the potential at large distances by this fit.[69] Recall that for observables in momentum space we take the renormalization scale entering our criteria as $\mu = q$, Eq. (304). The analysis (as in ETM 11C [792]) is dominated by the data at the smallest lattice spacing, where a controlled determination of the overall scale is difficult due to possible finite-size effects. Karbstein 18 [790] is a reanalysis of Karbstein 14 and supersedes it. Some data with a different discretization of the static quark is added (on the same configurations) and the discrete lattice results for the static potential in position space are first parametrized by a continuous function, which then allows for an analytical Fourier transformation to momentum space.

Similarly also for Takaura 18 [786,787] the momentum space potential $\tilde{V}(Q)$ is the central object. Namely, they assume that renormalon/power-law effects are absent in $\tilde{V}(Q)$ and only come in through the Fourier transformation. They provide evidence that renormalon effects (both $u = 1/2$ and $u = 3/2$) can be subtracted and arrive at a nonperturbative term $k\Lambda^3_{\overline{\rm MS}} r^2$. Two different analyses are carried out with the final result taken from "Analysis II." Our numbers including the evaluation of the criteria refer to it. Together with the perturbative 3-loop (including the $\alpha_s^4 \log \alpha_s$ term) expression, this term is fitted to the nonperturbative results for the potential in the region $0.04\ \text{fm} \le r \le 0.35\ \text{fm}$, where 0.04 fm is $r = a$ on the finest lattice. The nonperturbative potential data originates from JLQCD ensembles (Symanzik-improved gauge action and Möbius domain-wall quarks) at three lattice spacings with a pion mass around 300 MeV. Since at the maximal distance in the analysis we find $\alpha_{\overline{\rm MS}}(2/r) = 0.43$, the renormalization-scale criterion yields a ■. The perturbative behavior is ○ because of the high orders in perturbation theory known. The continuum-limit criterion yields a ○.

One of the main issues for all these computations is whether the perturbative running of the coupling constant has been reached. While for $N_f = 0$ fermions Brambilla 10 [795] reports agreement with perturbative behavior at the smallest distances, Husung 17 (which goes to shorter distances) finds relatively large corrections beyond the 3-loop $\alpha_{\rm qq}$. For dynamical fermions, Bazavov 12 [789] and Bazavov 14 [788] report good agreement with perturbation theory after the renormalon is subtracted or eliminated.

A second issue is the coverage of configuration space in some of the simulations, which use very small lattice spacings with periodic boundary conditions. Affected are the smallest two lattice spacings of Bazavov 14 [788] where very few tunnelings of the topological charge occur [117]. With present knowledge, it also seems possible that the older data by Refs. [720,785] used by Brambilla 10 [795] are partially obtained with (close to) frozen topology.

[69]Note that at large distances, where string breaking is known to occur, this is not any more the ground-state potential defined by Eq. (333).

The computation in Husung 17 [794], for $N_f = 0$ flavors, first determines the coupling $\bar{g}^2_{\rm qq}(r, a)$ from the force and then performs a continuum extrapolation on lattices down to $a \approx 0.015$ fm, using a step-scaling method at short distances, $r/r_0 \lesssim 0.5$. Using the 4-loop $\beta^{\rm qq}$ function this allows $r_0\Lambda_{\rm qq}$ to be estimated, which is then converted to the $\overline{\rm MS}$ scheme. $\alpha_{\rm eff} = \alpha_{\rm qq}$ ranges from ~0.17 to large values; we give ○ for renormalization scale and ★ for perturbative behavior. The range $a\mu = 2a/r \approx 0.37$–0.14 leads to a ★ in the continuum extrapolation. Recently these calculations have been extended in Husung 20 [793]. A finer lattice spacing of $a = 0.01$ fm (scale from $r_0 = 0.5$ fm) is reached and lattice volumes up to $L/a = 192$ are simulated (in Ref. [794] the smallest lattice spacing is 0.015 fm). The Wilson action is used despite its significantly larger cutoff effects compared to Symanzik-improved actions; this avoids unitarity violations, thus allowing for a clean ground-state extraction via a generalized eigenvalue problem. Open boundary conditions are used to avoid the topology-freezing problem. Furthermore, new results for the continuum approach are employed, which determine the cutoff dependence at $\mathcal{O}(a^2)$ including the exact coupling-dependent terms, in the asymptotic region where the Symanzik effective theory is applicable [772]. An *Ansatz* for the remaining higher-order cutoff effects at $\mathcal{O}(a^4)$ is propagated as a systematic error to the data, which effectively discards data for $r/a < 3.5$. The large-volume step-scaling function with step factor 3/4 is computed and compared to perturbation theory. For $\alpha_{qq} > 0.2$ there is a noticeable difference between the 2-loop and 3-loop results. Furthermore, the ultra-soft contributions at 4-loop level give a significant contribution to the static $Q\bar{Q}$ force. While this study is for $N_f = 0$ flavors it does raise the question whether the weak-coupling expansion for the range of r-values used in present analyses of α_s is sufficiently reliable. Around $\alpha_{\rm qq} \approx 0.21$ the differences get smaller but the error increases significantly, mainly due to the propagated lattice artifacts. The dependence of $\Lambda^{(N_f=0)}_{\overline{\rm MS}}\sqrt{8t_0}$ on $\alpha^3_{\rm qq}$ is very similar to the one observed in the previous study but no value for its $\alpha_{qq} \to 0$ limit is quoted. Husung 20 [793] is more pessimistic about the error on the Λ parameter stating the relative error has to be 5% or larger, while Husung 17 quotes a relative error of 3%.

In $2+1$-flavor QCD two new papers appeared on the determination of the strong coupling constant from the static quark anti-quark potential after the FLAG 19 report [82,83]. In TUMQCD 19 [83][70] the 2014 analysis of Bazavov 14 [788] has been extended by including three finer lattices with lattice spacing $a = 0.035$, 0.030 and 0.025 fm as well as lattice results on the free energy of static quark anti-quark pair at nonzero temperature. On the new fine lattices the effect of freezing topology has been

[70]The majority of authors are the same as in [788].

observed, however, it was verified that this does not affect the potential within the estimated errors [797,798]. The comparison of the lattice result on the static potential has been performed in the interval $[r_{\rm min}, r_{\rm max}]$, with $r_{\rm max} = 0.131$, 0.121, 0.098, 0.073 and 0.055 fm. The main result quoted in the paper is based on the analysis with $r_{\rm max} = 0.073$ fm [83]. Since the new study employs a much wider range in r than the previous one [788] we give it a ★ for the perturbative behavior. Since $\alpha_{\rm eff} = \alpha_{qq}$ varies in the range 0.2–0.4 for the r values used in the main analysis we give ○ for the renormalization scale. Several values of $r_{\rm min}$ have been used in the analysis, the largest being $r_{\rm min}/a = \sqrt{8} \simeq 2.82$, which corresponds to $a\mu \simeq 0.71$. Therefore, we give a ○ for continuum extrapolation in this case. An important difference compared to the previous study [788] is the variation of the renormalization scale. In Ref. [788] the renormalization scale was varied by a factor of $\sqrt{2}$ around the nominal value of $\mu = 1/r$, in order to exclude very low scales, for which the running of the strong coupling constant is no longer perturbative. In the new analysis the renormalization scale was varied by a factor of two. As the result, despite the extended dataset and shorter distances used in the new study the perturbative error did not decrease [83]. We also note that the scale dependence turned out to be nonmonotonic in the range $\mu = 1/(2r)$–$2/r$ [83]. The final result reads ("us" stands for "ultra-soft"),

$$\begin{aligned}\Lambda_{\overline{\rm MS}}^{(N_f=3)} &= 314.0 \pm 5.8({\rm stat}) \pm 3.0({\rm lat}) \\ &\quad \pm 1.7({\rm scale})^{+13.4}_{-1.8}({\rm pert}) \pm 4.0({\rm pert.\,us})\ {\rm MeV} \\ &= 314^{+16}_{-08}\ {\rm MeV}, \end{aligned} \tag{336}$$

where all errors were combined in quadrature. This is in very good agreement with the previous determination [788].

The analysis was also applied to the singlet static quark anti-quark free energy at short distances. At short distances the free energy is expected to be the same as the static potential. This is verified numerically in the lattice calculations TUMQCD 19 [83] for $rT < 1/4$ with T being the temperature. Furthermore, this is confirmed by the perturbative calculations at $T > 0$ at NLO [799]. The advantage of using the free energy is that it gives access to much shorter distances. On the other hand, one has fewer data points because the condition $rT < 1/4$ has to be satisfied. The analysis based on the free energy gives

$$\begin{aligned}\Lambda_{\overline{\rm MS}}^{(N_f=3)} &= 310.9 \pm 11.3({\rm stat}) \pm 3.0({\rm lat}) \\ &\quad \pm 1.7({\rm scale})^{+5.6}_{-0.8}({\rm pert}) \pm 2.1({\rm pert.\,us})\ {\rm MeV} \\ &= 311(13)\ {\rm MeV}, \end{aligned} \tag{337}$$

in good agreement with the above result and thus, providing additional confirmation of it.

The analysis of Ayala 20 [82] uses a subset of data presented in TUMQCD 19 [83] with the same correction of the lattice effects. For this reason the continuum extrapolation gets ○, too. They match to perturbation theory for $1/r > 2$ GeV, which corresponds to $\alpha_{\rm eff} = \alpha_{qq} = 0.2$–$0.4$. Therefore, we give ○ for the renormalization scale. They verify the perturbative behavior in the region $1\ {\rm GeV} < 1/r < 2.9\ {\rm GeV}$, which corresponds to variation of $\alpha^3_{\rm eff}$ by a factor of 3.34. However, the relative error on the final result has $\delta\Lambda/\Lambda \simeq 0.035$ which is larger than $\alpha^3_{\rm eff} = 0.011$. Therefore, we give a ★ for the perturbative behavior in this case. The final result for the Λ-parameter reads

$$\begin{aligned}\Lambda_{\overline{\rm MS}}^{(N_f=3)} &= 338 \pm 2({\rm stat}) \pm 8({\rm matching}) \pm 10({\rm pert})\ {\rm MeV} \\ &= 338(13)\ {\rm MeV}. \end{aligned} \tag{338}$$

This is quite different from the above result. This difference is mostly due to the organization of the perturbative series. The authors use ultra-soft (log) resummation, i.e., they resum the terms $\alpha_s^{3+n} \ln^n \alpha_s$ to all orders instead of using fixed-order perturbation theory. They also include what is called the terminant of the perturbative series associated to the leading renormalon of the force [82]. When they use fixed-order perturbation theory they obtain very similar results to Refs. [83,788]. It has been argued that log resummation cannot be justified since for the distance range available in the lattice studies α_s is not small enough and the logarithmic and nonlogarithmic higher-order terms are of a similar size [788]. On the other hand, the resummation of ultra-soft logs does not lead to any anomalous behavior of the perturbative expansion like large scale dependence or bad convergence [82].

To obtain the value of $\Lambda_{\overline{\rm MS}}^{(N_f=3)}$ from the static potential we combine the results in Eqs. (336) and (338) using the weighted average with the weight given by the perturbative error and using the difference in the central value as the error estimate. This leads to

$$\Lambda_{\overline{\rm MS}}^{(N_f=3)} = 330(24)\ {\rm MeV}, \tag{339}$$

from the static potential determination. In the case of TUMQCD 19, where the perturbative error is very asymmetric we used the larger upper error for the calculation of the corresponding weight.

A new analysis with $N_f = 0$ has been presented in Brambilla 23 [197] where gradient flow is used to study the static force. The use of gradient flow allows an improved determination of the static force while adding to the problem a new scale, the gradient flow time τ_F. The lattice volumes used are 40×20^3, 52×26^3, 60×30^2 and 80×40^3, with corresponding lattice spacings ranging from

0.06 to 0.03 fm, using the Wilson action. On the finest lattice an increase in the autocorrelation of the topological charge is observed and taken into account by increasing the Monte Carlo time in-between measurements. The reference scale t_0, used throughout the analysis, is obtained from a measurement of the action density by imposing

$$\tau_F \left\langle \frac{1}{4} G_{\mu\nu} G^{\mu\nu} \right\rangle \Big|_{\tau_F = t_0} = 0.3. \tag{340}$$

The static force is computed from the insertion of the chromoelectric field in the expectation value of the Wilson loop,

$$F(r) = -i \lim_{T\to\infty} \frac{\langle \mathrm{Tr}[W_{r\times T} \hat{\mathbf{r}} \cdot g\mathbf{E}(\mathbf{r}, \mathbf{t})] \rangle}{\langle \mathrm{Tr} W_{r\times T} \rangle}, \tag{341}$$

and tree-level improvement is used to improve the extrapolation to the continuum limit. The dimensionless product $r^2 F(r)$ yields the observable used for the extraction of α_s.

Results extrapolated to $\tau_F = 0$ are used for a conventional analysis along the lines of previous publications using the static force. The fit uses the perturbative expansion of the force including 3-loop contributions and leading ultrasoft logarithms. Data points with $r/\sqrt{t_0} \in [0.80, 1.15]$ are included in the fit, which yields

$$\sqrt{8t_0}\Lambda_{\overline{\mathrm{MS}}}^{(N_f=0)} = 0.6353 \pm 0.0032(\mathrm{stat}) \pm 0.0013(\mathrm{AIC}), \tag{342}$$

where the label AIC refers to the Bayesian procedure for combining results from different fit ranges based on Akaike's information criterion, as proposed in Ref. [800]. Note that the error on this result is still dominated by statistics rather than the systematics related to the choice of fitting range. The matching scale in these fits is the usual scale $\mu = 1/r$.

Measurements at $\tau_F \neq 0$ allow an alternative way to extract the strong coupling constant by fitting to the perturbative expression for the force at finite flow time. The latter perturbative expansion is only known at 1-loop, which is used as a correction of the higher-order result at $\tau_F = 0$. The best result is obtained by fitting the r-dependence at fixed values of τ_F, which yields

$$\sqrt{8t_0}\Lambda_{\overline{\mathrm{MS}}}^{(N_f=0)} = 0.629^{+22}_{-26}. \tag{343}$$

The scale of perturbative matching is defined as

$$\mu = \frac{1}{\sqrt{sr^2 + 8b\tau_F}}. \tag{344}$$

The uncertainty related to the truncation of the perturbative expansion is estimated by scale variations, where $b = 0$ and s is varied by a factor $\sqrt{2}$ in the zero-flow-time part of the perturbative expansion, while $s = 1$ and $b = 0, 1, -0.5$ in the finite-flow-time part. The central value corresponds to $s = 1$, $b = 0$. The error on the result above is dominated by the s-scale variation. The ratio $\sqrt{t_0}/r_0$ is computed in Brambilla 23 and allows us to quote a final result in units of r_0,

$$r_0\Lambda_{\overline{\mathrm{MS}}}^{(N_f=0)} = 0.657^{+23}_{-28}. \tag{345}$$

The continuum extrapolation is based on four lattice spacings. From the data reported in the figures, we see that for $r = 0.7323\sqrt{t_0}$, the effective coupling is below the requested threshold of 0.03, while the lattice spacing is such that $0.2321 \leq \mu a \leq 0.4916$. Therefore, we can give a ★ for the continuum extrapolation. Fits to the perturbative behavior are performed for $0.27 \leq \alpha_{\mathrm{eff}} \leq 0.36$ and $n_l = 3$ in the perturbative expansion. Hence, $\alpha_{\mathrm{eff}}^{n_l}$ changes by a factor of 2.37, which is 5% above the threshold of $(3/2)^2$. We feel in this case we can award a ○ for the perturbative behavior. Finally, given the range of values for α_{eff} quoted above, we give a ○ for the renormalization scale.

Scale variations. The perturbative matching for the static potential is done at lower scales, $\mu = 1.5, 2.5, 5.0$ GeV. We have computed the change in the determination of $\alpha_{\overline{\mathrm{MS}}}(M_Z)$ as explained in Sec. IX A. The systematic errors depend on the value of the perturbative matching scale. We obtain

$Q = 1.5$ GeV

$$\delta_{(2)} = 2.6\% \qquad \delta^*_{(2)} = 2.7\%. \tag{346}$$

The value of $\delta^*_{(4)}$ cannot be computed in this case, because the matching scale is low, already at the boundary of the region where the perturbative expansion can be trusted.

$Q = 2.5$ GeV

$$\delta^*_{(4)} = 0.9\%, \quad \delta_{(2)} = 1.5\% \quad \delta^*_{(2)} = 1.5\%. \tag{347}$$

$Q = 5.0$ GeV

$$\delta^*_{(4)} = 0.4\%, \quad \delta_{(2)} = 0.8\% \quad \delta^*_{(2)} = 0.8\%. \tag{348}$$

Note that in the last two cases it was possible to compute $\delta^*_{(4)}$.

For the larger values of Q, the error obtained from scale variations is very similar to the error quoted in previous editions of FLAG, where scale variations were not performed systematically. For $Q = 1.5$ GeV the error is larger, as expected since the matching of perturbation theory happens at lower energy.

F. α_s from the light-quark vacuum polarization in momentum/position space

1. General considerations

Except for the calculation Cali 20 [84], where position space is used (see below), the light-flavor-current two-point function is usually evaluated in momentum space, in terms of the vacuum-polarization function. Assuming $N_f = 3$ flavors in the isospin limit, with flavor nonsinglet currents consisting of up and down quarks, J^a_μ $(a = 1, \ldots, 3)$, the momentum representation takes the form

$$\langle J^a_\mu J^b_\nu \rangle = \delta^{ab}[(\delta_{\mu\nu}Q^2 - Q_\mu Q_\nu)\Pi^{(1)}_J(Q) - Q_\mu Q_\nu \Pi^{(0)}_J(Q)], \tag{349}$$

where Q_μ is a space-like momentum and $J_\mu \equiv V_\mu$ for a vector current and $J_\mu \equiv A_\mu$ for an axial-vector current.[71] Defining $\Pi_J(Q) \equiv \Pi^{(0)}_J(Q) + \Pi^{(1)}_J(Q)$, the operator product expansion (OPE) of $\Pi_{V/A}(Q)$ is given by

$$\begin{aligned}\Pi_{V/A}|_{\mathrm{OPE}}(Q^2, \alpha_s) &= c + C^{V/A}_1(Q^2) + C^{V/A}_m(Q^2)\frac{\bar{m}^2(Q)}{Q^2} \\ &+ \sum_{q=u,d,s} C^{V/A}_{\bar{q}q}(Q^2)\frac{\langle m_q \bar{q}q\rangle}{Q^4} + C^{V/A}_{GG}(Q^2)\frac{\langle \alpha_s GG\rangle}{Q^4} \\ &+ \mathcal{O}(Q^{-6}),\end{aligned} \tag{350}$$

for large Q^2. The perturbative coefficient functions $C^{V/A}_X(Q^2)$ for the operators X ($X = 1$, $\bar{q}q$, GG) are given as $C^{V/A}_X(Q^2) = \sum_{i\geq 0}(C^{V/A}_X)^{(i)}\alpha^i_s(Q^2)$ and $\bar{m}$ is the running mass of the mass-degenerate up and down quarks. $C^{V/A}_1$ is known including α^4_s in a continuum renormalization scheme such as the $\overline{\mathrm{MS}}$ scheme [802–805]. Nonperturbatively, there are terms in $C^{V/A}_X$ that do not have a series expansion in α_s. For an example for the unit operator see Ref. [806]. The term c is Q-independent and divergent in the limit of infinite ultraviolet cutoff. However the Adler function defined as

$$D(Q^2) \equiv -Q^2\frac{d\Pi(Q^2)}{dQ^2}, \tag{351}$$

is a scheme-independent finite quantity, which gives rise to an effective coupling. Therefore, one can determine the running coupling constant in the $\overline{\mathrm{MS}}$ scheme from the vacuum-polarization function computed by a lattice-QCD simulation. Of course, there is the choice whether to use the vector or the axial-vector channel, or both, the canonical choice being $\Pi_{V+A} = \Pi_V + \Pi_A$. While perturbation theory does not distinguish between these channels, the nonperturbative contributions are different, and the quality of lattice data may differ, too. For a given choice, the lattice data of the vacuum polarization is fitted with the perturbative formula Eq. (350) with fit parameter $\Lambda_{\overline{\mathrm{MS}}}$ parametrizing the running coupling $\alpha_{\overline{\mathrm{MS}}}(Q^2)$.

While there is no problem in discussing the OPE at the nonperturbative level, the condensates such as $\langle \alpha_s GG\rangle$ are ambiguous, since they mix with lower-dimensional operators including the unity operator. Therefore, one should work in the high-Q^2 regime where power corrections are negligible within the given accuracy. Thus setting the renormalization scale as $\mu \equiv \sqrt{Q^2}$, one should seek, as always, the window $\Lambda_{\mathrm{QCD}} \ll \mu \ll a^{-1}$.

2. Definitions in position space

The two-point current correlation functions in position space contain the same physical information as in momentum space, but the technical details are sufficiently different to warrant a separate discussion. The (Euclidean) current-current correlation function for $J^\mu_{ff'}$ (with flavor indices f, f') is taken to be either the flavor nondiagonal vector or axial-vector current, with the Lorentz indices contracted,

$$\begin{aligned}C_{\mathrm{A,V}}(x) &= -\sum_\mu \langle J^\mu_{ff'\mathrm{A,V}}(x) J^\mu_{f'f\mathrm{A,V}}(0)\rangle \\ &= \frac{6}{\pi^4 (x^2)^3}\left(1 + \frac{\alpha_s}{\pi} + \mathcal{O}(\alpha^2)\right).\end{aligned} \tag{352}$$

In the chiral limit, the perturbative expansion is known to α^4_s [807], and is identical for vector and axial-vector correlators. The only scale is set by the Euclidean distance $\mu = 1/|x|$ and the effective coupling can thus be defined as

$$\alpha_{\mathrm{eff}}(\mu = 1/|x|) = \pi[(x^2)^3(\pi^4/6)C_{\mathrm{A,V}}(x) - 1]. \tag{353}$$

As communicated to us by the authors of [84], there is a typo in Eq. (35) of [807]. For future reference, the numerical coefficients for the 3-loop conversion

$$\alpha_{\mathrm{eff}}(\mu) = \alpha_{\overline{\mathrm{MS}}}(\mu) + c_1\alpha^2_{\overline{\mathrm{MS}}}(\mu) + c_2\alpha^3_{\overline{\mathrm{MS}}}(\mu) + c_3\alpha^4_{\overline{\mathrm{MS}}}(\mu), \tag{354}$$

should read

$$c_1 = -1.4346, \quad c_2 = 0.16979, \quad c_3 = 3.21120. \tag{355}$$

3. Discussion of computations

Results using this method in momentum space are, to date, only available using overlap fermions or domain-wall fermions. Cali 20 [84] consider vacuum polarization in

[71] For the general mass-nondegenerate case with SU(3) flavor nonsinglet currents see, for example, Ref. [801].

TABLE 59. Results from the vacuum polarization in both momentum and position space.

Collaboration	Ref.	N_f	Publication status	Renormalization scale	Perturbative behavior	Continuum extrapolation	Scale	$\Lambda_{\overline{\text{MS}}}$ [MeV]	$r_0\Lambda_{\overline{\text{MS}}}$
Cali 20	[84]	$2+1$	A	○	★	★	m_Υ [a]	342(17)	0.818(41)[c]
Hudspith 18	[733]	$2+1$	P	○	○	■	m_Ω [b]	337(40)	0.806(96)[d]
Hudspith 15	[809]	$2+1$	C	○	○	■	m_Ω [b]	300(24)[e]	0.717(58)
JLQCD 10	[732]	$2+1$	A	■	■	■	$r_0 = 0.472$ fm	247(5)[f]	0.591(12)
JLQCD/TWQCD 08C	[808]	2	A	○	■	■	$r_0 = 0.49$ fm	$234(9)(^{+16}_{-0})$	$0.581(22)(^{+40}_{-0})$

[a] via t_0/a^2, still unpublished. We use $r_0 = 0.472$ fm

[b] Determined in [12].

[c] Evaluates to $\alpha^{(5)}_{\overline{\text{MS}}}(M_Z) = 0.11864(114)$
In conversion to $r_0\Lambda$ we used $r_0 = 0.472$ fm.

[d] $\alpha^{(5)}_{\overline{\text{MS}}}(M_Z) = 0.1181(27)(^{+8}_{-22})$. $\Lambda_{\overline{\text{MS}}}$ determined by us from $\alpha^{(3)}_{\overline{\text{MS}}}(2\text{ GeV}) = 0.2961(185)$. In conversion to $r_0\Lambda$ we used $r_0 = 0.472$ fm.

[e] Determined by us from $\alpha^{(3)}_{\overline{\text{MS}}}(2\text{ GeV}) = 0.279(11)$. Evaluates to $\alpha^{(5)}_{\overline{\text{MS}}}(M_Z) = 0.1155(18)$.

[f] $\alpha^{(5)}_{\overline{\text{MS}}}(M_Z) = 0.1118(3)(^{+16}_{-17})$.

position space using $\mathcal{O}(a)$-improved Wilson fermions. The results are collected in Table 59 for $N_f = 2$, JLQCD/TWQCD 08C [808] and for $N_f = 2+1$, JLQCD 10 [732], Hudspith 18 [733] and Cali 20 [84].

We first discuss the results of JLQCD/TWQCD 08C [808] and JLQCD 10 [732]. The fit to Eq. (350) is done with the 4-loop relation between the running coupling and $\Lambda_{\overline{\text{MS}}}$. It is found that without introducing fit parameters for condensate contributions, the momentum scale where the perturbative formula gives good agreement with the lattice results is very narrow, $aQ \simeq 0.8$–1.0. When fit parameters for condensate contributions are included the perturbative formula gives good agreement with the lattice results for the extended range $aQ \simeq 0.6$–1.0. Since there is only a single lattice spacing $a \approx 0.11$ fm there is a ■ for the continuum limit. The renormalization scale μ is in the range of $Q = 1.6$–2 GeV. Approximating $\alpha_{\text{eff}} \approx \alpha_{\overline{\text{MS}}}(Q)$, we estimate that $\alpha_{\text{eff}} = 0.25$–$0.30$ for $N_f = 2$ and $\alpha_{\text{eff}} = 0.29$–$0.33$ for $N_f = 2+1$. Thus we give a ○ and ■ for $N_f = 2$ and $N_f = 2+1$, respectively, for the renormalization scale and a ■ for the perturbative behavior.

A further investigation of this method was initiated in Hudspith 15 [809] and completed by Hudspith 18 [733] (see also [810]) based on domain-wall fermion configurations at three lattice spacings, $a^{-1} = 1.78$, 2.38, 3.15 GeV, with three different light-quark masses on the two coarser lattices and one on the fine lattice. An extensive discussion of condensates, using continuum finite-energy sum rules was employed to estimate where their contributions might be negligible. It was found that even up to terms of $O((1/Q^2)^8)$ (a higher order than depicted in Eq. (350) but with constant coefficients) no single condensate dominates and apparent convergence was poor for low Q^2 due to cancellations between contributions of similar size with alternating signs. (See, e.g., the list given by Hudspith 15 [809].) Choosing Q^2 to be at least ~ 3.8 GeV^2 mitigated the problem, but then the coarsest lattice had to be discarded, due to large lattice artefacts. So this gives a ■ for continuum extrapolation. With the higher Q^2 the quark-mass dependence of the results was negligible, so ensembles with different quark masses were averaged over. A range of Q^2 from 3.8–16 GeV^2 gives $\alpha_{\text{eff}} = 0.31$–$0.22$, so there is a ○ for the renormalization scale. The value of α^3_{eff} reaches $\Delta\alpha_{\text{eff}}/(8\pi b_0 \alpha_{\text{eff}})$ and thus gives a ○ for perturbative behavior. In Hudspith 15 [809] (superseded by Hudspith 18 [733]) about a 20% difference in $\Pi_V(Q^2)$ was seen between the two lattice spacings and a result is quoted only for the smaller a.

4. Vacuum polarization in position space

Cali 20 [84] evaluate the light-current two-point function in position space. The two-point functions for the

nonperturbatively renormalized (nonsinglet) flavor currents is computed for distances $|x|$ between 0.1 and 0.25 fm and extrapolated to the chiral limit. The available CLS configurations are used for this work, with lattice spacings between 0.039 and 0.086 fm. Despite fully nonperturbative renormalization and $\mathcal{O}(a)$ improvement, the remaining $\mathcal{O}(a^2)$ effects, as measured by $O(4)$ symmetry violations, are very large, even after subtraction of tree-level lattice effects. Therefore the authors performed a numerical stochastic perturbation theory (NSPT) simulation in order to determine the lattice artifacts at $\mathcal{O}(g^2)$. Only after subtraction of these effects the constrained continuum extrapolations from three different lattice directions to the same continuum limit are characterized by reasonable χ^2-values, so the feasibility of the study crucially depends on this step. Interestingly, there is no subtraction performed of nonperturbative effects. For instance, chiral symmetry breaking would manifest itself in a difference between the vector and the axial-vector two-point functions, and is invisible to perturbation theory, where these two-point functions are known to α_s^4 [807]. According to the authors, phenomenological estimates suggest that a difference of 1.5% between the continuum correlators would occur around 0.3 fm and this difference would not be resolvable by their lattice data. Equality within their errors is confirmed for shorter distances. We note, however, that chiral symmetry breaking effects are but one class of nonperturbative effects, and their smallness does not allow for the conclusion that such effects are generally small. In fact, the need for explicit subtractions in momentum space analyses may lead one to suspect that such effects are not negligible at the available distance scales. For the determination of $\Lambda_{\overline{\text{MS}}}^{(N_f=3)}$ the authors limit the range of distances to 0.13–0.19 fm, where $\alpha_{\text{eff}} \in [0.2354, 0.3075]$ (private communication by the authors). These effective couplings are converted to $\overline{\text{MS}}$ couplings at the same scales $\mu = 1/|x|$ by solving Eq. (354) numerically. Central values for the Λ-parameter thus obtained are in the range 325–370 MeV (using the β-function at 5-loop order) and a weighted average yields the quoted result 342(17) MeV, where the average emphasizes the data around $|x| = 0.16$ fm, or $\mu = 1.3$ GeV.

Applying the FLAG criteria the range of lattice spacings yields ★ for the continuum extrapolation. However, the FLAG criterion implicitly assumes that the remaining cutoff effects after nonperturbative $\mathcal{O}(a)$ improvement are small, which is not the case here. Some hypercubic lattice artefacts are still rather large even after 1-loop subtraction, but these are not used for the analysis. As for the renormalization scale, the lowest effective coupling entering the analysis is $0.235 < 0.25$, so we give ○. As for perturbative behavior, for the range of couplings in the above interval α_{eff}^3 changes by $(0.308/0.235)^3 \approx 2.2$, marginally reaching $(3/2)^2 = 2.25$. The errors $\Delta\alpha_{\text{eff}}$ after continuum and chiral extrapolations are 4–6% (private communication by the authors) and the induced uncertainty in Λ is comfortably above $2\alpha_{\text{eff}}^3$, which gives a ★ according to FLAG criteria.

Although the current FLAG criteria are formally passed by this result, the quoted error of 5% for Λ seems very optimistic. We have performed a simple test, converting to the $\overline{\text{MS}}$ scheme by inverting Eq. (354) perturbatively (instead of solving the fixed-order equation numerically). The differences between the couplings are of order α_s^5 and thus indicative of the sensitivity to perturbative truncation errors. The resulting Λ-parameter estimates are now in the range 409–468 MeV, i.e., ca. 15–30% larger than before. While the difference between both estimates decreases proportionally to the expected α_{eff}^3, an extraction of the Λ-parameter in this energy range is *a priori* affected by systematic uncertainties corresponding to such differences. The FLAG criterion might fail to capture this, e.g., if the assumption of an $\mathcal{O}(1)$ coefficient for the asymptotic α_{eff}^3 behavior is not correct. Some indication for a problematic behavior is indeed seen when perturbatively inverting Eq. (354) to order α_s^3. The resulting $\overline{\text{MS}}$ couplings are then closer to the values used in Cali 20, although the difference is formally $O(\alpha_s^4)$ rather than $O(\alpha_s^5)$.

Scale variations. Using scale variations to determine the systematic error due to the truncation of the perturbative series only makes sense when the extrapolation of the observable to the continuum limit is under control. Therefore, we apply our common procedure only to the results in Cali 20 [84]. Using $\mu \approx 1.3$ GeV as the typical scale set by the inverse of the distance, yields

$$\delta^*_{(4)} = 1.0\%, \qquad \delta_{(2)} = 11.6\% \qquad \delta^*_{(2)} = 0.6\%. \tag{356}$$

The discrepancy between the variation around Q, $\delta_{(2)} = 11.6\%$, and the variation around the scale of fastest apparent convergence, $\delta^*_{(2)} = 0.6\%$, is due to the large value of the factor $s^*_{\text{ref}} = 2.72$. As a consequence the scale of fastest apparent convergence is artificially large compared to the actual scale where the lattice observables is computed. The large value of $\delta_{(2)}$, obtained for $s_{\text{ref}} = 1$, shows that the scale of the lattice observable is too low to keep the systematic errors under control.

G. α_s from observables at the lattice spacing scale

1. General considerations

The general method is to evaluate a short-distance quantity $\mathcal{Q}$ at the scale of the lattice spacing $\sim 1/a$ and then determine its relationship to $\alpha_{\overline{\text{MS}}}$ via a perturbative expansion.

This is epitomized by the strategy of the HPQCD collaboration [734,811], discussed here for illustration,

which computes and then fits to a variety of short-distance quantities

$$Y = \sum_{n=1}^{n_{\max}} c_n \alpha_{\mathrm{V}'}^n(q^*). \tag{357}$$

The quantity Y is taken as the logarithm of small Wilson loops (including some nonplanar ones), Creutz ratios, tadpole-improved Wilson loops and the tadpole-improved or boosted bare coupling ($\mathcal{O}(20)$ quantities in total). The perturbative coefficients c_n (each depending on the choice of Y) are known to $n = 3$ with additional coefficients up to $n_{\max}$ being fitted numerically. The running coupling $\alpha_{\mathrm{V}'}$ is related to α_{V} from the static-quark potential (see Sec. IX E).[72]

The coupling constant is fixed at a scale $q^* = d/a$. The latter is chosen as the mean value of $\ln q$ with the one-gluon loop as measure [735,812]. (Thus a different result for d is found for every short-distance quantity.) A rough estimate yields $d \approx \pi$, and in general the renormalization scale is always found to lie in this region.

For example, for the Wilson loop $W_{mn} \equiv \langle W(ma, na)\rangle$ we have

$$\ln\left(\frac{W_{mn}}{u_0^{2(m+n)}}\right) = c_1\alpha_{\mathrm{V}'}(q^*) + c_2\alpha_{\mathrm{V}'}^2(q^*) + c_3\alpha_{\mathrm{V}'}^3(q^*) + \cdots, \tag{358}$$

for the tadpole-improved version, where $c_1, c_2, \ldots$ are the appropriate perturbative coefficients and $u_0 = W_{11}^{1/4}$. Substituting the nonperturbative simulation value in the left hand side, we can determine $\alpha_{\mathrm{V}'}(q^*)$, at the scale q^*. Note that one finds empirically that perturbation theory for these tadpole-improved quantities have smaller c_n coefficients and so the series has a faster apparent convergence compared to the case without tadpole improvement.

Using the β-function in the V′ scheme, results can be run to a reference value, chosen as $\alpha_0 \equiv \alpha_{\mathrm{V}'}(q_0)$, $q_0 = 7.5$ GeV. This is then converted perturbatively to the continuum $\overline{\mathrm{MS}}$ scheme

$$\alpha_{\overline{\mathrm{MS}}}(q_0) = \alpha_0 + d_1\alpha_0^2 + d_2\alpha_0^3 + \cdots, \tag{359}$$

where d_1, d_2 are known 1-and 2-loop coefficients.

Other collaborations have focused more on the bare boosted coupling constant and directly determined its relationship to $\alpha_{\overline{\mathrm{MS}}}$. Specifically, the boosted coupling is defined by

$$\alpha_{\mathrm{P}}(1/a) = \frac{1}{4\pi}\frac{g_0^2}{u_0^4}, \tag{360}$$

again determined at a scale $\sim 1/a$. As discussed previously, since the plaquette expectation value in the boosted coupling contains the tadpole-diagram contributions to all orders, which are dominant contributions in perturbation theory, there is an expectation that the perturbation theory using the boosted coupling has smaller perturbative coefficients [735], and hence smaller perturbative errors.

2. Continuum limit

Lattice results always come along with discretization errors, which one needs to remove by a continuum extrapolation. As mentioned previously, in this respect the present method differs in principle from those in which α_s is determined from physical observables. In the general case, the numerical results of the lattice simulations at a value of μ fixed in physical units can be extrapolated to the continuum limit, and the result can be analyzed as to whether it shows perturbative running as a function of μ in the continuum. For observables at the cutoff-scale ($q^* = d/a$), discretization effects cannot easily be separated out from perturbation theory, as the scale for the coupling comes from the lattice spacing. Therefore the restriction $a\mu \ll 1$ (the continuum-extrapolation criterion) is not applicable here. Discretization errors of order a^2 are, however, present. Since $a \sim \exp(-1/(2b_0 g_0^2)) \sim \exp(-1/(8\pi b_0 \alpha(q^*))$, these errors now appear as power corrections to the perturbative running, and have to be taken into account in the study of the perturbative behavior, which is to be verified by changing a. One thus usually fits with power corrections in this method.

In order to keep a symmetry with the continuum-extrapolation criterion for physical observables and to remember that discretization errors are, of course, relevant, we replace it here by one for the lattice spacings used:

(i) Lattice spacings
- ★ 3 or more lattice spacings, at least 2 points below $a = 0.1$ fm
- ○ 2 lattice spacings, at least 1 point below $a = 0.1$ fm
- ■ otherwise

3. Discussion of computations

Note that due to $\mu \sim 1/a$ being relatively large the results easily have a ★ or ○ in the rating on renormalization scale.

The work of El-Khadra 92 [820] employs a 1-loop formula to relate $\alpha_{\overline{\mathrm{MS}}}^{(0)}(\pi/a)$ to the boosted coupling for three lattice spacings $a^{-1} = 1.15$, 1.78, 2.43 GeV. (The lattice spacing is determined from the charmonium 1S-1P splitting.) They obtain $\Lambda_{\overline{\mathrm{MS}}}^{(0)} = 234$ MeV, corresponding to $\alpha_{\mathrm{eff}} = \alpha_{\overline{\mathrm{MS}}}^{(0)}(\pi/a) \approx 0.15$–$0.2$. The work of Aoki 94 [817]

[72] $\alpha_{\mathrm{V}'}$ is defined by $\Lambda_{\mathrm{V}'} = \Lambda_{\mathrm{V}}$ and $b_i^{\mathrm{V}'} = b_i^{\mathrm{V}}$ for $i = 0, 1, 2$ but $b_i^{\mathrm{V}'} = 0$ for $i \geq 3$.

calculates $\alpha_V^{(2)}$ and $\alpha_{\overline{\rm MS}}^{(2)}$ for a single lattice spacing $a^{-1} \sim 2$ GeV, again determined from charmonium 1S-1P splitting in two-flavor QCD. Using 1-loop perturbation theory with boosted coupling, they obtain $\alpha_V^{(2)} = 0.169$ and $\alpha_{\overline{\rm MS}}^{(2)} = 0.142$. Davies 94 [816] gives a determination of $\alpha_{\rm V}$ from the expansion

$$-\ln W_{11} \equiv \frac{4\pi}{3}\alpha_{\rm V}^{(N_f)}(3.41/a) \times [1-(1.185+0.070N_f)\alpha_{\rm V}^{(N_f)}], \tag{361}$$

neglecting higher-order terms. They compute the Υ spectrum in $N_f = 0$, 2 QCD for single lattice spacings at $a^{-1} = 2.57$, 2.47 GeV and obtain $\alpha_{\rm V}(3.41/a) \simeq 0.15$, 0.18, respectively. Extrapolating the inverse coupling linearly in N_f, a value of $\alpha_{\rm V}^{(3)}(8.3\ \text{GeV}) = 0.196(3)$ is obtained. SESAM 99 [814] follows a similar strategy, again for a single lattice spacing. They linearly extrapolated results for $1/\alpha_{\rm V}^{(0)}$, $1/\alpha_{\rm V}^{(2)}$ at a fixed scale of 9 GeV to give $\alpha_{\rm V}^{(3)}$, which is then perturbatively converted to $\alpha_{\overline{\rm MS}}^{(3)}$. This finally gave $\alpha_{\overline{\rm MS}}^{(5)}(M_Z) = 0.1118(17)$. Wingate 95 [815] also follows this method. With the scale determined from the charmonium 1S-1P splitting for single lattice spacings in $N_f = 0$, 2 giving $a^{-1} \simeq 1.80$ GeV for $N_f = 0$ and $a^{-1} \simeq 1.66$ GeV for $N_f = 2$, they obtain $\alpha_{\rm V}^{(0)}(3.41/a) \simeq 0.15$ and $\alpha_{\rm V}^{(2)} \simeq 0.18$, respectively. Extrapolating the inverse coupling linearly in N_f, they obtain $\alpha_{\rm V}^{(3)}(6.48\ \text{GeV}) = 0.194(17)$.

The QCDSF/UKQCD collaboration, QCDSF/UKQCD 05 [813,821,823], use the 2-loop relation (rewritten here in terms of α)

$$\frac{1}{\alpha_{\overline{\rm MS}}(\mu)} = \frac{1}{\alpha_{\rm P}(1/a)} + 4\pi(2b_0 \ln a\mu - t_1^{\rm P}) + (4\pi)^2(2b_1 \ln a\mu - t_2^{\rm P})\alpha_{\rm P}(1/a), \tag{362}$$

where $t_1^{\rm P}$ and $t_2^{\rm P}$ are known. (A 2-loop relation corresponds to a 3-loop lattice β-function.) This was used to directly compute $\alpha_{\overline{\rm MS}}$, and the scale was chosen so that the $\mathcal{O}(\alpha_{\rm P}^0)$ term vanishes, i.e.,

$$\mu^* = \frac{1}{a}\exp\left[t_1^{\rm P}/(2b_0)\right] \approx \begin{cases} 2.63/a & N_f = 0 \\ 1.4/a & N_f = 2 \end{cases}. \tag{363}$$

The method is to first compute $\alpha_{\rm P}(1/a)$ and from this, using Eq. (362) to find $\alpha_{\overline{\rm MS}}(\mu^*)$. The RG equation, Eq. (285), then determines $\mu^*/\Lambda_{\overline{\rm MS}}$ and hence using Eq. (363) leads to the result for $r_0\Lambda_{\overline{\rm MS}}$. This avoids giving the scale in MeV until the end. In the $N_f = 0$ case seven lattice spacings were used [720], giving a range $\mu^*/\Lambda_{\overline{\rm MS}} \approx 24$–$72$ (or $a^{-1} \approx 2$–7 GeV) and $\alpha_{\rm eff} = \alpha_{\overline{\rm MS}}(\mu^*) \approx 0.15$–$0.10$. Neglecting higher-order perturbative terms (see discussion after Eq. (364) below) in Eq. (362) this is sufficient to allow a continuum extrapolation of $r_0\Lambda_{\overline{\rm MS}}$. A similar computation for $N_f = 2$ by QCDSF/UKQCD 05 [813] gave $\mu^*/\Lambda_{\overline{\rm MS}} \approx 12$–$17$ (or roughly $a^{-1} \approx 2$–3 GeV) and $\alpha_{\rm eff} = \alpha_{\overline{\rm MS}}(\mu^*) \approx 0.20$–$0.18$. The $N_f = 2$ results of QCDSF/UKQCD 05 [813] are affected by an uncertainty which was not known at the time of publication: It has been realized that the values of r_0/a of Ref. [813] were significantly too low [717]. As this effect is expected to depend on a, it influences the perturbative behavior leading us to assign a ■ for that criterion.

Results for the $N_f = 0$ Λ-parameter by FlowQCD 15 [819], later updated and published in Kitazawa 16 [818], are obtained following the same strategy, cf. Eqs. (362), (363), except that the scale r_0 is replaced by the gradient flow scale w_0, leading to a determination of $w_0\Lambda_{\overline{\rm MS}}$. The continuum limit is estimated by extrapolating the data at six lattice spacings linearly in a^2. The data range used is $\mu^*/\Lambda_{\overline{\rm MS}} \approx 50$–$120$ (or $a^{-1} \approx 5$–11 GeV) and $\alpha_{\overline{\rm MS}}(\mu^*) \approx 0.12$–$0.095$. Since a very small value of $\alpha_{\overline{\rm MS}}$ is reached, there is a ★ in the perturbative behavior. Note that our conversion to the common r_0 scale unfortunately leads to a significant increase of the error of the Λ parameter compared to using w_0 directly [824]. Again we note that the results of QCDSF/UKQCD 05 [813] ($N_f = 0$) and Kitazawa 16 [818] may be affected by frozen topology as they have lattice spacings significantly below $a = 0.05$ fm. Kitazawa 16 [818] investigate this by evaluating w_0/a in a fixed topology and estimate any effect at about ∼1%.

The work of HPQCD 05A [811] (which supersedes the original work [825]) uses three lattice spacings $a^{-1} \approx 1.2$, 1.6, 2.3 GeV for $2+1$ flavor QCD. Typically the renormalization scale $q \approx \pi/a \approx 3.50$–$7.10$ GeV, corresponding to $\alpha_{\rm V'} \approx 0.22$–$0.28$.

In the later update HPQCD 08A [734] twelve datasets (with six lattice spacings) are now used reaching up to $a^{-1} \approx 4.4$ GeV, corresponding to $\alpha_{\rm V'} \approx 0.18$. The values used for the scale r_1 were further updated in HPQCD 10 [15]. Maltman 08 [87] uses most of the same lattice ensembles as HPQCD 08A [734], but not the one at the smallest lattice spacing, $a \approx 0.045$ fm. Maltman 08 [87] also considers a much smaller set of quantities (three versus 22) that are less sensitive to condensates. They also use different strategies for evaluating the condensates and for the perturbative expansion, and a slightly different value for the scale r_1. The central values of the final results from Maltman 08 [87] and HPQCD 08A [734] differ by 0.0009 (which would be decreased to 0.0007 taking into account a reduction of 0.0002 in the value of the r_1 scale used by Maltman 08 [87]).

As mentioned before, the perturbative coefficients are computed through 3-loop order [826], while the

higher-order perturbative coefficients c_n with $n_{\max} \geq n > 3$ (with $n_{\max} = 10$) are numerically fitted using the lattice-simulation data for the lattice spacings with the help of Bayesian methods. It turns out that corrections in Eq. (358) are of order $|c_i/c_1|\alpha^i = 5\%$–15% and 3%–10% for $i = 2$, 3, respectively. The inclusion of a fourth-order term is necessary to obtain a good fit to the data, and leads to a shift of the result by 1–2 sigma. For all but one of the 22 quantities, central values of $|c_4/c_1| \approx 2$–4 were found, with errors from the fits of ≈ 2. It should be pointed out that the description of lattice results for the short-distance quantities does not require Bayesian priors, once the term proportional to c_4 is included [87]. We also stress that different short-distance quantities have quite different nonperturbative contributions [827]. Hence the fact that different observables lead to consistent α_s values is a nontrivial check of the approach.

An important source of uncertainty is the truncation of perturbation theory. In HPQCD 08A [734], HPQCD 10 [15] it is estimated to be about 0.4% of $\alpha_{\overline{\rm MS}}(M_Z)$. In FLAG 13 we included a rather detailed discussion of the issue with the result that we prefer for the time being a more conservative error based on the above estimate $|c_4/c_1| = 2$. From Eq. (357) this gives an estimate of the uncertainty in $\alpha_{\rm eff}$ of

$$\Delta\alpha_{\rm eff}(\mu_1) = \left|\frac{c_4}{c_1}\right| \alpha^4_{\rm eff}(\mu_1), \tag{364}$$

at the scale μ_1 where $\alpha_{\rm eff}$ is computed from the Wilson loops. This can be used with a variation in Λ at lowest order of perturbation theory and also applied to α_s evolved to a different scale μ_2,[73]

$$\frac{\Delta\Lambda}{\Lambda} = \frac{1}{8\pi b_0 \alpha_s}\frac{\Delta\alpha_s}{\alpha_s}, \qquad \frac{\Delta\alpha_s(\mu_2)}{\Delta\alpha_s(\mu_1)} = \frac{\alpha_s^2(\mu_2)}{\alpha_s^2(\mu_1)}. \tag{365}$$

With $\mu_2 = M_Z$ and $\alpha_s(\mu_1) = 0.2$ (a typical value extracted from Wilson loops in HPQCD 10 [15], HPQCD 08A [734] at $\mu = 5$ GeV) we have

$$\Delta\alpha_{\overline{\rm MS}}(m_Z) = 0.0012, \tag{366}$$

which we shall later use as the typical perturbative uncertainty of the method with $2 + 1$ fermions.

Table 60 summarizes the results. Within the errors of 3%–5% $N_f = 3$ determinations of $r_0\Lambda$ nicely agree.

Scale variations. As discussed above, the short-distance observables are fitted to a perturbative expansion where the higher-order coefficients are actual parameters in the fit. Here instead we follow the exact same procedure introduced for all the observables, and we describe the observables using only the known perturbative coefficients. For illustration, we report the result of the scale variations for two observables, namely the simple 1×1 plaquette and the 2×1 Wilson loop. The perturbative coefficients are reported in Table 55 and the typical scale is $\mu \approx 2.4/a \approx 4.4$ GeV. With these values we obtain the following results.

— $-\log W_{11}$

$$\delta^*_{(4)} = 2.8\%, \quad \delta_{(2)} = 3.3\% \quad \delta^*_{(2)} = 2.5\%. \tag{367}$$

— $-\log W_{112}/u_0^6$

$$\delta^*_{(4)} = 3.5\%, \quad \delta_{(2)} = 3.2\% \quad \delta^*_{(2)} = 3.1\%. \tag{368}$$

This analysis suggests a systematic error around 3% for these kind of analyses on the available ensembles.

H. α_s from heavy-quark current two-point functions

1. General considerations

The method has been introduced in HPQCD 08, Ref. [244], and updated in HPQCD 10, Ref. [15], see also Ref. [828]. In addition there is a $2 + 1 + 1$-flavor result, HPQCD 14A [18].

The basic observable is constructed from a current,

$$J(x) = iam_c\bar{\psi}_c(x)\gamma_5\psi_{c'}(x), \tag{369}$$

of two mass-degenerate heavy-valence quarks, c, c', usually taken to be at or around the charm-quark mass. The pre-factor m_c denotes the bare mass of the quark. When the lattice discretization respects chiral symmetry, $J(x)$ is a renormalization group invariant local field, i.e., it requires no renormalization. Staggered fermions and twisted-mass fermions have such a residual chiral symmetry. The (Euclidean) time-slice correlation function

$$G(x_0) = a^6\sum_{\vec{x}}\langle J^\dagger(x)J(0)\rangle, \tag{370}$$

$[J^\dagger(x) = iam_c\bar{\psi}_{c'}(x)\gamma_5\psi_c(x)]$ has a $\sim x_0^{-3}$ singularity at short distances and moments

$$G_n = a\sum_{x_0=-(T/2-a)}^{T/2-a} x_0^n G(x_0) \tag{371}$$

are nonvanishing for even n and furthermore finite for $n \geq 4$ in the $a \to 0$ limit. Here T is the time extent of the lattice. The moments are dominated by contributions at x_0 of order $1/m_c$. For large mass m_c these are short distances and the moments become increasingly perturbative for decreasing n. Denoting the lowest-order perturbation

[73] From Eq. (292) we see that at low order in PT the coupling α_s is continuous and differentiable across the mass thresholds (at the same scale). Therefore to leading order α_s and $\Delta\alpha_s$ are independent of N_f.

TABLE 60. Wilson loop results. Some early results for $N_f = 0$, 2 did not determine $\Lambda_{\overline{\rm MS}}$.

Collaboration	Ref.	N_f	Publication status	Renormalization scale	Perturbative behavior	Lattice spacings	Scale	$\Lambda_{\overline{\rm MS}}$ [MeV]	$r_0\Lambda_{\overline{\rm MS}}$
HPQCD 10[ab]	[15]	$2+1$	A	○	★	★	$r_1 = 0.3133(23)$ fm	340(9)	0.812(22)
HPQCD 08A[a]	[734]	$2+1$	A	○	★	★	$r_1 = 0.321(5)$ fm[e]	338(12)[d]	0.809(29)
Maltman 08[a]	[87]	$2+1$	A	○	○	★	$r_1 = 0.318$ fm	352(17)[c]	0.841(40)
HPQCD 05A[a]	[811]	$2+1$	A	○	○	○	r_1[e]	319(17)[f]	0.763(42)
QCDSF/UKQCD 05	[813]	2	A	★	■	★	$r_0 = 0.467(33)$ fm	261(17)(26)	0.617(40)(21)[g]
SESAM 99[h]	[814]	2	A	○	■	■	$c\bar{c}$ (1S-1P)		
Wingate 95[i]	[815]	2	A	★	■	■	$c\bar{c}$ (1S-1P)		
Davies 94[j]	[816]	2	A	★	■	■	Υ		
Aoki 94[k]	[817]	2	A	★	■	■	$c\bar{c}$ (1S-1P)		
Kitazawa 16	[818]	0	A	★	★	★	w_0	260(5)[o]	0.621(11)[o]
FlowQCD 15	[819]	0	P	★	★	★	$w_{0.4}$[n]	258(6)[n]	0.618(11)[n]
QCDSF/UKQCD 05	[813]	0	A	★	○	★	$r_0 = 0.467(33)$ fm	259(1)(20)	0.614(2)(5)[g]
SESAM 99[h]	[814]	0	A	★	■	■	$c\bar{c}$ (1S-1P)		
Wingate 95[i]	[815]	0	A	★	■	■	$c\bar{c}$ (1S-1P)		
Davies 94[j]	[816]	0	A	★	■	■	Υ		
El-Khadra 92[l]	[820]	0	A	★	■	○	$c\bar{c}$ (1S-1P)	234(10)	0.560(24)[m]

[a]The numbers for Λ have been converted from the values for $\alpha_s^{(5)}(M_Z)$.

[b]$\alpha_{\overline{\rm MS}}^{(3)}(5\text{ GeV}) = 0.2034(21)$, $\alpha_{\overline{\rm MS}}^{(5)}(M_Z) = 0.1184(6)$, only update of intermediate scale and c-, b-quark masses, supersedes HPQCD 08A.

[c]$\alpha_{\overline{\rm MS}}^{(5)}(M_Z) = 0.1192(11)$.

[d]$\alpha_V^{(3)}(7.5\text{ GeV}) = 0.2120(28)$, $\alpha_{\overline{\rm MS}}^{(5)}(M_Z) = 0.1183(8)$, supersedes HPQCD 05.

[e]Scale is originally determined from Υ mass splitting. r_1 is used as an intermediate scale. In conversion to $r_0\Lambda_{\overline{\rm MS}}$, r_0 is taken to be 0.472 fm.

[f]$\alpha_V^{(3)}(7.5\text{ GeV}) = 0.2082(40)$, $\alpha_{\overline{\rm MS}}^{(5)}(M_Z) = 0.1170(12)$.

[g]This supersedes Refs. [821–823]. $\alpha_{\overline{\rm MS}}^{(5)}(M_Z) = 0.112(1)(2)$. The $N_f = 2$ results were based on values for r_0/a which have later been found to be too small [717]. The effect will be of the order of 10–15%, presumably an increase in Λr_0.

[h]$\alpha_{\overline{\rm MS}}^{(5)}(M_Z) = 0.1118(17)$.

[i]$\alpha_V^{(3)}(6.48\text{ GeV}) = 0.194(7)$ extrapolated from $N_f = 0$, 2. $\alpha_{\overline{\rm MS}}^{(5)}(M_Z) = 0.107(5)$.

[j]$\alpha_P^{(3)}(8.2\text{ GeV}) = 0.1959(34)$ extrapolated from $N_f = 0$, 2. $\alpha_{\overline{\rm MS}}^{(5)}(M_Z) = 0.115(2)$.

[k]Estimated $\alpha_{\overline{\rm MS}}^{(5)}(M_Z) = 0.108(5)(4)$.

[l]This early computation violates our requirement that scheme conversions are done at the 2-loop level. $\Lambda_{\overline{\rm MS}}^{(4)} = 160(^{+47}_{-37})$ MeV, $\alpha_{\overline{\rm MS}}^{(4)}(5\text{ GeV}) = 0.174(12)$. We converted this number to give $\alpha_{\overline{\rm MS}}^{(5)}(M_Z) = 0.106(4)$.

[m]We used $r_0 = 0.472$ fm to convert to $r_0\Lambda_{\overline{\rm MS}}$.

[n]Reference scale $w_{0.4}$ where w_x is defined by $t\partial_t[t^2\langle E(t)\rangle]|_{t=w_x^2} = x$ in terms of the action density $E(t)$ at positive flow time t [819]. Our conversion to r_0 scale using [819] $r_0/w_{0.4} = 2.587(45)$ and $r_0 = 0.472$ fm.

[o]Our conversion from $w_0\Lambda_{\overline{\rm MS}} = 0.2154(12)$ to r_0 scale using $r_0/w_0 = (r_0/w_{0.4})\cdot(w_{0.4}/w_0) = 2.885(50)$ with the factors cited by the collaboration [819] and with $r_0 = 0.472$ fm.

theory moments by $G_n^{(0)}$, one defines the normalized moments

$$R_n = \begin{cases} G_4/G_4^{(0)} & \text{for } n = 4, \\ \frac{am_{\eta_c}}{2am_c}\left(\frac{G_n}{G_n^{(0)}}\right)^{1/(n-4)} & \text{for } n \geq 6, \end{cases} \tag{372}$$

of even order n. Note that Eq. (369) contains the variable (bare) heavy-quark mass m_c. The normalization $G_n^{(0)}$ is introduced to help in reducing lattice artifacts. In addition, one can also define moments with different normalizations,

$$\tilde{R}_n = 2R_n/m_{\eta_c} \quad \text{for } n \geq 6. \tag{373}$$

While $\tilde{R}_n$ also remains renormalization-group invariant, it now also has a scale which might introduce an additional ambiguity [30].

The normalized moments can then be parametrized in terms of functions

$$R_n \equiv \begin{cases} r_4(\alpha_s(\mu)) & \text{for } n = 4, \\ \frac{m_{\eta_c}}{2\bar{m}_c(\mu_m)} r_n(\alpha_s(\mu)) & \text{for } n \geq 6, \end{cases} \tag{374}$$

with $\bar{m}_c(\mu_m)$ being the renormalized heavy-quark mass. The scale μ_m at which the heavy-quark mass is defined could be different from the scale μ at which α_s is defined [829]. The HPQCD collaboration, however, used the choice $\mu = \mu_m = 3m_c(\mu)$. This ensures that the renormalization scale is never too small. The reduced moments r_n have a perturbative expansion

$$r_n = 1 + r_{n,1}\alpha_s + r_{n,2}\alpha_s^2 + r_{n,3}\alpha_s^3 + \ldots, \tag{375}$$

where the written terms $r_{n,i}(\mu/\bar{m}_c(\mu))$, $i \leq 3$ are known for low n from Refs. [736,830–833]. In practice, the expansion is performed in the $\overline{\text{MS}}$ scheme. Matching nonperturbative lattice results for the moments to the perturbative expansion, one determines an approximation to $\alpha_{\overline{\text{MS}}}(\mu)$ as well as $\bar{m}_c(\mu)$. With the lattice spacing (scale) determined from some extra physical input, this calibrates μ. As usual suitable pseudoscalar masses determine the bare-quark masses, here in particular the charm-quark mass, and then through Eq. (374) the renormalized charm-quark mass.

A difficulty with this approach is that large masses are needed to enter the perturbative domain. Lattice artifacts can then be sizeable and have a complicated form. The ratios in Eq. (372) use the tree-level lattice results in the usual way for normalization. This results in unity as the leading term in Eq. (375), suppressing some of the kinematical lattice artifacts. We note that in contrast to, e.g., the definition of α_{qq}, here the cutoff effects are of order $a^k\alpha_s$, while there the tree-level term defines α_s and therefore the cutoff effects after tree-level improvement are of order $a^k\alpha_s^2$. To obtain the continuum results for the moments it is important to perform fits with high powers of a. This implies many fit parameters. To deal with this problem the HPQCD collaboration used Bayesian fits of their lattice results. More recent analyses of the moments, however, did not rely on Bayesian fits [30,31,81,230].

Finite-size effects (FSE) due to the omission of $|x_0| > T/2$ in Eq. (371) grow with n as $(m_{\eta_c}T/2)^n \exp(-m_{\eta_c}T/2)$. In practice, however, since the (lower) moments are short-distance dominated, the FSE are expected to be small at the present level of precision. Possible exception could be the ratio R_8/R_{10}, where the finite-volume effects could be significant as discussed below.

Moments of correlation functions of the quark's electromagnetic current can also be obtained from experimental data for e^+e^- annihilation [834,835]. This enables a nonlattice determination of α_s using a similar analysis method. In particular, the same continuum perturbation-theory computation enters both the lattice and the phenomenological determinations.

2. Discussion of computations

The determination of the strong coupling constant from the moments of quarkonium correlators by HPQCD collaboration have been discussed in detail in the FLAG 16 and 19 reports. Therefore, we only give the summary of these determinations in Table 61. There were no new determinations of the strong coupling constant in $2 + 1$ flavor QCD by other groups since the FLAG 21 report. The only new development was that Petreczky 20 [81] is now published and therefore this determination enters the FLAG average. The determinations of α_s by Maezawa 16, JLQCD16, Petreczky 19 and Boito 20 have been discussed in detail in the FLAG 21 report, so we do not discuss them here again and only give the summary of these determinations in Table 61. We will only discuss the results of Petreczky 20 [81] here.

Petreczky 20 is based on the same lattice data as Petreczky 19 [31]. Here the pseudo-scalar correlation functions have been computed using HISQ ensembles from HotQCD Collaboration [117] for physical strange-quark mass and light-quark masses corresponding to the pion mass of 160 MeV in the continuum limit, and lattice spacings $a^{-1} = 1.81$, 2.07, 2.39, 2.67, 3.01, 3.28, 4.00 and 4.89 GeV. Additional calculations have been performed for light-quark mass corresponding to the pion mass of 300 MeV and lattice spacings $a^{-1} = 2.39$, 4.89, 5.58, 6.62 and 7.85 GeV using the gauge configurations from the study of QCD equation of state at high temperatures [797]. No significant light-quark-mass dependence of heavy pseudo-scalar correlators have been observed [31]. Therefore, the results for the two light-quark masses have been combined into a single analysis. Calculations have been performed at four values of the heavy-quark mass equal to the physical charm-quark mass, one and half times the charm-quark mass, two times the charm-quark mass

TABLE 61. Heavy-quark current two-point function results. Note that all analysis using $2+1$ flavor simulations perturbatively add a dynamical charm quark. Partially they then quote results in four-flavor QCD, which we converted back to $N_f = 3$, corresponding to the nonperturbative sea quark content.

Collaboration	Ref.	N_f	Publication status	Renormalization scale	Perturbative behavior	Continuum extrapolation	Scale	$\Lambda_{\overline{\rm MS}}$ [MeV]	$r_0\Lambda_{\overline{\rm MS}}$
HPQCD 14A	[18]	$2+1+1$	A	○	★	○	$w_0 = 0.1715(9)$ fm[a]	294(11)[bc]	0.703(26)
Petreczky 20	[81]	$2+1$	A	○	○	★	$r_1 = 0.3106(18)$ fm	332(17)[h]	0.792(41)[g]
Boito 20	[836]	$2+1$	A	■	■	○	$m_c(m_c) = 1.28(2)$ GeV	328(30)[h]	0.785(72)
Petrezcky 19, $m_h = m_c$	[31]	$2+1$	A	■	■	★	$r_1 = 0.3106(18)$ fm[g]	314(10)	0.751(24)[g]
Petrezcky 19, $\frac{m_h}{m_c} = 1.5$	[31]	$2+1$	A	■	■	○	$r_1 = 0.3106(18)$ fm[g]	310(10)	0.742(24)[g]
Maezawa 16	[230]	$2+1$	A	■	■	○	$r_1 = 0.3106(18)$ fm[d]	309(10)[e]	0.739(24)[e]
JLQCD 16	[30]	$2+1$	A	■	○	○	$\sqrt{t_0} = 0.1465(25)$ fm	331(38)[f]	0.792(89)[f]
HPQCD 10	[15]	$2+1$	A	○	★	○	$r_1 = 0.3133(23)$ fm[j]	338(10)[i]	0.809(25)
HPQCD 08B	[244]	$2+1$	A	■	■	■	$r_1 = 0.321(5)$ fm[j]	325(18)[k]	0.777(42)

[a]Scale determined in [42] using f_π.
[b]$\alpha^{(4)}_{\overline{\rm MS}}(5\text{ GeV}) = 0.2128(25)$, $\alpha^{(5)}_{\overline{\rm MS}}(M_Z) = 0.11822(74)$.
[c]We evaluated $\Lambda^{(4)}_{\overline{\rm MS}}$ from $\alpha^{(4)}_{\overline{\rm MS}}$. We also used $r_0 = 0.472$ fm.
[d]Scale is determined from f_π.
[e]$\alpha^{(3)}_{\overline{\rm MS}}(m_c = 1.267\text{ GeV}) = 0.3697(85)$, $\alpha^{(5)}_{\overline{\rm MS}}(M_Z) = 0.11622(84)$. Our conversion with $r_0 = 0.472$ fm.
[f]We evaluated $\Lambda^{(3)}_{\overline{\rm MS}}$ from the given $\alpha^{(4)}_{\overline{\rm MS}}(3\text{ GeV}) = 0.2528(127)$. $\alpha^{(5)}_{\overline{\rm MS}}(M_Z) = 0.1177(26)$. We also used $r_0 = 0.472$ fm to convert.
[g]We used $r_0 = 0.472$ fm to convert.
[h]We back-engineered from $\alpha^{(5)}_{\overline{\rm MS}}(M_Z) = 0.1177(20)$. We used $r_0 = 0.472$ fm to convert.
[i]$\alpha^{(3)}_{\overline{\rm MS}}(5\text{ GeV}) = 0.2034(21)$, $\alpha^{(5)}_{\overline{\rm MS}}(M_Z) = 0.1183(7)$.
[j]Scale is determined from Υ mass splitting.
[k]We evaluated $\Lambda^{(3)}_{\overline{\rm MS}}$ from the given $\alpha^{(4)}_{\overline{\rm MS}}(3\text{ GeV}) = 0.251(6)$. $\alpha^{(5)}_{\overline{\rm MS}}(M_Z) = 0.1174(12)$.

and three times the charm-quark mass. In this study random-color wall sources which greatly reduced the statistical errors were used. In fact, the statistical errors on the moments were completely negligible compared to other sources of errors. The strong coupling constant was extracted from R_4 [81]. To obtain the continuum limit the lattice-spacing dependence of the results of R_4 at different quark masses was fitted simultaneously in a similar manner as in the HPQCD 10 and HPQCD 14 analyses, but without using Bayesian priors. In extracting α_s several choices of the renormalization scale μ in the range $2/3m_h$–$3m_h$ have been considered. The perturbative truncation error was estimated by varying the coefficient of the unknown 4-loop term in Eq. (375) between $-1.6r_3$ and $+1.6r_3$. However, the uncertainty of the results due to the scale variation was larger than the estimated perturbative truncation error. The final error of the result $\Lambda^{N_f=3}_{\overline{\rm MS}} = 331(17)$ MeV comes mostly from the scale variation [81]. Since there are three lattice spacing available with $a\mu < 0.5$ we give ★ for continuum extrapolation. Because $\alpha_{\rm eff} = 0.22$–0.38 we give ○ for the renormalization scale. Finally, since $(\Delta\Lambda/\Lambda)_{\Delta\alpha} > \alpha^2_{\rm eff}$ for the smallest $\alpha_{\rm eff}$ value we give ○ for the perturbative behavior. In addition to R_4 Petreczky 20 also considered using R_6/R_8 and R_8/R_{10} for the α_s determination. It was pointed out that the lattice spacing dependence of R_6/R_8 is quite subtle and therefore reliable continuum extrapolations for this ratio are not possible for $m_h \geq 2m_c$ [81]. For $m_h = m_c$ and $1.5m_c$ the ratio R_6/R_8 leads to α_s values that are consistent with the ones from R_4. Furthermore, it was argued that finite-volume effects in the case of R_8/R_{10} are large for $m_h = m_c$ and therefore the corresponding data are not suitable for extracting α_s. This observation may explain why the central values of α_s extracted from R_8/R_{10} in some previous studies were systematically lower [31,230,244]. On the other hand for $m_h \geq 1.5m_c$ the finite-volume effects are sufficiently small

TABLE 62. Moments and the ratios of the moments from $N_f = 3$ simulations at the charm-quark mass.

	HPQCD 08	HPQCD 10	Maezawa 16	JLQCD 16	Petreczky 19	Petreczky 20
R_4	1.272(5)	1.282(4)	1.265(7)	⋯	1.279(4)	1.278(2)
R_6	1.528(11)	1.527(4)	1.520(4)	1.509(7)	1.521(3)	1.522(2)
R_8	1.370(10)	1.373(3)	1.367(8)	1.359(4)	1.369(3)	1.368(3)
R_{10}	1.304(9)	1.304(2)	1.302(8)	1.297(4)	1.311(7)	1.301(3)
R_6/R_8	1.113(2)	⋯	1.114(2)	1.111(2)	1.1092(6)	1.10895(32)
R_8/R_{10}	1.049(2)	⋯	1.0495(7)	1.0481(9)	1.0485(8)	⋯

in the continuum extrapolated results if some small-volume lattice data are excluded from the analysis [81]. The α_s obtained from R_8/R_{10} with $m_h \geq 1.5m_c$ were consistent with the ones obtained from R_4.

Aside from the final results for $\alpha_s(m_Z)$ obtained by matching with perturbation theory, it is interesting to make a comparison of the short distance quantities in the continuum limit R_n which are available from HPQCD 08 [244], JLQCD 16 [30], Maezawa 16 [230], Petreczky 19 [31] and Petreczky 20 [81] (all using $2+1$ flavors). This comparison is shown in Table 62. The results are in quite good agreement with each other. For future studies it is of course interesting to check agreement of these numbers before turning to the more involved determination of α_s.

While there have been no new determinations of α_s from the moments of the heavy-quark current two-point functions in $2+1+1$ flavor or $2+1$ flavor QCD since the FLAG 21 report, this method has been scrutinized in quenched QCD ($N_f = 0$) in three conference proceedings [707,837,838]. In these works the Wilson gauge action was used for several values of the lattices spacings, down to lattice spacing of $a = 0.01$ fm, which is 2.5 times smaller than the smallest lattice spacing used in $2+1$ flavor QCD. The box size was sufficiently large for the heavy-quark current two-point functions, namely $L = 2$ fm was used. In the temporal direction open boundary conditions have been used, and the extent in the time direction was 6 fm. For heavy-quark twisted-mass fermion formulation was used at the maximal twist. Five different heavy-quark masses have been used in these studies, namely $0.77M_c, 1.16M_c$, $1.55M_c, 2.32M_c$ and $3.48M_c$, with M_c being the physical charm-quark RGI mass [707,837,838]. The continuum extrapolation of R_4 has been performed and from it the value of $\Lambda_{\overline{\rm MS}}^{(N_f=0)}$ was obtained for different heavy-quark masses and different choices of μ. It turned out, however, that the results obtained for different heavy-quark masses and values of μ are not consistent with each other and often are not compatible with the value determined from step scaling [763]. It was argued that this is due to the log-enhanced discretization errors in R_4, i.e., discretization errors that are proportional to $a^2\log(am_c)$ [838], and that reliable continuum extrapolation of R_4 is not possible for this lattice setup. A practical way to circument this problem was also proposed in Ref. [838] and relies on considering a special combination of R_4 evaluated at two heavy-quark masses. The ratios R_6/R_8 and R_8/R_{10} do not have log-enhanced discretization effects [707,838] and therefore, can be used to obtain $\Lambda_{\overline{\rm MS}}^{(N_f=0)}$. Such an analysis was performed in Ref. [707]. Here to deal with perturbative error it was assumed that $\Lambda_{\overline{\rm MS}}^{(N_f=0)}\sqrt{8t_0}$ obtained at different renormalization scales μ is linear in $\alpha_s^2(\mu)$ as expected from 3-loop perturbative calculations. Performing linear extrapolations in $\alpha_s^2(\mu)$ the final values of $\Lambda_{\overline{\rm MS}}^{(N_f=0)}\sqrt{8t_0}$ have been obtained. The corresponding results for the Λ-parameter agree with the result of the step-scaling analysis but have much larger errors, and thus are not competitive [707].

Scale variations. Moments of heavy-quark correlators are computed at scales that are set by the mass of the charm quark. We compute scale variations for the moments r_4, r_6 and r_8 at different values of the matching scale.

HQ $r_4, \mu = m_c$

$$\delta_{(2)} = 2.7\% \quad \delta^*_{(2)} = 2.8\%. \tag{376}$$

HQ $r_4, \mu = 2m_c$

$$\delta^*_{(4)} = 1.2\%, \qquad \delta_{(2)} = 1.5\% \qquad \delta^*_{(2)} = 1.6\%. \tag{377}$$

HQ $r_6, \mu = 2m_c$

$$\delta_{(2)} = 2.3\% \qquad \delta^*_{(2)} = 1.2\%. \tag{378}$$

HQ $r_6, \mu = 2m_c$

$$\delta_{(2)} = 2.8\% \qquad \delta^*_{(2)} = 4.8\%. \tag{379}$$

We note here that the errors from the scale variations are in the same ballpark as previous estimates published in FLAG reviews. The moment r_4 computed at the scale $Q = 2m_c$ happens to have a systematic error in the range 1–2%.

I. Gradient flow schemes

1. General considerations

The gradient flow [365,751] (cf. the paragraph around Eq. (317) for the basic equations) allows for the definition of many new observables, both in pure gauge theory and QCD, which are gauge invariant and automatically renormalized after the standard QCD renormalizations of parameters and composite fields have been carried out. This has been established perturbatively to all orders in Ref. [839] and confirmed up to 2-loop level in practical calculations [739]. It is generally assumed to be valid beyond perturbation theory and many simulation results corroborate this assumption.

The gradient flow comes with the flow-time parameter, t, which has dimensions of length squared and thus introduces a new energy scale which is, by analogy with the diffusion equation, naturally identified as $\mu = 1/\sqrt{8t}$ (in four dimensions). The most widely used observable is the action density at finite flow time,

$$E(t,x) = -\frac{1}{2}\mathrm{tr}\{G_{\mu\nu}(t,x)G_{\mu\nu}(x)\}. \tag{380}$$

Its expectation value has a perturbative expansion starting at $O(\alpha)$, which gives rise to the definition of the coupling in the GF scheme,

$$\alpha_{\mathrm{GF}}(\mu) \equiv \frac{\bar{g}^2_{\mathrm{GF}}(\mu)}{4\pi} = \frac{4\pi t^2}{3}\langle E(t,x)\rangle \tag{381}$$

and is known to 3-loop order,

$$\alpha_{\mathrm{GF}}(\mu = 1/\sqrt{8t}) = \alpha_{\overline{\mathrm{MS}}}(\mu) + k_1\alpha_{\overline{\mathrm{MS}}}(\mu)^2 + k_2\alpha_{\overline{\mathrm{MS}}}(\mu)^3 + \ldots \tag{382}$$

with k_1 and k_2 computed in Refs. [365,739], respectively (cf. Table 55). Note that the GF coupling directly relates to the scale t_0; its definition is equivalent to $\bar{g}^2_{\mathrm{GF}}(1/\sqrt{8t_0}) = 15.8$. With the flow time setting the renormalization scale, the β-function is readily obtained during the numerical integration of the flow equation, by also tracking the flow-time derivative of $\langle E(t,x)\rangle$,

$$\beta_{\mathrm{GF}}(\bar{g}_{\mathrm{GF}}) = -2t\frac{d}{dt}\bar{g}_{\mathrm{GF}}(1/\sqrt{8t}), \tag{383}$$

and the 3-loop β-function coefficient b_2 is known. In the pure gauge theory is given by

$$b_2^{\mathrm{GF}} = -1.90395(4)/(4\pi)^3, \quad (N_f = 0). \tag{384}$$

This is almost three times larger in magnitude than in the $\overline{\mathrm{MS}}$ scheme and of opposite sign. One naturally worries about higher-order corrections being large, too. As a result, making contact with perturbation theory requires very small couplings. To quantify the problem, we have done the following exercises (all for $N_f = 0$): First one may evaluate the difference in $\sqrt{8t}\Lambda_{\mathrm{GF}}$ obtained by integrating the perturbative β-function at 2- vs. 3-loop order from zero coupling to a reference value $\bar{g}^2_{\mathrm{GF}}(1/\sqrt{8t}) = 1.2$, which corresponds to the smallest coupling reached in the works discussed below. We find that this difference is about 11 percent, again about three times larger than with the $\overline{\mathrm{MS}}$ scheme. In order to vary the scale we convert to the $\overline{\mathrm{MS}}$ scheme,

$$\alpha_{\mathrm{GF}}(\mu) = \alpha_{\overline{\mathrm{MS}}}(s\mu) + k_1(s)\alpha^2_{\overline{\mathrm{MS}}}(s\mu) + k_2(s)\alpha^3_{\overline{\mathrm{MS}}}(s\mu) + \mathrm{O}(\alpha^4_{\overline{\mathrm{MS}}}), \tag{385}$$

where the s-dependence of the coefficients is given as

$$\begin{aligned} k_1(s) - k_1(1) &= 8\pi b_0 \ln(s), \\ k_2(s) - k_2(1) &= 32\pi^2 b_1 \ln(s) + k_1(s)^2 - k_1(1)^2. \end{aligned} \tag{386}$$

In order to obtain the $\overline{\mathrm{MS}}$ coupling in terms of the reference coupling one needs to invert Eq. (385), which we do either perturbatively or numerically for the truncated equation. We then compute,

$$\sqrt{8t}\Lambda_{\overline{\mathrm{MS}}} = s \times \varphi_{\overline{\mathrm{MS}}}(\bar{g}_{\overline{\mathrm{MS}}}(s/\sqrt{8t})), \tag{387}$$

for scale factors $s = 1/2$, 1, 2, using the 5-loop β-function in the $\overline{\mathrm{MS}}$ scheme. We find that the resulting variation in the Λ-parameter depends on how the $\overline{\mathrm{MS}}$-coupling is obtained: With perturbative inversion, the variation is plus 7.5 and minus 4 percent, with numerical inversion, one obtains plus 2.5 and plus 3.3 percent, i.e., even monotony is lost. The central values for $s = 1$ differ by 5 percent. As an alternative, we consider the scale factor $s^* = 0.534$ which implies $k_1(s^*) = 0$. Varying by a factor two around s^* one finds that the difference in central values reduces to 1.3 percent, and the Λ-parameter changes by minus 6 percent and plus 4 percent for perturbative inversion, and by plus 9.7% and minus 2.7% for numerical inversion.

We conclude that at this reference coupling a determination of the Λ-parameter to better than five percent seems impossible.

2. Discussion of computations

A determination of the β-function directly from the flow-time dependence of the GF coupling requires a controlled infinite-volume extrapolation. This was first suggested in Ref. [840], where the strategy was applied to a BSM model. Since then, two works have applied this scheme to the pure gauge theory (QCD with $N_f = 0$), namely Hasenfratz 23 [705] and Wong 23 [706], in a proceedings contribution. We mainly discuss Hasenfratz 23 who provide more

details: the data produced for the GF coupling ranges from 15.8 down to 1.2, lattice sizes vary between $L/a = 20$ and $L/a = 48$, depending on the β-value, and periodic boundary conditions are imposed on the gauge field. Wong 23 do have data for larger lattices up to $L/a = 64$ and even $L/a = 80$, 96 at selected bare couplings. The data for both $\bar{g}^2_{\rm GF}$ and $\beta_{\rm GF}$ are extrapolated to the infinite-volume limit at fixed lattice spacing, assuming corrections $\propto (a/L)^4$, with Wong 23 also allowing for a subleading $(a/L)^6$ term. Then the continuum limit is taken for a^2/t-values in the range 0.25–0.5, corresponding to $a\mu$-values in the range 0.177–0.25, and a somewhat wider range in Wong 23. The continuum extrapolation data for the β-function at fixed GF coupling are shown in plots. For Hasenfratz 23 these extrapolations look fine and would pass any reasonable data-driven criterion. Wong 23 only show the extrapolation at the largest GF coupling which looks fine, too. Hence we give ★ for the continuum extrapolation and also for renormalization scale, given that $\alpha_{\rm eff}$ reaches down to below 0.1. Regarding the formal FLAG criterion for perturbative behavior, Hasenfratz 23 give an overall error of 0.6% for $\alpha_{\rm GF}$. Using this error we have, at the smallest couplings reached, $\alpha^{n_l}_{\rm eff} = (0.1)^2 < 0.006 \times 2.85 = 0.017$, which satisfies the criterion comfortably. This warrants a ★ for Hasenfratz 23. For Wong 23 the accuracy of $\alpha_{\rm GF}$ is not given but they quote a per-mille accuracy for the beta function at $\bar{g}^2_{\rm GF} = 15.8$; we assign a ○, which assumes their coupling data is perhaps a factor 2 but still less than a factor 3–4 more accurate relative to the 0.6% of Hasenfratz 23.

Unfortunately, the formal FLAG criteria do not capture the anomalously bad behavior of the GF scheme. As discussed above, even at $\alpha_{\rm eff} = 0.1$ the estimate of the Λ-parameter is ambiguous at the level of about 5 percent.

Contact to perturbation theory is not really established, as the obtained β-function seems to show a slope that is different from the perturbative expectation. Imposing perturbative asymptotics and evaluating the integral over the beta function numerically leads to the estimate $\sqrt{8t_0}\Lambda_{\overline{\rm MS}} = 0.622(10)$. Wong 23 obtain an even smaller error, $\sqrt{8t_0}\Lambda_{\overline{\rm MS}} = 0.632(7)$.[74] Note that both values are in agreement with each other and with Dalla Brida 19 [who obtained 0.623(10)] and would lend support to the high central value compared to older results in the literature. Despite this consistency, the claimed high accuracy seems at odds with the bad perturbative behavior of this scheme.

Regarding the infinite-volume limit, the main problem is the lack of guidance from theory regarding the fit *Ansatz*. With $N_f = 0$ and in the hadronic regime, one may expect an exponential approach to the infinite-volume limit $\propto \exp(-m_G L)$, with m_G the 0^{++} glueball mass. At high energies one is necessarily in small volumes where hadrons cannot form, and leading effects $\propto (a/L)^4$ are used as a plausible *Ansatz* by both groups of authors. However, there is an intermediate regime where the situation is quite unclear, and even at high energies, once the volume is large enough to contain hadrons, the large-volume asymptotics should be expected to change. The situation may be even more complicated in full QCD, where massless pions are expected at low energies. Chiral perturbation theory may help but only as long as pions are relevant degrees of freedom.

Note that boundary conditions should not matter in the infinite-volume limit, so that any of the GF finite-volume couplings that have been used in step-scaling studies (cf. Sec. IX C) could be used to improve our understanding of it. In fact, the first discussion can be found in Ref. [750], there with open-SF boundary conditions. In Dalla Brida 19, two different finite-volume schemes are considered which should both converge to the infinite-volume GF scheme.

In step-scaling studies, the gradient-flow scale is fixed in units of L to a constant $c = \sqrt{8t}/L$, with typical values around $c = 0.3$. This means that the β-function cannot be obtained directly and a detour via the step-scaling function is used in practice [763] Since the schemes are defined in a finite volume, c becomes an integral part of the scheme definition as do the boundary conditions (SF, twisted periodic, etc.). In particular, the perturbative 2-loop result in Eq. (382) cannot be used. For $N_f = 0$ and twisted periodic boundary conditions there is a 1-loop computation [757] while for $N_f = 0$ and SF boundary conditions there is a 2-loop result obtained using a stochastic perturbative approach [756]. As in infinite volume, the perturbative behavior of the finite-volume gradient-flow schemes is quite bad [763]. This problem was circumvented in Refs. [704,755,763] by matching nonperturbatively to the SF scheme, in order to benefit from its good perturbative behavior. The option of such a matching is also mentioned in Hasenfratz 23 where it is left to future work.

In Table 63 we list these results.

Scale variations. As discussed in the general considerations of the previous subsection, the matching with perturbation theory is performed for $\bar{g}^2_{\rm GF}(1/\sqrt{8t}) = 1.2$. The corresponding energy scale $\mu = 1/\sqrt{8t}$ is not given in the publications, preventing us from using the generic procedure that we used for the majority of the observables. Instead, we defined an alternative procedure to estimate the effect of scale variations directly on the ratio of Λ-parameters, as discussed in Sec. IX I 1.

J. Summary

Having reviewed the individual computations, we are now in a position to discuss the overall result. We first look at the current results of the Λ-parameter for QCD with $N_f = 0, 2, 3, 4$ flavors in units of the scale r_0 (and $\sqrt{8t_0}$ for $N_f = 0$). These results are directly obtained from lattice

[74] Wong 23 write $t_0\Lambda_{\overline{\rm MS}}$, instead of $\sqrt{8t_0}\Lambda_{\overline{\rm MS}}$, which we interpret as a typo.

TABLE 63. Results for the GF scheme in infinite volume.

Collaboration	Ref.	N_f	Publication status	Renormalization scale	Perturbative behavior	Continuum extrapolation	Scale	$\sqrt{8t_0}\Lambda_{\overline{\rm MS}}$	$r_0\Lambda_{\overline{\rm MS}}$[a]
Hasenfratz 23	[705]	0	A	★	★	★	$\sqrt{t_0}$	0.622(10)	0.659(11)
Wong 23	[706]	0	C	★	○	★	$\sqrt{t_0}$	0.632(7)	0.670(8)

[a] $r_0\Lambda_{\overline{\rm MS}}$ determined by us using $\sqrt{8t_0}/r_0 = 0.9435(97)$ from Dalla Brida 19 [763] without propagating the error.

simulations of QCD with given N_f. For the Λ-parameter with $N_f = 0$ we present a more in depth discussion. As emphasized in our last report, even though $N_f = 0$ is unphysical, the Λ-parameter enters into the decoupling result, which is one of the most accurate lattice determinations of $\alpha^{(5)}_{\overline{\rm MS}}(m_Z)$. Fortunately, this has motivated several collaborations to help clarify the situation, which is characterized by many historical results, with a large spread of central values, that are mutually incompatible due to the smallness of some error estimates. We have decided to estimate ranges for different methods and give a corresponding FLAG estimate.

Then we discuss the central $\alpha_{\overline{\rm MS}}(m_Z)$ results in five-flavor QCD. We give ranges for each sub-group discussed previously, and give a final FLAG average as well as an overall average together with the current PDG nonlattice numbers. In the end, we return to the Λ-parameter; for $N_f = 3$, 4, 5 we derive their values from the FLAG estimate of $\alpha_{\overline{\rm MS}}(m_Z)$.

We end with an outlook and some concluding remarks.

1. Ranges for $[r_0\Lambda_{\overline{\rm MS}}]^{(N_f)}$ and $\Lambda^{(N_f)}_{\overline{\rm MS}}$

In the present situation, we give ranges for $[r_0\Lambda_{\overline{\rm MS}}]^{(N_f)}$ and $\Lambda_{\overline{\rm MS}}$, discussing their determination case by case. We include results with $N_f < 3$ because it is interesting to see the N_f-dependence of the connection of low- and high-energy QCD. This aids our understanding of the field theory and helps in finding possible ways to tackle it beyond the lattice approach. It is also of interest in providing an impression on the size of the vacuum-polarization effects of quarks, in particular with an eye on the still difficult-to-treat heavier charm and bottom quarks. Most importantly, however, the decoupling strategy described in Sec. IX D means that Λ-parameters at different N_f can be connected by a nonperturbative matching computation. Thus, even results at unphysical flavor numbers, in particular $N_f = 0$, may enter results for the physically interesting case. Rather than phasing out results for "unphysical flavor numbers," continued scrutiny by FLAG will be necessary. Having said this, we emphasize that results for $[r_0\Lambda_{\overline{\rm MS}}]^{(0)}$ and $[r_0\Lambda_{\overline{\rm MS}}]^{(2)}$ are *not* meant to be used directly for phenomenology.

For the ranges we obtain

$$[r_0\Lambda_{\overline{\rm MS}}]^{(4)} = 0.70(3), \tag{388}$$

$$[r_0\Lambda_{\overline{\rm MS}}]^{(3)} = 0.809(23), \tag{389}$$

$$[r_0\Lambda_{\overline{\rm MS}}]^{(2)} = 0.79(^{+5}_{-15}), \tag{390}$$

$$[r_0\Lambda_{\overline{\rm MS}}]^{(0)} = 0.647(11). \tag{391}$$

No change has occurred since FLAG 21 for $N_f = 2$, 4, so we refer to the respective discussions in earlier FLAG reports.

For $N_f = 2 + 1$, we take as a central value the weighted average of ALPHA 22 [80], Petreczky 20 [81], Cali 20 [84], Ayala 20 [82], TUMQCD 19 [83], ALPHA 17 [85], HPQCD 10 [15], PACS-CS 09A [86] and Maltman 08 [87], and arrive at our range,

$$[r_0\Lambda_{\overline{\rm MS}}]^{(3)} = 0.809(23), \tag{392}$$

where the error is the one from the weighted average of those results, which are statistics-dominated, namely PACS-CS 09A, ALPHA 17 and ALPHA 22, and the known correlation between the latter two is taken into account. This is to be compared with the much smaller error of 0.010, as obtained from the weighted average. There is good agreement with all $2 + 1$ results without red tags. In physical units, using $r_0 = 0.472$ fm and neglecting its error, we get

$$\Lambda^{(3)}_{\overline{\rm MS}} = 338(10)\ \text{MeV}, \tag{393}$$

whereas the error of the straight weighted average is around 4 MeV.

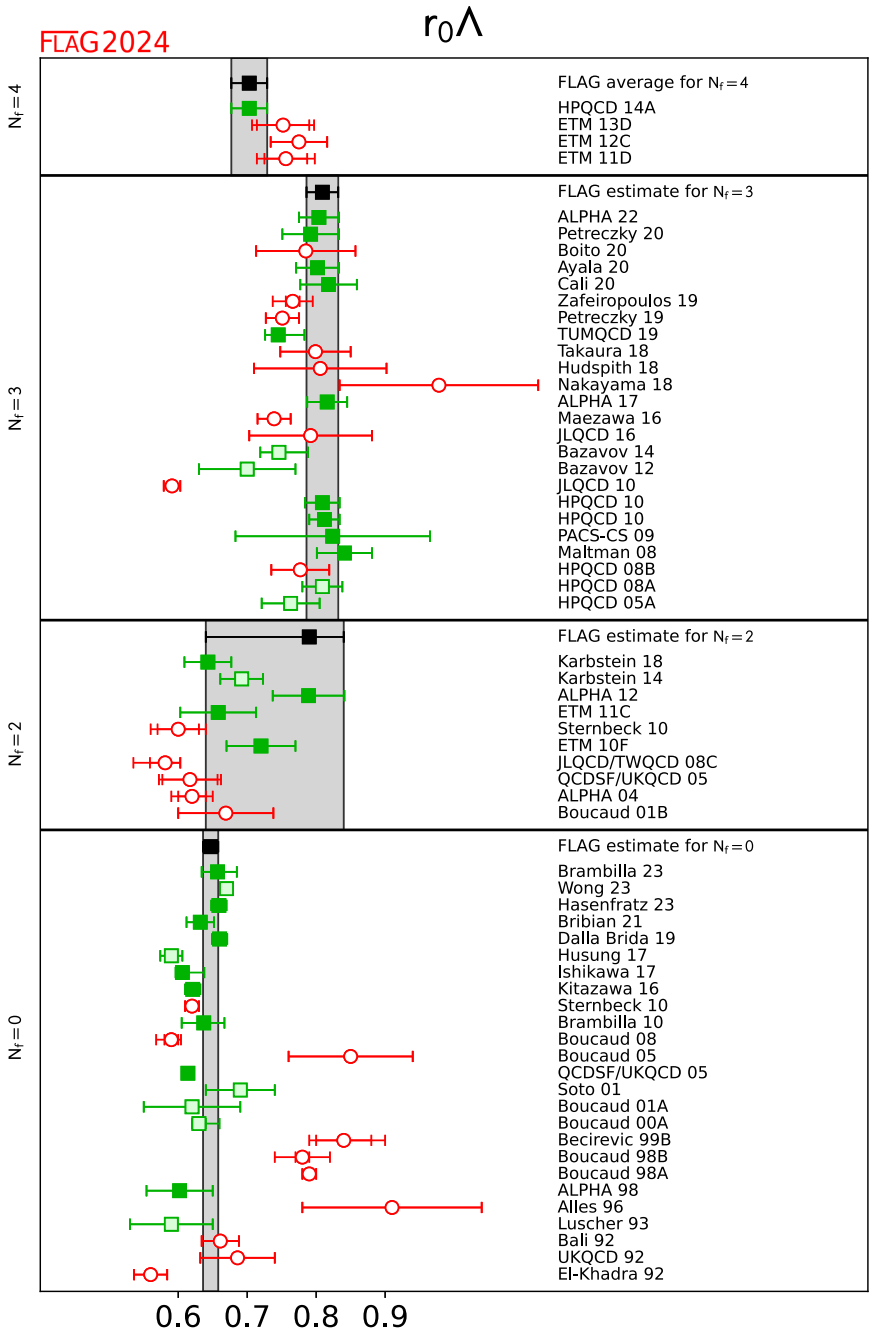


FIG. 38. $r_0\Lambda_{\overline{\rm MS}}$ estimates for $N_f = 0, 2, 3, 4$ flavors. Full green squares are used in our final ranges, pale green squares also indicate that there are no red squares in the color coding but the computations were superseded by later more complete ones or not published, while red open circles mean that there is at least one red square in the color coding.

For $N_f = 0$ there are now 12 results which pass the FLAG criteria, four of which are new since FLAG 21. Instead of averaging individual results we will group them by method, produce pre-ranges and a final estimate for the range from combining the pre-ranges. There are four different methods used:

(i) Step scaling: Combining Dalla Brida 19 with Bribian 21, Ishikawa 17 (with symmetrized larger error) and ALPHA 98 in a weighted average, we obtain

$$[r_0\Lambda_{\overline{\rm MS}}]^{(0)} = 0.648(11). \tag{394}$$

Leaving out Ishikawa 17 with its asymmetric error, this would change to 0.651(11). For the error we take the statistics-dominated one from Dalla Brida 19.

(ii) Static potential/force: We combine Brambilla 10 with Brambilla 23 (both with symmetrized error, using the larger ones) in a weighted average,

$$[r_0\Lambda_{\overline{\rm MS}}]^{(0)} = 0.648(28), \tag{395}$$

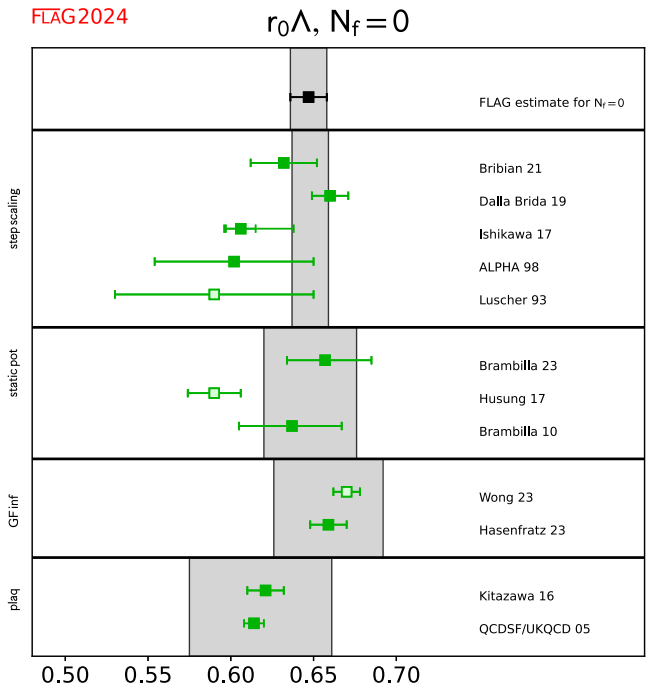


FIG. 39. $r_0\Lambda_{\overline{\rm MS}}$ estimates for $N_f = 0$ flavors. As discussed in the text, we group the results by method and estimate pre-ranges. Only full green squares are used in our final ranges, pale green squares indicate that the computations were not published or superseded by later more complete ones.

where we use the error of the newer result for our estimate of the range.

(iii) There are two new determinations with the GF scheme in infinite volume and continuous β-function, by Wong 23 and Hasenfratz 23. We use the central value of the published paper by Hasenfratz 23 and include a perturbative uncertainty of five percent as discussed in Sec. IX I, and obtain,

$$[r_0\Lambda_{\overline{\rm MS}}]^{(0)} = 0.659(33). \tag{396}$$

(iv) Wilson loops: There are two results which are, due to their tiny errors, causing the tension noticed in our previous FLAG report. We performed a scale-variation analysis, similar to the one explained in Sec. IX I for the GF scheme. Variations around the scale of fastest apparent convergence (cf. Sec. IX B 3) result in changes of up to 13 percent even at the finest available lattice spacings. Another way to look at the data is to note that both works perform continuum extrapolations of the Λ-parameter assuming an a^2-behavior. On the other hand, there is a parametric uncertainty of $O(\alpha_P^2(1/a))$ which is neglected. If included as a second term in a fit, the error gets much larger, and central values tend to increase. Stopping short of changing central values, we take the (unweighted) average central value and include a symmetric range of ± 7 percent as perturbative uncertainty,

$$[r_0\Lambda_{\overline{\rm MS}}]^{(0)} = 0.618(43). \tag{397}$$

With these pre-ranges we perform a weighted average to obtain the central value, and then take the statistics-dominated Dalla Brida 19 step-scaling error as our estimate of the range,

$$[r_0\Lambda_{\overline{\rm MS}}]^{(0)} = 0.647(11) \Rightarrow [\sqrt{8t_0}\Lambda_{\overline{\rm MS}}]^{(0)} = 0.610(10). \tag{398}$$

All results are shown in Fig. 38 and the $N_f = 0$ results, with our pre-range by method are shown in Fig. 39.

2. Our range for $\alpha_{\overline{\rm MS}}^{(5)}$

We now turn to the status of the essential result for phenomenology, $\alpha_{\overline{\rm MS}}^{(5)}(M_Z)$. We only consider lattice results with $N_f = 3$ or $N_f = 4$ sea quarks. Converting a Λ-parameter to $\alpha_{\overline{\rm MS}}^{(5)}(M_Z)$ involves the perturbative matching of the coupling across the charm- and bottom-quark thresholds, which is available up to 4-loop order [696,697]. Note that perturbative matching at 4-loops is consistent with using the β-function at 5-loop order, which is also available in the $\overline{\rm MS}$ scheme [693,847]. One then needs the Z-boson mass and the charm- and bottom-quark masses as additional input. For definiteness, we use $m_Z = 91.1876$ GeV, and, for the $\overline{\rm MS}$ quark masses at

their own scale, $m_c = 1.275(13)$ GeV and $m_b = 4.203(11)$ GeV [5]. Fortunately, the exact choices are almost irrelevant at the current accuracy: A change in the charm-quark mass by one percent shifts the value of $\alpha_s(m_Z)$ by 3×10^{-5}, and the effect for the bottom-quark mass is even smaller. This is down by over a factor of 20 compared to the current best total errors on α_s. The combined perturbative uncertainty of decoupling across both the charm- and the bottom-quark threshold is around 25×10^{-5}, if one takes the difference between 3-loop and 5-loop order as estimate, as was done, for example, in ALPHA 17 [85]. Even this generous estimate is still a factor 2–3 below the best total errors. Incidentally we also note that perturbative decoupling has been tested nonperturbatively [200]. It was found that the decoupling of a heavy quark in gluonic observables (such as the ones used to define $\alpha_{\rm eff}$), is well described by perturbation theory. Even for the charm quark the nonperturbative effects are expected to be at the few per-mille level. This result justifies the use of $N_f = 3$ QCD to obtain $\alpha^{(5)}_{\overline{\rm MS}}(M_Z)$, and it motivated the development of the decoupling method used in ALPHA 22 [80].

As can be seen from the tables and figures, several computations satisfy the FLAG criteria for inclusion in the FLAG average. Since FLAG 21 the contribution by Petreczky 20 [81] has been published and is now included in the average and there is the first result from the decoupling method by the ALPHA collaboration, ALPHA 22 [80].

We now explain the determination of our range. We only include those results without a red tag and that are published in a refereed journal.

A general issue with most determinations of $\alpha_{\overline{\rm MS}}$, both lattice and nonlattice, is that they are dominated by perturbative truncation errors, which are difficult to estimate. Further, all results discussed here except for those of Secs. IX C, IX G, IX D are based on extractions of $\alpha_{\overline{\rm MS}}$ that are largely influenced by data with $\alpha_{\rm eff} \geq 0.3$. At smaller α_s the momentum scale μ quickly gets at or above a^{-1}. We have included computations using $a\mu$ up to 1.5 and $\alpha_{\rm eff}$ up to 0.4, but one would ideally like to be significantly below that. Accordingly, we choose to not simply perform weighted averages with the individual errors estimated by each group. Rather, we use our own more conservative estimates of the perturbative truncation errors in the weighted average. In order to improve our assessment we have also performed scale variations as is commonly done in phenomenology. In Table 65, we provide a summary of the variations in $\alpha^{(5)}_{\overline{\rm MS}}(M_Z)$ obtained from the procedure explained in Sec. IX A and suggested in Ref. [688].

In the following we first obtain separate estimates for α_s from each of the six methods with results that pass the FLAG criteria: step scaling, decoupling, the heavy-quark potential, Wilson loops, heavy-quark current two-point functions and vacuum polarization. In a second step we combine them to obtain the overall FLAG estimate. All results are collected in Table 64.

(i) *Step scaling*

The step-scaling computations of PACS-CS 09A [86] and ALPHA 17 [85] reach energies around the Z-mass where perturbative uncertainties in the three-flavor theory are negligible. We form a weighted average of the two results and obtain $\alpha_{\overline{\rm MS}} = 0.11848(81)$, where the error is dominated by the statistical error from the simulations.

(ii) *Decoupling*

There is a single result which has been discussed in Sec. IX D. The result is $\alpha_{\overline{\rm MS}} = 0.11823(84)$ with a statistics-dominated error.

(iii) *Static-quark potential computations*

Brambilla 10 [795], ETM 11C [792] and Bazavov 12 [789] give evidence that they have reached distances where perturbation theory can be used. However, in addition to Λ, a scale is introduced into the perturbative prediction by the process of subtracting the renormalon contribution. This subtraction is avoided in Bazavov 14 [788] by using the force and again agreement with perturbative running is reported. Husung 17 [794] (unpublished) studied the reliability of perturbation theory in the pure gauge theory with lattice spacings down to 0.015 fm and found that at weak coupling there is a downward trend in the Λ-parameter with a slope $\Delta\Lambda/\Lambda \approx 9\alpha_s^3$. The downward trend is broadly confirmed in Husung 20 [793] albeit with larger errors.

Bazavov 14 [788] satisfies all of the criteria to enter the FLAG average for α_s but has been superseded by TUMQCD 19 [83]. Moreover, there is another study, Ayala 20 [82] who use the very same data as TUMQCD 19, but treat perturbation theory differently, resulting in a rather different central value. This shows that perturbative truncation errors are the main source of errors. We combine the results for $\Lambda^{(N_f=3)}_{\overline{\rm MS}}$ from both groups as a weighted average (with the larger upward error of TUMQCD 19) and take the difference of the central values as the uncertainty of the average. We obtain $\Lambda^{(N_f=3)}_{\overline{\rm MS}} = 330(24)$ MeV, which translates to $\alpha_s(m_Z) = 0.11782(165)$. This uncertainty of 1.4 percent is in line with estimates from scale variations.

(iv) *Small Wilson loops*

Here the situation is unchanged since FLAG 16. In the determination of α_s from observables at the lattice spacing scale, there is an interplay of higher-order perturbative terms and lattice artifacts. In

TABLE 64. Results for $\alpha_{\overline{\rm MS}}(M_Z)$. Different methods are listed separately and they are combined to a pre-range when computations are available without any ■. The FLAG estimate is given by 0.11833(67), where the error is the statistics-dominated error of the combined decoupling and step-scaling results.

Collaboration	Ref.	N_f	Publication status	Renormalization scale	Perturbative behavior	Continuum extrapolation	$\alpha_{\overline{\rm MS}}(M_Z)$	Remark	Table
ALPHA 17	[85]	2+1	A	★	★	★	0.11852(84)	step scaling	56
PACS-CS 09A	[86]	2 + 1	A	★	★	○	0.11800(300)	step scaling	56
pre-range (average)							0.11848(81)		
AlPHA 22	[80]	2+1	A	★	★	★	0.11823(84)	decoupling $N_f=3$ to $N_f=0$ & step scaling	57
pre-range (average)							0.11823(84)		
Ayala 20	[82]	2+1	A	○	★	○	0.11836(88)	$Q-\bar{Q}$ potential	58
TUMQCD 19	[83]	2+1	A	○	★	○	$0.11671(^{+110}_{-57})$	$Q-\bar{Q}$ potential (and free energy)	58
Takaura 18	[786,787]	2+1	A	■	○	○	$0.11790(70)(^{+130}_{-120})$	$Q-\bar{Q}$ potential	58
Bazavov 14	[788]	2+1	A	○	★	○	0.11660(100)	$Q-\bar{Q}$ potential	58
Bazavov 12	[789]	2+1	A	○	○	○	$0.11560(^{+210}_{-220})$	$Q-\bar{Q}$ potential	58
pre-range with estimated pert. error							0.11782(165)		
Cali 20	[84]	2+1	A	○	★	★	0.11863(114)	vacuum pol. (position space)	59
Hudspith 18	[733]	2+1	P	○	★	■	$0.11810(270)(^{+80}_{-220})$	vacuum polarization	59
JLQCD 10	[732]	2+1	A	■	○	■	$0.11180(30)(^{+160}_{-170})$	vacuum polarization	59
pre-range with estimated pert. error							0.11863(360)		
HPQCD 10	[15]	2+1	A	○	★	★	0.11840(60)	Wilson loops	60
Maltman 08	[87]	2+1	A	○	○	★	0.11920(110)	Wilson loops	60
pre-range with estimated pert. error							0.11871(128)		
Petreczky 20	[81]	2+1	A	○	○	★	0.11773(119)	heavy current two points	61
Boito 20	[836,841]	2+1	A	■	■	○	0.1177(20)	use published lattice data	61
Petreczky 19	[31]	2+1	A	■	■	★	0.1159(12)	heavy current two points	61
JLQCD 16	[30]	2+1	A	■	○	○	0.11770(260)	heavy current two points	61
Maezawa 16	[230]	2+1	A	■	■	○	0.11622(84)	heavy current two points	61
HPQCD 14A	[18]	2+1+1	A	○	★	○	0.11822(74)	heavy current two points	61
HPQCD 10	[15]	2+1	A	○	★	○	0.11830(70)	heavy current two points	61
HPQCD 08B	[244]	2+1	A	■	■	■	0.11740(120)	heavy current two points	61
pre-range with estimated pert. error							0.11818(119)		
Zafeiropoulos 19	[842]	2+1	A	■	■	■	0.1172(11)	gluon-ghost vertex	66 in [5]
ETM 13D	[843]	2+1+1	A	○	○	■	0.11960(40)(80)(60)	gluon-ghost vertex	66 in [5]
ETM 12C	[844]	2+1+1	A	○	○	■	0.12000(140)	gluon-ghost vertex	66 in [5]
ETM 11D	[845]	2 + 1 + 1	A	○	○	■	$0.11980(90)(50)(^{+0}_{-50})$	gluon-ghost vertex	66 in [5]
Nakayama 18	[846]	2+1	A	★	○	■	0.12260(360)	Dirac eigenvalues	67 in [5]

HPQCD 05A [811], HPQCD 08A [734] and Maltman 08 [87] both lattice artifacts (which are power corrections in this approach) and higher-order perturbative terms are fitted. We note that Maltman 08 [87] and HPQCD 08A [734] analyze largely the same dataset but use different versions of the perturbative expansion and treatments of nonperturbative terms. After adjusting for the slightly different lattice scales used, the values of $\alpha_{\overline{\rm MS}}(M_Z)$ differ by 0.0004 to 0.0008 for the three quantities considered. In fact the largest of these differences (0.0008) comes from a tadpole-improved loop, which is expected to be best behaved perturbatively. We therefore replace the perturbative-truncation errors

TABLE 65. Summary of the results of scale variations. We report results for those observables for which we could use the common procedure introduced earlier.

Observable	loops	Q [GeV]	$\delta^*_{(4)}$[%]	$\delta_{(2)}$[%]	$\delta^*_{(2)}$[%]	Ref.
Step scaling	2	80	0.1	0.2	0.2	[725,726]
Potential	3	1.5		2.6	2.7	[727–731]
		2.5	0.9	1.5	1.5	
		5.0	0.4	0.8	0.8	
Vacuum polarization	3	1.3	1.0	11.6	0.6	[84]
$-\log W_{11}$	2	4.4	2.8	3.3	2.5	[734,735]
$-\log W_{12}/u_0^6$		4.4	3.5	3.2	3.1	
HQ r_4	2	m_c		2.7	2.8	[736–738]
HQ r_4		$2m_c$	1.2	1.5	1.6	
HQ r_6		$2m_c$		2.3	1.2	
HQ r_8		$2m_c$		2.8	4.8	

from [15,87] with our estimate of the perturbative uncertainty Eq. (366). Taking the perturbative errors to be 100% correlated between the results, we obtain for the weighted average $\alpha_{\overline{\rm MS}} = 0.11871(128)$. We note that this assessment, taken over from FLAG 21, seems optimistic in the light of the uncertainty induced by scale variations, which are at the level of three percent for the plaquette and rectangle Wilson loops. One may expect that simultaneous consideration of many quantities stabilizes the estimates as do terms of higher order in α. It would be interesting to see a new study of this kind, possibly with a different action. We may have to revise our range in the future.

(v) *Heavy-quark current two-point functions*

Further computations with small errors are HPQCD 10 [15] and HPQCD 14A [18], where correlation functions of heavy valence quarks are used to construct short-distance quantities. Due to the large quark masses needed to reach the region of small coupling, considerable discretization errors are present, see Fig. 30 of FLAG 16. These are treated by fits to the perturbative running (a 5-loop running $\alpha_{\overline{\rm MS}}$ with a fitted 5-loop coefficient in the β-function is used) with high-order terms in a double expansion in $a^2\Lambda^2$ and $a^2m_c^2$ supplemented by priors which limit the size of the coefficients. The priors play an especially important role in these fits given the much larger number of fit parameters than data points. We note, however, that the size of the coefficients does not prevent high-order terms from contributing significantly, since the data includes values of am_c that are rather close to one.

From a physics perspective it seems natural to use the renormalization scale set by the charm-quark mass; however, this implies $\alpha_{\rm eff} \simeq 0.38$, which is the reason why JLQCD 16, Petreczky 19 [31] and Boito 20 [836] do not pass the FLAG criteria. Still some valuable insight can be gained from these works. While Petreczky 19/Petreczky 20 share the same lattice data for heavy quark masses in the range $m_h = m_c$–$4m_c$ they use a different strategy for continuum extrapolations and a different treatment of perturbative uncertainties. Petreczky 19 [31] perform continuum extrapolation separately for each value of the valence-quark mass, while Petreczky 20 rely on joint continuum extrapolations of the lattice data at different heavy-quark masses, similar to the analysis of HPQCD, but without Bayesian priors. It is concluded that reliable continuum extrapolations for $m_h \geq 2m_c$ require a joint fit to the data. This limits the eligible α_s determinations in Petreczky 19 [31] to $m_h = m_c$ and $1.5m_c$, for which, however, the FLAG criteria are not satisfied. There is also a difference in the choice of renormalization scale between both analyses: Petreczky 19 [31] uses $\mu = m_h$, while Petreczky 20 [81] considers several choices of μ in the range $\mu = 2/3m_h$–$3m_h$, which leads to larger perturbative uncertainties in the determination of α_s [81]. Boito 20 [836] use published continuum extrapolated lattice results for $m_h = m_c$ and performs their own extraction of α_s. Limiting the choice of m_h to the charm-quark mass means that the FLAG criteria are not met ($\alpha_{\rm eff} \simeq 0.38$). However, their analysis gives valuable insight into the perturbative error. In addition

to the renormalization scale μ, Boito 20 also vary the renormalization scale μ_m at which the charm-quark mass is defined. The corresponding result $\alpha_s(M_Z) = 0.1177(20)$ agrees well with previous lattice determination but has a larger error, which is dominated by the perturbative uncertainty due to the variation of both scales.

Since the FLAG 21 report the results of Petreczky 20 have been published and pass all FLAG criteria. There are now three determinations of α_s from the heavy-quark current two-point functions that satisfy all the FLAG criteria and enter the FLAG average: $\alpha_{\overline{\rm MS}}(M_Z) = 0.11773(119)$ from Petreczky 20 [81], $\alpha_{\overline{\rm MS}}(M_Z) = 0.11822(74)$ from HPQCD 14 [18] and $\alpha_{\overline{\rm MS}}(M_Z) = 0.11830(70)$ from HPQCD 10 [15]. All three determinations agree well with each other within errors. Since these determinations are uncorrelated we take the weighted average of these results as an estimate for the strong coupling constants from the heavy-quark current two-point functions. The analysis in Petreczky 20 does not use Bayesian priors and considers five different choices of the renormalization scale, while HPQCD 10 and HPQCD 14 analyses use $\mu = 3m_c$. Therefore, the error of Petreczky 20 can be considered to be more conservative and we take it as the range for $\alpha_{\overline{\rm MS}}(m_Z)$. With this we arrive at $\alpha_{\overline{\rm MS}}(M_Z) = 0.11818(119)$ from the method of the heavy-quark current two-point functions. Comparing with the scale variations, the perturbative uncertainty is estimated to be 1–2 percent so a one percent range is roughly in line.

(vi) *Light-quark vacuum polarization*

Cali 20 [84] use the light-quark current two-point functions in position space, evaluated on a subset of CLS configurations for lattice spacings in the range 0.038–0.076 fm, and for Euclidean distances 0.13–0.19 fm, corresponding to renormalization scales $\mu = 1$–1.5 GeV. Both flavor-nonsinglet vector and axial-vector currents are considered and their difference is shown to vanish within errors. After continuum and chiral limits are taken, the effective coupling from the axial-vector two-point function is converted at 3-loop order to $\alpha_{\overline{\rm MS}}(\mu)$. The authors do this by numerical solution for $\alpha_{\overline{\rm MS}}$ and then perform a weighted average of the Λ-parameter estimates for the available energy range, which yields $\Lambda_{\overline{\rm MS}}^{(N_f=3)} = 342(17)$ MeV. Note that this is the first calculation in the vacuum polarization category that passes the current FLAG criteria. Yet the renormalization scales are rather low and one might suspect that nonperturbative effects that do not break chiral symmetry may still be sizeable. Our main issue is a rather optimistic estimate of perturbative truncation errors, based only on the variation of the Λ-parameter from the range of effective couplings considered. If the solution for the $\overline{\rm MS}$ coupling is done by series expansion in $\alpha_{\rm eff}$, the differences in $\alpha_{\overline{\rm MS}}$, formally of order $\alpha_{\rm eff}^5$, are still large at the scales considered. Hence, as a measure of the systematic uncertainty we take the difference $409 - 355$ MeV between $\Lambda_{\overline{\rm MS}}^{(N_f=3)}$ estimates at $\mu = 1.5$ GeV as a proxy for the total error, i.e., $\Lambda_{\overline{\rm MS}}^{(N_f=3)} = 342(54)$ MeV, which translates to our pre-range, $\alpha_s(m_Z) = 0.11863(360)$, from vacuum polarization. Looking at scale variation it appears that these are of O(10) percent if the scale is identified as done by the authors. The scale is simply too low for perturbation theory. It is an interesting observation that a variation around the scale of fastest apparent convergence, cf. Sec. IX B 3, yields much smaller ambiguities of the order of one percent. A reanalysis of the data might be warranted.

(vii) *Other methods*

Computations using other methods do not qualify for an average yet, predominantly due to a lacking ○ in the continuum extrapolation.

We form the average in two steps, due to the known correlation between ALPHA 17 and ALPHA 22. We thus first combine these two results by combining the respective Λ-parameters and then obtain $\alpha_s(m_Z) = 0.11836(69)$. Next we combine with the step-scaling result by PACS CS-09A, and get $\alpha_{\overline{\rm MS}}^{(5)}(m_Z) = 0.11834(67)$. This average is interesting as it combines the three results where the error is dominated by statistics. A weighted average with the remaining pre-ranges yields the central value, we quote as the new FLAG estimate,

$$\alpha_{\overline{\rm MS}}^{(5)}(M_Z) = 0.11833(67) = 0.1183(7). \quad (399)$$

where we have used the above statistics-dominated error as our range, rather than the 25 percent smaller error from the weighted average. All central values are remarkably consistent, as can also be seen in Fig. 40.

3. Conclusions

With the present results our range for the strong coupling is [repeating Eq. (399)]

$$\alpha_{\overline{\rm MS}}^{(5)}(M_Z) = 0.1183(7) \quad \text{Refs. [15, 18, 80–87]},$$

and the associated Λ-parameters

$$\Lambda_{\overline{\rm MS}}^{(5)} = 213(8)\ \text{MeV} \quad \text{Refs. [15, 18, 80–87]}, \quad (400)$$

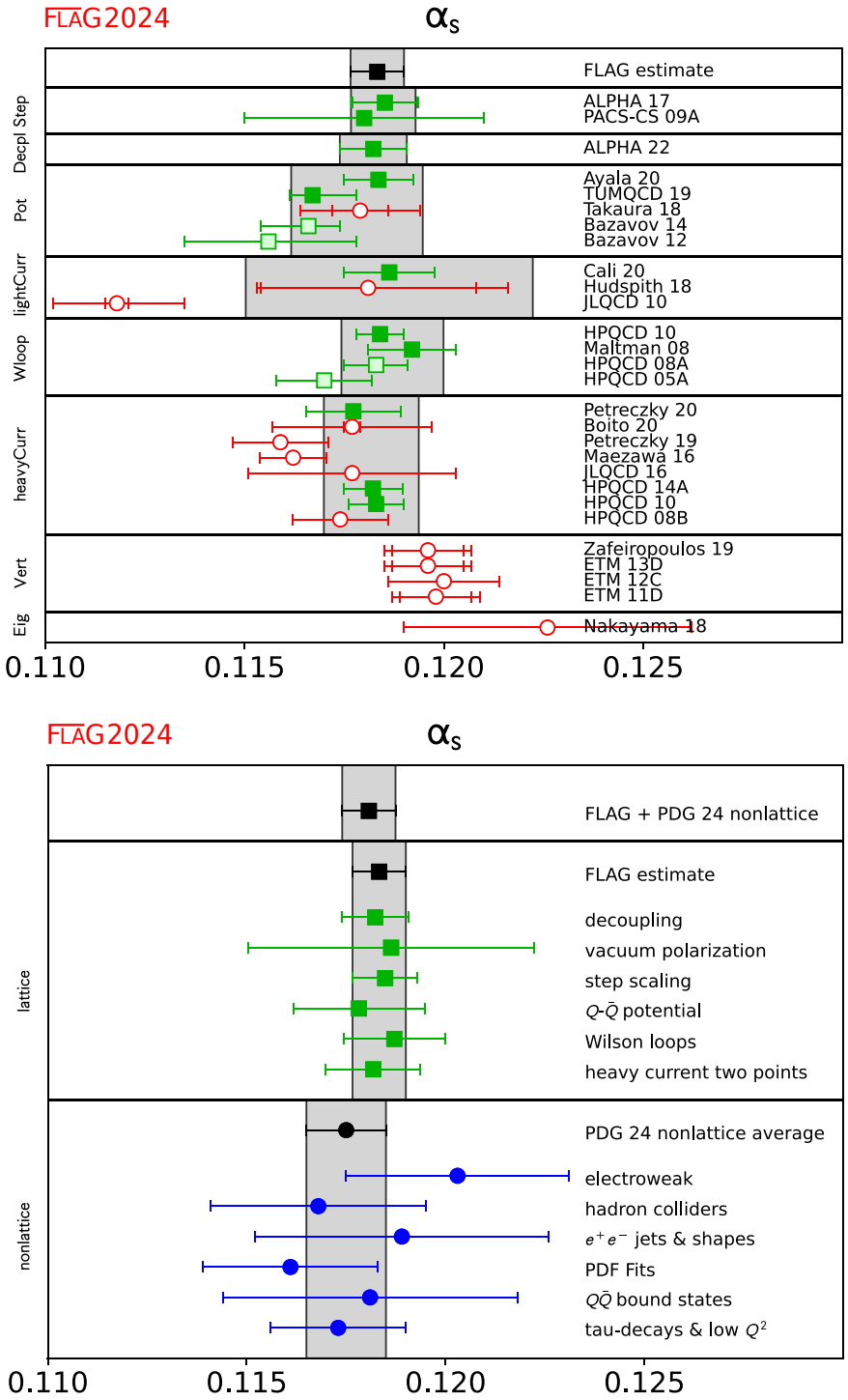


FIG. 40. $\alpha^{(5)}_{\overline{\text{MS}}}(M_Z)$, the coupling constant in the $\overline{\text{MS}}$ scheme at the Z-boson mass. Top: lattice results, pre-ranges from different calculation methods, and final average. Bottom: Comparison of the lattice pre-ranges and average with the nonlattice ranges and average. The first PDG 24 entry gives the outcome of their analysis excluding lattice results. At the very top we display the weighted average of PDG 24 nonlattice and FLAG lattice estimates, with the error taken from the FLAG estimate (statistics dominated), see Sec. IX J 3.

$$\Lambda^{(4)}_{\overline{\rm MS}} = 295(10)\ \text{MeV} \quad \text{Refs. [15, 18, 80–87]}, \tag{401}$$

$$\Lambda^{(3)}_{\overline{\rm MS}} = 338(10)\ \text{MeV} \quad \text{Refs. [15, 18, 80–87]}, \tag{402}$$

Compared with FLAG 21, the central values have only moved slightly and the errors have been reduced by ca. 15–20 percent. Overall we find excellent agreement between all published results that pass the FLAG criteria. The error for the reference value $\alpha_{\overline{\rm MS}}(M_Z)$ has reached the level of 0.6 percent, and, as we emphasize again, is dominated by the statistical errors originating from the stochastic process inherent in lattice simulations. The same cannot be said about nonlattice determinations, for which PDG 24 quote the value $\alpha^{(5)}_{\overline{\rm MS}}(M_Z) = 0.1175(10)$. Combining FLAG and PDG nonlattice estimates, we obtain

$$\alpha^{(5)}_{\overline{\rm MS}}(M_Z) = 0.1181(7), \qquad \text{FLAG 24} + \text{PDG 24}, \tag{403}$$

where we assign the error of the FLAG estimate as our range. In Fig. 40, we have collected and summarized the results that go into the FLAG estimate and the PDG 24 average. The agreement with nonlattice results is very good. Despite our conservative error estimate the FLAG lattice estimate has an error that is 30% smaller than the PDG 24 nonlattice result. Compared to high-energy experiments, lattice QCD has the advantage that the complicated transition between hadronic and quark and gluon degrees of freedom never needs to be dealt with explicitly. All hadronic input quantities are very well measured properties of hadrons, such as their masses and decay widths. We would like to encourage experimentalists and phenomenologists at collider experiments to make use of the FLAG lattice estimate. The higher accuracy and precision, with improvements still possible and expected in the near future, may help our understanding of other important physics aspects at the LHC and in other experiments. Currently, many experiments attempt their own determination of α_s, and the spread of the results is then taken as indication of the size of systematic effects. While this provides valuable information, one may ask whether one can learn more from the data about the origin of the systematic uncertainties, by using the precise lattice result for α_s as input for the analysis. This may clarify where tensions or inconsistencies arise and help our understanding of nonperturbative effects, e.g., in hadronization processes, or in some corners of parameter space. There is also the theoretical possibility that QCD does not provide the full picture of the strong interactions. While experimental data would be affected by any new physics, lattice QCD, by design, excludes such effects. Hence, any inconsistencies encountered in the analysis might also point to such new effects.

We finish by commenting on perspectives for the future. This edition of the FLAG report has seen the first result from the decoupling strategy, which complements the step-scaling result. In fact, the decoupling result also relies on the step-scaling technique, however, here it is applied in the $N_f = 0$ theory and therefore technically simpler, and with different systematics. The nice agreement between $N_f = 3$ step-scaling and decoupling results is therefore a very strong consistency check. Of course, further results with different schemes and systematics would be very welcome. For step scaling with $N_f = 0$, Dalla Brida 19 have used two different finite-volume schemes with SF boundary conditions, and there is now a new result by Bribian 21 with twisted periodic b.c.'s. There are also results with the GF scheme in infinite volume, where the β-function can be measured directly, by Hasenfratz 23 and Wong 23. In some sense, the case of $N_f = 0$ flavors is more difficult than full QCD, in that the asymptotic regime is often harder to reach. Of course, part of the problem lies in the smallness of statistical errors, which means that even moderate systematic errors easily stand out. In particular, in GF schemes, both in finite and infinite volume, the parametric uncertainties in the Λ-parameter of order α^{n_l}, Eq. (291), can be still quite large at the largest scales reached while showing the expected asymptotic behavior $\propto \alpha^{n_l}$ over a wide range. Rather than assigning a large systematic uncertainty at the highest scale reached, one might be inclined to allow for an extrapolation in α^{n_l}, together with a data-driven criterion to assess its quality. We will reconsider this issue in the next edition of the FLAG report.

Finally we emphasize the importance that errors remain dominated by statistics. Only in this case a probabilistic interpretation is obvious. This is currently not the case for the majority of lattice calculations, the exception being the step-scaling and decoupling approaches. For those determinations, further improvements will require access to higher energy scales, for instance, by implementing some elements of the step-scaling approach.

X. NUCLEON MATRIX ELEMENTS

Working group members: S. Collins, R. Gupta, A. Nicholson, H. Wittig

A large number of experiments testing the Standard Model (SM) and searching for physics beyond the Standard Model (BSM) involve either free nucleons (proton and neutron beams) or the scattering of electrons, muons, neutrinos and dark matter off nuclear targets. Necessary ingredients in the analysis of the experimental results are the matrix elements of various probes (fundamental currents or operators in a low-energy effective theory) between nucleon or nuclear states. The goal of lattice-QCD calculations in this context is to provide high-precision predictions of these matrix elements, the simplest of which give the nucleon charges and form factors. Determinations of the charges, the first Mellin moments of parton distribution functions, are the most mature and in this review we update results for twelve quantities, the isovector and flavor-diagonal axial vector, scalar and tensor charges,

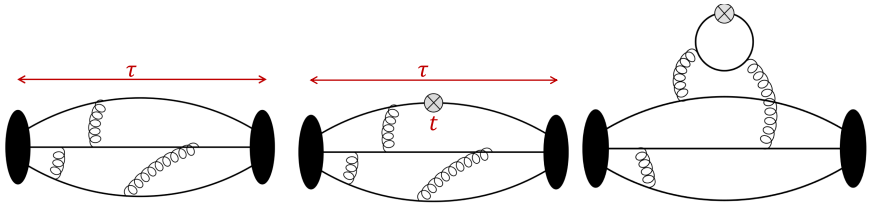


FIG. 41. The two- and three-point correlation functions (illustrated by Feynman diagrams) that need to be calculated to extract the ground-state nucleon matrix elements. Left: the nucleon two-point function. Middle: the connected three-point function with source-sink separation τ and operator-insertion time slice t. Right: the quark-disconnected three-point function with operator insertion at t.

given in the two previous FLAG reports in 2019 and 2021 [4,5]. In this edition in Sec. X E, we also add a review of the second Mellin moments for the vector, axial and tensor currents that give the momentum fraction, the helicity moment and the transversity moment as a sufficient number of calculations have been performed and the results are considered robust.

Other quantities that are not being reviewed but for which significant progress has been made in the last five years are the nucleon axial vector and electromagnetic form factors [90,91,93,848–858] and parton distribution functions from matrix elements of nonlocal operators [859–865]. The more challenging calculations of nuclear matrix elements that are needed, for example, to calculate the cross-sections of neutrinos or dark matter scattering off nuclear targets, are proceeding along three paths. The first is based on direct evaluations of matrix elements calculated with initial and final states consisting of multiple nucleons [866,867]. The second proceeds by matching few-nucleon observables computed in lattice QCD to nuclear effective field theories and extrapolating in the mass number A, while the third strategy uses the HAL QCD method [868] or the direct method [869] to extract nuclear forces and currents from lattice calculations as input for *ab initio* many-body methods. We expect future FLAG reviews to include results on these quantities once a sufficient level of control over all the systematics is reached.

A. Isovector and flavor-diagonal charges of the nucleon

The simplest nucleon matrix elements are composed of local quark-bilinear operators, $\overline{q_i}\Gamma_\alpha q_j$, where Γ_α can be any of the sixteen Dirac matrices. In this report, we consider two types of flavor structures: (a) when $i = u$ and $j = d$. These $\overline{u}\Gamma_\alpha d$ operators arise in $W^\pm$ mediated weak interactions such as in neutron or pion decay. We restrict the discussion to the matrix elements of the axial-vector (A), scalar (S) and tensor (T) currents, which give the isovector charges, $g^{u-d}_{A,S,T}$.[75] (b) When $i = j$ for $j \in \{u, d, s\}$, there is no change of flavor, e.g., in processes mediated via the electromagnetic or weak neutral interaction or dark matter. These γ or Z^0 or possible dark matter mediated processes couple to all flavors with their corresponding charges. Since these probes interact with nucleons within nuclear targets, one has to include the effects of QCD (to go from the couplings defined at the quark and gluon level to those for nucleons) and nuclear forces in order to make contact with experiments. The isovector and flavor-diagonal charges, given by the matrix elements of the corresponding operators calculated between nucleon states, are these nucleon level couplings. Here we review results for the light and strange flavors, $g^u_{A,S,T}$, $g^d_{A,S,T}$, and $g^s_{A,S,T}$ and the isovector charges $g^{u-d}_{A,S,T}$.

The isovector and flavor-diagonal operators also arise in BSM theories due to the exchange of novel force carriers or as effective interactions due to loop effects. The associated couplings are defined at the energy scale $\Lambda_{\rm BSM}$, while lattice-QCD calculations of matrix elements are carried out at a hadronic scale, μ, of a few GeV. The tool for connecting the couplings at the two scales is the renormalization group. Since the operators of interest are composed of quark fields (and more generally also of gluon fields), the predominant change in the corresponding couplings under a scale transformation is due to QCD. To define the operators and their couplings at the hadronic scale μ, one constructs renormalized operators, whose matrix elements are finite in the continuum limit. This requires calculating both multiplicative renormalization factors, including the anomalous dimensions and finite terms, and the mixing with other operators. We discuss the details of the renormalization factors needed for each of the six operators reviewed in this report in Sec. X A 3.

Once renormalized operators are defined, the nucleon matrix elements of interest are extracted using expectation values of two-point and three-point correlation functions illustrated in Fig. 41, where the latter can have both quark-line connected and disconnected contributions. In order to isolate the ground-state matrix element, these correlation functions are analyzed using their spectral decomposition. The current practice is to fit the n-point correlation functions (or ratios involving three- and two-point functions) including contributions from one or two excited

[75] In the isospin-symmetric limit $\langle p|\bar{u}\Gamma d|n\rangle = \langle p|\bar{u}\Gamma u - \bar{d}\Gamma d|p\rangle = \langle n|\bar{d}\Gamma d - \bar{u}\Gamma u|n\rangle$ for nucleon and proton states $|p\rangle$ and $|n\rangle$, respectively. The latter two (equivalent) isovector matrix elements are computed on the lattice.

states. In some cases, such as axial and vector operators, Ward identities provide relations between correlation functions, or ground-state matrix elements, or facilitate the calculation of renormalization factors. It is important to ensure that all such Ward identities are satisfied in lattice calculations, especially as in the case of axial form factors where they provide checks of whether excited-state contamination has been removed in obtaining matrix elements within ground-state nucleons [92,848,870].

The ideal situation occurs if the time separation τ between the nucleon source and sink positions, and the distance of the operator-insertion time from the source and the sink, t and $\tau - t$, respectively, are large enough such that the contribution of all excited states is negligible. In the limit of large τ, the ratio of noise to signal in the nucleon two- and three-point correlation functions grows exponentially as $e^{(M_N - \frac{3}{2}M_\pi)\tau}$ [470,871], where M_N and M_π are the masses of the nucleon and the pion, respectively. Therefore, in particular at small pion masses, maintaining reasonable errors for large τ is challenging, with most current calculations limited to $\tau \lesssim 1.5$ fm. In addition, the mass gap between the ground and excited (including multiparticle) states is smaller than in the meson sector and at these separations, excited-state effects can be significant. The approach commonly taken is to first obtain results with high statistics at multiple values of τ, using the methods described in Sec. X A 1. Then, as mentioned above, excited-state contamination is removed by fitting the data using a fit form involving one or two excited states. The different strategies that have been employed to minimize excited-state contamination are discussed in Sec. X A 2.

Usually, the quark-connected part of the three-point function (corresponding to the plot in the centre of Fig. 41) is computed via the so-called "sequential propagator method," which uses the product of two quark propagators between the positions of the initial and the final nucleons as a source term for another inversion of the lattice Dirac operator. This implies that the position of the sink time slice is fixed at some chosen value. Varying the value of the source-sink separation τ then requires the calculation of another sequential propagator.

The evaluation of quark-disconnected contributions is computationally more challenging as the disconnected loop (which contains the operator insertion, as illustrated in Fig. 41 right) is needed at all points on a particular time slice or, in general, over the whole lattice. The quark loop is computed stochastically and then correlated with the nucleon two-point function before averaging this three-point function over the ensemble of gauge configurations. The associated statistical error, therefore, is a combination of that due to the stochastic evaluation (on each configuration) and that from the gauge average. The number of stochastic sources employed on each configuration is, typically, optimized to reduce the overall error for a given computational cost. The statistical errors of the connected contributions, in contrast, usually come only from the ensemble average since they are often evaluated exactly on each configuration, for a small number of source positions. If these positions are well-separated in space and time, then each measurement is statistically independent. The methodology applied for these calculations and the variance reduction techniques are summarized in Sec. X A 1. By construction, arbitrary values of τ across the entire temporal extent of the lattice can be realized when computing the quark-disconnected contribution, since the source-sink separation is determined by the part of the diagram that corresponds to the two-point nucleon correlator. However, in practice, statistical fluctuations of both the connected and disconnected contributions increase sharply, so that the signal is lost in the statistical noise for $\tau \gtrsim 1.5$ fm.

The lattice calculation is performed for a given number of quark flavors and at a number of values of the lattice spacing a, the pion mass M_π, and the lattice size, represented by $M_\pi L$. The results need to be extrapolated to the physical point defined by $a = 0$, $M_\pi = 135$ MeV and $M_\pi L \to \infty$. This is done by fitting the data simultaneously in these three variables using a theoretically motivated *Ansatz*. The *Ansätze* used and the fitting strategy are described in Sec. X A 4.

The procedure for rating the various calculations and the criteria specific to this chapter are discussed in Sec. X B, which also includes a brief description of how the final averages are constructed. The physics motivation for computing the isovector charges, $g_{A,S,T}^{u-d}$, and the review of the lattice results are presented in Sec. X C. This is followed by a discussion of the relevance of the flavor-diagonal charges, $g_{A,S,T}^{u,d,s}$, and a presentation of the lattice results in Sec. X D.

1. Technical aspects of the calculations of nucleon matrix elements

The calculation of n-point functions needed to extract nucleon matrix elements requires making four essential choices. The first involves choosing between the suite of background gauge field ensembles one has access to. The range of lattice parameters should be large enough to facilitate the extrapolation to the continuum and infinite-volume limits, and, ideally, the evaluation at the physical pion mass taken to be $M_\pi = 135$ MeV. Such ensembles have been generated with a variety of discretization schemes for the gauge and fermion actions that have different levels of improvement and preservation of continuum symmetries. The actions employed at present include (i) Wilson gauge with nonperturbatively improved Sheikholeslami-Wohlert fermions (nonperturbatively improved clover fermions) [718,872–877], (ii) Iwasaki gauge with nonperturbatively improved clover fermions [878,879], (iii) Iwasaki gauge with twisted-mass fermions with a clover term [880–884], (iv) tadpole Symanzik

improved gauge with highly improved staggered quarks (HISQ) [88,99,100,885–890], (v) Iwasaki gauge with domain-wall fermions (DW) [92,104,891–895] and (vi) Iwasaki gauge with overlap fermions [896–898]. For details of the lattice actions, see the glossary in the Appendix A. 1 of FLAG 19 [4].

The second choice is of the valence-quark action. Here there are two choices, to maintain a unitary formulation by choosing exactly the same action as is used in the generation of gauge configurations or to choose a different action and tune the quark masses to match the pseudoscalar meson spectrum in the two theories. Such mixed-action formulations are nonunitary but are expected to have the same continuum limit as QCD. The reason for choosing a mixed-action approach is expediency. For example, the generation of $2+1+1$ flavor HISQ and $2+1$ flavor DW ensembles with physical quark masses has been possible even at the coarse lattice spacing of $a = 0.15$ fm and there are indications that cutoff effects are reasonably small. These ensembles have been analyzed using clover-improved Wilson fermions, DW and overlap fermions since the construction of baryon correlation functions with definite spin and parity is much simpler compared to staggered fermions.

The third choice is the combination of the algorithm for inverting the Dirac matrix and variance reduction techniques. Efficient inversion and variance reduction techniques are needed for the calculation of nucleon correlation functions with high precision because the signal-to-noise ratio degrades exponentially as $e^{(\frac{3}{2}M_\pi - M_N)\tau}$ with the source-sink separation τ. Thus, the number of measurements needed for high precision is much larger than in the meson sector. Commonly used inversion algorithms include the multigrid [899] and the deflation-accelerated Krylov solvers [900], which can handle linear systems with large condition numbers very efficiently, thereby enabling calculations of correlation functions at the physical pion mass.

The sampling of the path integral is limited by the number N_{conf} of gauge configurations generated. One requires sufficiently large N_{conf} such that the phase space (for example, different topological sectors) has been adequately sampled and all the correlation functions satisfy the expected lattice symmetries such as C, P, T, momentum and translation invariance. Thus, one needs gauge field generation algorithms that give decorrelated large-volume configurations cost-effectively. On such large lattices, to reduce errors one can exploit the fact that the volume is large enough to allow multiple measurements of nucleon correlation functions that are essentially statistically independent. Two other common variance reduction techniques that reduce the cost of multiple measurements on each configuration are the truncated solver with bias correction method [901] and deflation of the Dirac matrix for the low-lying modes followed by sloppy solution with bias correction for the residual matrix consisting predominately of the high-frequency modes [901,902].

A number of other variance reduction methods are also being used and developed. These include deflation with hierarchical probing for disconnected diagrams [903,904], the coherent source sequential propagator method [905,906], low-mode averaging [907,908], the hopping-parameter expansion [909,910] and partitioning [911] (also known as dilution [912]).

The final choice is of the interpolating operator used to create and annihilate the nucleon state, and of the operator used to calculate the matrix element. Along with the choice of the interpolating operator (or operators if a variational method is used) one also chooses a "smearing" of the source used to construct the quark propagator. By tuning the width of the smearing, one can optimize the spatial extent of the nucleon interpolating operator to reduce the overlap with the excited states. Two common smearing algorithms that are equally performant are Gaussian (Wuppertal) [913] and Jacobi [914] smearing. Specific smearing techniques for hadrons boosted to (large) nonzero momentum have also been designed [562,915,916].

Having made all the above choices, for which a reasonable recipe exists, one calculates a statistical sample of correlation functions from which the desired ground-state nucleon matrix element is extracted. Excited states, unfortunately, contribute significantly to nucleon correlation functions in present studies. To remove their contributions, calculations are performed with multiple source-sink separations τ and fits are made to the correlation functions using their spectral decomposition as discussed in the next section.

2. Controlling excited-state contamination

Nucleon matrix elements are determined from a combination of two- and three-point correlation functions. To be more specific, let $B^\alpha(\vec{x}, t)$ denote an interpolating operator for the nucleon. Placing the initial state at time slice $t = 0$, the two-point correlation function of a nucleon with momentum $\vec{p}$ reads

$$C_2(\vec{p};\tau) = \sum_{\vec{x},\vec{y}} e^{i\vec{p}\cdot(\vec{x}-\vec{y})} \mathbb{P}_{\beta\alpha} \langle B^\alpha(\vec{x},\tau)\bar{B}^\beta(\vec{y},0)\rangle, \quad (404)$$

where the projector $\mathbb{P}$ selects the polarization, and α, β denote Dirac indices. The three-point function of two nucleons and a quark-bilinear operator O_Γ is defined as

$$C_3^\Gamma(\vec{q};t,\tau) = \sum_{\vec{x},\vec{y},\vec{z}} e^{i\vec{p}'\cdot(\vec{x}-\vec{z})} e^{-i\vec{p}\cdot(\vec{y}-\vec{z})} \times \mathbb{P}_{\beta\alpha} \langle B^\alpha(\vec{x},\tau) O_\Gamma(\vec{z},t) \bar{B}^\beta(\vec{y},0)\rangle, \quad (405)$$

where $\vec{p}, \vec{p}'$ denote the momenta of the nucleons at the source and sink, respectively, and $\vec{q} \equiv \vec{p}' - \vec{p}$ is the momentum transfer. The bilinear operator is inserted at

time slice t, and τ denotes the source-sink separation. The corresponding quark-line diagrams for both C_2 and C_3^Γ, in terms of the nonperturbative quark propagators, $D^{-1}(y,x)$ where D denotes the lattice Dirac operator, are shown in Fig. 41.

The framework for the analysis of excited-state contamination is based on spectral decomposition. After inserting complete sets of eigenstates of the transfer matrix, the expressions for the correlators C_2 and C_3^Γ read

$$C_2(\vec{p};\tau) = \frac{1}{L^3}\sum_n \mathbb{P}_{\beta\alpha}\langle\Omega|B^\alpha|n\rangle\langle n|\bar{B}^\beta|\Omega\rangle e^{-E_n\tau}, \quad (406)$$

$$C_3^\Gamma(\vec{q};t,\tau) = \frac{1}{L^3}\sum_{n,m}\mathbb{P}_{\beta\alpha}\langle\Omega|B^\alpha|n\rangle\langle n|O_\Gamma|m\rangle \times \langle m|\bar{B}^\beta|\Omega\rangle e^{-E_n(\tau-t)}e^{-E_m t}, \quad (407)$$

where $|\Omega\rangle$ denotes the vacuum state, and E_n represents the energy of the nth eigenstate $|n\rangle$ in the nucleon channel. Here we restrict the discussion to vanishing momentum transfer, i.e., the forward limit $\vec{q}=0$, and label the ground state by $n=0$. The matrix element of interest $g_\Gamma \equiv \langle 0|O_\Gamma|0\rangle$ can, for instance, be obtained from the asymptotic behavior of the ratio

$$R_\Gamma(t,\tau) \equiv \frac{C_3^\Gamma(\vec{q}=0;t,\tau)}{C_2(\vec{p}=0;\tau)} \overset{t,(\tau-t)\to\infty}{\longrightarrow} g_\Gamma + \mathrm{O}(e^{-\Delta t}, e^{-\Delta(\tau-t)}, e^{-\Delta\tau}), \quad (408)$$

where $\Delta \equiv E_1 - E_0$ denotes the energy gap between the ground state and the first excitation. We also assume that the bilinear operator O_Γ is appropriately renormalized (see Sec. X A 3).

Excited states with the same quantum numbers as the nucleon include resonances such as a Roper-like state with a mass of about 1.5 GeV, or multi-particle states consisting of a nucleon and one or more pions [917,918]. The latter can provide significant contributions to the two- and three-point correlators in Eqs. (404) and (405) or their ratios (408) as the pion mass approaches its physical value. Ignoring the interactions between the individual hadrons, one can easily identify the lowest-lying multi-particle states: they include the $N\pi\pi$ state with all three particles at rest at $\sim$1.2 GeV, as well as $N\pi$ states with both hadrons having nonzero and opposite momentum. Depending on the spatial box size L in physical units (with the smallest nonzero momentum equal to $2\pi/L$), there may be a dense spectrum of $N\pi$ states before the first nucleon resonance is encountered. Corrections to nucleon correlation functions due to the pion continuum have been studied using chiral effective theory [917–920] and Lüscher's finite-volume quantization condition [921].

The well-known noise problem of baryonic correlation functions implies that the long-distance regime, $t,(\tau-t)\to\infty$, where the correlators are dominated by the ground state, is difficult to reach. Current lattice calculations of baryonic three-point functions are typically confined to source-sink separations of $\tau \lesssim 1.5$ fm, despite the availability of efficient noise reduction methods. In view of the dense excitation spectrum encountered in the nucleon channel, one has to demonstrate that the contributions from excited states are sufficiently suppressed to guarantee an unbiased determination of nucleon matrix elements. There are several strategies to address this problem:

(i) Multi-state fits to correlator ratios or individual two- and three-point functions;
(ii) Three-point correlation functions summed over the operator-insertion time t;
(iii) Increasing the projection of the interpolator B^α onto the ground state.

The first of the above methods includes excited state contributions explicitly when fitting to the spectral decomposition of the correlation functions, Eqs. (406), (407) or, alternatively, their ratio [see Eq. (408)]. In its simplest form, the resulting expression for R_Γ includes the contributions from the first excited state, i.e.,

$$R_\Gamma(t,\tau) = g_\Gamma + c_{01}e^{-\Delta t} + c_{10}e^{-\Delta(\tau-t)} + c_{11}e^{-\Delta\tau} + \ldots, \quad (409)$$

where c_{01}, c_{10}, c_{11} and Δ are treated as additional parameters when fitting $R_\Gamma(t,\tau)$ simultaneously over intervals in the source-sink separation τ and the operator-insertion time slice t. Multi-exponential fits become more difficult to stabilize for a growing number of excited states, since an increasing number of free parameters must be sufficiently constrained by the data. Therefore, a high level of comparable statistical precision over several source-sink separations is required. One common way to address this issue is to introduce Bayesian constraints, as described in [922]. Alternatively, one may try to reduce the number of free parameters, for instance, by determining the energy gap Δ from nucleon two-point function and/or using a common gap for several different nucleon matrix elements [923].

Ignoring the explicit contributions from excited states and fitting $R_\Gamma(t,\tau)$ to a constant in t for fixed τ amounts to applying what is called the "plateau method." The name derives from the ideal situation that sufficiently large source-sink separations τ can be realized, which would cause $R_\Gamma(t,\tau)$ to exhibit a plateau in t independent of τ. The ability to control excited-state contamination is rather limited in this approach, since the only option is to check for consistency in the estimate of the plateau as τ is varied. In view of the exponential degradation of the statistical

signal for increasing τ, such stability checks are difficult to perform reliably.

Summed operator insertions, originally proposed in Ref. [924], have also emerged as a widely used method to address the problem of excited-state contamination. One way to implement this method [925,926] proceeds by summing $R_\Gamma(t,\tau)$ over the insertion time t, resulting in the correlator ratio $S_\Gamma(\tau)$,

$$S_\Gamma(\tau) \equiv \sum_{t=a}^{\tau-a} R_\Gamma(t,\tau). \tag{410}$$

The asymptotic behavior of $S_\Gamma(\tau)$, including sub-leading terms, for large source-sink separations τ can be easily derived from the spectral decomposition of the correlators and is given by [927]

$$S_\Gamma(\tau) \overset{\tau \gg 1/\Delta}{\longrightarrow} K_\Gamma + (\tau-a) g_\Gamma + (\tau-a) e^{-\Delta\tau} d_\Gamma + e^{-\Delta\tau} f_\Gamma + \ldots, \tag{411}$$

where K_Γ is a constant, and the coefficients d_Γ and f_Γ contain linear combinations of transition matrix elements involving the ground and first excited states. Thus, the matrix element of interest g_Γ is obtained from the linear slope of $S_\Gamma(\tau)$ with respect to the source-sink separation τ. While the leading corrections from excited states $e^{-\Delta\tau}$ are smaller than those of the original ratio $R_\Gamma(t,\tau)$ [see Eq. (408)], extracting the slope from a linear fit to $S_\Gamma(\tau)$ typically results in relatively large statistical errors. In principle, one could include the contributions from excited states explicitly in the expression for $S_\Gamma(\tau)$. However, in practice it is often difficult to constrain an enlarged set of parameters reliably, in particular if one cannot afford to determine $S_\Gamma(\tau)$ except for a handful of source-sink separations.

The original summed operator-insertion technique described in Refs. [913,924,928,929] avoids the explicit summation over the operator-insertion time t at every fixed value of τ. Instead, one replaces one of the quark propagators that appear in the representation of the two-point correlation function $C_2(t)$ by a "sequential" propagator, according to

$$D^{-1}(y,x) \to D_\Gamma^{-1}(y,x) = \sum_z D^{-1}(y,z)\Gamma D^{-1}(z,x). \tag{412}$$

In this expression, the position $z \equiv (\vec{z},t)$ of the insertion of the quark-bilinear operator is implicitly summed over, by inverting the lattice Dirac operator D on the source field $\Gamma D^{-1}(z,x)$. While this gives access to all source-sink separations $0 \le \tau \le T$, where T is the temporal extent of the lattice, the resulting correlator also contains contact terms, as well as contributions from $\tau < t < T$ that must be controlled. This method has been adopted recently by the CalLat collaboration in their calculation of the isovector axial charge [88,889].[76]

As in the case of explicitly summing over the operator-insertion time, the matrix element of interest is determined from the slope of the summed correlator. For instance, in Ref. [88], the axial charge was determined from the summed three-point correlation function, by fitting to its asymptotic behavior [930] including sub-leading terms.

In practice, one often uses several methods simultaneously, e.g., multi-state fits and the summation method based on Eq. (411), in order to check the robustness of the result. All of the approaches for controlling excited-state contributions proceed by fitting data obtained in a finite interval in τ to a function that describes the approach to the asymptotic behavior derived from the spectral decomposition. Obviously, the accessible values of τ must be large enough so that the model function provides a good representation of the data that enter such a fit. It is then reasonable to impose a lower threshold on τ above which the fit model is deemed reliable. We will return to this issue when explaining our quality criteria in Sec. X B.

The third method for controlling excited-state contamination aims at optimizing the projection onto the ground state in the two-point and three-point correlation functions [875,906,933,934]. The RQCD collaboration has chosen to optimize the parameters in the Gaussian smearing procedure, so that the overlap of the nucleon interpolating operator onto the ground state is maximized [875]. In this way it may be possible to use shorter source-sink separations without incurring a bias due to excited states.

The variational method, originally designed to provide detailed information on energy levels of the ground and excited states in a given channel [935–938], has also been adapted to the determination of hadron-to-hadron transition elements [927]. In the case of nucleon matrix elements, the authors of Ref. [933] have employed a basis of operators to construct interpolators that couple to individual eigenstates in the nucleon channel. The method has produced promising results when applied to calculations of the axial and other forward matrix elements at a fixed value of the pion mass [906,933,934,939]. However, a more comprehensive study aimed at providing an estimate at the physical point has, until now, not been performed.

The investigation of excited-state effects is an active subfield in calculations of nucleon matrix elements, and many refinements and extensions have been implemented since the first edition of the FLAG report. For instance, it has been shown that the previously observed failure of the axial and pseudoscalar form factors to satisfy the PCAC relation linking them could be avoided by including the

[76] In Ref. [930] it is shown that the method can be linked to the Feynman-Hellmann theorem. A direct implementation of the Feynman-Hellmann theorem by means of a modification of the lattice action is discussed and applied in Refs. [931,932].

enhanced contribution of $N\pi$ excitations, either by including additional information on the nucleon excitation spectrum extracted from the three-point function of the axial current [870], or with guidance from chiral effective field theory analyses of nucleon three-point functions [848]. Following this, in Refs. [940,941] it has been demonstrated that this enhanced $N\pi$ contribution can be significantly reduced when performing a GEVP analysis with a basis that includes a five-quark/antiquark interpolator with the quantum numbers of the nucleon in addition to a three-quark interpolator. For the flavor-diagonal u- and d-quark scalar operators, a χPT study of excited-state corrections [101] suggests that there is a significant enhancement of the disconnected contribution, which impacts the calculation of the pion-nucleon sigma term $\sigma_{\pi N}$ as discussed in Sec. X D 2.

The variety of methods that are employed to address the problem of excited-state contamination has greatly improved our understanding of and control over excited-state effects in calculations of nucleon matrix elements. However, there is still room for further improvement: For instance, dedicated calculations of the excitation spectrum using the variational method could replace the often rudimentary spectral information gained from multi-state fits to the two- and three-point functions used primarily for the determination of the matrix elements. In general, the development of methods to explicitly include multi-particle states, such as $N\pi$ and $N\pi\pi$ with appropriate momentum configurations, coupled with the determination of the associated (transition) matrix elements, is needed to significantly enhance the precision of a variety of nucleon matrix elements. Such approaches would, to some extent, eliminate the need to extend the source-sink separation τ into a regime that is currently inaccessible due to the signal-to-noise problem.

Since the ongoing efforts to study excited-state contamination are producing deeper insights, we have decided to follow a more cautious approach in the assessment of available calculations of nucleon matrix elements. This is reflected in a modification of the quality criterion for excited-state contamination that is described and discussed in Sec. X B.

3. Renormalization and Symanzik improvement of local currents

In this section, we discuss the renormalization of lattice operators and their matching to a continuum reference scheme such as $\overline{\text{MS}}$, and the application of Symanzik improvement to remove $\mathcal{O}(a)$ contributions. For the charges, the relevant operators are the axial (A_μ), tensor ($T_{\mu\nu}$) and scalar (S) local operators of the form $\mathcal{O}_\Gamma = \bar{q}\Gamma q$, with $\Gamma = \gamma_\mu\gamma_5$, $i\sigma_{\mu\nu}$ and 1, respectively, whose matrix elements are evaluated in the forward limit. The steps in the renormalization of the 1-link operators, defined in Sec. X E, used to calculate the second Mellin moments of distribution functions are similar to those for the charges and we refer readers to Refs. [923,942].

For the charges, the general form for renormalized operators in the isovector flavor combination, at a scale μ, reads

$$\mathcal{O}_\Gamma^{\overline{\text{MS}}}(\mu) = Z_{\mathcal{O}}^{\overline{\text{MS}},\text{Latt}}(\mu a, g^2)[\mathcal{O}_\Gamma(a) + ab_{\mathcal{O}} m\mathcal{O}_\Gamma(a) + ac_{\mathcal{O}}\mathcal{O}_\Gamma^{\text{imp}}(a)] + \mathcal{O}(a^2), \tag{413}$$

where $Z_{\mathcal{O}}^{\overline{\text{MS}},\text{Latt}}(\mu a, g^2)$ denotes the multiplicative renormalization factor determined in the chiral limit, $m \to 0$, and the second and third terms represent all possible quark-mass-dependent and -independent Symanzik improvement terms, respectively, at $\mathcal{O}(a)$.[77] The chiral properties of overlap, domain-wall fermions (with improvement up to $\mathcal{O}(m_{\text{res}}^n)$ where m_{res} is the residual mass) and twisted-mass fermions (at maximal twist [947,948]) mean that the $\mathcal{O}(a)$-improvement terms are absent, while for nonperturbatively improved Sheikholeslami-Wohlert-Wilson (nonperturbatively improved clover) fermions all terms appear in principle. For the operators of interest here there are several mass-dependent terms but at most one dimension-four $\mathcal{O}_\Gamma^{\text{imp}}$; see, e.g., Refs. [949,950]. However, the latter involve external derivatives whose corresponding matrix elements vanish in the forward limit. Note that no mention is made of staggered fermions as they are not, currently, widely employed as valence quarks in nucleon matrix element calculations.

In order to illustrate the above remarks we consider the renormalization and improvement of the isovector axial current. This current has no anomalous dimension and hence the renormalization factor, $Z_A = Z_A^{\overline{\text{MS}},\text{Latt}}(g^2)$, is independent of the scale. The factor is usually computed nonperturbatively via the axial Ward identity [951] or the Rome-Southampton method [383] (see Sec. A. 3 of FLAG 19 [4] for details). In some studies, the ratio with the corresponding vector renormalization factor, Z_A/Z_V, is determined for which some of the systematics cancel. In this case, one constructs the combination $Z_A g_A/(Z_V g_V)$, where $Z_V g_V = 1$ and g_A and g_V are the lattice forward matrix elements, to arrive at the renormalized axial charge [888]. For domain-wall fermions the ratio is employed in order to remove $\mathcal{O}(am_{\text{res}})$ terms and achieve leading discretization effects starting at $\mathcal{O}(a^2)$ [12]. Thus, as mentioned above, $\mathcal{O}(a)$-improvement terms are only

[77]Here, $a(g^2)$ refers to the lattice spacing in the chiral limit, however, lattice simulations are usually carried out by fixing the value of g^2 while varying the quark masses. This means $a = a(\tilde{g}^2)$ where $\tilde{g}^2 = g^2(1 + b_g am_q)$ [943,944] is the improved coupling that varies with the average sea-quark mass m_q. The difference between the renormalization factors calculated with respect to g^2 and $\tilde{g}^2$ can effectively be absorbed into the $b_{\mathcal{O}}$ coefficients [945,946].

present for nonperturbatively improved clover fermions. For the axial current, Eq. (413) takes the explicit form,

$$A_\mu^{\overline{\rm MS}}(\mu) = Z_A^{\overline{\rm MS},\rm Latt}(g^2)[(1 + ab_A m_{\rm val} + 3a\tilde{b}_A m_{\rm sea})A_\mu(a) + ac_A\partial_\mu P(a)] + \mathcal{O}(a^2), \tag{414}$$

where $m_{\rm val}$ and $m_{\rm sea}$ are the average valence- and sea-quark masses derived from the vector Ward identity [944,950,951], and P is the pseudoscalar operator $\bar{q}\gamma_5 q$. The matrix element of the derivative term is equivalent to $q_\mu\langle N(p')|P|N(p)\rangle$ and hence vanishes in the forward limit when the momentum transfer $q_\mu = 0$. The improvement coefficients b_A and $\tilde{b}_A$ are known perturbatively for a variety of gauge actions [949,952,953] and nonperturbatively for the tree-level Symanzik-improved gauge action for $N_f = 2 + 1$ [954].

Turning to operators for individual quark flavors, these can mix under renormalization and the singlet and nonsinglet renormalization factors can differ. For the axial current, such mixing occurs for all fermion formulations just like in the continuum, where the singlet combination acquires an anomalous dimension due to the $U_A(1)$ anomaly. The ratio of singlet to nonsinglet renormalization factors, $r_{\mathcal{O}} = Z_{\mathcal{O}}^{\rm s.}/Z_{\mathcal{O}}^{\rm n.s.}$ for $\mathcal{O} = A$ differs from 1 at $\mathcal{O}(\alpha_s^2)$ in perturbation theory (due to quark loops), suggesting that the mixing is a small effect. The nonperturbative determinations performed so far find $r_A \approx 1$ [882,955], supporting this. For the tensor current the disconnected diagram vanishes in the continuum due to chirality and consequently on the lattice $r_T = 1$ holds for overlap and DW fermions (assuming $m_{\rm res} = 0$ for the latter). For twisted-mass and clover fermions the mixing is expected to be small with $r_T = 1 + \mathcal{O}(\alpha_s^3)$ [956] and this is confirmed by the nonperturbative studies of Refs. [884,957].

The scalar operators for the individual quark flavors, $\bar{q}q$, are relevant not only for the corresponding scalar charges, but also for the sigma terms $\sigma_q = m_q\langle N|\bar{q}q|N\rangle$ when combined with the quark masses m_q. For overlap and DW fermions $r_S = 1$, like in the continuum and all $\bar{q}q$ renormalize multiplicatively with the isovector Z_S. The latter is equal to the inverse of the mass renormalization and hence $m_q\bar{q}q$ is renormalization group (RG) invariant. For twisted-mass fermions, through the use of Osterwalder-Seiler valence fermions, the operators $m_{ud}(\bar{u}u + \bar{d}d)$ and $m_s\bar{s}s$ are also invariant [958].[78] In contrast, the lack of good chiral properties leads to significant mixing between quark flavors for clover fermions. Nonperturbative determinations via the axial Ward identity [717,876] have found the ratio r_S to be much larger than the perturbative expectation $1 + \mathcal{O}(\alpha_s^2)$ [956] may suggest. While the sum over the quark flavors which appear in the action $\sum_q^{N_f} m_q\bar{q}q$ is RG invariant, large cancellations between the contributions from individual flavors can occur when evaluating, e.g., the strange sigma term. Note that for twisted-mass and clover fermions there is also an additive contribution $\propto a^{-3}\mathbf{1}$ (or $\propto \mu a^{-2}\mathbf{1}$) to the scalar operator. This contribution is removed from the nucleon scalar matrix elements by working with the subtracted current, $\bar{q}q - \langle\bar{q}q\rangle$, where $\langle\bar{q}q\rangle$ is the vacuum expectation value of the current [950].

Symanzik improvement for the singlet currents follows the same pattern as in the isovector case with $\mathcal{O}(a)$ terms only appearing for nonperturbatively improved clover fermions. For the axial and tensor operators only mass-dependent terms are relevant in the forward limit while for the scalar there is an additional gluonic operator $\mathcal{O}_S^{\rm imp} = {\rm Tr}(F_{\mu\nu}F_{\mu\nu})$ with a coefficient of $\mathcal{O}(\alpha_s)$ in perturbation theory. When constructing the sigma terms from the quark masses and the scalar operator, the improvement terms remain and they must be included to remove all $\mathcal{O}(a)$ effects for nonperturbatively improved clover fermions, see Ref. [950] for a discussion.

4. Extrapolations in a, M_π and $M_\pi L$

To obtain physical results that can be used to compare to or make predictions for experiment, all quantities must be extrapolated to the continuum and infinite-volume limits. In general, either a chiral extrapolation or interpolation must also be made to the physical pion mass. These extrapolations need to be performed simultaneously since discretization and finite-volume effects are themselves dependent upon the pion mass. Furthermore, in practice it is not possible to hold the pion mass fixed while the lattice spacing is varied, as some variation in a occurs when tuning the quark masses at fixed gauge coupling. Thus, one performs a simultaneous extrapolation in all three variables using a theoretically motivated formula of the form,

$$g(M_\pi, a, L) = g_{\rm phys} + \delta_{M_\pi} + \delta_a + \delta_L, \tag{415}$$

where $g_{\rm phys}$ is the desired extrapolated result, and δ_{M_π}, δ_a, δ_L are the deviations due to the pion mass, the lattice spacing, and the volume, respectively. Below we outline the forms for each of these terms.

All observables discussed in this section are dimensionless, therefore the extrapolation formulas may be parametrized by a set of dimensionless variables

$$\epsilon_\pi = \frac{M_\pi}{\Lambda_\chi}, \qquad M_\pi L, \qquad \epsilon_a = \Lambda_a a. \tag{416}$$

[78]Note that for twisted-mass fermions the pseudoscalar renormalization factor is the relevant factor for the scalar operator. The isovector (isosinglet) scalar current in the physical basis becomes the isosinglet (isovector) pseudoscalar current in the twisted basis. Perturbatively $r_P = 1 + \mathcal{O}(\alpha_s^3)$ and nonperturbative determinations have found $r_P \approx 1$ [884].

Here, $\Lambda_\chi \sim 1$ GeV is a chiral symmetry breaking scale, which, for example, can be set to $\Lambda_\chi = 4\pi F_\pi$, where $F_\pi = 92.2$ MeV is the pion decay constant, and Λ_a is a discretization scale, e.g., $\Lambda_a = \frac{1}{4\pi w_0}$, where w_0 is a gradient-flow scale [115].

Effective field theory methods may be used to determine the form of each of these extrapolations. For the single nucleon charges, heavy-baryon χPT (HBχPT) is a common choice [959,960], however, other variants, such as unitarized [961] or covariant χPT [962,963], are also employed. Various formulations of HBχPT exist, including those for two and three flavors, as well as with and without explicit Δ baryon degrees of freedom. Two-flavor HBχPT is typically used due to issues with convergence of the three-flavor theory [878,964–967]. The convergence properties of all known formulations for baryon χPT, even at the physical pion mass, have not been well established.

To $\mathcal{O}(\epsilon_\pi^2)$, the two-flavor chiral expansion for the nucleon charges is known to be of the form [968],

$$g = g_0 + g_1\epsilon_\pi + g_2\epsilon_\pi^2 + \tilde{g}_2\epsilon_\pi^2 \ln(\epsilon_\pi^2), \tag{417}$$

where $g_1 = 0$ for all charges g except $g_S^{u,d}$. The dimensionless coefficients $g_{0,1,2}, \tilde{g}_2$ are assumed to be different for each of the different charges. The coefficients in front of the logarithms, $\tilde{g}_2$, are known functions of the low-energy constants (LECs), and do not represent new, independent LECs. Mixed-action calculations will have further dependence upon the mixed valence-sea pion mass, m_{vs}.

Given the potential difficulties with convergence of the chiral expansion, known values of the $\tilde{g}_2$ in terms of LECs are not typically used, but are left as free fit parameters. Furthermore, many quantities have been found to display mild pion-mass dependence, such that Taylor expansions, i.e., neglecting logarithms in the above expressions, are also often employed. The lack of a rigorously established theoretical basis for the extrapolation in the pion mass thus requires data close to the physical pion mass for obtaining high-precision extrapolated/interpolated results.

Discretization effects depend upon the lattice action used in a particular calculation, and their form may be determined using the standard Symanzik power counting. In general, for an unimproved action, the corrections due to discretization effects δ_a include terms of the form,

$$\delta_a = c_1\epsilon_a + c_2\epsilon_a^2 + \cdots, \tag{418}$$

where $c_{1,2}$ are dimensionless coefficients. Additional terms of the form $\tilde{c}_n(\epsilon_\pi\epsilon_a)^n$, where n is an integer whose lowest value depends on the combined discretization and chiral properties, will also appear. Improved actions systematically remove correction terms, e.g., an $\mathcal{O}(a)$-improved action, combined with a similarly improved operator, will contain terms in the extrapolation *Ansatz* beginning at ϵ_a^2 (see Sec. X A 3).

Finite volume corrections δ_L may be determined in the usual way from effective field theory, by replacing loop integrals over continuous momenta with discrete sums. Finite volume effects therefore introduce no new undetermined parameters to the extrapolation. For example, at next-to-leading order, and neglecting contributions from intermediate Δ baryons, the finite-volume corrections for the axial charge in two-flavor HBχPT take the form [969],

$$\begin{aligned}\delta_L &\equiv g_A(L) - g_A(\infty) \\ &= \frac{8}{3}\epsilon_\pi^2[g_{A,0}^3 F_1(M_\pi L) + g_{A,0}F_3(M_\pi L)],\end{aligned} \tag{419}$$

where

$$\begin{aligned}F_1(mL) &= \sum_{\mathbf{n}\neq\mathbf{0}}\left[K_0(mL|\mathbf{n}|) - \frac{K_1(mL|\mathbf{n}|)}{mL|\mathbf{n}|}\right], \\ F_3(mL) &= -\frac{3}{2}\sum_{\mathbf{n}\neq\mathbf{0}}\frac{K_1(mL|\mathbf{n}|)}{mL|\mathbf{n}|},\end{aligned} \tag{420}$$

and $K_\nu(z)$ are the modified Bessel functions of the second kind. Some extrapolations are performed using the form for asymptotically large $M_\pi L$,

$$K_0(z) \to \frac{e^{-z}}{\sqrt{z}}, \tag{421}$$

and neglecting contributions due to K_1. Care must, however, be taken to establish that these corrections are negligible for all included values of $M_\pi L$. The numerical coefficients, for example, $8/3$ in Eq. (419), are often taken to be additional free fit parameters, due to the question of convergence of the theory discussed above.

Given the lack of knowledge about the convergence of the expansions and the resulting plethora of possibilities for extrapolation models at differing orders, it is important to include statistical tests of model selection for a given set of data. Bayesian model averaging [970] or use of the Akaike information criterion [971] are common choices which penalize over-parametrized models.

B. Quality criteria for nucleon matrix elements and averaging procedure

There are two specific issues that call for a modification and extension of the FLAG quality criteria listed in Sec. II. The first concerns the rating of the chiral extrapolation: The FLAG criteria reflect the ability of χPT to provide accurate descriptions of the pion-mass dependence of observables. Clearly, this ability is linked to the convergence properties of χPT in a particular mass range. Quantities extracted from nucleon matrix elements are extrapolated to the physical pion mass using some variant of baryonic χPT, whose convergence is not well established as compared to the mesonic sector. Therefore, we have opted for stricter

quality criteria, $200\ \text{MeV} \leq M_{\pi,\text{min}} \leq 300\ \text{MeV}$, for a green circle in the chiral extrapolation of nucleon matrix elements, i.e.,

★ $M_{\pi,\text{min}} < 200$ MeV with three or more pion masses used in the extrapolation, *or* two values of M_π with one lying within 10 MeV of 135 MeV (the physical neutral pion mass) and the other one below 200 MeV.

○ $200\ \text{MeV} \leq M_{\pi,\text{min}} \leq 300\ \text{MeV}$ with three or more pion masses used in the extrapolation;
or two values of M_π with $M_{\pi,\text{min}} < 200$ MeV;
or a single value of M_π lying within 10 MeV of 135 MeV (the physical neutral pion mass)

■ Otherwise

In Sec. X A 2 we have discussed that insufficient control over excited-state contributions, arising from the noise problem in baryonic correlation functions, may lead to a systematic bias in the determination of nucleon matrix elements. We therefore introduce an additional criterion that rates the efforts to suppress excited-state contamination in the final result. As described in Sec. X A 2, the applied methodology to control excited-state contamination is quite diverse. Since a broad consensus on the question which procedures should be followed has yet to emerge, our criterion is expressed in terms of simulation parameters that can be straightforwardly extracted on the basis of publications. Furthermore, the criterion must also be readily applicable to a variety of different local operators whose matrix elements are discussed in this chapter. These requirements are satisfied by the source-sink separation τ, i.e., the Euclidean distance between the initial and final nucleons. The discussion at the end of Sec. X A 2 shows that there is room for improvement in the ability to control excited-state contamination. Hence, we have reverted to a binary system, based on the range of source-sink separations of a given calculations. While we do not award the highest category—a green star—in this edition, we stress that the adoption of the modified criterion for excited-state contamination has not led to a situation where calculations that were previously rated with a green star are now excluded from FLAG averages. The rating scale concerning control over excited-state contributions is thus

○ Three or more source-sink separations τ, at least two of which must be above 1.0 fm.

■ Otherwise

We will continue to monitor the situation concerning excited-state contamination and, if necessary, adapt the criteria further in future editions of the FLAG report.

As explained in Sec. II, FLAG averages are distinguished by the sea-quark content. Hence, for a given configuration of the quark sea (i.e., for $N_f = 2$, $2+1$, $2+1+1$, or $1+1+1+1$), we first identify those calculations that pass the FLAG and the additional quality criteria defined in this section, i.e., excluding any calculation that has a red tag in one or more of the categories. We then add statistical and systematic errors in quadrature and perform a weighted average. If the fit is of bad quality (i.e., if $\chi^2_{\text{min}}/\text{dof} > 1$), the errors of the input quantities are scaled by $\sqrt{\chi^2/\text{dof}}$. In the following step, correlations among different calculations are taken into account in the error estimate by applying Schmelling's procedure [203].

C. Isovector charges

The axial, scalar and tensor isovector charges are needed to interpret the results of many experiments and phenomena mediated by weak interactions, including probes of new physics. The most natural process from which isovector charges can be measured is neutron beta decay ($n \to p^+ e^- \bar{\nu}_e$). At the quark level, this process occurs when a down quark in a neutron transforms into an up quark due to weak interactions, in particular due to the axial-current interaction. While scalar and tensor currents have not been observed in nature, effective scalar and tensor interactions arise in the SM due to loop effects. At the TeV and higher scales, contributions to these three currents could arise due to new interactions and/or loop effects in BSM theories. These super-weak corrections to standard weak decays can be probed through high-precision measurements of the neutron decay distribution by examining deviations from SM predictions as described in Ref. [972]. The lattice-QCD methodology for the calculation of isovector charges is well established, and the control over statistical and systematic uncertainties has become quite robust since the first edition of the FLAG report that featured nucleon matrix elements [4].

The axial charge g_A^{u-d} is an important parameter that encapsulates the strength of weak interactions of nucleons. It enters in many analyses of nucleon structure and of SM and BSM physics. For example, it enters in (i) the extraction of V_{ud} and tests of the unitarity of the CKM matrix; (ii) the analysis of neutrinoless double-beta decay, (iii) neutrino-nucleus quasi-elastic scattering cross-section; (iv) the rate of proton-proton fusion, the first step in the thermonuclear reaction chains that power low-mass hydrogen-burning stars like the Sun; (v) solar and reactor neutrino fluxes; (vi) muon capture rates, etc. Currently the best determination of the ratio of the axial to the vector charge, g_A/g_V, comes from measurement of neutron beta decay using polarized ultracold neutrons by the UCNA collaboration, 1.2772(20) [973,974], and by PERKEO II, 1.2761^{+14}_{-17} [975]. Note that, in the SM, $g_V = 1$ up to second-order corrections in isospin breaking [976,977] as a result of the conservation of the vector current. The percent-level contributions of radiative corrections discussed in Ref. [978] will need to be considered once the accuracy of the lattice-QCD calculations reaches that of g_A^{u-d} measured in experiments. The current goal is to calculate it directly with $\mathcal{O}(1\%)$ accuracy using lattice QCD.

Isovector scalar or tensor interactions contribute to the helicity-flip parameters, called b and B, in the neutron decay distribution. By combining the calculation of the scalar and tensor charges with the measurements of b and B, one can put constraints on novel scalar and tensor interactions at the TeV scale as described in Ref. [972]. To optimally bound such scalar and tensor interactions using measurements of b and B parameters in planned experiments targeting 10^{-3} precision [979–981], we need to determine g_S^{u-d} and g_T^{u-d} at the 10% level as explained in Refs. [888,972]. Future higher-precision measurements of b and B would require correspondingly higher-precision calculations of the matrix elements to place even more stringent bounds on these couplings at the TeV-scale.

One can estimate g_S^{u-d} via the conserved vector current (CVC) relation, $g_S/g_V = (M_{\text{neutron}} - M_{\text{proton}})^{\text{QCD}}/(m_d - m_u)^{\text{QCD}}$, as done by Gonzalez-Alonso *et al.* [982]. In their analysis, they took estimates of the two mass differences on the right-hand side from the global lattice-QCD data [2] and obtained $g_S^{u-d} = 1.02(8)(7)$.

The tensor charge g_T^{u-d} can be extracted experimentally from semi-inclusive deep-inelastic scattering (SIDIS) data [983–986]. A sample of these phenomenological estimates is shown in Fig. 44, and the noteworthy feature is that the current uncertainty in these phenomenological estimates is large. More recent phenomenological analyses include lattice values for the tensor charges as constraints in their global fits [985,987,988].

1. Results for g_A^{u-d}, g_S^{u-d} and g_T^{u-d}

Results for the isovector axial, scalar and tensor charges are presented in Tables 66, 67 and 68, respectively. Compared with previous editions of the FLAG report, we have made two changes: First, we have stopped listing results for isovector charges from simulations in two-flavor QCD, since no new results have been reported since 2018. Second, for simulations using $2+1$ or $2+1+1$ flavors of dynamical quarks, we have imposed a cutoff to focus on results published after 2014. For full listings, including results obtained in two-flavor QCD [872–875,877,880,882,884,992] or published prior to our cutoff date [885,891–893,905,993–995], we refer to earlier editions of the FLAG report.

For the sake of brevity, only calculations completed after FLAG 21 and calculations that meet the criteria for inclusion in averages are described below. For detailed descriptions of past calculations and those that do not meet the criteria, the reader is again referred to earlier editions of FLAG. The final results for the scalar and tensor charges, g_S^{u-d} and g_T^{u-d}, are presented in the $\overline{\text{MS}}$-scheme at a reference scale of 2 GeV by all collaborations.

The $2+1$-flavor calculation of the scalar and tensor charges by χQCD 21A [97] was performed using a mixed-action approach with domain-wall fermion gauge configurations generated by the RBC/UKQCD collaboration and overlap valence quarks. They include five pion masses ranging from $m_\pi \sim 140$ MeV to 370 MeV, four lattice spacings ($a \sim 0.06$, 0.08, 0.11, and 0.14 fm), thereby considerably extending the parameter range in their earlier calculation of the axial charge in χQCD 18 [92]. Matrix elements are computed for three to six different valence-quark masses on each ensemble. The extrapolation to the physical pion mass, continuum and infinite-volume limits is obtained by a global fit of all data to a partially quenched chiral perturbation theory *Ansatz*. Excited-state contamination is assessed using three to five sink-source separations and multi-state fits. Renormalization factors were determined nonperturbatively using the RI/MOM prescription.

The NME 21 [93] $2+1$-flavor calculation utilized seven ensembles of $\mathcal{O}(a)$-improved Wilson fermions. Three lattice spacings, ranging from $a \sim 0.07$ fm to 0.13 fm, several pion masses, $m_\pi \sim 165$ MeV to 285 MeV, and volumes corresponding to $m_\pi L \sim 3.75$ to 6.15 were used. Combined continuum, chiral, and infinite-volume extrapolations were performed to the physical point using leading-order fit functions. Several fitting strategies were explored using four to six source-sink separations ranging from 0.7–1.8 fm. Final results are quoted by averaging results from two of these fitting strategies, in which the excited-state energy for the three-point function is fixed using two alternative choices of priors. Renormalization is nonperturbative (RI-SMOM) using two strategies.

PACS 22B [990] reports estimates for the scalar and tensor charges, computed on two ensembles with nonperturbatively improved Wilson quark and Iwasaki gauge action at a single lattice spacing of 0.085 fm, pion mass near physical value, and two volumes with $m_\pi L \sim 3.7$ and 7.4. Two to four source-sink separations ranging from 0.85–1.36 fm were used to estimate contributions from excited states. They employ the RI-SMOM$_{\gamma_\mu}$ renormalization procedure. Due to the use of only a single lattice spacing, this calculation does not meet the criteria for inclusion in the average. In PACS 23 [855], another ensemble was considered for the calculation of the axial charge and form factors, which features a smaller lattice spacing of 0.063 fm, a 10 fm spatial box size and a near-physical pion mass of 138 MeV. The range of source-sink separations matches the choice in PACS 22B. The size of discretization effects is estimated by the difference between results at fine and coarser lattice spacings. Since these results are based on only two lattice spacings, they do not qualify for an average.

The calculation of all three isovector charges by QCDSF/UKQCD/CSSM 23 [94] used a Feynman-Hellmann approach to determine matrix elements from derivatives of energies produced via a variation of the action. These energies were determined from fits to two-point correlation functions, where a weighted average is taken of the results

TABLE 66. Overview of results for g_A^{u-d}.

Collaboration	Ref.	N_f	Publication status	Continuum extrapolation	Chiral extrapolation	Finite volume	Renormalization	Excited states	g_A^{u-d}
ETM 23	[91]	$2+1+1$	A	★	★	★	★	○	1.245(28)(14)[c]
PNDME 23[a]	[90]	$2+1+1$	A	★[e]	★	★	★	○	1.292(53)(24)[c]
CalLat 19	[89]	$2+1+1$	C	○	★	★	★	○	1.2642(93)
ETM 19	[989]	$2+1+1$	A	■	○	★	★	○	1.286(23)
PNDME 18[a]	[890]	$2+1+1$	A	★[e]	★	★	★	○	1.218(25)(30)
CalLat 18	[88]	$2+1+1$	A	○	★	★	★	○	1.271(10)(7)
CalLat 17	[889]	$2+1+1$	P	○	★	★	★	○	1.278(21)(26)
PNDME 16[a]	[888]	$2+1+1$	A	○[e]	★	★	★	○	1.195(33)(20)
Mainz 24	[96]	$2+1$	A	★	★	★	★	○	1.254(19)(15)
PACS 23	[855]	$2+1$	A	■	○	★	★	○	1.264(14)(3)
RQCD 23	[95]	$2+1$	A	★	★	★	★	○	$1.284(^{+0.028}_{-0.027})$
QCDSF/UKQCD/CSSM 23	[94]	$2+1$	A	★	○	★	★	○	1.253(63)(41)[d]
PACS 22B	[990]	$2+1$	A	■	○	★	★	○	1.288(14)(9)
Mainz 22	[854]	$2+1$	A	★	★	★	★	○	1.225(39)(25)[c]
NME 21[a]	[93]	$2+1$	A	○[e]	★	★	★	○	1.31(6)(5)
RQCD 19	[848]	$2+1$	A	★	★	★	★	○	1.302(45)(73)[c]
LHPC 19	[850]	$2+1$	A	■[e]	★	★	★	○	1.265(49)
Mainz 19	[923]	$2+1$	A	★	○	★	★	○	$1.242(25)(^{+0}_{-0.030})$
PACS 18A	[991]	$2+1$	A	■	★	★	★	○	1.273(24)(5)(9)
PACS 18	[879]	$2+1$	A	■	■	★	★	■	1.163(75)(14)
χQCD 18	[92]	$2+1$	A	○	★	★	★	○	1.254(16)(30)[f]
JLQCD 18	[898]	$2+1$	A	■	○	○	★	○	1.123(28)(29)(90)

[a]The improvement coefficient in the valence-quark action is set to its tadpole-improved tree-level value.

[b]The quark action is tree-level improved.

[c]Determination includes data for nonforward matrix elements.

[d]Feynman-Hellmann theorem is used to determine the matrix element.

[e]The rating takes into account that the action is not fully $\mathcal{O}(a)$-improved by requiring an additional lattice spacing.

[f]For this partially quenched analysis the criteria are applied to the unitary points.

TABLE 67. Overview of results for g_S^{u-d}.

Collaboration	Ref.	N_f	Publication status	Continuum extrapolation	Chiral extrapolation	Finite volume	Renormalization	Excited states	g_S^{u-d}
PNDME 23	[90]	$2+1+1$	A	★[b]	★	★	★	○	1.085(50)(103)
ETM 19	[989]	$2+1+1$	A	■	○	★	★	○	1.35(17)
PNDME 18	[890]	$2+1+1$	A	★[b]	★	★	★	○	1.022(80)(60)
PNDME 16	[888]	$2+1+1$	A	○[b]	★	★	★	○	0.97(12)(6)
Mainz 24	[96]	$2+1$	A	★	★	★	★	○	1.203(77)(81)
RQCD 23	[95]	$2+1$	A	★	★	★	★	○	1.11^{+14}_{-16}
QCDSF/UKQCD/CSSM 23	[94]	$2+1$	A	★	○	★	★	○[a]	1.08(21)(03)[a]
PACS 22B	[990]	$2+1$	A	■	○	★	★	○	0.927(83)(22)
NME 21	[93]	$2+1$	A	○[b]	★	★	★	○	1.06(9)(6)
χQCD 21A	[97]	$2+1$	A	★	★	★	★	○	0.94(10)(08)[c]
RBC/UKQCD 19	[996]	$2+1$	A	■	○	★	★	■	0.9(3)
Mainz 19	[923]	$2+1$	A	★	○	★	★	○	$1.13(11)(^{7}_{6})$
LHPC 19	[850]	$2+1$	A	■[b]	★	★	★	○	0.927(303)
JLQCD 18	[898]	$2+1$	A	■	○	○	★	○	0.88(8)(3)(7)

[a]Feynman-Hellmann theorem is used.

[b]The rating takes into account that the action is not fully $\mathcal{O}(a)$-improved by requiring an additional lattice spacing.

[c]For this partially quenched analysis the criteria are applied to the unitary points.

TABLE 68. Overview of results for g_T^{u-d}.

Collaboration	Ref.	N_f	Publication status	Continuum extrapolation	Chiral extrapolation	Finite volume	Renormalization	Excited states	g_T^{u-d}
PNDME 23	[90]	$2+1+1$	A	★[b]	★	★	★	○	0.991(21)(10)
ETM 22	[98]	$2+1+1$	A	★	★	★	★	○	0.924(54)
ETM 19	[989]	$2+1+1$	A	■	○	★	★	○	0.936(25)
PNDME 18	[890]	$2+1+1$	A	★[b]	★	★	★	○	0.989(32)(10)
PNDME 16	[888]	$2+1+1$	A	○[b]	★	★	★	○	0.987(51)(20)
PNDME 15, 15A	[886,887]	$2+1+1$	A	○[b]	★	★	★	○	1.020(76)
Mainz 24	[96]	$2+1$	A	★	★	★	★	○	0.993(15)(05)
RQCD 23	[95]	$2+1$	A	★	★	★	★	○	0.984^{+19}_{-29}

(Table continued)

TABLE 68. *(Continued)*

Collaboration	Ref.	N_f	Publication status	Continuum extrapolation	Chiral extrapolation	Finite volume	Renormalization	Excited states	g_T^{u-d}
QCDSF/UKQCD/CSSM 23	[94]	$2+1$	A	★	○	★	★	○[a]	1.010(21)(12)
PACS 22B	[990]	$2+1$	A	■	○	★	★	○	1.036(6)(20)
NME 21	[93]	$2+1$	A	○[b]	★	★	★	○	0.95(5)(2)
RBC/UKQCD 19	[996]	$2+1$	A	■	○	★	★	■	1.04(5)
Mainz 19	[923]	$2+1$	A	★	○	★	★	○	$0.965(38)(^{13}_{41})$
LHPC 19	[850]	$2+1$	A	■[b]	★	★	★	○	0.972(41)
JLQCD 18	[898]	$2+1$	A	■	○	○	★	○	1.08(3)(3)(9)

[a]Feynman-Hellmann theorem is used.

[b]The rating takes into account that the action is not fully $\mathcal{O}(a)$-improved by requiring an additional lattice spacing.

obtained when varying the fitting range. The computations utilized the $2+1$-flavor stout-link nonperturbative clover action with Wilson-clover valence quarks. Pion masses range from 220–468 MeV, using a flavor-breaking expansion around the flavor SU(3) point to extrapolate to physical pion mass. Combined pion-mass, lattice-spacing, and volume extrapolations were performed, using multiple volumes ranging from $m_\pi L \sim 3.2$–9, and five lattice spacings, 0.052–0.082 fm. Only the leading discretization effects and asymptotic form of the volume extrapolation, Eq. (421), were included. They employ the RI'-MOM prescription for nonperturbative renormalization.

The calculations of g_A^{u-d}, g_S^{u-d} and g_T^{u-d} published by RQCD 23 [95] and Mainz 24 [96] are both based on $2+1$-flavor ensembles generated by the CLS effort using nonperturbatively improved Wilson fermions. The subsets of ensembles used in the two calculations partly overlap. The 48 ensembles used by RQCD 23 [95] span six values of the lattice spacing, from 0.039–0.098 fm, pion masses from 130 MeV up to 430 MeV, and volumes corresponding to $m_\pi L \sim 3$–6.5. Excited states are controlled using simultaneous two- and three-state fits of up to four different observables using four time separations, $t \approx 0.7$–1.2 fm, with a number of fit strategies employed. Extrapolations to the physical point were performed using leading-order chiral expressions for the pion mass, the leading asymptotic form for finite-volume corrections, and terms up to a^2 in the lattice spacing. Renormalization uses the nonperturbative RI'-SMOM scheme. In an earlier paper (RQCD 19 [848]), the Regensburg group computed the axial form factor on a subset of the ensembles that enter RQCD 23. The estimate for g_A^{u-d} from an analysis including matrix elements for nonforward kinematics is also listed in Table 66 but has been superseded by the result in RQCD 23.

The Mainz 24 [96] calculation, which supersedes Mainz 19 [923], uses four lattice spacings ($a \sim 0.05$ fm to 0.086 fm) from the CLS set of ensembles, pion masses ranging from ∼130 MeV to ∼350 MeV, and volumes corresponding to $m_\pi L \sim 3$–5.4. Physical-point extrapolations were performed simultaneously in the lattice spacing, pion mass, and volume. In Mainz 24, the range of source-sink separations used was enlarged to 0.2–1.4 fm, which allowed for the inclusion of sub-leading terms in the summation method for improved control over excited-state effects. Renormalization was performed nonperturbatively using the RI-SMOM scheme. The Mainz group has also performed a calculation of the axial form factor (Mainz 22 [854]) on the same set of ensembles, by incorporating the summation method directly into the z-expansion used to describe the Q^2-dependence. The corresponding estimate for g_A^{u-d} from an analysis including nonforward matrix elements has larger errors than the most recent result [96].

New results for $N_f = 2+1+1$ flavors of dynamical fermions have been published by PNDME [90] and ETM [91,98]. The mixed-action calculation by PNDME 23 [90], which supersedes PNDME 18 [890] and PNDME 16 [888], was performed using the MILC HISQ ensembles, with a clover valence action. As in PNDME 18 [890], the 11 ensembles used include three pion-mass values, $M_\pi \sim 135$, 225, 320 MeV, and four lattice spacings, $a \sim 0.06$, 0.09, 0.12, 0.15 fm. Note that four lattice spacings are required to meet the green star criteria, as this calculation is not fully

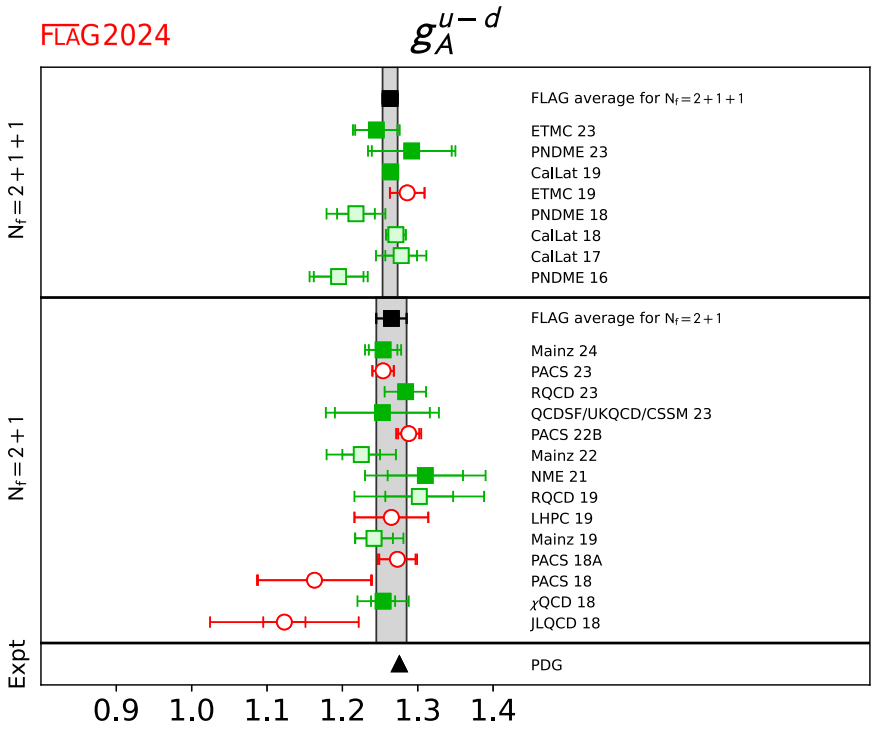


FIG. 42. Lattice results and FLAG averages for the isovector axial charge g_A^{u-d} for $2+1$ and $2+1+1$ flavor calculations. Also shown is the experimental result as quoted in the PDG [205].

$\mathcal{O}(a)$-improved. Lattice size ranges between $3.3 \lesssim M_\pi L \lesssim 5.5$. Physical-point extrapolations were performed simultaneously, keeping only the leading-order terms in the various expansion parameters. For the finite-volume extrapolation, the asymptotic limit of the χPT prediction, Eq. (421), was used. PNDME 23 [90] adds a study of sensitivity to excited-state contamination using between three and five source-sink time separations from $0.72 \lesssim \tau \lesssim 1.68$ fm, and several strategies, including removing $N\pi$ contributions. Renormalization was performed nonperturbatively using the RI-SMOM scheme.

The ETM collaboration has presented new results for the tensor charge (ETM 22 [98]) and for the axial charge (ETM 23 [91]). Both calculations use three ensembles with $2+1+1$-flavor twisted-mass fermions with close-to-physical pion masses at $a = 0.057$, 0.069 and 0.080 fm, with volumes corresponding to $m_\pi L \sim 3.6$–3.9. These results supersede those in [989] based on the single ensemble at $a = 0.080$ fm. To control excited-state effects, they compared results from the plateau, summation method and two-state fits. After applying nonperturbative renormalization via the RI'-MOM method supplemented by a perturbative subtraction of lattice artefacts [997,998], they perform the extrapolation to the continuum limit via a fit which is linear in a^2.

We now proceed to discussing global averages for the isovector charges. The compilation of results for the axial charge g_A^{u-d}, plotted in Fig. 42, shows that the situation has greatly improved in terms of stability and precision thanks to several new calculations that have been added since FLAG 21. For QCD with $N_f = 2+1+1$ dynamical quarks, the latest calculations by ETM 23 [91], PNDME 23 [90] and CalLat 19 [89] pass all quality criteria. Since PNDME and CalLat both use gauge ensembles produced by MILC, we assume that the quoted errors are 100% correlated, even though the range of pion masses and lattice spacings explored in Refs. [90] and [88,89] is not exactly identical. The two results are fully consistent within errors, which is an improvement, since FLAG 21 reported a slight tension between CalLat 19 [89] and PNDME 18 [890]. The calculation by ETM 23 [91] uses an independent set of ensembles. Performing a weighted average yields $g_A^{u-d} = 1.2633(100)$ with $\chi^2/\mathrm{dof} = 0.30$. The result by CalLat dominates the $2+1+1$ weighted average due to its smaller error. Values for $\delta(a_{\min})$ for the two $N_f = 2+1+1$ calculations that enter the averages vary between 1.0–1.5 (PNDME 23: 1.0, CalLat 19: 1.5).

For QCD with $N_f = 2+1$ dynamical quarks, we compute a weighted average from the results χQCD 18 [92], NME 21 [93], QCDSF/UKQCD/CSSM 23 [94], RQCD 23 [95] and Mainz 24 [96]. Since the calculations by the Mainz group and RQCD were both performed on ensembles generated by the CLS effort, we treat the results RQCD 23 [95] and Mainz 24 [96] as 100% correlated. This yields $g_A^{u-d} = 1.265(20)$ with $\chi^2/\mathrm{dof} = 0.28$. Values for $\delta(a_{\min})$ for the qualified calculations for $N_f = 2+1$

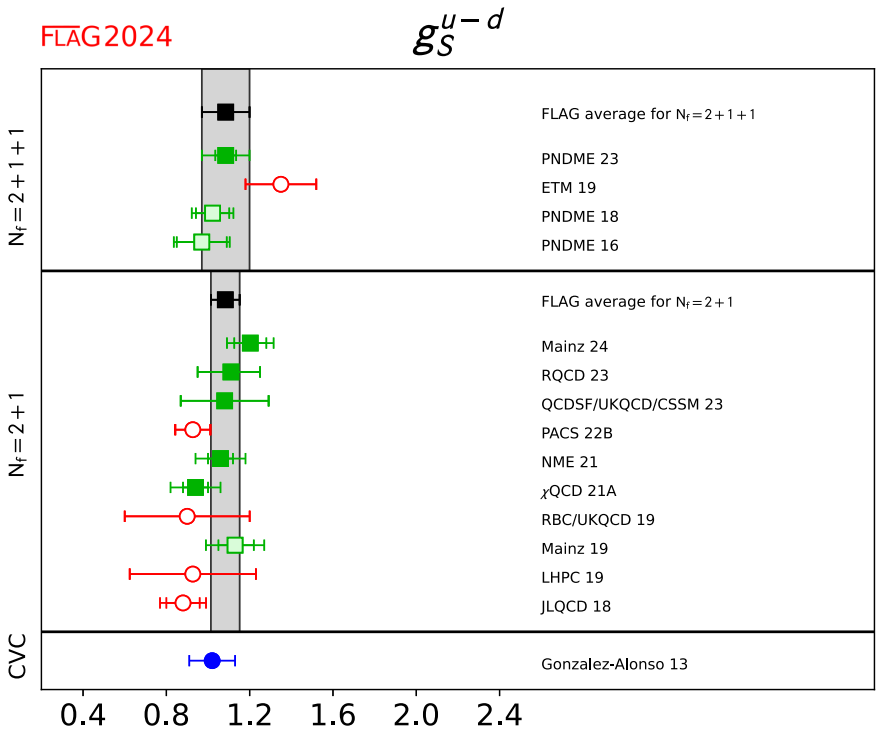


FIG. 43. Lattice results and FLAG averages for the isovector scalar charge g_S^{u-d} for $N_f = 2+1$ and $2+1+1$ flavor calculations. Also shown is a phenomenological result obtained using the conserved vector current (CVC) relation [982] (circle).

suggest that discretization effects are under good control (NME 21: 0.15, QCDSF/UKQCD/CSSM 23: 0.6, RQCD 23: 2.0, Mainz 24: 2.3). From the information provided in the paper, it is not possible to infer $\delta(a_{\min})$ for χQCD 18.

To summarize, the FLAG averages for the axial charge read

$$N_f = 2+1+1: \quad g_A^{u-d} = 1.263(10) \quad \text{Refs. [88–91]}, \tag{422}$$

$$N_f = 2+1: \quad g_A^{u-d} = 1.265(20) \quad \text{Refs. [92–96]}. \tag{423}$$

The averages computed for QCD with $N_f = 2+1+1$ and $N_f = 2+1$ flavors are in excellent agreement, with a relative precision of 0.8% and 1.5%, respectively. The average for $2+1+1$ flavors exhibits a mild tension of 1.25σ with the experimental value of $g_A^{u-d} = 1.2756(13)$ quoted by the PDG. While lattice QCD is able to determine the axial charge with a total relative uncertainty at the percent level, the experimental result is more precise by an order of magnitude. We conclude with the remark that there has been enormous progress in calculating this important benchmark quantity in lattice QCD over the course of the past 10–15 years, owing to a variety of methods to control excited-state effects, higher statistical precision, as well as much better control over the extrapolation to the physical point.

Turning now to the isovector scalar charge, we note that —in addition to the direct three-point method—its value can also be determined indirectly via the conserved vector current (CVC) relation from results for the neutron-proton mass difference [185,211,212,259,999–1003] and the down- and up-quark-mass difference (see Sec. IV A 3). For comparison, the compilation in Fig. 43 also shows the indirect determination by Gonzalez-Alonso *et al.* [982] obtained using lattice and phenomenological input.

For $2+1+1$ flavors, only PNDME 23 [90], which supersedes PNDME 18 [890] and PNDME 16 [888], meets all the criteria for inclusion in the average. Consequently we identify the result from PNDME 23 with the global average.

There are five $2+1$-flavor calculations which satisfy all criteria required for inclusion in the average, i.e., χQCD 21A [97], NME 21 [93], QCDSF/UKQCD/CSSM 23 [94], RQCD 23 [95] and Mainz 24 [96]. The calculations by PACS 22B [990] and LHP 19 [850] have been performed at fewer than three lattice spacings and therefore do not meet the criteria. As in the case of the isovector axial charge, we assume 100% correlation between the results reported by Mainz 24 and RQCD 23, since the calculations were both performed on the CLS set of ensembles. Values of $\delta(a_{\min})$ for the qualified calculations range from 0.4–2.4 (PNDME 23: 1.6, NME 21: 2.4, RQCD 23: 0.4, Mainz 24: 0.5). It is not possible based on the information given to determine $\delta(a_{\min})$ for χQCD 21 or QCDSF/UKQCD/CSSM 23,

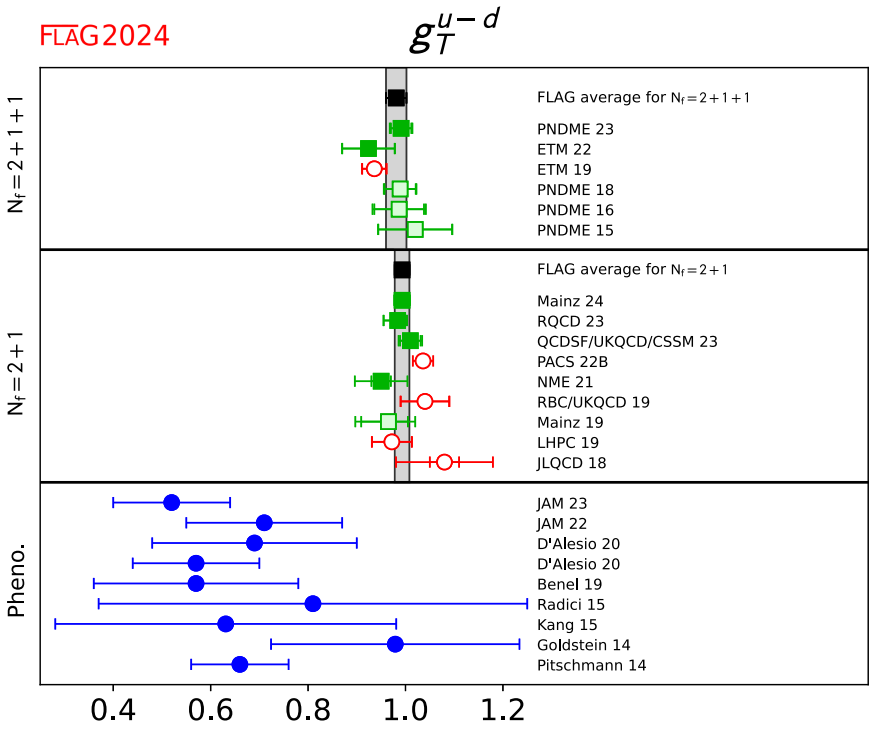


FIG. 44. Lattice results and FLAG averages for the isovector tensor charge g_T^{u-d} for $N_f = 2+1$ and $2+1+1$ flavor calculations. Also shown are phenomenological results using measures of transversity [987,988,1004–1010] (circles). To maintain the independence of lattice QCD and phenomenological results, the JAM22 (private communication supplementing [987]) and JAM23 [988] values shown are those obtained without including input from lattice QCD.

however, in the former calculation it is noted that all data on the finest lattice spacing is within one sigma of the quoted final result, while for the latter extrapolations performed without accounting for discretization effects give results within one sigma of the final quoted result. Thus it is likely that in these cases $\delta(a_{\min})$ is within a reasonable range.

The final FLAG values for g_S^{u-d} are

$$N_f = 2+1+1: \quad g_S^{u-d} = 1.085(114) \quad \text{Ref. [90]}, \tag{424}$$

$$N_f = 2+1: \quad g_S^{u-d} = 1.083(69) \quad \text{Refs. [93–97]}, \tag{425}$$

so that the total relative error for $N_f = 2+1+1$ and $2+1$ is about 10.5% and 6.4%, respectively. This implies that the relevant precision target for current experimental searches for new scalar interactions has been met.

Estimates of the isovector tensor charge are generally at a high level of precision, with values that are stable over time, as can be seen from the compilation given in Table 68 and plotted in Fig. 44. This is a consequence of the smaller statistical fluctuations in the raw data and the very mild dependence on a, M_π, and the lattice size $M_\pi L$. As a result, the uncertainty due to the various extrapolations is small. Also shown for comparison in Fig. 44 are phenomenological results using measures of transversity [987,988,1004–1010].

For $N_f = 2+1+1$ flavors, two calculations meet all the criteria for inclusion in the average: PNDME 23 [90], which supersedes PNDME 18 [890] and PNDME 16 [888], and ETM 22 [98]. Computational details for PNDME 23 and ETM 22 have already been described above.

Using $N_f = 2+1$ flavors, four calculations meet all criteria for inclusion in the average: NME 21 [93], QCDSF/UKQCD/CSSM 23 [94], RQCD 23 [95], and Mainz 24 [96] calculation, which supersedes Mainz 19 [923]. Details of these calculations, as well as the PACS 22B [990] calculation which does not meet all criteria for inclusion in the average, have been described above. As in the cases of the axial and scalar charge, we assume 100% correlation between the Mainz 24 and RQCD 23 calculations. Values of $\delta(a_{\min})$ for the qualified calculations range from 0.03–2 (PNDME 23: 2, NME 21: 0.5, RQCD 23: 0.03, Mainz 24: 0.5). Similarly to the case for g_S, it is not possible based on the information given to determine $\delta(a_{\min})$ for χQCD 21 or QCDSF/UKQCD/CSSM 23. However, in the former calculation it is noted that all data on the finest lattice spacing is within one sigma of the quoted final result, while for the latter extrapolations performed without accounting for discretization give results within one sigma of the final quoted result. Thus, it is likely that in these cases $\delta(a_{\min})$ is within a reasonable range.

The final FLAG values for g_T^{u-d} are

$$N_f = 2+1+1: \quad g_T^{u-d} = 0.981(21) \quad \text{Refs. [90,98]}, \tag{426}$$

$$N_f = 2+1: \quad g_T^{u-d} = 0.993(15) \quad \text{Refs. [93–96]}, \tag{427}$$

which implies that the isovector tensor charge is determined at the level of 1.5%–2.0% relative precision.

D. Flavor-diagonal charges

Three examples of interactions for which matrix elements of flavor-diagonal operators ($q\Gamma q$ where Γ defines the Lorentz structure of the bilinear quark operator) are needed are the neutral-current interactions of neutrinos, elastic scattering of electrons off nuclei, and the scattering of dark matter off nuclei. In addition, these matrix elements also probe intrinsic properties of nucleons (the spin, the nucleon sigma term and strangeness content, and the contribution of the electric dipole moment (EDM) of the quarks to the nucleon EDM) as explained below. For brevity, all operators are assumed to be appropriately renormalized as discussed in Sec. X A 3.

The matrix elements of the scalar operator $\bar{q}q$ with flavor q give the rate of change in the nucleon mass due to nonzero values of the corresponding quark mass. This relationship is given by the Feynman-Hellmann theorem. The quantities of interest are the nucleon σ-term, $\sigma_{\pi N}$, and the strange and charm content of the nucleon, σ_s and σ_c,

$$\sigma_{\pi N} = m_{ud}\langle N|\bar{u}u + \bar{d}d|N\rangle, \tag{428}$$

$$\sigma_s = m_s\langle N|\bar{s}s|N\rangle, \tag{429}$$

$$\sigma_c = m_c\langle N|\bar{c}c|N\rangle. \tag{430}$$

Here, m_{ud} is the average of the up- and down-quark masses and m_s, m_c are the strange- and charm-quark masses. The $\sigma_{\pi N,s,c}$ give the shift in M_N due to nonzero light-, strange- and charm-quark masses. The same matrix elements are also needed to quantify the spin-independent interaction of dark matter with nucleons. Note that, while σ_b and σ_t are also phenomenologically interesting, they are unlikely to be calculated on the lattice due to the expected tiny signal in the matrix elements. In principle, the heavy sigma terms can be estimated using $\sigma_{u,d,s}$ by exploiting the heavy-quark limit [1011–1013].

The matrix elements of the axial operator $\bar{q}\gamma_\mu\gamma_5 q$ give the contribution Δq of quarks of flavor q to the spin of the nucleon

$$\langle N|\bar{q}\gamma_\mu\gamma_5 q|N\rangle = g_A^q \bar{u}_N\gamma_\mu\gamma_5 u_N,$$
$$g_A^q \equiv \Delta q = \int_0^1 dx(\Delta q(x) + \Delta\bar{q}(x)). \tag{431}$$

The charge g_A^q is thus the contribution of the spin of a quark of flavor q to the spin of the nucleon. It is also related to the first Mellin moment of the polarized parton distribution function (PDF) Δq as shown in the second line in Eq. (431). Measurements by the European Muon collaboration in 1987 of the spin asymmetry in polarized deep inelastic scattering showed that the sum of the spins of the quarks contributes less than half of the total spin of the proton [1014]. To understand this unexpected result, called the "proton spin crisis," it is common to start with Ji's sum rule [1015], which provides a gauge invariant decomposition of the nucleon's total spin, as

$$\frac{1}{2} = \sum_{q=u,d,s,c,\cdot}\left(\frac{1}{2}\Delta q + L_q\right) + J_g, \tag{432}$$

where $\Delta q/2 \equiv g_A^q/2$ is the contribution of the intrinsic spin of a quark with flavor q; L_q is the orbital angular momentum of that quark; and J_g is the total angular momentum of the gluons. Thus, to obtain the spin of the proton starting from QCD requires calculating the contributions of the three terms: the spin and orbital angular momentum of the quarks, and the angular momentum of the gluons. Lattice-QCD calculations of the various matrix elements needed to extract the three contributions are underway. An alternate decomposition of the spin of the proton has been provided by Jaffe and Manohar [1016]. The two formulations differ in the decomposition of the contributions of the quark orbital angular momentum and of the gluons. The contribution of the quark spin, which is the subject of this review and given in Eq. (431), is the same in both formulations.

The tensor charges are defined as the matrix elements of the tensor operator $\bar{q}\sigma^{\mu\nu}q$ with $\sigma^{\mu\nu} = \{\gamma_\mu, \gamma_\nu\}/2$

$$g_T^q \bar{u}_N\sigma_{\mu\nu}u_N = \langle N|\bar{q}\sigma_{\mu\nu}q|N\rangle. \tag{433}$$

These flavor-diagonal tensor charges $g_T^{u,d,s,c}$ quantify the contributions of the u, d, s, c quark EDM to the neutron electric dipole moment (nEDM) [886,1017]. Since particles can have an EDM only due to P- and T- (or CP- assuming CPT is a good symmetry) violating interactions, the nEDM is a very sensitive probe of new sources of CP violation that arise in most extensions of the SM designed to explain nature at the TeV scale. The current experimental bound on the nEDM is $d_n < 1.8 \times 10^{-26}$ e cm [1018,1019], while the known CP violation in the SM implies $d_n < 10^{-31}$ e cm [1020]. A nonzero result over the intervening five orders of magnitude would signal new physics. Planned experiments aim to reduce the bound to around 10^{-28} e cm. A discovery or reduction in the bound from these experiments will put stringent constraints on many BSM theories, provided the matrix elements of novel CP-violating interactions, of

TABLE 69. Overview of results for g_A^q.

Collaboration	Ref.	N_f	Publication status	Continuum extrapolation	Chiral extrapolation	Finite volume	Renormalization	Excited states	g_A^u	g_A^d
PNDME 20	[1021]	$2+1+1$	C	★[b]	★	★	★	○	0.790(23)(30)	−0.425(15)(30)
ETM 19	[989]	$2+1+1$	A	■	○	★	★	○	0.862(17)	−0.424(16)
PNDME 18A	[99]	$2+1+1$	A	★[b]	★	★	★	○	0.777(25)(30)[a]	−0.438(18)(30)[a]
Mainz 19A	[1022]	$2+1$	C	★	○	★	★	○	0.84(3)(4)	−0.40(3)(4)
χQCD 18	[92]	$2+1$	A	○	★	★	★	○	0.847(18)(32)[c]	−0.407(16)(18)[c]
									g_A^s	
PNDME 20	[1021]	$2+1+1$	C	★[b]	★	★	★	○	−0.053(7)	
ETM 19	[989]	$2+1+1$	A	■	○	★	★	○	−0.0458(73)	
PNDME 18A	[99]	$2+1+1$	A	★[b]	★	★	★	○	−0.053(8)[a]	
Mainz 19A	[1022]	$2+1$	C	★	○	★	★	○	−0.044(4)(5)	
χQCD 18	[92]	$2+1$	A	○	★	★	★	○	−0.035(6)(7)[c]	
JLQCD 18	[898]	$2+1$	A	■	○	○	★	○	−0.046(26)(9)[a]	
χQCD 15	[895]	$2+1$	A	■	○	■	★	○	−0.0403(44)(78)[a]	

[a]Assumed that $Z_A^{\text{n.s.}} = Z_A^s$.

[b]The rating takes into account that the action is not fully $\mathcal{O}(a)$-improved by requiring an additional lattice spacing.

[c]For this partially quenched analysis the criteria are applied to the unitary points.

which the quark EDM is one, are calculated with the required precision.

One can also extract these tensor charges from the zeroth moment of the transversity distributions that are measured in many experiments including Drell-Yan and semi-inclusive deep inelastic scattering (SIDIS). Of particular importance is the active program at Jefferson Lab (JLab) to measure them [983,984]. Transversity distributions describe the net transverse polarization of quarks in a transversely polarized nucleon. Their extraction from the data taken over a limited range of Q^2 and Bjorken x is, however, not straightforward and requires additional phenomenological modeling. At present, lattice-QCD estimates of $g_T^{u,d,s}$, presented in the next section, are more accurate than these phenomenological estimates [988,1004–1010]. Future experiments will significantly improve the extraction of the transversity distributions. Thus, accurate calculations of the tensor charges using lattice QCD will continue to help elucidate the structure of the nucleon in terms of quarks and gluons and provide a benchmark against which phenomenological estimates utilizing measurements at JLab and other experimental facilities worldwide can be compared.

The methodology for the calculation of flavor-diagonal charges is well established. The major challenges are the much larger statistical errors in the disconnected contributions for the same computational cost and the need for the additional calculations of the isosinglet renormalization factors. In this report, we present results for the axial and tensor charges in the same section X D 1 since they are mostly calculated together and because the statistical and systematic uncertainties are similar. The calculation of the scalar charges can, however, be done in two ways and the results are therefore presented separately in Sec. X D 2.

1. Results for $g_A^{u,d,s}$ and $g_T^{u,d,s}$

A compilation of results for the flavor-diagonal axial (tensor) charges for the proton is given in Table 69 (Table 70), and are plotted in Fig. 45. Results for the neutron can be obtained by interchanging the u- and d-flavor indices. To keep the report current, publications from before 2014 that do not satisfy one or more of the FLAG criteria and the $N_f = 2$ results have been removed. They can be obtained from the FLAG 19 [4] and FLAG 21 [5] reports.

TABLE 70. Overview of results for g_T^q.

Collaboration	Ref.	N_f	Publication status	Continuum extrapolation	Chiral extrapolation	Finite volume	Renormalization	Excited states	g_T^u	g_T^d
PNDME 20	[1021]	$2+1+1$	C	★[a]	★	★	★	○	0.783(27)(10)	−0.205(10)(10)
ETM 19	[989]	$2+1+1$	A	■	○	★	★	○	0.729(22)	−0.2075(75)
PNDME 18B	[100]	$2+1+1$	A	★[a]	★	★	★	○	0.784(28)(10)[b]	−0.204(11)(10)[b]
PNDME 16	[888]	$2+1+1$	A	○[a]	★	★	★	○	0.792(42)[bc]	−0.194(14)[bc]
PNDME 15	[886,887]	$2+1+1$	A	○[a]	★	★	★	○	0.774(66)[b]	−0.233(28)[b]
Mainz 19A	[1022]	$2+1$	C	★	○	★	★	○	0.77(4)(6)	−0.19(4)(6)
JLQCD 18	[898]	$2+1$	A	■	○	○	★	○	0.85(3)(2)(7)	−0.24(2)(0)(2)
									g_T^s	
PNDME 20	[1021]	$2+1+1$	C	★[a]	★	★	★	○	−0.0022(12)	
ETM 19	[989]	$2+1+1$	A	■	○	★	★	○	−0.00268(58)	
PNDME 18B	[100]	$2+1+1$	A	★[a]	★	★	★	○	−0.0027(16)[b]	
PNDME 15	[886,887]	$2+1+1$	A	○[a]	★	★	★	○	0.008(9)[b]	
Mainz 19A	[1022]	$2+1$	C	★	○	★	★	○	−0.0026(73)(42)	
JLQCD 18	[898]	$2+1$	A	■	○	○	★	○	−0.012(16)(8)	

[a]The rating takes into account that the action is not fully $\mathcal{O}(a)$-improved by requiring an additional lattice spacing.

[b]Assumed that $Z_T^{\text{n.s.}} = Z_T^s$.

[c]Disconnected terms omitted.

There are no new results that qualify for FLAG averages, so the FLAG values for the proton in the $\overline{\text{MS}}$ scheme at 2 GeV remain the same as in FLAG 19 [4] and FLAG 21 [5]. For $g_A^{u,d,s}$, only the PNDME 18A [99] calculation qualifies for the $2+1+1$-flavor theory, and only the χQCD 18 [92] for $2+1$ flavors.

The PNDME 18A [99] results were obtained using the $2+1+1$-flavor clover-on-HISQ formulation. The connected contributions were obtained on 11 HISQ ensembles generated by the MILC collaboration with $a \approx 0.057$, 0.87, 0.12 and 0.15 fm, $M_\pi \approx 135$, 220 and 320 MeV, and $3.3 < M_\pi L < 5.5$. The light disconnected contributions were obtained on six of these ensembles with the lowest pion mass $M_\pi \approx 220$ MeV, while the strange disconnected contributions were obtained on seven ensembles, i.e., including an additional one at $a \approx 0.087$ fm and $M_\pi \approx 135$ MeV. The excited-state and the chiral-continuum fits were done separately for the connected and disconnected contributions, which introduces a systematic that is hypothesized to be small as explained in Ref. [99]. The analysis of the excited-state contamination, discussed in Sec. X A 2, was done using three-state fits for the connected contribution and two-state fits for the disconnected contributions. Isovector renormalization factors, calculated on the lattice in the RI-SMOM scheme and converted to $\overline{\text{MS}}$, are used for the flavor-diagonal operators, i.e., assuming $Z_{A,S,T}^{u-d} = Z_{A,S,T}^{u,d,s}$. The chiral-continuum extrapolation was done keeping the leading correction terms proportional to M_π^2 and a, and the leading finite-volume correction in $M_\pi L$ was included in the analysis of the connected contributions. The continuum-limit criteria, $\delta(a_{\text{min}})$, can only be extracted for g_A^s from PNDME 18A and is 0.3.

The PNDME 20 [1021] and the more recent conference proceedings, [1023,1024], are updates. They extend the disconnected calculations to eight ensembles, perform fits to the sum of the connected and disconnected contributions, and also show, through explicit calculations, that flavor mixing in the calculation of renormalization factors in the RI-sMOM scheme is small, and the isovector renormalization factor is a good approximation for renormalizing flavor-diagonal axial and tensor charges as discussed in

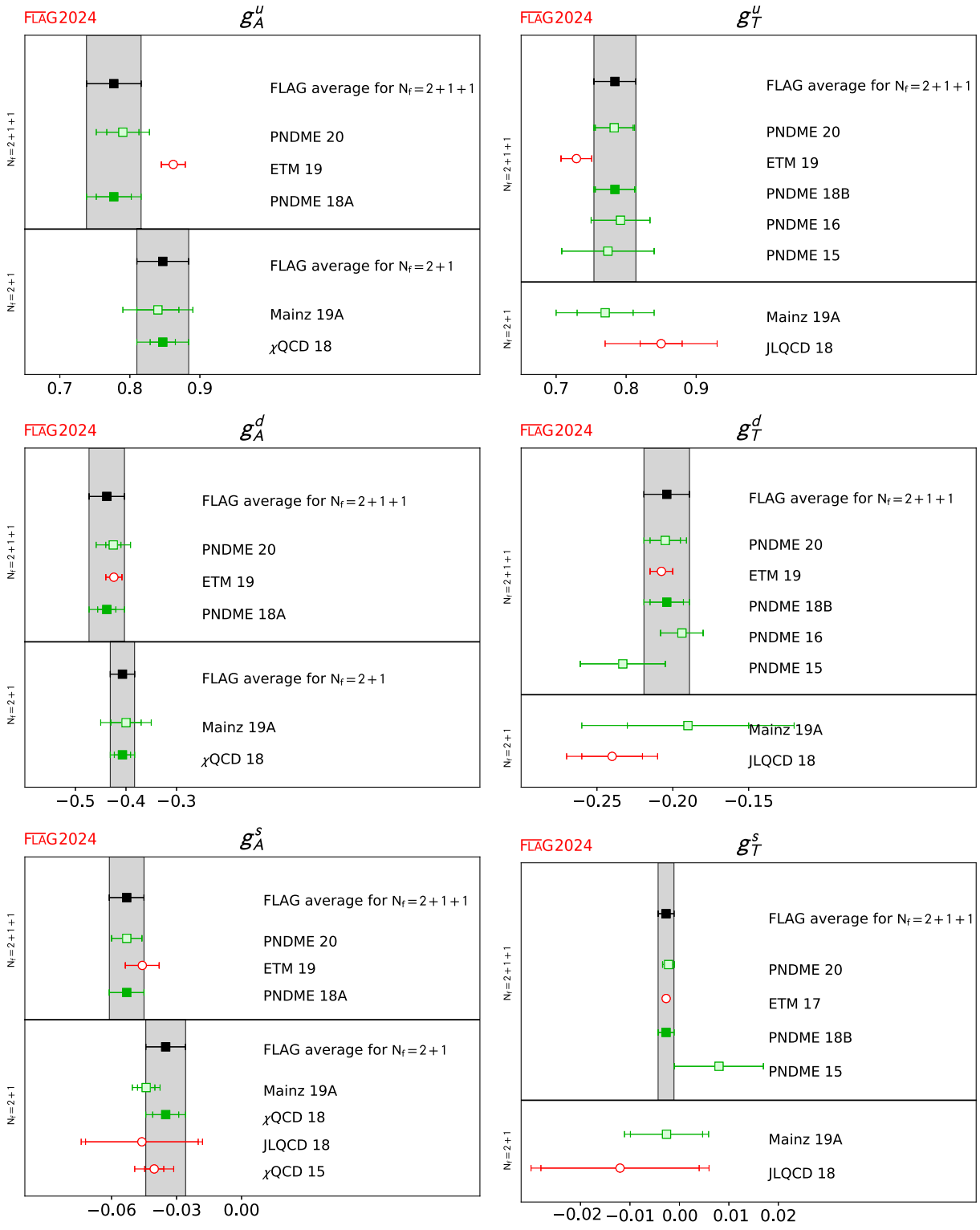


FIG. 45. Lattice results and FLAG averages for $g_A^{u,d,s}$ (left) and $g_T^{u,d,s}$ (right) for the $N_f = 2+1$ and $2+1+1$-flavor calculations.

Sec. X A 3. These updates are, however, not included in Table 70 as they are preliminary.

The ETM 19 [989] results for $g_A^{u,d,s,c}$ are from a single ensemble with $2+1+1$-flavor twisted-mass fermions with a clover term at $a = 0.0801(4)$ fm and $M_\pi = 139.3(7)$ MeV. These are not considered for the averages as they do not satisfy the criteria for the continuum extrapolation.

The $2+1+1$-flavor FLAG values for the axial charges $g_A^{u,d,s}$ of the proton are the PNDME 18A results given in Table 69

$$N_f = 2+1+1: \quad g_A^u = 0.777(25)(30) \quad \text{Ref. [99]}, \tag{434}$$

$$N_f = 2+1+1: \quad g_A^d = -0.438(18)(30) \quad \text{Ref. [99]}, \tag{435}$$

$$N_f = 2+1+1: \quad g_A^s = -0.053(8) \quad \text{Ref. [99]}. \tag{436}$$

The $2+1$-flavor FLAG results from χQCD 18 [92] were obtained using the overlap-on-domain-wall formalism. Three domain-wall ensembles with lattice spacings 0.143, 0.11 and 0.083 fm and sea-quark pion masses $M_\pi = 171$, 337 and 302 MeV, respectively, were analyzed. In addition to the three approximately unitary points, the paper presents data for an additional 4–5 valence-quark masses on each ensemble, i.e., partially quenched data. Separate excited-state fits were done for the connected and disconnected contributions. The continuum, chiral and volume extrapolation to the combined unitary and nonunitary data is made including terms proportional to both $M^2_{\pi,\text{valence}}$ and $M^2_{\pi,\text{sea}}$, and two $\mathcal{O}(a^2)$ discretization terms for the two different domain-wall actions. With just three unitary points, not all the coefficients are well constrained. The $M_{\pi,\text{sea}}$-dependence is omitted and considered as a systematic, and a prior is used for the coefficients of the a^2-terms to stabilize the fit. The continuum-limit criteria, $\delta(a_{\min})$, could not be extracted for these results from χQCD 18.

These χQCD 18 $2+1$-flavor results for the proton, which supersede the χQCD 15 [895] analysis, are

$$N_f = 2+1: \quad g_A^u = 0.847(18)(32) \quad \text{Ref. [92]}, \tag{437}$$

$$N_f = 2+1: \quad g_A^d = -0.407(16)(18) \quad \text{Ref. [92]}, \tag{438}$$

$$N_f = 2+1: \quad g_A^s = -0.035(6)(7) \quad \text{Ref. [92]}. \tag{439}$$

The results for $g_A^{u,d,s}$ from Mainz 19A [1022] satisfy all the criteria, however, they are not included in the averages as [1022] is a conference proceeding. The JLQCD 18 [898], ETM 17C [883] and Engelhardt 12 [1025] calculations were not considered for the averages as they did not satisfy the criteria for the continuum extrapolation. All three calculations were done at a single lattice spacing. The JLQCD 18 calculation used overlap fermions and the Iwasaki gauge action. They perform a chiral fit using data at four pion masses in the range 290–540 MeV. Finite-volume corrections are assumed to be negligible since each of the two pairs of points on different lattice volumes satisfy $M_\pi L \geq 4$. The ETM 17C calculation is based on a single twisted-mass ensemble with $M_\pi = 130$ MeV, $a = 0.094$ and a relatively small $M_\pi L = 2.98$. Engelhardt 12 [1025] calculation was done on three asqtad ensembles with $M_\pi = 293$, 356 and 495 MeV, but all at a single lattice spacing $a = 0.124$ fm.

Results for g_A^s are also presented by LHPC in Ref. [955]. However, this calculation is not included in Table 69 as it has been performed on a single ensemble with $a = 0.114$ fm and a heavy pion mass, $M_\pi \approx 317$ MeV.

Switching to the tensor charges, $g_T^{u,d,s}$, only one calculation, the PNDME 18B [100], qualifies for the FLAG averaging. These $2+1+1$-flavor theory results, which use the same ensembles already discussed for $g_A^{u,d,s}$, supersede those in PNDME 16 [888] and PNDME 15 [886]. The continuum-limit criteria, $\delta(a_{\min})$, can only be extracted for g_T^s from PNDME 18B and is 0.5. Again, results in the more recent conference proceedings, [1023,1024], are not discussed here as they are preliminary.

The FLAG values for the proton in the $\overline{\text{MS}}$ scheme at 2 GeV, which remain the same as in FLAG 19 and FLAG 21, are

$$N_f = 2+1+1: \quad g_T^u = 0.784(28)(10) \quad \text{Ref. [100]}, \tag{440}$$

$$N_f = 2+1+1: \quad g_T^d = -0.204(11)(10) \quad \text{Ref. [100]}, \tag{441}$$

$$N_f = 2+1+1: \quad g_T^s = -0.0027(16) \quad \text{Ref. [100]}. \tag{442}$$

The ensembles and the analysis strategy used in PNDME 18B is the same as described in PNDME 18A for $g_A^{u,d,s}$. The only difference for the tensor charges was that a one-state (constant) fit was used for the disconnected contributions as the data did not show significant excited-state contamination. The isovector renormalization factors, used for all three flavor-diagonal tensor operators, were calculated on the lattice in the RI-SMOM scheme and converted to $\overline{\text{MS}}$ at 2 GeV using 2-loop perturbation theory [1026]. The proceeding [1024] extends the calculation to eight ensembles and reports that flavor mixing in the calculation of renormalization factors is small, and the isovector renormalization factor, which was used for renormalizing the flavor-diagonal tensor charges in PNDME 18B, is a good approximation.

The ETM 19 [989] results for $g_T^{u,d,s,c}$ are from a single ensemble with $2+1+1$-flavor twisted-mass fermions with a clover term at $a = 0.0801(4)$ fm and $M_\pi = 139.3(7)$ MeV. It was not considered for the final averages because it did not satisfy the criteria for the continuum extrapolation. The same applies to the JLQCD 18 [898] and ETM 17 [884] calculations. The Mainz 19A [1022] results with $2+1$-flavor ensembles of clover fermions are not included in the averages as Ref. [1022] is a conference proceeding.

2. Results for $g_S^{u,d,s}$ from direct and hybrid calculations of the matrix elements

The sigma terms $\sigma_q = m_q \langle N|\bar{q}q|N\rangle = m_q g_S^q$ or the quark-mass fractions $f_{T_q} = \sigma_q / M_N$ are normally computed

TABLE 71. Overview of results for $\sigma_{\pi N}$ and σ_s from the direct approach (above) and σ_s from the hybrid approach (below). The renormalization criteria is given for $\sigma_{\pi N}$ (first) and σ_s (second). The label "na" indicates that no renormalization is required.

Collaboration	Ref.	N_f	Publication status	Continuum extrapolation	Chiral extrapolation	Finite volume	Renormalization	Excited states	$\sigma_{\pi N}$ [MeV]	σ_s [MeV]
PNDME 21	[101]	$2+1+1$	A	○[b]	★	★	[a]/–	○	59.6(7.4)	···
ETM 19	[989]	$2+1+1$	A	■	○	★	na/na	○	41.6(3.8)	45.6(6.2)
Mainz 23	[106]	$2+1$	A	★[b]	★	★	★/★	○	43.7(3.6)	28.6(9.3)
JLQCD 18	[898]	$2+1$	A	■	○	○	na/na	○	26(3)(5)(2)	17(18)(9)
χQCD 15A	[104]	$2+1$	A	○	★	★	na/na	○	45.9(7.4)(2.8)[c]	40.2(11.7)(3.5)[c]
MILC 12C	[107]	$2+1+1$	A	★	★	★	–/○	○	···	$0.44(8)(5) \times m_s$[de]
MILC 12C	[107]	$2+1$	A	★	○	★	–/○	○	···	$0.637\,(55)(74) \times m_s$[de]
MILC 09D	[1027]	$2+1$	A	★	○	★	–/na	○	···	59(6)(8)[d]

[a]Mixing between quark flavors is found to be small and is neglected.

[b]The rating takes into account that the scalar current is not fully $\mathcal{O}(a)$-improved by requiring an additional lattice spacing. The gluonic operator that appears in the $\mathcal{O}(a)$ improvement for Wilson fermions is not implemented. The effect of this term is expected to be small.

[c]For this partially quenched analysis the criteria are applied to the unitary points.

[d]This study employs a hybrid method, see Ref. [1027].

[e]The matrix element $\langle N|\bar{s}s|N\rangle$ at the scale $\mu = 2$ GeV in the $\overline{\text{MS}}$ scheme is computed.

rather than g_S^q. These combinations have the advantage of being renormalization group invariant in the continuum, and this holds on the lattice for actions with good chiral properties, see Sec. X A 3 for a discussion. In order to aid comparison with phenomenological estimates, e.g., from $\pi - N$ scattering [1028–1030], the light-quark sigma terms are usually added to give the πN sigma term, $\sigma_{\pi N} = \sigma_u + \sigma_d$. The direct evaluation of the sigma terms involves the calculation of the corresponding three-point correlation functions for different source-sink separations τ. For $\sigma_{\pi N}$ there are both connected and disconnected contributions, while for most lattice fermion formulations only disconnected contributions are needed for σ_s. The techniques typically employed lead to the availability of a wider range of τ for the disconnected contributions compared to the connected ones (both, however, suffer from signal-to-noise problems for large τ, as discussed in Sec. X A) and we only comment on the range of τ computed for the latter in the following.

Recent $N_f = 2+1$ and $N_f = 2+1+1$ results for $\sigma_{\pi N}$ and σ_s from the direct approach are compiled in Table 71. In the following, we summarize new results that have appeared since the last FLAG report and previous studies that enter the averages. Details of ETM 19 [989] and JLQCD 18 [898] can be found in the FLAG 21 report. As there have been no new $N_f = 2$ studies of the sigma terms since the introduction of the section on nucleon matrix elements [876,881], we also refer the reader to the previous report for a discussion of these results and other early three- and four-flavor works with at least one red square [894,897,1025].

Starting with $N_f = 2+1+1$, there is a new study from PNDME [101]. This calculation is based on a mixed-action set-up of $\mathcal{O}(a)$-improved Wilson valence fermions on top of staggered (HISQ) gauge ensembles generated by the MILC collaboration. Six ensembles are utilized with lattice spacings, $a \approx 0.12$, 0.09 and 0.06 fm and pion masses $M_\pi \approx 315$, 230 and 138 MeV. The two-point and three-point correlation functions are fitted simultaneously including contributions from four and three states, respectively, where wide-width priors are used for the excited-state masses entering the fits. Four to five values of the source-sink separation are utilized with the largest $\tau \approx 1.5$ fm. The fitting procedure is repeated using a narrow-width prior for the first excited state which is set to the energy of the lowest multi-hadron state ($N\pi$ or $N\pi\pi$, see Sec. X A 2). This choice is motivated by a χPT analysis [101], which indicates that excited-state contributions arising from

low-lying $N\pi$ and $N\pi\pi$ states can be significant on close-to-physical pion mass ensembles. In particular, there is a significant enhancement of the disconnected contribution due to the large QCD condensate. The quality of the fits is, however, similar for both a narrow- and wide-width prior for the first excited state. Combined continuum- and chiral-limit fits are performed with a parametrization composed of a term linear in the lattice spacing and the NNLO SU(2) baryon χPT expression for the pion-mass dependence. Finite-volume effects are not resolved. The result from the narrow-width first-excited-state prior analysis is chosen as the final value, while the wide-width prior analysis (which has a first-excited-state energy significantly above the lowest $N\pi$ or $N\pi\pi$ noninteracting level) gives $\sigma_{\pi N} \approx 42$ MeV.

Moving on to the $N_f = 2+1$ results, Mainz 23 [106] is a new study employing 16 nonperturbatively $\mathcal{O}(a)$-improved Wilson fermion ensembles from the CLS consortium. The flavor average of the light- and strange-quark mass is held constant in the simulations as the pion mass varies in the range $350 \gtrsim M_\pi \gtrsim 130$ MeV. Four lattice spacings are realized, with $a = 0.050$–0.086 fm. The connected three-point functions are computed for a large number of source-sink separations (between 9 and 17 values of τ, depending on the ensemble) where the largest $\tau = 1.4$–1.5 fm. The ground-state matrix elements are extracted employing two analysis strategies: one employing the summation method (with only the ground-state terms) and the other performing two-state fits to correlator ratios. For the latter, the mass gap to the first excited state is set with a prior equal to twice the pion mass. As both the light- and strange-quark masses vary in the simulations, $\sigma_{\pi N}$ and σ_s are fitted simultaneously with the quark-mass dependence parametrized by SU(3) $\mathcal{O}(p^3)$ covariant baryon χPT. Combined continuum, chiral and finite-volume fits are performed, where cuts are made on the dataset entering the fit which depend on the lattice spacing, finite volume and pion mass. Akaike information criterion [971] averages of the results are computed for the two analysis choices separately. The two results are then combined to form the final values.

The χQCD 15A [104] study also qualifies for global averaging. In this mixed-action study, three RBC/UKQCD $N_f = 2+1$ domain-wall ensembles are analyzed comprising two lattice spacings, $a = 0.08$ fm with $M_{\pi,\text{sea}} = 300$ MeV and $a = 0.11$ fm with $M_{\pi,\text{sea}} = 330$ MeV and 139 MeV. Overlap fermions are employed with a number of nonunitary valence-quark masses. The connected three-point functions are measured with three values of τ in the range 0.9–1.4 fm. A combined chiral, continuum and volume extrapolation is performed for all data with $M_\pi < 350$ MeV. The leading-order expressions are taken for the lattice-spacing and volume dependence while partially quenched SU(2) HBχPT up to M_π^3-terms models the chiral behavior for $\sigma_{\pi N}$. The strange-quark sigma term has a milder dependence on the pion mass and only the leading-order quadratic terms are included in this case.

MILC has also computed σ_s using a hybrid method [1027] which makes use of the Feynman-Hellmann (FH) theorem and involves evaluating the nucleon matrix element $\langle N|\int d^4x\bar{s}s|N\rangle$.[79] This method is applied in MILC 09D [1027] to the $N_f = 2+1$ asqtad ensembles with lattice spacings $a = 0.06, 0.09, 0.12$ fm and values of M_π ranging down to 224 MeV. A continuum and chiral extrapolation is performed including terms linear in the light-quark mass and quadratic in a. As the coefficient of the discretization term is poorly determined, a Bayesian prior is used, with a width corresponding to a 10% discretization effect between the continuum limit and the coarsest lattice spacing.[80] A similar updated analysis is presented in MILC 12C [107], with an improved evaluation of $\langle N|\int d^4x\bar{s}s|N\rangle$ on a subset of the $N_f = 2+1$ asqtad ensembles. The study is also extended to HISQ $N_f = 2+1+1$ ensembles comprising four lattice spacings with $a = 0.06$–0.15 fm and a minimum pion mass of 131 MeV. Results are presented for $g_S^s = \langle N|\bar{s}s|N\rangle$ (in the $\overline{\text{MS}}$ scheme at 2 GeV) rather than for σ_s. The scalar matrix element is renormalized for both three and four flavors using the 2-loop factor for the asqtad action [238]. The error incurred by applying the same factor to the HISQ results is expected to be small.[81]

Both MILC 09D and MILC 12C achieve green tags for all the criteria, see Table 71. As the same set of asqtad ensembles is utilized in both studies we take MILC 12C as superseding MILC 09D for the three-flavor case. The global averaging is discussed in Sec. X D 4.

3. Results for $g_S^{u,d,s}$ using the Feynman-Hellmann theorem

An alternative approach for accessing the sigma terms is to determine the slope of the nucleon mass as a function of the quark masses, or equivalently, the squared pseudoscalar meson masses. The FH theorem gives

$$\sigma_{\pi N} = m_u \frac{\partial M_N}{\partial m_u} + m_d \frac{\partial M_N}{\partial m_d} \approx M_\pi^2 \frac{\partial M_N}{\partial M_\pi^2},$$
$$\sigma_s = m_s \frac{\partial M_N}{\partial m_s} \approx M_{\bar{s}s}^2 \frac{\partial M_N}{\partial M_{\bar{s}s}^2}, \tag{443}$$

where the fictitious $\bar{s}s$ meson has a mass squared $M_{\bar{s}s}^2 = 2M_K^2 - M_\pi^2$. In principle this is a straightforward method as the nucleon mass can be extracted from fits to

[79] Note that in the direct method the matrix element $\langle N|\int d^3x\bar{s}s|N\rangle$, involving the spatial-volume sum, is evaluated for a fixed time slice.

[80] This is consistent with discretization effects observed in other quantities at $a = 0.12$ fm.

[81] At least at 1-loop the renormalization factors for HISQ and asqtad are very similar, cf. Ref. [1031].

TABLE 72. Overview of results for $\sigma_{\pi N}$ and σ_s from the Feynman-Hellmann approach.

Collaboration	Ref.	N_f	Publication status	Continuum extrapolation	Chiral extrapolation	Finite volume	$\sigma_{\pi N}$ [MeV]	σ_s [MeV]
BMW 20A	[1032]	$1+1+1+1$	P	★[b]	★	★	$0.0398(32)(44) \times m_N$[a]	$0.0577\,(46)(33) \times m_N$[a]
ETM 14A	[26]	$2+1+1$	A	★	○	○	64.9(1.5)(13.2)[c]	–
RQCD 22	[105]	$2+1$	A	★	★	★	43.9(4.7)	$16(^{58}_{68})$
BMW 15	[103]	$2+1$	A	★[b]	★	★	38(3)(3)	105(41)(37)
Junnarkar 13	[108]	$2+1$	A	○	○	○	–	48(10)(15)
BMW 11A	[102]	$2+1$	A	○[b]	★	○	$39(4)(^{18}_{7})$	$67(27)(^{55}_{47})$

[a]The quark fractions $f_{T_{ud}} = f_{T_u} + f_{T_d} = \sigma_{\pi N}/m_N$ and $f_{T_s} = \sigma_s/m_N$ are computed.

[b]The rating takes into account that the action is not fully O(a) improved by requiring an additional lattice spacing.

[c]Two results for $\sigma_{\pi N}$ are quoted arising from different fit *Ansätze* to the nucleon mass. The systematic error is the same as in Ref. [1033] for a combined $N_f = 2$ and $N_f = 2+1+1$ analysis [1034].

two-point correlation functions, and a further fit to M_N as a function of M_π (and also M_K for σ_s) provides the slope. Nonetheless, this approach presents its own challenges: a functional form for the chiral behavior of the nucleon mass is needed, and while baryonic χPT (BχPT) is the natural choice, the convergence properties of the different formulations are not well established. Results are sensitive to the formulation chosen and the order of the expansion employed. If there is an insufficient number of data points when implementing higher-order terms, the coefficients are sometimes fixed using additional input, e.g., from analyses of experimental data. This may influence the slope extracted. Simulations with pion masses close to or bracketing the physical point can alleviate these difficulties. In some studies the nucleon mass is used to set the lattice spacing. This naturally forces the fit to reproduce the physical nucleon mass at the physical point and may affect the extracted slope. Note that, if the nucleon mass is fitted as a function of the pion and kaon masses, the dependence of the meson masses on the quark masses also, in principle, needs to be considered in order to extract the sigma terms.

An overview of recent three- and four-flavor determinations of $\sigma_{\pi N}$ and σ_s is given in Table 72. All the results are eligible for global averaging, with RQCD 22 [105] being the sole new work. For details of earlier works (published before 2014) with at least one red square [878,897,964,1035–1037] and all $N_f = 2$ [718,896] works we refer the reader to the FLAG 21 report. Note that the renormalization criterion is not included in Table 72 as renormalization is not normally required when computing the sigma terms in the Feynman-Hellmann approach.[82] At present, a rating indicating control over excited-state contamination is also not considered since a wide range of source-sink separations are available for nucleon two-point functions and ground-state dominance is normally achieved. This issue may be revisited in the future as statistical precision improves and this systematic is further investigated.

We first summarize the determinations of $\sigma_{\pi N}$. BMW have performed a $N_f = 1+1+1+1$ study BMW 20A [1032] which follows a two-step analysis procedure: the dependence of the nucleon mass on the pion and kaon masses is determined on HEX-smeared clover ensembles with $a = 0.06$–0.1 fm and pion masses in the range $M_\pi = 195$–420 MeV. The meson masses as a function of the quark masses are evaluated on stout-staggered ensembles with a similar range in a and quark masses which bracket their physical values. As [1032] is a preprint, their results (for both sigma terms) are not considered for global averaging.

Regarding $N_f = 2+1+1$, there is only one recent study. In ETM 14A [26], fits are performed to the nucleon mass utilizing SU(2) χPT for data with $M_\pi \geq 213$ MeV as part of an analysis to set the lattice spacing. The expansion is considered to $\mathcal{O}(p^3)$ and $\mathcal{O}(p^4)$, with two and three of the coefficients as free parameters, respectively. The

[82]An exception to this is when clover fermions are employed. In this case one must take care of the mixing between quark flavors when renormalizing the quark masses that appear in Eq. (443).

difference between the two fits is taken as the systematic error. No discernable discretization or finite-volume effects are observed where the lattice spacing is varied over the range $a = 0.06$–0.09 fm and the spatial volumes cover $M_\pi L = 3.4$ up to $M_\pi L > 5$. The results are unchanged when a near-physical-point $N_f = 2$ ensemble is added to the analysis in Ref. [1033].

Turning to $N_f = 2 + 1$, RQCD 22 [105] utilizes 49 nonperturbatively $\mathcal{O}(a)$-improved Wilson fermion CLS ensembles, with six lattice spacings in the range $0.04 \leq a \leq 0.1$ fm and $M_\pi \sim 130$–410 MeV. The ensembles lie on three trajectories in the quark-mass plane, two of which meet at the physical point. Simultaneous fits to the bayon octet are performed, employing SU(3) $\mathcal{O}(p^3)$ covariant baryon χPT, heavy baryon χPT and Taylor-expansion fit forms for the quark-mass dependence. The final values at the physical point in the continuum and infinite-volume limits are obtained by performing an Akaike-information-criterion [971] average of the covariant baryon χPT fits to various reduced datasets. These fits include finite-volume terms to $\mathcal{O}(p^3)$ as well as terms quadratic in the lattice spacing in order to model cutoff effects.

In BMW 11A [102], stout-smeared tree-level clover fermions are employed on 15 ensembles with simulation parameters encompassing $a = 0.06$–0.12 fm, $M_\pi \sim$ 190–550 MeV and $M_\pi L \gtrsim 4$. Taylor, Padé and covariant SU(3) BχPT fit forms are considered. Due to the use of smeared gauge links, discretization effects are found to be mild even though the fermion action is not fully $\mathcal{O}(a)$-improved. Fits are performed including an $\mathcal{O}(a)$ or $\mathcal{O}(a^2)$ term and also without a lattice-spacing-dependent term. Finite-volume effects were assessed to be small in an earlier work [1038]. The final results are computed considering all combinations of the fit *Ansatz* weighted by the quality of the fit. In BMW 15 [103], a more extensive analysis on 47 ensembles is presented for HEX-smeared clover fermions involving five lattice spacings and pion masses reaching down to 120 MeV. Bracketing the physical point reduces the reliance on a chiral extrapolation. Joint continuum, chiral and infinite-volume extrapolations are carried out for a number of fit parametrizations with the final results determined via the Akaike-information-criterion procedure. Although only $\sigma_{\pi N}$ is accessible in the FH approach in the isospin limit, the individual quark fractions $f_{T_q} = \sigma_q / M_N$ for $q = u, d$ for the proton and the neutron are also quoted in BMW 15, using isospin relations.[83]

With one exception, all of the above studies have also determined the strange-quark sigma term, while Junnarkar 13 [108] only presents results for σ_s. This quantity is difficult to access via the Feynman-Hellmann method since in most simulations the physical point is approached by varying the light-quark mass, keeping m_s approximately constant. While additional ensembles can be generated, it is hard to resolve a small slope with respect to m_s. Such problems are illustrated by the large uncertainties in the results from BMW 11A and BMW 15. Alternative approaches have been pursued where the physical point is approached along a trajectory keeping the average of the light- and strange-quark masses fixed [1036], and where quark-mass reweighting is applied [897]. One can also fit to the whole baryon octet and apply SU(3) flavor-symmetry constraints as investigated in RQCD 22 [105] and Refs. [102,1035–1037].

Junnarkar 13 [108] is a mixed-action study which utilizes domain-wall valence fermions on MILC $N_f = 2 + 1$ asqtad ensembles. The derivative $\partial M_N / \partial m_s$ is determined from simulations above and below the physical strange-quark mass for M_π around 240–675 MeV. The resulting values of σ_s are extrapolated quadratically in M_π. The quark fraction $f_{T_s} = \sigma_s / M_N$ exhibits a milder pion-mass dependence and extrapolations of this quantity were also performed using *Ansätze* linear and quadratic in M_π. A weighted average of all three fits was used to form the final result. Two lattice spacings were analyzed, with a around 0.09 fm and 0.12 fm, however, discretization effects could not be resolved.

The global averaging of the results is discussed in the next section.

4. Summary of results for $g_S^{u,d,s}$

We consider computing global averages of results determined via the direct, hybrid and FH methods. Beginning with $\sigma_{\pi N}$, Tables 71 and 72 show that for $N_f = 2 + 1 + 1$ ETM 14A (FH) and PNDME 21 (direct) satisfy the selection criteria. The FLAG average for the four-flavor case reads

$$N_f = 2+1+1: \quad \sigma_{\pi N} = 60.9(6.5)\ \text{MeV} \quad \text{Refs. [26,101]}. \tag{444}$$

We remark that although the $N_f = 1 + 1 + 1 + 1$ BMW 20A study [1032] also satisfies the criteria, it is not considered for averaging as it is a preprint. For $N_f = 2 + 1$ we form an average from the BMW 11A (FH), BMW 15 (FH), χQCD 15A (direct), RQCD 22 (FH) and Mainz 23 (direct) results, yielding

$$N_f = 2+1: \quad \sigma_{\pi N} = 42.2(2.4)\ \text{MeV} \quad \text{Refs. [102–106]}. \tag{445}$$

Note that both BMW results are included as they were obtained on independent sets of ensembles (employing different fermion actions). The RQCD 22 and Mainz 23 studies both utilize CLS $N_f = 2 + 1$ ensembles (the latter utilizes a subset of the ensembles employed by the former). To be conservative we take the statistical errors for these

[83] These isospin relations were also derived in Ref. [1039].

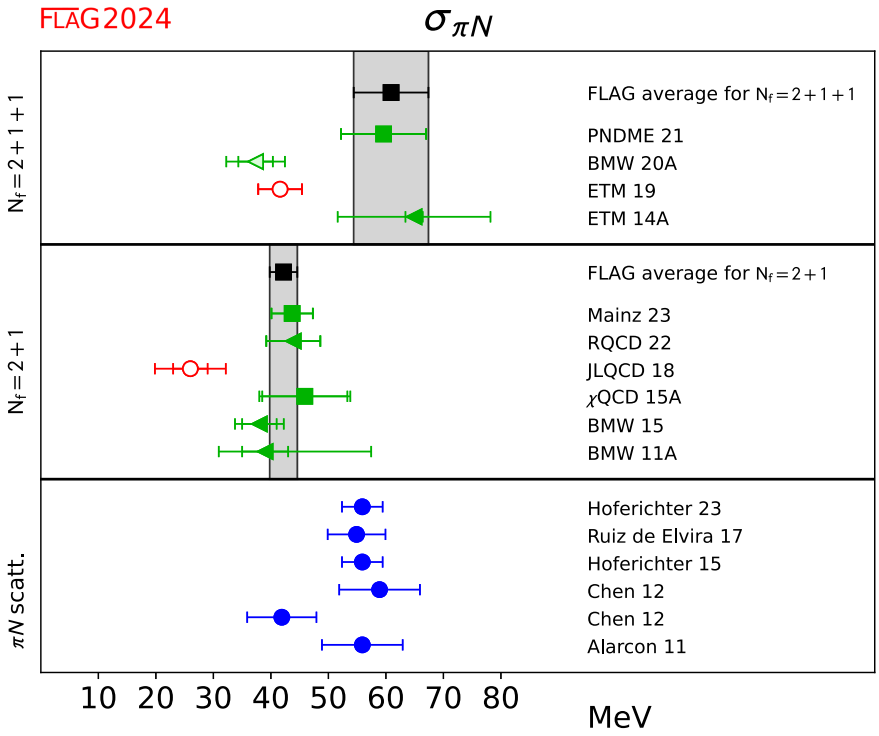


FIG. 46. Lattice results and FLAG averages for the nucleon sigma term, $\sigma_{\pi N}$, for the $N_f = 2+1$, and $2+1+1$ flavor calculations. Determinations via the direct approach are indicated by squares and circles, and the Feynman-Hellmann method by triangles. Results from recent analyses of $\pi - N$ scattering [1028–1030,1040,1041] (filled blue circles) are shown for comparison. Note that the charged pion is used to define the isospin limit in these phenomenological analyses, while the neutral pion with $M_\pi \sim 135$ MeV is usually used to define the physical point in lattice simulations. We adjust the results to be consistent with the latter, applying the correction for the different conventions determined in Ref. [1041].

two studies to be 100% correlated. The FLAG result for $N_f = 2$ can be found in the FLAG 21 report [5].

Moving on to σ_s and the calculations detailed in Table 71, for $N_f = 2+1+1$ MILC 12C (hybrid) and BMW 20A satisfy the quality criteria, however, the latter is a preprint and is not considered for averaging. In order to convert the result for $\langle N|\bar{s}s|N\rangle$ given in MILC 12C to a value for σ_s, we multiply by the appropriate FLAG average for m_s given in Eq. (35) of FLAG 19. This gives our result for four flavors, which is unchanged since the last FLAG report,

$$N_f = 2+1+1\text{:}\quad \sigma_s = 41.0(8.8)\,\text{MeV}\quad \text{Ref. [107]}. \tag{446}$$

For $N_f = 2+1$ we perform a weighted average of BMW 11A (FH), MILC 12C (hybrid), Junnarkar 13 (FH), BMW 15 (FH), χQCD 15A (direct), RQCD 22 (FH) and Mainz 23 (direct). MILC 09D [1027] also passes the FLAG selection rules, however, this calculation is superseded by MILC 12C. As for Eq. (446), the strangeness scalar matrix element determined in the latter study is multiplied by the three-flavor FLAG average for m_s given in Eq. (33) of FLAG 19. There are correlations between the MILC 12C and Junnarkar 13 results as there is some overlap between the sets of asqtad ensembles used in both cases. We take the statistical errors for these two studies to be 100% correlated and, similarly, for the Mainz 23 and RQCD 22 studies (as for $\sigma_{\pi N}$). The global average is

$$N_f = 2+1\text{:}\quad \sigma_s = 44.9(6.4)\,\text{MeV}\quad \text{Refs. [102–108]}, \tag{447}$$

where the error has been increased by around 10% because $\chi^2/\text{dof} = 1.2317$ for the weighted average. For all the other averages presented above, the χ^2/dof is less than one and no rescaling of the error is applied. There are no $N_f = 2$ studies of σ_s which pass the FLAG quality criteria, see the FLAG 21 report for further details.

We remark that it was not possible to determine $\delta(a_{\min})$ for the above works based on the information provided.

All the results for $\sigma_{\pi N}$ and σ_s are displayed in Figs. 46 and 47 along with the averages given above. Note that where $f_{T_{ud}} = f_{T_u} + f_{T_d}$ or f_{T_s} is quoted in Tables 71 and 72, we multiply by the experimental proton mass in order to include the results in the figures. For $\sigma_{\pi N}$, the averages are consistent with the respective FLAG 21 values, however, the errors are significantly reduced. For four flavors, this is due to the PNDME 21 direct result, which dominates the average. The results that enter the average for three flavors,

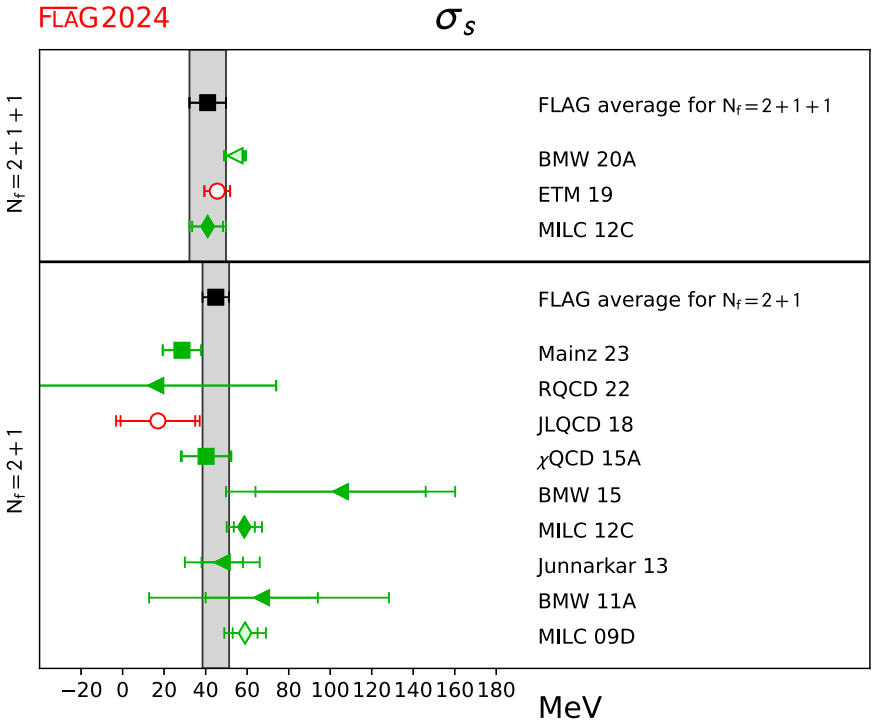


FIG. 47. Lattice results and FLAG averages for σ_s for the $N_f = 2+1$, and $2+1+1$ flavor calculations. Determinations via the direct approach are indicated by squares and circles, the Feynman-Hellmann method by triangles and the hybrid approach by diamonds.

are all consistent with each other and the addition of the RQCD 22 and Mainz 23 studies reduces the uncertainty. The latter is the most precise result to date which passes all the FLAG quality criteria. Notably, there is now a 2.7σ difference between the $N_f = 2+1$ and $N_f = 2+1+1$ FLAG averages. This is unlikely to be due to the inclusion of charm quarks in the sea. The control of excited-state contributions remains an issue. In particular, the PNDME 21 study utilizes a narrow-width prior in their fitting analysis set to the lowest multi-hadron ($N\pi$ or $N\pi\pi$) excited-state energy. This is motivated by a χPT analysis which indicates that these multi-hadron contributions are significant at physical pion masses. If this constraint is relaxed then a sigma term of around 42 MeV is obtained. Mainz 23 also find an increase in the sigma term if such a prior is included in the fitting procedure; however, the shift is much less pronounced. Although progress is being made in terms of improving the statistical precision of the correlation functions and realizing more source-sink separations (with the maximum separation currently around 1.5 fm), more work needs to be done in order to control excited-state contributions at close-to-physical pion masses. We caution the reader that as more results for both $\sigma_{\pi N}$ and σ_s become available the averages may change.

Also shown for comparison in the figures are determinations of $\sigma_{\pi N}$ from recent analyses of $\pi - N$ scattering [1028–1030,1040,1041]. The $N_f = 2+1+1$ lattice average is in agreement with Hoferichter *et al.* [1041] (Hoferichter 23 in Fig. 46), while there is some tension, at the level of around three standard deviations, with the lattice average for $N_f = 2+1$.[84]

For the strangeness sigma term, the four-flavor average is unchanged from the previous FLAG report, while the three-flavor average has decreased by 1σ and there is a small reduction in the error. There is a slight tension between the Mainz 23 and MILC 12C $N_f = 2+1$ results, however, both FLAG averages are consistent with each other.

Finally we remark that, by exploiting the heavy-quark limit, the light- and strange-quark sigma terms can be used to estimate σ_q for the charm, bottom and top quarks [1011–1013]. The resulting estimate for the charm quark, see, e.g., the RQCD 16 $N_f = 2$ analysis of Ref. [876] that reports $f_{T_c} = 0.075(4)$ or $\sigma_c = 70(4)$ MeV, is consistent with the direct determinations of ETM 19 [989] for $N_f = 2+1+1$ of $\sigma_c = 107(22)$ MeV, ETM 16A [881] for $N_f = 2$ of $\sigma_c = 79(21)(^{12}_{8})$ MeV and χQCD 13A [894] for $N_f = 2+1$ of $\sigma_c = 94(31)$ MeV. BMW in BMW 20A [1032] employing the Feynman-Hellmann approach obtain $f_{T_c} = \sigma_c/m_N = 0.0734(45)(55)$ for $N_f = 1+1+1+1$. MILC in MILC 12C [107] find $\langle N|\bar{c}c|N\rangle = 0.056(27)$ in the $\overline{\text{MS}}$ scheme at a scale of 2 GeV for $N_f = 2+1+1$ via the

[84]We adjust the result of Ref. [1041] such that it is consistent with defining the isospin limit using the mass of the neutral pion.

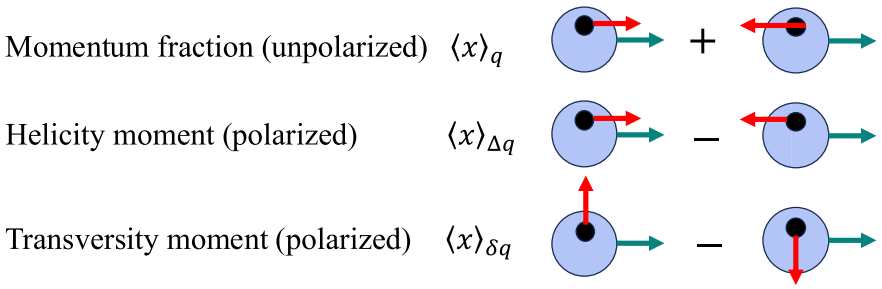


FIG. 48. A pictorial description of the three moments showing the direction of the spin of the quark (red arrow) with respect to the nucleon momentum (green arrow).

hybrid method. Considering the large uncertainty, this is consistent with the other results once multiplied by the charm-quark mass.

E. Isovector second Mellin moments $\langle x \rangle_{u-d}$, $\langle x \rangle_{\Delta u-\Delta d}$ and $\langle x \rangle_{\delta u-\delta d}$

This section introduces the basics of the calculation of the momentum fraction carried by the quarks and the transversity and helicity moments in the isovector channel. These moments of spin-independent (i.e., unpolarized), $q = q_\uparrow + q_\downarrow$, helicity (i.e., polarized), $\Delta q = q_\uparrow - q_\downarrow$, and transversity, $\delta q = q_\top + q_\perp$ distributions, are defined as

$$\langle x \rangle_q = \int_0^1 x[q(x) + \bar{q}(x)]dx, \tag{448}$$

$$\langle x \rangle_{\Delta q} = \int_0^1 x[\Delta q(x) + \Delta\bar{q}(x)]dx, \tag{449}$$

$$\langle x \rangle_{\delta q} = \int_0^1 x[\delta q(x) + \delta\bar{q}(x)]dx, \tag{450}$$

where $q_{\uparrow(\downarrow)}$ corresponds to quarks with helicity aligned (anti-aligned) with that of a longitudinally polarized target, and $q_{\top(\perp)}$ corresponds to quarks with spin aligned (anti-aligned) with that of a transversely polarized target. These alignments are shown pictorially in Fig. 48.

At leading twist, these moments can be extracted from the forward matrix elements of one-derivative vector, axial-vector and tensor operators within ground-state nucleons. The complete set of the relevant twist-two operators are

$$\begin{aligned}
\mathcal{O}^{\mu\nu}_{V^a} &= \bar{q}\gamma^{\{\mu}\overleftrightarrow{D}^{\nu\}}\tau^a q, \\
\mathcal{O}^{\mu\nu}_{A^a} &= \bar{q}\gamma^{\{\mu}\overleftrightarrow{D}^{\nu\}}\gamma^5\tau^a q, \\
\mathcal{O}^{\mu\nu\rho}_{T^a} &= \bar{q}\sigma^{[\mu\{\nu]}\overleftrightarrow{D}^{\rho\}}\tau^a q,
\end{aligned} \tag{451}$$

where $q = \{u, d\}$ is the isodoublet of light quarks and $\sigma^{\mu\nu} = (\gamma^\mu\gamma^\nu - \gamma^\nu\gamma^\mu)/2$. The derivative $\overleftrightarrow{D}^\nu \equiv \frac{1}{2}(\vec{D}^\nu - \overleftarrow{D}^\nu)$ consists of four terms defined in Ref. [109]. Lorentz indices within $\{\}$ in Eq. (451) are symmetrized and within $[]$ are antisymmetrized. It is also implicit that, where relevant, the traceless part of the above operators is taken.

The methodology for nonperturbative renormalization of these operators is very similar to that for the charges. Details of these twist-two operators and their renormalization can be found in Refs. [923,942].

In numerical calculations, it is typical to set the spin of the nucleon in a given direction. Choosing the spin to be in the "3" direction and restricting to the isovector case, $\tau^a = \tau^3$, the explicit operators become

$$\mathcal{O}^{44}_{V^3} = \bar{q}\left(\gamma^4\overleftrightarrow{D}^4 - \frac{1}{3}\gamma\cdot\overleftrightarrow{\mathbf{D}}\right)\tau^3 q, \tag{452}$$

$$\mathcal{O}^{34}_{A^3} = \bar{q}\gamma^{\{3}\overleftrightarrow{D}^{4\}}\gamma^5\tau^3 q, \tag{453}$$

$$\mathcal{O}^{124}_{T^3} = \bar{q}\sigma^{[1\{2]}\overleftrightarrow{D}^{4\}}\tau^3 q. \tag{454}$$

The isovector moments are then obtained from their forward matrix elements within the nucleon ground state using the following relations:

$$\langle 0|\mathcal{O}^{44}_{V^3}|0\rangle = -M_N\langle x\rangle_{u-d}, \tag{455}$$

$$\langle 0|\mathcal{O}^{34}_{A^3}|0\rangle = -\frac{iM_N}{2}\langle x\rangle_{\Delta u-\Delta d}, \tag{456}$$

$$\langle 0|\mathcal{O}^{124}_{T^3}|0\rangle = -\frac{iM_N}{2}\langle x\rangle_{\delta u-\delta d}. \tag{457}$$

1. Results for the isovector moments $\langle x \rangle_{u-d}$, $\langle x \rangle_{\Delta u-\Delta d}$ and $\langle x \rangle_{\delta u-\delta d}$

A summary of results for these three moments is given in Tables 73 and 74 and the values including the FLAG averages are shown in Fig. 49. Results from $N_f = 2$ simulations and publications prior to 2014 have been included as this is the first review of these quantities. For the momentum fraction and helicity moment, we have also included phenomenological estimates. Lattice values

TABLE 73. Overview of results for $\langle x\rangle_{u-d}$ and $\langle x\rangle_{\Delta u-\Delta d}$. The $N_f = 2$ results and publications prior to 2014 are included as this is the first review of these quantities.

Collaboration	Ref.	N_f	Publication status	Continuum extrapolation	Chiral extrapolation	Finite volume	Renormalization	Excited states	$\langle x\rangle_{u-d}$	$\langle x\rangle_{\Delta u-\Delta d}$
ETM 22	[98]	$2+1+1$	A	★	★	★	★	○	0.126(32)	
PNDME 20A	[109]	$2+1+1$	A	★[a]	★	★	★	○	0.173(14)(07)	0.213(15)(22)
ETM 20C	[1042]	$2+1+1$	A	■	○	★	★	○	0.171(18)	
ETM 19A	[1043]	$2+1+1$	A	■	○	★	★	○	0.178(16)	0.193(18)
Mainz 24	[96]	$2+1$	A	★[a]	★	★	★	○	0.153(15)(10)	0.207(15)(06)
LHPC 24	[1044]	$2+1$	A	■[a]	★	★	★	○	0.200(17)	0.213(16)
NME 21A	[1045]	$2+1$	C	★[a]	★	★	★	○	0.156(12)(20)	0.185(12)(20)
NME 20	[110]	$2+1$	A	○[a]	★	★	★	○	0.155(17)(20)	0.183(14)(20)
Mainz 19	[923]	$2+1$	A	★[a]	○	★	★	○	$0.180(25)(^{14}_{6})$	$0.221(25)(^{10}_{0})$
χQCD 18A	[111]	$2+1$	A	○	★	★	★	○	0.151(28)(29)	
LHPC 12A	[994]	$2+1$	A	■[a]	★	★	★	○	0.140(21)	
LHPC 10	[905]	$2+1$	A	■[a]	○	■	★	■	0.1758(20)	0.1972(55)
RBC/UKQCD 10D	[893]	$2+1$	A	■	■	○	★	■	0.140–0.237	0.180–0.279
RQCD 18	[1046]	2	A	○[a]	★	★	★	■	0.195(7)(15)	0.271(14)(16)
ETM 17C	[883]	2	A	■	○	○	★	○	0.194(9)(11)	
ETM 15D	[880]	2	A	■	○	○	★	○	0.208(24)	0.229(30)
RQCD 14A	[1047]	2	A	○[a]	★	★	★	■	0.217(9)	

[a]The rating takes into account that the moments are not fully $\mathcal{O}(a)$-improved by requiring an additional lattice spacing.

for the momentum fraction are consistent with phenomenology but have larger errors. Results for the helicity moment, $\langle x\rangle_{\Delta u-\Delta d}$, are consistent and have similar uncertainties. Lattice results for the transversity moment are a prediction.

We discuss results for these three moments together as the methodology for their calculations and the analysis is the same, and the systematics are similar. All results presented in this section are in the $\overline{\text{MS}}$ scheme at 2 GeV.

For the $2+1+1$-theory, the ETM 22 and PNDME 20A results in [98,109] qualify for the averages. The PNDME 20A results are from nine HISQ ensembles analyzed using clover fermions. The operators are renormalized nonperturbatively using the RI'-MOM scheme, and the chiral-continuum-finite-volume extrapolation is done keeping the leading-order corrections in each of the three variables. Analyses of excited-state contamination are done using three strategies that differ in the selection of the first excited-state mass. The final results are from a three-state fit to the three-point function with the spectrum taken from the two-point function, i.e., assuming no enhanced contribution from multihadron excited states. An additional systematic uncertainty is assigned to cover the spread of these three estimates.

The ETM collaboration has presented new results from three ensembles with $2+1+1$-flavor twisted-mass fermions with close-to-physical pion masses at $a = 0.057$, 0.069 and 0.80 fm in [98]. These results supersede those in [1042,1043] based on the single ensemble at $a = 0.080$ fm for the momentum fraction and the transversity moment. To control excited-state contamination, they compare results from the plateau, summation and two-state methods with the final values taken from the two-state fit. Operators are renormalized nonperturbatively via the RI'-MOM scheme supplemented by perturbative subtraction of lattice artefacts. The continuum extrapolation, which keeps the leading correction $\propto a^2$, shows a significant slope for $\langle x\rangle_{u-d}$, which reduces the continuum-limit value.

When determining the final results to quote for the $2+1+1$ theory, we note the large difference between the

TABLE 74. Overview of results for $\langle x \rangle_{\delta u - \delta d}$. The $N_f = 2$ results and publications prior to 2014 are included as this is the first review of these quantities.

Collaboration	Ref.	N_f	Publication status	Continuum extrapolation	Chiral extrapolation	Finite volume	Renormalization	Excited states	$\langle x \rangle_{\delta u - \delta d}$
ETM 22	[98]	$2+1+1$	A	★	★	★	★	○	0.168(44)
PNDME 20A	[109]	$2+1+1$	A	★[a]	★	★	★	○	0.208(19)(24)
ETM 19A	[1043]	$2+1+1$	A	■	○	★	★	○	0.204(23)
Mainz 24	[96]	$2+1$	A	★[a]	★	★	★	○	0.195(17)(15)
LHPC 24	[1044]	$2+1$	A	■[a]	★	★	★	○	0.219(21)
NME 21A	[1045]	$2+1$	C	★[a]	★	★	★	○	0.209(15)(20)
NME 20	[110]	$2+1$	A	○[a]	★	★	★	○	0.220(18)(20)
Mainz 19	[923]	$2+1$	A	★[a]	○	★	★	○	$0.212(32)(^{+20}_{-20})$
RQCD 18	[1046]	2	A	○[a]	★	★	★	■	0.266(8)(4)
ETM 15D	[880]	2	A	■	○	○	★	○	0.306(29)

[a]The rating takes into account that the moments are not fully $\mathcal{O}(a)$-improved by requiring an additional lattice spacing.

results from Refs. [98,109] for the momentum fraction. Our conservative approach is to construct the interval defined by the PNDME 20A value plus error and the ETM 22 value, i.e., 0.126–0.189, and then take the mean of the interval for the central value and half the spread for the error as shown in Fig. 49. For the transversity moment we perform the FLAG averaging assuming no correlations between the two calculations. For the helicity fraction we quote the PNDME 20A [109] values. The values of $\delta(a_{\min})$ for the three moments for the PNDME 20A calculation [109] are 0.6, 0.3 and 0.13, and those for ETM 22 are roughly 0.8 (momentum fraction) and 0.0 (transversity). The FLAG averages are

$$N_f = 2+1+1 : \langle x \rangle_{u-d} = 0.158(32) \text{ Refs. } [98,109], \quad (458)$$

$$N_f = 2+1+1 : \langle x \rangle_{\Delta u - \Delta d} = 0.213(27) \text{ Ref. } [109], \quad (459)$$

$$N_f = 2+1+1 : \langle x \rangle_{\delta u - \delta d} = 0.195(25) \text{ Refs. } [98,109]. \quad (460)$$

Five calculations qualify for averages for the $2+1$-flavor theory: the Mainz [96,923], the NME [110,1045], and χQCD [111]. Of these, the Mainz 24 [96] supersedes the Mainz 19 [923], and while the NME 21A [1045] is an update of NME 20 [110], it is a conference proceeding.

The Mainz 24 results are based on fifteen $N_f = 2+1$ ensembles produced by the CLS collaboration covering the ranges $0.05 \le a \le 0.09$ fm and $130 \le M_\pi \le 360$ MeV. A two-state summation method is used to control excited-state contamination. In the continuum-chiral-finite-volume extrapolation, leading-order corrections are used for the continuum and finite-volume corrections and up to NNLO results from SU(2) baryon chiral perturbation theory for the chiral part.

The NME 20 [110] results are based on seven $N_f = 2+1$ clover ensembles produced by the JLab/W&M/LANL/MIT collaborations. They cover the range $0.07 \le a \le 0.13$ fm and $170 \le M_\pi \le 280$ MeV. The analysis methodology is the same as in Ref. [109] already discussed above.

The χQCD [111] calculation uses four domain-wall ensembles that have been generated by the RBC/UKQCD collaboration that cover the range $0.08 \le a \le 0.14$ fm and $139 \le M_\pi \le 330$ MeV. A number of values of overlap-valence-quark masses, in addition to those close to the unitary point $M_\pi^{\text{sea}} = M_\pi^{\text{valence}}$, are used. The renormalization is carried out nonperturbatively. The continuum-chiral-finite-volume extrapolation is carried out using the leading corrections plus terms accounting for partial quenching, i.e., the leading terms in the difference $M_\pi^{\text{sea}} - M_\pi^{\text{valence}}$.

The three older calculations, LHPC 12A [994], LHPC 10 [905] and RBC/UKQCD [893], do not meet the criteria of control over the continuum limit. Similarly, the $N_f = 2$ calculations fail to satisfy one or more of the FLAG criteria.

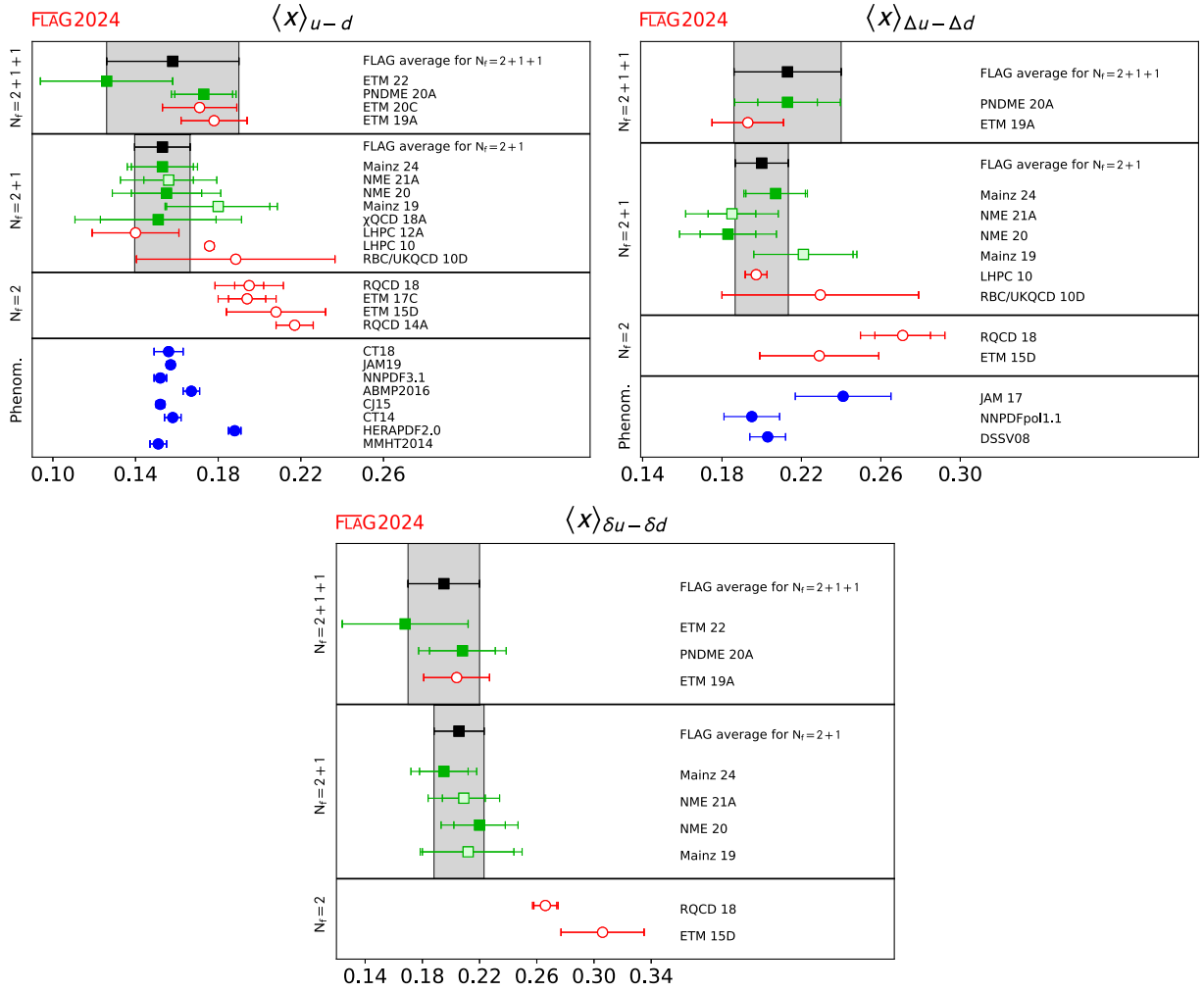


FIG. 49. Lattice-QCD results for the second Mellin moments $\langle x \rangle_{u-d}$, $\langle x \rangle_{\Delta u-\Delta d}$ and $\langle x \rangle_{\delta u-\delta d}$. Results from $N_f = 2$ simulations and publications prior to 2014 have been included as this is the first review of these quantities. For the momentum-fraction and helicity moment, we have also included phenomenological estimates [1048–1058]. For reference, a recent analysis [1059], using a combined set of World DIS data, found $\langle x \rangle_{u-d} = 0.143(5)$ at $Q^2 = 4$ GeV^2 (not shown).

The $2+1$-flavor FLAG averages for the momentum fraction, $\langle x \rangle_{u-d}$, are constructed using the Mainz 24 [96], NME 20 [110] and χQCD 18A [111] values assuming zero correlations between them. The results for the helicity and transversity moments are the FLAG averages of the Mainz 24 [96] and NME 20 [110] values again assuming zero correlations. The values of $\delta(a_{\min})$ for the Mainz 24 [96] for the three moments are 1.5, 0.2, 0.1 and those for the NME 20 are 0.5, 1.0 and 0.2. The χQCD 18A work does not provide enough information to determine $\delta(a_{\min})$. The FLAG averages are

$$N_f = 2+1: \quad \langle x \rangle_{u-d} = 0.153(13) \quad \text{Refs. [96,110,111]}, \tag{461}$$

$$N_f = 2+1: \quad \langle x \rangle_{\Delta u-\Delta d} = 0.200(13) \quad \text{Refs. [96,110]}, \tag{462}$$

$$N_f = 2+1: \quad \langle x \rangle_{\delta u-\delta d} = 0.206(17) \quad \text{Refs. [96,110]}. \tag{463}$$

XI. SCALE SETTING

Working group members: R. Sommer, N. Tantalo, U. Wenger

Matching QCD to nature requires fixing the quark masses and matching an overall scale to experiment. That overall energy scale $\mathcal{S}$ may be taken, for example, as the nucleon mass. This process is referred to as scale setting.

A. Impact

The scale setting procedure, described in some detail below, is a rather technical step necessary to obtain predictions from QCD. What may easily be overlooked

is that the exact predictions obtained from the theory, including many in this review, may depend rather sensitively on the scale.

As long as the theory is incomplete, e.g., because we have predictions from $N_f = 2+1$ QCD, results will depend on which physics scale is used. Whenever a theory scale (see Sec. XI D) is used, it matters which value one imposes. Thus, to know whether computations of a particular quantity agree or not, one should check which (value for a) scale was used.

The sensitivity of predictions to the scale vary with the observable. For example, the Λ parameter of the theory has a linear dependence,

$$\frac{\delta\Lambda}{\Lambda} \approx \frac{\delta\mathcal{S}}{\mathcal{S}}, \tag{464}$$

because Λ has mass dimension one and other hidden dependencies on the scale are (usually) suppressed. Let us preview the results. The present precision on the most popular theory scale, w_0 in Eq. (500) is about 0.4% and for $\sqrt{t_0}$ it is 0.6%. On the Λ parameter it is about 3%. Thus, we would think that the scale uncertainty is irrelevant. However, in Sec. XI G we will discuss that differences between $N_f = 2+1$ and $2+1+1$ numbers for $\sqrt{t_0}$ are at around 2%, which *does matter.*

Also, light-quark masses have an approximatively linear dependence on the scale (roughly speaking one determines, e.g., $m_{ud} = \frac{1}{\mathcal{S}} \times [M_\pi^2]_{\rm exp} \times [\frac{m_{ud}\mathcal{S}}{M_\pi^2}]_{\rm lat}$) and scale uncertainties may play an important role in the discussion of agreement vs. disagreement of computations within their error budget.

The list of quantities where scale setting is very important may be continued; we just want to mention an observable very much discussed at present, the hadronic vacuum-polarization contribution to the anomalous magnetic moment of the muon [206]. It is easily seen that the dependence on the scale is about quadratic in that case [1060],

$$\frac{\delta a_\mu^{\rm HVP}}{a_\mu^{\rm HVP}} \approx 2\frac{\delta\mathcal{S}}{\mathcal{S}}. \tag{465}$$

This fact means that scale setting has to be precise at the few per-mille precision for the $a_\mu^{\rm HVP}$ lattice determination to be relevant in the comparison with experiment.

B. Scale setting as part of hadronic renormalization schemes

We consider QCD with N_f quarks and without a θ-parameter. This theory is completely defined by its coupling constant as well as N_f quark masses. After these parameters are specified all other properties of the theory are predictions. Coupling and quark masses depend on a renormalization scale μ as well as on a renormalization scheme. The most popular scheme in the framework of perturbative computations is the $\overline{\rm MS}$ scheme, but one may also define nonperturbative renormalization schemes, see Secs. IV and IX.

In principle, a lattice computation may, therefore, use these $N_f + 1$ parameters as input together with the renormalization scale μ to fix the bare quark masses and coupling of the discretized Lagrangian, perform continuum and infinite-volume limit and obtain desired results, e.g., for decay rates.[85] However, there are various reasons why this strategy is inefficient. The most relevant one is that unless one uses lattice gauge theory to compute them, coupling and quark masses cannot be obtained from experiments without invoking perturbation theory and thus necessarily truncation errors. Moreover, these parameters are naturally short-distance quantities, since this is where perturbation theory applies. Lattice QCD on the other hand is most effective at long distances, where the lattice spacing plays a minor role. Therefore, it is more natural to proceed differently.

Namely, we may fix $N_f + 1$ nonperturbative, long-distance observables to have the values found in nature. An obvious choice are $N_f + 1$ hadron masses that are stable in the absence of weak interactions. This hadronic renormalization scheme is defined by

$$\frac{M_i(g_0, \{am_{0,\rm j}\})}{M_1(g_0, \{am_{0,\rm j}\})} = \frac{M_i^{\rm exp}}{M_1^{\rm exp}}, \quad i = 2 \ldots N_f + 1, \quad j = 1 \ldots N_f. \tag{466}$$

Here, M_i are the chosen hadron masses, g_0 is the bare coupling, and $am_{0,j}$ are the bare quark masses in lattice units. The ratio M_i/M_1 is, precisely speaking, defined through the hadron masses in lattice units, but in infinite volume. In QCD (without QED), all particles are massive. Therefore, the infinite volume limit of the properties of stable particles is approached with exponentially small corrections, which are assumed to be estimated reliably. The power-like finite-volume corrections in QCD + QED are discussed in Sec. XI B 2. For fixed g_0, Eq. (466) needs to be solved for the bare quark masses,

$$am_{0,\rm j} = \mu_j(g_0). \tag{467}$$

The functions μ_j define a line in the bare parameter space, called the line of constant physics. Its dependence on the set of masses $\{M_i\}$ is suppressed. The continuum limit is obtained as $g_0 \to 0$ with the lattice spacing shrinking roughly as $aM_1 \sim {\rm e}^{-1/(2b_0 g_0^2)}$. More precisely, consider

[85] At first sight this seems like too many inputs, but note that it is the scale μ, at which $\alpha(\mu)$ has a particular value, which is the input. The coupling α by itself can have any (small) value as it runs.

observables $\mathcal{O}$ with mass dimension $d_\mathcal{O}$. One defines their dimensionless ratio

$$\hat{\mathcal{O}}(aM_1) = \left.\frac{\mathcal{O}}{M_1^{d_\mathcal{O}}}\right|_{am_{0,j}=\mu_j(g_0)}, \tag{468}$$

and obtains the continuum prediction as

$$\mathcal{O}^{\text{cont}} = (M_1^{\text{exp}})^{d_\mathcal{O}} \lim_{aM_1\to 0} \hat{\mathcal{O}}(aM_1) \tag{469}$$

which explains why the determination and use of aM_1 is referred to as scale setting.

Equation (467) has to be obtained from numerical results. Therefore, it is easiest and most transparent if the ith mass ratio depends predominantly on the ith quark mass. Remaining for a while in the isospin-symmetric theory with $m_{0,1} = m_{0,2}$ (we enumerate the quark masses in the order up, down, strange, charm, bottom and ignore the top quark), we have natural candidates for the numerators as the pseudoscalar masses in the associated flavor sectors, i.e., π, K, D, B. The desired strong dependence on light-(strange-)quark masses of π- (K-)meson masses derives from their pseudo-Goldstone nature of the approximate $\mathrm{SU(3)_L \times SU(3)_R}$ symmetry of the massless QCD Lagrangian, which predicts that M_π^2 is roughly proportional to the light-quark mass and M_K^2 to the sum of light- and strange-quark masses. For D and B mesons approximate heavy-quark symmetry predicts M_D and M_B to be proportional to charm- and bottom-quark masses. Also other heavy-light bound states have this property. There is another important feature, which singles out pseudoscalar masses. Because they are the lightest particles with the given flavor quantum numbers, their correlation functions have the least signal/noise problem in the Monte Carlo evaluation of the path integral [470,1061].

Still restricting ourselves to isospin-symmetric QCD (isoQCD, see Sec. III), we thus take it for granted that the choice M_i, $i \geq 2$ is easy, and we do not need to discuss it in detail: the pseudoscalar meson masses are very good choices, and some variations for heavy quarks may provide further improvements.

The choice of M_1 is more difficult. From the point of view of physics, a natural choice is the nucleon mass, $M_1 = M_{\text{nucl}}$. Unfortunately it has a rather bad signal/noise problem when quark masses are close to their physical values. The ratio of signal to noise of the correlation function at time x_0 from N measurements behaves as [470]

$$R_{S/N}^{\text{nucl}\,x_0} \overset{\text{large}}{\sim} \sqrt{N}\exp\left(-\left(M_{\text{nucl}} - \frac{3}{2}M_\pi\right)x_0\right) \approx \sqrt{N}\exp(-x_0/0.27\ \text{fm}), \tag{470}$$

where the numerical value of 0.27 fm uses the experimental masses. The behavior in practice, but at still favorably large quark masses, is illustrated in Fig. 50. Because this property leads to large statistical errors and it is further difficult to control excited-state contaminations when statistical errors are large, it is useful to search for alternative physics scales. The community has gone this way, and we discuss some of them below. For illustration, here we just give one example: the decay constants of leptonic π or K decays have mass dimension one and can directly replace M_1 above. Figure 50 demonstrates their long and precise plateaux as a function of the Euclidean time. Advantages and disadvantages of this choice and others are discussed more systematically in Sec. XI C.

1. Theory scales

Since the signal/noise problem of physics scales is rather severe, they were already replaced by theory scales in the very first days of lattice QCD. These scales cannot be determined from experiment alone. Rather, their values have to be computed by lattice QCD using a physics scale as input.

Creutz already used the string tension in his seminal paper on SU(2) Yang Mills theory [1065], because it is far easier to determine than glueball masses. A further step was made by the potential scale r_0, defined in terms of the static force $F(r)$ as [708]

$$r_0^2 F(r_0) = 1.65. \tag{471}$$

Even though r_0 can vaguely be related to the phenomenology of charmonium and bottomonium states, its precise definition is in terms of $F(r)$ which can be obtained accurately from Monte Carlo lattice computations with (improvable) control over the uncertainties, but not from experiment. In that sense, it is a prototype of a theory scale.

Useful properties of a good theory scale are high statistical precision, easy to control systematics, e.g., weak volume dependence, quark-mass dependence only due to the fermion determinant, and low numerical cost for its evaluation. These properties are realized to varying degrees by the different theory scales covered in this section and, in this respect, they are much preferred compared to physics scales. Consequently, the physics scale M_1 has often been replaced by a theory scale as, e.g., $\mathcal{S} = r_0^{-1}$ in the form

$$\mathcal{O}^{\text{cont}} = (\mathcal{S}^{\text{phys}})^{d_\mathcal{O}} \lim_{a\mathcal{S}\to 0} \hat{\mathcal{O}}_\mathcal{S}(a\mathcal{S}) \quad \text{with}$$
$$\hat{\mathcal{O}}_\mathcal{S}(a\mathcal{S}) = [\mathcal{S}^{-d_\mathcal{O}}\mathcal{O}]_{am_{0,j}=\mu_j(g_0)}, \tag{472}$$

and

$$\mathcal{S}^{\text{phys}} = (M_1^{\text{exp}}) \lim_{aM_1\to 0} \hat{\mathcal{S}}_{M_1}(aM_1). \tag{473}$$

In this section, we review the determination of numerical results for the values of various theory scales in physical units, Eq. (473). The main difficulty is that a physics scale

M_1 has to be determined first in order to connect to nature and, in particular, that the continuum limit of the theory scale in units of the physics scale has to be taken.

2. Isospin breaking

For simplicity and because it is a very good approximation, we have assumed above that all other interactions except for QCD can be ignored when hadron masses and many other properties of hadrons are considered. This is a natural point of view because QCD is a renormalizable field theory and thus provides unique results.

However, we must be aware that while it is true that the predictions (e.g., for hadron masses $M_i, i > N_f + 1$) are unique once Eq. (466) is specified, they will change when we change the inputs $M_i^{\rm exp}$. These ambiguities are due to the neglected electroweak and gravitational interactions, namely because QCD is only an approximate—even if precise—theory of hadrons. At the sub-percent level, QED effects and isospin violations due to $m_u \neq m_d$ must be included. At that level one has a very precise description of nature, where weak decays or weak effects, in general, can be included perturbatively and systematically in an effective-field-theory description through the weak-effective-interaction Hamiltonian, while gravity may be ignored.

Scale setting is then part of the renormalization of QCD + QED, and in principle it is quite analogous to the previous discussion. Triviality of QED does not play a role at small enough α: we may think of replacing the continuum limit $a \to 0$ by a limit $a \to a_{\rm w}$ with $a_{\rm w}$ nonzero but very far below all physical QCD + QED scales treated. The definition and implementation of a hadronic renormalization scheme of QCD + QED defined on the lattice is discussed in Sec. III. The electric charge appears as a new parameter and is conveniently fixed in the Thomson limit. Care needs to be taken in the separate definition of QED effects and strong isospin-breaking effects due to the up/down quark-mass difference. Here, we repeat Eq. (23),

$$X^{\phi} = \bar{X} + X_{\gamma} + X_{\rm SU(2)}, \tag{474}$$

and again emphasize that the split of physical observables X^{ϕ} into their isoQCD part, $\bar{X}$, the QED contributions, X_{γ}, and the strong IB effects, $X_{\rm SU(2)}$, is scheme dependent. In order to hopefully avoid confusion and to make it possible to average results also when they have a precision where the small IB-breaking effects matter, a particular scheme has been defined in Sec. III. For quantities that enter in the averages, the schemes used in the computations are listed in Table 75. In this way, we can, to some degree, judge whether differences of results may also be due to the scheme used.

As a matter of fact, many existing lattice calculations have been performed in the isospin-symmetric limit, but not all the results considered in this review correspond to the very same definition of QCD. The different choices of experimental inputs are perfectly legitimate if QED radiative corrections are neglected, but in principle, predictions of isoQCD do depend on these choices, and it is not meaningful to average numbers obtained with different inputs. However, at the present level of precision the sub-percent differences in the inputs are most likely not relevant, and we will average and compare isoQCD results irrespective of these differences. The issue will become important when results become significantly more precise. Of course, the different inputs may not be ignored, when radiative corrections, Eq. (23), from various collaborations are directly compared. In this case, we strongly suggest to compare results for the unambiguous full theory observable or sticking to a standard.

C. Physical scales

The purpose of this short section is to summarize the most popular scales and give a short discussion of their advantages and disadvantages. We restrict ourselves to those used in more recent computations and, thus, the list is short.

1. The mass of the Ω baryon

As already discussed, masses of hadrons that are stable in QCD + QED and have a small width, in general, are very good candidates for physical scales since there are no QED infrared divergences to be discussed. Furthermore, remaining within this class, the radiative corrections are expected to be small. Furthermore, the Ω baryon has a significantly better noise/signal ratio than the nucleon (see Fig. 50). It also has little dependence on up- and down-quark masses, since it is composed entirely of strange valence quarks.

Still, one has to be aware that the mass is not extracted from the plateau region but from a modeling of the approach to a plateau in the form of fits [12,112,115,116,119,235]. In this sense, the noise/signal ratio problem may persist. The use of various interpolating fields for the Ω helps in constraining such analyses, but it would be desirable to have a theoretical understanding of multi-hadron (or in QCD + QED multi-hadron + photon) contributions as for the nucleon [1068] discussed in Sec. X. In the present review, we take the estimates of the collaborations at face value and do not try to apply a rating or an estimate of systematic error due to excited-state contributions.

2. Pion and kaon leptonic decay rates

These decay rates play a prominent role in scale setting, in (pure) QCD because excited-state contaminations can simply be avoided by going to sufficiently large Euclidean time. As a downside, QED radiative corrections need to be taken into account in the values assigned to the associated decay constants. Therefore, we briefly summarize the

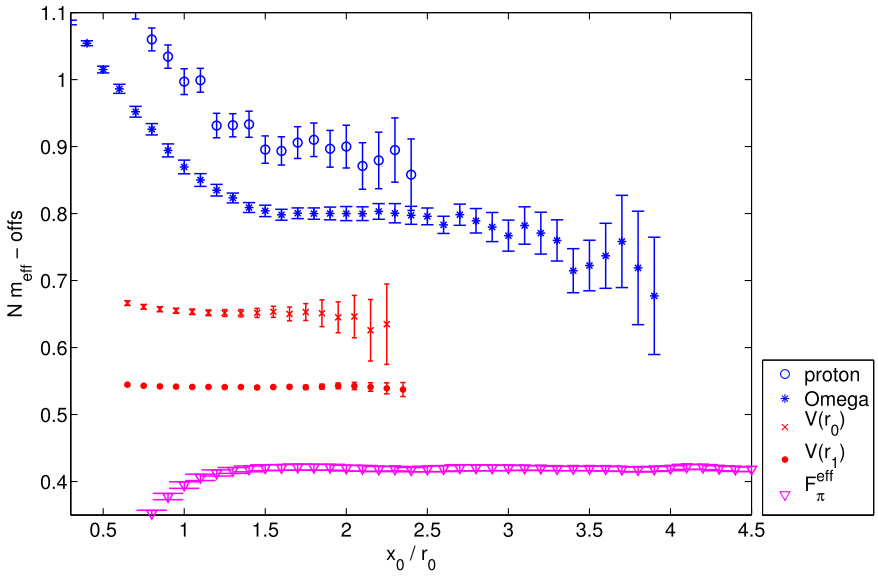


FIG. 50. Effective masses for M_{proton} [1062], M_Ω [1063], $V(\approx r_0)$, $V(\approx r_1)$ [717] and f_π [1064] on $N_f = 2$ CLS ensemble N6 with $a = 0.045$ fm, $M_\pi = 340$ MeV on a $48^3 \times 96$ lattice [1064]. All effective "masses" have been scaled such that the errors in the graph reflect directly the errors of the determined scales. They are shifted vertically by arbitrary amounts. Figure from Ref. [824]. Note that this example is at still favorably large quark masses. The situation for M_{proton} becomes worse closer to the physical point, but may be changed by algorithmic improvements.

knowledge of QED radiative corrections and the definition of decay constants. More details are found in the previous edition of this review.

The physical observable is the decay rate $\Gamma^{\text{QCD+QED}}[\pi^- \mapsto \mu\bar{\nu}_\mu(\gamma), E_\gamma]$ of a pion at rest. It depends on the maximum energy E_γ of photons emitted in the decay and registered in the experimental measurement. These soft and hard photons cannot be avoided since the cross-section vanishes as $E_\gamma \to 0$ and, e.g., the fixed-order cross-section without final-state photons is infrared divergent. However, apart from the dependence on E_γ, there are no ambiguities in the definition of $\Gamma^{\text{QCD+QED}}$.

In QCD, the leptonic decay rate is,

$$\Gamma^{\text{QCD}}[\pi \mapsto \mu\bar{\nu}_\mu] = \frac{G_F^2}{8\pi}|V_{ud}|^2 M_{\pi^-}^{\text{exp}}(m_\mu^{\text{exp}})^2\left[1-\frac{(m_\mu^{\text{exp}})^2}{(M_{\pi^-}^{\text{exp}})^2}\right](f_\pi^{\text{QCD}})^2, \tag{475}$$

where one naturally introduces the decay constant,

$$f_\pi^{\text{QCD}} = \frac{\langle 0|\bar{u}\gamma^0\gamma^5 d|\pi\rangle^{\text{QCD}}}{M_\pi^{\text{QCD}}}. \tag{476}$$

of the pion. Radiative corrections to f_π^{QCD} are then defined by

$$\delta f_\pi^{\text{QCD}}(E_\gamma) = \sqrt{\frac{\Gamma^{\text{QCD+QED}}[\pi^- \mapsto \mu\bar{\nu}_\mu(\gamma), E_\gamma]}{\Gamma^{\text{QCD}}[\pi \mapsto \mu\bar{\nu}_\mu]}} - 1, \tag{477}$$

such that

$$\Gamma^{\text{QCD+QED}}[\pi^- \mapsto \mu\bar{\nu}_\mu(\gamma), E_\gamma] = \Gamma^{\text{QCD}}[\pi \mapsto \mu\bar{\nu}_\mu][1+\delta f_\pi^{\text{QCD}}(E_\gamma)]^2. \tag{478}$$

Common practice is to set

$$E_\gamma = E_\gamma^{\max} = \frac{M_{\pi^-}^{\text{exp}}}{2}\left[1-\frac{(m_\mu^{\text{exp}})^2}{(M_{\pi^-}^{\text{exp}})^2}\right], \tag{479}$$

the maximum energy allowed for a single photon in the case of negligible $\mathcal{O}(\alpha_{\text{em}}^2)$ corrections.

As discussed in Sec. III, $\delta f_\pi^{\text{QCD}}(E_\gamma)$ depends on the scheme used to define QCD. However, the RM123 lattice determination in the electro-quenched approximation [217] found the scheme dependence to be irrelevant at the level of their result, $\delta f_\pi^{\text{isoQCD}}(E_\gamma^{\max}) = 0.0076(9)$.[86] Additionally this agrees well with the estimate, $\delta f_\pi^{\text{isoQCD}}(E_\gamma^{\max}) = 0.0088(11)$ from ChPT [282,1069,1070]. Taking V_{ud} from the PDG [225] (beta decays) and the ChPT number for δf_π, one has

$$f_\pi^{\text{isoQCD}} = 130.56(2)_{\text{exp}}(13)_{\text{QED}}(2)_{V_{ud}}\text{MeV}.$$

[86]More precisely, both a hadronic scheme and a so-called GRS scheme were tested, where as a simplification one may replace constant $\alpha_s(\mu_{\text{ref}})$ across theories by constant lattice spacing in the electro-quenched approximation.

With the Edinburgh consensus Sec. III, the scale of isoQCD is *defined* by

$$f_\pi^{\mathrm{isoQCD}} \equiv 130.5\ \mathrm{MeV}. \tag{480}$$

At the present level of accuracy the difference between the determined value (with a scheme uncertainty of around 1 per mille) and the defining value (480) is irrelevant.

Some scale determinations use also the kaon decay constant. There the understanding of QED radiative corrections is not yet as good as for pion decays. The ChPT estimate is $\delta f_K^{\mathrm{isoQCD}}(E_\gamma^{\max}) = 0.0053(11)$ [282,1069,1070], while the electro-quenched lattice computation yielded $\delta f_K^{\mathrm{isoQCD}}(E_\gamma^{\max}) = 0.0012(5)$ [217]. As a slight update of the previous review, here we opt for a more conservative number of

$$\delta f_K^{\mathrm{isoQCD}}(E_\gamma^{\max}) = 0.003(3), \tag{481}$$

encompassing both estimates. Together with $V_{us} = 0.2232(6)$ from Sec. V ($f_+(0)$ for $N_f = 2+1+1$) and the PDG decay rate, we have

$$f_K^{\mathrm{isoQCD}} = 157.4(2)_{\mathrm{exp}}(4)_{\mathrm{QED}}(4)_{V_{us}}\ \mathrm{MeV}. \tag{482}$$

Depending on the lattice formulation, there is also a nontrivial renormalization of the axial current. Since it is easily determined from a chiral Ward identity, it does not play an important role. When it is present, it is assumed to be accounted for in the statistical errors.

3. Other physics scales

Scales derived from bottomonium have been used in the past, in particular, the splitting $\Delta M_\Upsilon = M_{\Upsilon(2s)} - M_{\Upsilon(1s)}$. They have very little dependence on the light-quark masses, but need an input for the b-quark mass. In all relevant cases, the b quark is treated by NRQCD.

D. Theory scales

In the following, we consider in more detail the two classes of theory scales that are most commonly used in typical lattice computations. The first class consists of scales related to the static quark-antiquark potential [708]. The second class is related to the action density renormalized through the gradient flow [365].

1. Potential scales

In this approach, lattice scales are derived from the properties of the static quark-antiquark potential. In particular, a scale can be defined by fixing the force $F(r)$ between a static quark and antiquark separated by the distance r in physical units [708]. Advantages of using the potential include the ease and accuracy of its computation, and its mild dependence on the valence-quark mass. In general, a potential scale r_c can be fixed through the condition that the static force takes a predescribed value, i.e.,

$$r_c^2 F(r_c) = X_c, \tag{483}$$

where X_c is a suitably chosen number. Phenomenological and computational considerations suggest that the optimal choice for X_c is in the region where the static force turns over from Coulomb-like to linear behavior and before string breaking occurs. In the original work [708], it was suggested to use $X_0 = 1.65$ leading to the condition

$$r_0^2 F(r_0) = 1.65. \tag{484}$$

In Ref. [709], the value $X_1 = 1.0$ was proposed yielding the scale r_1.

The static force is the derivative of the static quark-antiquark potential $V(r)$ which can be determined through the calculation of Wilson loops. More specifically, the potential at distance r is extracted from the asymptotic time dependence of the $r \times t$-sized Wilson loops $W(r,t)$,

$$V(r) = -\lim_{t\to\infty} \frac{d}{dt} \log\langle W(r,t)\rangle. \tag{485}$$

The derivative of the potential needed for the force is then determined through the derivative of a suitable local parametrization of the potential as a function of r, e.g.,

$$V(r) = C_- \frac{1}{r} + C_0 + C_+ r, \tag{486}$$

and estimating uncertainties due to the parametrization. In some calculations, the gauge field is fixed to Coulomb or temporal gauge in order to ease the computation of the potential at arbitrary distances.

In order to optimize the overlap of the Wilson loops with the ground state of the potential, one can use different types and levels of spatial gauge-field smearing and extract the ground-state energy from the corresponding correlation matrix by solving a generalized eigenvalue problem [936,937,1071]. Finally, one can also make use of the noise reduction proposed in Refs. [1072,1073]. It includes a smearing of the temporal parallel transporter [1074] in the lattice definition of the discretized loops and thus yields a different discretization of the continuum force.

2. Gradient flow scales

The gradient flow $B_\mu(t,x)$ of gauge fields is defined in the continuum by the flow equation

$$\dot{B}_\mu = D_\nu G_{\nu\mu}, \qquad B_\mu|_{t=0} = A_\mu, \tag{487}$$

$$G_{\mu\nu} = \partial_\mu B_\nu - \partial_\nu B_\mu + [B_\mu, B_\nu], \quad D_\mu = \partial_\mu + [B_\mu, \cdot], \tag{488}$$

TABLE 75. isoQCD schemes used in different computations as well as the Edinburgh consensus (see Sec. III). We do not list the choice for M_π. It is $M_\pi = 135.0$ MeV throughout. As all quantities refer to the light sector of QCD only, charm quarks only enter through sea-quark effects. We therefore do not list which quantity is used to fix the charm-quark mass at the present stage.

Collaboration	Ref.	N_f	M_K [MeV]	Scale	Scale [MeV]
ETM 21	[45]	$2+1+1$	494.2	f_π	130.4
CalLat 20A	[112]	$2+1+1$	494.2	M_Ω	1672.5
MILC 15	[113]	$2+1+1$	494.5	$F_{p4s}(f_\pi)$	$153.90(9)(^{+21}_{-28})$
HPQCD 13A	[42]	$2+1+1$	494.6	f_π	130.4
Hudspith 24	[1066]	$2+1$	494.2	M_Ω	1672.5
RQCD 22	[105]	$2+1$	494.2	M_Ξ	1316.9
CLS 21	[1067]	$2+1$	497.6	$\frac{1}{3}(f_\pi+2f_K)$	148.3
CLS 16	[114]	$2+1$	494.2	$\frac{1}{3}(f_\pi+2f_K)$	147.6
RBC/UKQCD 14B	[12]	$2+1$	495.7	M_Ω	1672.5
HotQCD 14	[117]	$2+1$	n/a[a]	$r_1(f_\pi)$	0.3106 fm
BMW 12A	[115]	$2+1$	494.2	M_Ω	1672.5
Edinburgh consensus			494.6	f_π	130.5

[a]The scheme uses $M_{\eta_{s\bar{s}}} \approx 695$ MeV instead of fixing M_K.

where A_μ is the fundamental gauge field, $G_{\mu\nu}$ the field-strength tensor, and D_μ the covariant derivative [365]. At finite lattice spacing, a possible form of Eqs. (487) and (488) is

$$a^2 \frac{d}{dt} V_t(x,\mu) = -g_0^2 \cdot \partial_{x,\mu} S_G(V_t) \cdot V_t(x,\mu), \tag{489}$$

where $V_t(x,\mu)$ is the flow of the original gauge field $U(x,\mu)$ at flow time t, S_G is an arbitrary lattice discretization of the gauge action, and $\partial_{x,\mu}$ denotes the su(3)-valued differential operator with respect to $V_t(x,\mu)$. An important point to note is that the flow time t has the dimension of a length squared, i.e., $t \sim a^2$, and hence provides a means for setting the scale.

One crucial property of the gradient flow is that any function of the gauge fields evaluated at flow times $t > 0$ is renormalized [839] by just renormalizing the gauge coupling. Therefore, one can define a scale by keeping a suitable gluonic observable defined at constant flow time t, e.g., the action density $E = -\frac{1}{2}\mathrm{Tr} G_{\mu\nu} G_{\mu\nu}$ [365], fixed in physical units. This can, for example, be achieved through the condition

$$t_c^2 \langle E(t_c,x)\rangle = c, \quad E(t,x) = -\frac{1}{2}\mathrm{Tr} G_{\mu\nu}(t,x) G_{\mu\nu}(t,x), \tag{490}$$

where $G_{\mu\nu}(t,x)$ is the field-strength tensor evaluated on the flowed gauge field V_t. Then, the lattice scale a can be determined from the dimensionless flow time in lattice units, $\hat{t}_c = a^2 t_c$. The original proposal in [365] was to use $c = 0.3$ yielding the scale t_0,

$$t_0^2 \langle E(t_0)\rangle = 0.3. \tag{491}$$

For convenience one sometimes also defines $s_0 = \sqrt{t_0}$.

An alternative scale w_0 has been introduced in Ref. [115]. It is defined by fixing a suitable derivative of the action density,

$$W(t_c) = t_c \cdot \partial_t (t^2 \langle E(t)\rangle)_{t=t_c} = c. \tag{492}$$

Setting $c = 0.3$ yields the scale w_0 through

$$W(w_0^2) = 0.3. \tag{493}$$

In addition to the lattice scales from t_0 and w_0, one can also consider the scale from the dimensionful combination t_0/w_0. This combination is observed to have a very weak dependence on the quark mass [45,1075,1076].

A useful property of the gradient-flow scales is the fact that their quark-mass dependence is known from χPT [1077].

Since the action density at $t \sim t_0 \sim w_0^2$ usually suffers from large autocorrelation [1075,1078], the calculation of the statistical error needs special care.

Lattice artefacts in the gradient-flow scales originate from different sources [1079], which are systematically discussed by considering t as a coordinate in a fifth dimension. First, there is the choice of the action S_G for $t > 0$. Second, there is the discretization of $E(t,x)$. Third, due to the discretization of the four-dimensional quantum action, and fourth, contributions of terms localized at the boundary $t = 0_+$. The interplay between the different

sources of lattice artefacts turns out to be rather subtle [1079].

Removing discretization errors due to the first two sources requires only classical (g_0-independent) improvement. Those due to the quantum action are common to all $t = 0$ observables, but the effects of the boundary terms are not easily removed in practice. At tree level, the Zeuthen flow [1079] removes these effects completely, but none of the computations reviewed here have used it. Discretization effects due to S_G can be removed by using an improved action such as the tree-level Symanzik-improved gauge action [115,1080]. More phenomenological attempts of improving the gradient-flow scales consist of applying a t-shift [1081], or tree-level improvement [1082].

3. Other theory scales

The MILC collaboration has been using another set of scales, the partially quenched pseudoscalar decay constant f_{p4s} with degenerate valence quarks with a mass $m_q = 0.4 \cdot m_{\text{strange}}$, and the corresponding partially quenched pseudoscalar mass M_{p4s}. So far it has been a quantity only used by the MILC collaboration [20,21,183]. We do not perform an in-depth discussion or an average but will list numbers in the results section.

Yet another scale that has been used is the leptonic decay constant of the η_s. This fictitious particle is a pseudoscalar made of a valence quark-antiquark pair with different (fictitious) flavors which are mass-degenerate with the strange quark [120,122,1083].

E. List of computations and results

1. Gradient-flow scales

We now turn to a review of the calculations of the gradient-flow scales $\sqrt{t_0}$ and w_0. The results are compiled in Table 76 and shown in Fig. 51. In the following, we briefly discuss the calculations in the order that they appear in the table and figure.

ETM 21 [45] finalizes and supersedes ETM 20 discussed below. It determines the scales $\sqrt{t_0}, w_0$, also $t_0/w_0 = 0.11969(62)$ fm, and the ratio $\sqrt{t_0}/w_0 = 0.82930(65)$, cf. also HPQCD 13A [42]. Since ETM 21 is now published, the values replace the ones of ETM 20 in the previous FLAG average.

CalLat 20A [112] use Möbius Domain-Wall valence fermions on HISQ ensembles generated by the MILC and CalLat collaborations. The gauge fields entering the Möbius domain-wall operator are gradient-flow smeared with $t = a^2$. They compute the Ω mass and the scales w_0, t_0 and perform global fits to determine $w_0 M_\Omega$ and $\sqrt{t_0} M_\Omega$ at the physical point. The flow is discretized with the Symanzik tree-level improved action and the clover discretization of $E(t)$ is used. A global fit with Bayesian priors is performed including terms derived from χPT for finite-volume and quark-mass dependencies, as well as a^2 and $a^2\alpha_s(1.5/a)$ terms for discretization errors. Also, a tree-level improved definition of the GF scales is used where the leading-in-g^2 cutoff effects are removed up to and including $\mathcal{O}(a^8/t^4)$.

BMW 20 [116] presents a result for w_0 in the context of their staggered-fermion calculation of the muon anomalous magnetic moment. It is the first computation that takes QED and isospin-breaking corrections into account. The simulations are performed by using staggered fermions with stout gauge-field smearing with six lattice spacings and several pion masses around the physical point with M_π between 110 and 140 MeV. Volumes are around $L = 6$ fm. At the largest lattice spacing, it is demonstrated how the effective masses of the Ω correlator almost reach the plateau value extracted from a four-state fit (two states per parity). Within the range where the data are fit, the deviation of data points from the estimated plateau is less than a percent. Isospin-breaking corrections are computed by Taylor expansion around isoQCD with QED treated as QED_L [263]. Finite-volume effects in QED are taken from the $1/L, 1/L^2$ universal corrections and $\mathcal{O}(1/L^3)$ effects are neglected. The results for $M_\Omega w_0$ are extrapolated to the continuum by a fit with a^2 and a^4 terms.

ETM 20 [1084] presents in their proceedings contribution a preliminary analysis of their $N_f = 2 + 1 + 1$ Wilson twisted-mass fermion simulations at maximal twist (i.e., automatic $\mathcal{O}(a)$ improved), at three lattice spacings and pion masses at the physical point. Their determination of $w_0 = 0.1706(18)$ fm from f_π using an analysis in terms of M_π is the value quoted above. They obtain the consistent value $w_0 = 0.1703(18)$ fm from an analysis in terms of the renormalized light quark mass.

MILC 15 [113] sets the physical scale using the fictitious pseudoscalar decay constant $F_{p4s} = 153.90(9)(+21/-28)$ MeV with degenerate valence quarks of mass $m_v = 0.4 m_s$ and physical sea-quark masses [183]. (F_{p4s} has strong dependence on the valence-quark mass and is determined from f_π.) They use a definition of the flow scales where the tree-level lattice artefacts up to $\mathcal{O}(a^4/t^2)$ are divided out. Charm-quark mass mistunings are between 1% and 11%. They are taken into account at leading order in $1/m_c$ through $\Lambda^{(3)}_{\text{QCD}}$ applied directly to F_{p4s} and $1/m_c$ corrections are included as terms in the fits. They use elaborate variations of fits in order to estimate extrapolation errors (both in GF scales and F_{p4s}). They include errors from FV effects and experimental errors in f_π in F_{p4s}.

HPQCD 13A [42] uses eight MILC-HISQ ensembles with lattice spacings $a = 0.088, 0.121, 0.151$ fm. Values of L are between 2.5 fm and 5.8 fm with $M_\pi L = 3.3$–4.6. Pion masses range between 128 and 306 MeV. QCD is defined by using the inputs $M_\pi = 134.98(32)$ MeV, $M_K = 494.6(3)$ MeV, $f_{\pi^+} = 130.4(2)$ MeV derived by

model subtractions of IB effects. Additional scale ratios are given: $\sqrt{t_0}/w_0 = 0.835(8)$, $r_1/w_0 = 1.789(26)$.

Hudspith 24 [1066] computes the mass of the omega baryon on CLS $N_f = 2+1$ configurations along the trajectories with approximately constant trace of the bare quark-mass matrix. They use 27 ensembles with six different values of the lattice spacing from $a = 0.09$ fm to $a = 0.04$ fm. They compute the (nonpositive) correlation function $C_\Omega(x_0)$ of a local field with a gauge-fixed wall-source, which results in a very good statistical precision. It is analyzed directly with a two-state fit describing the data over a large range. In addition they also extract M_Ω by constructing a 2×2 generalized pencil-of-functions matrix correlator from $C_\Omega(x_0), C_\Omega(x_0+a)$, $C_\Omega(x_0+2a)$. Projecting with a GEVP eigenvector (from a fixed-time GEVP) a correlation function with a long plateau of the effective mass is found. Precisions for the Omega mass on various ensembles range from a few per mille to below a per mille.

These masses, together with the scale t_0 are subsequently fit using a phenomenology- and ChPT-motivated form where a few parameters are taken from previous ChPT fits [1086] to baryon masses computed on CLS ensembles by RQCD [105]. The dependence on t_0 is in the higher-order chiral-correction terms which include NNNLO. There is no term in the fit which allows for discretization effects in the chiral corrections. Their absence is justified by the results of previous fits in [1086]. Given the unconventional analysis carried out in this work, the WG hopes that additional technical information will be provided in the published version of the paper (in particular concerning the direction in parameter space of the global fit of the Ω, kaon and pion masses from which the continuum value of t_0 is extracted) and may reconsider the ★ assigned in this review, on the basis of the standard continuum-limit criterion, once the paper is published and eligible to enter the average. Once the precision for the raw values of am_Ω is independently confirmed, this paper [1066], possibly with a new analysis, may lead to very high-precision determinations of the theory scales.

RQCD 22 [105] is an independent analysis of CLS ensembles employing $N_f = 2+1$ nonperturbatively improved Wilson fermions and the tree-level Symanzik improved gauge action. It uses a multitude of quark-mass combinations at six different values of the lattice spacing, ranging from $a \lesssim 0.098$ fm down to $a < 0.039$ fm. Near-physical quark masses are realized at $a = 0.064$ fm and $a = 0.085$ fm. The input quantities used to fix the physical point and to set the scale are $M_\pi = 134.8(3)$ MeV, $M_K = 494.2(3)$ MeV, and $m_\Xi = 1316.9(3)$ MeV (last line of pg. 33 in [105]). As RQCD 22 has been published since the last update, the result for $\sqrt{t_0}$ is now included in the FLAG average.

CLS 21 [1067] is a proceedings contribution describing a preliminary analysis following the one in CLS 16 [114], cf. the description below. CLS 21 includes about twice the number of ensembles as compared to CLS 16, in particular, ensembles at two more lattice spacings and two ensembles at the physical point. As a consequence, this analysis is not considered a straightforward update and hence does not supersede the result of CLS 16.

CLS 16 [114] uses CLS configurations of $2+1$ non-perturbatively $\mathcal{O}(a)$-improved Wilson fermions. There are a few pion masses with the strange mass adjusted along a line of $m_u + m_d + m_s = \text{const}$. Three different lattice spacings are used. They determine t_0 at the physical point defined by π and K masses and the linear combination $f_K + \frac{1}{2} f_\pi$. They use the Wilson flow with the clover definition of $E(t)$.

QCDSF 15B [1085,1087] results, unpublished, are obtained by simulating $N_f = 2+1$ QCD with the tree-level Symanzik-improved gauge action and clover Wilson fermions with single-level stout smearing for the hopping terms together with unsmeared links for the clover term (SLiNC action). Simulations are performed at four different lattice spacings, in the range [0.06, 0.08] fm, with $M_{\pi,\min} = 228$ MeV and $M_{\pi,\min} L = 4.1$. The results for the gradient-flow scales have been obtained by relying on the observation that flavor-symmetric quantities get corrections of $\mathcal{O}((\Delta m_q)^2)$ where Δm_q is the difference of the quark mass from the SU(3)-symmetric value. The $\mathcal{O}(\Delta m_q^2)$ terms are not detected in the data and subsequently neglected.

RBC/UKQCD 14B [12] presents results for $\sqrt{t_0}$ and w_0 obtained in QCD with $2+1$ dynamical flavors. The simulations are performed by using domain-wall fermions on six ensembles with lattice spacing $a^{-1} = 1.38$, 1.73, 1.78, 2.36, 2.38, and 3.15 GeV, pion masses in the range $M_\pi^{\text{unitary}} \in [139, 360]$ MeV. The simulated volumes are such that $M_\pi L > 3.9$. The effective masses of the Ω correlator are extracted with two-state fits and it is shown, by using two different nonlocal interpolating operators at the source, that the correlators almost reach a pleateau. In the calculation of $\sqrt{t_0}$ and w_0, the clover definition of $E(t)$ is used. The values given are $\sqrt{t_0} = 0.7292(41)$ GeV^{-1} and $w_0 = 0.8742(46)$ GeV^{-1} which we converted to the values in Table 76.

HotQCD 14 [117] determines the equation of state with $N_f = 2+1$ flavors using highly improved staggered quarks (HISQ/tree). As a byproduct, they update the results of HotQCD 11 [719] by adding simulations at four new values of β, for a total of 24 ensembles, with lattice spacings in the range [0.04, 0.25] fm and volumes in the range [2.6, 6.1] fm with $M_\pi = 160$ MeV. They obtain values for the scale parameters r_0 and w_0, via the ratios $r_0/r_1, w_0/r_1$ and using $r_1 = 0.3106(14)(8)(4)$ fm from MILC 10 [47]. They obtain for the ratios $(r_0/r_1)_{\text{cont}} = 1.5092(39)$ and $(w_0/r_1)_{\text{cont}} = 0.5619(21)$ in the continuum. They crosscheck their determination of the scale r_1 using the hadronic quantities f_K, f_η from

TABLE 76. Results for gradient flow scales at the physical point, cf. Eq. (473). Note that BMW 20 [116] take IB and QED corrections into account. An additional result for the ratio of scales is ETM 21 [45]: $t_0/w_0 = 0.11969(62)$ fm.

Collaboration	Ref.	N_f	Publication status	Chiral extrapolation	Continuum extrapolation	Finite volume	Physical scale	$\sqrt{t_0}$ [fm]	w_0 [fm]
ETM 21	[45]	$2+1+1$	A	★	★	★	f_π	0.14436(61)	0.17383(63)
CalLat 20A	[112]	$2+1+1$	A	★	★	★	M_Ω	0.1422(14)	0.1709(11)
BMW 20	[116]	$1+1+1+1$	A	★	★	★	M_Ω		0.17236(29)(63)[70]
ETM 20	[1084]	$2+1+1$	C	★	★	★	f_π		0.1706(18)
MILC 15	[113]	$2+1+1$	A	★	★	★	$F_{p4s}(f_\pi)$[a]	0.1416(+8/−5)	0.1714(+15/−12)
HPQCD 13A	[42]	$2+1+1$	A	★	○	★	f_π	0.1420(8)	0.1715(9)
Hudspith 24	[1066]	$2+1$	P	★	★	★	[b]	0.14480(32)(6)	
RQCD 22	[105]	$2+1$	A	★	★	★	M_Ξ	0.1449(+7/−9)	
CLS 21	[1067]	$2+1$	C	★	★	★	f_π, f_K	0.1443(7)(13)	
CLS 16	[114]	$2+1$	A	○	★	★	f_π, f_K	0.1467(14)(7)	
QCDSF/UKQCD 15B	[1085]	$2+1$	P	○	○	○	$M_P^{\mathrm{SU}(3)}$	0.1511(22)(6)(5)(3)	0.1808(23)(5)(6)(4)
RBC/UKQCD 14B	[12]	$2+1$	A	★	★	★	M_Ω	0.14389(81)	0.17250(91)
HotQCD 14	[117]	$2+1$	A	★	★	★	$r_1(f_\pi)$[a]		0.1749(14)
BMW 12A	[115]	$2+1$	A	★	★	★	M_Ω	0.1465(21)(13)	0.1755(18)(4)

[a]These scales are not physical scales and have been determined from f_π.

[b]There is no physical scale as such. The input is the quark-mass dependence of M_Ω.

HPQCD 09B [122] and the experimental value of M_φ, and find good agreement.

BMW 12A [115] is the work in which w_0 was introduced. Simulations with 2HEX smeared Wilson fermions and two-level stout-smeared rooted staggered fermions are done. The Wilson flow with clover $E(t)$ is used, and a test of the Symanzik flow is carried out. They take the results with Wilson fermions as their central value, because those "do not rely on the 'rooting' of the fermion determinant." Staggered fermion results agree within uncertainties.

2. Potential scales

We now turn to a review of the calculations of the potential scales r_0 and r_1. The results are compiled in Table 77 and shown in Fig. 52. With the exception of TUMQCD 22 [118], the most recent calculations date back to 2014, and we discuss them in the order that they appear in the table and the figure.

Asmussen 23 [1088] perform a computation of the potential at five lattice spacings down to $a = 0.04$ fm on CLS ensembles. The ground-state level is extracted from a GEVP, starting from smeared Wilson loops with different levels of smearing. The results are thus far only available as a conference proceedings. The final result for r_0 originates from a global fit incorporating the pion-mass dependence and the lattice-spacing dependence.

TUMQCD 22 [118] uses HISQ ensembles generated by MILC at six lattice spacings ranging from $a = 0.15$ fm to $a = 0.03$ fm to compute the potential. Scale setting is performed through f_{p4s} [20]. In contrast to other determinations, the static potential is extracted using Coulomb-gauge fixing on two time-slices and the Wilson lines connecting the two time slices. Thus, there is no variational method but fits are performed with up to three energy levels. Both continuum extrapolations with a^2 corrections and $\alpha^2(1/a)a^2$ are performed, where there is a pre-selection of the direction $\vec{r}/r$ and direction-dependent discretization effects are assumed to be sufficiently reduced by the use of the tree-level improved r_{I} [708]. The final results come from a Bayesian model average.

ETM 14 [8] uses $N_f = 2+1+1$ Wilson twisted-mass fermions at maximal twist (i.e., automatic $\mathcal{O}(a)$-improved), three lattice spacings and pion masses reaching down to $M_\pi = 211$ MeV. They determine the scale r_0 through $f_\pi = f_{\pi^+} = 130.41$ MeV. A crosscheck of the so-obtained lattice spacings with the ones obtained via the fictitious

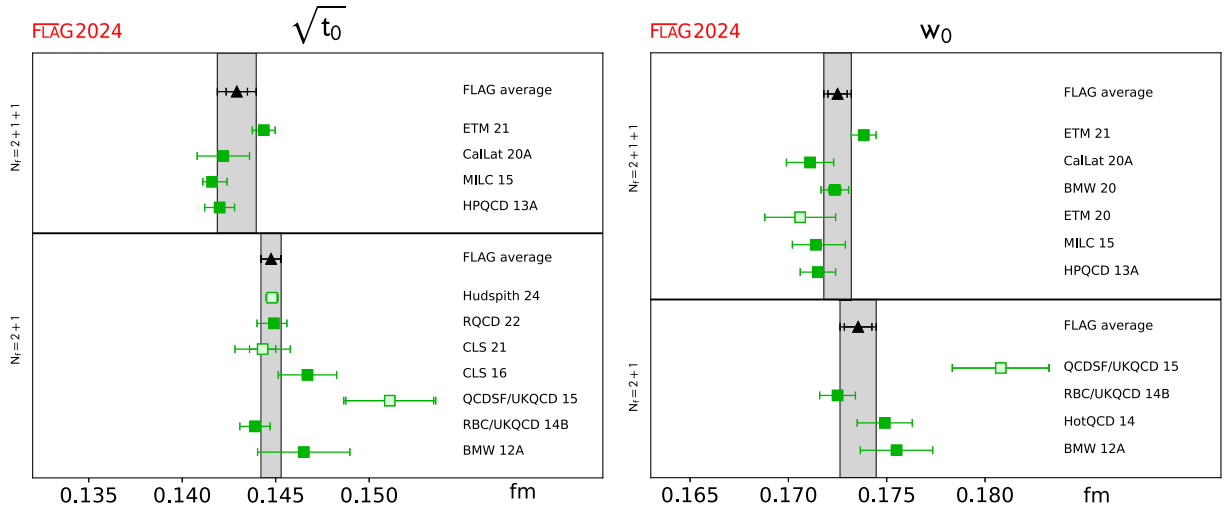


FIG. 51. Results for gradient flow scales.

pseudoscalar meson $M_{s's'}$ made of two strange-like quarks gives consistent results. The crosscheck is done using the dimensionless combinations $r_0 M_{s's'}$ (with r_0 in the chiral limit) and $f_\pi/M_{s's'}$ determined in the continuum, and then using r_0/a and the value of $M_{s's'}$ obtained from the experimental value of f_π. We also note that in Ref. [1075] using the same ensembles the preliminary value $w_0 = 0.1782$ fm is determined, however, without error due to the missing or incomplete investigation of the systematic effects.

HPQCD 13A [42] was already discussed above in connection with the gradient flow scales.

HPQCD 11B [1083] uses five MILC-HISQ ensembles and determines r_1 from $M_{\Upsilon(2s)} - M_{\Upsilon(1s)}$ and the decay constant f_{η_s} (see HPQCD 09B). The valence b quark is treated by NRQCD, while the light valence quarks have the HISQ discretization, identical to the sea quarks.

HotQCD 14 [117] was already discussed in connection with the gradient flow scales.

χQCD 14 [29] uses overlap fermions as valence quarks on $N_f = 2+1$ domain-wall fermion gauge configurations generated by the RBC/UKQCD collaboration [119]. Using the physical masses of D_s, D_s^* and J/ψ as inputs, the strange- and charm-quark masses and the decay contant f_{D_s} are determined as well as the scale r_0.

HotQCD 11 [719] uses configurations with tree-level improved Symanzik gauge action and HISQ staggered quarks in addition to previously generated ensembles with p4 and asqtad staggered quarks. In this calculation, QCD is defined by generating lines of constant physics with $m_l/m_s = \{0.2, 0.1, 0.05, 0.025\}$ and setting the strange-quark mass by requiring that the mass of a fictitious $\eta_{s\bar{s}}$ meson is $M_{\eta_{s\bar{s}}} = \sqrt{2M_K^2 - M_\pi^2}$. The physical point is taken to be at $m_l/m_s = 0.037$. The physical scale is set by using the value $r_1 = 0.3106(8)(18)(4)$ fm obtained in Ref. [47] by using f_π as physical input. In the paper, this result is shown to be consistent within the statistical and systematic errors with the choice of f_K as physical input. The result $r_0/r_1 = 1.508(5)$ is obtained by averaging over 12 ensembles at $m_l/m_s = 0.05$ with lattice spacings in the range [0.066, 0.14] fm. This result is then used to get $r_0 = 0.468(4)$ fm. Finite-volume effects have been monitored with 20 ensembles in the range [3.2, 6.1] fm with $M_\pi L > 2.6$.

RBC/UKQCD 10A [119] uses $N_f = 2+1$ flavors of domain-wall quarks and the Iwasaki gauge action at two values of the lattice spacing with unitary pion masses in the approximate range [290, 420] MeV. They use the masses of π and K meson and of the Ω baryon to determine the physical quark masses and the lattice spacings, and so obtain estimates of the scales r_0, r_1 and the ratio r_1/r_0 from a combined chiral and continuum extrapolation.

MILC 10 [47] presents a further update of r_1 with asqtad-staggered-quark ensembles with $a \in \{0.045, 0.06, 0.09\}$ fm. It supersedes MILC 09 [19,196,1089].

MILC 09 [196] presents an $N_f = 2+1$ calculation of the potential scales on asqtad-staggered-quark ensembles with $a \in \{0.045, 0.06, 0.09, 0.12, 0.15, 0.18\}$ fm. The continuum extrapolation is performed by using Goldstone-boson pions as light as $M_\pi = 224$ MeV (RMS pion mass of 258 MeV). The physical scale is set from f_π. The result for r_1 obtained in the published paper [196] is then updated and, therefore, superseded by the conference proceedings MILC 09A and 09B [19,1089].

HPQCD 09B [122] is an extension of HPQCD 05B [120] and uses HISQ valence quarks instead of asqtad quarks. The scale r_1 is obtained from three different inputs.

TABLE 77. Results for potential scales at the physical point, cf. Eq. (473). $\Delta M_\Upsilon = M_{\Upsilon(2s)} - M_{\Upsilon(1s)}$.

Collaboration	Ref.	N_f	Publication status	Chiral extrapolation	Continuum extrapolation	Finite volume	Physical scale	r_0 [fm]	r_1 [fm]
TUMQCD 22	[118]	$2+1+1$	A	★	★	★	f_{p4s} ([20]) [b]	0.4547(64)	0.3037(25)
ETM 14	[8]	$2+1+1$	A	○	★	★	f_π	0.474(14)	
HPQCD 13A	[42]	$2+1+1$	A	★	○	★	f_π		0.3112(30)
HPQCD 11B	[1083]	$2+1+1$	A	○	○	○	ΔM_Υ, f_{η_s}		0.3209(26)
Asmussen 23	[1088]	$2+1$	C	★	★	★	f_π, f_K	0.4671(64)	
HotQCD 14	[117]	$2+1$	A	★	★	★	r_1 ([47])[a]	0.4671(41)	
χQCD 14	[29]	$2+1$	A	○	○	○	three inputs[c]	0.465(4)(9)	
HotQCD 11	[719]	$2+1$	A	★	★	★	f_π	0.468(4)	
RBC/UKQCD 10A	[119]	$2+1$	A	○	○	○	M_Ω	0.487(9)	0.333(9)
MILC 10	[47]	$2+1$	C	○	★	★	f_π		0.3106(8)(14)(4)
MILC 09	[196]	$2+1$	A	○	★	★	f_π		$0.3108(15)(^{+26}_{-79})$
MILC 09A	[19]	$2+1$	C	○	★	★	f_π		$0.3117(6)(^{+12}_{-31})$
HPQCD 09B	[122]	$2+1$	A	○	★	○	three inputs		0.3133(23)(3)
PACS-CS 08	[235]	$2+1$	A	★	■	■	M_Ω	$0.4921(64)(^{+74}_{-2})$	
HPQCD 05B	[120]	$2+1$	A	○	○	○	ΔM_Υ	0.469(7)	0.321(5)
Aubin 04	[121]	$2+1$	A	○	○	○	ΔM_Υ	0.462(11)(4)	0.317(7)(3)

[a]This theory scale was determined in turn from r_1 [47].
[b]This theory scale was determined in turn from f_π.
[c]$M_{D_s^*}, M_{D_s^*} - M_{D_s}, M_{J/\psi}$.

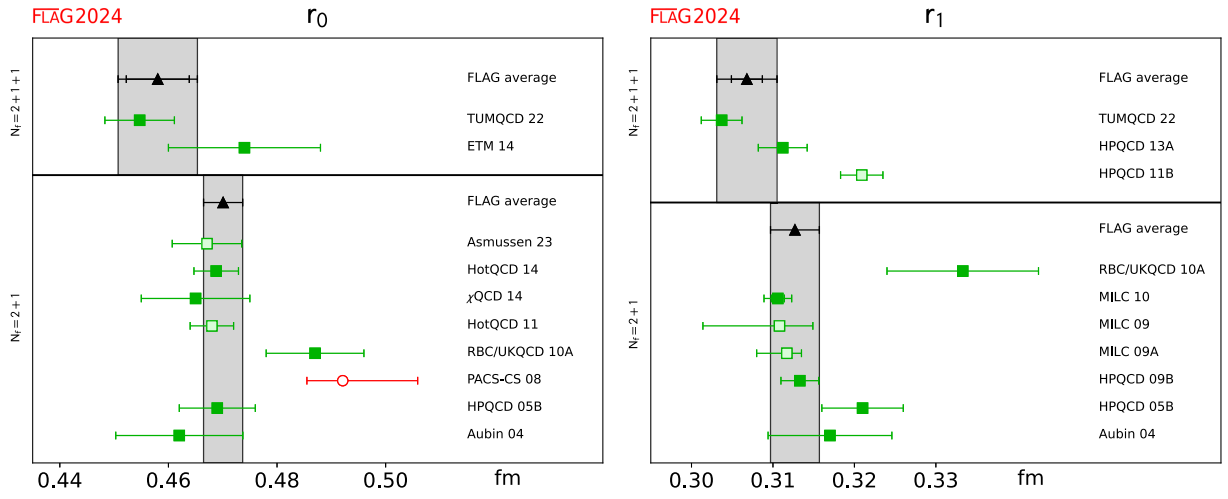


FIG. 52. Results for potential scales.

First $r_1 = 0.309(4)$ fm from the splitting of 2S and 1S Υ states as in Ref. [120], second $r_1 = 0.316(5)$ fm from $M_{D_s} - M_{\eta_s}/2$ and third $r_1 = 0.315(3)$ fm from the decay constant of the η_s. The fictitious η_s state is operationally defined by setting quark masses to the s-quark mass and dropping disconnected diagrams. Its mass and decay constant are obtained from a partially quenched-chiral-perturbation-theory analysis using the pion and kaon states from experiment together with various partially quenched lattice data. The three results are combined to $r_1 = 0.3133(23)(3)$ fm.

PACS-CS 08 [235] presents a calculation of r_0 in $N_f = 2+1$ QCD by using NP $\mathcal{O}(a)$-improved clover Wilson quarks and Iwasaki gauge action. The calculation is done at fixed lattice spacing $a = 0.09$ fm and is extrapolated to the physical point from (unitary) pion masses in the range [156, 702] MeV. The $N_f = 2+1$ theory is defined by fixing M_π, M_K, and M_Ω to 135.0,497.6, and 1672.25 MeV, respectively. The effective masses of smeared-local Ω correlators averaged over the four spin polarizations show quite good plateaux.

RBC/Bielefeld 07 [1090] performed calculations of the equation of state with two light-quark flavors and a heavier strange quark using improved staggered fermions. Zero-temperature calculations including the static-quark potential were used to set the temperature scale for the thermodynamic observables. The lattice cutoff changes by a factor 6 from $a \simeq 0.3$ fm down to $a \simeq 0.05$ fm while the pion mass is kept fixed at $M_\pi \simeq 220(4)$ MeV. Apart from the dimensionless ratio $r_0/r_1 = 1.4636(60)$ they also provide a result for the ratio $r_0\sqrt{\sigma} = 1.1034(40)$

HPQCD 05B [120] performed the first bottomonium spectrum calculation in full QCD with $N_f = 2+1$ on MILC asqtad configurations and the b quark treated by NRQCD. They find agreement of the low lying Υ states with experiment and also compare to quenched and $N_f = 2$ results. They determined r_0 and r_1 from the splitting of 2S and 1S states.

Aubin 04 [121] presents an $N_f = 2+1$ calculation of the potential scales by using asqtad staggered quark ensembles with $a = 0.09$ and 0.12 fm. The continuum extrapolation is performed by using Goldstone-boson pions as light as $M_\pi = 250$ MeV. The physical scale is set from the Υ 2S-1S and 1P-1S splittings computed with NRQCD by HPQCD [1091].

3. Ratios of scales

It is convenient in many cases to also have ratios of scales at hand. In addition to translating from one scale to another, the ratios provide important crosschecks between different determinations. Results on ratios provided by the collaborations are compiled in Table 78 and Fig. 53. The details of the computations were already discussed in the previous sections.

F. Averages

1. Data-driven continuum-limit criterion

As discussed in Sec. II A 2, we evaluate the inflation factor

$$s(a) = \max[1, 1 + 2(\delta(a) - 3)/3],$$
$$\delta(a) = \frac{|Q(a) - Q(0)|}{\sigma_Q}, \tag{494}$$

where Q is the quantity for which we perform an average, and σ_Q is the uncertainty estimated by the collaboration for its continuum limit. If $s(a_{\min})$ exceeds one, i.e., if the continuum limit is more than three σ_Q from the result at smallest lattice spacing, $a_{\min}$, the error of the computation is inflated by $s(a_{\min})$ before taking the average. For our quantities $s(a_{\min}) = 1$ except for few cases. We therefore report explicitly values of $s(a_{\min})$ only where $s(a_{\min}) > 1$.

2. Gradient flow scale $\sqrt{t_0}$

For $N_f = 2+1+1$, we have two recent calculations from ETM 21 [45] and CalLat 20A [112], and two less recent ones from MILC 15 [113] and HPQCD 13A [42] fulfilling the FLAG criteria to enter the average. The latter two and CalLat 20A are based on the same MILC-HISQ gauge-field ensembles, hence we consider their statistical errors to be 100% correlated.

For $N_f = 2+1$, we have four calculations from RQCD 22 [105], CLS 16 [114], RBC/UKQCD 14B [12], and BMW 12A [115] which enter the FLAG average. RQCD 22 and CLS 16 are based on the same gauge-field ensembles, hence we consider their statistical errors to be 100% correlated. The other two are independent computations, so there is no correlation to be taken into account. QCDSF/UKQCD 15B [1085] does not contribute to the average, because it is not published. CLS 21 [1067] is a proceedings contribution based on double the number of ensembles. It is therefore not a straightforward update and does not supersede CLS 16 [114]. Performing the weighted and correlated average we obtain

$N_f = 2+1+1$:

$$\sqrt{t_0} = 0.14292(104)\ \text{fm}\ \ \text{Refs. [42,45,112,113]}, \tag{495}$$

$N_f = 2+1$:

$$\sqrt{t_0} = 0.14474(57)\ \text{fm}\ \ \text{Refs. [12,105,114,115]}. \tag{496}$$

We note that the $N_f = 2+1+1$ results of staggered fermions and the twisted-mass result are not well compatible. The resulting stretching factor based on the χ^2 value from the weighted average for $N_f = 2+1+1$ is 1.81. It causes the error to be increased compared to FLAG 21. For the $N_f = 2+1$ average the stretching factor is 1.04. We hope that the differences for $N_f = 2+1+1$ get resolved in the near future and the uncertainty of the average decreases.

3. Gradient flow scale w_0

For $N_f = 1+1+1+1$, including QED, there is a single calculation, BMW 20 [116] with the result

$$N_f = 1+1+1+1+\text{QED}: \quad w_0 = 0.17236(70)\ \text{fm} \quad \text{Ref. [116]}. \tag{497}$$

For $N_f = 2+1+1$ we now have four calculations ETM 21 [45], CalLat 20A [112], MILC 15 [113], and HPQCD 13A [42] entering the FLAG average. The proceedings ETM 20 is superseded by ETM 21. As discussed above in connection with $\sqrt{t_0}$, we assume 100% correlation between the statistical errors of CalLat 20A, MILC 15, and HPQCD 13A.

For $N_f = 2+1$, we have three calculations RBC/UKQCD 14B [12], HotQCD 14 [117], and BMW 12A [115] that enter the FLAG average. These calculations are independent, and no correlation is used. QCDSF/UKQCD 15B [1085] does not contribute to the average, because it is not published.

Performing the weighted and correlated average, we obtain

$$N_f = 2+1+1: \quad w_0 = 0.17256(103)\ \text{fm} \quad \text{Refs. [42,45,112,113]}, \tag{498}$$

$$N_f = 2+1: \quad w_0 = 0.17355(92)\ \text{fm} \quad \text{Refs. [12,115,117]}. \tag{499}$$

As above, $N_f = 2+1+1$ results of staggered fermions and the twisted-mass result are not well compatible. The resulting stretching factor based on the χ^2 value from the weighted average is 1.67. It causes the error to be slightly increased compared to FLAG 21. For the $N_f = 2+1$ average the stretching factor is 1.23. We hope that the differences for $N_f = 2+1+1$ get resolved in the near future and the uncertainty of the average decreases.

Isospin-breaking and electromagnetic corrections are expected to be small at the level of present uncertainties. This is also confirmed by the explicit computation by BMW 12A. Therefore, we also perform an average over all $N_f > 2+1$ computations and obtain

$$N_f > 2+1: \quad w_0 = 0.17250(70)\ \text{fm} \quad \text{Refs. [42,45,112,113,116]}. \tag{500}$$

For the $N_f > 2+1$ average the rescaling factor is 1.45.

4. Gradient flow scale t_0/w_0

Currently, there is only one calculation of the scale t_0/w_0 available from ETM 21 [45] which forms the FLAG average

$$N_f = 2+1+1: \quad t_0/w_0 = 0.11969(62)\ \text{fm} \quad \text{Ref. [45]}. \tag{501}$$

5. Potential scale r_0

For $N_f = 2+1+1$, there are two determinations of r_0 from ETM 14 [8] and TUMQCD 22 [118], which contribute to the FLAG average and these are uncorrelated.

TABLE 78. Results for dimensionless ratios of scales.

Collaboration	Ref.	N_f	Publication status	Chiral extrapolation	Continuum extrapolation	Finite volume	$\sqrt{t_0}/w_0$	r_0/r_1	r_1/w_0
TUMQCD 22	[118]	$2+1+1$	A	★	★	★		1.4968(69)	
ETM 21	[45]	$2+1+1$	A	★	★	★	0.82930(65)		
HPQCD 13A	[42]	$2+1+1$	A	★	○	★	0.835(8)		1.789(26)
HotQCD 14	[117]	$2+1$	A	★	★	★			1.7797(67)
HotQCD 11	[719]	$2+1$	A	★	★	★		1.508(5)	
RBC/UKQCD 10A	[119]	$2+1$	A	○	○	○		1.462(32)[a]	
RBC/Bielefeld 07	[1090]	$2+1$	A	■	★	★		1.4636(60)	
Aubin 04	[121]	$2+1$	A	○	○	○		1.474(7)(18)	

[a]This value is obtained from $r_1/r_0 = 0.684(15)(0)(0)$.

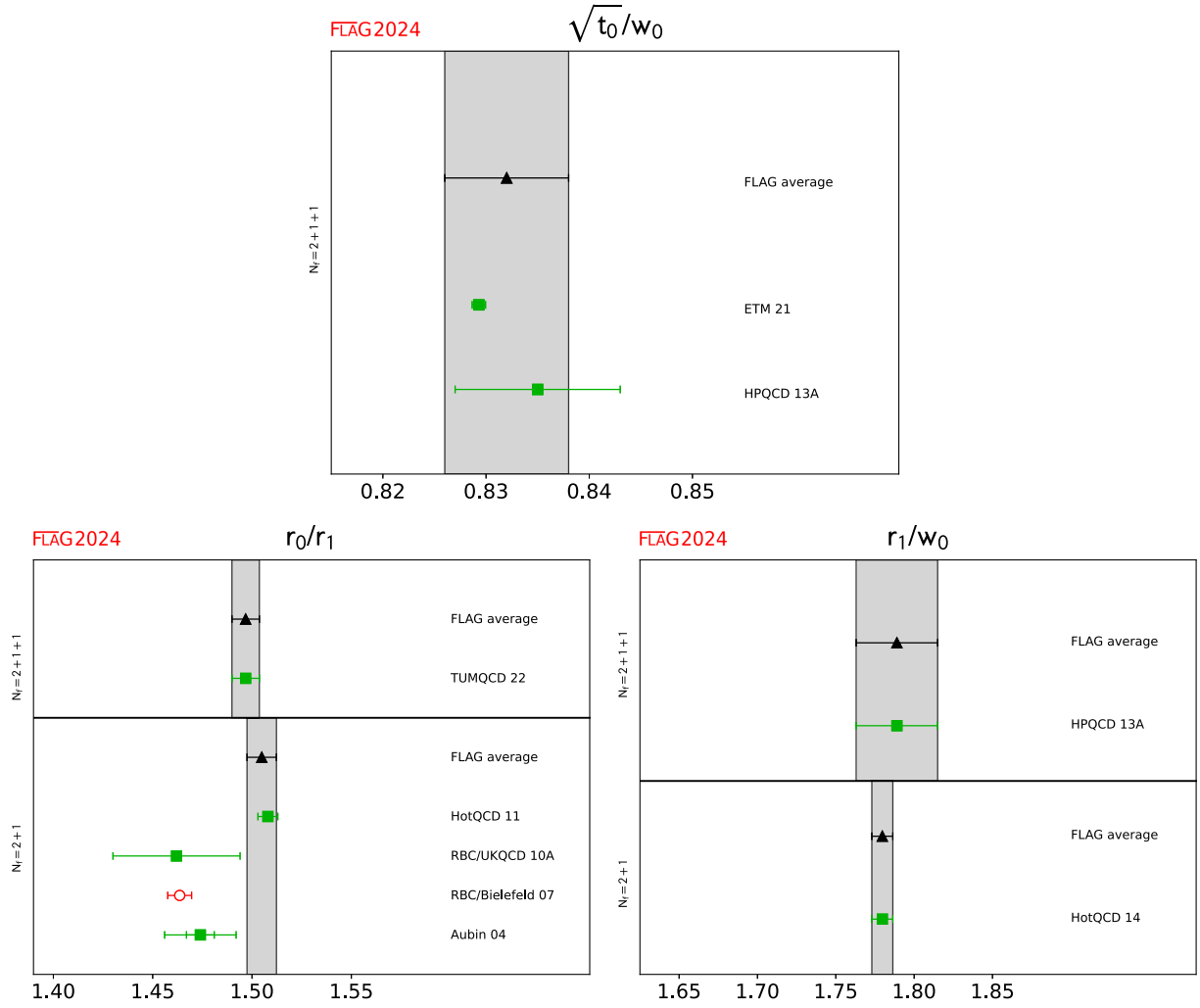


FIG. 53. Results for dimensionless ratios of scales.

For $N_f = 2+1$, all but one calculation fulfill all the criteria to enter the FLAG average. HotQCD 14 [117] is essentially an update of HotQCD 11 [719] by enlarging the set of ensembles used in the computation. Therefore, the result from HotQCD 14 supersedes the one from HotQCD 11 and, hence, we only use the former in the average. The computation of χQCD [29] is based on the configurations produced by RBC/UKQCD 10A [119], and we, therefore, assume a 100% correlation between the statistical errors of the two calculations. HPQCD 05B [120] enhances the calculation of Aubin 04 [121] by adding ensembles at a coarser lattice spacing and using the same discretization for the valence fermion. Therefore, we consider the full errors (statistical and systematic) on the results from Aubin 04 and HPQCD 05B to be 100% correlated.

Performing the weighted (and correlated) average, we obtain

$$N_f = 2+1+1: \quad r_0 = 0.4580(73)\ \text{fm} \quad \text{Refs. [8, 118]}, \tag{502}$$

$$N_f = 2+1: \quad r_0 = 0.4701(36)\ \text{fm} \quad \text{Refs. [29, 117, 119–121]}. \tag{503}$$

We note that for the $N_f = 2+1+1$ average, the stretching factor based on the χ^2-value from the weighted average is 1.25, while for the $N_f = 2+1$ average it is 1.14.

6. Potential scale r_1

For $N_f = 2+1+1$, there are three works that fulfill the criteria to enter the FLAG average, namely TUMQCD 22 [118], HPQCD 13A [42] and HPQCD 11B [1083]. They are all based on a varying number of MILC-HISQ ensembles and we therefore assume 100% correlation between the statistical errors. The result from HPQCD 13A supersedes the result from HPQCD 11B (in line with a corresponding statement in HPQCD 13A), hence TUMQCD 22 and HPQCD 13A form the FLAG average.

For $N_f = 2+1$, all the results quoted in Table 77 fulfill the FLAG criteria, but not all of them enter the average. The

published result from MILC 09 [196] is superseded by the result in the proceedings MILC 10 [47], while MILC 09A [19] is a proceedings contribution and does not enter the average. HPQCD 09B [122] uses HISQ valence quarks instead of asqtad valence quarks as in HPQCD 05B [120]. Therefore, we have RBC/UKQCD 10A [119], MILC 10, HPQCD 09B, HPQCD 05B, and Aubin 04 entering the average. However, since the latter four calculations are based on the aqtad MILC ensembles, we attribute 100% correlation on the statistical error between them and 100% correlation on the systematic error between HPQCD 05B and Aubin 04 as discussed above in connection with r_0.

Performing the weighted and correlated average, we obtain

$$N_f = 2+1+1: \quad r_1 = 0.3068(37)\ \text{fm} \quad \text{Refs. [42, 118]}, \tag{504}$$

$$N_f = 2+1: \quad r_1 = 0.3127(30)\ \text{fm} \quad \text{Refs. [47, 119–122]}. \tag{505}$$

We note that for the $N_f = 2+1+1$ average the stretching factor based on the χ^2-value from the weighted average is 1.92, while for the $N_f = 2+1$ average it is 1.57. While it is not entirely clear what the reasons are for the discrepancies encoded in these stretching factors, excited-state contaminations are likely to play a role. Also for the potential, states with additional pions will play an increasingly important role at small pion masses and are not easily captured.

7. The scales M_{p4s} and f_{p4s}

As mentioned in Sec. XI D 3, these scales have been used only by the MILC and FNAL/MILC collaborations [20,21,183]. The latest numbers from Ref. [20] are $f_{4ps} = 153.98(11)(^{+2}_{-12})(12)[4]$ MeV and $M_{p4s} = 433.12(14)(^{+17}_{-6})(4)[40]$ MeV and, hence, we have

$$N_f = 2+1+1: \quad f_{4ps} = 153.98(20)\ \text{MeV} \quad \text{Ref. [20]}, \tag{506}$$

$$N_f = 2+1+1: \quad M_{4ps} = 433.12(30)\ \text{MeV} \quad \text{Ref. [20]}. \tag{507}$$

8. Dimensionless ratios of scales

We start with the ratio $\sqrt{t_0}/w_0$ for which two $N_f = 2+1+1$ calculations from ETM 21 [45] and HPQCD 13A [42] are available and form the FLAG average

$$N_f = 2+1+1: \quad \sqrt{t_0}/w_0 = 0.832(6) \quad \text{Refs. [42, 45]}. \tag{508}$$

Here we found a large stretching factor $s(a_{\min}) = 12.3$ for [45]. It was applied to the uncertainty before performing the weighted average and has a large effect. In fact, in the web-update after FLAG 21 the error was an order of magnitude smaller due to the very small error of ETM 21. This is now compensated by the large stretching factor.

For the ratio r_0/r_1 there is only one $N_f = 2+1+1$ calculation available from TUMQCD 22 [118], which fulfills the FLAG criteria and therefore forms the FLAG average. For $N_f = 2+1$ there are three calculations from HotQCD 11 [719], RBC/UKQCD 10A [119], and Aubin 04 [121] available. They all fulfill the FLAG criteria and enter the FLAG average of this ratio,

$$N_f = 2+1+1: \quad r_0/r_1 = 1.4968(69) \quad \text{Ref. [118]}, \tag{509}$$

$$N_f = 2+1: \quad r_0/r_1 = 1.5049(74) \quad \text{Refs. [119, 121, 716]}. \tag{510}$$

We note that for $N_f = 2+1$, the stretching factor based on the χ^2-value from the weighted average is 1.54.

Finally, for the ratio r_1/w_0 there is one computation from HotQCD 14 [117] for $N_f = 2+1+1$, and one from HPQCD 13A [42] for $N_f = 2+1$ fulfilling the FLAG criteria, and, hence, forming the FLAG values

$$N_f = 2+1+1: \quad r_1/w_0 = 1.789(26) \quad \text{Ref. [42]}, \tag{511}$$

$$N_f = 2+1: \quad r_1/w_0 = 1.7797(67) \quad \text{Ref. [117]}. \tag{512}$$

G. Observations and conclusions

Unfortunately the different computations for theory scales reported here are generally not in good agreement within each set of $N_f = 2+1+1$ and $2+1$ flavor content. As a measure we list here the stretching factors above one. We remind the reader that their squares are equal to the χ^2/dof of the weighted averages. Quantitatively, the stretching factors are for $N_f = 2+1$: 1.2 (w_0), 1.1 (r_0), 1.6 (r_1), 1.5 (r_0/r_1). For $N_f = 2+1+1$ the numbers are larger: 1.8 ($\sqrt{t_0}$), 1.7 (w_0) 1.3 (r_0) 1.9 (r_1), and due to differences which exist between present-days twisted-mass QCD results and staggered results. Of course, the limited number of large-scale QCD simulations that are available means that there are only a small number of truly independent determinations of the scales. For example,

three out of the five computations entering our average for w_0 are based on the same HISQ rooted staggered fermion configurations and thus their differences are only due to the choice of the physical scale (M_Ω vs. f_π), the valence quark action (Möbius domain-wall valence fermions vs. staggered fermions) employed to compute it and different analysis of continuum limit, etc.

Due to the publication of ETM 21, differences between $N_f = 2+1$ and $2+1+1$ QCD are now smaller and (within their errors) in agreement with expectations [198,199]. The effect of the charm quark is $-0.6(8)\%$ on w_0 and $-1.2(9)\%$ on $\sqrt{t_0}$ as computed from the FLAG averages, while precision studies of the decoupling of charm quarks predicted generic effects of a magnitude of only $\approx 0.2\%$ [198,199] for low-energy quantities. However, the agreement within errors is due to large stretching factors. Taking just the individual results, they do not agree. The differences are between $N_f = 2+1$ calculations and $2+1+1$ calculations, but one can also interpret them as a difference between staggered fermion simulations and Wilson-type ones. Since the FLAG averages have changed quite a bit due to one more computation entering the averages, we are looking forward to further and more precise results to see whether the numbers hold up over time. In this respect, it is highly desirable for future computations to also publish ratios such as $\sqrt{t_0}/w_0$ for which there are few numbers so far.

Such ratios of gradient flow scales are also of high interest in order to better understand the specific discretization errors of gradient flow observables. So far, systematic studies and information on the different contributions (see Sec. XI D 2 and Ref. [1079]) are missing. A worrying result is, for example, the scale-setting study of Ref. [226] on ratios of scales. The authors find indications that the asymptotic $\sim a^2$ scaling does not set in before $a \approx 0.05$ fm and the $a = 0.04$ fm data has a relevant influence on their continuum extrapolations.

A final word concerns the physics scales that all results depend on. While the mass of the Ω baryon is more popular than the leptonic decay rate of the pion, both have systematics which are difficult to estimate. For the Ω baryon it is the contaminations by excited states and for the decay rates it is the QED effects $\delta f_\pi^{\mathrm{isoQCD}}$. The uncertainty in V_{ud} is *not* relevant at this stage, but means that one is relying more on the standard model being an accurate low-energy theory than in the case of the Ω mass. In principle, excited-state effects are controlled by just going to large Euclidean time, but, in practice, this yields errors that are too large. One, therefore, performs fits with a very small number of excitations while theoretically there is a multitude of multi-hadron states that are expected to contribute. For the leptonic decay rate of the pion, the situation is quite reversed, namely, the problematic QED contributions have a well-motivated theory: chiral perturbation theory. The needed combination of low-energy constants is not accessible from experiment but its large-N estimate [1069] has been (indirectly) confirmed by the recent computation of $\delta f_\pi^{\mathrm{isoQCD}}$ [217]. Unfortunately the same comparison is not so favorable for the leptonic kaon decay.

ACKNOWLEDGMENTS

We are very grateful to the external reviewers for providing detailed comments and suggestions on the draft of this review. These reviewers were Martin Beneke, Aoife Bharucha, Chris Bouchard, Vincenzo Cirigliano, Martha Constantinou, Evgeny Epelbaum, Martin Gorbahn, André Hoang, Christian Hoelbling, Weonjong Lee, Laurent Lellouch, Zoltan Ligeti, Agostino Patella, Chris Sachrajda, and Takeshi Yamazaki. We are grateful to Anthony Grebe for help in making the figures more suitable for readers with color blindness. We also wish to thank Silvano Simula for his valuable contributions in the early stages of preparing the report, and Takumi Doi for correspondence and helpful comments. The kick-off meeting for the present review was held at CERN in January 2023. The mid-review meeting was held in January 2024 at the Johannes Gutenberg University in Mainz and was supported by the Mainz Institute for Theoretical Physics. We thank our hosts for their hospitality and financial support is gratefully acknowledged. Members of FLAG were supported by funding agencies; in particular: X. F. is supported in part by NSFC of China under Grants No. 12125501 and No. 12141501, and National Key Research and Development Program of China under No. 2020YFA0406400. M. G. was supported in part by the United States Department of Energy Grant No. DE-SC0013682. S. G. acknowledges support from the United States Department of Energy through Grant No. DE-SC0010120. G. H. acknowledges support from the grant No. PID2021-127526NB-I00, funded by MCIN/AEI/10.13039/501100011033 and by "ERDF A way of making Europe," and by the Spanish Research Agency (Agencia Estatal de Investigación) through grant IFT Centro de Excelencia Severo Ochoa No. CEX2020-001007-S, funded by MCIN/AEI/10.13039/501100011033. C. J. M. was supported in part by the United States Department of Energy under Grant No. DE-SC0023047. T. K. was supported in part by JSPS KAKENHI Grants No. JP22K21347 and No. JP23K20846, and by "Program for Promoting Researches on the Supercomputer Fugaku" (Simulation for basic science: approaching the new quantum era, JPMXP1020230411) through the Joint Institute for Computational Fundamental Science (JICFuS). S. M. was supported by the United States Department of Energy, Office of Science, Office of High Energy Physics under Award Number DE-SC0009913. A. P. was supported in part by funding from the European Research Council (ERC) under the European Union's Horizon 2020 research and innovation programme under Grant Agreements No. 757646 and

No. 813942, UK STFC Grant No. ST/X000494/1, and long-term Invitational Fellowship L23530 from the Japan Society for the Promotion of Science. P. P. was supported by the U.S. Department of Energy under Contract No. DE-SC0012704. S. S. acknowledges partial support by the H2020 program in the Europlex training network, Grant Agreement No. 813942. S. R. S. was supported in part by the United States Department of Energy Grant No. DE-SC0011637. S. S. acknowledges support from the EU H2020-MSCA-ITN-2018-813942 (EuroPLEx). A. V. was supported by the Spanish Research Agency (Agencia Estatal de Investigación) under Grant No. RYC2020-030244-I/AEI/10.13039/501100011033. U. W. was supported by the Swiss National Science Foundation (SNSF) Project No. 200020_208222.

XII. DATA AVAILABILITY

The data supporting this study's findings are available within the article.

APPENDIX A: LIST OF ACRONYMS

BχPT	baryonic chiral perturbation theory
BCL	Bourrely-Caprini-Lellouch
BGL	Boyd-Grinstein-Lebed
BK	Becirevic-Kaidalov
BSM	beyond standard model
BZ	Ball-Zwicky
χPT	chiral perturbation theory
CKM	Cabibbo-Kobayashi-Maskawa
CLN	Caprini-Lellouch-Neubert
CP	charge-parity
CPT	charge-parity-time reversal
CVC	conserved vector current
DSDR	dislocation suppressing determinant ratio
DW	domain wall
DWF	domain wall fermion
EDM	electric dipole moment
EFT	effective field theory
EM	electromagnetic
ESC	excited state contributions
EW	electroweak
FCNC	flavor-changing neutral current
FH	Feynman-Hellman
FSE	finite-size effects
FV	finite volume
GF	gradient flow
GGOU	Gambino-Giordano-Ossola-Uraltsev
GRS	Gasser-Rusetsky-Scimemi
HEX	hypercubic stout
HISQ	highly improved staggered quarks
HMχPT	heavy-meson chiral perturbation theory
HMC	hybrid Monte Carlo
HMrSχPT	heavy-meson rooted staggered chiral perturbation theory
HQET	heavy-quark effective theory
IR	infrared
isoQCD	isospin-symmetric QCD
LD	long distance
LEC	low-energy constant
LO	leading order
LW	Lüscher-Weisz
MC	Monte Carlo
MM	minimal MOM
MOM	momentum subtraction
$\overline{\text{MS}}$	modified minimal substraction scheme
NDR	naive dimensional regularization
nEDM	nucleon electric dipole moment
NGB	Nambu-Goldstone bosons
NLO	next-to-leading order
NME	nucleon matrix elements
NNLO	next-to-next-to-leading order
NP	nonperturbative
npHQET	nonperturbative heavy-quark effective theory
NRQCD	nonrelativistic QCD
NSPT	numerical stochastic perturbation theory
OPE	operator product expansion
PCAC	partially conserved axial current
PDF	parton distribution function
PDG	particle data group
QCD	quantum chromodynamics
QED	quantum electrodynamics
QED_{L}	formulation of QED in finite volume (see [263])
QED_{TL}	formulation of QED in finite volume (see [1092])
RG	renormalization group
RGI	renormalization group invariant
RH	R. Hill
RHQ	relativistic heavy-quark
RHQA	relativistic heavy-quark action
RI-MOM	regularization-independent momentum subtraction (also RI/MOM)
RI-SMOM	regularization-independent symmetric momentum (also RI/SMOM)
RMS	root mean square
SχPT	staggered chiral perturbation theory
SD	short distance
SF	Schrödinger functional
SIDIS	semi-inclusive deep-inelastic scattering
SM	standard model

(Continued)

SSF	step-scaling function
SUSY	supersymmetric
SW	Sheikholeslami-Wohlert
UT	unitarity triangle
UV	ultraviolet

APPENDIX B

1. Inclusion of electromagnetic effects

Electromagnetism on a lattice can be formulated using a naive discretization of the Maxwell action $S[A_\mu] = \frac{1}{4}\int d^4x \sum_{\mu,\nu}[\partial_\mu A_\nu(x) - \partial_\nu A_\mu(x)]^2$. Even in its noncompact form, the action remains gauge invariant. This is not the case for non-Abelian theories for which one uses the traditional compact Wilson gauge action (or an improved version of it). Compact actions for QED feature spurious photon-photon interactions which vanish only in the continuum limit. This is one of the main reason why the noncompact action is the most popular so far. It was used in all the calculations presented in this review. Gauge-fixing is necessary for noncompact actions because of the usual infinite measure of equivalent gauge orbits which contribute to the path integral. It was shown [1093,1094] that gauge-fixing is not necessary with compact actions, including in the construction of interpolating operators for charged states.

Although discretization is straightforward, simulating QED in a finite volume is more challenging. Indeed, the long range nature of the interaction suggests that important finite-size effects have to be expected. In the case of periodic boundary conditions, the situation is even more critical: a naive implementation of the theory features an isolated zero-mode singularity in the photon propagator. It was first proposed in [338] to fix the global zero-mode of the photon field $A_\mu(x)$ in order to remove it from the dynamics. This modified theory is generally named $\mathrm{QED_{TL}}$. Although this procedure regularizes the theory and has the right classical infinite-volume limit, it is nonlocal because of the zero-mode fixing. As first discussed in [185], the nonlocality in time of $\mathrm{QED_{TL}}$ prevents the existence of a transfer matrix, and therefore a quantum-mechanical interpretation of the theory. Another prescription named $\mathrm{QED_L}$, proposed in [263], is to remove the zero-mode of $A_\mu(x)$ independently for each time slice. This theory, although still nonlocal in space, is local in time and has a well-defined transfer matrix. Whether these nonlocalities constitute an issue to extract infinite-volume physics from lattice-QCD+$\mathrm{QED_L}$ simulations is, at the time of this review, still an open question. However, it is known through analytical calculations of electromagnetic finite-size effects at $\mathcal{O}(\alpha)$ in hadron masses [185–188,212,263,1095,1096], meson leptonic decays [187,1096], and the hadronic vacuum polarization [1097] that $\mathrm{QED_L}$ does not suffer from a problematic (e.g., UV divergent) coupling of short- and long-distance physics due to its nonlocality, and is likely safe to use for these quantities. Another strategy, first proposed in [1098] and used by the QCDSF collaboration, is to bound the zero-mode fluctuations to a finite range. Although more minimal, it is still a nonlocal modification of the theory and so far finite-size effects for this scheme have not been investigated. Two proposals for local formulations of finite-volume QED emerged. The first one described in [1099] proposes to use massive photons to regulate zero-mode singularities, at the price of (softly) breaking gauge invariance. The second one presented in [1094], based on earlier works [1100,1101], avoids the zero-mode issue by using anti-periodic boundary conditions for $A_\mu(x)$. In this approach, gauge invariance requires the fermion field to undergo a charge conjugation transformation over a period, breaking electric charge conservation. These local approaches have the potential to constitute cleaner approaches to finite-volume QED. They have led to first numerical studies at unphysical masses [1102,1103], but were not used in any calculation reviewed in this paper.

Once a finite-volume theory for QED is specified, there are various ways to compute QED effects themselves on a given hadronic quantity. The most direct approach, first used in [338], is to include QED directly in the lattice simulations and assemble correlation functions from charged quark propagators. Another approach proposed in [212], is to exploit the perturbative nature of QED, and compute the leading-order corrections directly in pure QCD as matrix elements of the electromagnetic current. Both approaches have their advantages and disadvantages and as shown in [23], are not mutually exclusive. A critical comparative study can be found in [1104].

Finally, most of the calculations presented here made the choice of computing electromagnetic corrections in the electro-quenched approximation. In this limit, one assumes that only valence quarks are charged, which is equivalent to neglecting QED corrections to the fermionic determinant. This approximation reduces dramatically the cost of lattice-QCD+QED calculations since it allows the reuse of previously generated QCD configurations. If QED is introduced perturbatively through current insertions, the electro-quenched approximation avoids computing disconnected contributions coming from the electromagnetic current in the vacuum, which are generally challenging to determine precisely. The electromagnetic contributions from sea quarks to hadron-mass splittings are known to be flavor-SU(3) and large-N_c suppressed, thus electro-quenched simulations are expected to have an $\mathcal{O}(10\%)$ accuracy for the leading electromagnetic effects. This suppression is in principle rather

weak and results obtained from electro-quenched simulations might feature uncontrolled systematic errors. For this reason, the use of the electro-quenched approximation constitutes the difference between ★ and ○ in the FLAG criterion for the inclusion of isospin-breaking effects.

2. Parametrizations of semileptonic form factors

In this section, we discuss the description of the q^2-dependence of form factors, using the vector form factor f_+ of $B \to \pi\ell\nu$ decays as a benchmark case. Since in this channel the parametrization of the q^2-dependence is crucial for the extraction of $|V_{ub}|$ from the existing measurements (involving decays to light leptons), as explained above, it has been studied in great detail in the literature. Some comments about the generalization of the techniques involved will follow.

a. The vector form factor for $B \to \pi\ell\nu$

All form factors are analytic functions of q^2 outside physical poles and inelastic threshold branch points; in the case of $B \to \pi\ell\nu$, the only pole expected below the $B\pi$ production region, starting at $q^2 = t_+ = (m_B + m_\pi)^2$, is the B^*. A simple *Ansatz* for the q^2-dependence of the $B \to \pi\ell\nu$ semileptonic form factors that incorporates vector-meson dominance is the Bečirević-Kaidalov (BK) parametrization [573], which for the vector form factor reads

$$f_+(q^2) = \frac{f(0)}{(1 - q^2/m_{B^*}^2)(1 - \alpha q^2/m_{B^*}^2)}. \tag{B1}$$

Because the BK *Ansatz* has few free parameters, it has been used extensively to parametrize the shape of experimental branching-fraction measurements and theoretical form-factor calculations. A variant of this parametrization proposed by Ball and Zwicky (BZ) adds extra pole factors to the expressions in Eq. (B1) in order to mimic the effect of multiparticle states [1105]. A similar idea, extending the use of effective poles also to $D \to \pi\ell\nu$ decays, is explored in Ref. [1106]. Finally, yet another variant (RH) has been proposed by Hill in Ref. [574]. Although all of these parametrizations capture some known properties of form factors, they do not manifestly satisfy others. For example, perturbative QCD scaling constrains the behavior of f_+ in the deep Euclidean region [1107–1109], and angular momentum conservation constrains the asymptotic behavior near thresholds—e.g., $\mathrm{Im}\, f_+(q^2) \sim (q^2 - t_+)^{3/2}$ (see, e.g., Ref. [1110]). Most importantly, these parametrizations do not allow for an easy quantification of systematic uncertainties.

A more systematic approach that improves upon the use of simple models for the q^2 behavior exploits the positivity and analyticity properties of two-point functions of vector currents to obtain optimal parametrizations of form factors [575,1109,1111–1115]. Any form factor f can be shown to admit a series expansion of the form

$$f(q^2) = \frac{1}{B(q^2)\phi(q^2, t_0)} \sum_{n=0}^{\infty} a_n(t_0) z(q^2, t_0)^n, \tag{B2}$$

where the squared momentum transfer is replaced by the variable

$$z(q^2, t_0) = \frac{\sqrt{t_+ - q^2} - \sqrt{t_+ - t_0}}{\sqrt{t_+ - q^2} + \sqrt{t_+ - t_0}}. \tag{B3}$$

This is a conformal transformation, depending on an arbitrary real parameter $t_0 < t_+$, that maps the q^2 plane cut for $q^2 \geq t_+$ onto the disk $|z(q^2, t_0)| < 1$ in the z complex plane. The function $B(q^2)$ is called the *Blaschke factor*, and contains poles and cuts below t_+—for instance, in the case of $B \to \pi$ decays,

$$B(q^2) = \frac{z(q^2, t_0) - z(m_{B^*}^2, t_0)}{1 - z(q^2, t_0) z(m_{B^*}^2, t_0)} = z(q^2, m_{B^*}^2). \tag{B4}$$

Finally, the quantity $\phi(q^2, t_0)$, called the *outer function*, is some otherwise arbitrary function that does not introduce further poles or branch cuts. The crucial property of this series expansion is that the sum of the squares of the coefficients

$$\sum_{n=0}^{\infty} a_n^2 = \frac{1}{2\pi i} \oint \frac{dz}{z} |B(z)\phi(z) f(z)|^2, \tag{B5}$$

is a finite quantity. Therefore, by using this parametrization an absolute bound to the uncertainty induced by truncating the series can be obtained. The aim in choosing ϕ is to obtain a bound that is useful in practice, while (ideally) preserving the correct behavior of the form factor at high q^2 and around thresholds.

The simplest form of the bound would correspond to $\sum_{n=0}^{\infty} a_n^2 = 1$. *Imposing* this bound yields the following "standard" choice for the outer function

$$\begin{aligned}\phi(q^2, t_0) = {} & \sqrt{\frac{1}{32\pi\chi_{1^-}(0)}} \left(\sqrt{t_+ - q^2} + \sqrt{t_+ - t_0}\right) \\ & \times \left(\sqrt{t_+ - q^2} + \sqrt{t_+ - t_-}\right)^{3/2} \\ & \times \left(\sqrt{t_+ - q^2} + \sqrt{t_+}\right)^{-5} \frac{t_+ - q^2}{(t_+ - t_0)^{1/4}},\end{aligned} \tag{B6}$$

where $t_- = (m_B - m_\pi)^2$, and $\chi_{1^-}(0)$ is the derivative of the transverse component of the polarization function (i.e., the Fourier transform of the vector two-point function) $\Pi_{\mu\nu}(q)$ at Euclidean momentum $Q^2 = -q^2 = 0$. It is computed perturbatively, using operator product expansion techniques, by relating the $B \to \pi\ell\nu$ decay amplitude to

$\ell\nu \to B\pi$ inelastic scattering via crossing symmetry and reproducing the correct value of the inclusive $\ell\nu \to X_b$ amplitude. We will refer to the series parametrization with the outer function in Eq. (B6) as Boyd, Grinstein, and Lebed (BGL). The perturbative and OPE truncations imply that the bound is not strict, and one should take it as

$$\sum_{n=0}^{N} a_n^2 \lesssim 1, \tag{B7}$$

where this holds for any choice of N. Since the values of $|z|$ in the kinematical region of interest are well below 1 for judicious choices of t_0, this provides a very stringent bound on systematic uncertainties related to truncation for $N \geq 2$. On the other hand, the outer function in Eq. (B6) is somewhat unwieldy and, more relevantly, spoils the correct large q^2 behavior and induces an unphysical singularity at the $B\pi$ threshold.

A simpler choice of outer function has been proposed by Bourrely, Caprini and Lellouch (BCL) in Ref. [1110], which leads to a parametrization of the form

$$f_+(q^2) = \frac{1}{1 - q^2/m_{B^*}^2} \sum_{n=0}^{N} a_n^+(t_0) z(q^2, t_0)^n. \tag{B8}$$

This satisfies all the basic properties of the form factor, at the price of changing the expression for the bound to

$$\sum_{j,k=0}^{N} B_{jk}(t_0) a_j^+(t_0) a_k^+(t_0) \leq 1. \tag{B9}$$

The constants B_{jk} can be computed and shown to be $|B_{jk}| \lesssim \mathcal{O}(10^{-2})$ for judicious choices of t_0; therefore, one again finds that truncating at $N \geq 2$ provides sufficiently stringent bounds for the current level of experimental and theoretical precision. It is actually possible to optimize the properties of the expansion by taking

$$t_0 = t_{\rm opt} = (m_B + m_\pi)(\sqrt{m_B} - \sqrt{m_\pi})^2, \tag{B10}$$

which for physical values of the masses results in the semileptonic domain being mapped onto the symmetric interval $|z| \lesssim 0.279$ (where this range differs slightly for the $B^\pm$ and B^0 decay channels), minimizing the maximum truncation error. If one also imposes that the asymptotic behavior $\mathrm{Im}\, f_+(q^2) \sim (q^2 - t_+)^{3/2}$ near threshold is satisfied, then the highest-order coefficient is further constrained as

$$a_N^+ = -\frac{(-1)^N}{N} \sum_{n=0}^{N-1} (-1)^n n a_n^+. \tag{B11}$$

Substituting the above constraint on a_N^+ into Eq. (B8) leads to the constrained BCL parametrization

$$f_+(q^2) = \frac{1}{1 - q^2/m_{B^*}^2} \sum_{n=0}^{N-1} a_n^+ \left[z^n - (-1)^{n-N} \frac{n}{N} z^N \right], \tag{B12}$$

which is the standard implementation of the BCL parametrization used in the literature.

Parameterizations of the BGL and BCL kind, to which we will refer collectively as "z-parametrizations," have already been adopted by the *BABAR* and Belle collaborations to report their results, and also by the Heavy Flavour Averaging Group (HFAG, later renamed HFLAV). Some lattice collaborations, such as FNAL/MILC and ALPHA, have already started to report their results for form factors in this way. The emerging trend is to use the BCL parametrization as a standard way of presenting results for the q^2-dependence of semileptonic form factors. Our policy will be to quote results for z-parametrizations when the latter are provided in the paper (including the covariance matrix of the fits); when this is not the case, but the published form factors include the full correlation matrix for values at different q^2, we will perform our own fit to the constrained BCL *Ansatz* in Eq. (B12); otherwise no fit will be quoted. We however stress the importance of providing, apart from parametrization coefficients, values for the form factors themselves (in the continuum limit and at physical quark masses) for a number of values of q^2, so that the results can be independently parametrized by the readers if so wished.

b. The scalar form factor for $B \to \pi\ell\nu$

The discussion of the scalar $B \to \pi$ form factor is very similar. The main differences are the absence of a constraint analog to Eq. (B11) and the choice of the overall pole function. In our fits we adopt the simple expansion

$$f_0(q^2) = \sum_{n=0}^{N-1} a_n^0 z^n. \tag{B13}$$

We do impose the exact kinematical constraint $f_+(0) = f_0(0)$ by expressing the a_{N-1}^0 coefficient in terms of all remaining a_n^+ and a_n^0 coefficients. This constraint introduces important correlations between the a_n^+ and a_n^0 coefficients; thus only lattice calculations that present the correlations between the vector and scalar form factors can be used in an average that takes into account the constraint at $q^2 = 0$.

Finally we point out that we do not need to use the same number of parameters for the vector and scalar form factors. For instance, with $(N^+ = 3, N^0 = 3)$ we have $a_{0,1,2}^+$ and $a_{0,1}^0$, while with $(N^+ = 3, N^0 = 4)$ we have $a_{0,1,2}^+$ and $a_{0,1,2}^0$ as independent fit parameters. In our average we will choose the combination that optimizes uncertainties.

c. Extension to other form factors

The discussion above largely extends to form factors for other semileptonic transitions (e.g., $B_s \to K$ and $B_{(s)} \to D_{(s)}^{(*)}$, and semileptonic D and K decays). Details are discussed in the relevant sections.

A general discussion of semileptonic meson decay in this context can be found, e.g., in Ref. [1116]. Extending what has been discussed above for $B \to \pi$, the form factors for a generic $H \to L$ transition will display a cut starting at the production threshold t_+, and the optimal value of t_0 required in z-parametrizations is $t_0 = t_+(1 - \sqrt{1 - t_-/t_+})$ (where $t_\pm = (m_H \pm m_L)^2$). For unitarity bounds to apply, the Blaschke factor has to include all sub-threshold poles with the quantum numbers of the hadronic current—i.e., vector (resp. scalar) resonances in $B\pi$ scattering for the vector (resp. scalar) form factors of $B \to \pi$, $B_s \to K$, or $\Lambda_b \to p$; and vector (resp. scalar) resonances in $B_c\pi$ scattering for the vector (resp. scalar) form factors of $B \to D$ or $\Lambda_b \to \Lambda_c$.[87] Thus, as emphasized above, the control over systematic uncertainties brought in by using z-parametrizations strongly depends on implementation details. This has practical consequences, in particular, when the resonance spectrum in a given channel is not sufficiently well known. Caveats may also apply for channels where resonances with a non-negligible width appear. A further issue is whether $t_+ = (m_H + m_L)^2$ is the proper choice for the start of the cut in cases such as $B_s \to K\ell\nu$ and $B \to D\ell\nu$, where there are lighter two-particle states that project on the current (B,π and B_c,π for the two processes, respectively).[88] In any such situation, it is not clear *a priori* that a given z-parametrization will satisfy strict bounds, as has been seen, e.g., in determinations of the proton charge radius from electron-proton scattering [1117–1119].

The HPQCD collaboration pioneered a variation on the z-parametrization approach, which they refer to as a "modified z-expansion," that is used to simultaneously extrapolate their lattice simulation data to the physical light-quark masses and the continuum limit, and to interpolate/extrapolate their lattice data in q^2. This entails allowing the coefficients a_n to depend on the light-quark masses, squared lattice spacing, and, in some cases the charm-quark mass and pion or kaon energy. Because the modified z-expansion is not derived from an underlying effective field theory, there are several potential concerns with this approach that have yet to be studied. The most significant is that there is no theoretical derivation relating the coefficients of the modified z-expansion to those of the physical coefficients measured in experiment; it therefore introduces an unquantified model dependence in the form-factor shape. As a result, the applicability of unitarity bounds has to be examined carefully. Related to this, z-parametrization coefficients implicitly depend on quark masses, and particular care should be taken in the event that some state can move across the inelastic threshold as quark masses are changed (which would in turn also affect the form of the Blaschke factor). Also, the lattice-spacing dependence of form factors provided by Symanzik effective theory techniques may not extend trivially to z-parametrization coefficients. The modified z-expansion is now being utilized by collaborations other than HPQCD and for quantities other than $D \to \pi\ell\nu$ and $D \to K\ell\nu$, where it was originally employed. We advise treating results that utilize the modified z-expansion to obtain form-factor shapes and CKM matrix elements with caution, however, since the systematics of this approach warrant further study.

d. Choice of form-factor basis for chiral-continuum extrapolations

For pseudoscalar-to-pseudoscalar transitions $P_1 \to P_2$ (such as $B \to \pi$ or $B_s \to K$), the chiral and continuum extrapolations have often been performed in a different basis $f_\parallel$, $f_\perp$ given by [1120]

$$\langle P_2(p')|V^\mu|P_1(p)\rangle = \sqrt{2M_1}[v^\mu f_\parallel(E_2) + p'^\mu_\perp f_\perp(E_2)]. \tag{B14}$$

Here, $v^\mu = p^\mu/M_1$ is the initial-meson four-velocity, $p'^\mu_\perp = p'^\mu - (v\cdot p')v^\mu$ is the projection of the final-meson momentum in the direction perpendicular to v^μ, and the form factors are taken to be functions of $E_2 = v\cdot p'$ (the energy of the final-state meson in the initial-meson rest frame). After the chiral and continuum extrapolations, the standard form factors are then constructed as the linear combinations

$$f_0(q^2) = \frac{\sqrt{2M_1}}{M_1^2 - M_2^2}[(M_1 - E_2)f_\parallel(E_2) + (E_2^2 - M_K^2)f_\perp(E_2)], \tag{B15}$$

$$f_+(q^2) = \frac{1}{\sqrt{2M_1}}[f_\parallel(E_2) + (M_1 - E_2)f_\perp(E_2)]. \tag{B16}$$

The decomposition (B14) is motivated by heavy-meson chiral perturbation theory and is also convenient for the extraction of the form factors from the correlation functions. For example, for $B \to \pi$, heavy-meson chiral perturbation theory predicts, at leading-order in both the chiral and the heavy-quark expansion,

$$f_\perp(E_\pi) = \frac{1}{f_\pi}\frac{g_{B^*B\pi}}{E_\pi + \Delta_{B^*}}, \tag{B17}$$

[87] A more complicated analytic structure may arise in other cases, such as channels with vector mesons in the final state. We will however not discuss form-factor parametrizations for any such process.

[88] We are grateful to G. Herdoíza, R.J. Hill, A. Kronfeld and A. Szczepaniak for illuminating discussions on this issue.

$$f_\parallel(E_\pi) = \frac{1}{f_\pi}, \tag{B18}$$

where $\Delta_{B^*} = M_{B^*} - M_B$. For a general transition $P_1 \to P_2$, the chiral and continuum extrapolations were therefore commonly performed by fitting functions of the form

$$f_\perp(E_2) = \frac{1}{E_2 + \Delta_\perp}[\ldots] \tag{B19}$$

and

$$f_\parallel(E_2) = \frac{1}{E_2 + \Delta_\parallel}[\ldots] \quad \text{or} \quad f_\parallel(E_2) = [\ldots] \tag{B20}$$

with $\Delta_\perp = M_{1^-} - M_1$ and $\Delta_\parallel = M_{0^+} - M_1$, where M_{1^-} and M_{0^+} denote the masses of the bound states with $J^P = 1^-$ and $J^P = 0^+$ that couple to the weak current, and the ellipsis in the brackets denote terms describing the remaining dependence on the quark masses, lattice spacing, and kinematics. The terms in front of the brackets introduce poles at $E_2 = -\Delta$, which corresponds to $q^2 \approx M_{J^P}^2$ for large M_1. Depending on the process, there may be no QCD-stable bound state with $J^P = 0^+$, in which case this pole factor for $f_\parallel$ is usually omitted.

A problem with the above prescription is that, for finite heavy-quark mass, the J^P quantum numbers of the poles appearing in the form factors are definite only in the helicity basis of the form factors, with $J^P = 1^-$ for f_+ and $J^P = 0$ for f_0. In particular, the form factor $f_\parallel$, being a linear combination of f_+ and f_0, also has a pole at the lower mass M_{1^-} that is neglected when using the above functions. The alternative is to perform the chiral-continuum extrapolations for f_+ and f_0 using

$$f_+(E_2) = \frac{1}{E_2 + \Delta_+}[\ldots] \tag{B21}$$

and

$$f_0(E_2) = \frac{1}{E_2 + \Delta_0}[\ldots] \quad \text{or} \quad f_0(E_2) = [\ldots], \tag{B22}$$

where $\Delta_+ = M_{1^-} - M_1$ and $\Delta_0 = M_{0^+} - M_1$ now truly correspond to the lowest pole in each form factor. The authors of Ref. [128] found that this method (in the case of $B_s \to K$ form factors) yields significantly different results for the extrapolated f_0 when compared to extrapolating $f_\parallel$, $f_\perp$ and then reconstructing f_+ and f_0. Lattice determinations of the form factors based on extrapolations of $f_\parallel$, $f_\perp$ may therefore have an uncontrolled systematic error, and directly extrapolating f_+ and f_0 appears to be the better choice.

3. Explicit parametrizations used in the form factor fits

In order to reconstruct the form factors from the results of fits performed using a z-parametrization it is necessary not only to use the correct version of the parametrization but also to adopt *exactly* the same numerical values for all ancillary quantities that enter the fit (e.g., location of poles). In particular, users must avoid utilizing the most updated numerical inputs for these quantities with z-coefficients extracted using older values. The purpose of this appendix is to eliminate all ambiguities in the implementation of the fit results presented in Secs. VII and VIII.

a. $D \to K$ form factors

BCL parametrization

$$f_+(q^2) = \frac{1}{1 - q^2/m_{D_s^*}^2} \sum_{n=0}^{N^+-1} a_n^+ \left[z^n - (-1)^{n-N^+} \frac{n}{N^+} z^N \right], \tag{B23}$$

$$f_0(q^2) = \frac{1}{1 - q^2/m_{D_s^*(0^+)}^2} \sum_{n=0}^{N^0-1} a_n^0 z^n. \tag{B24}$$

The kinematical constraint $f_+(0) = f_0(0)$ is implemented expressing $a_{N^0-1}^0$ in terms of the other coefficients. We use $t_+ = (m_D + m_K)^2$, $t_- = (m_D - m_K)^2$ and $t_0 = t_+ - \sqrt{t_+(t_+ - t_-)}$. The numerical inputs are $m_D = 1.87265$ GeV, $m_{D_s^*} = 2.1122$ GeV, $m_{D_s^*(0^+)} = 2.317$ GeV, and $m_K = 0.495644$ GeV.

b. $B \to \pi$ form factors

BCL parametrization

$$f_+(q^2) = \frac{1}{1 - q^2/m_{B^*}^2} \sum_{n=0}^{N^+-1} a_n^+ \left[z^n - (-1)^{n-N^+} \frac{n}{N^+} z^N \right], \tag{B25}$$

$$f_0(q^2) = \sum_{n=0}^{N^0-1} a_n^0 z^n. \tag{B26}$$

The kinematical constraint $f_+(0) = f_0(0)$ is implemented expressing $a_{N^0-1}^0$ in terms of the other coefficients. We use $t_+ = (m_B + m_\pi)^2$ and $t_0 = (m_B + m_\pi)(\sqrt{m_B} - \sqrt{m_\pi})$. The numerical inputs are $m_{B^*} = 5.32471$ GeV, $m_B = 5.27934$ GeV and $m_\pi = 0.1349768$ GeV.

Results for the form factor f_T are taken directly from Ref. [129] where we refer the reader for details on the parametrization.

c. $B_s \to K$ form factors

BCL parametrization

$$f_+(q^2) = \frac{1}{1 - q^2/m^2_{B^*}} \sum_{n=0}^{N^+-1} a_n^+ \left[z^n - (-1)^{n-N^+} \frac{n}{N^+} z^N \right], \tag{B27}$$

$$f_0(q^2) = \frac{1}{1 - q^2/m^2_{B^*(0^+)}} \sum_{n=0}^{N^0-1} a_n^0 z^n. \tag{B28}$$

The kinematical constraint $f_+(0) = f_0(0)$ is implemented expressing $a^0_{N^0-1}$ in terms of the other coefficients. We use $t_+ = (m_B + m_\pi)^2$, $t_- = (m_{B_s} - m_K)^2$ and $t_0 = t_+ - \sqrt{t_+(t_+ - t_-)}$. The numerical inputs are $m_B = 5.27931$ GeV, $m_{B^*} = 5.3251$ GeV, $m_{B_s} = 5.36688$ GeV, $m_{B^*(0^+)} = 5.68$ GeV, $m_K = 0.493677$ GeV and $m_\pi = 0.1349766$ GeV.

d. $B \to K$ form factors

BCL parametrization

$$f_+(q^2) = \frac{1}{1 - q^2/m^2_{B_s^*}} \sum_{n=0}^{N^+-1} a_n^+ \left[z^n - (-1)^{n-N^+} \frac{n}{N^+} z^N \right], \tag{B29}$$

$$f_0(q^2) = \frac{1}{1 - q^2/m^2_{B_s^*(0^+)}} \sum_{n=0}^{N^0-1} a_n^0 z^n, \tag{B30}$$

$$f_T(q^2) = \frac{1}{1 - q^2/m^2_{B_s^*}} \sum_{n=0}^{N^T-1} a_n^T z^n. \tag{B31}$$

The kinematical constraint $f_+(0) = f_0(0)$ is implemented expressing $a^0_{N^0-1}$ in terms of the other coefficients. We use $t_+ = (m_B + m_K)^2$ and $t_0 = (m_B + m_K)(\sqrt{m_B} - \sqrt{m_K})^2$. The numerical inputs are $m_B = 5.27931$ GeV, $m_{B_s^*} = 5.4154$ GeV, $m_{B_s^*(0^+)} = 5.718$ GeV and $m_K = 0.493677$ GeV.

e. $B \to D$ form factors

BCL parametrization

$$f_+(q^2) = \sum_{n=0}^{N^+-1} a_n^+ \left[z^n - (-1)^{n-N^+} \frac{n}{N^+} z^N \right], \tag{B32}$$

$$f_0(q^2) = \sum_{n=0}^{N^0-1} a_n^0 z^n. \tag{B33}$$

The kinematical constraint $f_+(0) = f_0(0)$ is implemented expressing $a^0_{N^0-1}$ in terms of the other coefficients. We use $t_+ = (m_B + m_D)^2$ and $t_0 = (m_B + m_D)(\sqrt{m_B} - \sqrt{m_D})$. The numerical inputs are $m_B = 5.27931$ GeV and $m_D = (1.86483 + 1.86965)/2$ GeV.

f. $B_s \to D_s$ form factors

Results for the form factors are taken directly from Table VIII of Ref. [134] where we refer the reader for details on the parametrization.

g. $B \to D^*$ form factors

We adopt the BGL parametrization used in Ref. [136]: the form factors are given in Eqs. (63) and (64), the poles for the Blaschke factors are given in Table 9, the four outer functions in Eqs. (67)–(70) and the remaining numerical inputs in Table 10. We impose the kinematic constraints at zero and max recoil (see Eqs. (72) and (73) of Ref. [136]) by eliminating the coefficients $a_0^{F_1}$ and $a_0^{F_2}$.

h. $B_s \to D_s^*$ form factors

We adopt the same BGL parametrization described in Sec. B 3 g. Both the outer functions and the location of the poles are identical to the $B \to D^*$ case, and the kinematical constraints are imposed in the same way. The only difference are the masses $m_{B_s} = 5.36688$ GeV and $m_{D_s^*} = 2.112$ GeV.

APPENDIX C: NOTES

In the following Appendices we provide more detailed information on the simulations used to calculate the quantities discussed in Secs. IV–XI, see Tables 79–189. We present this information only for results that are new with respect to FLAG 21. For all other results the information is available in the corresponding Appendices C.1–C.9 in FLAG 21 [5], B.1–B.8 in FLAG 19 [4], and B.1–B.7 in FLAG 16 [3].

1. Notes to Sec. IV on quark masses

TABLE 79. Continuum extrapolations/estimation of lattice artifacts in determinations of m_{ud}, m_s and, in some cases m_u and m_d, with $N_f = 2 + 1$ quark flavors.

Collab.	Ref.	N_f	a [fm]	Description
CLQCD 23	[10]	$2 + 1$	0.052, 0.077, 0.11	Smeared Wilson-clover/Symanzik

TABLE 80. Chiral extrapolation/minimum pion mass in determinations of m_{ud}, m_s, and in some cases m_u and m_d, with $N_f = 2 + 1$ quark flavors.

Collab.	Ref.	N_f	$M_{\pi,\min}$ [MeV]	Description
CLQCD 23	[10]	$2 + 1$	135.5	

TABLE 81. Finite-volume effects in determinations of m_{ud}, m_s and, in some cases m_u and m_d, with $N_f = 2 + 1$ quark flavors.

Collab.	Ref.	N_f	L [fm]	$M_{\pi,\min}L$	Description
CLQCD 23	[10]	$2 + 1$	2.5–5.1	3.45	

TABLE 82. Renormalization in determinations of m_{ud}, m_s and, in some cases m_u and m_d, with $N_f = 2 + 1$ quark flavors.

Collab.	Ref.	N_f	Description
CLQCD 23	[10]	$2 + 1$	RI/MOM

TABLE 83. Continuum extrapolations/estimation of lattice artifacts in the determinations of m_c with $N_f = 2 + 1$ quark flavors.

Collab.	Ref.	N_f	a [fm]	Description
ALPHA 23	[28]	$2 + 1$	0.085, 0.075, 0.064, 0.049	$\mathcal{O}(a^2)$ terms, with mass-dependent coefficients, are included in the chiral-continuum extrapolation. t_0 is used as intermediate scale with the physical scale set by a combination of f_π and f_K in the isosymmetric limit.

TABLE 84. Chiral extrapolation/minimum pion mass in the determinations of m_c with $N_f = 2 + 1$ quark flavors.

Collab.	Ref.	N_f	$M_{\pi,\min}$ [MeV]	Description
ALPHA 23	[28]	$2 + 1$	200	

TABLE 85. Finite-volume effects in the determinations of m_c with $N_f = 2 + 1$ quark flavors.

Collab.	Ref.	N_f	L [fm]	$M_{\pi,\min}L$	Description
ALPHA 23	[28]	$2 + 1$	2.7, 2.4, 3.1/4.1, 2.4/3.1	3.9, 5.1, 4.2, 4.1	No explicit discussion of FSE.

TABLE 86. Renormalization in the determinations of m_c with $N_f = 2 + 1$ quark flavors.

Collab.	Ref.	N_f	Description
ALPHA 23	[28]	$2 + 1$	Schrödinger functional

2. Notes to Sec. V on $|V_{ud}|$ and $|V_{us}|$

TABLE 87. Continuum extrapolations/estimation of lattice artifacts in the determinations of $f_+(0)$.

Collab.	Ref.	N_f	a [fm]	Description
PACS 22	[342]	$2+1$	0.085, 0.063	Nonperturbative $\mathcal{O}(a)$ clover quark action. Scale set from Ξ-baryon mass.

TABLE 88. Chiral extrapolation/minimum pion mass in determinations of $f_+(0)$.

Collab.	Ref.	N_f	$M_{\pi,\mathrm{min}}$ [MeV]	Description
PACS 22	[342]	$2+1$	135	Physical point simulation at a single pion mass 135 MeV.

TABLE 89. Finite-volume effects in determinations of $f_+(0)$.

Collab.	Ref.	N_f	L [fm]	$M_{\pi,\mathrm{min}}L$	Description
PACS 22	[342]	$2+1$	10.9	7.5	

TABLE 90. Continuum extrapolations/estimation of lattice artifacts in determinations of f_K/f_π.

Collab.	Ref.	N_f	a [fm]	Description
ETM 21	[45]	$2+1+1$	0.07, 0.08, 0.09	Wilson-clover twisted mass quark action. Relative scale through gradient flow scale w_0 and absolute scale through f_π.
CLQCD 23	[10]	$2+1$	0.105, 0.077, 0.052	Tadpole-improved clover quark action with one-step stout smearing. Scale set through gradient-flow scale w_0.

TABLE 91. Chiral extrapolation/minimum pion mass in determinations of f_K/f_π.

Collab.	Ref.	N_f	$M_{\pi,\mathrm{min}}$ [MeV]	Description
ETM 21	[45]	$2+1+1$	134	Chiral extrapolation based on NLO SU(2) χPT.
CLQCD 23	[10]	$2+1$	135.5	Two additional partially quenched quark masses on each ensemble. Chiral extrapolation based on NLO SU(2) partially quenched χPT for f_π and a polynomial extrapolation for f_K.

TABLE 92. Finite-volume effects in determinations of f_K/f_π.

Collab.	Ref.	N_f	L [fm]	$M_{\pi,\mathrm{min}}L$	Description
ETM 21	[45]	$2+1+1$	2.0–5.6	3.8	Three different volumes at $M_\pi = 253$ MeV and $a = 0.08$ fm.
CLQCD 23	[10]	$2+1$	2.5–5.1	3.5	Two volumes at four simulation points with $M_\pi = 200$–300 MeV on two coarser lattices.

3. Notes to Sec. VI on kaon mixing

a. Kaon B-parameter B_K

TABLE 93. Continuum extrapolations/estimation of lattice artifacts in determinations of B_K.

Collab.	Ref.	N_f	a [fm]	Description
RBC/UKQCD 24	[56]	$2+1$	0.114, 0.084, 0.073	Combined continuum and chiral [NLO SU(2)] extrapolation fits. Assigned systematic error at the per-mille level.

TABLE 94. Chiral extrapolation/minimum pion mass in determinations of B_K.

Collab.	Ref.	N_f	$M_{\pi,\mathrm{min}}$ [MeV]	Description
RBC/UKQCD 24	[56]	$2+1$	139, 139, 232	Chiral extrapolations based on SU(2)-χPT fits at NLO. Systematic uncertainties amount to less than half a per cent.

TABLE 95. Finite-volume effects in determinations of B_K.

Collab.	Ref.	N_f	L [fm]	$M_{\pi,\mathrm{min}}L$	Description
RBC/UKQCD 24	[56]	$2+1$	5.5, 5.4, 3.5, 2.6	3.9, 3.8, 4.1	Finite-volume effects are found to be negligible compared to other systematic effects and are thus omitted in the final error budget.

TABLE 96. Running and matching in determinations of B_K.

Collab.	Ref.	N_f	Renormalization	Running match.	Description
RBC/UKQCD 24	[56]	$2+1$	RI	PT1ℓ	Two different RI-SMOM schemes used to estimate a 1% systematic error owing to the perturbative matching to $\overline{\mathrm{MS}}$.

b. Kaon BSM B-parameters

TABLE 97. Continuum extrapolations/estimation of lattice artifacts in determinations of the BSM B_i parameters.

Collab.	Ref.	N_f	a [fm]	Description
RBC/UKQCD 24	[56]	$2+1$	0.114, 0.084, 0.073	Systematic uncertainties ranging from a minimum of 0.4% (for the case of B_2) to 1.9% (for the case of B_3).

TABLE 98. Chiral extrapolation/minimum pion mass in determinations of the BSM B_i parameters.

Collab.	Ref.	N_f	$M_{\pi,\mathrm{min}}$ [MeV]	Description
RBC/UKQCD 24	[56]	$2+1$	139, 139, 232	Chiral extrapolations based on SU(2)-χPT fits at NLO. Systematic uncertainties amount to less than half a percent.

TABLE 99. Finite-volume effects in determinations of the BSM B_i parameters.

Collab.	Ref.	N_f	L [fm]	$M_{\pi,\mathrm{min}}L$	Description
RBC/UKQCD 24	[56]	$2+1$	5.5, 5.4, 3.5 2.6	3.9, 3.8, 4.1	Finite-volume effects are at most at the 2 per-mille level. They are negligible compared to other systematic effects and are therefore omitted in the error budget.

TABLE 100. Running and matching in determinations of the BSM B_i parameters.

Collab.	Ref.	N_f	Renormalization	Running match.	Description
RBC/UKQCD 24	[56]	$2+1$	RI	PT1ℓ	Two different RI-SMOM schemes used to estimate the systematic error owing to the perturbative matching to $\overline{\mathrm{MS}}$; minimal value of about 0.7% for the case of B_2 and maximal of 2.4% for B_3.

c. $K \to \pi\pi$ decay amplitudes

TABLE 101. Continuum extrapolations/estimation of lattice artifacts in determinations of the $K \to \pi\pi$ decay amplitudes.

Collab.	Ref.	N_f	a [fm]	Description
RBC/UKQCD 23A	[415]	$2+1$	0.193	Single lattice spacing.

TABLE 102. Chiral extrapolation/minimum pion mass in determinations of the $K \to \pi\pi$ decay amplitudes.

Collab.	Ref.	N_f	$M_{\pi,\mathrm{min}}$ [MeV]	Description
RBC/UKQCD 23A	[415]	$2+1$	142.6	Single pion mass value, close to the physical point.

TABLE 103. Finite-volume effects in determinations of the $K \to \pi\pi$ decay amplitudes.

Collab.	Ref.	N_f	L [fm]	$M_{\pi,\mathrm{min}}L$	Description
RBC/UKQCD 23A	[415]	$2+1$	4.6	3.3	Finite-volume effects amount to a 7% systematic error contribution to the final error budget of A_0 and A_2.

TABLE 104. Running and matching in determinations of the $K \to \pi\pi$ decay amplitudes.

Collab.	Ref.	N_f	Renormalization	Running match.	Description
RBC/UKQCD 23A	[415]	$2+1$	RI	PT1ℓ	Two different RI-SMOM schemes are used. One of the two schemes is used for the final analysis. A systematic error ranging from 6% to 16%, depending on the considered case, is included based on the dispersion of other sets of intermediate scheme and scales. Systematic uncertainties arising from the computation of the Wilson coefficients in the $\overline{\text{MS}}$ scheme amount to 12%.

4. Notes to Sec. VII on D-meson decay constants and form factors

TABLE 105. Chiral extrapolation/minimum pion mass in $N_f = 2+1+1$ determinations of the D- and D_s-meson decay constants. For actions with multiple species of pions, masses quoted are the RMS pion masses. The different $M_{\pi,\text{min}}$ entries correspond to the different lattice spacings.

Collab.	Ref.	N_f	$M_{\pi,\text{min}}$ [MeV]	Description
ETM 13F ETM 14E ETM 21B	[43,356,458]	$2+1+1$	245, 239, 211 167, 137, 134	$f_{D_s}\sqrt{m_{D_s}}$ in ETM 13F and f_{D_s}/m_{D_s} in ETM 14E are extrapolated using both a quadratic and a linear fit in m_l plus $O(a^2)$ terms. In ETM 21B either w_0 or the $D_{(s)}$ meson mass are used as scaling variables in the chiral-continuum extrapolations.

TABLE 106. Chiral extrapolation/minimum pion mass in $N_f = 2+1$ determinations of the D- and D_s-meson decay constants. For actions with multiple species of pions, masses quoted are the RMS pion masses. The different $M_{\pi,\text{min}}$ entries correspond to the different lattice spacings.

Collab.	Ref.	N_f	$M_{\pi,\text{min}}$ [MeV]	Description
RQCD/ALPHA 24	[461]	$2+1$	335, 129, 155, 130, 175, 337	The dependence on light and strange quark masses is described using fit *Ansätze* inspired by NLO HMχPT.
ALPHA 23	[28]	$2+1$	277, 415, 200, 257	HMχPT expressions are used for the quantities $(8t_0)^{3/4} f_{D_{(s)}}\sqrt{m_{D_{(s)}}}$.

TABLE 107. Finite-volume effects in $N_f = 2+1+1$ determinations of the D- and D_s-meson decay constants. Each L-entry corresponds to a different lattice spacing, with multiple spatial volumes at some lattice spacings. For actions with multiple species of pions, the lightest masses are quoted.

Collab.	Ref.	N_f	L [fm]	$M_{\pi,\text{min}}L$	Description
ETM 13F ETM 14E ETM 21B	[43,356,458]	$2+1+1$	2.3/4.6, 2.6/5.2, 3.3/5.5	3.8, 3.6, 3.7	The comparison of two different volumes at the two largest lattice spacings indicates that FV effects are below the statistical errors. No explicit discussion of FSE in ETM 21B.

TABLE 108. Finite-volume effects in $N_f = 2 + 1$ determinations of the D- and D_s-meson decay constants. Each L-entry corresponds to a different lattice spacing, with multiple spatial volumes at some lattice spacings. For actions with multiple species of pions, the lightest masses are quoted.

Collab.	Ref.	N_f	L [fm]	$M_{\pi,\mathrm{min}}L$	Description
RQCD/ALPHA 24	[461]	$2+1$	2.34, 2.05/5.46, 2.4/4.8, 2.0/6.1, 2.4/4.8, 2.48	4, 3.6, 3.8, 4.05, 4.2, 4.2	By comparing different volumes (up to 5) at fixed pion mass, FSE are estimated to be negligible once the cut $m_\pi L \geq 3.5$ or $L \geq 2.3$ fm is imposed.
ALPHA 23	[28]	$2+1$	2.7, 2.4, 3.1/4.1, 2.4/3.1	3.9, 5.1, 4.2, 4.1	No explicit discussion of FSE.

TABLE 109. Lattice spacings and description of actions used in $N_f = 2 + 1 + 1$ determinations of the D- and D_s-meson decay constants.

Collab.	Ref.	N_f	a [fm]	Continuum extrapolation	Scale setting
ETM 13F ETM 14E ETM 21B	[43,356,458]	$2+1+1$	0.095, 0.081, 0.069	Chiral and continuum extrapolations performed simultaneously by adding an $O(a^2)$ term to the chiral fits.	Relative scale set through w_0 or $M_{c's'}$, the mass of a fictitious meson made of valence quarks of mass $r_0 m_{s'} = 0.22$ and $r_0 m_{c'} = 2.4$. Absolute scale through f_π^{iso}.

TABLE 110. Lattice spacings and description of actions used in $N_f = 2 + 1$ determinations of the D- and D_s-meson decay constants.

Collab.	Ref.	N_f	a [fm]	Continuum extrapolation	Scale Setting
RQCD/ALPHA 24	[461]	$2+1$	0.098, 0.085, 0.075, 0.064, 0.049, 0.039	Terms up to a^4 (possibly with mass-dependent coefficients) are included in the chiral-continuum extrapolation.	t_0 is used as intermediate scale with the physical scale set by a combination of f_π and f_K in the isosymmetric limit.
ALPHA 23	[28]	$2+1$	0.085, 0.075, 0.064, 0.049	$\mathcal{O}(a^2)$ terms, with mass-dependent coefficients, are included in the chiral-continuum extrapolation.	t_0 is used as intermediate scale with the physical scale set by a combination of f_π and f_K in the isosymmetric limit.

TABLE 111. Operator renormalization in $N_f = 2 + 1 + 1$ determinations of the D- and D_s-meson decay constants.

Collab.	Ref.	N_f	Renormalization	Description
ETM 13F ETM 14E ETM 21B	[43,356,458]	$2+1+1$	⋯	The axial current is absolutely normalized.

TABLE 112. Operator renormalization in $N_f = 2 + 1$ determinations of the D- and D_s-meson decay constants.

Collab.	Ref.	N_f	Renormalization	Description
RQCD/ALPHA 24	[461]	$2+1$	SF	The axial current is nonperturbatively improved and renormalized.
ALPHA 23	[28]	$2+1$	⋯	The axial current is absolutely normalized.

TABLE 113. Heavy-quark treatment in $N_f = 2+1+1$ determinations of the D-and D_s-meson decay constants.

Collab.	Ref.	N_f	Action	Description
ETM 13F ETM 14E ETM 21B	[43,356,458]	$2+1+1$	tmWil	$0.15 \lesssim am_h \lesssim 0.28$.

TABLE 114. Heavy-quark treatment in $N_f = 2+1$ determinations of the D- and D_s-meson decay constants.

Collab.	Ref.	N_f	Action	Description
RQCD/ALPHA 24	[461]	$2+1$	npSW	$0.1 \leq am_h \leq 0.3$.
ALPHA 23	[28]	$2+1$	tmWil on npSW	$0.13 \leq am_h \leq 0.26$

a. Form factors for semileptonic decays of charmed hadrons

TABLE 115. Continuum extrapolations/estimation of lattice artifacts in $N_f = 2+1+1$ determinations of form factors for semileptonic decays of charmed hadrons. For HPQCD 22, see Table 141.

Collab.	Ref.	N_f	a [fm]	Continuum extrapolation	Scale setting
FNAL/MILC 22	[123]	$2+1+1$	0.12, 0.088, 0.057, 0.042	Combined chiral-continuum extrapolation using SU(2) heavy-meson rooted staggered chiral perturbation theory.	Scale setting using gradient flow w_0 with physical scale from f_π.
Meinel 21B	[503]	$2+1$	0.0828(3), 0.1106(3)	Combined chiral-continuum extrapolation as part of the expansion of form factor shape in powers of $w-1$. Systematics estimated by varying fit form.	Scale setting using Ω mass in Ref. [12].
HPQCD 21A	[65]	$2+1+1$	0.042, 0.06, 0.09, 0.12, 0.15	Modified z-expansion fit combining the continuum and chiral extrapolations and the momentum-transfer dependence. Discretization effects assumed dominated by the charm scale. Discretization errors on form factors between 0.4% and 1.2% as a function of the momentum transfer.	Scale setting from f_π via the flow quantity w_0[18,42,1121].
Zhang 21	[500]	$2+1$	0.080, 0.11	Continuum extrapolation combined with fit to q^2-dependence of form factors in a "modified" z-expansion. Systematics estimated from difference between extrapolated results and results at smallest lattice spacing, and difference between two current renormalization methods.	Set from Wilson-flow quantity w_0.
HPQCD 20	[493]	$2+1+1$	0.06, 0.09, 0.12, 0.15	Modified z-expansion fit combining the continuum and chiral extrapolations and the momentum-transfer dependence, and, for the heavy-HISQ spectator b quark, the dependence on $1/m_Q$. The analysis combines data with NRQCD b quarks and data with HISQ heavy quarks.	Scale setting from f_π via the flow quantity w_0[18,42,1121].

TABLE 116. Chiral extrapolation/minimum pion mass in determinations of form factors for semileptonic decays of charmed hadrons. For actions with multiple species of pions, masses quoted are the RMS pion masses for $N_f = 2+1$ and the Goldstone mode mass for $N_f = 2+1+1$. The different $M_{\pi,\mathrm{min}}$ entries correspond to the different lattice spacings. For HPQCD 22, see Table 142.

Collab.	Ref.	N_f	$M_{\pi,\mathrm{min}}$ [MeV]	Description
FNAL/MILC 22	[123]	$2+1+1$	135, 130, 134, 308	Combined chiral-continuum extrapolation using SU(2) heavy-meson rooted staggered chiral perturbation theory at NLO, including NNLO analytic terms.
Meinel 21B	[503]	$2+1$	303, 340	Combined chiral-continuum extrapolation as part of the expansion of form factor shape in powers of $w-1$. Systematic uncertainty estimated by repeating fit with added higher-order terms.
HPQCD 21A	[65]	$2+1+1$	315, 329, 129, 132, 131	Modified z-expansion fit combining the continuum and chiral extrapolations and the momentum-transfer dependence. Polynomial dependence on quark masses, supplemented by a pion chiral logarithm. Fit result compared with alternative approach based on cubic splines in q^2.
Zhang 21	[500]	$2+1$	300, 290	Dependence on pion mass neglected. No estimate of resulting systematic uncertainty.
HPQCD 20	[493]	$2+1+1$	329, 316, 132/305, 131/305	Modified z-expansion fit combining the continuum and chiral extrapolations and the momentum-transfer dependence, and, for the heavy-HISQ spectator b quark, the dependence on $1/m_Q$. The analysis combines data with NRQCD b quarks and data with HISQ heavy quarks.

TABLE 117. Finite-volume effects in determinations of form factors for semileptonic decays of charmed hadrons. Each L-entry corresponds to a different lattice spacing, with multiple spatial volumes at some lattice spacings. For actions with multiple species of pions, the lightest pion masses are quoted. For HPQCD 22, see Table 143.

Collab.	Ref.	N_f	L [fm]	$M_{\pi,\mathrm{min}}L$	Description
FNAL/MILC 22	[123]	$2+1+1$	5.76, 4.22/5.63, 2.74/3.65/5.47, 2.69	3.95, 3.72, 3.72, 4.20	Finite-volume effects removed by correction to chiral logs due to sums over discrete momenta; corrections are $\mathcal{O}(0.01)\%$ overall. Effect of frozen topological charge at finest lattice spacing also corrected using χPT and found to be $\lesssim 0.03\%$.
Meinel 21B	[503]	$2+1$	2.7, 2.7	4.1, 4.6	Finite-volume effects not quantified. Effects from unstable $\Lambda^*(1520)$ not quantified.
HPQCD 21A	[65]	$2+1+1$	2.73, 2.72, 2.81/5.62, 2.93/5.87, 2.45/4.89	$\gtrsim 3.7$	Finite-volume correction included in chiral fit, claimed to be a negligible effect. Effect of frozen topology in finest ensemble not discussed.
Zhang 21	[500]	$2+1+1$	2.6, 2.6	$\gtrsim 3.8$	No discussion of finite-volume effects.
HPQCD 20	[493]	$2+1+1$	2.72, 2.81, 2.93/5.87, 2.45/4.89	$\gtrsim 3.8$	Physical point ensemble at $a \simeq 0.15$ fm has $m_\pi L = 3.3$; the statement $m_\pi L \gtrsim 3.8$ applies to the other five ensembles.

TABLE 118. Operator renormalization in determinations of form factors for semileptonic decays of charmed hadrons. For HPQCD 22, see Table 144.

Collab.	Ref.	N_f	Renormalization	Description
FNAL/MILC 22	[123]	$2+1+1$	NPR	Nonperturbative renormalization by imposing the PCVC relation.
Meinel 21B	[503]	$2+1$	mNPR	Residual matching factors ρ computed at 1-loop for vector and axial-vector currents, but at tree-level only for tensor currents. A systematic uncertainty is assigned to $\rho_{T^{\mu\nu}}$ as the double of $\max(\lvert\rho_{A^\mu}-1\rvert, \lvert\rho_{V^\mu}-1\rvert)$.
HPQCD 21A	[65]	$2+1+1$	NP	Vector current normalized by imposing Ward identity at zero recoil.
Zhang 21	[500]	$2+1$	NP	Local vector current renormalized using ratio to conserved vector current. Axial current renormalized using ratio of off-shell quark matrix elements.
HPQCD 20	[493]	$2+1+1$	NP	Vector current normalized by imposing Ward identity at zero recoil.

TABLE 119. Heavy-quark treatment in determinations of form factors for semileptonic decays of charmed hadrons. For HPQCD 22, see Table 145.

Collab.	Ref.	N_f	Action	Description
FNAL/MILC 22	[123]	$2+1+1$	HISQ	Valence heavy-quark masses range from 0.9 to 2 times the physical charm mass, with $0.164 \le am_h \le 0.8935$
Meinel 21B	[503]	$2+1$	Columbia RHQ for both the b and c quarks.	Discretization errors discussed as part of combined chiral-continuum-w fit. Higher-order fit also includes $\mathcal{O}(\alpha_s a\lvert\mathbf{p}\rvert)$ terms to account for missing radiative corrections to $\mathcal{O}(a)$ improvement of the currents.
HPQCD 21A	[65]	$2+1+1$	HISQ	Bare charm-quark mass $0.194 \lesssim am_c \lesssim 0.8605$.
Zhang 21	[500]	$2+1+1$	SW	Bare charm-quark mass $0.235 \lesssim am_c \lesssim 0.485$. No $\mathcal{O}(a)$ improvement of currents.
HPQCD 20	[493]	$2+1+1$	Charm: HISQ Bottom (spectator): HISQ and NRQCD	Bare charm-quark HIQS mass $0.274 \lesssim am_c \lesssim 0.827$. Bare bottom-quark HIQS mass $0.274 \lesssim am_b \lesssim 0.8$.

5. Notes to Sec. VIII on B-meson decay constants, mixing parameters and form factors

a. $B_{(s)}$-meson decay constants

TABLE 120. Chiral extrapolation/minimum pion mass in determinations of the B- and B_s-meson decay constants for $N_f = 2+1+1$ simulations. The different $M_{\pi,\mathrm{min}}$ entries correspond to the different lattice spacings.

Collab.	Ref.	N_f	$M_{\pi,\mathrm{min}}$ [MeV]	Description
Frezzotti 24	[532]	$2+1+1$	175, 140, 137, 141	One light-quark mass per lattice spacing. Chiral effects expected to be subdominant compared to other effects.

TABLE 121. Chiral extrapolation/minimum pion mass in determinations of the B- and B_s-meson decay constants for $N_f = 2+1$ simulations. The different $M_{\pi,\mathrm{min}}$ entries correspond to the different lattice spacings.

Collab.	Ref.	N_f	$M_{\pi,\mathrm{min}}$ [MeV]	Description
QCDSF/UKQCD/CSSM 22	[548]	$2+1$	280, 155, 226, 290	Between one and three light-quark masses per lattice spacing. Generic fits to $(M_\pi^2/X_\pi^2 - 1)^2$ and $a^2(M_\pi^2/X_\pi^2 - 1)$ in the combined chiral-continuum extrapolation, with systematic errors estimated to be from 1.3% in f_{B_s}/f_B.
RBC/UKQCD 22	[550]	$2+1$	340, 302, 267, 371	Between one and three light-quark masses per lattice spacing. Combined chiral-continuum extrapolation using NLO SU(2) heavy-meson χPT. No explicit estimate of systematic errors.

TABLE 122. Finite-volume effects in determinations of the B- and B_s-meson decay constants for $N_f = 2+1+1$ simulations. Each L-entry corresponds to a different lattice spacing.

Collab.	Ref.	N_f	L [fm]	$M_{\pi,\mathrm{min}}L$	Description
Frezzotti 24	[532]	$2+1+1$	4.36, 5.09, 5.46, 5.46	3.9, 3.6, 3.8, 3.9	Finite-volume effects estimated to be subdominant to other sources of uncertainty, based in part on calculations in a larger ensemble in [467]

TABLE 123. Finite-volume effects in determinations of the B- and B_s-meson decay constants for $N_f = 2+1$ simulations. Each L-entry corresponds to a different lattice spacing, with multiple spatial volumes at some lattice spacings.

Collab.	Ref.	N_f	L [fm]	$M_{\pi,\mathrm{min}}L$	Description
QCDSF/UKQCD/CSSM 22	[548]	$2+1$	2.62, 2.36/3.55, 3.26/4.35, 2.83	3.86, 3.10/4.07, 4.37/3.42, 4.03	Final result for f_{B_s}/f_B includes fits to ensembles with $M_\pi L > 4$. No explicit estimate of FV effects.
RBC/UKQCD 22	[550]	$2+1$	2.65, 2.65, 3.40, 2.00	4.57, 4.06, 4.60, 3.77	No explicit estimate of FV effects.

TABLE 124. Continuum extrapolations/estimation of lattice artifacts in determinations of the B- and B_s-meson decay constants for $N_f = 2+1+1$ simulations.

Collab.	Ref.	N_f	a [fm]	Continuum extrapolation	Scale setting
Frezzotti 24	[532]	$2+1+1$	0.091, 0.080, 0.068, 0.057	Continuum extrapolation linear in a^2.	Scale set by w_0, with details described in Ref. [7].

TABLE 125. Continuum extrapolations/estimation of lattice artifacts in determinations of the B and B_s meson decay constants for $N_f = 2+1$ simulations.

Collab.	Ref.	N_f	a [fm]	Continuum extrapolation	Scale setting
QCDSF/UKQCD/CSSM 22	[548]	$2+1$	0.082, 0.074, 0.068, 0.059	Combined continuum and chiral extrapolation omits the term linear in a^2. Systematic errors associated with discretization effects subdominant in f_{B_s}/f_B.	Scale setting procedure and scale uncertainty are not discussed.
RBC/UKQCD 22	[550]	$2+1$	0.11, 0.083, 0.071, 0.063	Combined continuum and chiral extrapolation includes term linear in a^2. No estimate of systematic errors associated with discretization effects.	Scale setting procedure and scale uncertainty are not discussed.

TABLE 126. Description of the renormalization/matching procedure adopted in the determinations of the B- and B_s-meson decay constants for $N_f = 2+1+1$ simulations.

Collab.	Ref.	N_f	Renormalization	Description
Frezzotti 24	[532]	$2+1+1$	⋯	Nonperturbative operator renormalization provided by ETMC by private communication and unpublished at the time of this review.

TABLE 127. Description of the renormalization/matching procedure adopted in the determinations of the B- and B_s-meson decay constants for $N_f = 2+1$ simulations.

Collab.	Ref.	N_f	Renormalization	Description
QCDSF/UKQCD/CSSM 22	[548]	$2+1$	mNPR	Operator renormalization is calculated partially nonperturbatively as $Z_{B_q} = \rho_A^{bq}\sqrt{Z_V^{bb}Z_V^{qq}}$, with perturbative contribution neglected, $\rho_A^{bq} = 1$.
RBC/UKQCD 22	[550]	$2+1$	mNPR	Operator renormalization is calculated partially nonperturbatively as $Z_{B_q} = \rho_A^{bq}\sqrt{Z_V^{bb}Z_V^{qq}}$.

TABLE 128. Heavy-quark treatment in determinations of the B- and B_s-meson decay constants for $N_f = 2+1+1$ simulations.

Collab.	Ref.	N_f	Action	Description
Frezzotti 24	[532]	$2+1+1$	tmWil	Heavy-strange meson extrapolated to physical B_s mass using HQET scaling linear in B/m_{H_s}, with contributions from QCD-HQET current matching and HQET axial current anomalous dimension at 1-loop.

TABLE 129. Heavy-quark treatment in $N_f = 2+1$ determinations of the B-and B_s-meson decay constants.

Collab.	Ref.	N_f	Action	Description
QCDSF/UKQCD/CSSM 22	[548]	$2+1$	RHQ	HQ tuning effects are estimated to be 0.06% in f_{B_s}/f_B. HQ discretization effects not explicitly estimated, although the continuum-limit fits do not indicate a strong a^2 dependence.
RBC/UKQCD 22	[550]	$2+1$	RHQ	HQ tuning and discretization effects not explicitly estimated. HQ tuning of new finest ensemble ongoing.

b. $B_{(s)}$-meson mixing matrix elements

TABLE 130. Continuum extrapolations/estimation of lattice artifacts in determinations of the neutral B-meson mixing matrix elements for $N_f = 2+1+1$ simulations.

Collab.	Ref.	N_f	a [fm]	Continuum extrapolation	Scale setting
HPQCD 19A	[77]	$2+1+1$	0.15, 0.12, 0.09	Discretization errors start from $\alpha_s a^2$ and are included in the systematic error. It is estimated as 1.8% for individual bag parameters. Residual $\alpha_s a^2$ and a^4 errors from wrong-spin contributions are subtracted by including them in the chiral fit.	Scale setting done using Υ and Υ' mass splitting [1083].

TABLE 131. Continuum extrapolations/estimation of lattice artifacts in determinations of the neutral B-meson mixing matrix elements for $N_f = 2+1$ simulations.

Collab.	Ref.	N_f	a [fm]	Continuum extrapolation	Scale setting
RBC/UKQCD 18A	[76]	$2+1$	0.11, 0.08, 0.07	Combined continuum (a^2) and heavy quark ($1/m_H$) extrapolation with the LO pion mass dependence (m_π^2) in the global fit.	Lattice scale and target quark masses are set using Ω, K and π masses [12,61,119].

TABLE 132. Chiral extrapolation/minimum pion mass in determinations of the neutral B-meson mixing matrix elements. For actions with multiple species of pions, masses quoted are the RMS pion masses (where available). The different $M_{\pi,\mathrm{min}}$ entries correspond to the different lattice spacings.

Collab.	Ref.	N_f	$M_{\pi,\mathrm{min}}$ [MeV]	Description
HPQCD 19A	[77]	$2+1+1$	311, 241, –	Pion mass in the Goldstone channel is as small as 130 MeV for two coarser lattices. NLO HMrSχPT is used with NNLO analytic terms and other discretization errors. Staggered wrong-spin contributions are included.
RBC/UKQCD 18A	[76]	$2+1$	139, 139, 234	Combined continuum (a^2) and heavy quark ($1/m_H$) extrapolation with the LO pion mass dependence (m_π^2) in the global fit.

TABLE 133. Finite-volume effects in determinations of the neutral B-meson mixing matrix elements. Each L-entry corresponds to a different lattice spacing, with multiple spatial volumes at some lattice spacings. For actions with multiple species of pions, masses quoted are the RMS pion masses (where available).

Collab.	Ref.	N_f	L [fm]	$M_{\pi,\mathrm{min}}L$	Description
HPQCD 19A	[77]	$2+1+1$	2.4/3.5/4.6, 2.9/3.8/5.7, 2.8	7.3, 7.0, –	FV error is estimated to be negligible from FV HMχPT.
RBC/UKQCD 18A	[76]	$2+1$	2.7/5.5, 2.6/5.3, 3.5	3.9, 3.8, 4.0	FV error is estimated to be less than 0.18% for SU(3)-breaking ratios from FV HMχPT.

TABLE 134. Operator renormalization in determinations of the neutral B-meson mixing matrix elements.

Collab.	Ref.	N_f	Renormalization	Description
HPQCD 19A	[77]	$2+1+1$	PT1ℓ	HISQ-NRQCD 4-quark operators are matched through $O(1/M)$ and renormalized to 1-loop: included are those of $O(\alpha_s)$, $O(\Lambda_{\rm QCD}/M)$, $O(\alpha_s/aM)$, $O(\alpha_s\Lambda_{\rm QCD}/M)$. Remnant error is dominated by $O(\alpha_s\Lambda_{\rm QCD}/M)$ 2.9% and $O(\alpha_s^2)$ 2.1% for individual bag parameters. Associated error for their SU(3) breaking ratio are negligible.
RBC/UKQCD 18A	[76]	$2+1$	$\cdots$	Operators are renormalized multiplicatively due to chiral symmetry of DWF. No need to calculate the renormalization factor since only the SU(3) breaking ratios are examined.

TABLE 135. Heavy-quark treatment in determinations of the neutral B-meson mixing matrix elements.

Collab.	Ref.	N_f	Action	Description
HPQCD 19A	[77]	$2+1+1$	NRQCD	See the entry in Table 134.
RBC/UKQCD 18A	[76]	$2+1$	DWF	Domain-wall fermion with 3 stout-smearing extends the reach to heavy mass, allowing to simulate up to half of the b-quark mass. Heavy mass errors on ξ are estimated as 0.8% from fitting range and 0.4% from higher order $(1/M^2)$ by power counting.

c. Form factors entering determinations of $|V_{ub}|$ ($B \to \pi\ell\nu$, $B_s \to K\ell\nu$, $\Lambda_b \to p\ell\bar{\nu}$)

TABLE 136. Continuum extrapolations/estimation of lattice artifacts in determinations of $B \to \pi\ell\nu$, $B_s \to K\ell\nu$, and $\Lambda_b \to p\ell\bar{\nu}$ form factors.

Collab.	Ref.	N_f	a [fm]	Continuum extrapolation	Scale setting
RBC/UKQCD 23	[128]	$2+1$	0.071, 0.083, 0.11	Joint chiral-continuum extrapolation using SU(2) hard-pion HMχPT. Systematic uncertainty estimated by varying fit *Ansatz* and form of coefficients, as well as implementing different cuts on data.	Scale implicitly set in the light-quark sector using the Ω^- mass, cf. [12,61,76].
JLQCD 22	[126]	$2+1$	0.044, 0.055, 0.080	Discretization effects treated using overall factors of $(1 + C_{a^2}(\Lambda_{\rm QCD}a)^2 + C_{(am_Q)^2}(am_Q)^2)$, with independent coefficients for the two form factors. Systematic uncertainties estimated by adding $C_{a^4}(\Lambda_{\rm QCD}a)^4$ or $C_{(am_Q)^4}(am_Q)^4)$ terms.	Relative scale set using gradient-flow time $t_0^{1/2}/a$. Absolute scale $t_0^{1/2}$ taken from Ref. [115].
FNAL/MILC 19	[592]	$2+1$	0.06, 0.09, 0.12	HMrSχPT expansion used at next-to-leading order in SU(2) and leading order in $1/M_B$, including next-to-next-to-leading-order (NNLO) analytic and generic discretization terms. Hard kaons assumed to decouple. Systematic uncertainties estimated by varying fit *Ansatz* and data range. The (stat + chiral extrap + HQ discretization + g_π) uncertainty dominates the error budget, ranging from 2%–3% at $q^2 \gtrsim 21$ GeV^2 to up to 8%–10% in the lower end of the accessed q^2 interval.	Relative scale r_1/a set from the static-quark potential. Absolute scale r_1, including related uncertainty estimates, taken from [60].

TABLE 137. Chiral extrapolation/minimum pion mass in determinations of $B \to \pi\ell\nu$, $B_s \to K\ell\nu$, and $\Lambda_b \to p\ell\bar{\nu}$ form factors. For actions with multiple species of pions, masses quoted are the RMS pion masses. The different $M_{\pi,\mathrm{min}}$ entries correspond to the different lattice spacings.

Collab.	Ref.	N_f	$M_{\pi,\mathrm{min}}$ [MeV]	Description
RBC/UKQCD 23	[128]	$2+1$	268, 301, 340	Joint chiral-continuum extrapolation using SU(2) hard-pion HMχPT. Systematic uncertainty estimated by varying fit *Ansatz* and form of coefficients, as well as implementing different cuts on data.
JLQCD 22	[126]	$2+1$	300, 300, 230	Chiral extrapolation uses SU(2) hard-pion heavy-meson chiral perturbation theory at next-to-leading order. Systematic uncertainty estimated by adding M_π^4 terms or by making the coefficients of the chiral logs fit parameters.
FNAL/MILC 19	[592]	$2+1$	255, 277, 456	HMrSχPT expansion used at next-to-leading order in SU(2) and leading order in $1/M_B$, including next-to-next-to-leading-order (NNLO) analytic and generic discretization terms. Hard kaons assumed to decouple. Systematic uncertainties estimated by varying fit *Ansatz* and data range.

TABLE 138. Finite-volume effects in determinations of $B \to \pi\ell\nu$, $B_s \to K\ell\nu$, and $\Lambda_b \to p\ell\bar{\nu}$ form factors. Each L-entry corresponds to a different lattice spacing, with multiple spatial volumes at some lattice spacings. For actions with multiple species of pions, the lightest masses are quoted.

Collab.	Ref.	N_f	L [fm]	$M_{\pi,\mathrm{min}}L$	Description
RBC/UKQCD 23	[128]	$2+1$	3.4, 2.7, 2.6	4.6, 4.0, 4.4	Finite-volume effects removed by correction to chiral logs due to sums over discrete momenta; quoted maximum corrections are 0.13% for f_+ and 0.06% for f_0.
JLQCD 22	[126]	$2+1$	2.6, 3.9	$\gtrsim$4.0	Finite-volume effects in form factors deemed negligible. Bias in pion mass due to topology freezing at finest lattice spacing estimated to be $\sim$0.1%.
FNAL/MILC 19	[592]	$2+1$	3.8, 2.5/2.9/3.6/5.8, 2.9	$\gtrsim$3.8	Finite-volume effects estimated by comparing infinite volume integrals with finite sums in HMrSχPT, found to be negligible.

TABLE 139. Operator renormalization in determinations of $B \to \pi\ell\nu$, $B_s \to K\ell\nu$, and $\Lambda_b \to p\ell\bar{\nu}$ form factors.

Collab.	Ref.	N_f	Renormalization	Description
RBC/UKQCD 23	[128]	$2+1$	mNPR	Perturbative truncation error estimated as full size of $O(\alpha_s)$ correction at the 0.083 fm lattice spacing.
JLQCD 22	[126]	$2+1$	NPR	$Z_{V_{qq}}$ obtained using position-space current-current correlators. For heavier quark masses, $\sqrt{Z_{V_{QQ}}Z_{V_{qq}}}$ is used, where $Z_{V_{QQ}}$ is the renormalization factor of the flavor-conserving temporal vector current, determined using charge conservation.
FNAL/MILC 19	[592]	$2+1$	mNPR	Perturbative truncation error estimated at 1% with size of 1-loop correction on next-to-finest ensemble.

TABLE 140. Heavy-quark treatment in determinations of $B \to \pi\ell\nu$, $B_s \to K\ell\nu$, and $\Lambda_b \to p\ell\bar{\nu}$ form factors.

Collab.	Ref.	N_f	Action	Description
RBC/UKQCD 23	[128]	$2+1$	Columbia RHQ	Heavy-quark discretization errors estimated by power counting.
JLQCD 22	[126]	$2+1$	DWF	Bare heavy-quark masses satisfy $am_Q < 0.7$ and reach from the charm mass up to 2.44 times the charm mass. Form factors extrapolated linearly in $1/m_Q$ to the bottom mass.
FNAL/MILC 19	[592]	$2+1$	Fermilab	(See comments for continuum limit extrapolation.)

d. Form factors for rare decays of beauty hadrons

TABLE 141. Continuum extrapolations/estimation of lattice artifacts in determinations of form factors for rare decays of beauty hadrons.

Collab.	Ref.	N_f	a [fm]	Continuum extrapolation	Scale setting
HPQCD 22	[492]	$2+1+1$	0.15, 0.12, 0.090, 0.088, 0.059, 0.044	Combined extrapolation in lattice spacing, light-quark mass, strange-quark mass, heavy-quark mass, and momentum transfer using modified z expansion. Stability tested by varying fit form, changing prior widths, and removing data subsets.	Scale setting using gradient flow w_0 with physical scale from f_π.
Meinel 20, Meinel 21B	[503,670]	$2+1$	0.0828(3), 0.1106(3)	Combined chiral-continuum extrapolation as part of the expansion of form factor shape in powers of $w-1$. Systematic uncertainty estimated by repeating fit with added higher-order terms.	Scale setting using Ω mass in Ref. [12].

TABLE 142. Chiral extrapolation/minimum pion mass in determinations of form factors for rare decays of beauty hadrons. For actions with multiple species of pions, masses quoted are the RMS pion masses for $N_f = 2+1$ and the Goldstone mode mass for $N_f = 2+1+1$. The different $M_{\pi,\mathrm{min}}$ entries correspond to the different lattice spacings.

Collab.	Ref.	N_f	$M_{\pi,\mathrm{min}}$ [MeV]	Description
HPQCD 22	[492]	$2+1+1$	131, 132, 313, 128, 325, 308	Combined extrapolation in lattice spacing, light-quark mass, strange-quark mass, heavy-quark mass, and momentum transfer using modified z expansion. Logarithms from hard-pion χPT included. Stability tested by varying fit form, changing prior widths, and removing data subsets.
Meinel 20, Meinel 21B	[503,670]	$2+1$	303, 340	Combined chiral-continuum extrapolation as part of the expansion of form factor shape in powers of $w-1$. Systematic uncertainty estimated by repeating fit with added higher-order terms.

TABLE 143. Finite-volume effects in determinations of form factors for rare decays of beauty hadrons. Each L-entry corresponds to a different lattice spacing, with multiple spatial volumes at some lattice spacings. For actions with multiple species of pions, masses quoted are the RMS pion masses for $N_f = 2+1$ and the Goldstone mode mass for $N_f = 2+1+1$.

Collab.	Ref.	N_f	L [fm]	$M_{\pi,\mathrm{min}}L$	Description
HPQCD 22	[492]	$2+1+1$	2.4/4.8, 2.88/5.76, 2.88, 5.63, 2.83, 2.82	3.19, 3.86, 4.57, 3.66, 4.67, 4.41	Finite-volume effects included in fit by replacing infinite-volume chiral logs with sums over discrete momenta.
Meinel 20, Meinel 21B	[503,670]	$2+1$	2.7, 2.7	4.1, 4.6	Finite-volume effects not quantified. Effects from unstable $\Lambda^*(1520)$ not quantified.

TABLE 144. Operator renormalization in determinations of form factors for rare decays of beauty hadrons.

Collab.	Ref.	N_f	Renormalization	Description
HPQCD 22	[492]	$2+1+1$	NPR	Z_V and Z_A obtained from Ward identities. Z_T determined using RI-SMOM.
Meinel 20, Meinel 21B	[503,670]	$2+1$	mNPR	Residual matching factors ρ computed at 1-loop for vector and axial-vector currents, but at tree-level only for tensor currents. A systematic uncertainty is assigned to $\rho_{T^{\mu\nu}}$ as the double of $\max(\lvert\rho_{A^\mu}-1\rvert, \lvert\rho_{V^\mu}-1\rvert)$.

TABLE 145. Heavy-quark treatment in determinations of form factors for rare decays of beauty hadrons.

Collab.	Ref.	N_f	Action	Description
HPQCD 22	[492]	$2+1+1$	HISQ	Extrapolation to the physical b-quark mass using terms with powers and logarithms of the inverse heavy-meson mass in the modified z-expansion fit. Heavy-quark masses in lattice units satisfy $am_h \leq 0.9$. The heavy-light pseudoscalar meson mass reaches $\approx 0.94\, M_{B,\mathrm{phys}}$.
Meinel 20, Meinel 21B	[503,670]	$2+1$	Columbia RHQ	Discretization errors discussed as part of combined chiral-continuum-w fit. Higher-order fit also includes $\mathcal{O}(\alpha_s a\lvert\mathbf{p}\rvert)$ terms to account for missing radiative corrections to $\mathcal{O}(a)$ improvement of the currents.

e. Form factors entering determinations of $|V_{cb}|$ ($B_{(s)} \to D_{(s)}^{(*)}\ell\nu$, $\Lambda_b \to \Lambda_c^{(*)}\ell\bar{\nu}$) and $R(D_{(s)})$

TABLE 146. Continuum extrapolations/estimation of lattice artifacts in $N_f = 2+1$ determinations of $B_{(s)} \to D_{(s)}^{(*)}\ell\nu$ and $\Lambda_b \to \Lambda_c^{(*)}\ell\bar{\nu}$ form factors, and of $R(D_{(s)})$.

Collab.	Ref.	N_f	a [fm]	Continuum extrapolation	Scale setting
HPQCD 23	[135]	$2+1+1$	0.044, 0.058, 0.088	Combined chiral-continuum and heavy-quark extrapolations using HMrSχPT. The recoil dependence in powers of $(w-1)$ is fitted using BGL-inspired coefficients. Zero-recoil uncertainty negligible compared to other sources of error.	Scale setting from Wilson flow, fixing the slope $t\frac{d}{dt}\{t^2\langle E(t)\rangle\}|_{t=w_0^2} = 0.3$, with w_0 taken from [42]. Uncertainty related to scale setting estimated at ≈0.5%.
JLQCD 23	[137]	$2+1$	0.044, 0.055, 0.080	Combined chiral-continuum and heavy-quark extrapolations using HMχPT. Each form factor is extrapolated separately. Zero-recoil uncertainty estimated at ≈0.9%.	Scale setting from Wilson flow, fixing the slope $t\frac{d}{dt}\{t^2\langle E(t)\rangle\}|_{t=w_0^2} = 0.3$, with w_0 taken from [115]. Uncertainty related to scale setting estimated at ≈1.7%.
FNAL/MILC 21	[136]	$2+1$	0.045, 0.06, 0.09, 0.12, 0.15	Combined chiral-continuum extrapolation using HMrSχPT. Total uncertainty quoted at 0.7%.	Relative scale r_1/a set from the static-quark potential. Absolute scale r_1, including related uncertainty estimates, taken from [60]. Uncertainty related to scale setting estimated at less than 0.1%.
Meinel 21, Meinel 21B	[503,659]	$2+1$	0.0828(3), 0.1106(3)	Combined chiral-continuum extrapolation as part of the expansion of form factor shape in powers of $w-1$. Systematics estimated by varying fit form.	Scale setting using Ω mass in Ref. [12].

TABLE 147. Chiral extrapolation/minimum pion mass in $N_f = 2+1$ determinations of $B_{(s)} \to D_{(s)}^{(*)}\ell\nu$ and $\Lambda_b \to \Lambda_c^{(*)}\ell\bar{\nu}$ form factors, and of $R(D_{(s)})$. For actions with multiple species of pions, masses quoted are the RMS pion masses for $N_f = 2+1$ and the Goldstone mode mass for $N_f = 2+1+1$. The different $M_{\pi,\mathrm{min}}$ entries correspond to the different lattice spacings.

Collab.	Ref.	N_f	$M_{\pi,\mathrm{min}}$ [MeV]	Description
HPQCD 23	[135]	$2+1+1$	315, 135, 129	Combined chiral-continuum and heavy-quark extrapolations using HMrSχPT. The recoil dependence in powers of $(w-1)$ is fitted using BGL-inspired coefficients. Zero-recoil uncertainty negligible compared to other sources of error.
JLQCD 23	[137]	$2+1$	284, 300, 226	Combined chiral-continuum and heavy-quark extrapolations using HMχPT. Each form factor is extrapolated separately. Zero-recoil uncertainty estimated at $\approx$0.9%.
FNAL/MILC 21	[136]	$2+1$	320, 220, 180, 270, 340	Combined chiral-continuum extrapolation using HMrSχPT. Systematic errors estimated by adding higher-order analytic terms and varying the $D^* - D - \pi$ coupling. Total uncertainty quoted at 0.7%.
Meinel 21, Meinel 21B	[503,659]	$2+1$	303, 340	Combined chiral-continuum extrapolation as part of the expansion of form factor shape in powers of $w-1$. Systematic uncertainty estimated by repeating fit with added higher-order terms.

TABLE 148. Finite-volume effects in determinations of $B_{(s)} \to D_{(s)}^{(*)}\ell\nu$ and $\Lambda_b \to \Lambda_c^{(*)}\ell\bar{\nu}$ form factors, and of $R(D_{(s)})$. Each L-entry corresponds to a different lattice spacing, with multiple spatial volumes at some lattice spacings. For actions with multiple species of pions, the lightest pion masses are quoted.

Collab.	Ref.	N_f	L [fm]	$M_{\pi,\mathrm{min}}L$	Description
HPQCD 23	[135]	$2+1+1$	2.8, 2.8–5.5, 2.8–5.6	4.5, 3.7, 3.7	Finite-volume effects expected to be negligible, including the effect of frozen topology in the finest ensemble, according to [123].
JLQCD 23	[137]	$2+1$	2.8, 2.6, 2.6–3.9	4.0, 4.0, 4.4	Study effects of topology freezing and compare ensembles with similar parameters but different volumes.
FNAL/MILC 21	[136]	$2+1$	4.6, 4.3–6.3, 4.1–5.8, 3.8–6.2, 3.9	$\gtrsim$3.8	Finite-volume error estimated to be negligible at zero recoil using HMrSχPT. Given the values $m_\pi L \gtrsim 3.7$ and the smallness of the chiral logs, expectations are that finite-volume errors remain negligible in the whole recoil range.
Meinel 21, Meinel 21B	[503,659]	$2+1$	2.7, 2.7	4.1, 4.6	Finite-volume effects not quantified. Effects from unstable Λ_c^* not quantified.

TABLE 149. Operator renormalization in determinations of $B_{(s)} \to D_{(s)}^{(*)}\ell\nu$ and $\Lambda_b \to \Lambda_c^{(*)}\ell\bar{\nu}$ form factors, and of $R(D_{(s)})$.

Collab.	Ref.	N_f	Renormalization	Description
HPQCD 23	[135]	$2+1+1$	NPR	Vector (axial) currents renormalized nonperturbatively using the PCVC (PCAC) relation.
JLQCD 23	[137]	$2+1$	mNPR	Majority of current renormalization factor cancels in ratio of lattice correlation functions. Remaining correction expected to behave better than $O(a)$, and vanishes in the continuum limit.
FNAL/MILC 21	[136]	$2+1$	mNPR	Majority of current renormalization factor cancels in double ratio of lattice correlation functions. Remaining correction calculated with 1-loop tadpole-improved lattice perturbation theory. Systematic uncertainty estimated at 0.1%.
Meinel 21, Meinel 21B	[503,659]	$2+1$	mNPR	Residual matching factors ρ computed at 1-loop for vector and axial-vector currents, but at tree-level only for tensor currents. A systematic uncertainty is assigned to $\rho_{T^{\mu\nu}}$ as the double of $\max(\lvert\rho_{A^\mu}-1\rvert, \lvert\rho_{V^\mu}-1\rvert)$.

TABLE 150. Heavy-quark treatment in determinations of $B_{(s)} \to D_{(s)}^{(*)}\ell\nu$ and $\Lambda_b \to \Lambda_c^{(*)}\ell\bar{\nu}$ form factors, and of $R(D_{(s)})$.

Collab.	Ref.	N_f	Action	Description
HPQCD 23	[135]	$2+1+1$	HISQ for both the b and c quarks.	Values of bare heavy-quark masses up to $am_h = 0.8$. The error from continuum limit and extrapolation to physical b mass at zero recoil is quite small, but it becomes dominant at mid-recoil.
JLQCD 23	[137]	$2+1$	Möbius domain-wall for both the b and c quarks.	Values of bare heavy-quark masses up to $am_h = 0.69$. The systematics associated to the extrapolation to physical b mass stays under 4% for all form factors in the whole recoil range.
FNAL/MILC 21	[136]	$2+1$	Fermilab RHQ for both the b and c quarks.	Discretization errors discussed as part of combined chiral-continuum stemming from $\alpha_s a$, a^2 and a^3 terms.
Meinel 21, Meinel 21B	[503,659]	$2+1$	Columbia RHQ for both the b and c quarks.	Discretization errors discussed as part of combined chiral-continuum-w fit. Higher-order fit also includes $\mathcal{O}(\alpha_s a\lvert\mathbf{p}\rvert)$ terms to account for missing radiative corrections to $\mathcal{O}(a)$ improvement of the currents.

6. Notes to Sec. IX on the strong coupling α_s

a. Renormalization scale and perturbative behavior

TABLE 151. Renormalization scale and perturbative behavior of α_s determinations for $N_f = 0$.

Collab.	Ref.	N_f	$\alpha_{\rm eff}$	n_l	Description
Hasenfratz 23	[705]	0	$0.095 < \alpha_{\rm eff} < 1.26$	2	GF scheme does not reach perturbative asymptotics.
Wong 23	[706]	0	$0.095 < \alpha_{\rm eff} < 1.26$	2	GF scheme does not reach perturbative asymptotics.
Brambilla 23	[197]	0	$0.27 < \alpha_{\rm eff} < 0.36$	3	Static force using operator insertion.
Chimirri 23	[707]	0	$0.17 < \alpha_{\overline{\rm MS}} < 0.25$	2	Values for α read off from figure.
Bribian 21	[704]	0	SF: 0.07–0.19 TGF: 0.05–0.92	2	Step scaling with TGF, nonpert. matching to SF.

TABLE 152. Renormalization scale and perturbative behavior of α_s determinations for $N_f = 3$.

Collab.	Ref.	N_f	$\alpha_{\rm eff}$	n_l	Description
ALPHA 22	[80]	$2+1$, 0	0.08–0.95	2	Decoupling $N_f = 3 \to N_f = 0$; uses $N_f = 0$ step-scaling from Dalla Brida 19 [763].

b. Continuum limit

TABLE 153. Continuum limit for α_s determinations with $N_f = 0$.

Collab.	Ref.	N_f	$a\mu$	Description
Hasenfratz 23	[705]	0	$0.158 < a/\sqrt{8t} < 0.29$	GF scheme, infinite-volume extrapolation, direct determination of the β-function.
Wong 23	[706]	0	$0.16 < a/\sqrt{8t} < 0.28$	GF scheme, infinite-volume extrapolation, direct determination of the β-function.
Brambilla 23	[197]	0	$0.23 < a\mu < 0.49$	Force between static quarks using operator insertion.
Chimirri 23	[707]	0	$0.8m_c < \mu < 3.5m_c$	Lattice spacings a in the range 0.01–0.07 fm; Scale defined by $\mu = s \times \bar{m}_{\overline{\rm MS},c}(\mu)$.
Bribian 21	[704]	0	TGF: $0.041 < a\mu < 0.083$ SF: $0.063 < a\mu < 0.17$	Step scaling TGF scheme, nonpert. matching to SF scheme.

TABLE 154. Continuum limit for α_s determinations with $N_f = 3$.

Collab.	Ref.	N_f	$a\mu$	Description
ALPHA 22	[80]	$2+1$, 0	$0.021 < a\mu_{\rm dec} < 0.083$	Decoupling $N_f = 3 \to N_f = 0$; continuum limit subject to cutoff $aM < 0.4$, $z = M/\mu_{\rm dec} = 4 - 12$.

7. Notes to Sec. X on nucleon matrix elements

TABLE 155. Continuum extrapolations/estimation of lattice artifacts in determinations of the isovector axial, scalar and tensor charges with $N_f = 2 + 1 + 1$ quark flavors.

Collab.	Ref.	N_f	a [fm]	Description
ETM 23	[91]	$2 + 1 + 1$	0.057, 0.069, 0.080	Extrapolation via a fit which is linear in a^2.
PNDME 23	[90]	$2 + 1 + 1$	0.06, 0.09, 0.12, 0.15	Physical-point extrapolations performed simultaneously, keeping only the leading-order terms in the various expansion parameters.
ETM 22	[98]	$2 + 1 + 1$	0.057, 0.069, 0.080	Extrapolation via a fit which is linear in a^2.

TABLE 156. Continuum extrapolations/estimation of lattice artifacts in determinations of the isovector axial, scalar and tensor charges with $N_f = 2 + 1$ quark flavors.

Collab.	Ref.	N_f	a [fm]	Description
Mainz 24	[96]	$2 + 1$	0.049, 0.064, 0.076, 0.086	Extrapolation performed as part of a simultaneous fit in a, M_π and $M_\pi L$.
PACS 23	[855]	$2 + 1$	0.063, 0.085	Discretization effects estimated by difference between two ensembles.
RQCD 23	[95]	$2 + 1$	0.039, 0.049, 0.064, 0.076, 0.086, 0.098	Extrapolation performed using terms up to a^2 in the lattice spacing.
QCDSF/ UKQCD/ CSSM 23	[94]	$2 + 1$	0.052, 0.059, 0.068, 0.074, 0.082	Extrapolation performed including leading discretization effects.
PACS 22B	[990]	$2 + 1$	0.085	Single lattice spacing.
Mainz 22	[854]	$2 + 1$	0.049, 0.064, 0.076, 0.086	Extrapolation performed as part of a simultaneous fit in a, M_π and $M_\pi L$.

TABLE 157. Chiral extrapolation/minimum pion mass in determinations of the isovector axial, scalar and tensor charges with $N_f = 2 + 1 + 1$ quark flavors.

Collab.	Ref.	N_f	$M_{\pi,\mathrm{min}}$ [MeV]	Description
ETM 23	[91]	$2 + 1 + 1$	140, 138, 141	Three pion masses within 3% of the physical value.
PNDME 23	[90]	$2 + 1 + 1$	321, 228, 138, 136	Fit performed including leading-order pion-mass dependence.
ETM 22	[98]	$2 + 1 + 1$	140, 138, 141	Three pion masses within 3% of the physical value.

TABLE 158. Chiral extrapolation/minimum pion mass in determinations of the isovector axial, scalar and tensor charges with $N_f = 2 + 1$ quark flavors.

Collab.	Ref.	N_f	$M_{\pi,\mathrm{min}}$ [MeV]	Description
Mainz 24	[96]	$2 + 1$	176, 130, 218, 228	Physical-point extrapolations were performed simultaneously in the lattice spacing, pion mass, and volume.
PACS 23	[855]	$2 + 1$	138, 135	Three near-physical pion masses.
RQCD 23	[95]	$2 + 1$	336, 176, 131, 156, 127, 338	Extrapolations performed using leading-order chiral expressions for the pion mass.
QCDSF/ UKQCD/ CSSM 23	[94]	$2 + 1$	290, 315, 270, 220, 280, 347	Combined pion-mass, lattice-spacing, and volume extrapolations, performed around chiral SU(3) point.
PACS 22B	[990]	$2 + 1$	135	Two near-physical pion masses.
Mainz 22	[854]	$2 + 1$	176, 130,218,228	Physical-point extrapolations were performed simultaneously in the lattice spacing, pion mass, and volume.

TABLE 159. Finite-volume effects in determinations of the isovector axial, scalar and tensor charges with $N_f = 2 + 1 + 1$ quark flavors.

Collab.	Ref.	N_f	L [fm]	$M_{\pi,\mathrm{min}}L$	Description
ETM 23	[91]	$2 + 1 + 1$	5.1, 5.4, 5.5	3.6, 3.8, 3.9	No extrapolation performed.
PNDME 23	[90]	$2 + 1 + 1$	2.4, 2.9–4.8, 2.9–5.8, 2.9–5.8	3.62, 2.98	Physical-point extrapolations performed simultaneously, using the leading-order terms in the various expansion parameters.
ETM 22	[98]	$2 + 1 + 1$	5.1, 5.4, 5.5	3.62, 2.98	No extrapolation performed.

TABLE 160. Finite-volume effects in determinations of the isovector axial, scalar and tensor charges with $N_f = 2 + 1$ quark flavors.

Collab.	Ref.	N_f	L [fm]	$M_{\pi,\mathrm{min}}L$	Description
Mainz 24	[96]	$2 + 1$	4.14.8, 6.1, 4.7	4.7, 5.4, 4.0, 4.2	Extrapolation performed including a term of the form $M_\pi^2 e^{-M_\pi L}/\sqrt{M_\pi L}$ as part of a simultaneous fit in a, M_π and $M_\pi L$.
PACS 23	[855]	$2 + 1$	5.5–10.9, 10.9	3.8–7.5, 7.5	Negligible finite-volume effects seen between volumes.
RQCD 23	[95]	$2 + 1$	4.8, 2.75–11, 4.9–9.7, 4.1–12.3, 6.3–9.4, 7.5	4.0, 3.5, 3.8, 4.1, 4.3, 4.3	Leading asymptotic form for finite-volume corrections used for extrapolation.
QCDSF/ UKQCD/ CSSM 23	[94]	$2 + 1$	2.6, 2.4, 3.3–4.4, 2.8, 2.5	4.0, 3.9	Combined pion-mass, lattice-spacing, and volume extrapolations performed.
PACS 22B	[990]	$2 + 1$	5.5–10.9	3.8–7.5	Negligible finite-volume effects seen between volumes.
Mainz 22	[854]	$2 + 1$	4.14.8, 6.1, 4.7	4.7, 5.4, 4.0, 4.2	Extrapolation performed including a term of the form $M_\pi^2 e^{-M_\pi L}/\sqrt{M_\pi L}$ as part of a simultaneous fit in a, M_π and $M_\pi L$.

TABLE 161. Renormalization in determinations of the isovector axial, scalar and tensor charges with $N_f = 2+1+1$ quark flavors.

Collab.	Ref.	N_f	Renormalization
ETM 23	[91]	$2+1+1$	RI'-MOM
PNDME 23	[90]	$2+1+1$	RI-SMOM
ETM 22	[98]	$2+1+1$	RI'-MOM

TABLE 162. Renormalization in determinations of the isovector axial, scalar and tensor charges with $2+1$ quark flavors.

Collab.	Ref.	N_f	Renormalization
Mainz 24	[96]	$2+1$	RI-SMOM
PACS 23	[855]	$2+1$	RI-SMOM
RQCD 23	[95]	$2+1$	RI'-SMOM
QCDSF/ UKQCD/ CSSM 23	[94]	$2+1$	RI'-MOM
PACS 22B	[990]	$2+1$	RI-SMOM
Mainz 22	[854]	$2+1$	RI-SMOM

TABLE 163. Control of excited-state contamination in determinations of the isovector axial, scalar and tensor charges with $N_f = 2+1+1$ quark flavors. The comma-separated list of numbers in square brackets denote the range of source-sink separations τ (in Fermi) at each value of the bare coupling.

Collab.	Ref.	N_f	τ [fm]	Description
ETM 23	[91]	$2+1+1$	[0.6–1.6]	Compared results from the plateau, summation method and two-state fits.
PNDME 23	[90]	$2+1+1$	[0.8–1.4]	Several strategies to remove excited-state contributions, including removing $N\pi$ contributions.
ETM 22	[98]	$2+1+1$	[0.6–1.6]	Compared results from the plateau, summation method and two-state fits.

TABLE 164. Control of excited-state contamination in determinations of the isovector axial, scalar and tensor charges with $N_f = 2+1$ quark flavors. The comma-separated list of numbers in square brackets denote the range of source-sink separations τ (in Fermi) at each value of the bare coupling.

Collab.	Ref.	N_f	τ [fm]	Description
Mainz 24	[96]	$2+1$	[0.4–1.5, 0.4–1.5, 0.4–1.5, 0.4–1.5]	Two-state fits to the summation method.
PACS 23	[855]	$2+1$	[0.8–1.1]	Excited-state contributions estimated using different time separations and smearings.
RQCD 23	[95]	$2+1$	[0.7–1.3, 0.7–1.3, 0.7–1.3]	Simultaneous two- and three-state fits of up to four different observables using four time separations.
QCDSF/ UKQCD/ CSSM 23	[94]	$2+1$	all	Energies from fits to two-point correlation functions, where a weighted average is taken of the results obtained when varying the fitting range.

(Table continued)

TABLE 164. *(Continued)*

Collab.	Ref.	N_f	τ [fm]	Description
PACS 22B	[990]	$2+1$	[0.9–1.4]	Excited-state contributions estimated using different time separations and smearings.
Mainz 22	[854]	$2+1$	[0.4–1.5, 0.4–1.5, 0.4–1.5, 0.4–1.5]	Two-state fits to the summation method.

TABLE 165. Continuum extrapolation/estimation of lattice artifacts in direct determinations of $\sigma_{\pi N}$ and σ_s.

Collab.	Ref.	N_f	a [fm]	Description
PNDME 21	[101]	$2+1+1$	0.12, 0.09, 0.06	Joint continuum and chiral fit includes a aM_π^2 term.
Mainz 23	[106]	$2+1$	0.08, 0.07, 0.06, 0.05	Joint continuum, chiral and finite-volume (correlated) fit of $\sigma_{\pi N}$ and σ_s includes a $aM_{\pi,K}^2$ term. Fits are performed including and excluding this term.

TABLE 166. Chiral extrapolation/minimum pion mass in direct determinations of $\sigma_{\pi N}$ and σ_s.

Collab.	Ref.	N_f	$M_{\pi,\mathrm{min}}$ [MeV]	Description
PNDME 21	[101]	$2+1+1$	228, 138, 235	Joint continuum and chiral fit including the SU(2) NNLO baryon χPT [1122] terms.
Mainz 23	[106]	$2+1$	219, 154, 128, 174	Joint continuum, chiral and finite-volume (correlated) fit of $\sigma_{\pi N}$ and σ_s utilizing SU(3) NNLO covariant baryon χPT with the EOMS loop regularization scheme [963,1123,1124]. Cuts on the pion mass excluding ensembles with $M_\pi > 220$, 285 or 360 MeV are made.

TABLE 167. Finite-volume effects in direct determinations of $\sigma_{\pi N}$ and σ_s.

Collab.	Ref.	N_f	L [fm]	$M_{\pi,\mathrm{min}}L$	Description
PNDME 21	[101]	$2+1+1$	2.9–3.8	4.4	Finite-volume terms are not included in the joint continuum-chiral extrapolation.
			2.8–5.6	3.9	
			2.8–3.7	4.4	
Mainz 23	[106]	$2+1$	2.7–4.1	4.6	Joint continuum, chiral and finite-volume (correlated) fit of $\sigma_{\pi N}$ and σ_s includes a term derived from the SU(2) finite-volume expression for the nucleon mass in Ref. [1125]. Fits are performed including and excluding this term.
			2.4–4.8	3.8	
			2.0–6.1	4.0	
			2.4–4.7	4.2	

TABLE 168. Renormalization for direct determinations of $\sigma_{\pi N}$ and σ_s. The type of renormalization (Ren.) is given for $\sigma_{\pi N}$ first and σ_s second. The label na indicates that no renormalization is required.

Collab.	Ref.	N_f	Ren.	Description
PNDME 21	[101]	$2+1+1$	⋯	Flavor mixing occurs due to breaking of chiral symmetry. The ratio of Z^{ns}/Z^s is estimated to be close to 1 and the mixing is neglected.
Mainz 23	[106]	$2+1$	NP/NP	Flavor mixing occurs due to breaking of chiral symmetry. The mixing is implemented using ratios of the light- and strange-quark masses rather than utilizing Z^{ns}/Z^s.

TABLE 169. Control of excited-state contamination in direct determinations of $\sigma_{\pi N}$ and σ_s. The comma-separated list of numbers in square brackets denote the range of source-sink separations τ (in Fermi) at each value of the bare coupling. The range of τ for the connected (disconnected) contributions to the three-point correlation functions is given first (second). If a wide range of τ values is available this is indicated by "all" in the table.

Collab.	Ref.	N_f	τ [fm]	Description
PNDME 21	[101]	$2+1+1$	[1.0–1.7, 1.0–1.7]/all [0.9–1.4, 0.9–1.4]/all [1.1–1.4, 1.1–1.4]/all	The two- and three-point functions are fitted simultaneously including four and three states, respectively. The final results are obtained using a narrow-width prior to set the first excited-state energy to that of the lowest $N\pi$ state.
Mainz 23	[106]	$2+1$	[0.3–1.5]/all [0.3–1.5]/all [0.3–1.5]/all [0.3–1.5]/all	Summation method including the ground-state terms and ratio fits including an excited state with the energy fixed with a prior to the lowest $N\pi$ energy are considered. The final result combines results from both fit types.

TABLE 170. Continuum extrapolations/estimation of lattice artifacts in determinations of $\sigma_{\pi N}$ and σ_s from the Feynman-Hellmann method.

Collab.	Ref.	N_f	a [fm]	Description
RQCD 22	[105]	$2+1$	0.10, 0.09, 0.08, 0.06, 0.05, 0.04	Combined continuum, chiral and volume fit to the baryon octet. Leading $O(a^2)$ terms are included in the parametrization. Fits are performed also excluding the coarsest lattice spacing.

TABLE 171. Chiral extrapolation/minimum pion mass in determinations of $\sigma_{\pi N}$ and σ_s from the Feynman-Hellmann method.

Collab.	Ref.	N_f	$M_{\pi,\mathrm{min}}$ [MeV]	Description
RQCD 22	[105]	$2+1$	338, 127, 216131, 176, 336	Combined continuum, chiral and volume fit to the baryon octet. Fits utilizing SU(3) NNLO covariant baryon χPT with the EOMS loop regularization scheme [963,1123,1124] are performed. Cuts on the flavor average meson mass squared are made.

TABLE 172. Finite-volume effects in determinations of $\sigma_{\pi N}$ and σ_s from the Feynman-Hellmann method.

Collab.	Ref.	N_f	L [fm]	$M_{\pi,\min}L$	Description
RQCD 22	[105]	$2+1$	2.3, 2.0–5.5, 2.4–4.8, 2.0–6.1, 2.4–4.7 2.5	4.0, 3.5, 5.3, 4.0, 4.2, 4.2	Combined continuum, chiral and volume fit to the baryon octet. Finite-volume terms from NNLO covariant baryon χPT (with no new fit parameters) are included in the fit [1126–1128]. Ensembles with $L < 2.3$ fm are excluded from the analysis.

TABLE 173. Continuum extrapolations/estimation of lattice artifacts in determinations of the isovector unpolarized, helicity and transversity second moments with $N_f = 2+1+1$ quark flavors.

Collab.	Ref.	N_f	a [fm]	Description
ETM 22	[98]	$2+1+1$	0.08, 0.07, 0.06	Linear extrapolation in a^2.
PNDME 20A	[109]	$2+1+1$	0.15, 0.12, 0.09, 0.06	Extrapolation performed using a linear term in a as part of a simultaneous fit in a, M_π and $M_\pi L$.
ETM 20C	[1042]	$2+1+1$	0.08	Single lattice spacing.
ETM 19A	[1043]	$2+1+1$	0.08	Single lattice spacing.

TABLE 174. Continuum extrapolations/estimation of lattice artifacts in determinations of the isovector unpolarized, helicity and transversity second moments with $N_f = 2+1$ quark flavors.

Collab.	Ref.	N_f	a [fm]	Description
Mainz 24	[96]	$2+1$	0.09, 0.08, 0.06, 0.05	A number of simultaneous a, M_π and $M_\pi L$ fits are performed using a linear term in a. The final results are obtained from a weighted average.
LHPC 24	[1044]	$2+1$	0.12, 0.09	A Bayesian fit is performed including an a and an a^2 term.
NME 21A	[1045]	$2+1$	0.127, 0, 09, 0.07	Extrapolation performed using a linear term in a as part of a simultaneous fit in a, M_π and $M_\pi L$.
NME 20	[110]	$2+1$	0.127, 0, 09, 0.07	Extrapolation performed using a linear term in a as part of a simultaneous fit in a, M_π and $M_\pi L$.
Mainz 19	[923]	$2+1$	0.05, 0.06, 0.08, 0.09	Extrapolation performed as part of a simultaneous fit in a, M_π and $M_\pi L$.
χQCD 18A	[111]	$2+1$	0.143, 0.11, 0.114, 0.083	Partially quenched calculation. Extrapolation performed as part of a simultaneous fit in a^2, M_π and $M_\pi L$ using expression from HBChPT.
LHPC 12A	[994]	$2+1$	0.12, 0.09	No statistically significant discretization effects observed. Results assumed to be constant in a.
LHPC 10	[905]	$2+1$	0.12	Single lattice spacing.
RBC/UKQCD 10D	[893]	$2+1$	0.11	Single lattice spacing.

TABLE 176. Chiral extrapolation/minimum pion mass in determinations of the isovector unpolarized, helicity and transversity second moments with $N_f = 2 + 1 + 1$ quark flavors.

Collab.	Ref.	N_f	$M_{\pi,\mathrm{min}}$ [MeV]	Description
ETM 22	[98]	$2 + 1 + 1$	140, 137, 141	Simulate close to M_π^{phys}.
PNDME 20A	[109]	$2 + 1 + 1$	321, 228, 138, 136	Extrapolation performed using a linear term in M_π^2 as part of a simultaneous fit in a, M_π and $M_\pi L$.
ETM 20C	[1042]	$2 + 1 + 1$	139	Single pion mass within 3% of the physical value.
ETM 19A	[1043]	$2 + 1 + 1$	139	Single pion mass within 3% of the physical value.

TABLE 177. Chiral extrapolation/minimum pion mass in determinations of the isovector unpolarized, helicity and transversity second moments with $N_f = 2 + 1$ quark flavors.

Collab.	Ref.	N_f	$M_{\pi,\mathrm{min}}$ [MeV]	Description
Mainz 24	[96]	$2 + 1$	228, 218, 130, 176	A number of simultaneous a, M_π and $M_\pi L$ fits are performed using terms which appear in the SU(2) NNLO ChPT expression for the axial charge and (alternatively) a linear term in M_π^2. The final results are obtained from a weighted average.
LHPC 24	[1044]	$2 + 1$	136, 133	Simulate close to M_π^{phys}.
NME 21A	[1045]	$2 + 1$	285, 169, 167	Extrapolation performed using a linear term in M_π^2 as part of a simultaneous fit in a, M_π and $M_\pi L$.
NME 20	[110]	$2 + 1$	285, 169, 167	Extrapolation performed using a linear term in M_π^2 as part of a simultaneous fit in a, M_π and $M_\pi L$.
Mainz 19	[923]	$2 + 1$	290, 200, 260	Extrapolation performed using logarithmic and quadratic terms in M_π as part of a simultaneous fit in a, M_π and $M_\pi L$.
χQCD 18A	[111]	$2 + 1$	171, 330, 139, 300	Partially quenched calculation. Extrapolation performed as part of a simultaneous fit in a^2, M_π and $M_\pi L$ using expression from HBChPT.
LHPC 12A	[994]	$2 + 1$	149, 317	Chiral fit formula based on the "small-scale expansion" to order ϵ^3 with some coefficients fixed.
LHPC 10	[905]	$2 + 1$	293	Chiral fit formula based on the "small-scale expansion" to order ϵ^3 with some coefficients fixed.
RBC/UKQCD 10D	[893]	$2 + 1$	329, 416, 555, 668	Constant fit to heaviest three and linear fit to lightest two pion masses gives the quoted range.

TABLE 178. Chiral extrapolation/minimum pion mass in determinations of the isovector unpolarized, helicity and transversity second moments with $N_f = 2$ quark flavors.

Collab.	Ref.	N_f	$M_{\pi,\min}$ [MeV]	Description
RQCD 18	[1046]	2	280, 150, 260	Chiral fit using BChPT. Kept terms up to $O(M_\pi^3)$.
ETM 17C	[883]	2	≈135	Single ensemble within 3% of physical pion mass.
ETM 15D	[880]	2	131	Single ensemble within 3% of physical pion mass.
RQCD 14A	[1047]	2	280, 150, 260	No significant dependence on pion mass observed.

TABLE 179. Finite-volume effects in determinations of the isovector unpolarized, helicity and transversity second moments with $N_f = 2 + 1 + 1$ quark flavors.

Collab.	Ref.	N_f	L [fm]	$M_{\pi,\min}L$	Description
ETM 22	[98]	$2+1+1$	5.1, 5.5, 5.5	3.6, 3.8, 3.9	Finite-volume effects not estimated.
PNDME 20A	[109]	$2+1+1$	2.4, 4.8, 5.6, 5.5	3.9, 5.5, 3.9, 3.7	Fit performed using a term of the form $M_\pi^2 e^{-M_\pi L}/\sqrt{M_\pi L}$ as part of a simultaneous fit in a, M_π and $M_\pi L$.
ETM 20C	[1042]	$2+1+1$	5.1	3.6	Finite-volume effects not estimated.
ETM 19A	[1043]	$2+1+1$	5.1	3.6	Finite-volume effects not estimated.

TABLE 180. Finite-volume effects in determinations of the isovector unpolarized, helicity and transversity second moments with $N_f = 2 + 1$ quark flavors.

Collab.	Ref.	N_f	L [fm]	$M_{\pi,\min}L$	Description
Mainz 24	[96]	$2+1$	4.1, 4.8, 6.1, 4.7	4.7, 5.4, 4.0, 4.2	A number of simultaneous a, M_π and $M_\pi L$ fits are performed using term of the form $M_\pi^2 e^{-M_\pi L}/\sqrt{M_\pi L}$. The final results are obtained from a weighted average.
LHPC 24	[1044]	$2+1$	5.6, 5.9	3.9, 4.0	Finite-volume effects are not estimated.
NME 21A	[1045]	$2+1$	4.1, 3.0–5.8, 3.5–5.1	5.9, 5.1, 4.3	Fit performed using a term of the form $M_\pi^2 e^{-M_\pi L}/\sqrt{M_\pi L}$ as part of a simultaneous fit in a, M_π and $M_\pi L$.
NME 20	[110]	$2+1$	4.1, 3.0–5.8, 3.5–5.1	5.9, 5.1, 4.3	Fit performed using a term of the form $M_\pi^2 e^{-M_\pi L}/\sqrt{M_\pi L}$ as part of a simultaneous fit in a, M_π and $M_\pi L$.
Mainz 19	[923]	$2+1$	2.8–4.1, 2.4–3.6, 2.1–4.1, 2.4–3.2	4.7, 5.3, 4.2, 4.3	Extrapolation performed including a term of the form $M_\pi^2 e^{-M_\pi L}/\sqrt{M_\pi L}$ as part of a simultaneous fit in a^2, M_π and $M_\pi L$.

(Table continued)

TABLE 180. *(Continued)*

Collab.	Ref.	N_f	L [fm]	$M_{\pi,\min}L$	Description
χQCD 18A	[111]	$2+1$	4.6, 2.7, 5.5, 2.6	4.0, 4.4, 3.9, 4.0	Extrapolation performed including a term of the form $e^{-M_\pi L}$ as part of a simultaneous fit in a^2, M_π and $M_\pi L$.
LHPC 12A	[994]	$2+1$	2.8–5.6, 2.9	4.2, 4.6	Finite-volume effects investigated and found to be negligible.
LHPC 10	[905]	$2+1$	2.5–3.5	3.7	Finite-volume effects included in chiral fit formula and found to be negligible.
RBC/UKQCD 10D	[893]	$2+1$	2.7	4.6	No uncertainty estimated. Comparison between two volumes for the three heaviest pion masses shows no deviation within statistical errors.

TABLE 181. Finite-volume effects in determinations of the isovector unpolarized, helicity and transversity second moments with $N_f = 2$ quark flavors.

Collab.	Ref.	N_f	L [fm]	$M_{\pi,\min}L$	Description
RQCD 18	[1046]	2	2.6, 1.7–4.6, 1.9–2.9	3.7, 2.8, 3.8	No significant finite-volume effects observed.
ETM 17C	[883]	2	4.5	3.1	Single ensemble
ETM 15D	[880]	2	4.5	3.0	Single ensemble
RQCD 14A	[1047]	2	2.6, 1.7–4.6, 1.9–2.9	3.7, 2.8, 3.8	No significant finite-volume effects observed.

TABLE 182. Renormalization in determinations of the isovector unpolarized, helicity and transversity second moments with $N_f = 2+1+1$, $N_f = 2+1$ and $N_f = 2$ quark flavors.

Collab.	Ref.	N_f	Renormalization
ETM 22	[98]	$2+1+1$	RI′-MOM
PNDME 20A	[109]	$2+1+1$	RI′-MOM
ETM 20C	[1042]	$2+1+1$	RI′-MOM
ETM 19A	[1043]	$2+1+1$	RI′-MOM
Mainz 24	[96]	$2+1$	RI-MOM
LHPC 24	[1044]	$2+1$	RI′-MOM/RI-SMOM
NME 21A	[1045]	$2+1$	RI′-MOM
NME 20	[110]	$2+1$	RI′-MOM

(Table continued)

TABLE 182. *(Continued)*

Collab.	Ref.	N_f	Renormalization
Mainz 19	[923]	$2+1$	RI-MOM
χQCD 18A	[111]	$2+1$	RI-MOM
LHPC 12A	[994]	$2+1$	RI-MOM
LHPC 10	[905]	$2+1$	RI-MOM
RBC/UKQCD 10D	[893]	$2+1$	RI-MOM
RQCD 18	[1046]	2	RI′-MOM
ETM 17C	[883]	2	RI′-MOM
ETM 15D	[880]	2	RI′-MOM
RQCD 14A	[1047]	2	RI′-MOM

TABLE 183. Control of excited-state contamination in determinations of the isovector unpolarized, helicity and transversity second moments with $N_f = 2+1+1$ quark flavors. The comma-separated list of numbers in square brackets denote the range of source-sink separations τ (in Fermi) at each value of the bare coupling.

Collab.	Ref.	N_f	τ [fm]	Description
ETM 22	[98]	$2+1+1$	[0.6–1.6] [0.6–1.5] [0.5–1.2]	Two-state fit to all τ. A comparison is made with plateau fits and the summation method.
PNDME 20A	[109]	$2+1+1$	[0.8–1.4] [1.0–1.7, 1.0–1.7] [0.9–1.4, 0.9–1.4, 0.9–1.4] [1.0–1.4, 0.9–1.3]	Fits to the τ- and t-dependence of three-point correlators using two or three lowest-lying states.
ETM 20C	[1042]	$2+1+1$	[0.6–1.6]	Two-state fit to all τ. A comparison is made with plateau fits and the summation method.
ETM 19A	[1043]	$2+1+1$	[0.6–1.6]	Two-state fit to all τ. A comparison is made with plateau fits and the summation method.

TABLE 184. Control of excited-state contamination in determinations of the isovector unpolarized, helicity and transversity second moments with $N_f = 2 + 1$ quark flavors. The comma-separated list of numbers in square brackets denote the range of source-sink separations τ (in Fermi) at each value of the bare coupling.

Collab.	Ref.	N_f	τ [fm]	Description
Mainz 24	[96]	$2+1$	[0.4–1.5, 0.4–1.5, 0.4–1.5, 0.4–1.5] [0.3–1.5, 0.3–1.5,0.3–1.5] [0.3–1.4,0.3–1.4,0.3– 1.4,0.3–1.4,0.3–1.4] [0.2–1.4,0.2–1.4,0.2–1.4]	Two-state summation method.
LHPC 24	[1044]	$2+1$	[0.3–1.4] [0.9–1.5]	Two-state fits to the three-point function and the summation method are utilized, with the final results obtained from a weighted average.
NME 21A	[1045]	$2+1$	[1.3–1.8] [1.1–1.5,1.3–1.7,1.1– 1.5,1.1–1.5] [1.1–1.4,1.2–1.5]	Fits to the τ- and t-dependence of three-point correlators using two or three lowest-lying states.
NME 20	[110]	$2+1$	[1.3–1.8] [1.1–1.5,1.3–1.7,1.1– 1.5,1.1–1.5] [1.1–1.4,1.2–1.5]	Fits to the τ- and t-dependence of three-point correlators using two or three lowest-lying states.
Mainz 19	[923]	$2+1$	[1.0–1.4, 1.0–1.4, 1.0–1.4] [1.0–1.5,1.0–1.5] [1.0–1.4,1.0–1.4,1.0– 1.4,1.0–1.4] [1.0–1.4,1.0–1.3]	Fits to the τ- and t-dependence of correlator ratios using the two lowest-lying states.
χQCD 18A	[111]	$2+1$	[0.7–1.5]	Two-state fits to the three-point function.
LHPC 12A	[994]	$2+1$	[0.9–1.4, 0.9–1.4, 0.9–1.4, 0.9–1.4, 0.9–1.4] [0.9–1.4]	Fits to the leading (ground state) τ-dependence of summed correlator ratios.
LHPC 10	[905]	$2+1$	[1.1, 1.1, 1.1, 1.1, 1.1–1.2, 1.1]	Plateau fits of correlator ratio at $\tau = 1.1$ fm. Larger source-sink separation on one ensemble as cross check.
RBC/UKQCD 10D	[893]	$2+1$	[1.4, 1.4, 1.4, 1.4]	Single source-sink separation considered.

TABLE 185. Control of excited-state contamination in determinations of the isovector unpolarized, helicity and transversity second moments with $N_f = 2$ quark flavors. The comma-separated list of numbers in square brackets denote the range of source-sink separations τ (in Fermi) at each value of the bare coupling.

Collab.	Ref.	N_f	τ [fm]	Description
RQCD 18	[1046]	2	Not given	Analysis limited by statistics
ETM 17C	[883]	2	[0.9–1.5]	Result from plateau method with $\tau/a = 14$. Consistent with estimates from summation and two-state fit methods.
ETM 15D	[880]	2	[0.9–1.3]	Result from plateau method with $\tau/a = 14$. Consistent with estimate from the summation method.
RQCD 14A	[1047]	2	Not given	Plateau value at larger τ/a consistent with two-state fit.

8. Notes to Sec. XI on scale setting

TABLE 186. Continuum extrapolations/estimation of lattice artifacts in scale determinations with $N_f = 2+1+1$ quark flavors.

Collab.	Ref.	N_f	a [fm]	Description
TUMQCD 22	[118]	$2+1+1$	0.15294, 0.12224, 0.08786, 0.05662, 0.0426, 0.03216	MILC ensembles from on-shell Symanzik-improved gauge action and rooted HISQ fermions
ETM 21	[45]	$2+1+1$	0.069, 0.079, 0.097	

TABLE 187. Continuum extrapolations/estimation of lattice artifacts in scale determinations with $N_f = 2+1$ quark flavors.

Collab.	Ref.	N_f	a [fm]	Description
Hudspith 24	[1066]	$2+1$	0.098, 0.085, 0.075, 0.064, 0.049, 0.039	NP $\mathcal{O}(a)$-improved Wilson fermions with tree-level Symanzik improved gauge action.
Asmussen 23	[1088]	$2+1$	0.085, 0.075, 0.064, 0.049, 0.039	NP $\mathcal{O}(a)$-improved Wilson fermions with tree-level Symanzik improved gauge action.
RQCD 22	[105]	$2+1$	0.098, 0.085, 0.075, 0.064, 0.049, 0.039	NP $\mathcal{O}(a)$-improved Wilson fermions with tree-level Symanzik improved gauge action.
RBC/Bielefeld 07	[1090]	$2+1$	0.3–0.05	Simulations with improved staggered fermions (p4fat3-action: smeared 1-link term and bent 3-link terms) at 27 different values of β.

TABLE 188. Chiral extrapolation and finite-volume effects in scale determinations with $N_f = 2+1+1$ quark flavors. We list the minimum pion mass $M_{\pi,\mathrm{min}}$ and $M_\pi L \equiv M_{\pi,\mathrm{min}}[L(M_{\pi,\mathrm{min}})]_{\mathrm{max}}$ is evaluated at the maximum value of L available at $M_\pi = M_{\pi,\mathrm{min}}$.

Collab.	Ref.	N_f	$M_{\pi,\mathrm{min}}$ [MeV]	$M_\pi L$	Description
TUMQCD 22	[118]	$2+1+1$	129	3.25 – 4.17	At the physical point.
ETM 21	[45]	$2+1+1$	134.2	3.78	

TABLE 189. Chiral extrapolation and finite-volume effects in scale determinations with $N_f = 2+1$ quark flavors. We list the minimum pion mass $M_{\pi,\mathrm{min}}$ and $M_\pi L \equiv M_{\pi,\mathrm{min}}[L(M_{\pi,\mathrm{min}})]_{\mathrm{max}}$ is evaluated at the maximum value of L available at $M_\pi = M_{\pi,\mathrm{min}}$.

Collab.	Ref.	N_f	$M_{\pi,\mathrm{min}}$ [MeV]	$M_\pi L$	Description
Hudspith 24	[1066]	$2+1$	127/131	3.51/4.05	At $m = m_{\mathrm{symm}}$.
Asmussen 23	[1088]	$2+1$	127/131	3.51/4.05	At $m = m_{\mathrm{symm}}$.
RQCD 22	[105]	$2+1$	127/131 200	3.51/4.05 4.14	At $m = m_{\mathrm{symm}}$. At $\tilde{m}_s = \tilde{m}_{s,\mathrm{phys}}$
RBC/Bielefeld 07	[1090]	$2+1$	220	5.456	

[1] [FLAG 10] G. Colangelo, S. Dürr, A. Jüttner, L. Lellouch, H. Leutwyler *et al.*, Review of lattice results concerning low energy particle physics, Eur. Phys. J. C **71**, 1695 (2011).

[2] [FLAG 13] S. Aoki, Y. Aoki, C. Bernard, T. Blum, G. Colangelo *et al.*, Review of lattice results concerning low-energy particle physics, Eur. Phys. J. C **74**, 2890 (2014).

[3] [FLAG 16] S. Aoki *et al.*, Review of lattice results concerning low-energy particle physics, Eur. Phys. J. C **77**, 112 (2017).

[4] [FLAG 19] S. Aoki *et al.*, FLAG review 2019: Flavour lattice averaging group (FLAG), Eur. Phys. J. C **80**, 113 (2020).

[5] [FLAG 21] Y. Aoki *et al.*, FLAG review 2021, Eur. Phys. J. C **82**, 869 (2022).

[6] Flavour Lattice Averaging Group (FLAG), FLAG Review, http://flag.itp.unibe.ch.

[7] [ETM 21A] C. Alexandrou *et al.*, Quark masses using twisted mass fermion gauge ensembles, Phys. Rev. D **104**, 074515 (2021).

[8] [ETM 14] N. Carrasco *et al.*, Up, down, strange and charm quark masses with $N_f = 2 + 1 + 1$ twisted mass lattice QCD, Nucl. Phys. **B887**, 19 (2014).

[9] [FNAL/MILC/TUMQCD 18] A. Bazavov *et al.*, Up-, down-, strange-, charm-, and bottom-quark masses from four-flavor lattice QCD, Phys. Rev. D **98**, 054517 (2018).

[10] [CLQCD 23] Zhi-Cheng Hu *et al.*, Quark masses and low-energy constants in the continuum from the tadpole-improved clover ensembles, Phys. Rev. D **109**, 054507 (2024).

[11] [ALPHA 19] M. Bruno, I. Campos, P. Fritzsch, J. Koponen, C. Pena, D. Preti, A. Ramos, and A. Vladikas, Light quark masses in $N_f = 2 + 1$ lattice QCD with Wilson fermions, Eur. Phys. J. C **80**, 169 (2020).

[12] [RBC/UKQCD 14B] T. Blum *et al.*, Domain wall QCD with physical quark masses, Phys. Rev. D **93**, 074505 (2016).

[13] [BMW 10A] S. Dürr, Z. Fodor, C. Hoelbling, S. Katz, S. Krieg, T. Kurth, L. Lellouch, T. Lippert, K. K. Szabo, and G. Vulvert, Lattice QCD at the physical point: Light quark masses, Phys. Lett. B **701**, 265 (2011).

[14] [BMW 10B] S. Dürr, Z. Fodor, C. Hoelbling, S. Katz, S. Krieg, T. Kurth, L. Lellouch, T. Lippert, K. K. Szabó, and G. Vulvert, Lattice QCD at the physical point: Simulation and analysis details, J. High Energy Phys. 08 (2011) 148.

[15] [HPQCD 10] C. McNeile, C. T. H. Davies, E. Follana, K. Hornbostel, and G. P. Lepage, High-precision c and b masses and QCD coupling from current-current correlators in lattice and continuum QCD, Phys. Rev. D **82**, 034512 (2010).

[16] [MILC 10A] A. Bazavov *et al.*, Staggered chiral perturbation theory in the two-flavor case and SU(2) analysis of the MILC data, Proc. Sci., LAT2010 (**2010**) 083 [arXiv:1011.1792].

[17] [HPQCD 18] A. T. Lytle, C. T. H. Davies, D. Hatton, G. P. Lepage, and C. Sturm, Determination of quark masses from $n_f = 4$ lattice QCD and the RI-SMOM intermediate scheme, Phys. Rev. D **98**, 014513 (2018).

[18] [HPQCD 14A] B. Chakraborty, C. T. H. Davies, G. C. Donald, R. J. Dowdall, B. Galloway, P. Knecht *et al.*, High-precision quark masses and QCD coupling from $n_f = 4$ lattice QCD, Phys. Rev. D **91**, 054508 (2015).

[19] [MILC 09A] A. Bazavov *et al.*, MILC results for light pseudoscalars, *Proc. Sci.*, CD09 (2009) 007 [arXiv:0910.2966].

[20] [FNAL/MILC 17] A. Bazavov *et al.*, B- and D-meson leptonic decay constants from four-flavor lattice QCD, Phys. Rev. D **98**, 074512 (2018).

[21] [FNAL/MILC 14A] A. Bazavov *et al.*, Charmed and light pseudoscalar meson decay constants from four-flavor lattice QCD with physical light quarks, Phys. Rev. D **90**, 074509 (2014).

[22] [ALPHA 19B] M. Bruno, I. Campos, J. Koponen, C. Pena, D. Preti, A. Ramos *et al.*, Light and strange quark masses from $N_f = 2 + 1$ simulations with Wilson fermions, Proc. Sci., LATTICE2018 (**2019**) 220 [arXiv:1903.04094].

[23] [RM123 17] D. Giusti, V. Lubicz, C. Tarantino, G. Martinelli, S. Sanfilippo, S. Simula, and N. Tantalo, Leading isospin-breaking corrections to pion, kaon and charmed-meson masses with twisted-mass fermions, Phys. Rev. D **95**, 114504 (2017).

[24] [BMW 16A] Z. Fodor, C. Hoelbling, S. Krieg, L. Lellouch, T. Lippert, A. Portelli, A. Sastre, K. K. Szabo, and L. Varnhorst, Up and down quark masses and corrections to Dashen's theorem from lattice QCD and quenched QED, Phys. Rev. Lett. **117**, 082001 (2016).

[25] [MILC 18]S. Basak *et al.*, Lattice computation of the electromagnetic contributions to kaon and pion masses, Phys. Rev. D **99**, 034503 (2019).

[26] [ETM 14A] C. Alexandrou, V. Drach, K. Jansen, C. Kallidonis, and G. Koutsou, Baryon spectrum with $N_f = 2 + 1 + 1$ twisted mass fermions, Phys. Rev. D **90**, 074501 (2014).

[27] [HPQCD 20A] D. Hatton, C. T. H. Davies, B. Galloway, J. Koponen, G. P. Lepage, and A. T. Lytle, Charmonium properties from lattice $QCD + QED$: Hyperfine splitting, J/ψ leptonic width, charm quark mass, and a_μ^c, Phys. Rev. D **102**, 054511 (2020).

[28] [ALPHA 23] A. Bussone, A. Conigli, J. Frison, G. Herdoíza, C. Pena, D. Preti, A. Sáez, and J. Ugarrio, Hadronic physics from a Wilson fermion mixed-action approach: Charm quark mass and $D_{(s)}$ meson decay constants, Eur. Phys. J. C **84**, 506 (2024).

[29] [χQCD 14] Y. Yi-Bo *et al.*, Charm and strange quark masses and f_{D_s} from overlap fermions, Phys. Rev. D **92**, 034517 (2015).

[30] [JLQCD 16] K. Nakayama, B. Fahy, and S. Hashimoto, Short-distance charmonium correlator on the lattice with Möbius domain-wall fermion and a determination of charm quark mass, Phys. Rev. D **94**, 054507 (2016).

[31] P. Petreczky and J. Weber, Strong coupling constant and heavy quark masses in $(2 + 1)$-flavor QCD, Phys. Rev. D **100**, 034519 (2019).

[32] [ALPHA 21] J. Heitger, F. Joswig, and S. Kuberski, Determination of the charm quark mass in lattice QCD

with $2+1$ flavours on fine lattices, J. High Energy Phys. 05 (2021) 288.
[33] [HPQCD 09A] C. T. H. Davies, C. McNeile, K. Y. Wong, E. Follana, R. Horgan, K. Hornbostel, G. P. Lepage, J. Shigemitsu, and H. Trottier, Precise charm to strange mass ratio and light quark masses from full lattice QCD, Phys. Rev. Lett. **104**, 132003 (2010).
[34] [HPQCD 21] D. Hatton, C. T. H. Davies, J. Koponen, G. P. Lepage, and A. T. Lytle, Determination of $\bar{m}_b/\bar{m}_c$ and $\bar{m}_b$ from $n_f = 4$ lattice QCD + QED, Phys. Rev. D **103**, 114508 (2021).
[35] [HPQCD 14B] B. Colquhoun, R. J. Dowdall, C. T. H. Davies, K. Hornbostel, and G. P. Lepage, Υ and Υ' leptonic widths, a_μ^b and m_b from full lattice QCD, Phys. Rev. D **91**, 074514 (2015).
[36] [ETM 16B] A. Bussone *et al.*, Mass of the b quark and B-meson decay constants from $N_f = 2+1+1$ twisted-mass lattice QCD, Phys. Rev. D **93**, 114505 (2016).
[37] P. Gambino, A. Melis, and S. Simula, Extraction of heavy-quark-expansion parameters from unquenched lattice data on pseudoscalar and vector heavy-light meson masses, Phys. Rev. D **96**, 014511 (2017).
[38] [ETM 16] N. Carrasco, P. Lami, V. Lubicz, L. Riggio, S. Simula, and C. Tarantino, $K \to \pi$ semileptonic form factors with $N_f = 2+1+1$ twisted mass fermions, Phys. Rev. D **93**, 114512 (2016).
[39] [FNAL/MILC 18] A. Bazavov *et al.*, $|V_{us}|$ from $K_{\ell 3}$ decay and four-flavor lattice QCD, Phys. Rev. D **99**, 114509 (2019).
[40] [FNAL/MILC 12I] A. Bazavov, C. Bernard, C. Bouchard, C. DeTar, D. Du *et al.*, Kaon semileptonic vector form factor and determination of $|V_{us}|$ using staggered fermions, Phys. Rev. D **87**, 073012 (2013).
[41] [RBC/UKQCD 15A Collaboration] P. A. Boyle *et al.*, The kaon semileptonic form factor in $N_f = 2+1$ domain wall lattice QCD with physical light quark masses, J. High Energy Phys. 06 (2015) 164.
[42] [HPQCD 13A] R. Dowdall, C. Davies, G. Lepage, and C. McNeile, V_{us} from π and K decay constants in full lattice QCD with physical u, d, s and c quarks, Phys. Rev. D **88**, 074504 (2013).
[43] [ETM 14E] N. Carrasco, P. Dimopoulos, R. Frezzotti, P. Lami, V. Lubicz *et al.*, Leptonic decay constants f_K, f_D and f_{D_s} with $N_f = 2+1+1$ twisted-mass lattice QCD, Phys. Rev. D **91**, 054507 (2015).
[44] [CalLat 20] N. Miller *et al.*, F_K/F_π from Möbius domain-wall fermions solved on gradient-flowed HISQ ensembles, Phys. Rev. D **102**, 034507 (2020).
[45] [ETM 21] C. Alexandrou *et al.*, Ratio of kaon and pion leptonic decay constants with $N_f = 2+1+1$ Wilson-clover twisted-mass fermions, Phys. Rev. D **104**, 074520 (2021).
[46] [HPQCD/UKQCD 07] E. Follana, C. T. H. Davies, G. P. Lepage, and J. Shigemitsu, High precision determination of the π, K, D and D_s decay constants from lattice QCD, Phys. Rev. Lett. **100**, 062002 (2008).
[47] [MILC 10] A. Bazavov *et al.*, Results for light pseudoscalar mesons, Proc. Sci., LAT2010 (**2010**) 074 [arXiv:1012.0868].
[48] [BMW 10] S. Dürr, Z. Fodor, C. Hoelbling, S. Katz, S. Krieg *et al.*, The ratio F_K/F_π in QCD, Phys. Rev. D **81**, 054507 (2010).
[49] [BMW 16] S. Dürr *et al.*, Leptonic decay-constant ratio f_K/f_π from lattice QCD using $2+1$ clover-improved fermion flavors with 2-HEX smearing, Phys. Rev. D **95**, 054513 (2017).
[50] [QCDSF/UKQCD 16] V. G. Bornyakov, R. Horsley, Y. Nakamura, H. Perlt, D. Pleiter, P. E. L. Rakow, G. Schierholz, A. Schiller, H. Stüben, and J. M. Zanotti, Flavour breaking effects in the pseudoscalar meson decay constants, Phys. Lett. B **767**, 366 (2017).
[51] [RBC/UKQCD 15F] T. Blum *et al.*, $K \to \pi\pi\Delta I = 3/2$ decay amplitude in the continuum limit, Phys. Rev. D **91**, 074502 (2015).
[52] [ETM 15] N. Carrasco, P. Dimopoulos, R. Frezzotti, V. Lubicz, G. C. Rossi, S. Simula, and C. Tarantino, $\Delta S = 2$ and $\Delta C = 2$ bag parameters in the Standard Model and beyond from $N_f = 2+1+1$ twisted-mass lattice QCD, Phys. Rev. D **92**, 034516 (2015).
[53] [BMW 11] S. Dürr, Z. Fodor, C. Hoelbling, S. Katz, S. Krieg *et al.*, Precision computation of the kaon bag parameter, Phys. Lett. B **705**, 477 (2011).
[54] J. Laiho and R. S. Van de Water, Pseudoscalar decay constants, light-quark masses and B_K from mixed-action lattice QCD, Proc. Sci., LATTICE2011 (**2011**) 293 [arXiv:1112.4861].
[55] [SWME 15A] Y.-C. Jang *et al.*, Kaon BSM B-parameters using improved staggered fermions from $N_f = 2+1$ unquenched QCD, Phys. Rev. D **93**, 014511 (2016).
[56] [RBC/UKQCD 24] P. Boyle, Felix, J. M. Flynn, N. Garron, J. Kettle, R. Mukherjee, and J. T. Tsang, Kaon mixing beyond the Standard Model with physical masses, Phys. Rev. D **110**, 034501 (2024).
[57] [ETM 12D] V. Bertone *et al.*, Kaon mixing beyond the SM from $N_f = 2$ tmQCD and model independent constraints from the UTA, J. High Energy Phys. 03 (2013) 089; J. High Energy Phys. 07 (2013) 143(E).
[58] [RBC/UKQCD 16] N. Garron, R. J. Hudspith, and A. T. Lytle, Neutral kaon mixing beyond the standard model with $n_f = 2+1$ chiral fermions part 1: Bare matrix elements and physical results, J. High Energy Phys. 11 (2016) 001.
[59] [HPQCD 12A] H. Na, C. T. Davies, E. Follana, G. P. Lepage, and J. Shigemitsu, $|V_{cd}|$ from D meson leptonic decays, Phys. Rev. D **86**, 054510 (2012).
[60] [FNAL/MILC 11] A. Bazavov *et al.*, B- and D-meson decay constants from three-flavor lattice QCD, Phys. Rev. D **85**, 114506 (2012).
[61] [RBC/UKQCD 17] P. A. Boyle, L. Del Debbio, A. Jüttner, A. Khamseh, F. Sanfilippo, and J. T. Tsang, The decay constants $\mathbf{f_D}$ and $\mathbf{f_{D_s}}$ in the continuum limit of $\mathbf{N_f = 2+1}$ domain wall lattice QCD, J. High Energy Phys. 12 (2017) 008.
[62] [HPQCD 10A] C. T. H. Davies, C. McNeile, E. Follana, G. Lepage, H. Na, and J. Shigemitsu, Update: Precision D_s decay constant from full lattice QCD using very fine lattices, Phys. Rev. D **82**, 114504 (2010).
[63] [ETM 17D] V. Lubicz, L. Riggio, G. Salerno, S. Simula, and C. Tarantino, Scalar and vector form factors of

$D \to \pi(K)\ell\nu$ decays with $N_f = 2+1+1$ twisted fermions, Phys. Rev. D **96**, 054514 (2017).
[64] [HPQCD 11] H. Na, C. T. H. Davies, E. Follana, J. Koponen, G. Peter Lepage, and J. Shigemitsu, $D \to \pi\ell\nu$ semileptonic decays, $|V_{cd}|$ and 2nd row unitarity from lattice QCD, Phys. Rev. D **84**, 114505 (2011).
[65] [HPQCD 21A] B. Chakraborty, W. G. Parrott, C. Bouchard, C. T. H. Davies, J. Koponen, and G. P. Lepage, Improved V_{cs} determination using precise lattice QCD form factors for $D \to K\ell\nu$, Phys. Rev. D **104**, 034505 (2021).
[66] [HPQCD 10B] H. Na, C. T. H. Davies, E. Follana, G. P. Lepage, and J. Shigemitsu, The $D \to K\ell\nu$ semileptonic decay scalar form factor and $|V_{cs}|$ from lattice QCD, Phys. Rev. D **82**, 114506 (2010).
[67] [HPQCD 13] R. J. Dowdall, C. Davies, R. Horgan, C. Monahan, and J. Shigemitsu, B-meson decay constants from improved lattice NRQCD and physical u, d, s and c sea quarks, Phys. Rev. Lett. **110**, 222003 (2013).
[68] [HPQCD 17A] C. Hughes, C. T. H. Davies, and C. J. Monahan, New methods for B meson decay constants and form factors from lattice NRQCD, Phys. Rev. D **97**, 054509 (2018).
[69] [HPQCD 11A] C. McNeile, C. T. H. Davies, E. Follana, K. Hornbostel, and G. P. Lepage, High-precision f_{B_s} and HQET from relativistic lattice QCD, Phys. Rev. D **85**, 031503 (2012).
[70] [HPQCD 12] H. Na, C. J. Monahan, C. T. Davies, R. Horgan, G. P. Lepage, and J. Shigemitsu, The B and B_s meson decay constants from lattice QCD, Phys. Rev. D **86**, 034506 (2012).
[71] [RBC/UKQCD 14A] Y. Aoki, T. Ishikawa, T. Izubuchi, C. Lehner, and A. Soni, Neutral B meson mixings and B meson decay constants with static heavy and domain-wall light quarks, Phys. Rev. D **91**, 114505 (2015).
[72] [RBC/UKQCD 14] N. H. Christ, J. M. Flynn, T. Izubuchi, T. Kawanai, C. Lehner *et al.*, B-meson decay constants from $2+1$-flavor lattice QCD with domain-wall light quarks and relativistic heavy quarks, Phys. Rev. D **91**, 054502 (2015).
[73] [ETM 13B] N. Carrasco *et al.*, B-physics from $N_f = 2$ tmQCD: The standard model and beyond, J. High Energy Phys. 03 (2014) 016.
[74] [ALPHA 14] F. Bernardoni *et al.*, Decay constants of B-mesons from non-perturbative HQET with two light dynamical quarks, Phys. Lett. B **735**, 349 (2014).
[75] R. Balasubramamian and B. Blossier, Decay constant of B_s and B_s^* mesons from $N_f = 2$ lattice QCD, Eur. Phys. J. C **80**, 412 (2020).
[76] [RBC/UKQCD 18A] P. A. Boyle, L. Del Debbio, N. Garron, A. Juttner, A. Soni, J. T. Tsang *et al.*, SU(3)-breaking ratios for $D_{(s)}$ and $B_{(s)}$ mesons, arXiv:1812.08791.
[77] [HPQCD 19A] R. J. Dowdall, C. T. H. Davies, R. R. Horgan, G. P. Lepage, C. J. Monahan, J. Shigemitsu *et al.*, Neutral B-meson mixing from full lattice QCD at the physical point, Phys. Rev. D **100**, 094508 (2019).
[78] [HPQCD 09] E. Gamiz, C. T. Davies, G. P. Lepage, J. Shigemitsu, and M. Wingate, Neutral B meson mixing in unquenched lattice QCD, Phys. Rev. D **80**, 014503 (2009).
[79] [FNAL/MILC 16] A. Bazavov *et al.*, $B^0_{(s)}$-mixing matrix elements from lattice QCD for the Standard Model and beyond, Phys. Rev. D **93**, 113016 (2016).
[80] [ALPHA 22] M. Dalla Brida, R. Höllwieser, F. Knechtli, T. Korzec, A. Nada, A. Ramos, S. Sint, and R. Sommer, Determination of $\alpha_s(m_Z)$ by the non-perturbative decoupling method, Eur. Phys. J. C **82**, 1092 (2022).
[81] P. Petreczky and J. H. Weber, Strong coupling constant from moments of quarkonium correlators revisited, Eur. Phys. J. C **82**, 64 (2022).
[82] C. Ayala, X. Lobregat, and A. Pineda, Determination of $\alpha(M_z)$ from an hyperasymptotic approximation to the energy of a static quark-antiquark pair, J. High Energy Phys. 09 (2020) 016.
[83] [TUMQCD 19] A. Bazavov, N. Brambilla, X. Garcia i Tormo, P. Petreczky, J. Soto, A. Vairo, and J. H. Weber, Determination of the QCD coupling from the static energy and the free energy, Phys. Rev. D **100**, 114511 (2019).
[84] S. Cali, K. Cichy, P. Korcyl, and J. Simeth, Running coupling constant from position-space current-current correlation functions in three-flavor lattice QCD, Phys. Rev. Lett. **125**, 242002 (2020).
[85] [ALPHA 17] M. Bruno, M. Dalla Brida, P. Fritzsch, T. Korzec, A. Ramos, S. Schaefer, H. Simma, S. Sint, and R. Sommer, QCD coupling from a nonperturbative determination of the three-flavor Λ parameter, Phys. Rev. Lett. **119**, 102001 (2017).
[86] [PACS-CS 09A] S. Aoki *et al.*, Precise determination of the strong coupling constant in $N_f = 2+1$ lattice QCD with the Schrödinger functional scheme, J. High Energy Phys. 10 (2009) 053.
[87] K. Maltman, D. Leinweber, P. Moran, and A. Sternbeck, The realistic lattice determination of $\alpha_s(M_Z)$ revisited, Phys. Rev. D **78**, 114504 (2008).
[88] [CalLat 18] C. C. Chang *et al.*, A percent-level determination of the nucleon axial coupling from quantum chromodynamics, Nature (London) **558**, 91 (2018).
[89] [CalLat 19] A. Walker-Loud *et al.*, Lattice QCD determination of g_A, Proc. Sci., CD2018 (**2020**) 020 [arXiv:1912.08321].
[90] [PNDME 23] Y.-C. Jang, R. Gupta, T. Bhattacharya, B. Yoon, and H.-W. Lin, Nucleon isovector axial form factors, Phys. Rev. D **109**, 014503 (2024).
[91] [ETM 23] C. Alexandrou, S. Bacchio, M. Constantinou, J. Finkenrath, R. Frezzotti, B. Kostrzewa, G. Koutsou, G. Spanoudes, and C. Urbach, Nucleon axial and pseudoscalar form factors using twisted-mass fermion ensembles at the physical point, Phys. Rev. D **109**, 034503 (2024).
[92] [χQCD 18] J. Liang, Y.-B. Yang, T. Draper, M. Gong, and K.-F. Liu (, Quark spins and anomalous ward identity, Phys. Rev. D **98**, 074505 (2018).
[93] [NME 21] S. Park, R. Gupta, B. Yoon, S. Mondal, T. Bhattacharya, Y.-C. Jang *et al.*, Precision nucleon charges and form factors using $2+1$-flavor lattice QCD, Phys. Rev. D **105**, 054505 (2022).
[94] [QCDSF/UKQCD/CSSM 23] R. E. Smail *et al.*, Constraining beyond the Standard Model nucleon isovector charges, Phys. Rev. D **108**, 094511 (2023).
[95] [RQCD 23] G. S. Bali, S. Collins, S. Heybrock, M. Löffler, R. Rödl, W. Söldner, and S. Weishäupl, Octet baryon

isovector charges from $N_f = 2 + 1$ lattice QCD, Phys. Rev. D **108**, 034512 (2023).
[96] [Mainz 24] D. Djukanovic, G. von Hippel, H. B. Meyer, K. Ottnad, and H. Wittig, Improved analysis of isovector nucleon matrix elements with $N_f = 2 + 1$ flavors of $O(a)$ improved Wilson fermions, Phys. Rev. D **109**, 074507 (2024).
[97] [χQCD 21A] L. Liu, T. Chen, T. Draper, J. Liang, K.-F. Liu, G. Wang *et al.*, Nucleon isovector scalar charge from overlap fermions, Phys. Rev. D **104**, 094503 (2021).
[98] [ETM 22] C. Alexandrou *et al.*, Moments of the nucleon transverse quark spin densities using lattice QCD, Phys. Rev. D **107**, 054504 (2023).
[99] [PNDME 18A] H.-W. Lin, R. Gupta, B. Yoon, Y.-C. Jang, and T. Bhattacharya, Quark contribution to the proton spin from $2 + 1 + 1$-flavor lattice QCD, Phys. Rev. D **98**, 094512 (2018).
[100] [PNDME 18B] R. Gupta, B. Yoon, T. Bhattacharya, V. Cirigliano, Y.-C. Jang, and H.-W. Lin, Flavor diagonal tensor charges of the nucleon from $(2 + 1 + 1)$-flavor lattice QCD, Phys. Rev. D **98**, 091501 (2018).
[101] [PNDME 21] R. Gupta, S. Park, M. Hoferichter, E. Mereghetti, B. Yoon, and T. Bhattacharya, Pion—nucleon sigma term from lattice QCD, Phys. Rev. Lett. **127**, 242002 (2021).
[102] [BMW 11A] S. Dürr *et al.*, Sigma term and strangeness content of octet baryons, Phys. Rev. D **85**, 014509 (2012); Phys. Rev. D **93**, 039905(E) (2016).
[103] [BMW 15] S. Dürr *et al.*, Lattice computation of the nucleon scalar quark contents at the physical point, Phys. Rev. Lett. **116**, 172001 (2016).
[104] [χQCD 15A] Y.-B. Yang, A. Alexandru, T. Draper, J. Liang, and K.-F. Liu, πN and strangeness sigma terms at the physical point with chiral fermions, Phys. Rev. D **94**, 054503 (2016).
[105] [RQCD 22] G. S. Bali, S. Collins, P. Georg, D. Jenkins, P. Korcyl, A. Schäfer, E E. Scholz, J. Simeth, W. Söldner, and S. Weishäupl, Scale setting and the light baryon spectrum in $N_f = 2 + 1$ QCD with Wilson fermions, J. High Energy Phys. 05 (2023) 035.
[106] [Mainz 23] A. Agadjanov, D. Djukanovic, G. von Hippel, H. B. Meyer, K. Ottnad, and H. Wittig, Nucleon sigma terms with $N_f = 2 + 1$ flavors of $O(a)$-improved Wilson fermions, Phys. Rev. Lett. **131**, 261902 (2023).
[107] [MILC 12C] W. Freeman and D. Toussaint, Intrinsic strangeness and charm of the nucleon using improved staggered fermions, Phys. Rev. D **88**, 054503 (2013).
[108] P. Junnarkar and A. Walker-Loud, Scalar strange content of the nucleon from lattice QCD, Phys. Rev. D **87**, 114510 (2013).
[109] [PNDME 20A] S. Mondal, R. Gupta, S. Park, B. Yoon, T. Bhattacharya, and H.-W. Lin, Moments of nucleon isovector structure functions in $2 + 1 + 1$-flavor QCD, Phys. Rev. D **102**, 054512 (2020).
[110] [PNDME 20A] S. Mondal, R. Gupta, S. Park, B. Yoon, T. Bhattacharya, B. Joó, and F. Winter, Nucleon momentum fraction, helicity and transversity from $2 + 1$-flavor lattice QCD, J. High Energy Phys. 04 (2020) 004.
[111] [χQCD 18A] Y.-B. Yang, J. Liang, Y.-J. Bi, Y. Chen, T. Draper, K.-F. Liu, and Z. Liu, Proton mass decomposition from the QCD energy momentum tensor, Phys. Rev. Lett. **121**, 212001 (2018).
[112] [CalLat 20A] N. Miller *et al.*, Scale setting the Möbius domain wall fermion on gradient-flowed HISQ action using the omega baryon mass and the gradient-flow scales t_0 and w_0, Phys. Rev. D **103**, 054511 (2021).
[113] [MILC 15] A. Bazavov *et al.*, Gradient flow and scale setting on MILC HISQ ensembles, Phys. Rev. D **93**, 094510 (2016).
[114] [CLS 16] M. Bruno, T. Korzec, and S. Schaefer, Setting the scale for the CLS $2 + 1$ flavor ensembles, Phys. Rev. D **95**, 074504 (2017).
[115] [BMW 12A] S. Borsanyi, S. Dürr, Z. Fodor, C. Hoelbling, S. D. Katz *et al.*, High-precision scale setting in lattice QCD, J. High Energy Phys. 09 (2012) 010.
[116] [BMW 20] Sz. Borsanyi *et al.*, Leading hadronic contribution to the muon magnetic moment from lattice QCD, Nature (London) **593**, 51 (2021).
[117] [HotQCD 14] A. Bazavov *et al.*, Equation of state in $(2 + 1)$-flavor QCD, Phys. Rev. D **90**, 094503 (2014).
[118] [TUMQCD 22] N. Brambilla, R. L. Delgado, A. S. Kronfeld, V. Leino, P. Petreczky, S. Steinbeißer, A. Vairo, and J. H. Weber, Static energy in $(2 + 1 + 1)$-flavor lattice QCD: Scale setting and charm effects, Phys. Rev. D **107**, 074503 (2023).
[119] [RBC/UKQCD 10A] Y. Aoki *et al.*, Continuum limit physics from $2 + 1$ flavor domain wall QCD, Phys. Rev. D **83**, 074508 (2011).
[120] [HPQCD 05B] A. Gray *et al.*, The upsilon spectrum and m_b from full lattice QCD, Phys. Rev. D **72**, 094507 (2005).
[121] C. Aubin *et al.*, Light hadrons with improved staggered quarks: Approaching the continuum limit, Phys. Rev. D **70**, 094505 (2004).
[122] [HPQCD 09B] C. T. H. Davies, E. Follana, I. Kendall, G. P. Lepage, and C. McNeile, Precise determination of the lattice spacing in full lattice QCD, Phys. Rev. D **81**, 034506 (2010).
[123] [FNAL/MILC 22] A. Bazavov *et al.*, D-meson semileptonic decays to pseudoscalars from four-flavor lattice QCD, Phys. Rev. D **107**, 094516 (2023).
[124] [FNAL/MILC 15] J. A. Bailey *et al.*, $|V_{ub}|$ from $B \to \pi \ell \nu$ decays and $(2 + 1)$-flavor lattice QCD, Phys. Rev. D **92**, 014024 (2015).
[125] [RBC/UKQCD 15] J. M. Flynn, T. Izubuchi, T. Kawanai, C. Lehner, A. Soni, R. S. Van de Water, and O. Witzel, $B \to \pi \ell \nu$ and $B_s \to K \ell \nu$ form factors and $|V_{ub}|$ from $2 + 1$-flavor lattice QCD with domain-wall light quarks and relativistic heavy quarks, Phys. Rev. D **91**, 074510 (2015).
[126] [JLQCD 22] B. Colquhoun, S. Hashimoto, T. Kaneko, and J. Koponen, Form factors of $B \to \pi \ell \nu$ and a determination of $|V_{ub}|$ with Möbius domain-wall fermions, Phys. Rev. D **106**, 054502 (2022).
[127] [HPQCD 14] C. M. Bouchard, G. P. Lepage, C. Monahan, H. Na, and J. Shigemitsu, $B_s \to K \ell \nu$ form factors from lattice QCD, Phys. Rev. D **90**, 054506 (2014).
[128] [RBC/UKQCD 23] J. M. Flynn, R. C. Hill, A. Jüttner, A. Soni, J. T. Tsang, and O. Witzel, Exclusive semileptonic $B_s \to K \ell \nu$ decays on the lattice, Phys. Rev. D **107**, 114512 (2023).

[129] [FNAL/MILC 15E] J. A. Bailey *et al.*, $B \to \pi \ell \ell$ form factors for new-physics searches from lattice QCD, Phys. Rev. Lett. **115**, 152002 (2015).

[130] [HPQCD 13E] C. Bouchard, G. P. Lepage, C. Monahan, H. Na, and J. Shigemitsu, Rare decay $B \to K \ell^+ \ell^-$ form factors from lattice QCD, Phys. Rev. D **88**, 054509 (2013); Phys. Rev. D **88**, 079901(E) (2013).

[131] [FNAL/MILC 15D] J. A. Bailey *et al.*, $B \to K l^+ l^-$ decay form factors from three-flavor lattice QCD, Phys. Rev. D **93**, 025026 (2016).

[132] [FNAL/MILC 15C] J. A. Bailey *et al.*, $B \to D \ell \nu$ form factors at nonzero recoil and $|V_{cb}|$ from $2+1$-flavor lattice QCD, Phys. Rev. D **92**, 034506 (2015).

[133] [HPQCD 15] H. Na, C. M. Bouchard, G. P. Lepage, C. Monahan, and J. Shigemitsu, $B \to D \ell \nu$ form factors at nonzero recoil and extraction of $|V_{cb}|$, Phys. Rev. D **92**, 054510 (2015).

[134] [HPQCD 19] E. McLean, C. T. H. Davies, J. Koponen, and A. T. Lytle, $B_s \to D_s \ell \nu$ form factors for the full q^2 range from lattice QCD with non-perturbatively normalized currents, Phys. Rev. D **101**, 074513 (2020).

[135] [HPQCD 23] J. Harrison and C. T. H. Davies, $B \to D^*$ and $B_s \to D_s^*$ vector, axial-vector and tensor form factors for the full q^2 range from lattice QCD, Phys. Rev. D **109**, 094515 (2024).

[136] [FNAL/MILC 21] A. Bazavov *et al.*, Semileptonic form factors for $B \to D^* \ell \nu$ at nonzero recoil from $2+1$-flavor lattice QCD, Eur. Phys. J. C **82**, 1141 (2022); Eur. Phys. J. C **83**, 21(E) (2023).

[137] [JLQCD 23] Y. Aoki, B. Colquhoun, H. Fukaya, S. Hashimoto, T. Kaneko, R. Kellermann, J. Koponen, and E. Kou, $B \to D^* \ell \nu_\ell$ semileptonic form factors from lattice QCD with Möbius domain-wall quarks, Phys. Rev. D **109**, 074503 (2024).

[138] *BABAR* Collaboration, Study of $B \to \pi \ell \nu$ and $B \to \rho \ell \nu$ decays and determination of $|V_{ub}|$, Phys. Rev. D **83**, 032007 (2011).

[139] *BABAR* Collaboration, Branching fraction and form-factor shape measurements of exclusive charmless semileptonic B decays, and determination of $|V_{ub}|$, Phys. Rev. D **86**, 092004 (2012).

[140] Belle Collaboration, Measurement of the decay $B^0 \to \pi^- \ell^+ \nu$ and determination of $|V_{ub}|$, Phys. Rev. D **83**, 071101 (2011).

[141] Belle Collaboration, Study of exclusive $B \to X_u \ell \nu$ decays and extraction of $\|V_{ub}\|$ using full reconstruction tagging at the Belle experiment, Phys. Rev. D **88**, 032005 (2013).

[142] *BABAR* Collaboration, Measurement of $|V_{cb}|$ and the form-factor slope in $\bar{B} \to D \ell^- \bar{\nu}_\ell$ decays in events tagged by a fully reconstructed B meson, Phys. Rev. Lett. **104**, 011802 (2010).

[143] Belle Collaboration, Measurement of the decay $B \to D \ell \nu_\ell$ in fully reconstructed events and determination of the Cabibbo-Kobayashi-Maskawa matrix element $|V_{cb}|$, Phys. Rev. D **93**, 032006 (2016).

[144] Belle Collaboration, Measurement of the CKM matrix element $|V_{cb}|$ from $B^0 \to D^{*-} \ell^+ \nu_\ell$ at Belle, Phys. Rev. D **100**, 052007 (2019); Phys. Rev. D **103**, 079901(E) (2021).

[145] Belle Collaboration, Measurement of differential distributions of $B \to D^* \ell \bar{\nu}_\ell$ and implications on $|V_{cb}|$, Phys. Rev. D **108**, 012002 (2023).

[146] Belle-II Collaboration, Determination of $|V_{cb}|$ using $\bar{B}^0 \to D^{*,+} \ell^- \bar{\nu}_\ell$ decays with Belle II, Phys. Rev. D **108**, 092013 (2023).

[147] Belle-II Collaboration, Measurement of the semileptonic $\bar{B}^0 \to D^{*+} \ell^- \nu_\ell$ branching fraction with fully reconstructed B meson decays and 34.6 fb^{-1} of Belle II data, arXiv:2008.10299.

[148] HFLAV Collaboration, Averages of b-hadron, c-hadron, and τ-lepton properties as of 2021, Phys. Rev. D **107**, 052008 (2023).

[149] K. Symanzik, Continuum limit and improved action in lattice theories. 1. Principles and ϕ^4 theory, Nucl. Phys. **B226**, 187 (1983).

[150] K. Symanzik, Continuum limit and improved action in lattice theories. 2. O(N) nonlinear sigma model in perturbation theory, Nucl. Phys. **B226**, 205 (1983).

[151] [RBC 07A] D. J. Antonio *et al.*, Localization and chiral symmetry in 3 flavor domain wall QCD, Phys. Rev. D **77**, 014509 (2008).

[152] [MILC 10] A. Bazavov *et al.*, Topological susceptibility with the asqtad action, Phys. Rev. D **81**, 114501 (2010).

[153] [ALPHA 10C] S. Schaefer, R. Sommer, and F. Virotta, Critical slowing down and error analysis in lattice QCD simulations, Nucl. Phys. **B845**, 93 (2011).

[154] M. Lüscher, Topology, the Wilson flow, and the HMC algorithm, Proc. Sci., LATTICE2010 (**2010**) 015 [arXiv:1009.5877].

[155] S. Schaefer, Algorithms for lattice QCD: Progress and challenges, AIP Conf. Proc. **1343**, 93 (2011).

[156] A. Chowdhury, A. Harindranath, J. Maiti, and P. Majumdar, Topological susceptibility in lattice Yang-Mills theory with open boundary condition, J. High Energy Phys. 02 (2014) 045.

[157] [LSD 14] R. C. Brower *et al.*, Maximum-likelihood approach to topological charge fluctuations in lattice gauge theory, Phys. Rev. D **90**, 014503 (2014).

[158] [JLQCD 15] H. Fukaya, S. Aoki, G. Cossu, S. Hashimoto, T. Kaneko, and J. Noaki, η' meson mass from topological charge density correlator in QCD, Phys. Rev. D **92**, 111501 (2015).

[159] L. Del Debbio, H. Panagopoulos, and E. Vicari, Theta dependence of SU(N) gauge theories, J. High Energy Phys. 08 (2002) 044.

[160] C. Bernard *et al.*, Topological susceptibility with the improved Asqtad action, Phys. Rev. D **68**, 114501 (2003).

[161] M. Lüscher and S. Schaefer, Lattice QCD without topology barriers, J. High Energy Phys. 07 (2011) 036.

[162] C. Bonanno, G. Clemente, M. D'Elia, L. Maio, and L. Parente, Full QCD with milder topological freezing, J. High Energy Phys. 08 (2024) 236.

[163] M. G. Endres, R. C. Brower, W. Detmold, K. Orginos, and A. V. Pochinsky, Multiscale Monte Carlo equilibration: Pure Yang-Mills theory, Phys. Rev. D **92**, 114516 (2015).

[164] W. Detmold and M. G. Endres, Scaling properties of multiscale equilibration, Phys. Rev. D **97**, 074507 (2018).

[165] S. Mages, B. C. Toth, S. Borsanyi, Z. Fodor, S. Katz, and K. K. Szabo, Lattice QCD on non-orientable manifolds, Phys. Rev. D **95**, 094512 (2017).
[166] A. Francis, P. Fritzsch, M. Lüscher, and A. Rago, Master-field simulations of O(a)-improved lattice QCD: Algorithms, stability and exactness, Comput. Phys. Commun. **255**, 107355 (2020).
[167] P. Fritzsch, J. Bulava, M. Cè, A. Francis, M. Lüscher, and A. Rago, Master-field simulations of QCD, Proc. Sci., LATTICE2021 (**2022**) 465 [arXiv:2111.11544].
[168] M. Lüscher, Trivializing maps, the Wilson flow, and the HMC algorithm, Commun. Math. Phys. **293**, 899 (2010).
[169] M. S. Albergo, G. Kanwar, and P. E. Shanahan, Flow-based generative models for Markov Chain Monte Carlo in lattice field theory, Phys. Rev. D **100**, 034515 (2019).
[170] G. Kanwar, M. S. Albergo, D. Boyda, K. Cranmer, D. C. Hackett, S. Racanière, D. J. Rezende, and P. E. Shanahan, Equivariant flow-based sampling for lattice gauge theory, Phys. Rev. Lett. **125**, 121601 (2020).
[171] D. Boyda, G. Kanwar, S. Racanière, D. J. Rezende, M. S. Albergo, K. Cranmer, D. C. Hackett, and P. E. Shanahan, Sampling using $SU(N)$ gauge equivariant flows, Phys. Rev. D **103**, 074504 (2021).
[172] M. Gerdes, P. de Haan, C. Rainone, R. Bondesan, and M. C. N. Cheng, Learning lattice quantum field theories with equivariant continuous flows, SciPost Phys. **15**, 238 (2023).
[173] S. Bacchio, P. Kessel, S. Schaefer, and L. Vaitl, Learning trivializing gradient flows for lattice gauge theories, Phys. Rev. D **107**, L051504 (2023).
[174] R. Abbott *et al.*, Normalizing flows for lattice gauge theory in arbitrary space-time dimension, arXiv:2305.02402.
[175] K. Holland, A. Ipp, D. I. Müller, and U. Wenger, Machine learning a fixed point action for SU(3) gauge theory with a gauge equivariant convolutional neural network, Phys. Rev. D **110**, 074502 (2024).
[176] R. Brower, S. Chandrasekharan, J. W. Negele, and U. Wiese, QCD at fixed topology, Phys. Lett. B **560**, 64 (2003).
[177] S. Aoki, H. Fukaya, S. Hashimoto, and T. Onogi, Finite volume QCD at fixed topological charge, Phys. Rev. D **76**, 054508 (2007).
[178] I. Bautista, W. Bietenholz, A. Dromard, U. Gerber, L. Gonglach, C. P. Hofmann, H. Mejía-Díaz, and M. Wagner, Measuring the topological susceptibility in a fixed sector, Phys. Rev. D **92**, 114510 (2015).
[179] W. Bietenholz, C. Czaban, A. Dromard, U. Gerber, C. P. Hofmann, H. Mejía-Díaz, and M. Wagner, Interpreting numerical measurements in fixed topological sectors, Phys. Rev. D **93**, 114516 (2016).
[180] C. Bernard and D. Toussaint, Effects of nonequilibrated topological charge distributions on pseudoscalar meson masses and decay constants, Phys. Rev. D **97**, 074502 (2018).
[181] S. Duane, A. D. Kennedy, B. J. Pendleton, and D. Roweth, Hybrid Monte Carlo, Phys. Lett. B **195**, 216 (1987).
[182] M. A. Clark and A. D. Kennedy, Accelerating staggered fermion dynamics with the rational hybrid Monte Carlo (RHMC) algorithm, Phys. Rev. D **75**, 011502 (2007).
[183] [MILC 12B] A. Bazavov *et al.*, Lattice QCD ensembles with four flavors of highly improved staggered quarks, Phys. Rev. D **87**, 054505 (2013).
[184] G. Colangelo, S. Dürr, and C. Haefeli, Finite volume effects for meson masses and decay constants, Nucl. Phys. **B721**, 136 (2005).
[185] [BMW 14] Sz. Borsanyi *et al.*, Ab initio calculation of the neutron-proton mass difference, Science **347**, 1452 (2015).
[186] Z. Davoudi and M. J. Savage, Finite-volume electromagnetic corrections to the masses of mesons, baryons and nuclei, Phys. Rev. D **90**, 054503 (2014).
[187] V. Lubicz, G. Martinelli, C. T. Sachrajda, F. Sanfilippo, S. Simula, and N. Tantalo, Finite-volume QED corrections to decay amplitudes in lattice QCD, Phys. Rev. D **95**, 034504 (2017).
[188] Z. Davoudi, J. Harrison, A. Jüttner, A. Portelli, and M. J. Savage, Theoretical aspects of quantum electrodynamics in a finite volume with periodic boundary conditions, Phys. Rev. D **99**, 034510 (2019).
[189] [ETM 07A] Ph. Boucaud *et al.*, Dynamical twisted mass fermions with light quarks, Phys. Lett. B **650**, 304 (2007).
[190] [ETM 09C] R. Baron *et al.*, Light meson physics from maximally twisted mass lattice QCD, J. High Energy Phys. 08 (2010) 097.
[191] O. Bär, Chiral logs in twisted mass lattice QCD with large isospin breaking, Phys. Rev. D **82**, 094505 (2010).
[192] S. Dürr, Theoretical issues with staggered fermion simulations, Proc. Sci., LAT2005 (**2006**) 021 [arXiv:hep-lat/0509026].
[193] S. R. Sharpe, Rooted staggered fermions: Good bad or ugly?, Proc. Sci., LAT2006 (**2006**) 022 [arXiv:hep-lat/0610094].
[194] A. S. Kronfeld, Lattice gauge theory with staggered fermions: How, where, and why (not), Proc. Sci., LAT2007 (**2007**) 016 [arXiv:0711.0699].
[195] M. Golterman, QCD with rooted staggered fermions, Proc. Sci., CONFINEMENT8 (**2008**) 014 [arXiv:0812.3110].
[196] [MILC 09] A. Bazavov *et al.*, Full nonperturbative QCD simulations with $2+1$ flavors of improved staggered quarks, Rev. Mod. Phys. **82**, 1349 (2010).
[197] N. Brambilla, V. Leino, J. Mayer-Steudte, and A. Vairo, Static force from generalized Wilson loops on the lattice using the gradient flow, Phys. Rev. D **109**, 114517 (2024).
[198] [ALPHA 14A] M. Bruno, J. Finkenrath, F. Knechtli, B. Leder, and R. Sommer, Effects of heavy sea quarks at low energies, Phys. Rev. Lett. **114**, 102001 (2015).
[199] [ALPHA 17A] F. Knechtli, T. Korzec, B. Leder, and G. Moir, Power corrections from decoupling of the charm quark, Phys. Lett. B **774**, 649 (2017).
[200] A. Athenodorou, J. Finkenrath, F. Knechtli, T. Korzec, B. Leder, M. K. Marinkovic *et al.*, How perturbative are heavy sea quarks?, Nucl. Phys. **B943**, 114612 (2019).
[201] S. Cali, F. Knechtli, and T. Korzec, How much do charm sea quarks affect the charmonium spectrum?, Eur. Phys. J. C **79**, 607 (2019).
[202] [ALPHA 21A] S. Cali, K. Eckert, J. Heitger, F. Knechtli, and T. Korzec, Charm sea effects on charmonium decay constants and heavy meson masses, Eur. Phys. J. C **81**, 733 (2021).

[203] M. Schmelling, Averaging correlated data, Phys. Scr. **51**, 676 (1995).
[204] J. L. Rosner, S. Stone, and R. S. Van de Water, Leptonic decays of charged pseudoscalar mesons, in review of particle physics [243] 2015 update, arXiv:1509.02220.
[205] Particle Data Group, Review of particle physics, Prog. Theor. Exp. Phys. **2022**, 083C01 (2022).
[206] T. Aoyama *et al.*, The anomalous magnetic moment of the muon in the standard model, Phys. Rep. **887**, 1 (2020).
[207] N. Tantalo, Matching lattice QC + ED to Nature, Proc. Sci., LATTICE2022 (**2023**) 249 [arXiv:2301.02097].
[208] J. Gasser and H. Leutwyler, Quark masses, Phys. Rep. **87**, 77 (1982).
[209] J. Gasser, A. Rusetsky, and I. Scimemi, Electromagnetic corrections in hadronic processes, Eur. Phys. J. C **32**, 97 (2003).
[210] J. Gasser and G. R. S. Zarnauskas, On the pion decay constant, Phys. Lett. B **693**, 122 (2010).
[211] [BMW 13A] Sz. Borsanyi *et al.*, Isospin splittings in the light baryon octet from lattice QCD and QED, Phys. Rev. Lett. **111**, 252001 (2013).
[212] [RM123 13] G. M. de Divitiis, R. Frezzotti, V. Lubicz, G. Martinelli, R. Petronzio, G. C. Rossi, F. Sanfilippo, S. Simula, and N. Tantalo, Leading isospin breaking effects on the lattice, Phys. Rev. D **87**, 114505 (2013).
[213] N. Tantalo, Isospin breaking effects on the lattice, Proc. Sci., LATTICE2013 (**2014**) 007 [arXiv:1311.2797].
[214] A. Portelli, Inclusion of isospin breaking effects in lattice simulations, Proc. Sci., LATTICE2014 (**2015**) 013 [arXiv:1505.07057].
[215] [QCDSF/UKQCD 15A] R. Horsley *et al.*, QED effects in the pseudoscalar meson sector, J. High Energy Phys. 04 (2016) 093.
[216] A. Bussone *et al.*, On the definition of schemes for computing leading order isospin breaking corrections, Proc. Sci., LATTICE2018 (**2018**) 293 [arXiv:1810.11647].
[217] M. Di Carlo, D. Giusti, V. Lubicz, G. Martinelli, C. Sachrajda, F. Sanfilippo, S. Simula, and N. Tantalo, Light-meson leptonic decay rates in lattice QCD+QED, Phys. Rev. D **100**, 034514 (2019).
[218] C. T. Sachrajda, Isospin breaking in lattice QCD computations of decay amplitudes, Acta Phys. Pol. B **52**, 175 (2021).
[219] M. Cè *et al.*, Window observable for the hadronic vacuum polarization contribution to the muon g-2 from lattice QCD, Phys. Rev. D **106**, 114502 (2022).
[220] P. Boyle *et al.*, Isospin-breaking corrections to light-meson leptonic decays from lattice simulations at physical quark masses, J. High Energy Phys. 02 (2023) 242.
[221] A. Boccaletti *et al.*, High precision calculation of the hadronic vacuum polarization contribution to the muon anomaly, arXiv:2407.10913.
[222] [RM123 11] G. M. de Divitiis, P. Dimopoulos, R. Frezzotti, V. Lubicz, G. Martinelli *et al.*, Isospin breaking effects due to the up-down mass difference in lattice QCD, J. High Energy Phys. 04 (2012) 124.
[223] D. Giusti, V. Lubicz, G. Martinelli, C. T. Sachrajda, F. Sanfilippo, S. Simula, and N. Tantalo, First lattice calculation of the QED corrections to leptonic decay rates, Phys. Rev. Lett. **120**, 072001 (2018).
[224] A. Portelli, Estimation of scheme ambiguities in the separation of isospin-breaking effects in lattice QCD calculations, Lattice 2022, 2022, https://indico.hiskp.uni-bonn.de/event/40/contributions/542/.
[225] Particle Data Group, Review of particle physics, Prog. Theor. Exp. Phys. **2020**, 083C01 (2020).
[226] [ALPHA 20] R. Höllwieser, F. Knechtli, and T. Korzec, Scale setting for $N_f = 3 + 1$ QCD, Eur. Phys. J. C **80**, 349 (2020).
[227] P. A. Baikov, K. G. Chetyrkin, and J. H. Kühn, Quark mass and field anomalous dimensions to $\mathcal{O}(\alpha_s^5)$, J. High Energy Phys. 10 (2014) 076.
[228] M. Gell-Mann, R. J. Oakes, and B. Renner, Behavior of current divergences under SU(3) × SU(3), Phys. Rev. **175**, 2195 (1968).
[229] [RBC/UKQCD 12] R. Arthur *et al.*, Domain wall QCD with near-physical pions, Phys. Rev. D **87**, 094514 (2013).
[230] Y. Maezawa and P. Petreczky, Quark masses and strong coupling constant in 2 + 1 flavor QCD, Phys. Rev. D **94**, 034507 (2016).
[231] [PACS-CS 12] S. Aoki, K.-I. Ishikawa, N. Ishizuka, K. Kanaya, Y. Kuramashi *et al.*, 1 + 1 + 1 flavor QCD + QED simulation at the physical point, Phys. Rev. D **86**, 034507 (2012).
[232] [PACS-CS 10] S. Aoki *et al.*, Non-perturbative renormalization of quark mass in $N_f = 2 + 1$ QCD with the Schrödinger functional scheme, J. High Energy Phys. 08 (2010) 101.
[233] T. Blum *et al.*, Electromagnetic mass splittings of the low lying hadrons and quark masses from 2 + 1 flavor lattice QCD + QED, Phys. Rev. D **82**, 094508 (2010).
[234] [PACS-CS 09] S. Aoki *et al.*, Physical point simulation in 2 + 1 flavor lattice QCD, Phys. Rev. D **81**, 074503 (2010).
[235] [PACS-CS 08] S. Aoki *et al.*, 2 + 1 flavor lattice QCD toward the physical point, Phys. Rev. D **79**, 034503 (2009).
[236] [RBC/UKQCD 08] C. Allton *et al.*, Physical results from 2 + 1 flavor domain wall QCD and SU(2) chiral perturbation theory, Phys. Rev. D **78**, 114509 (2008).
[237] [CP-PACS/JLQCD 07] T. Ishikawa *et al.*, Light quark masses from unquenched lattice QCD, Phys. Rev. D **78**, 011502 (2008).
[238] [HPQCD 05] Q. Mason, H. D. Trottier, R. Horgan, C. T. H. Davies, and G. P. Lepage, High-precision determination of the light-quark masses from realistic lattice QCD, Phys. Rev. D **73**, 114501 (2006).
[239] [MILC 04] C. Aubin, C. Bernard, C. DeTar, J. Osborn, Steven Gottlieb, E. B. Gregory, D. Toussaint, U. M. Heller, J. E. Hetrick, and R. Sugar, Light pseudoscalar decay constants, quark masses and low energy constants from three-flavor lattice QCD, Phys. Rev. D **70**, 114501 (2004).
[240] [HPQCD/MILC/UKQCD 04] C. Aubin *et al.*, First determination of the strange and light quark masses from full lattice QCD, Phys. Rev. D **70**, 031504 (2004).
[241] T. van Ritbergen, J. A. M. Vermaseren, and S. A. Larin, The four-loop β-function in quantum chromodynamics, Phys. Lett. B **400**, 379 (1997).

[242] K. G. Chetyrkin and A. Retey, Renormalization and running of quark mass and field in the regularization invariant and $\overline{\text{MS}}$ schemes at three and four loops, Nucl. Phys. **B583**, 3 (2000).

[243] Particle Data Group, Review of particle physics, Chin. Phys. C **38**, 090001 (2014) and 2015 update.

[244] [HPQCD 08B] I. Allison *et al.*, High-precision charm-quark mass from current-current correlators in lattice and continuum QCD, Phys. Rev. D **78**, 054513 (2008).

[245] M. Bruno *et al.*, Simulation of QCD with $N_f = 2 + 1$ flavors of non-perturbatively improved Wilson fermions, J. High Energy Phys. 02 (2015) 043.

[246] [ALPHA 18C] I. Campos, P. Fritzsch, C. Pena, D. Preti, A. Ramos, and A. Vladikas, Non-perturbative quark mass renormalisation and running in $N_f = 3$ QCD, Eur. Phys. J. C **78**, 387 (2018).

[247] C. A. Dominguez, N. F. Nasrallah, R. Röntsch, and K. Schilcher, Light quark masses from QCD sum rules with minimal hadronic bias, Nucl. Phys. B, Proc. Suppl. **186**, 133 (2009).

[248] K. G. Chetyrkin and A. Khodjamirian, Strange quark mass from pseudoscalar sum rule with $O(\alpha_s^4)$ accuracy, Eur. Phys. J. C **46**, 721 (2006).

[249] M. Jamin, J. A. Oller, and A. Pich, Scalar $K\pi$ form factor and light quark masses, Phys. Rev. D **74**, 074009 (2006).

[250] S. Narison, Strange quark mass from e^+e^- revisited and present status of light quark masses, Phys. Rev. D **74**, 034013 (2006).

[251] A. I. Vainshtein *et al.*, Sum rules for light quarks in quantum chromodynamics, Sov. J. Nucl. Phys. **27**, 274 (1978).

[252] K. Maltman and J. Kambor, $m_u + m_d$ from isovector pseudoscalar sum rules, Phys. Lett. B **517**, 332 (2001).

[253] J. A. Oller and L. Roca, Non-perturbative study of the light pseudoscalar masses in chiral dynamics, Eur. Phys. J. A **34**, 371 (2007).

[254] R. Kaiser, The η and the η' at large N_c, diploma work, University of Bern, 1997; H. Leutwyler, On the 1/N-expansion in chiral perturbation theory, Nucl. Phys. B, Proc. Suppl. **64**, 223 (1998).

[255] H. Leutwyler, The ratios of the light quark masses, Phys. Lett. B **378**, 313 (1996).

[256] S. Weinberg, The problem of mass, Trans. N.Y. Acad. Sci. **38**, 185 (1977).

[257] R. F. Dashen, Chiral $\text{SU}(3) \times \text{SU}(3)$ as a symmetry of the strong interactions, Phys. Rev. **183**, 1245 (1969).

[258] [MILC 16] S. Basak *et al.*, Electromagnetic effects on the light pseudoscalar mesons and determination of m_u/m_d, Proc. Sci., LATTICE2015 (**2016**) 259 [arXiv:1606.01228].

[259] [QCDSF/UKQCD 15] R. Horsley *et al.*, Isospin splittings of meson and baryon masses from three-flavor lattice QCD + QED, J. Phys. G **43**, 10LT02 (2016).

[260] [ALPHA 05] M. Della Morte *et al.*, Non-perturbative quark mass renormalization in two-flavor QCD, Nucl. Phys. **B729**, 117 (2005).

[261] H. Leutwyler, Light quark masses, Proc. Sci., CD09 (**2009**) 005 [arXiv:0911.1416].

[262] [RBC 07] T. Blum, T. Doi, M. Hayakawa, T. Izubuchi, and N. Yamada, Determination of light quark masses from the electromagnetic splitting of pseudoscalar meson masses computed with two flavors of domain wall fermions, Phys. Rev. D **76**, 114508 (2007).

[263] M. Hayakawa and S. Uno, QED in finite volume and finite size scaling effect on electromagnetic properties of hadrons, Prog. Theor. Phys. **120**, 413 (2008).

[264] [ETM 10] R. Baron *et al.*, Light hadrons from lattice QCD with light (u, d), strange and charm dynamical quarks, J. High Energy Phys. 06 (2010) 111.

[265] J. Bijnens and N. Danielsson, Electromagnetic corrections in partially quenched chiral perturbation theory, Phys. Rev. D **75**, 014505 (2007).

[266] [BMW 12] A. Portelli, S. Dürr, Z. Fodor, J. Frison, C. Hoelbling *et al.*, Systematic errors in partially-quenched QCD plus QED lattice simulations, Proc. Sci., LAT2011 (**2011**) 136 [arXiv:1201.2787].

[267] J. Gasser and H. Leutwyler, $\eta \to 3\pi$ to one loop, Nucl. Phys. **B250**, 539 (1985).

[268] G. Colangelo, S. Lanz, H. Leutwyler, and E. Passemar, Dispersive analysis of $\eta \to 3\pi$, Eur. Phys. J. C **78**, 947 (2018).

[269] G. Amoros, J. Bijnens, and P. Talavera, QCD isospin breaking in meson masses, decay constants and quark mass ratios, Nucl. Phys. **B602**, 87 (2001).

[270] [HPQCD 13B] A. J. Lee, C. J. Monahan, R. R. Horgan, C. T. H. Davies, R. J. Dowdall, and J. Koponen, Mass of the b quark from lattice NRQCD and lattice perturbation theory, Phys. Rev. D **87**, 074018 (2013).

[271] [ALPHA 13C] F. Bernardoni *et al.*, The b-quark mass from non-perturbative $N_f = 2$ heavy quark effective theory at $O(1/m_h)$, Phys. Lett. B **730**, 171 (2014).

[272] [ETM 11A] P. Dimopoulos *et al.*, Lattice QCD determination of m_b, f_B and f_{B_s} with twisted mass Wilson fermions, J. High Energy Phys. 01 (2012) 046.

[273] [ETM 14B] A. Bussone *et al.*, Heavy flavour precision physics from $N_f = 2 + 1 + 1$ lattice simulations, in *International Conference on High Energy Physics 2014 (ICHEP 2014) Valencia, Spain, 2014* (2016), Vol. 273–275, pp. 273–275, arXiv:1411.0484.

[274] Particle Data Group, Review of particle physics, Phys. Rev. D **110**, 030001 (2024).

[275] M. Moulson, Experimental determination of V_{us} from kaon decays, Proc. Sci., CKM2016 (**2017**) 033 [arXiv:1704.04104].

[276] Particle Data Group, Review of particle physics, Chin. Phys. C **40**, 100001 (2016).

[277] A. Rusetsky, Isospin symmetry breaking, Proc. Sci., CD09 (**2009**) 071 [arXiv:0910.5151].

[278] J. Gasser, Theoretical progress on cusp effect and $K_{\ell 4}$ decays, Proc. Sci., KAON07 (**2008**) 033 [arXiv:0710.3048].

[279] V. Cirigliano, M. Knecht, H. Neufeld, H. Rupertsberger, and P. Talavera, Radiative corrections to $K_{\ell 3}$ decays, Eur. Phys. J. C **23**, 121 (2002).

[280] V. Cirigliano, H. Neufeld, and H. Pichl, K_{e3} decays and CKM unitarity, Eur. Phys. J. C **35**, 53 (2004).

[281] V. Cirigliano, M. Giannotti, and H. Neufeld, Electromagnetic effects in $K_{\ell 3}$ decays, J. High Energy Phys. 11 (2008) 006.
[282] V. Cirigliano and H. Neufeld, A note on isospin violation in $P_{\ell 2}(\gamma)$ decays, Phys. Lett. B **700**, 7 (2011).
[283] N. Carrasco, V. Lubicz, G. Martinelli, C. T. Sachrajda, N. Tantalo, C. Tarantino, and M. Testa, QED corrections to hadronic processes in lattice QCD, Phys. Rev. D **91**, 074506 (2015).
[284] N. Hermansson-Truedsson, M. Di Carlo, M. T. Hansen, and A. Portelli, Structure-dependent electromagnetic finite-volume effects through order $1/L^3$, Proc. Sci., LATTICE2023 (**2024**) 265 [arXiv:2310.13358].
[285] C. Y. Seng, M. Gorchtein, and M. J. Ramsey-Musolf, Dispersive evaluation of the inner radiative correction in neutron and nuclear β decay, Phys. Rev. D **100**, 013001 (2019).
[286] C.-Y. Seng, M. Gorchtein, H. H. Patel, and M. J. Ramsey-Musolf, Reduced hadronic uncertainty in the determination of V_{ud}, Phys. Rev. Lett. **121**, 241804 (2018).
[287] W. J. Marciano and A. Sirlin, Improved calculation of electroweak radiative corrections and the value of V_{ud}, Phys. Rev. Lett. **96**, 032002 (2006).
[288] A. Czarnecki, W. J. Marciano, and A. Sirlin, Radiative corrections to neutron and nuclear beta decays revisited, Phys. Rev. D **100**, 073008 (2019).
[289] P.-X. Ma, X. Feng, M. Gorchtein, L.-C. Jin, K.-F. Liu, C.-Y. Seng, B-G. Wang, and Z.-L. Zhang, Lattice QCD calculation of electroweak box contributions to superallowed nuclear and neutron beta decays, Phys. Rev. Lett. **132**, 191901 (2024).
[290] I. S. Towner and J. C. Hardy, An improved calculation of the isospin-symmetry-breaking corrections to superallowed Fermi β decay, Phys. Rev. C **77**, 025501 (2008).
[291] G. A. Miller and A. Schwenk, Isospin-symmetry-breaking corrections to superallowed Fermi β decay: Formalism and schematic models, Phys. Rev. C **78**, 035501 (2008).
[292] N. Auerbach, Coulomb corrections to superallowed β decay in nuclei, Phys. Rev. C **79**, 035502 (2009).
[293] H. Liang, N. Van Giai, and J. Meng, Isospin corrections for superallowed Fermi β decay in self-consistent relativistic random-phase approximation approaches, Phys. Rev. C **79**, 064316 (2009).
[294] G. A. Miller and A. Schwenk, Isospin-symmetry-breaking corrections to superallowed Fermi β decay: Radial excitations, Phys. Rev. C **80**, 064319 (2009).
[295] I. Towner and J. Hardy, Comparative tests of isospin-symmetry-breaking corrections to superallowed $0^+ \to 0^+$ nuclear β decay, Phys. Rev. C **82**, 065501 (2010).
[296] J. C. Hardy and I. S. Towner, Superallowed $0^+ \to 0^+$ nuclear β decays: 2014 critical survey, with precise results for V_{ud} and CKM unitarity, Phys. Rev. C **91**, 025501 (2015).
[297] J. Hardy and I. S. Towner, $|V_{ud}|$ from nuclear β decays, Proc. Sci., CKM2016 (**2016**) 028.
[298] M. Gorchtein, γW box inside out: Nuclear polarizabilities distort the beta decay spectrum, Phys. Rev. Lett. **123**, 042503 (2019).
[299] J. C. Hardy and I. S. Towner, Superallowed $0^+ \to 0^+$ nuclear β decays: 2020 critical survey, with implications for V_{ud} and CKM unitarity, Phys. Rev. C **102**, 045501 (2020).
[300] E. Gamiz, M. Jamin, A. Pich, J. Prades, and F. Schwab, Determination of m_s and $|V_{us}|$ from hadronic τ decays, J. High Energy Phys. 01 (2003) 060.
[301] E. Gamiz, M. Jamin, A. Pich, J. Prades, and F. Schwab, V_{us} and m_s from hadronic τ decays, Phys. Rev. Lett. **94**, 011803 (2005).
[302] K. Maltman, A mixed τ-electroproduction sum rule for V_{us}, Phys. Lett. B **672**, 257 (2009).
[303] A. Pich and R. Kass, Talks Given at CKM 2008, http://ckm2008.roma1.infn.it.
[304] E. Gamiz, M. Jamin, A. Pich, J. Prades, and F. Schwab, Theoretical progress on the V_{us} determination from τ decays, Proc. Sci., KAON07 (**2008**) 008 [arXiv:0709.0282].
[305] E. Gamiz, $|V_{us}|$ from hadronic τ decays, CKM 2012, arXiv:1301.2206.
[306] K. Maltman, C. E. Wolfe, S. Banerjee, J. M. Roney, and I. Nugent, Status of the hadronic τ determination of V_{us}, Int. J. Mod. Phys. A **23**, 3191 (2008).
[307] K. Maltman, C. E. Wolfe, S. Banerjee, I. M. Nugent, and J. M. Roney, Status of the hadronic τ decay determination of $|V_{us}|$, Nucl. Phys. B, Proc. Suppl. **189**, 175 (2009).
[308] [HFLAV 18] Y. Amhis *et al.*, Averages of b-hadron, c-hadron, and τ-lepton properties as of 2018, Eur. Phys. J. C **81**, 226 (2021).
[309] K. Maltman, P. Boyle, R. Hudspith, T. Izubuchi, A. Juttner, C. Lehner *et al.*, Current status of inclusive hadronic tau determinations of $|V_{us}|$, SciPost Phys. Proc., **6** (2019).
[310] [RBC/UKQCD 18] P. Boyle, R. J. Hudspith, T. Izubuchi, A. Jüttner, C. Lehner, R. Lewis *et al.*, Novel $|V_{us}|$ Determination Using Inclusive Strange τ decay and lattice hadronic vacuum polarization functions, Phys. Rev. Lett. **121**, 202003 (2018).
[311] A. Crivellin, M. Kirk, T. Kitahara, and F. Mescia, Global fit of modified quark couplings to EW gauge bosons and vector-like quarks in light of the Cabibbo angle anomaly, J. High Energy Phys. 03 (2023) 234.
[312] M. T. Hansen, H. B. Meyer, and D. Robaina, From deep inelastic scattering to heavy-flavor semileptonic decays: Total rates into multihadron final states from lattice QCD, Phys. Rev. D **96**, 094513 (2017).
[313] P. Gambino and S. Hashimoto, Inclusive semileptonic decays from lattice QCD, Phys. Rev. Lett. **125**, 032001 (2020).
[314] [ETM 23A] A. Evangelista, R. Frezzotti, N. Tantalo, G. Gagliardi, F. Sanfilippo, S. Simula, and V. Lubicz, Inclusive hadronic decay rate of the τ lepton from lattice QCD, Phys. Rev. D **108**, 074513 (2023).
[315] [ETM 24] C. Alexandrou *et al.*, Inclusive hadronic decay rate of the τ lepton from lattice QCD: The $\bar{u}s$ flavour channel and the Cabibbo angle, Phys. Rev. Lett. **132**, 261901 (2024).
[316] M. Antonelli *et al.*, An evaluation of $|V_{us}|$ and precise tests of the standard model from world data on leptonic and semileptonic kaon decays, Eur. Phys. J. C **69**, 399 (2010).

[317] T. Ishikawa, T. Blum, M. Hayakawa, T. Izubuchi, C. Jung, and R. Zhou, Full QED + QCD low-energy constants through reweighting, Phys. Rev. Lett. **109**, 072002 (2012).
[318] T. Izubuchi, Lattice $QCD + QED$-from Isospin breaking to g-2 light-by-light, Talk Given at Lattice 2012, Cairns, Australia, http://www.physics.adelaide.edu.au/cssm.au/cssm/lattice2012.
[319] N. H. Christ, X. Feng, L.-C. Jin, C. T. Sachrajda, and T. Wang, Radiative corrections to leptonic decays using infinite-volume reconstruction, Phys. Rev. D **108**, 014501 (2023).
[320] N. H. Christ, X. Feng, L. Jin, C. T. Sachrajda, and T. Wang, Lattice calculation of electromagnetic corrections to $K_{\ell 3}$ decay, Proc. Sci., LATTICE2023 (**2024**) 266 [arXiv:2402.08915].
[321] C.-Y. Seng, X. Feng, M. Gorchtein, L.-C. Jin, and U.-G. Meißner, New method for calculating electromagnetic effects in semileptonic beta-decays of mesons, J. High Energy Phys. 10 (2020) 179.
[322] P.-X. Ma, X. Feng, M. Gorchtein, L.-C. Jin, and C.-Y. Seng, Lattice QCD calculation of the electroweak box diagrams for the kaon semileptonic decays, Phys. Rev. D **103**, 114503 (2021).
[323] C.-Y. Seng, D. Galviz, M. Gorchtein, and U.-G. Meißner, Improved K_{e3} radiative corrections sharpen the $K_{\mu 2}$–K_{l3} discrepancy, J. High Energy Phys. 11 (2021) 172.
[324] M. Ademollo and R. Gatto, Nonrenormalization theorem for the strangeness violating vector currents, Phys. Rev. Lett. **13**, 264 (1964).
[325] J. Gasser and H. Leutwyler, Low-energy expansion of meson form factors, Nucl. Phys. **B250**, 517 (1985).
[326] G. Furlan, F. Lannoy, C. Rossetti, and G. Segré, Symmetry-breaking corrections to weak vector currents, Nuovo Cimento **38**, 1747 (1965).
[327] J. Gasser and H. Leutwyler, Chiral perturbation theory: Expansions in the mass of the strange quark, Nucl. Phys. **B250**, 465 (1985).
[328] C. Bernard, J. Bijnens, and E. Gamiz, Semileptonic kaon decay in staggered chiral perturbation theory, Phys. Rev. D **89**, 054510 (2014).
[329] [RBC 08A] J. M. Flynn and C. T. Sachrajda, SU(2) chiral perturbation theory for $K_{\ell 3}$ decay amplitudes, Nucl. Phys. **B812**, 64 (2009).
[330] H. Leutwyler and M. Roos, Determination of the elements V_{us} and V_{ud} of the Kobayashi-Maskawa matrix, Z. Phys. C **25**, 91 (1984).
[331] P. Post and K. Schilcher, K_{l3} form factors at order p^6 in chiral perturbation theory, Eur. Phys. J. C **25**, 427 (2002).
[332] J. Bijnens and P. Talavera, K_{l3} decays in chiral perturbation theory, Nucl. Phys. **B669**, 341 (2003).
[333] M. Jamin, J. A. Oller, and A. Pich, Order p^6 chiral couplings from the scalar $K\pi$ form factor, J. High Energy Phys. 02 (2004) 047.
[334] V. Cirigliano, G. Ecker, M. Eidemüller, R. Kaiser, A. Pich, and J. Portolés, The Green function and SU(3) breaking in $K_{\ell 3}$ decays, J. High Energy Phys. 04 (2005) 006.
[335] A. Kastner and H. Neufeld, The K_{l3} scalar form factors in the standard model, Eur. Phys. J. C **57**, 541 (2008).
[336] [JLQCD 17] S. Aoki, G. Cossu, X. Feng, H. Fukaya, S. Hashimoto, T. Kaneko, J. Noaki, and T. Onogi, Chiral behavior of $K \to \pi l \nu$ decay form factors in lattice QCD with exact chiral symmetry, Phys. Rev. D **96**, 034501 (2017).
[337] V. Bernard and E. Passemar, Matching chiral perturbation theory and the dispersive representation of the scalar $K\pi$ form-factor, Phys. Lett. B **661**, 95 (2008).
[338] A. Duncan, E. Eichten, and H. Thacker, Electromagnetic splittings and light quark masses in lattice QCD, Phys. Rev. Lett. **76**, 3894 (1996).
[339] [MILC 08] S. Basak *et al.*, Electromagnetic splittings of hadrons from improved staggered quarks in full QCD, Proc. Sci., LAT2008 (**2008**) 127 [arXiv:0812.4486].
[340] [BMW 10C] A. Portelli *et al.*, Electromagnetic corrections to light hadron masses, Proc. Sci., LAT2010 (**2010**) 121 [arXiv:1011.4189].
[341] [FNAL/MILC 13E] A. Bazavov *et al.*, Determination of $|V_{us}|$ from a lattice-QCD calculation of the $K \to \pi \ell \nu$ semileptonic form factor with physical quark masses, Phys. Rev. Lett. **112**, 112001 (2014).
[342] [PACS 22] K.-I. Ishikawa, N. Ishizuka, Y. Kuramashi, Y. Namekawa, Y. Taniguchi, N. Ukita *et al.*, $K_{\ell 3}$ form factors at the physical point: Toward the continuum limit, Phys. Rev. D **106**, 094501 (2022).
[343] [PACS 19] J. Kakazu, K.-i. Ishikawa, N. Ishizuka, Y. Kuramashi, Y. Nakamura, Y. Namekawa *et al.*, $K_{\ell 3}$ form factors at the physical point on $(10.9\ \mathrm{fm})^3$ volume, Phys. Rev. D **101**, 094504 (2020).
[344] [RBC/UKQCD 13] P. A. Boyle, J. M. Flynn, N. Garron, A. Jüttner, C. T. Sachrajda, K. Sivalingam, and J. M. Zanotti, The kaon semileptonic form factor with near physical domain wall quarks, J. High Energy Phys. 08 (2013) 132.
[345] [JLQCD 12] T. Kaneko *et al.*, Chiral behavior of kaon semileptonic form factors in lattice QCD with exact chiral symmetry, Proc. Sci., LAT2012 (**2012**) 111 [arXiv:1211.6180].
[346] [JLQCD 11] T. Kaneko *et al.*, Kaon semileptonic form factors in QCD with exact chiral symmetry, Proc. Sci., LAT2011 (**2011**) 284 [arXiv:1112.5259].
[347] [RBC/UKQCD 10] P. A. Boyle, J. M. Flynn, A. Jüttner, C. Kelly, C. Maynard, H. Pedroso de Lima, C. T. Sachrajda, and J. M. Zanotti, $K \to \pi$ form factors with reduced model dependence, Eur. Phys. J. C **69**, 159 (2010).
[348] [RBC/UKQCD 07] P. A. Boyle, A. Jüttner, R. Kenway, C. Sachrajda, S. Sasaki, A. Soni, R. J. Tweedie, and J. M. Zanotti, K_{l3} semileptonic form-factor from $2 + 1$ flavour lattice QCD, Phys. Rev. Lett. **100**, 141601 (2008).
[349] D. Guadagnoli, F. Mescia, and S. Simula, Lattice study of semileptonic form-factors with twisted boundary conditions, Phys. Rev. D **73**, 114504 (2006).
[350] [UKQCD 07] P. A. Boyle, J. Flynn, A. Jüttner, C. Sachrajda, and J. Zanotti, Hadronic form factors in lattice QCD at small and vanishing momentum transfer, J. High Energy Phys. 05 (2007) 016.
[351] [ETM 10J] V. Lubicz, F. Mescia, L. Orifici, S. Simula, and C. Tarantino, Improved analysis of the scalar and vector form factors of kaon semileptonic decays with $N_f = 2$ twisted-mass fermions, Proc. Sci., LATTICE2010 (**2010**) 316 [arXiv:1012.3573].

[352] [SPQcdR 04] D. Bećirević *et al.*, The $K \to \pi$ vector form factor at zero momentum transfer on the lattice, Nucl. Phys. **B705**, 339 (2005).
[353] [ETM 09K] V. Lubicz, F. Mescia, S. Simula, and C. Tarantino, $K \to \pi l \nu$ semileptonic form factors from two-flavor lattice QCD, Phys. Rev. D **80**, 111502 (2009).
[354] C. Bernard, J. Bijnens, E. Gámiz, and J. Relefors, Twisted finite-volume corrections to K_{l3} decays with partially-quenched and rooted-staggered quarks, J. High Energy Phys. 03 (2017) 120.
[355] [PACS 23A] T. Yamazaki, K.-i. Ishikawa, N. Ishizuka, Y. Kuramashi, Y. Namekawa, Y. Taniguchi *et al.*, $|V_{us}|$ from kaon semileptonic form factor in $N_f = 2 + 1$ QCD at the physical point on $(10\ \mathrm{fm})^4$, Proc. Sci., LATTICE2023 (**2024**) 276 [arXiv:2311.16755].
[356] [ETM 13F] P. Dimopoulos, R. Frezzotti, P. Lami, V. Lubicz, E. Picca *et al.*, Pseudoscalar decay constants f_K/f_π, f_D and f_{D_s} with $N_f = 2 + 1 + 1$ ETMC configurations, Proc. Sci., LATTICE2013 (**2014**) 314 [arXiv:1311.3080].
[357] [MILC 13A] A. Bazavov, C. Bernard, C. DeTar, J. Foley, W. Freeman *et al.*, Leptonic decay-constant ratio f_{K^+}/f_{π^+} from lattice QCD with physical light quarks, Phys. Rev. Lett. **110**, 172003 (2013).
[358] [MILC 11] A. Bazavov *et al.*, Properties of light pseudoscalars from lattice QCD with HISQ ensembles, Proc. Sci., LAT2011 (**2011**) 107 [arXiv:1111.4314].
[359] [ETM 10E] F. Farchioni, G. Herdoíza, K. Jansen, M. Petschlies, C. Urbach *et al.*, Pseudoscalar decay constants from $N_f = 2 + 1 + 1$ twisted mass lattice QCD, Proc. Sci., LAT2010 (**2010**) 128 [arXiv:1012.0200].
[360] E. E. Scholz and S. Dürr, Leptonic decay-constant ratio f_K/f_π from clover-improved $N_f = 2 + 1$ QCD, Proc. Sci., LATTICE2016 (**2016**) 283 [arXiv:1610.00932].
[361] [JLQCD/TWQCD 10] J. Noaki *et al.*, Chiral properties of light mesons in $N_f = 2 + 1$ overlap QCD, Proc. Sci., LAT2010 (**2010**) 117.
[362] C. Aubin, J. Laiho, and R. S. Van de Water, Light pseudoscalar meson masses and decay constants from mixed action lattice QCD, Proc. Sci., LAT2008 (**2008**) 105 [arXiv:0810.4328].
[363] B. Ananthanarayan, J. Bijnens, S. Friot, and S. Ghosh, Analytic representation of F_k/F_π in two loop chiral perturbation theory, Phys. Rev. D **97**, 091502 (2018).
[364] B. Sheikholeslami and R. Wohlert, Improved continuum limit lattice action for QCD with Wilson fermions, Nucl. Phys. **B259**, 572 (1985).
[365] M. Lüscher, Properties, and uses of the Wilson flow in lattice QCD, J. High Energy Phys. 08 (2010) 071; J. High Energy Phys. 03 (2014) 092.
[366] D. Giusti, V. Lubicz, G. Martinelli, F. Sanfilippo, S. Simula, N. Tantalo *et al.*, Leading isospin-breaking corrections to meson masses on the lattice, EPJ Web Conf. **175**, 06002 (2018).
[367] [JLQCD 15C] B. Fahy, G. Cossu, S. Hashimoto, T. Kaneko, J. Noaki, and M. Tomii, Decay constants and spectroscopy of mesons in lattice QCD using domain-wall fermions, Proc. Sci., LATTICE2015 (**2016**) 074 [arXiv:1512.08599].
[368] G. C. Branco, L. Lavoura, and J. P. Silva, *CP* violation, Int. Ser. Monogr. Phys. **103**, 1 (1999).
[369] M. Sozzi, *Discrete Symmetries and CP Violation: From Experiment to Theory* (Oxford University Press, New York, 2008).
[370] A. Buras, *Gauge Theories of Weak Decays* (Cambridge University Press, Cambridge, England, 2020).
[371] G. Buchalla, A. J. Buras, and M. E. Lautenbacher, Weak decays beyond leading logarithms, Rev. Mod. Phys. **68**, 1125 (1996).
[372] A. J. Buras, Weak Hamiltonian, CP violation, and rare decays, arXiv:hep-ph/9806471; Published in Les Houches 1997, Probing the Standard Model of Particle Interactions, Pt. 1, 281–539.
[373] L. Lellouch, Flavor physics, and lattice quantum chromodynamics, in *Modern perspectives in lattice QCD: Quantum Field Theory and High Performance Computing. Proceedings, International School, 93rd Session, Les Houches, France, 2009* (2011), pp. 629–698, arXiv:1104.5484.
[374] K. Anikeev *et al.*, *B* physics at the tevatron: Run II and beyond, arXiv:hep-ph/0201071.
[375] U. Nierste, Three lectures on meson mixing, and CKM phenomenology, published in Dubna 2008, Heavy Quark Physics (HQP08), pp. 1–39, arXiv:0904.1869.
[376] A. J. Buras and D. Guadagnoli, Correlations among new *CP* violating effects in $\Delta F = 2$ observables, Phys. Rev. D **78**, 033005 (2008).
[377] A. J. Buras, D. Guadagnoli, and G. Isidori, On ϵ_K beyond lowest order in the operator product expansion, Phys. Lett. B **688**, 309 (2010).
[378] T. Inami and C. S. Lim, Effects of superheavy quarks and leptons in low-energy weak processes $K_L \to \mu\bar{\mu}$, $K^+ \to \pi^+ \nu\bar{\nu}$ and $K^0 \leftrightarrow \bar{K}^0$, Prog. Theor. Phys. **65**, 297 (1981).
[379] [RBC/UKQCD 12F] N. H. Christ, T. Izubuchi, C. T. Sachrajda, A. Soni, and J. Yu, Long distance contribution to the $K_L - K_S$ mass difference, Phys. Rev. D **88**, 014508 (2013).
[380] J. Brod, M. Gorbahn, and E. Stamou, Standard-model prediction of ϵ_K with manifest CKM unitarity, Phys. Rev. Lett. **125**, 171803 (2020).
[381] J. Brod and M. Gorbahn, Next-to-next-to-leading-order charm-quark contribution to the *CP* violation parameter ϵ_K and ΔM_K, Phys. Rev. Lett. **108**, 121801 (2012).
[382] J. Brod and M. Gorbahn, ϵ_K at next-to-next-to-leading order: The charm-top-quark contribution, Phys. Rev. D **82**, 094026 (2010).
[383] G. Martinelli, C. Pittori, C. T. Sachrajda, M. Testa, and A. Vladikas, A general method for nonperturbative renormalization of lattice operators, Nucl. Phys. **B445**, 81 (1995).
[384] M. Lüscher, R. Narayanan, P. Weisz, and U. Wolff, The Schrödinger functional: A renormalizable probe for non-Abelian gauge theories, Nucl. Phys. **B384**, 168 (1992).
[385] [SWME 14] T. Bae *et al.*, Improved determination of B_K with staggered quarks, Phys. Rev. D **89**, 074504 (2014).

[386] [ALPHA 07A] P. Dimopoulos, G. Herdoíza, F.Palombi, M. Papinutto, C. Pena, A. Vladikas, and H. Wittig, Non-perturbative renormalisation of $\Delta F = 2$ four-fermion operators in two-flavour QCD, J. High Energy Phys. 05 (2008) 065.

[387] [ALPHA 18B] P. Dimopoulos, G. Herdoíza, M. Papinutto, C. Pena, D. Preti, and A. Vladikas, Non-perturbative renormalisation and running of BSM four-quark operators in $N_f = 2$ QCD, Eur. Phys. J. C **78**, 579 (2018).

[388] I. Campos Plasencia, M. Dalla Brida, G. M. de Divitiis, A. Lytle, R. Marinelli, M. Papinutto *et al.*, Non-perturbative mixing and renormalisation of $\Delta F = 2$ four-fermion operators, Proc. Sci., LATTICE2023 (**2024**) 270.

[389] L. Wolfenstein, Parametrization of the Kobayashi-Maskawa matrix, Phys. Rev. Lett. **51**, 1945 (1983).

[390] Z. Bai, N. H. Christ, J. M. Karpie, C. T. Sachrajda, A. Soni, and B. Wang, Long-distance contribution to ϵ_K from lattice QCD, Phys. Rev. D **109**, 054501 (2024).

[391] [SWME 23A] S. Jwa *et al.*, 2023 update of ε_K with lattice QCD inputs, Proc. Sci., LATTICE2023 (**2024**) 160 [arXiv:2312.02986].

[392] J. Brod, S. Kvedaraite, Z. Polonsky, and A. Youssef, Electroweak corrections to the charm-top-quark contribution to ϵ_K, J. High Energy Phys. 12 (2022) 014.

[393] [SWME 14D] W. Lee *et al.*, Current status of ε_K calculated with lattice QCD inputs, Proc. Sci., LATTICE2014 (**2014**) 371 [arXiv:1410.6995].

[394] [SWME 15B] J. A. Bailey, Y.-C. Jang, W. Lee, and S. Park, Standard Model evaluation of ε_K using lattice QCD inputs for $\hat{B}_K$ and V_{cb}, Phys. Rev. D **92**, 034510 (2015).

[395] [SWME 18] J. A. Bailey *et al.*, Updated evaluation of ϵ_K in the Standard Model with lattice QCD inputs, Phys. Rev. D **98**, 094505 (2018).

[396] UTfit Collaboration, New UTfit analysis of the unitarity triangle in the Cabibbo-Kobayashi-Maskawa scheme, Rend. Lincei Sci. Fis. Nat. **34**, 37 (2023).

[397] A. J. Buras and J. Girrbach, Stringent tests of constrained minimal flavor violation through $\Delta F = 2$ transitions, Eur. Phys. J. C **73**, 2560 (2013).

[398] [SWME 25A] S. Jwa *et al.*, 2024 update of ε_K with lattice QCD inputs, Proc. Sci., LATTICE2024 (**2024**) 433 [arXiv:2501.00215].

[399] [SWME 25B] S. Jwa *et al.*, 2025 update on ε_K in the standard model with lattice QCD inputs, arXiv:2503.00351.

[400] S. Hashimoto, Inclusive semi-leptonic B meson decay structure functions from lattice QCD, Prog. Theor. Exp. Phys. **2017**, 053B03 (2017).

[401] P. Gambino, S. Hashimoto, S. Mächler, M. Panero, F. Sanfilippo, S. Simula, A. Smecca, and N. Tantalo, Lattice QCD study of inclusive semileptonic decays of heavy mesons, J. High Energy Phys. 07 (2022) 083.

[402] A. Barone, S. Hashimoto, A. Jüttner, T. Kaneko, and R. Kellermann, Approaches to inclusive semileptonic $B_{(s)}$-meson decays from Lattice QCD, J. High Energy Phys. 07 (2023) 145.

[403] O. Cata and S. Peris, Long distance dimension eight operators in B_K, J. High Energy Phys. 03 (2003) 060.

[404] M. Ciuchini, E. Franco, V. Lubicz, G. Martinelli, L. Silvestrini, and C. Tarantino, Power corrections to the CP-violation parameter ε_K, J. High Energy Phys. 02 (2022) 181.

[405] V. Cirigliano, A. Pich, G. Ecker, and H. Neufeld, Isospin violation in epsilon-prime, Phys. Rev. Lett. **91**, 162001 (2003).

[406] V. Cirigliano, H. Gisbert, A. Pich, and A. Rodríguez-Sánchez, Isospin-violating contributions to ϵ'/ϵ, J. High Energy Phys. 02 (2020) 032.

[407] [RBC/UKQCD 20] R. Abbott *et al.*, Direct CP violation and the $\Delta I = 1/2$ rule in $K \to \pi\pi$ decay from the Standard Model, Phys. Rev. D **102**, 054509 (2020).

[408] [RBC/UKQCD 15G] Z. Bai *et al.*, Standard Model prediction for direct CP violation in $K \to \pi\pi$ decay, Phys. Rev. Lett. **115**, 212001 (2015).

[409] Particle Data Group, Review of particle physics, Phys. Rev. D **98**, 030001 (2018).

[410] Z. Bai, Long distance part of ϵ_K from lattice QCD, Proc. Sci., LATTICE2016 (**2017**) 309 [arXiv:1611.06601].

[411] Z. Bai, N. H. Christ, T. Izubuchi, C. T. Sachrajda, A. Soni, and J. Yu, $K_L - K_S$ mass difference from lattice QCD, Phys. Rev. Lett. **113**, 112003 (2014).

[412] N. H. Christ, X. Feng, G. Martinelli, and C. T. Sachrajda, Effects of finite volume on the $K_L - K_S$ mass difference, Phys. Rev. D **91**, 114510 (2015).

[413] B. Wang, Calculation of the $K_L - K_S$ mass difference for physical quark masses, Proc. Sci., LATTICE2019 (**2019**) 093 [arXiv:2001.06374].

[414] B. Wang, Calculating Δm_K with lattice QCD, Proc. Sci., LATTICE2021 (**2022**) 141 [arXiv:2301.01387].

[415] [RBC/UKQCD 23A] T. Blum, P. A. Boyle, D. Hoying, T. Izubuchi, L. Jin, C. Jung *et al.*, $\Delta I = 3/2$ and $\Delta I = 1/2$ channels of $K \to \pi\pi$ decay at the physical point with periodic boundary conditions, Phys. Rev. D **108**, 094517 (2023).

[416] Z. Bai *et al.*, Erratum: Standard-model prediction for direct CP violation in $K \to \pi\pi$ decay, arXiv:1603.03065.

[417] [RBC/UKQCD 23B] T. Blum *et al.*, Isospin 0 and 2 two-pion scattering at physical pion mass using all-to-all propagators with periodic boundary conditions in lattice QCD, Phys. Rev. D **107**, 094512 (2023).

[418] M. Gaillard and B. W. Lee, $\Delta I = 1/2$ rule for nonleptonic decays in asymptotically free field theories, Phys. Rev. Lett. **33**, 108 (1974).

[419] G. Altarelli and L. Maiani, Octet enhancement of non-leptonic weak interactions in asymptotically free gauge theories, Phys. Lett. **52B**, 351 (1974).

[420] [RBC/UKQCD 21] T. Blum *et al.*, Lattice determination of $I = 0$ and $2\pi\pi$ scattering phase shifts with a physical pion mass, Phys. Rev. D **104**, 114506 (2021).

[421] N. Ishizuka, K. I. Ishikawa, A. Ukawa, and T. Yoshié, Calculation of $K \to \pi\pi$ decay amplitudes with improved Wilson fermion action in lattice QCD, Phys. Rev. D **92**, 074503 (2015).

[422] N. Ishizuka, K. I. Ishikawa, A. Ukawa, and T. Yoshié, Calculation of $K \to \pi\pi$ decay amplitudes with improved Wilson fermion action in non-zero momentum frame in lattice QCD, Phys. Rev. D **98**, 114512 (2018).

[423] A. Donini, P. Hernández, C. Pena, and F. Romero-López, Nonleptonic kaon decays at large N_c, Phys. Rev. D **94**, 114511 (2016).

[424] A. Donini, P. Hernández, C. Pena, and F. Romero-López, Dissecting the $\Delta I = 1/2$ rule at large N_c, Eur. Phys. J. C **80**, 638 (2020).

[425] J. Baeza-Ballesteros, P. Hernández, and F. Romero-López, A lattice study of $\pi\pi$ scattering at large N_c, J. High Energy Phys. 06 (2022) 049.

[426] N. Christ and X. Feng, Including electromagnetism in $K \to \pi\pi$ decay calculations, EPJ Web Conf. **175**, 13016 (2018).

[427] Y. Cai and Z. Davoudi, QED-corrected Lellouch-Luescher formula for $K \to \pi\pi$ decay, Proc. Sci., LATTICE2018 (**2018**) 280 [arXiv:1812.11015].

[428] N. Christ, X. Feng, J. Karpie, and T. Nguyen, π-π scattering, QED, and finite-volume quantization, Phys. Rev. D **106**, 014508 (2022).

[429] D. Bećirević, Ph. Boucaud, V. Giménez, V. Lubicz, G. Martinelli, J. Micheli, and M. Papinutto, $K^0\bar{K}^0$ mixing with Wilson fermions without subtractions, Phys. Lett. B **487**, 74 (2000).

[430] [ALPHA 01] R. Frezzotti, P. A. Grassi, S. Sint, and P. Weisz, Lattice QCD with a chirally twisted mass term, J. High Energy Phys. 08 (2001) 058.

[431] [ALPHA 06] P. Dimopoulos *et al.*, A precise determination of B_K in quenched QCD, Nucl. Phys. **B749**, 69 (2006).

[432] [ALPHA 07] P. Dimopoulos *et al.*, Flavour symmetry restoration and kaon weak matrix elements in quenched twisted mass QCD, Nucl. Phys. **B776**, 258 (2007).

[433] R. S. Van de Water and S. R. Sharpe, B_K in staggered chiral perturbation theory, Phys. Rev. D **73**, 014003 (2006).

[434] J. A. Bailey, H.-J. Kim, W. Lee, and S. R. Sharpe, Kaon mixing matrix elements from beyond-the-Standard-Model operators in staggered chiral perturbation theory, Phys. Rev. D **85**, 074507 (2012).

[435] P. H. Ginsparg and K. G. Wilson, A remnant of chiral symmetry on the lattice, Phys. Rev. D **25**, 2649 (1982).

[436] Y. Aoki *et al.*, The Kaon B-parameter from quenched domain-wall QCD, Phys. Rev. D **73**, 094507 (2006).

[437] [RBC/UKQCD] N. Christ, Estimating domain wall fermion chiral symmetry breaking, Proc. Sci., LAT2005 (**2006**) 345.

[438] V. Cirigliano, J. F. Donoghue, and E. Golowich, Dimension eight operators in the weak OPE, J. High Energy Phys. 10 (2000) 048.

[439] A. J. Buras, M. Jamin, and P. H. Weisz, Leading and next-to-leading QCD corrections to ϵ parameter and $B_0 - \bar{B}_0$ mixing in the presence of a heavy top quark, Nucl. Phys. **B347**, 491 (1990).

[440] A. Suzuki, Y. Taniguchi, H. Suzuki, and K. Kanaya, Four quark operators for kaon bag parameter with gradient flow, Phys. Rev. D **102**, 034508 (2020).

[441] [SWME 13A] T. Bae *et al.*, Neutral kaon mixing from new physics: Matrix elements in $N_f = 2 + 1$ lattice QCD, Phys. Rev. D **88**, 071503 (2013).

[442] [SWME 13] T. Bae *et al.*, Update on B_K and ε_K with staggered quarks, Proc. Sci., LATTICE2013 (**2013**) 476 [arXiv:1310.7319].

[443] [SWME 11A] T. Bae *et al.*, Kaon B-parameter from improved staggered fermions in $N_f = 2 + 1$ QCD, Phys. Rev. Lett. **109**, 041601 (2012).

[444] [RBC/UKQCD 10B] Y. Aoki *et al.*, Continuum limit of B_K from $2 + 1$ flavor domain wall QCD, Phys. Rev. D **84**, 014503 (2011).

[445] [SWME 10] T. Bae, Y.-C. Jang, C. Jung, H.-J. Kim, J. Kim, J. Kim, K. Kim, W. Lee, S. R. Sharpe, and B. Yoon, B_K using HYP-smeared staggered fermions in $N_f = 2 + 1$ unquenched QCD, Phys. Rev. D **82**, 114509 (2010).

[446] C. Aubin, J. Laiho, and R. S. Van de Water, The neutral kaon mixing parameter B_K from unquenched mixed-action lattice QCD, Phys. Rev. D **81**, 014507 (2010).

[447] [ETM 10A] M. Constantinou *et al.*, B_K-parameter from $N_f = 2$ twisted mass lattice QCD, Phys. Rev. D **83**, 014505 (2011).

[448] [ETM 10C] M. Constantinou *et al.*, Non-perturbative renormalization of quark bilinear operators with $N_f = 2$ (tmQCD) Wilson fermions and the tree- level improved gauge action, J. High Energy Phys. 08 (2010) 068.

[449] F. Gabbiani, E. Gabrielli, A. Masiero, and L. Silvestrini, A complete analysis of FCNC and CP constraints in general SUSY extensions of the standard model, Nucl. Phys. **B477**, 321 (1996).

[450] [RBC/UKQCD 12E] P. A. Boyle, N. Garron, and R. J. Hudspith, Neutral kaon mixing beyond the Standard Model with $n_f = 2 + 1$ chiral fermions, Phys. Rev. D **86**, 054028 (2012).

[451] A. J. Buras, M. Misiak, and J. Urban, Two loop QCD anomalous dimensions of flavor changing four quark operators within and beyond the standard model, Nucl. Phys. **B586**, 397 (2000).

[452] C. R. Allton, L. Conti, A. Donini, V. Gimenez, L. Giusti, G. Martinelli, M. Talevi, and A. Vladikas, B parameters for $\Delta S = 2$ supersymmetric operators, Phys. Lett. B **453**, 30 (1999).

[453] A. Donini, V. Gimenez, L. Giusti, and G. Martinelli, Renormalization group invariant matrix elements of $\Delta S = 2$ and $\Delta I = 3/2$ four fermion operators without quark masses, Phys. Lett. B **470**, 233 (1999).

[454] R. Babich, N. Garron, C. Hoelbling, J. Howard, L. Lellouch, and C. Rebbi, $K^0 \to \bar{K}^0$ mixing beyond the Standard Model and CP-violating electroweak penguins in quenched QCD with exact chiral symmetry, Phys. Rev. D **74**, 073009 (2006).

[455] A. J. Buras and J.-M. Gérard, Dual QCD insight into BSM hadronic matrix elements for $K^0 - \bar{K}^0$ mixing from lattice QCD, Acta Phys. Pol. B **50**, 121 (2019).

[456] [SWME 14C] J. Leem *et al.*, Calculation of BSM Kaon B-parameters using staggered quarks, Proc. Sci., LATTICE2014 (**2014**) 370 [arXiv:1411.1501].

[457] [RBC/UKQCD 17A] P. Boyle, N. Garron, R. J. Hudspith, C. Lehner, and A. T. Lytle, Neutral kaon mixing beyond the standard model with $n_f = 2 + 1$ chiral fermions. Part 2: Non perturbative renormalisation of the $\Delta F = 2$ four-quark operators, J. High Energy Phys. 10 (2017) 054.

[458] [ETM 21B] P. Dimopoulos, R. Frezzotti, M. Garofalo, and S. Simula, K- and $D_{(s)}$-meson leptonic decay constants with physical light, strange and charm quarks by ETMC, Proc. Sci., LATTICE2021 (**2021**) 472 [arXiv:2110.01294].

[459] [FNAL/MILC 13] A. Bazavov *et al.*, Charmed and strange pseudoscalar meson decay constants from HISQ simulations, Proc. Sci., LATTICE2013 (**2014**) 405 [arXiv:1312.0149].

[460] [FNAL/MILC 12B] A. Bazavov *et al.*, Pseudoscalar meson physics with four dynamical quarks, Proc. Sci., LAT2012 (**2012**) 159 [arXiv:1210.8431].

[461] [RQCD/ALPHA 24] S. Kuberski, F. Joswig, S. Collins, J. Heitger, and W. Söldner, D and D_s decay constants in $N_f = 2 + 1$ QCD with Wilson fermions, J. High Energy Phys. 07 (2024) 090.

[462] [χQCD 20A] Y. Chen, W.-F. Chiu, M. Gong, Z. Liu, and Y. Ma, Charmed and ϕ meson decay constants from $2 + 1$-flavor lattice QCD, Chin. Phys. C **45**, 023109 (2021).

[463] [PACS-CS 11] Y. Namekawa *et al.*, Charm quark system at the physical point of $2 + 1$ flavor lattice QCD, Phys. Rev. D **84**, 074505 (2011).

[464] [FNAL/MILC 05] C. Aubin, C. Bernard, C. E. DeTar, M. Di Pierro, E. D. Freeland *et al.*, Charmed meson decay constants in three-flavor lattice QCD, Phys. Rev. Lett. **95**, 122002 (2005).

[465] [RQCD 21] G. S. Bali, V. Braun, S. Collins, A. Schäfer, and J. Simeth, Masses and decay constants of the η and η' mesons from lattice QCD, J. High Energy Phys. 08 (2021) 137.

[466] D. Giusti, C. F. Kane, C. Lehner, S. Meinel, and A. Soni, Methods for high-precision determinations of radiative-leptonic decay form factors using lattice QCD, Phys. Rev. D **107**, 074507 (2023).

[467] R. Frezzotti, N. Tantalo, G. Gagliardi, F. Sanfilippo, S. Simula, V. Lubicz, F. Mazzetti, G. Martinelli, and C. T. Sachrajda, Lattice calculation of the Ds meson radiative form factors over the full kinematical range, Phys. Rev. D **108**, 074505 (2023).

[468] A. Desiderio *et al.*, First lattice calculation of radiative leptonic decay rates of pseudoscalar mesons, Phys. Rev. D **103**, 014502 (2021).

[469] G. Parisi, The strategy for computing the hadronic mass spectrum, Phys. Rep. **103**, 203 (1984).

[470] G. P. Lepage, The analysis of algorithms for lattice field theory, in *Theoretical Advanced Study Institute in Elementary Particle Physics* (1989).

[471] A. Sirlin, Large m_W, m_Z behavior of the $O(\alpha)$ corrections to semileptonic processes mediated by W, Nucl. Phys. **B196**, 83 (1982).

[472] CLEO Collaboration, Improved measurements of D meson semileptonic decays to π and K mesons, Phys. Rev. D **80**, 032005 (2009).

[473] BESIII Collaboration, Measurement of $e^+e^- \to \pi^+\pi^-\psi(3686)$ from 4.008 to 4.600 GeV and observation of a charged structure in the $\pi^\pm\psi(3686)$ mass spectrum, Phys. Rev. D **96**, 032004 (2017).

[474] BESIII Collaboration, Measurement of the branching fraction for the semi-leptonic decay $D^{0(+)} \to \pi^{-(0)}\mu^+\nu_\mu$ and test of lepton universality, Phys. Rev. Lett. **121**, 171803 (2018).

[475] P. F. Bedaque, Aharonov-Bohm effect, and nucleon nucleon phase shifts on the lattice, Phys. Lett. B **593**, 82 (2004).

[476] C. Sachrajda and G. Villadoro, Twisted boundary conditions in lattice simulations, Phys. Lett. B **609**, 73 (2005).

[477] [ETM 11B] S. Di Vita, B. Haas, V. Lubicz, F. Mescia, S. Simula, and C. Tarantino, Form factors of the $D \to \pi$ and $D \to K$ semileptonic decays with $N_f = 2$ twisted mass lattice QCD, *Proc. Sci.*, LATTICE2010 (2010) 301 [arXiv:1104.0869].

[478] [HPQCD 11C] J. Koponen *et al.*, The D to K and D to π semileptonic decay form factors from lattice QCD, Proc. Sci., LAT2011 (**2011**) 286 [arXiv:1111.0225].

[479] [HPQCD 12B] J. Koponen, C. Davies, and G. Donald, D to K and D to π semileptonic form factors from lattice QCD, Charm 2012, arXiv:1208.6242.

[480] [HPQCD 13C] J. Koponen, C. T. H. Davies, G. C. Donald, E. Follana, G. P. Lepage *et al.*, The shape of the $D \to K$ semileptonic form factor from full lattice QCD and V_{cs}, arXiv:1305.1462.

[481] [ETM 18] V. Lubicz, L. Riggio, G. Salerno, S. Simula, and C. Tarantino, Tensor form factor of $D \to \pi(K)\ell\nu$ and $D \to \pi(K)\ell\ell$ decays with $N_f = 2 + 1 + 1$ twisted-mass fermions, Phys. Rev. D **98**, 014516 (2018).

[482] [FNAL/MILC 04] C. Aubin *et al.*, Semileptonic decays of D mesons in three-flavor lattice QCD, Phys. Rev. Lett. **94**, 011601 (2005).

[483] V. Lubicz, G. Martinelli, M. S. McCarthy, and C. T. Sachrajda, Semileptonic decays of D mesons in a lattice QCD, Phys. Lett. B **274**, 415 (1992).

[484] A. Abada, D. Becirevic, P. Boucaud, J. P. Leroy, V. Lubicz, and F. Mescia, Heavy → light semileptonic decays of pseudoscalar mesons from lattice QCD, Nucl. Phys. **B619**, 565 (2001).

[485] FOCUS Collaboration, Measurements of the q^2 dependence of the $D^0 \to K^-\mu^+\nu$ and $D^0 \to \pi^-\mu^+\nu$ form factors, Phys. Lett. B **607**, 233 (2005).

[486] Belle Collaboration, Measurement of $D^0 \to \pi l\nu(Kl\nu)$ and their form-factors, arXiv:hep-ex/0510003.

[487] [FNAL/MILC 12G] J. A. Bailey *et al.*, Charm semileptonic decays and $|V_{cs(d)}|$ from heavy clover quarks and $2 + 1$ flavor asqtad staggered ensembles, Proc. Sci., LAT2012 (**2012**) 272 [arXiv:1211.4964].

[488] [JLQCD 17B] T. Kaneko, B. Colquhoun, H. Fukaya, and S. Hashimoto, D meson semileptonic form factors in $N_f = 3$ QCD with Möbius domain-wall quarks, EPJ Web Conf. **175**, 13007 (2018).

[489] G. Colangelo, M. Procura, L. Rothen, R. Stucki, and J. Tarrus Castella, On the factorization of chiral logarithms in the pion form factors, J. High Energy Phys. 09 (2012) 081.

[490] M. Marshall, P. Boyle, L. Del Debbio, F. Erben, J. Flynn, A. Jüttner *et al.*, Semileptonic $D \to \pi\ell\nu$, $D \to K\ell\nu$ and $D_s \to K\ell\nu$ decays with $2 + 1f$ domain wall fermions, Proc. Sci., LATTICE2021 (**2022**) 416 [arXiv:2201.02680].

[491] J. Bijnens and I. Jemos, Hard pion chiral perturbation theory for $B \to \pi$ and $D \to \pi$ form factors, Nucl. Phys. **B840**, 54 (2010); Nucl. Phys. **B844**, 182(E) (2011).

[492] [HPQCD 22] W. G. Parrott, C. Bouchard, and C. T. H. Davies, $B \to K$ and $D \to K$ form factors from fully relativistic lattice QCD, Phys. Rev. D **107**, 014510 (2023).

[493] [HPQCD 20] L. J. Cooper, C. T. H. Davies, J. Harrison, J. Komijani, and M. Wingate, $B_c \to B_{s(d)}$ form factors from

lattice QCD, Phys. Rev. D **102**, 014513 (2020); Phys. Rev. D **103**, 099901(E) (2021).
[494] T. Feldmann and M. W. Y. Yip, Form factors for $\Lambda_b \to \Lambda$ transitions in SCET, Phys. Rev. D **85**, 014035 (2012); Phys. Rev. D **86**, 079901(E) (2012).
[495] S. Meinel, $\Lambda_c \to \Lambda l^+ \nu_l$ form factors and decay rates from lattice QCD with physical quark masses, Phys. Rev. Lett. **118**, 082001 (2017).
[496] BESIII Collaboration, Measurement of the absolute branching fraction for $\Lambda_c^+ \to \Lambda e^+ \nu_e$, Phys. Rev. Lett. **115**, 221805 (2015).
[497] BESIII Collaboration, Measurement of the absolute branching fraction for $\Lambda_c^+ \to \Lambda \mu^+ \nu_\mu$, Phys. Lett. B **767**, 42 (2017).
[498] S. Meinel, $\Lambda_c \to N$ form factors from lattice QCD and phenomenology of $\Lambda_c \to n \ell^+ \nu_\ell$ and $\Lambda_c \to p \mu^+ \mu^-$ decays, Phys. Rev. D **97**, 034511 (2018).
[499] W. Detmold, C. Lehner, and S. Meinel, $\Lambda_b \to p \ell^- \bar{\nu}_\ell$ and $\Lambda_b \to \Lambda_c \ell^- \bar{\nu}_\ell$ form factors from lattice QCD with relativistic heavy quarks, Phys. Rev. D **92**, 034503 (2015).
[500] Q.-A. Zhang, J. Hua, F. Huang, R. Li, Y. Li, C.-D. Lu, P. Sun, W. Sun, W. Wang, and Y. Yang, $\Xi_c \to \Xi$ form factors and $\Xi_c \to \Xi \ell^+ \nu_\ell$ decay rates from lattice QCD, Chin. Phys. C **46**, 011002 (2022).
[501] Belle Collaboration, Measurements of the branching fractions of semileptonic decays $\Xi_c^0 \to \Xi^- \ell^+ \nu_\ell$ and asymmetry parameter of $\Xi_c^0 \to \Xi^- \pi^+$ decay, Phys. Rev. Lett. **127**, 121803 (2021).
[502] C. Farrell and S. Meinel, Form factors for the charm-baryon semileptonic decay $\Xi_c \to \Xi \ell \nu$ from domain-wall lattice QCD, Proc. Sci., LATTICE2023 (**2024**) 210 [arXiv:2309.08107].
[503] S. Meinel and G. Rendon, $\Lambda_c \to \Lambda^*(1520)$ form factors from lattice QCD and improved analysis of the $\Lambda_b \to \Lambda^*(1520)$ and $\Lambda_b \to \Lambda_c^*(2595, 2625)$ form factors, Phys. Rev. D **105**, 054511 (2022).
[504] B. A. Dobrescu and A. S. Kronfeld, Accumulating evidence for nonstandard leptonic decays of D_s mesons, Phys. Rev. Lett. **100**, 241802 (2008).
[505] *BABAR* Collaboration, Measurement of the hadronic form-factor in $D^0 \to K^- e^+ \nu_e$ 1, Phys. Rev. D **76**, 052005 (2007).
[506] BESIII Collaboration, Study of dynamics of $D^0 \to K^- e^+ \nu_e$ and $D^0 \to \pi^- e^+ \nu_e$ decays, Phys. Rev. D **92**, 072012 (2015).
[507] BESIII Collaboration, Analysis of $D^+ \to \bar{K}^0 e^+ \nu_e$ and $D^+ \to \pi^0 e^+ \nu_e$ semileptonic decays, Phys. Rev. D **96**, 012002 (2017).
[508] BESIII Collaboration, Study of the $D^0 \to K^- \mu^+ \nu_\mu$ dynamics and test of lepton flavor universality with $D^0 \to K^- \ell^+ \nu_\ell$ decays, Phys. Rev. Lett. **122**, 011804 (2019).
[509] Belle Collaboration, Measurement of $D^0 \to \pi l \nu (K l \nu)$ form factors and absolute branching fractions, Phys. Rev. Lett. **97**, 061804 (2006).
[510] BESIII Collaboration, First measurement of the form factors in $D_s^+ \to K^0 e^+ \nu_e$ and $D_s^+ \to K^{*0} e^+ \nu_e$ decays, Phys. Rev. Lett. **122**, 061801 (2019).
[511] BESIII Collaboration, Study of the semileptonic decay $\Lambda_c^+ \to \Lambda e^+ \nu e$, Phys. Rev. Lett. **129**, 231803 (2022).
[512] BESIII Collaboration, Study of $\Lambda_c^+ \to \Lambda \mu^+ \nu_\mu$ and test of lepton flavor universality with $\Lambda_c^+ \to \Lambda \ell^+ \nu_\ell$ decays, Phys. Rev. D **108**, L031105 (2023).
[513] Belle-II Collaboration, Measurement of the Λ_c^+ lifetime, Phys. Rev. Lett. **130**, 071802 (2023).
[514] *BABAR* Collaboration, Evidence of $B \to \tau \nu$ decays with hadronic B tags, Phys. Rev. D **88**, 031102 (2013).
[515] Belle Collaboration, Measurement of the branching fraction of $B^+ \to \tau^+ \nu_\tau$ decays with the semileptonic tagging method, Phys. Rev. D **92**, 051102 (2015).
[516] G. Buchalla and A. J. Buras, QCD corrections to rare K and B decays for arbitrary top quark mass, Nucl. Phys. **B400**, 225 (1993).
[517] LHCb Collaboration, First evidence for the decay $B_s \to \mu^+ \mu^-$, Phys. Rev. Lett. **110**, 021801 (2013).
[518] LHCb and CMS Collaborations, Observation of the rare $B_s^0 \to \mu^+ \mu^-$ decay from the combined analysis of CMS and LHCb data, Nature (London) **522**, 68 (2015).
[519] ATLAS Collaboration, Study of the rare decays of B_s^0 and B^0 mesons into muon pairs using data collected during 2015 and 2016 with the ATLAS detector, J. High Energy Phys. 04 (2019) 098.
[520] CMS Collaboration, Measurement of properties of $\mathrm{B_s^0} \to \mu^+ \mu^-$ decays and search for $\mathrm{B^0} \to \mu^+ \mu^-$ with the CMS experiment, J. High Energy Phys. 04 (2020) 188.
[521] LHCb Collaboration, Measurement of the $B_s^0 \to \mu^+ \mu^-$ branching fraction and effective lifetime and search for $B^0 \to \mu^+ \mu^-$ decays, Phys. Rev. Lett. **118**, 191801 (2017).
[522] CMS Collaboration, Combination of the ATLAS, CMS, and LHCb results on the $B_{(s)}^0 \to \mu^+ \mu^-$ decays, Report No. CMS-PAS-BPH-20-003, 2020.
[523] M. Beneke, C. Bobeth, and R. Szafron, Power-enhanced leading-logarithmic QED corrections to $B_q \to \mu^+ \mu^-$, J. High Energy Phys. 10 (2019) 232.
[524] LHCb Collaboration, Measurement of the $B_s^0 \to \mu^+ \mu^-$ decay properties and search for the $B^0 \to \mu^+ \mu^-$ and $B_s^0 \to \mu^+ \mu^- \gamma$ decays, Phys. Rev. D **105**, 012010 (2022).
[525] CMS Collaboration, Measurement of the $\mathrm{B_S^0} \to \mu^+ \mu^-$ decay properties and search for the $\mathrm{B^0} \to \mu^+ \mu^-$ decay in proton-proton collisions at $\sqrt{s} = 13$ TeV, Phys. Lett. B **842**, 137955 (2023).
[526] W. Altmannshofer and P. Stangl, New physics in rare B decays after Moriond 2021, Eur. Phys. J. C **81**, 952 (2021).
[527] LHCb Collaboration, Analysis of neutral B-meson decays into two muons, Phys. Rev. Lett. **128**, 041801 (2022).
[528] T. Janowski, B. Pullin, and R. Zwicky, Charged and neutral $\bar{B}_{u,d,s} \to \gamma$ form factors from light cone sum rules at NLO, J. High Energy Phys. 12 (2021) 008.
[529] A. Kozachuk, D. Melikhov, and N. Nikitin, Rare FCNC radiative leptonic $B_{s,d} \to \gamma l^+ l^-$ decays in the Standard Model, Phys. Rev. D **97**, 053007 (2018).
[530] I. Belov, A. Berezhnoy, and D. Melikhov, Nonfactorizable charming-loop contribution to FCNC $B_s \to \gamma l^+ l^-$ decay, Phys. Rev. D **109**, 114012 (2024).
[531] D. Guadagnoli, C. Normand, S. Simula, and L. Vittorio, From $D_s \to \gamma$ in lattice QCD to $B_s \to \mu\mu\gamma$ at high q^2, J. High Energy Phys. 07 (2023) 112.
[532] R. Frezzotti, N. Tantalo, G. Gagliardi, F. Sanfilippo, S. Simula, V. Lubicz, G. Martinelli, and C. T. Sachrajda,

$B_s \to \mu^+\mu^-\gamma$ decay rate at large q^2 from lattice QCD, Phys. Rev. D **109**, 114506 (2024).
[533] CLEO Collaboration, Search for $B \to \mu\bar{\nu}_\mu\gamma$ and $B \to e\bar{\nu}_e\gamma$, Phys. Rev. D **56**, 11 (1997).
[534] *BABAR* Collaboration, A model-independent search for the decay $B^+ \to \ell^+\nu_\ell\gamma$, Phys. Rev. D **80**, 111105 (2009).
[535] Belle Collaboration, Search for $B^+ \to \ell^+\nu_\ell\gamma$ decays with hadronic tagging using the full Belle data sample, Phys. Rev. D **91**, 112009 (2015).
[536] Belle Collaboration, Search for the rare decay of $B^+ \to \ell^+\nu_\ell\gamma$ with improved hadronic tagging, Phys. Rev. D **98**, 112016 (2018).
[537] M. Beneke, V. M. Braun, Y. Ji, and Y.-B. Wei, Radiative leptonic decay $B \to \gamma\ell\nu_\ell$ with subleading power corrections, J. High Energy Phys. 07 (2018) 154.
[538] S. Zhao and A. V. Radyushkin, B-meson Ioffe-time distribution amplitude at short distances, Phys. Rev. D **103**, 054022 (2021).
[539] J. Xu, X.-R. Zhang, and S. Zhao, Inverse moment of the B-meson quasidistribution amplitude, Phys. Rev. D **106**, L011503 (2022).
[540] [ETM 13E] N. Carrasco, P. Dimopoulos, R. Frezzotti, V. Giménez, P. Lami *et al.*, A $N_f = 2 + 1 + 1$ 'twisted' determination of the b-quark mass, f_B and f_{B_s}, Proc. Sci., LATTICE2013 (**2014**) 313 [arXiv:1311.2837].
[541] [RBC/UKQCD 13A] O. Witzel, B-meson decay constants with domain-wall light quarks and nonperturbatively tuned relativistic b-quarks, Proc. Sci., LATTICE2013 (**2014**) 377 [arXiv:1311.0276].
[542] [ALPHA 13] F. Bernardoni, B. Blossier, J. Bulava, M. Della Morte, P. Fritzsch *et al.*, B-physics with $N_f = 2$ Wilson fermions, Proc. Sci., LATTICE2013 (**2014**) 381 [arXiv:1309.1074].
[543] [ETM 13C] N. Carrasco *et al.*, B-physics computations from $N_f = 2$ tmQCD, Proc. Sci., LATTICE2013 (**2014**) 382 [arXiv:1310.1851].
[544] [ALPHA 12A] F. Bernardoni, B. Blossier, J. Bulava, M. Della Morte, P. Fritzsch *et al.*, B-physics from HQET in two-flavour lattice QCD, Proc. Sci., LAT2012 (**2012**) 273 [arXiv:1210.7932].
[545] [ETM 12B] N. Carrasco, P. Dimopoulos, R. Frezzotti, V. Gimenez, G. Herdoíza *et al.*, B-physics from the ratio method with Wilson twisted mass fermions, Proc. Sci., LAT2012 (**2012**) 104 [arXiv:1211.0568].
[546] [ALPHA 11] B. Blossier, J. Bulava, M. Della Morte, M. Donnellan, P. Fritzsch *et al.*, M_b and f_B from non-perturbatively renormalized HQET with $N_f = 2$ light quarks, Proc. Sci., LAT2011 (**2011**) 280 [arXiv:1112.6175].
[547] [ETM 09D] B. Blossier *et al.*, A proposal for B-physics on current lattices, J. High Energy Phys. 04 (2010) 049.
[548] [QCDSF/UKQCD/CSSM 22] S. Hollitt *et al.*, Measurements of $SU(3)_f$ symmetry breaking in B meson decay constants, Proc. Sci., LATTICE2021 (**2022**) 549 [arXiv:2201.10779].
[549] [RBC/UKQCD 10C] C. Albertus *et al.*, Neutral B-meson mixing from unquenched lattice QCD with domain-wall light quarks and static b-quarks, Phys. Rev. D **82**, 014505 (2010).
[550] [RBC/UKQCD 22] M. Black and O. Witzel, B meson decay constants using relativistic heavy quarks, Proc. Sci., LATTICE2022 (**2023**) 405 [arXiv:2212.10125].
[551] [QCDSF/UKQCD 10] W. Bietenholz *et al.*, Tuning the strange quark mass in lattice simulations, Phys. Lett. B **690**, 436 (2010).
[552] [RBC/UKQCD 12A] Y. Aoki, N. H. Christ, J. M. Flynn, T. Izubuchi, C. Lehner, M. Li, H. Peng, A. Soni, R. S. Van de Water, and O. Witzel, Nonperturbative tuning of an improved relativistic heavy-quark action with application to bottom spectroscopy, Phys. Rev. D **86**, 116003 (2012).
[553] H. Akaike, A new look at the statistical model identification, IEEE Trans. Autom. Control **19**, 716 (1974).
[554] A. Lenz and U. Nierste, Theoretical update of $B_s - \bar{B}_s$ mixing, J. High Energy Phys. 06 (2007) 072.
[555] M. Beneke, G. Buchalla, and I. Dunietz, Width difference in the $B_s - \overline{B_s}$ system, Phys. Rev. D **54**, 4419 (1996).
[556] [FNAL/MILC 11A] C. M. Bouchard, E. Freeland, C. Bernard, A. El-Khadra, E. Gamiz *et al.*, Neutral B mixing from $2 + 1$ flavor lattice-QCD: the standard model and beyond, *Proc. Sci.*, LAT2011 (2011) 274 [arXiv:1112.5642].
[557] J. T. Tsang and M. Della Morte, B-physics from lattice gauge theory, Eur. Phys. J. Spec. Top. **233**, 253 (2024).
[558] [HPQCD 06A] E. Dalgic, A. Gray, E. Gamiz, C. T. Davies, G. P. Lepage, J. Shigemitsu, H. Trottier, and M. Wingate, $B_s^0 - \overline{B}_s^0$ mixing parameters from unquenched lattice QCD, Phys. Rev. D **76**, 011501 (2007).
[559] [ETM 12A] N. Carrasco *et al.*, Neutral meson oscillations in the standard model and beyond from $N_f = 2$ twisted mass lattice QCD, Proc. Sci., LAT2012 (**2012**) 105 [arXiv:1211.0565].
[560] [FNAL/MILC 12] A. Bazavov, C. Bernard, C. Bouchard, C. DeTar, M. Di Pierro *et al.*, Neutral B-meson mixing from three-flavor lattice QCD: Determination of the SU(3)-breaking ratio ξ, Phys. Rev. D **86**, 034503 (2012).
[561] P. Boyle, F. Erben, A. Jüttner, T. Kaneko, M. Marshall, A. Portelli *et al.*, BSM $B - \bar{B}$ mixing on JLQCD and RBC/UKQCD $N_f = 2 + 1$ DWF ensembles, Proc. Sci., LATTICE2021 (**2022**) 224 [arXiv:2111.11287].
[562] M. Della Morte, B. Jäger, T. Rae, and H. Wittig, Improved interpolating fields for hadrons at non-zero momentum, Eur. Phys. J. A **48**, 139 (2012).
[563] [HPQCD 06] E. Gulez, A. Gray, M. Wingate, C. T. H. Davies, G. Peter Lepage, and J. Shigemitsu, B meson semileptonic form-factors from unquenched lattice QCD, Phys. Rev. D **73**, 074502 (2006).
[564] [FNAL/MILC 08A] J. A. Bailey *et al.*, The $B \to \pi\ell\nu$ semileptonic form factor from three-flavor lattice QCD: A model-independent determination of $|V_{ub}|$, Phys. Rev. D **79**, 054507 (2009).
[565] Z. Gelzer *et al.*, Semileptonic B-meson decays to light pseudoscalar mesons on the HISQ ensembles, EPJ Web Conf. **175**, 13024 (2018).
[566] [FNAL/MILC 19A] Z. Gelzer *et al.*, B-meson semileptonic form factors on $(2 + 1 + 1)$-flavor HISQ ensembles, Proc. Sci., LATTICE2019 (**2019**) 236 [arXiv:1912.13358].
[567] J. Flynn, R. Hill, A. Jüttner, A. Soni, J. T. Tsang, and O. Witzel, Semileptonic $B \to \pi\ell\nu$, $B \to D\ell\nu$, $B_s \to K\ell\nu$, and

$B_s \to D_s \ell\nu$ decays, Proc. Sci., LATTICE2019 (**2019**) 184 [arXiv:1912.09946].
[568] [HPQCD 15A] B. Colquhoun, R. J. Dowdall, J. Koponen, C. T. H. Davies, and G. P. Lepage, $B \to \pi\ell\nu$ at zero recoil from lattice QCD with physical u/d quarks, Phys. Rev. D **93**, 034502 (2016).
[569] [HPQCD 12C] C. M. Bouchard, G. P. Lepage, C. J. Monahan, H. Na, and J. Shigemitsu, Form factors for B and B_s semileptonic decays with NRQCD/HISQ quarks, Proc. Sci., LAT2012 (**2012**) 118 [arXiv:1210.6992].
[570] [HPQCD 13F] C. M. Bouchard, G. P. Lepage, J. C. Monahan, H. Na, and J. Shigemitsu, B and B_s semileptonic decay form factors with NRQCD/HISQ quarks, Proc. Sci., LATTICE2013 (**2014**) 387 [arXiv:1310.3207].
[571] J. Flynn, R. Hill, A. Juettner, A. Soni, J. T. Tsang, and O. Witzel, Form factors for semileptonic $B \to \pi$, $B_s \to K$ and $B_s \to D_s$ decays, Proc. Sci., LATTICE2021 (**2022**) 306 [arXiv:2112.10580].
[572] P. Ball and R. Zwicky, $|V_{ub}|$ and constraints on the leading-twist pion distribution amplitude from $B \to \pi l\nu$, Phys. Lett. B **625**, 225 (2005).
[573] D. Bećirević and A. B. Kaidalov, Comment on the heavy → light form-factors, Phys. Lett. B **478**, 417 (2000).
[574] R. J. Hill, Heavy-to-light meson form-factors at large recoil, Phys. Rev. D **73**, 014012 (2006).
[575] C. G. Boyd, B. Grinstein, and R. F. Lebed, Constraints on form-factors for exclusive semileptonic heavy to light meson decays, Phys. Rev. Lett. **74**, 4603 (1995).
[576] Belle-II Collaboration, Reconstruction of $B \to \rho\ell\nu_\ell$ decays identified using hadronic decays of the recoil B meson in 2019–2021 Belle II data, arXiv:2211.15270.
[577] [UKQCD 04] K. C. Bowler, J. F. Gill, C. M. Maynard, and J. M. Flynn, $B \to \rho\ell\nu$ form-factors in lattice QCD, J. High Energy Phys. 05 (2004) 035.
[578] J. M. Flynn, Y. Nakagawa, J. Nieves, and H. Toki, $|V_{ub}|$ from exclusive semileptonic $B \to \rho$ decays, Phys. Lett. B **675**, 326 (2009).
[579] M. Lüscher, Volume dependence of the energy spectrum in massive quantum field theories. 2. Scattering states, Commun. Math. Phys. **105**, 153 (1986).
[580] M. Lüscher, Two particle states on a torus and their relation to the scattering matrix, Nucl. Phys. **B354**, 531 (1991).
[581] M. Lüscher, Signatures of unstable particles in finite volume, Nucl. Phys. **B364**, 237 (1991).
[582] M. Lage, U.-G. Meissner, and A. Rusetsky, A Method to measure the antikaon-nucleon scattering length in lattice QCD, Phys. Lett. B **681**, 439 (2009).
[583] V. Bernard, M. Lage, U. G. Meissner, and A. Rusetsky, Scalar mesons in a finite volume, J. High Energy Phys. 01 (2011) 019.
[584] M. Doring, U.-G. Meissner, E. Oset, and A. Rusetsky, Unitarized chiral perturbation theory in a finite volume: Scalar meson sector, Eur. Phys. J. A **47**, 139 (2011).
[585] M. T. Hansen and S. R. Sharpe, Multiple-channel generalization of Lellouch-Luscher formula, Phys. Rev. D **86**, 016007 (2012).
[586] R. A. Briceno and Z. Davoudi, Moving multichannel systems in a finite volume with application to proton-proton fusion, Phys. Rev. D **88**, 094507 (2013).
[587] [HS 14] J. J. Dudek, R. G. Edwards, C. E. Thomas, and D. J. Wilson, Resonances in coupled $\pi K - \eta K$ scattering from quantum chromodynamics, Phys. Rev. Lett. **113**, 182001 (2014).
[588] R. A. Briceño, M. T. Hansen, and A. Walker-Loud, Multichannel $1 \to 2$ transition amplitudes in a finite volume, Phys. Rev. D **91**, 034501 (2015).
[589] R. A. Briceño and M. T. Hansen, Multichannel $0 \to 2$ and $1 \to 2$ transition amplitudes for arbitrary spin particles in a finite volume, Phys. Rev. D **92**, 074509 (2015).
[590] L. Leskovec, S. Meinel, M. Petschlies, J. Negele, S. Paul, A. Pochinsky *et al.*, A lattice QCD study of the $B \to \pi\pi\ell\bar{\nu}$ transition, *Proc. Sci.*, LATTICE2022 (2023) 416 [arXiv:2212.08833].
[591] L. Leskovec, S. Meinel, M. Petschlies, J. Negele, S. Paul, A. Pochinsky *et al.*, Lattice outlook on $B \to \rho\ell\bar{\nu}$ and $B \to K^\star\ell\ell$, in *Proceedings of the 12th International Workshop on the CKM Unitarity Triangle* (2024), arXiv:2403.19543.
[592] [FNAL/MILC 19] A. Bazavov *et al.*, $B_s \to K\ell\nu$ decay from lattice QCD, Phys. Rev. D **100**, 034501 (2019).
[593] J. M. Flynn, A. Jüttner, and J. T. Tsang, Bayesian inference for form-factor fits regulated by unitarity and analyticity, J. High Energy Phys. 12 (2023) 175.
[594] T. Blake, S. Meinel, M. Rahimi, and D. van Dyk, Dispersive bounds for local form factors in $\Lambda_b \to \Lambda$ transitions, Phys. Rev. D **108**, 094509 (2023).
[595] [JLQCD 24] P. Mohanta, T. Kaneko, and S. Hashimoto, $B_s \to K\ell\nu$ form factors from lattice QCD with domain-wall heavy quarks, Proc. Sci., LATTICE2023 (**2024**) 267 [arXiv:2401.01570].
[596] H. Jeong, C. DeTar, A. X. El-Khadra, E. Gámiz, Z. Gelzer, S. Gottlieb *et al.*, Form factors for semileptonic B-decays with HISQ light quarks and clover b-quarks in Fermilab interpretation, Proc. Sci., LATTICE2023 (**2024**) 253 [arXiv:2402.14924].
[597] A. Lytle, C. DeTar, E. Gámiz, S. Gottlieb, W. Jay, A. X. El-Khadra *et al.*, B-meson semileptonic decays from highly improved staggered quarks, Proc. Sci., LATTICE2023 (**2024**) 240 [arXiv:2403.03959].
[598] F. Bahr, D. Banerjee, F. Bernardoni, M. Koren, H. Simma, and R. Sommer, Extraction of bare form factors for $B_s \to K\ell\nu$ decays in nonperturbative HQET, Int. J. Mod. Phys. A **34**, 1950166 (2019).
[599] [ALPHA 14B] F. Bahr, F. Bernardoni, J. Bulava, A. Joseph, A. Ramos, H. Simma *et al.*, Form factors for $B_s \to K\ell\nu$ decays in lattice QCD, in *Proceedings of the 8th International Workshop on the CKM Unitarity Triangle (CKM2014) Vienna, Austria, 2014* (2014), https://inspirehep.net/record/1328088/files/arXiv:1411.3916.pdf.
[600] M. Antonelli *et al.*, Flavor physics in the quark sector, Phys. Rep. **494**, 197 (2010).
[601] B. Grinstein and D. Pirjol, Exclusive rare $B \to K^*\ell^+\ell^-$ decays at low recoil: Controlling the long-distance effects, Phys. Rev. D **70**, 114005 (2004).

[602] M. Beylich, G. Buchalla, and T. Feldmann, Theory of $B \to K^{(*)}\ell^+\ell^-$ decays at high q^2: OPE and quark-hadron duality, Eur. Phys. J. C **71**, 1635 (2011).

[603] M. Beneke, T. Feldmann, and D. Seidel, Systematic approach to exclusive $B \to Vl^+l^-$, $V\gamma$ decays, Nucl. Phys. **B612**, 25 (2001).

[604] Z. Liu *et al.*, Form factors for rare B decays: Strategy, methodology, and numerical study, Proc. Sci., LAT2009 (**2009**) 242 [arXiv:0911.2370].

[605] [HPQCD 13D] C. Bouchard, G. P. Lepage, C. Monahan, H. Na, and J. Shigemitsu, Standard model predictions for $B \to Kll$ with form factors from lattice QCD, Phys. Rev. Lett. **111**, 162002 (2013); Phys. Rev. Lett. **112**, 149902(E) (2014).

[606] [FNAL/MILC 15F] D. Du, A. X. El-Khadra, S. Gottlieb, A. S. Kronfeld, J. Laiho, E. Lunghi, R. S. Van de Water, and R. Zhou, Phenomenology of semileptonic B-meson decays with form factors from lattice QCD, Phys. Rev. D **93**, 034005 (2016).

[607] LHCb Collaboration, First measurement of the differential branching fraction and CP asymmetry of the $B^\pm \to \pi^\pm\mu^+\mu^-$ decay, J. High Energy Phys. 10 (2015) 034.

[608] C. B. Lang, D. Mohler, S. Prelovsek, and R. M. Woloshyn, Predicting positive parity B_s mesons from lattice QCD, Phys. Lett. B **750**, 17 (2015).

[609] [HPQCD 20D] D. Hatton, C. T. H. Davies, G. P. Lepage, and A. T. Lytle, Renormalization of the tensor current in lattice QCD and the J/ψ tensor decay constant, Phys. Rev. D **102**, 094509 (2020).

[610] [HPQCD 22A] W. G. Parrott, C. Bouchard, and C. T. H. Davies, Standard Model predictions for $B \to K\ell^+\ell^-$, $B \to K\ell_1^-\ell_2^+$ and $B \to K\nu\bar{\nu}$ using form factors from $N_f = 2 + 1 + 1$ lattice QCD, Phys. Rev. D **107**, 014511 (2023); Phys. Rev. D **107**, 119903(E) (2023).

[611] R. R. Horgan, Z. Liu, S. Meinel, and M. Wingate, Lattice QCD calculation of form factors describing the rare decays $B \to K^*\ell^+\ell^-$ and $B_s \to \phi\ell^+\ell^-$, Phys. Rev. D **89**, 094501 (2014).

[612] R. R. Horgan, Z. Liu, S. Meinel, and M. Wingate, Calculation of $B^0 \to K^{*0}\mu^+\mu^-$ and $B_s^0 \to \phi\mu^+\mu^-$ observables using form factors from lattice QCD, Phys. Rev. Lett. **112**, 212003 (2014).

[613] R. R. Horgan, Z. Liu, S. Meinel, and M. Wingate, Rare B decays using lattice QCD form factors, Proc. Sci., LATTICE2014 (**2015**) 372 [arXiv:1501.00367].

[614] [RBC/UKQCD 15B] J. Flynn, A. Jüttner, T. Kawanai, E. Lizarazo, and O. Witzel, Hadronic form factors for rare semileptonic B decays, in *Proceedings, 33rd International Symposium on Lattice Field Theory (Lattice 2015)* (2016), Vol. LATTICE2015, p. 345, http://inspirehep.net/record/1405735/files/arXiv:1511.06622.pdf.

[615] J. Flynn, T. Izubuchi, A. Jüttner, T. Kawanai, C. Lehner, E. Lizarazo *et al.*, Form factors for semi-leptonic B decays, Proc. Sci., LATTICE2016 (**2016**) 296 [arXiv:1612.05112].

[616] E. Lizarazo and O. Witzel, Non-perturbative determinations of B-meson decay constants and semi-leptonic form factors, Proc. Sci., ICHEP2016 (**2016**) 558 [arXiv:1612.06113].

[617] M. E. Luke, Effects of subleading operators in the heavy quark effective theory, Phys. Lett. B **252**, 447 (1990).

[618] N. Isgur and M. B. Wise, Weak transition form-factors between heavy mesons, Phys. Lett. B **237**, 527 (1990).

[619] N. Isgur and M. B. Wise, Weak decays of heavy mesons in the static quark approximation, Phys. Lett. B **232**, 113 (1989).

[620] M. Neubert, Heavy quark symmetry, Phys. Rep. **245**, 259 (1994).

[621] A. F. Falk and M. Neubert, Second order power corrections in the heavy quark effective theory. 1. Formalism and meson form-factors, Phys. Rev. D **47**, 2965 (1993).

[622] M. Neubert, Short distance expansion of heavy quark currents, Phys. Rev. D **46**, 2212 (1992).

[623] M. Neubert, Higher order perturbative corrections to $b \to c$ transitions at zero recoil, Phys. Lett. B **341**, 367 (1995).

[624] A. S. Kronfeld, Application of heavy quark effective theory to lattice QCD. 1. Power corrections, Phys. Rev. D **62**, 014505 (2000).

[625] J. Harada, S. Hashimoto, A. S. Kronfeld, and T. Onogi, Application of heavy-quark effective theory to lattice QCD. 3. Radiative corrections to heavy-heavy currents, Phys. Rev. D **65**, 094514 (2002).

[626] S. Hashimoto, A. X. El-Khadra, A. S. Kronfeld, P. B. Mackenzie, S M. Ryan, and J. N. Simone, Lattice QCD calculation of $\bar{B} \to D\ell\bar{\nu}$ decay form factors at zero recoil, Phys. Rev. D **61**, 014502 (1999).

[627] [HPQCD 17] C. J. Monahan, H. Na, C. M. Bouchard, G. P. Lepage, and J. Shigemitsu, $B_s \to D_s\ell\nu$ form factors and the fragmentation fraction ratio f_s/f_d, Phys. Rev. D **95**, 114506 (2017).

[628] [HPQCD 20B] J. Harrison, C. T. H. Davies, and A. Lytle, $B_c \to J/\psi$ form factors for the full q^2 range from lattice QCD, Phys. Rev. D **102**, 094518 (2020).

[629] [FNAL/MILC 04A] M. Okamoto *et al.*, Semileptonic $D \to \pi/K$ and $B \to \pi/D$ decays in $2 + 1$ flavor lattice QCD, Nucl. Phys. B, Proc. Suppl. **140**, 461 (2005).

[630] [FNAL/MILC 13B] S.-W. Qiu, C. DeTar, A. X. El-Khadra, A. S. Kronfeld, J. Laiho *et al.*, Semileptonic decays $B \to D^{(*)}l\nu$ at nonzero recoil, Proc. Sci., LATTICE2013 (**2014**) 385 [arXiv:1312.0155].

[631] M. Atoui, V. Morenas, D. Becirevic, and F. Sanfilippo, $b_s \to d_s\ell\nu_\ell$ near zero recoil in and beyond the standard model, Eur. Phys. J. C **74**, 2861 (2014).

[632] C. J. Monahan, H. Na, C. M. Bouchard, G. P. Lepage, and J. Shigemitsu, $B_{(s)} \to D_{(s)}$ semileptonic decays with NRQCD-HISQ valence quarks, Proc. Sci., LATTICE2016 (**2016**) 298 [arXiv:1611.09667].

[633] LHCb Collaboration, Measurement of $|V_{cb}|$ with $B_s^0 \to D_s^{(*)-}\mu^+\nu_\mu$ decays, Phys. Rev. D **101**, 072004 (2020).

[634] LHCb Collaboration, Precise measurement of the f_s/f_d ratio of fragmentation fractions and of B_s^0 decay branching fractions, Phys. Rev. D **104**, 032005 (2021).

[635] T. Kaneko, Y. Aoki, B. Colquhoun, M. Faur, H. Fukaya, S. Hashimoto *et al.*, $B \to D^{(*)}\ell\nu$ semileptonic decays in lattice QCD with domain-wall heavy quarks, Proc. Sci., LATTICE2021 (**2022**) 561 [arXiv:2112.13775].

[636] J. G. Korner and G. A. Schuler, Exclusive semileptonic heavy meson decays including lepton mass effects, Z. Phys. C **46**, 93 (1990).

[637] D. Bigi, P. Gambino, and S. Schacht, A fresh look at the determination of $|V_{cb}|$ from $B \to D^* \ell \nu$, Phys. Lett. B **769**, 441 (2017).
[638] [FNAL/MILC 08] C. Bernard *et al.*, The $\bar{B} \to D^* \ell \bar{\nu}$ form factor at zero recoil from three-flavor lattice QCD: A model independent determination of $|V_{cb}|$, Phys. Rev. D **79**, 014506 (2009).
[639] [FNAL/MILC 14] J. A. Bailey *et al.*, Update of $|V_{cb}|$ from the $\bar{B} \to D^* \ell \bar{\nu}$ form factor at zero recoil with three-flavor lattice QCD, Phys. Rev. D **89**, 114504 (2014).
[640] J. Harrison, C. Davies, and M. Wingate, $|V_{cb}|$ from the $\bar{B}^0 \to D^{*+} \ell^- \bar{\nu}$ zero-recoil form factor using $2+1+1$ flavour HISQ and NRQCD, Proc. Sci., LATTICE2016 (**2017**) 287 [arXiv:1612.06716].
[641] [HPQCD 17B] J. Harrison, C. Davies, and M. Wingate, Lattice QCD calculation of the $B_{(s)} \to D^*_{(s)} \ell \nu$ form factors at zero recoil and implications for $|V_{cb}|$, Phys. Rev. D **97**, 054502 (2018).
[642] M. Neubert, Theoretical update on the model independent determination of $|V_{cb}|$ using heavy quark symmetry, Phys. Lett. B **338**, 84 (1994).
[643] S. Hashimoto, A. S. Kronfeld, P. B. Mackenzie, S. M. Ryan, and J. N. Simone, Lattice calculation of the zero recoil form-factor of $\bar{B} \to D^* \ell \bar{\nu}$: Toward a model independent determination of $|V_{cb}|$, Phys. Rev. D **66**, 014503 (2002).
[644] L. Randall and M. B. Wise, Chiral perturbation theory for $B \to D^*$ and $B \to D$ semileptonic transition matrix elements at zero recoil, Phys. Lett. B **303**, 135 (1993).
[645] M. J. Savage, Heavy meson observables at one loop in partially quenched chiral perturbation theory, Phys. Rev. D **65**, 034014 (2002).
[646] [HPQCD 19B] E. McLean, C. T. H. Davies, A. T. Lytle, and J. Koponen, Lattice QCD form factor for $B_s \to D_s^* l \nu$ at zero recoil with non-perturbative current renormalisation, Phys. Rev. D **99**, 114512 (2019).
[647] [HPQCD 21B] J. Harrison and C. T. H. Davies, $B_s \to D_s^*$ form factors for the full q^2 range from Lattice QCD, Phys. Rev. D **105**, 094506 (2022).
[648] T. Bhattacharya *et al.*, Current progress on the semileptonic form factors for $\bar{B} \to D^* \ell \bar{\nu}$ decay using the Oktay-Kronfeld action, Proc. Sci., LATTICE2023 (**2023**) 245 [arXiv:2401.01561].
[649] R. Fleischer, N. Serra, and N. Tuning, A new strategy for B_s branching ratio measurements and the search for new physics in $B_s^0 \to \mu^+ \mu^-$, Phys. Rev. D **82**, 034038 (2010).
[650] LHCb Collaboration, Determination of f_s/f_d for 7 TeV pp collisions and a measurement of the branching fraction of the decay $B_d \to D^- K^+$, Phys. Rev. Lett. **107**, 211801 (2011).
[651] [FNAL/MILC 12C] J. A. Bailey *et al.*, $B_s \to D_s / B \to D$ semileptonic form-factor ratios and their application to $\mathrm{BR}(B_s^0 \to \mu^+ \mu^-)$, Phys. Rev. D **85**, 114502 (2012).
[652] A. Lytle, B. Colquhoun, C. Davies, J. Koponen, and C. McNeile, Semileptonic B_c decays from full lattice QCD, Proc. Sci., BEAUTY2016 (**2016**) 069 [arXiv:1605.05645].
[653] [HPQCD 16] B. Colquhoun, C. Davies, J. Koponen, A. Lytle, and C. McNeile, B_c decays from highly improved staggered quarks and NRQCD, Proc. Sci., LATTICE2016 (**2016**) 281 [arXiv:1611.01987].
[654] [HPQCD 20C] J. Harrison, C. T. H. Davies, and A. Lytle, $R(J/\psi)$ and $B_c^- \to J/\psi \ell^- \bar{\nu}_\ell$ lepton flavor universality violating observables from lattice QCD, Phys. Rev. Lett. **125**, 222003 (2020).
[655] LHCb RICH Group Collaboration, Performance of the LHCb RICH detector at the LHC, Eur. Phys. J. C **73**, 2431 (2013).
[656] LHCb Collaboration, Determination of the quark coupling strength $|V_{ub}|$ using baryonic decays, Nat. Phys. **11**, 743 (2015).
[657] A. Datta, S. Kamali, S. Meinel, and A. Rashed, Phenomenology of $\Lambda_b \to \Lambda_c \tau \bar{\nu}_\tau$ using lattice QCD calculations, J. High Energy Phys. 08 (2017) 131.
[658] S. Meinel, Status of next-generation $\Lambda_b \to p, \Lambda, \Lambda_c$ form-factor calculations, Proc. Sci., LATTICE2023 (**2024**) 275 [arXiv:2309.01821].
[659] S. Meinel and G. Rendon, $\Lambda_b \to \Lambda_c^*(2595, 2625) \ell^- \bar{\nu}$ form factors from lattice QCD, Phys. Rev. D **103**, 094516 (2021).
[660] T. D. Cohen, H. Lamm, and R. F. Lebed, Precision model-independent bounds from global analysis of $b \to c \ell \nu$ form factors, Phys. Rev. D **100**, 094503 (2019).
[661] M. Papucci and D. J. Robinson, Form factor counting and HQET matching for new physics in $\Lambda_b \to \Lambda_c^* l \nu$, Phys. Rev. D **105**, 016027 (2022).
[662] V. Di Risi, D. Iacobacci, and F. Sannino, $\Lambda_b \to \Lambda_c^*$ at $1/m_c^2$ heavy quark mass order, Phys. Rev. D **109**, 036021 (2024).
[663] T. Blake and M. Kreps, Angular distribution of polarised Λ_b baryons decaying to $\Lambda \ell^+ \ell^-$, J. High Energy Phys. 11 (2017) 138.
[664] LHCb Collaboration, Angular moments of the decay $\Lambda_b^0 \to \Lambda \mu^+ \mu^-$ at low hadronic recoil, J. High Energy Phys. 09 (2018) 146.
[665] W. Detmold, C. J. D. Lin, S. Meinel, and M. Wingate, $\Lambda_b \to \Lambda \ell^+ \ell^-$ form factors and differential branching fraction from lattice QCD, Phys. Rev. D **87**, 074502 (2013).
[666] W. Detmold and S. Meinel, $\Lambda_b \to \Lambda \ell^+ \ell^-$ form factors, differential branching fraction, and angular observables from lattice QCD with relativistic b quarks, Phys. Rev. D **93**, 074501 (2016).
[667] T. Blake, S. Meinel, and D. van Dyk, Bayesian analysis of $b \to s \mu^+ \mu^-$ Wilson coefficients using the full angular distribution of $\Lambda_b \to \Lambda(\to p\pi^-)\mu^+\mu^-$ decays, Phys. Rev. D **101**, 035023 (2020).
[668] LHCb Collaboration, Differential branching fraction and angular analysis of $\Lambda_b^0 \to \Lambda \mu^+ \mu^-$ decays, J. High Energy Phys. 06 (2015) 115; J. High Energy Phys. 09 (2018) 145(E).
[669] M. Algueró, B. Capdevila, A. Crivellin, S. Descotes-Genon, P. Masjuan, J. Matias, and J. Virto, Emerging patterns of new physics with and without lepton flavour universal contributions, Eur. Phys. J. C **79**, 714 (2019); Eur. Phys. J. C **80**, 511(A) (2020).
[670] S. Meinel and G. Rendon, $\Lambda_b \to \Lambda^*(1520) \ell^+ \ell^-$ form factors from lattice QCD, Phys. Rev. D **103**, 074505 (2021).
[671] W. Detmold, C. J. D. Lin, S. Meinel, and M. Wingate, $\Lambda_b \to p l^- \bar{\nu}_\ell$ form factors from lattice QCD with static b quarks, Phys. Rev. D **88**, 014512 (2013).

[672] Belle Collaboration, Measurement of $B^- \to \tau^- \bar{\nu}_\tau$ with a hadronic tagging method using the full data sample of Belle, Phys. Rev. Lett. **110**, 131801 (2013).

[673] *BABAR* Collaboration, A search for $B^+ \to \ell^+ \nu_\ell$ recoiling against $B^- \to D^0 \ell^- \bar{\nu} X$, Phys. Rev. D **81**, 051101 (2010).

[674] D. Bigi and P. Gambino, Revisiting $B \to D \ell \nu$, Phys. Rev. D **94**, 094008 (2016).

[675] M. Bordone, B. Capdevila, and P. Gambino, Three loop calculations and inclusive V_{cb}, Phys. Lett. B **822**, 136679 (2021).

[676] LHCb Collaboration, First observation of the decay $B_s^0 \to K^- \mu^+ \nu_\mu$ and measurement of $|V_{ub}|/|V_{cb}|$, Phys. Rev. Lett. **126**, 081804 (2021).

[677] P. Gambino, K. J. Healey, and S. Turczyk, Taming the higher power corrections in semileptonic B decays, Phys. Lett. B **763**, 60 (2016).

[678] LHC Higgs Cross Section Working Group Collaboration, Handbook of LHC Higgs cross sections: 4. Deciphering the nature of the Higgs sector, CERN Yellow Rep. Monogr. **2**, 1 (2017).

[679] G. P. Salam, The strong coupling: A theoretical perspective, in *From My Vast Repertoire …: Guido Altarelli's Legacy*, edited by A. Levy, S. Forte, and G. Ridolfi (2019), pp. 101–121, arXiv:1712.05165.

[680] S. Dittmaier *et al.*, Handbook of LHC Higgs cross sections: 2. Differential distributions, arXiv:1201.3084.

[681] LHC Higgs Cross Section Working Group Collaboration, Handbook of LHC Higgs cross sections: 3. Higgs properties, arXiv:1307.1347.

[682] LBNE Collaboration, Scientific opportunities with the long-baseline neutrino experiment, arXiv:1307.7335.

[683] S. Dawson, A. Gritsan, H. Logan, J. Qian, C. Tully *et al.*, Higgs working group report of the snowmass 2013 community planning study, arXiv:1310.8361.

[684] A. Accardi *et al.*, A critical appraisal and evaluation of modern PDFs, Eur. Phys. J. C **76**, 471 (2016).

[685] G. P. Lepage, P. B. Mackenzie, and M. E. Peskin, Expected precision of Higgs boson partial widths within the standard model, arXiv:1404.0319.

[686] D. Buttazzo, G. Degrassi, P. P. Giardino, G. F. Giudice, F. Sala, A. Salvio, and A. Strumia, Investigating the near-criticality of the Higgs boson, J. High Energy Phys. 12 (2013) 089.

[687] J. R. Espinosa, Vacuum Stability and the Higgs Boson, Proc. Sci., LATTICE2013 (**2014**) 010 [arXiv:1311.1970].

[688] L. Del Debbio and A. Ramos, Lattice determinations of the strong coupling, Phys. Rep. **920**, 1 (2021).

[689] M. Dalla Brida, Past, present, and future of precision determinations of the QCD parameters from lattice QCD, Eur. Phys. J. A **57**, 66 (2021).

[690] S. Forte and Z. Kassabov, Why α_s cannot be determined from hadronic processes without simultaneously determining the parton distributions, Eur. Phys. J. C **80**, 182 (2020).

[691] M. Czakon, The four-loop QCD beta-function, and anomalous dimensions, Nucl. Phys. **B710**, 485 (2005).

[692] T. Luthe, A. Maier, P. Marquard, and Y. Schröder, Towards the five-loop Beta function for a general gauge group, J. High Energy Phys. 07 (2016) 127.

[693] F. Herzog, B. Ruijl, T. Ueda, J. A. M. Vermaseren, and A. Vogt, The five-loop beta function of Yang-Mills theory with fermions, J. High Energy Phys. 02 (2017) 090.

[694] P. A. Baikov, K. G. Chetyrkin, and J. H. Kuhn, Five-loop running of the QCD coupling constant, Phys. Rev. Lett. **118**, 082002 (2017).

[695] W. Bernreuther and W. Wetzel, Decoupling of heavy quarks in the minimal subtraction scheme, Nucl. Phys. **B197**, 228 (1982).

[696] K. Chetyrkin, J. H. Kuhn, and C. Sturm, QCD decoupling at four loops, Nucl. Phys. **B744**, 121 (2006).

[697] Y. Schröder and M. Steinhauser, Four-loop decoupling relations for the strong coupling, J. High Energy Phys. 01 (2006) 051.

[698] B. A. Kniehl, A. V. Kotikov, A. I. Onishchenko, and O. L. Veretin, Strong-coupling constant with flavor thresholds at five loops in the anti-MS scheme, Phys. Rev. Lett. **97**, 042001 (2006).

[699] A. G. Grozin, M. Hoeschele, J. Hoff, and M. Steinhauser, Simultaneous decoupling of bottom and charm quarks, J. High Energy Phys. 09 (2011) 066.

[700] K. G. Chetyrkin, J. H. Kuhn, and M. Steinhauser, RunDec: A Mathematica package for running and decoupling of the strong coupling and quark masses, Comput. Phys. Commun. **133**, 43 (2000).

[701] F. Herren and M. Steinhauser, Version 3 of RunDec and CRunDec, Comput. Phys. Commun. **224**, 333 (2018).

[702] A. H. Hoang, C. Lepenik, and V. Mateu, REvolver: Automated running and matching of couplings and masses in QCD, Comput. Phys. Commun. **270**, 108145 (2022).

[703] [ALPHA 19A] M. Dalla Brida, R. Höllwieser, F. Knechtli, T. Korzec, A. Ramos, and R. Sommer, Non-perturbative renormalization by decoupling, Phys. Lett. B **807**, 135571 (2020).

[704] E. I. Bribian, J. L. D. Golan, M. G. Perez, and A. Ramos, Memory efficient finite volume schemes with twisted boundary conditions, Eur. Phys. J. C **81**, 951 (2021).

[705] A. Hasenfratz, C. T. Peterson, J. van Sickle, and O. Witzel, Λ parameter of the SU(3) Yang-Mills theory from the continuous β function, Phys. Rev. D **108**, 014502 (2023).

[706] C. H. Wong, S. Borsanyi, Z. Fodor, K. Holland, and J. Kuti, Toward a novel determination of the strong QCD coupling at the Z-pole, Proc. Sci., LATTICE2022 (**2023**) 043 [arXiv:2301.06611].

[707] L. Chimirri, A quenched exploration of heavy quark moments, and their perturbative expansion, Proc. Sci., LATTICE2022 (**2023**) 350 [arXiv:2301.09959].

[708] R. Sommer, A new way to set the energy scale in lattice gauge theories and its applications to the static force and α_s in SU(2) Yang-Mills theory, Nucl. Phys. **B411**, 839 (1994).

[709] C. W. Bernard, T. Burch, K. Orginos, D. Toussaint, T. A. DeGrand, C. DeTar, S. Gottlieb, U. M. Heller, J. E. Hetrick, and B. Sugar, The static quark potential in three flavor QCD, Phys. Rev. D **62**, 034503 (2000).

[710] G. Martinelli and C. T. Sachrajda, On the difficulty of computing higher twist corrections, Nucl. Phys. **B478**, 660 (1996).

[711] S. Bethke, A. H. Hoang, S. Kluth, J. Schieck, I. W. Stewart *et al.*, Workshop on precision measurements of α_s, arXiv:1110.0016.
[712] A. H. Hoang and C. Regner, On the difference between FOPT and CIPT for hadronic tau decays, Eur. Phys. J. Spec. Top. **230**, 2625 (2021).
[713] M. A. Benitez-Rathgeb, D. Boito, A. H. Hoang, and M. Jamin, Reconciling the contour-improved and fixed-order approaches for τ hadronic spectral moments. Part II. Renormalon norm and application in α_s determinations, J. High Energy Phys. 09 (2022) 223.
[714] D. Boito, M. Golterman, K. Maltman, J. Osborne, and S. Peris, Strong coupling from the revised ALEPH data for hadronic τ decays, Phys. Rev. D **91**, 034003 (2015).
[715] D. Boito, M. Golterman, K. Maltman, and S. Peris, Strong coupling from hadronic τ decays: A critical appraisal, Phys. Rev. D **95**, 034024 (2017).
[716] [ETM 09J] B. Blossier *et al.*, Pseudoscalar decay constants of kaon and D-mesons from $N_f = 2$ twisted mass lattice QCD, J. High Energy Phys. 07 (2009) 043.
[717] [ALPHA 12] P. Fritzsch, F. Knechtli, B. Leder, M. Marinkovic, S. Schaefer *et al.*, The strange quark mass and the Λ parameter of two flavor QCD, Nucl. Phys. **B865**, 397 (2012).
[718] [QCDSF 12] G. Bali, P. Bruns, S. Collins, M. Deka, B. Glasle *et al.*, Nucleon mass and sigma term from lattice QCD with two light fermion flavors, Nucl. Phys. **B866**, 1 (2013).
[719] [HotQCD 11] A. Bazavov, T. Bhattacharya, M. Cheng, C. DeTar, H. Ding *et al.*, The chiral and deconfinement aspects of the QCD transition, Phys. Rev. D **85**, 054503 (2012).
[720] S. Necco and R. Sommer, The $N_f = 0$ heavy quark potential from short to intermediate distances, Nucl. Phys. **B622**, 328 (2002).
[721] M. Lüscher and P. Weisz, Quark confinement and the bosonic string, J. High Energy Phys. 07 (2002) 049.
[722] [ALPHA 16] M. Dalla Brida, P. Fritzsch, T. Korzec, A. Ramos, S. Sint, and R. Sommer, Determination of the QCD Λ-parameter and the accuracy of perturbation theory at high energies, Phys. Rev. Lett. **117**, 182001 (2016).
[723] [ALPHA 18] M. Dalla Brida, P. Fritzsch, T. Korzec, A. Ramos, S. Sint, and R. Sommer, A non-perturbative exploration of the high energy regime in $N_f = 3$ QCD, Eur. Phys. J. C **78**, 372 (2018).
[724] M. Cacciari and N. Houdeau, Meaningful characterisation of perturbative theoretical uncertainties, J. High Energy Phys. 09 (2011) 039.
[725] [ALPHA 98A] A. Bode, U. Wolff, and P. Weisz, Two loop computation of the Schrodinger functional in pure SU(3) lattice gauge theory, Nucl. Phys. **B540**, 491 (1999).
[726] [ALPHA 99] A. Bode, P. Weisz, and U. Wolff, Two loop computation of the Schrödinger functional in lattice QCD, Nucl. Phys. **B576**, 517 (2000).
[727] W. Fischler, Quark-antiquark potential in QCD, Nucl. Phys. **B129**, 157 (1977).
[728] M. Peter, The Static quark—anti-quark potential in QCD to three loops, Phys. Rev. Lett. **78**, 602 (1997).
[729] M. Peter, The static potential in QCD: A full two loop calculation, Nucl. Phys. **B501**, 471 (1997).
[730] A. V. Smirnov, V. A. Smirnov, and M. Steinhauser, Three-loop static potential, Phys. Rev. Lett. **104**, 112002 (2010).
[731] A. V. Smirnov, V. A. Smirnov, and M. Steinhauser, Fermionic contributions to the three-loop static potential, Phys. Lett. B **668**, 293 (2008).
[732] [JLQCD 10] E. Shintani, S. Aoki, H. Fukaya, S. Hashimoto, T. Kaneko, T. Onogi, and N. Yamada, Strong coupling constant from vacuum polarization functions in three-flavor lattice QCD with dynamical overlap fermions, Phys. Rev. D **82**, 074505 (2010); Phys. Rev. D **89**, 099903(E) (2014).
[733] R. J. Hudspith, R. Lewis, K. Maltman, and E. Shintani, α_s from the lattice hadronic vacuum polarisation, arXiv: 1804.10286.
[734] [HPQCD 08A] C. T. H. Davies, K. Hornbostel, I. D. Kendall, G. P. Lepage, C. McNeile, J. Shigemitsu, and H. Trottier, Update: Accurate determinations of α_s from realistic lattice QCD, Phys. Rev. D **78**, 114507 (2008).
[735] G. P. Lepage and P. B. Mackenzie, On the viability of lattice perturbation theory, Phys. Rev. D **48**, 2250 (1993).
[736] K. Chetyrkin, J. H. Kuhn, and C. Sturm, Four-loop moments of the heavy quark vacuum polarization function in perturbative QCD, Eur. Phys. J. C **48**, 107 (2006).
[737] K. G. Chetyrkin, J. H. Kuhn, and M. Steinhauser, Heavy quark current correlators to $O(\alpha_s^2)$, Nucl. Phys. **B505**, 40 (1997).
[738] D. J. Broadhurst, Three loop on-shell charge renormalization without integration: Lambda-MS (QED) to four loops, Z. Phys. C **54**, 599 (1992).
[739] R. V. Harlander and T. Neumann, The perturbative QCD gradient flow to three loops, J. High Energy Phys. 06 (2016) 161.
[740] M. Lüscher, P. Weisz, and U. Wolff, A numerical method to compute the running coupling in asymptotically free theories, Nucl. Phys. **B359**, 221 (1991).
[741] S. Sint, On the Schrödinger functional in QCD, Nucl. Phys. **B421**, 135 (1994).
[742] A. Coste, A. Gonzalez-Arroyo, J. Jurkiewicz, and C. Korthals Altes, Zero momentum contribution to Wilson loops in periodic boxes, Nucl. Phys. **B262**, 67 (1985).
[743] M. Lüscher, R. Sommer, P. Weisz, and U. Wolff, A precise determination of the running coupling in the $SU(3)$ Yang-Mills theory, Nucl. Phys. **B413**, 481 (1994).
[744] S. Sint and R. Sommer, The running coupling from the QCD Schrödinger functional: A one loop analysis, Nucl. Phys. **B465**, 71 (1996).
[745] [*CP*-PACS 04] S. Takeda, S. Aoki, M. Fukugita, K.-I. Ishikawa, N. Ishizuka *et al.*, A scaling study of the step scaling function in $SU(3)$ gauge theory with improved gauge actions, Phys. Rev. D **70**, 074510 (2004).
[746] M. Lüscher, A semiclassical formula for the topological susceptibility in a finite space-time volume, Nucl. Phys. **B205**, 483 (1982).
[747] P. Fritzsch, A. Ramos, and F. Stollenwerk, Critical slowing down and the gradient flow coupling in the Schrödinger functional, Proc. Sci., Lattice2013 (**2014**) 461 [arXiv: 1311.7304].
[748] M. Dalla Brida, P. Fritzsch, T. Korzec, A. Ramos, S. Sint, and R. Sommer, Slow running of the gradient flow

coupling from 200 MeV to 4 GeV in $N_f = 3$ QCD, Phys. Rev. D **95**, 014507 (2017).
[749] C. Bonanno, J. L. Dasilva Golán, M. D'Elia, M. García Pérez, and A. Giorgieri, The SU(3) twisted gradient flow strong coupling without topology freezing, Eur. Phys. J. C **84**, 916 (2024).
[750] M. Lüscher, Step scaling, and the Yang-Mills gradient flow, J. High Energy Phys. 06 (2014) 105.
[751] R. Narayanan and H. Neuberger, Infinite N phase transitions in continuum Wilson loop operators, J. High Energy Phys. 03 (2006) 064.
[752] Z. Fodor, K. Holland, J. Kuti, D. Nogradi, and C. H. Wong, The Yang-Mills gradient flow in finite volume, J. High Energy Phys. 11 (2012) 007.
[753] P. Fritzsch and A. Ramos, The gradient flow coupling in the Schrödinger functional, J. High Energy Phys. 10 (2013) 008.
[754] A. Ramos, The gradient flow running coupling with twisted boundary conditions, J. High Energy Phys. 11 (2014) 101.
[755] K.-I. Ishikawa, I. Kanamori, Y. Murakami, A. Nakamura, M. Okawa, and R. Ueno, Non-perturbative determination of the Λ-parameter in the pure SU(3) gauge theory from the twisted gradient flow coupling, J. High Energy Phys. 12 (2017) 067.
[756] M. Dalla Brida and M. Lüscher, SMD-based numerical stochastic perturbation theory, Eur. Phys. J. C **77**, 308 (2017).
[757] E. I. Bribian and M. Garcia Perez, The twisted gradient flow coupling at one loop, J. High Energy Phys. 03 (2019) 200.
[758] [ALPHA 10A] F. Tekin, R. Sommer, and U. Wolff, The running coupling of QCD with four flavors, Nucl. Phys. **B840**, 114 (2010).
[759] P. Perez-Rubio and S. Sint, Non-perturbative running of the coupling from four flavour lattice QCD with staggered quarks, *Proc. Sci.*, LAT2010 (2010) 236 [arXiv:1011.6580].
[760] [ALPHA 04] M. Della Morte *et al.*, Computation of the strong coupling in QCD with two dynamical flavours, Nucl. Phys. **B713**, 378 (2005).
[761] [ALPHA 01A] A. Bode *et al.*, First results on the running coupling in QCD with two massless flavors, Phys. Lett. B **515**, 49 (2001).
[762] A. Nada and A. Ramos, An analysis of systematic effects in finite size scaling studies using the gradient flow, Eur. Phys. J. C **81**, 1 (2021).
[763] M. Dalla Brida and A. Ramos, The gradient flow coupling at high-energy and the scale of SU(3) Yang—Mills theory, Eur. Phys. J. C **79**, 720 (2019).
[764] [ALPHA 98] S. Capitani, M. Lüscher, R. Sommer, and H. Wittig, Nonperturbative quark mass renormalization in quenched lattice QCD, Nucl. Phys. **B544**, 669 (1999).
[765] J. Bulava and S. Schaefer, Improvement of $N_f = 3$ lattice QCD with Wilson fermions and tree-level improved gauge action, Nucl. Phys. **B874**, 188 (2013).
[766] M. Lüscher and P. Weisz, On-shell improved lattice gauge theories, Commun. Math. Phys. **97**, 59 (1985).
[767] [JLQCD/CP-PACS 04] N. Yamada *et al.*, Non-perturbative O(a)-improvement of Wilson quark action in three-flavor QCD with plaquette gauge action, Phys. Rev. D **71**, 054505 (2005).
[768] A. Gonzalez-Arroyo and M. Okawa, The string tension from smeared Wilson loops at large N, Phys. Lett. B **718**, 1524 (2013).
[769] M. Gerlach, F. Herren, and M. Steinhauser, Wilson coefficients for Higgs boson production and decoupling relations to $\mathcal{O}(\alpha_s^4)$, J. High Energy Phys. 11 (2018) 141.
[770] J. Balog, F. Niedermayer, and P. Weisz, The Puzzle of apparent linear lattice artifacts in the 2d non-linear sigma-model and Symanzik's solution, Nucl. Phys. **B824**, 563 (2010).
[771] J. Balog, F. Niedermayer, and P. Weisz, Logarithmic corrections to $O(a^2)$ lattice artifacts, Phys. Lett. B **676**, 188 (2009).
[772] N. Husung, P. Marquard, and R. Sommer, Asymptotic behavior of cutoff effects in Yang—Mills theory and in Wilson's lattice QCD, Eur. Phys. J. C **80**, 200 (2020).
[773] N. Husung, P. Marquard, and R. Sommer, The asymptotic approach to the continuum of lattice QCD spectral observables, Phys. Lett. B **829**, 137069 (2022).
[774] N. Husung, Logarithmic corrections to $O(a)$ and $O(a^2)$) effects in lattice QCD with Wilson or Ginsparg—Wilson quarks, Eur. Phys. J. C **83**, 142 (2023); Eur. Phys. J. C **83**, 144(E) (2023).
[775] [ALPHA 24] M. Dalla Brida, R. Höllwieser, F. Knechtli, T. Korzec, S. Sint, and R. Sommer, Heavy Wilson quarks and O(a) improvement: Nonperturbative results for b_g, J. High Energy Phys. 01 (2024) 188.
[776] C. Michael, The running coupling from lattice gauge theory, Phys. Lett. B **283**, 103 (1992).
[777] [UKQCD 92] S. P. Booth, D. S. Henty, A. Hulsebos, A. C. Irving, C. Michael, and P. W. Stephenson, The running coupling from SU(3) lattice gauge theory, Phys. Lett. B **294**, 385 (1992).
[778] A. Billoire, How heavy must be quarks in order to build coulombic $q\bar{q}$ bound states, Phys. Lett. B **92**, 343 (1980).
[779] Y. Schröder, The static potential in QCD to two loops, Phys. Lett. B **447**, 321 (1999).
[780] N. Brambilla, A. Pineda, J. Soto, and A. Vairo, The infrared behavior of the static potential in perturbative QCD, Phys. Rev. D **60**, 091502 (1999).
[781] C. Anzai, Y. Kiyo, and Y. Sumino, Static QCD potential at three-loop order, Phys. Rev. Lett. **104**, 112003 (2010).
[782] N. Brambilla, A. Vairo, X. Garcia i Tormo, and J. Soto, The QCD static energy at NNNLL, Phys. Rev. D **80**, 034016 (2009).
[783] A. H. Hoang, A. V. Manohar, and I. W. Stewart, The running Coulomb potential and lamb shift in QCD, Phys. Rev. D **64**, 014033 (2001).
[784] A. H. Hoang and I. W. Stewart, Ultrasoft renormalization in nonrelativistic QCD, Phys. Rev. D **67**, 114020 (2003).
[785] S. Necco and R. Sommer, Testing perturbation theory on the $N_f = 0$ static quark potential, Phys. Lett. B **523**, 135 (2001).
[786] H. Takaura, T. Kaneko, Y. Kiyo, and Y. Sumino, Determination of α_s from static QCD potential with renormalon subtraction, Phys. Lett. B **789**, 598 (2019).

[787] H. Takaura, T. Kaneko, Y. Kiyo, and Y. Sumino, Determination of α_s from static QCD potential: OPE with renormalon subtraction and lattice QCD, J. High Energy Phys. 04 (2019) 155.
[788] A. Bazavov, N. Brambilla, X. Garcia i Tormo, P. Petreczky, J. Soto, and A. Vairo, Determination of α_s from the QCD static energy: An update, Phys. Rev. D **90**, 074038 (2014).
[789] A. Bazavov, N. Brambilla, X. Garcia i Tormo, P. Petreczky, J. Soto, and A. Vairo, Determination of α_s from the QCD static energy, Phys. Rev. D **86**, 114031 (2012).
[790] F. Karbstein, M. Wagner, and M. Weber, Determination of $\Lambda_{\overline{\rm MS}}^{(n_f=2)}$ and analytic parametrization of the static quark-antiquark potential, Phys. Rev. D **98**, 114506 (2018).
[791] F. Karbstein, A. Peters, and M. Wagner, $\Lambda_{\overline{\rm MS}}^{(n_f=2)}$ from a momentum space analysis of the quark-antiquark static potential, J. High Energy Phys. 09 (2014) 114.
[792] [ETM 11C] K. Jansen, F. Karbstein, A. Nagy, and M. Wagner, $\Lambda_{\overline{\rm MS}}$ from the static potential for QCD with $N_f = 2$ dynamical quark flavors, J. High Energy Phys. 01 (2012) 025.
[793] N. Husung, A. Nada, and R. Sommer, Yang Mills short distance potential and perturbation theory, Proc. Sci., LATTICE2019 (**2020**) 263.
[794] N. Husung, M. Koren, P. Krah, and R. Sommer, SU(3) Yang Mills theory at small distances and fine lattices, EPJ Web Conf. **175**, 14024 (2018).
[795] N. Brambilla, X. Garcia i Tormo, J. Soto, and A. Vairo, Precision determination of $r_0\Lambda_{\overline{\rm MS}}$ from the QCD static energy, Phys. Rev. Lett. **105**, 212001 (2010).
[796] G. S. Bali and K. Schilling, Running coupling and the Λ-parameter from $SU(3)$ lattice simulations, Phys. Rev. D **47**, 661 (1993).
[797] A. Bazavov, P. Petreczky, and J. Weber, Equation of state in $2+1$ flavor QCD at high temperatures, Phys. Rev. D **97**, 014510 (2018).
[798] J. H. Weber, A. Bazavov, and P. Petreczky, Equation of state in $(2+1)$ flavor QCD at high temperatures, Proc. Sci., Confinement2018 (**2019**) 166 [arXiv:1811.12902].
[799] M. Berwein, N. Brambilla, P. Petreczky, and A. Vairo, Polyakov loop correlator in perturbation theory, Phys. Rev. D **96**, 014025 (2017); Phys. Rev. D **101**, 099903(A) (2020).
[800] W. I. Jay and E. T. Neil, Bayesian model averaging for analysis of lattice field theory results, Phys. Rev. D **103**, 114502 (2021).
[801] R. Brüser, A. H. Hoang, and M. Stahlhofen, Three-loop OPE Wilson coefficients of dimension-four operators for (axial-)vector and (pseudo-)scalar current correlators, J. High Energy Phys. 12 (2024) 103.
[802] K. G. Chetyrkin, A. L. Kataev, and F. V. Tkachov, Higher order corrections to $\sigma_{\rm tot}(e^+e^- \to \text{Hadrons})$ in quantum chromodynamics, Phys. Lett. **85B**, 277 (1979).
[803] L. R. Surguladze and M. A. Samuel, Total hadronic cross-section in e^+e^- annihilation at the four loop level of perturbative QCD, Phys. Rev. Lett. **66**, 560 (1991); Phys. Rev. Lett. **66**, 2416(E) (1991).
[804] S. G. Gorishnii, A. L. Kataev, and S. A. Larin, The $O(\alpha_s^3)$ corrections to $\sigma_{\rm tot}(e^+e^- \to \text{hadrons})$ and $\Gamma(\tau^- \to \nu_\tau + \text{hadrons})$ in QCD, Phys. Lett. B **259**, 144 (1991).
[805] P. A. Baikov, K. G. Chetyrkin, and J. H. Kuhn, Order α_s^4 QCD corrections to Z and τ decays, Phys. Rev. Lett. **101**, 012002 (2008).
[806] I. Balitsky, M. Beneke, and V. M. Braun, Instanton contributions to the τ decay widths, Phys. Lett. B **318**, 371 (1993).
[807] K. Chetyrkin and A. Maier, Massless correlators of vector, scalar and tensor currents in position space at orders α_s^3 and α_s^4: Explicit analytical results, Nucl. Phys. **B844**, 266 (2011).
[808] [JLQCD/TWQCD 08C] E. Shintani, S. Aoki, T. W. Chiu, S. Hashimoto, T. H. Hsieh, T. Kaneko, H. Matsufuru, J. Noaki, T. Onogi, and N. Yamada, Lattice study of the vacuum polarization function and determination of the strong coupling constant, Phys. Rev. D **79**, 074510 (2009).
[809] R. J. Hudspith, R. Lewis, K. Maltman, and E. Shintani, Determining the QCD coupling from lattice vacuum polarization, in *Proceedings, 33rd International Symposium on Lattice Field Theory (Lattice 2015)* (2016), Vol. LATTICE2015, p. 268, http://inspirehep.net/record/1398355/files/arXiv:1510.04890.pdf.
[810] R. Hudspith, R. Lewis, K. Maltman, and E. Shintani, α_s from the hadronic vacuum polarisation, EPJ Web Conf. **175**, 10006 (2018).
[811] [HPQCD 05A] Q. Mason, H. D. Trottier, C. T. H. Davies, K. Foley, A. Gray, G. P. Lepage, M. Nobes, and J. Shigemitsu, Accurate determinations of α_s from realistic lattice QCD, Phys. Rev. Lett. **95**, 052002 (2005).
[812] K. Hornbostel, G. Lepage, and C. Morningstar, Scale setting for α_s beyond leading order, Phys. Rev. D **67**, 034023 (2003).
[813] [QCDSF/UKQCD 05] M. Göckeler, R. Horsley, A. Irving, D. Pleiter, P. Rakow, G. Schierholz *et al.*, A determination of the Lambda parameter from full lattice QCD, Phys. Rev. D **73**, 014513 (2006).
[814] [SESAM 99] A. Spitz, H. Hoeber, N. Eicker, S. Güsken, Th. Lippert, K. Schilling, T. Struckmann, P. Ueberholz, and J. Viehoff, α_s from upsilon spectroscopy with dynamical Wilson fermions, Phys. Rev. D **60**, 074502 (1999).
[815] M. Wingate, T. A. DeGrand, S. Collins, and U. M. Heller, From spectroscopy to the strong coupling constant with heavy Wilson quarks, Phys. Rev. D **52**, 307 (1995).
[816] C. T. H. Davies, K. Hornbostel, G. P. Lepage, A. Lidsey, J. Shigemitsu, and J. Sloan, A precise determination of α_s from lattice QCD, Phys. Lett. B **345**, 42 (1995).
[817] S. Aoki, M. Fukugita, S. Hashimoto, N. Ishizuka, H. Mino, M. Okawa, T. Onogi, and A. Ukawa, Manifestation of sea quark effects in the strong coupling constant in lattice QCD, Phys. Rev. Lett. **74**, 22 (1995).
[818] M. Kitazawa, T. Iritani, M. Asakawa, T. Hatsuda, and H. Suzuki, Equation of state for SU(3) gauge theory via the energy-momentum tensor under gradient flow, Phys. Rev. D **94**, 114512 (2016).
[819] [FlowQCD 15] M. Asakawa, T. Iritani, M. Kitazawa, and H. Suzuki, Determination of reference scales for Wilson gauge action from Yang–Mills gradient flow, arXiv:1503.06516.
[820] A. X. El-Khadra, G. Hockney, A. S. Kronfeld, and P. B. Mackenzie, A determination of the strong coupling

constant from the charmonium spectrum, Phys. Rev. Lett. **69**, 729 (1992).
[821] [QCDSF/UKQCD 04A] M. Göckeler, R. Horsley, A. Irving, D. Pleiter, P. E. L. Rakow, G. Schierholz, and H. Stüben, Determination of Λ in quenched and full QCD: An update, Nucl. Phys. B, Proc. Suppl. **140**, 228 (2005).
[822] S. Booth, M. Göckeler, R. Horsley, A. Irving, B. Joo, S. Pickles *et al.*, The strong coupling constant from lattice QCD with $N_f = 2$ dynamical quarks, Nucl. Phys. B, Proc. Suppl. **106**, 308 (2002).
[823] [QCDSF/UKQCD 01] S. Booth, M. Göckeler, R. Horsley, A. Irving, B. Joo, S. Pickles *et al.*, Determination of $\Lambda_{\overline{\rm MS}}$ from quenched and $N_f = 2$ dynamical QCD, Phys. Lett. B **519**, 229 (2001).
[824] R. Sommer, Scale setting in lattice QCD, Proc. Sci., LATTICE2013 (**2014**) 015 [arXiv:1401.3270].
[825] [HPQCD 03A] C. T. H. Davies *et al.*, High-precision lattice QCD confronts experiment, Phys. Rev. Lett. **92**, 022001 (2004).
[826] Q. J. Mason, High-precision lattice QCD: Perturbations in a non-perturbative world, Ph.D. thesis, Cornell University, LNS, 2004.
[827] K. Maltman, Two recent high-precision determinations of α_s, AIP Conf. Proc. **1261**, 159 (2010).
[828] A. Bochkarev and P. de Forcrand, Determination of the renormalized heavy quark mass in lattice QCD, Nucl. Phys. **B477**, 489 (1996).
[829] B. Dehnadi, A. H. Hoang, and V. Mateu, Bottom and charm mass determinations with a convergence test, J. High Energy Phys. 08 (2015) 155.
[830] R. Boughezal, M. Czakon, and T. Schutzmeier, Charm and bottom quark masses from perturbative QCD, Phys. Rev. D **74**, 074006 (2006).
[831] A. Maier, P. Maierhofer, and P. Marqaurd, The second physical moment of the heavy quark vector correlator at $O(\alpha_s^3)$, Phys. Lett. B **669**, 88 (2008).
[832] A. Maier, P. Maierhofer, P. Marquard, and A. Smirnov, Low energy moments of heavy quark current correlators at four loops, Nucl. Phys. **B824**, 1 (2010).
[833] Y. Kiyo, A. Maier, P. Maierhofer, and P. Marquard, Reconstruction of heavy quark current correlators at $O(\alpha_s^3)$, Nucl. Phys. **B823**, 269 (2009).
[834] J. H. Kühn, M. Steinhauser, and C. Sturm, Heavy quark masses from sum rules in four-loop approximation, Nucl. Phys. **B778**, 192 (2007).
[835] K. Chetyrkin, J. Kuhn, A. Maier, P. Maierhofer, P. Marquard, M. Steinhauser, and C. Sturm, Charm and bottom quark masses: An update, Phys. Rev. D **80**, 074010 (2009).
[836] D. Boito and V. Mateu, Precise determination of α_s from relativistic quarkonium sum rules, J. High Energy Phys. 03 (2020) 094.
[837] L. Chimirri and R. Sommer, Investigation of the perturbative expansion of moments of heavy quark correlators for $N_f = 0$, Proc. Sci., LATTICE2021 (**2022**) 354 [arXiv:2203.07936].
[838] R. Sommer, L. Chimirri, and N. Husung, Log-enhanced discretization errors in integrated correlation functions, Proc. Sci., LATTICE2022 (**2023**) 358 [arXiv:2211.15750].
[839] M. Lüscher and P. Weisz, Perturbative analysis of the gradient flow in non-Abelian gauge theories, J. High Energy Phys. 02 (2011) 051.
[840] Z. Fodor, K. Holland, J. Kuti, D. Nogradi, and C. H. Wong, A new method for the beta function in the chiral symmetry broken phase, EPJ Web Conf. **175**, 08027 (2018).
[841] D. Boito and V. Mateu, Precise α_s determination from charmonium sum rules, Phys. Lett. B **806**, 135482 (2020).
[842] S. Zafeiropoulos, P. Boucaud, F. De Soto, J. Rodríguez-Quintero, and J. Segovia, Strong running coupling from the gauge sector of domain wall lattice QCD with physical quark masses, Phys. Rev. Lett. **122**, 162002 (2019).
[843] [ETM 13D] B. Blossier *et al.*, High statistics determination of the strong coupling constant in Taylor scheme and its OPE Wilson coefficient from lattice QCD with a dynamical charm, Phys. Rev. D **89**, 014507 (2014).
[844] [ETM 12C] B. Blossier, P. Boucaud, M. Brinet, F. De Soto, X. Du, V. Morenas, O. Pène, K. Petrov, and J. Rodríguez-Quintero, The strong running coupling at τ and Z_0 mass scales from lattice QCD, Phys. Rev. Lett. **108**, 262002 (2012).
[845] [ETM 11D] B. Blossier, P. Boucaud, M. Brinet, F. De Soto, X. Du *et al.*, Ghost-gluon coupling, power corrections and $\Lambda_{\overline{\rm MS}}$ from lattice QCD with a dynamical charm, Phys. Rev. D **85**, 034503 (2012).
[846] K. Nakayama, H. Fukaya, and S. Hashimoto, Lattice computation of the Dirac eigenvalue density in the perturbative regime of QCD, Phys. Rev. D **98**, 014501 (2018).
[847] K. G. Chetyrkin, G. Falcioni, F. Herzog, and J. A. M. Vermaseren, Five-loop renormalisation of QCD in covariant gauges, J. High Energy Phys. 10 (2017) 179; J. High Energy Phys. 12 (2017) 006(A).
[848] [RQCD 19] G. S. Bali, L. Barca, S. Collins, M. Gruber, M. Löffler, A. Schäfer, W. Söldner, P. Wein, S. Weishäupl, and T. Wurm, Nucleon axial structure from lattice QCD, J. High Energy Phys. 05 (2020) 126.
[849] Y.-C. Jang, R. Gupta, H.-W. Lin, B. Yoon, and T. Bhattacharya, Nucleon electromagnetic form factors in the continuum limit from $(2 + 1 + 1)$-flavor lattice QCD, Phys. Rev. D **101**, 014507 (2020).
[850] [LHPC 19] N. Hasan, J. Green, S. Meinel, M. Engelhardt, S. Krieg, J. Negele, A. Pochinsky, and S. Syritsyn, Nucleon axial, scalar, and tensor charges using lattice QCD at the physical pion mass, Phys. Rev. D **99**, 114505 (2019).
[851] C. Alexandrou *et al.*, Nucleon axial and pseudoscalar form factors from lattice QCD at the physical point, Phys. Rev. D **103**, 034509 (2021).
[852] A. S. Meyer *et al.*, Nucleon axial form factor from domain wall on HISQ, Proc. Sci., LATTICE2021 (**2022**) 081 [arXiv:2111.06333].
[853] D. Djukanovic, T. Harris, G. von Hippel, P. M. Junnarkar, H. B. Meyer, D. Mohler, K. Ottnad, T. Schulz, J. Wilhelm, and H. Wittig, Isovector electromagnetic form factors of the nucleon from lattice QCD and the proton radius puzzle, Phys. Rev. D **103**, 094522 (2021).
[854] [Mainz 22] D. Djukanovic, G. von Hippel, J. Koponen, H. B. Meyer, K. Ottnad, T. Schulz, and H. Wittig, Isovector axial form factor of the nucleon from lattice QCD, Phys. Rev. D **106**, 074503 (2022).

[855] [PACS 23] R. Tsuji, Y. Aoki, K.-I. Ishikawa, Y. Kuramashi, S. Sasaki, K. Sato *et al.*, Nucleon form factors in $N_f = 2 + 1$ lattice QCD at the physical point: Finite lattice spacing effect on the root-mean-square radii, Phys. Rev. D **109**, 094505 (2024).
[856] D. Djukanovic, G. von Hippel, H. B. Meyer, K. Ottnad, M. Salg, and H. Wittig, Electromagnetic form factors of the nucleon from $Nf = 2 + 1$ lattice QCD, Phys. Rev. D **109**, 094510 (2024).
[857] D. Djukanovic, G. von Hippel, H. B. Meyer, K. Ottnad, M. Salg, and H. Wittig, Precision calculation of the electromagnetic radii of the proton and neutron from lattice QCD, Phys. Rev. Lett. **132**, 211901 (2024).
[858] D. Djukanovic, G. von Hippel, H. B. Meyer, K. Ottnad, M. Salg, and H. Wittig, Zemach and Friar radii of the proton and neutron from lattice QCD, Phys. Rev. D **110**, L011503 (2024).
[859] H.-W. Lin *et al.*, Parton distributions and lattice QCD calculations: A community white paper, Prog. Part. Nucl. Phys. **100**, 107 (2018).
[860] M. Constantinou, The x-dependence of hadronic parton distributions: A review on the progress of lattice QCD, Eur. Phys. J. A **57**, 77 (2021).
[861] M. Constantinou *et al.*, Parton distributions and lattice QCD calculations: Toward 3D structure, Prog. Part. Nucl. Phys. **121**, 103908 (2021).
[862] K. Cichy and M. Constantinou, A guide to light-cone PDFs from lattice QCD: An overview of approaches, techniques and results, Adv. High Energy Phys. **2019**, 3036904 (2019).
[863] C. Monahan, Recent developments in x-dependent structure calculations, Proc. Sci., LATTICE2018 (**2018**) 018 [arXiv:1811.00678].
[864] M. Constantinou *et al.*, Lattice QCD calculations of parton physics, arXiv:2202.07193.
[865] L. Del Debbio, An overview of lattice results for parton distribution functions, SciPost Phys. Proc. **15**, 028 (2024).
[866] M. J. Savage, Nuclear physics from lattice QCD, Prog. Part. Nucl. Phys. **67**, 140 (2012).
[867] [NPLQCD 17] E. Chang, Z. Davoudi, W. Detmold, A. S. Gambhir, K. Orginos, M. J. Savage, P. E. Shanahan, M. L. Wagman, and F. Winter, Scalar, axial, and tensor interactions of light nuclei from lattice QCD, Phys. Rev. Lett. **120**, 152002 (2018).
[868] T. Iritani, Two-baryon systems from HAL QCD method, and the mirage in the temporal correlation of the direct method, EPJ Web Conf. **175**, 05008 (2018).
[869] M. L. Wagman, F. Winter, E. Chang, Z. Davoudi, W. Detmold, K. Orginos, M. J. Savage, and P. E. Shanahan, Baryon-baryon interactions and spin-flavor symmetry from lattice quantum chromodynamics, Phys. Rev. D **96**, 114510 (2017).
[870] Y.-C. Jang, R. Gupta, B. Yoon, and T. Bhattacharya, Axial vector form factors from lattice QCD that satisfy the PCAC relation, Phys. Rev. Lett. **124**, 072002 (2020).
[871] H. W. Hamber, E. Marinari, G. Parisi, and C. Rebbi, Considerations on numerical analysis of QCD, Nucl. Phys. **B225**, 475 (1983).
[872] [QCDSF 06] A. A. Khan, M. Göckeler, P. Hägler, T. Hemmert, R. Horsley *et al.*, Axial coupling constant of the nucleon for two flavours of dynamical quarks in finite and infinite volume, Phys. Rev. D **74**, 094508 (2006).
[873] [QCDSF 13] R. Horsley, Y. Nakamura, A. Nobile, P. Rakow, G. Schierholz, and J. M. Zanotti, Nucleon axial charge and pion decay constant from two-flavor lattice QCD, Phys. Lett. B **732**, 41 (2014).
[874] [Mainz 12] S. Capitani, M. Della Morte, G. von Hippel, B. Jager, A. Jüttner, B. Knippschild, H. B. Meyer, and H. Wittig, The nucleon axial charge from lattice QCD with controlled errors, Phys. Rev. D **86**, 074502 (2012).
[875] [RQCD 14] G. S. Bali, S. Collins, B. Glässle, M. Göckeler, J. Najjar, R. H. Rödl *et al.*, Nucleon isovector couplings from $N_f = 2$ lattice QCD, Phys. Rev. D **91**, 054501 (2015).
[876] [RQCD 16] G. S. Bali, S. Collins, D. Richtmann, A. Schäfer, W. Söldner, and A. Sternbeck, Direct determinations of the nucleon and pion σ terms at nearly physical quark masses, Phys. Rev. D **93**, 094504 (2016).
[877] [Mainz 17] S. Capitani, M. Della Morte, D. Djukanovic, G. M. von Hippel, J. Hua, B. Jäger, P. M. Junnarkar, H. B. Meyer, T. D. Rae, and H. Wittig, Iso-vector axial form factors of the nucleon in two-flavor lattice QCD, Int. J. Mod. Phys. A **34**, 1950009 (2019).
[878] [PACS-CS 09] K.-I. Ishikawa *et al.*, SU(2) and SU(3) chiral perturbation theory analyses on baryon masses in $2 + 1$ flavor lattice QCD, Phys. Rev. D **80**, 054502 (2009).
[879] [PACS 18] K.-I. Ishikawa, Y. Kuramashi, S. Sasaki, N. Tsukamoto, A. Ukawa, and T. Yamazaki, Nucleon form factors on a large volume lattice near the physical point in $2 + 1$ flavor QCD, Phys. Rev. D **98**, 074510 (2018).
[880] [ETM 15D] A. Abdel-Rehim *et al.*, Nucleon and pion structure with lattice QCD simulations at physical value of the pion mass, Phys. Rev. D **92**, 114513 (2015); Phys. Rev. D **93**, 039904(E) (2016).
[881] [ETM 16A] A. Abdel-Rehim, C. Alexandrou, M. Constantinou, K. Hadjiyiannakou, K. Jansen, C. Kallidonis, G. Koutsou, and A. Vaquero Avilés-Casco, Direct evaluation of the quark content of nucleons from lattice QCD at the physical point, Phys. Rev. Lett. **116**, 252001 (2016).
[882] [ETM 17B] C. Alexandrou, M. Constantinou, K. Hadjiyiannakou, K. Jansen, C. Kallidonis, G. Koutsou *et al.*, Nucleon axial form factors using $N_f = 2$ twisted mass fermions with a physical value of the pion mass, Phys. Rev. D **96**, 054507 (2017).
[883] [ETM 17C] C. Alexandrou, M. Constantinou, K. Hadjiyiannakou, K. Jansen, C. Kallidonis, G. Koutsou, A. Vaquero Avilés-Casco, and C. Wiese, Nucleon spin and momentum decomposition using lattice QCD simulations, Phys. Rev. Lett. **119**, 142002 (2017).
[884] [ETM 17] C. Alexandrou *et al.*, Nucleon scalar and tensor charges using lattice QCD simulations at the physical value of the pion mass, Phys. Rev. D **95**, 114514 (2017); Phys. Rev. D **96**, 099906(E) (2017).
[885] [PNDME 13] T. Bhattacharya, S. D. Cohen, R. Gupta, A. Joseph, H.-W. Lin, and B. Yoon, Nucleon charges and electromagnetic form factors from $2 + 1 + 1$-flavor lattice QCD, Phys. Rev. D **89**, 094502 (2014).
[886] [PNDME 15A] T. Bhattacharya, V. Cirigliano, S. Cohen, R. Gupta, A. Joseph, H.-W. Lin *et al.*, Iso-vector and

Iso-scalar tensor charges of the nucleon from lattice QCD, Phys. Rev. D **92**, 094511 (2015).
[887] [PNDME 15] T. Bhattacharya, V. Cirigliano, R. Gupta, H.-W. Lin, and B. Yoon, Neutron electric dipole moment and tensor charges from lattice QCD, Phys. Rev. Lett. **115**, 212002 (2015).
[888] [PNDME 16] T. Bhattacharya, V. Cirigliano, S. Cohen, R. Gupta, H.-W. Lin, and B. Yoon, Axial, scalar and tensor charges of the nucleon from $2+1+1$-flavor lattice QCD, Phys. Rev. D **94**, 054508 (2016).
[889] [CalLat 17] E. Berkowitz *et al.*, An accurate calculation of the nucleon axial charge with lattice QCD, arXiv:1704.01114.
[890] [PNDME 18] R. Gupta, Y.-C. Jang, B. Yoon, H.-W. Lin, V. Cirigliano, and T. Bhattacharya, Isovector charges of the nucleon from $2+1+1$-flavor lattice QCD, Phys. Rev. D **98**, 034503 (2018).
[891] [RBC/UKQCD 08B] T. Yamazaki, Y. Aoki, T. Blum, H. W. Lin, M. F. Lin, S. Ohta, S. Sasaki, R. J. Tweedie, and J. M. Zanotti, Nucleon axial charge in $2+1$ flavor dynamical lattice QCD with domain wall fermions, Phys. Rev. Lett. **100**, 171602 (2008).
[892] [RBC/UKQCD 09B] T. Yamazaki, Y. Aoki, T. Blum, H.-W. Lin, S. Ohta, S. Sasaki, R. Tweedie, and J. Zanotti, Nucleon form factors with $2+1$ flavor dynamical domain-wall fermions, Phys. Rev. D **79**, 114505 (2009).
[893] [RBC/UKQCD 10D] Y. Aoki, T. Blum, H.-W. Lin, S. Ohta, S. Sasaki, R. Tweedie *et al.*, Nucleon isovector structure functions in $(2+1)$-flavor QCD with domain wall fermions, Phys. Rev. D **82**, 014501 (2010).
[894] [χQCD 13A] M. Gong *et al.*, Strangeness and charmness content of the nucleon from overlap fermions on $2+1$-flavor domain-wall fermion configurations, Phys. Rev. D **88**, 014503 (2013).
[895] [χQCD 15] M. Gong, Y.-B. Yang, J. Liang, A. Alexandru, T. Draper, and K.-F. Liu, Strange and charm quark spins from the anomalous Ward identity, Phys. Rev. D **95**, 114509 (2017).
[896] [JLQCD 08B] H. Ohki, H. Fukaya, S. Hashimoto, T. Kaneko, H. Matsufuru, J. Noaki *et al.*, Nucleon sigma term and strange quark content from lattice QCD with exact chiral symmetry, Phys. Rev. D **78**, 054502 (2008).
[897] [JLQCD 12A] H. Ohki, K. Takeda, S. Aoki, S. Hashimoto, T. Kaneko, H. Matsufuru, J. Noaki, and T. Onogi, Nucleon strange quark content from $N_f = 2+1$ lattice QCD with exact chiral symmetry, Phys. Rev. D **87**, 034509 (2013).
[898] [JLQCD 18] N. Yamanaka, S. Hashimoto, T. Kaneko, and H. Ohki, Nucleon charges with dynamical overlap fermions, Phys. Rev. D **98**, 054516 (2018).
[899] R. Babich, J. Brannick, R. C. Brower, M. A. Clark, T. A. Manteuffel, S. F. McCormick, J. C. Osborn, and C. Rebbi, Adaptive multigrid algorithm for the lattice Wilson-Dirac operator, Phys. Rev. Lett. **105**, 201602 (2010).
[900] M. Lüscher, Deflation acceleration of lattice QCD simulations, J. High Energy Phys. 12 (2007) 011.
[901] G. S. Bali, S. Collins, and A. Schafer, Effective noise reduction techniques for disconnected loops in lattice QCD, Comput. Phys. Commun. **181**, 1570 (2010).
[902] T. Blum, T. Izubuchi, and E. Shintani, New class of variance-reduction techniques using lattice symmetries, Phys. Rev. D **88**, 094503 (2013).
[903] A. Stathopoulos, J. Laeuchli, and K. Orginos, Hierarchical probing for estimating the trace of the matrix inverse on toroidal lattices, SIAM J. Sci. Comput. **35**, S299 (2013).
[904] A. S. Gambhir, A. Stathopoulos, K. Orginos, B. Yoon, R. Gupta, and S. Syritsyn, Algorithms for disconnected diagrams in lattice QCD, Proc. Sci., LATTICE2016 (**2016**) 265 [arXiv:1611.01193].
[905] [LHPC 10] J. D. Bratt *et al.*, Nucleon structure from mixed action calculations using $2+1$ flavors of asqtad sea and domain wall valence fermions, Phys. Rev. D **82**, 094502 (2010).
[906] B. Yoon *et al.*, Controlling excited-state contamination in nucleon matrix elements, Phys. Rev. D **93**, 114506 (2016).
[907] T. A. DeGrand and S. Schaefer, Improving meson two point functions in lattice QCD, Comput. Phys. Commun. **159**, 185 (2004).
[908] L. Giusti, P. Hernandez, M. Laine, P. Weisz, and H. Wittig, Low-energy couplings of QCD from current correlators near the chiral limit, J. High Energy Phys. 04 (2004) 013.
[909] R. Gupta, A. Patel, C. F. Baillie, G. Guralnik, G. W. Kilcup, and S. R. Sharpe, QCD with dynamical Wilson fermions, Phys. Rev. D **40**, 2072 (1989).
[910] C. Thron, S. Dong, K. Liu, and H. Ying, Pade—Z(2) estimator of determinants, Phys. Rev. D **57**, 1642 (1998).
[911] S. Bernardson, P. McCarty, and C. Thron, Monte Carlo methods for estimating linear combinations of inverse matrix entries in lattice QCD, Comput. Phys. Commun. **78**, 256 (1993).
[912] J. Foley, K. Jimmy Juge, A. Ó. Cais, M. Peardon, S. M. Ryan, and J.-I. Skullerud, Practical all-to-all propagators for lattice QCD, Comput. Phys. Commun. **172**, 145 (2005).
[913] S. Güsken, U. Löw, K. H. Mütter, R. Sommer, A. Patel, and K. Schilling, Nonsinglet axial vector couplings of the baryon octet in lattice QCD, Phys. Lett. B **227**, 266 (1989).
[914] C. Alexandrou, F. Jegerlehner, S. Gusken, K. Schilling, and R. Sommer, B meson properties from lattice QCD, Phys. Lett. B **256**, 60 (1991).
[915] D. S. Roberts, W. Kamleh, D. B. Leinweber, M. S. Mahbub, and B. J. Menadue, Accessing high momentum states in lattice QCD, Phys. Rev. D **86**, 074504 (2012).
[916] G. S. Bali, B. Lang, B. U. Musch, and A. Schäfer, Novel quark smearing for hadrons with high momenta in lattice QCD, Phys. Rev. D **93**, 094515 (2016).
[917] B. C. Tiburzi, Time dependence of nucleon correlation functions in chiral perturbation theory, Phys. Rev. D **80**, 014002 (2009).
[918] O. Bär, Multi-hadron-state contamination in nucleon observables from chiral perturbation theory, EPJ Web Conf. **175**, 01007 (2018).
[919] O. Bär, Nucleon-pion-state contribution in lattice calculations of the nucleon charges g_A, g_T and g_S, Phys. Rev. D **94**, 054505 (2016).
[920] O. Bär, Nucleon-pion-state contribution in lattice calculations of moments of parton distribution functions, Phys. Rev. D **95**, 034506 (2017).

[921] M. T. Hansen and H. B. Meyer, On the effect of excited states in lattice calculations of the nucleon axial charge, Nucl. Phys. **B923**, 558 (2017).
[922] B. Yoon *et al.*, Isovector charges of the nucleon from $2+1$-flavor QCD with clover fermions, Phys. Rev. D **95**, 074508 (2017).
[923] [Mainz 19] T. Harris, G. von Hippel, P. Junnarkar, H. B. Meyer, K. Ottnad, J. Wilhelm, H. Wittig, and L. Wrang, Nucleon isovector charges and twist-2 matrix elements with $N_f = 2+1$ dynamical Wilson quarks, Phys. Rev. D **100**, 034513 (2019).
[924] L. Maiani, G. Martinelli, M. L. Paciello, and B. Taglienti, Scalar densities and baryon mass differences in lattice QCD with Wilson fermions, Nucl. Phys. **B293**, 420 (1987).
[925] S. J. Dong, K. F. Liu, and A. G. Williams, Lattice calculation of the strangeness magnetic moment of the nucleon, Phys. Rev. D **58**, 074504 (1998).
[926] S. Capitani, B. Knippschild, M. Della Morte, and H. Wittig, Systematic errors in extracting nucleon properties from lattice QCD, Proc. Sci., LATTICE2010 (**2010**) 147 [arXiv:1011.1358].
[927] J. Bulava, M. Donnellan, and R. Sommer, On the computation of hadron-to-hadron transition matrix elements in lattice QCD, J. High Energy Phys. 01 (2012) 140.
[928] S. Güsken, K. Schilling, R. Sommer, K. H. Mütter, and A. Patel, Mass splittings in the baryon octet and the nucleon σ term in lattice QCD, Phys. Lett. B **212**, 216 (1988).
[929] R. Sommer, Current matrix elements with quenched Wilson fermions, Nucl. Phys. B, Proc. Suppl. **17**, 513 (1990).
[930] C. Bouchard, C. C. Chang, T. Kurth, K. Orginos, and A. Walker-Loud, On the Feynman-Hellmann theorem in quantum field theory and the calculation of matrix elements, Phys. Rev. D **96**, 014504 (2017).
[931] [CSSM/QCDSF/UKQCD 14] A. J. Chambers *et al.*, Feynman-Hellmann approach to the spin structure of hadrons, Phys. Rev. D **90**, 014510 (2014).
[932] A. J. Chambers *et al.*, Disconnected contributions to the spin of the nucleon, Phys. Rev. D **92**, 114517 (2015).
[933] B. J. Owen, J. Dragos, W. Kamleh, D. B. Leinweber, M. S. Mahbub, B. J. Menadue, and J. M. Zanott, Variational approach to the calculation of gA, Phys. Lett. B **723**, 217 (2013).
[934] C. Egerer, D. Richards, and F. Winter, Controlling excited-state contributions with distillation in lattice QCD calculations of nucleon isovector charges g_S^{u-d}, g_A^{u-d}, g_T^{u-d}, Phys. Rev. D **99**, 034506 (2019).
[935] G. Fox, R. Gupta, O. Martin, and S. Otto, Monte Carlo estimates of the mass gap of the O(2) and O(3) spin models in $(1+1)$-dimensions, Nucl. Phys. **B205**, 188 (1982).
[936] C. Michael, Adjoint sources in lattice gauge theory, Nucl. Phys. **B259**, 58 (1985).
[937] M. Lüscher and U. Wolff, How to calculate the elastic scattering matrix in two-dimensional quantum field theories by numerical simulation, Nucl. Phys. **B339**, 222 (1990).
[938] B. Blossier, M. Della Morte, G. von Hippel, T. Mendes, and R. Sommer, On the generalized eigenvalue method for energies and matrix elements in lattice field theory, J. High Energy Phys. 04 (2009) 094.
[939] J. Dragos, R. Horsley, W. Kamleh, D. B. Leinweber, Y. Nakamura, P. E. L. Rakow, G. Schierholz, R. D. Young, and J. M. Zanotti, Nucleon matrix elements using the variational method in lattice QCD, Phys. Rev. D **94**, 074505 (2016).
[940] L. Barca, G. Bali, and S. Collins, Toward N to $N\pi$ matrix elements from lattice QCD, Phys. Rev. D **107**, L051505 (2023).
[941] C. Alexandrou, G. Koutsou, Y. Li, M. Petschlies, and F. Pittler, Investigation of pion-nucleon contributions to nucleon matrix elements, Phys. Rev. D **110**, 094514 (2024).
[942] M. Göckeler, R. Horsley, E.-M. Ilgenfritz, H. Perlt, P. E. L. Rakow, G. Schierholz, and A. Schiller, Polarized and unpolarized nucleon structure functions from lattice QCD, Phys. Rev. D **53**, 2317 (1996).
[943] K. Jansen, C. Liu, M. Luscher, H. Simma, S. Sint, R. Sommer, P. Weisz, and U. Wolff, Nonperturbative renormalization of lattice QCD at all scales, Phys. Lett. B **372**, 275 (1996).
[944] M. Lüscher, S. Sint, R. Sommer, and P. Weisz, Chiral symmetry and O(a) improvement in lattice QCD, Nucl. Phys. **B478**, 365 (1996).
[945] [RQCD 16A] G. S. Bali, E. E. Scholz, J. Simeth, and W. Söldner, Lattice simulations with $N_f = 2+1$ improved Wilson fermions at a fixed strange quark mass, Phys. Rev. D **94**, 074501 (2016).
[946] A. Gerardin, T. Harris, and H. B. Meyer, Non-perturbative renormalization and O(a)-improvement of the non-singlet vector current with $N_{\mathrm{f}} = 2+1$ Wilson fermions and tree-level Symanzik improved gauge action, Phys. Rev. D **99**, 014519 (2019).
[947] R. Frezzotti and G. C. Rossi, Chirally improving Wilson fermions. I: O(a) improvement, J. High Energy Phys. 08 (2004) 007.
[948] R. Frezzotti and G. C. Rossi, Twisted mass lattice QCD with mass nondegenerate quarks, Nucl. Phys. B, Proc. Suppl. **128**, 193 (2004).
[949] S. Capitani, M. Göckeler, R. Horsley, H. Perlt, P. E. L. Rakow, G. Schierholz *et al.*, Renormalization and off-shell improvement in lattice perturbation theory, Nucl. Phys. **B593**, 183 (2001).
[950] T. Bhattacharya, R. Gupta, W. Lee, S. R. Sharpe, and J. M. S. Wu, Improved bilinears in lattice QCD with non-degenerate quarks, Phys. Rev. D **73**, 034504 (2006).
[951] M. Bochicchio, L. Maiani, G. Martinelli, G. C. Rossi, and M. Testa, Chiral symmetry on the lattice with Wilson fermions, Nucl. Phys. **B262**, 331 (1985).
[952] S. Sint and P. Weisz, Further results on O(a) improved lattice QCD to one loop order of perturbation theory, Nucl. Phys. **B502**, 251 (1997).
[953] Y. Taniguchi and A. Ukawa, Perturbative calculation of improvement coefficients to $O(g^2a)$ for bilinear quark operators in lattice QCD, Phys. Rev. D **58**, 114503 (1998).
[954] P. Korcyl and G. S. Bali, Non-perturbative determination of improvement coefficients using coordinate space correlators in $N_f = 2+1$ lattice QCD, Phys. Rev. D **95**, 014505 (2017).

[955] J. Green, N. Hasan, S. Meinel, M. Engelhardt, S. Krieg, J. Laeuchli, J.Negele, K. Orginos, A. Pochinsky, and S. Syritsyn, Up, down, and strange nucleon axial form factors from lattice QCD, Phys. Rev. D **95**, 114502 (2017).

[956] M. Constantinou, M. Hadjiantonis, H. Panagopoulos, and G. Spanoudes, Singlet versus nonsinglet perturbative renormalization of fermion bilinears, Phys. Rev. D **94**, 114513 (2016).

[957] G. S. Bali, S. Collins, M. Göckeler, S. Piemonte, and A. Sternbeck, Non-perturbative renormalization of flavor singlet quark bilinear operators in lattice QCD, Proc. Sci., LATTICE2016 (**2016**) 187 [arXiv:1703.03745].

[958] S. Dinter, V. Drach, R. Frezzotti, G. Herdoíza, K. Jansen, and G. Rossi, Sigma terms and strangeness content of the nucleon with $N_f = 2 + 1 + 1$ twisted mass fermions, J. High Energy Phys. 08 (2012) 037.

[959] E. E. Jenkins and A. V. Manohar, Baryon chiral perturbation theory using a heavy fermion Lagrangian, Phys. Lett. B **255**, 558 (1991).

[960] V. Bernard, N. Kaiser, and U.-G. Meissner, Chiral dynamics in nucleons and nuclei, Int. J. Mod. Phys. E **04**, 193 (1995).

[961] T. N. Truong, Chiral perturbation theory, and final state theorem, Phys. Rev. Lett. **61**, 2526 (1988).

[962] T. Becher and H. Leutwyler, Baryon chiral perturbation theory in manifestly Lorentz invariant form, Eur. Phys. J. C **9**, 643 (1999).

[963] T. Fuchs, J. Gegelia, G. Japaridze, and S. Scherer, Renormalization of relativistic baryon chiral perturbation theory and power counting, Phys. Rev. D **68**, 056005 (2003).

[964] A. Walker-Loud *et al.*, Light hadron spectroscopy using domain wall valence quarks on an Asqtad sea, Phys. Rev. D **79**, 054502 (2009).

[965] A. Torok, S. R. Beane, W. Detmold, T. C. Luu, K. Orginos, A. Parreno, M. J. Savage, and A. Walker-Loud, Meson-baryon scattering lengths from mixed-action lattice QCD, Phys. Rev. D **81**, 074506 (2010).

[966] E. E. Jenkins, A. V. Manohar, J. W. Negele, and A. Walker-Loud, A lattice test of $1/N_c$ baryon mass relations, Phys. Rev. D **81**, 014502 (2010).

[967] A. Walker-Loud, Evidence for non-analytic light quark mass dependence in the baryon spectrum, Phys. Rev. D **86**, 074509 (2012).

[968] V. Bernard, N. Kaiser, J. Kambor, and U. G. Meissner, Chiral structure of the nucleon, Nucl. Phys. **B388**, 315 (1992).

[969] S. R. Beane and M. J. Savage, Baryon axial charge in a finite volume, Phys. Rev. D **70**, 074029 (2004).

[970] R. E. Kass and A. E. Raftery, Bayes factors, J. Am. Stat. Assoc. **90**, 773 (1995).

[971] H. Akaike, A new look at the statistical model identification, IEEE Trans. Autom. Control **19**, 716 (1974).

[972] T. Bhattacharya, V. Cirigliano, S. D. Cohen, A. Filipuzzi, M. Gonzalez-Alonso *et al.*, Probing novel scalar and tensor interactions from (ultra)cold neutrons to the LHC, Phys. Rev. D **85**, 054512 (2012).

[973] UCNA Collaboration, Precision measurement of the neutron β-decay asymmetry, Phys. Rev. C **87**, 032501 (2013).

[974] UCNA Collaboration, New result for the neutron β-asymmetry parameter A_0 from UCNA, Phys. Rev. C **97**, 035505 (2018).

[975] D. Mund, B. Maerkisch, M. Deissenroth, J. Krempel, M. Schumann, H. Abele, A. Petoukhov, and T. Soldner, Determination of the weak axial vector coupling from a measurement of the beta-asymmetry parameter a in neutron beta decay, Phys. Rev. Lett. **110**, 172502 (2013).

[976] M. Ademollo and R. Gatto, Nonrenormalization theorem for the strangeness violating vector currents, Phys. Rev. Lett. **13**, 264 (1964).

[977] J. F. Donoghue and D. Wyler, Isospin breaking and the precise determination of V_{ud}, Phys. Lett. B **241**, 243 (1990).

[978] V. Cirigliano, J. de Vries, L. Hayen, E. Mereghetti, and A. Walker-Loud, Pion-induced radiative corrections to neutron β decay, Phys. Rev. Lett. **129**, 121801 (2022).

[979] R. Alarcon *et al.*, Precise Measurement of Neutron Decay Parameters, 2007, http://nab.phys.virginia.edu/nab_loi.pdf.

[980] W. Wilburn *et al.*, Measurement of the neutrino-spin correlation Parameter b in neutron decay using ultracold neutrons, Rev. Mex. Fis. **Suppl. 55**, 119 (2009).

[981] Nab Collaboration, Nab: Measurement principles, apparatus and uncertainties, Nucl. Instrum. Methods Phys. Res., Sect. A **611**, 211 (2009).

[982] M. Gonzalez-Alonso and J. Martin Camalich, Isospin breaking in the nucleon mass and the sensitivity of β decays to new physics, Phys. Rev. Lett. **112**, 042501 (2014).

[983] J. Dudek *et al.*, Physics opportunities with the 12 GeV upgrade at Jefferson Lab, Eur. Phys. J. A **48**, 187 (2012).

[984] Z. Ye, N. Sato, K. Allada, T. Liu, J.-P. Chen, H. Gao, Z.-B. Kang, A. Prokudin, P. Sun, and F. Yuan, Unveiling the nucleon tensor charge at Jefferson Lab: A study of the SoLID case, Phys. Lett. B **767**, 91 (2017).

[985] H.-W. Lin, W. Melnitchouk, A. Prokudin, N. Sato, and H. Shows, First Monte Carlo global analysis of nucleon transversity with lattice QCD constraints, Phys. Rev. Lett. **120**, 152502 (2018).

[986] M. Radici and A. Bacchetta, First extraction of transversity from a global analysis of electron-proton and proton-proton data, Phys. Rev. Lett. **120**, 192001 (2018).

[987] Jefferson Lab Angular Momentum (JAM), Jefferson Lab Angular Momentum Collaboration, Updated QCD global analysis of single transverse-spin asymmetries: Extracting $H^{\sim}$, and the role of the Soffer bound and lattice QCD, Phys. Rev. D **106**, 034014 (2022).

[988] JAM Collaboration, Transversity distributions and tensor charges of the nucleon: Extraction from dihadron production and their universal nature, Phys. Rev. Lett. **132**, 091901 (2024).

[989] [ETM 19] C. Alexandrou, S. Bacchio, M. Constantinou, J. Finkenrath, K. Hadjiyiannakou, K. Jansen *et al.*, Nucleon axial, tensor, and scalar charges and σ-terms in lattice QCD, Phys. Rev. D **102**, 054517 (2020).

[990] [PACS 22B] R. Tsuji, N. Tsukamoto, Y. Aoki, K.-I. Ishikawa, Y. Kuramashi, S. Sasaki *et al.*, Nucleon isovector couplings in $N_f = 2 + 1$ lattice QCD at the physical point, Phys. Rev. D **106**, 094505 (2022).

[991] [PACS 18A] E. Shintani, K.-I. Ishikawa, Y. Kuramashi, S. Sasaki, and T. Yamazaki, Nucleon form factors and root-mean-square radii on a $(10.8\ \mathrm{fm})^4$ lattice at the physical point, Phys. Rev. D **99**, 014510 (2019); Phys. Rev. D **102**, 019902(E) (2020).

[992] [RBC 08] H.-W. Lin, T. Blum, S. Ohta, S. Sasaki, and T. Yamazaki, Nucleon structure with two flavors of dynamical domain-wall fermions, Phys. Rev. D **78**, 014505 (2008).

[993] [LHPC 05] R. G. Edwards, G. T. Fleming, Ph. Hägler, J. W. Negele, K. Orginos, A. V. Pochinsky, D. B. Renner, D. G. Richards, and W. Schroers, The nucleon axial charge in full lattice QCD, Phys. Rev. Lett. **96**, 052001 (2006).

[994] [LHPC 12A] J. R. Green, M. Engelhardt, S. Krieg, J. W. Negele, A. V. Pochinsky, and S. N. Syritsyn, Nucleon structure from lattice QCD using a nearly physical pion mass, Phys. Lett. B **734**, 290 (2014).

[995] [LHPC 12] J. R. Green, J. W. Negele, A. V. Pochinsky, S. N. Syritsyn, M. Engelhardt, and S. Krieg, Nucleon scalar and tensor charges from lattice QCD with light Wilson quarks, Phys. Rev. D **86**, 114509 (2012).

[996] [RBC/UKQCD 19] M. Abramczyk, T. Blum, T. Izubuchi, C. Jung, M. Lin, A. Lytle, S. Ohta, and E. Shintani , Nucleon mass and isovector couplings in $2+1$-flavor dynamical domain-wall lattice QCD near physical mass, Phys. Rev. D **101**, 034510 (2020).

[997] M. Constantinou, R. Horsley, H. Panagopoulos, H. Perlt, P. E. L. Rakow, G. Schierholz *et al.*, Renormalization of local quark-bilinear operators for $N_f = 3$ flavors of stout link nonperturbative clover fermions, Phys. Rev. D **91**, 014502 (2015).

[998] [ETM 15F] C. Alexandrou, M. Constantinou, and H. Panagopoulos, Renormalization functions for $\mathrm{Nf} = 2$ and $\mathrm{Nf} = 4$ twisted mass fermions, Phys. Rev. D **95**, 034505 (2017).

[999] A. Walker-Loud, C. E. Carlson, and G. A. Miller, The electromagnetic self-energy contribution to $M_p - M_n$ and the isovector nucleon magneticpolarizability, Phys. Rev. Lett. **108**, 232301 (2012).

[1000] P. E. Shanahan, A. W. Thomas, and R. D. Young, Strong contribution to octet baryon mass splittings, Phys. Lett. B **718**, 1148 (2013).

[1001] S. R. Beane, K. Orginos, and M. J. Savage, Strong-isospin violation in the neutron proton mass difference from fully-dynamical lattice QCD and PQQCD, Nucl. Phys. **B768**, 38 (2007).

[1002] [QCDSF/UKQCD 12A] R. Horsley, J. Najjar, Y. Nakamura, D. Pleiter, P. E. L. Rakow, G. Schierholz, and J. M. Zanotti, Isospin breaking in octet baryon mass splittings, Phys. Rev. D **86**, 114511 (2012).

[1003] D. A. Brantley, B. Joo, E. V. Mastropas, E. Mereghetti, H. Monge-Camacho, B. C. Tiburzi *et al.*, Strong isospin violation and chiral logarithms in the baryon spectrum, arXiv:1612.07733.

[1004] M. Radici, A. Courtoy, A. Bacchetta, and M. Guagnelli, Improved extraction of valence transversity distributions from inclusive dihadron production, J. High Energy Phys. 05 (2015) 123.

[1005] Z.-B. Kang, A. Prokudin, P. Sun, and F. Yuan, Extraction of quark transversity distribution and collins fragmentation functions with QCD evolution, Phys. Rev. D **93**, 014009 (2016).

[1006] Z.-B. Kang (private communication).

[1007] G. R. Goldstein, J. O. Gonzalez Hernandez, and S. Liuti, Flavor dependence of chiral odd generalized parton distributions and the tensor charge from the analysis of combined π^0 and η exclusive electroproduction data, arXiv:1401.0438.

[1008] M. Pitschmann, C.-Y. Seng, C. D. Roberts, and S. M. Schmidt, Nucleon tensor charges and electric dipole moments, Phys. Rev. D **91**, 074004 (2015).

[1009] J. Benel, A. Courtoy, and R. Ferro-Hernandez, A constrained fit of the valence transversity distributions from dihadron production, Eur. Phys. J. C **80**, 465 (2020).

[1010] U. D'Alesio, C. Flore, and A. Prokudin, Role of the Soffer bound in determination of transversity and the tensor charge, Phys. Lett. B **803**, 135347 (2020).

[1011] M. A. Shifman, A. I. Vainshtein, and V. I. Zakharov, Remarks on Higgs boson interactions with nucleons, Phys. Lett. **78B**, 443 (1978).

[1012] K. G. Chetyrkin, B. A. Kniehl, and M. Steinhauser, Decoupling relations to $O(\alpha_s^3)$ and their connection to low-energy theorems, Nucl. Phys. **B510**, 61 (1998).

[1013] R. J. Hill and M. P. Solon, Standard Model anatomy of WIMP dark matter direct detection II: QCD analysis and hadronic matrix elements, Phys. Rev. D **91**, 043505 (2015).

[1014] European Muon Collaboration, A measurement of the spin asymmetry and determination of the structure function g(1) in deep inelastic muon-proton scattering, Phys. Lett. B **206**, 364 (1988).

[1015] X.-D. Ji, Gauge-invariant decomposition of nucleon spin, Phys. Rev. Lett. **78**, 610 (1997).

[1016] R. L. Jaffe and A. Manohar, The G(1) problem: Fact and fantasy on the spin of the proton, Nucl. Phys. **B337**, 509 (1990).

[1017] M. Pospelov and A. Ritz, Electric dipole moments as probes of new physics, Ann. Phys. (Amsterdam) **318**, 119 (2005).

[1018] C. Abel *et al.*, Measurement of the permanent electric dipole moment of the neutron, Phys. Rev. Lett. **124**, 081803 (2020).

[1019] C. Baker, D. Doyle, P. Geltenbort, K. Green, M. van der Grinten *et al.*, An improved experimental limit on the electric dipole moment of the neutron, Phys. Rev. Lett. **97**, 131801 (2006).

[1020] C.-Y. Seng, Reexamination of the standard model nucleon electric dipole moment, Phys. Rev. C **91**, 025502 (2015).

[1021] [PNDME 20] S. Park, T. Bhattacharya, R. Gupta, Y.-C. Jang, B. Joo, H.-W. Lin *et al.*, Nucleon charges and form factors using clover and HISQ ensembles, Proc. Sci., LATTICE2019 (**2020**) 136 [arXiv:2002.02147].

[1022] [Mainz 19A] D. Djukanovic, H. Meyer, K. Ottnad, G. von Hippel, J. Wilhelm, and H. Wittig, Strange nucleon form factors and isoscalar charges with $N_f = 2+1$ $\mathcal{O}(a)$-improved Wilson fermions, Proc. Sci., LATTICE2019 (**2019**) 158 [arXiv:1911.01177].

[1023] S. Park, T. Bhattacharya, R. Gupta, H.-W. Lin, S. Mondal, and B. Yoon, Update on flavor diagonal nucleon charges,

Proc. Sci., LATTICE2022 (**2023**) 118 [arXiv:2301.07890].
[1024] S. Park, T. Bhattacharya, R. Gupta, H.-W. Lin, S. Mondal, and B. Yoon, Update on flavor diagonal nucleon charges from clover fermions, Proc. Sci., LATTICE2023 (**2024**) 328 [arXiv:2401.00721].
[1025] M. Engelhardt, Strange quark contributions to nucleon mass, and spin from lattice QCD, Phys. Rev. D **86**, 114510 (2012).
[1026] B. A. Kniehl and O. L. Veretin, Bilinear quark operators in the RI/SMOM scheme at three loops, Phys. Lett. B **804**, 135398 (2020).
[1027] [MILC 09D] D. Toussaint and W. Freeman, The strange quark condensate in the nucleon in $2+1$ flavor QCD, Phys. Rev. Lett. **103**, 122002 (2009).
[1028] J. M. Alarcon, J. Martin Camalich, and J. A. Oller, The chiral representation of the πN scattering amplitude and the pion-nucleon sigma term, Phys. Rev. D **85**, 051503 (2012).
[1029] Y.-H. Chen, D.-L. Yao, and H. Q. Zheng, Analyses of pion-nucleon elastic scattering amplitudes up to $O(p^4)$ in extended-on-mass-shell subtraction scheme, Phys. Rev. D **87**, 054019 (2013).
[1030] M. Hoferichter, J. Ruiz de Elvira, B. Kubis, and U.-G. Meissner, High-precision determination of the pion-nucleon σ term from Roy-Steiner equations, Phys. Rev. Lett. **115**, 092301 (2015).
[1031] C. McNeile, A. Bazavov, C. T. H. Davies, R. J. Dowdall, K. Hornbostel, G. P. Lepage, and H. D. Trottier, Direct determination of the strange and light quark condensates from full lattice QCD, Phys. Rev. D **87**, 034503 (2013).
[1032] [BMW 20A] Sz. Borsanyi, Z. Fodor, C. Hoelbling, L. Lellouch, K. Szabo, C. Torrero *et al.*, Ab-initio calculation of the proton and the neutron's scalar couplings for new physics searches, arXiv:2007.03319.
[1033] [ETM 17A] C. Alexandrou and C. Kallidonis, Low-lying baryon masses using $N_f = 2$ twisted mass clover-improved fermions directly at the physical pion mass, Phys. Rev. D **96**, 034511 (2017).
[1034] C. Kallidonis (private communication).
[1035] J. Martin Camalich, L. S. Geng, and M. J. Vicente Vacas, The lowest-lying baryon masses in covariant SU(3)-flavor chiral perturbation theory, Phys. Rev. D **82**, 074504 (2010).
[1036] [QCDSF/UKQCD 11] R. Horsley, Y. Nakamura, H. Perlt, D. Pleiter, P. E. L. Rakow, G. Schierholz, A. Schiller, H. Stüben, F. Winter, and J. M. Zanotti, Hyperon sigma terms for $2+1$ quark flavours, Phys. Rev. D **85**, 034506 (2012).
[1037] P. E. Shanahan, A. W. Thomas, and R. D. Young, Sigma terms from an SU(3) chiral extrapolation, Phys. Rev. D **87**, 074503 (2013).
[1038] [BMW 08] S. Dürr *et al.*, Ab-initio determination of light hadron masses, Science **322**, 1224 (2008).
[1039] A. Crivellin, M. Hoferichter, and M. Procura, Accurate evaluation of hadronic uncertainties in spin-independent WIMP-nucleon scattering: Disentangling two- and three-flavor effects, Phys. Rev. D **89**, 054021 (2014).
[1040] J. Ruiz de Elvira, M. Hoferichter, B. Kubis, and U.-G. Meissner, Extracting the σ-term from low-energy pion-nucleon scattering, J. Phys. G **45**, 024001 (2018).
[1041] M. Hoferichter, J. R. de Elvira, B. Kubis, and U.-G. Meißner, On the role of isospin violation in the pion–nucleon σ-term, Phys. Lett. B **843**, 138001 (2023).
[1042] [ETM 20C] C. Alexandrou, S. Bacchio, M. Constantinou, J. Finkenrath, K. Hadjiyiannakou, K. Jansen *et al.*, Complete flavor decomposition of the spin and momentum fraction of the proton using lattice QCD simulations at physical pion mass, Phys. Rev. D **101**, 094513 (2020).
[1043] [ETM 19A] C. Alexandrou *et al.*, Moments of nucleon generalized parton distributions from lattice QCD simulations at physical pion mass, Phys. Rev. D **101**, 034519 (2020).
[1044] [LHPC 24] M. Rodekamp, M. Engelhardt, J. R. Green, S. Krieg, S. Liuti, S. Meinel, J. W. Negele, A. Pochinsky, and S. Syritsyn, Moments of nucleon unpolarized, polarized, and transversity parton distribution functions from lattice QCD at the physical point, Phys. Rev. D **109**, 074508 (2024).
[1045] [NME 21A] S. Mondal, T. Bhattacharya, R. Gupta, B. Joó, H.-W. Lin, S. Park *et al.*, Nucleon isovector momentum fraction, helicity and transversity moment using Lattice QCD, Proc. Sci., LATTICE2021 (**2021**) 513 [arXiv:2201.00067].
[1046] [RQCD 18] G. S. Bali, S. Collins, M. Göckeler, R. Rödl, A. Schäfer, and A. Sternbeck, Nucleon generalized form factors from two-flavor lattice QCD, Phys. Rev. D **100**, 014507 (2019).
[1047] [RQCD 14A] G. Bali, S. Collins, B. Gläßle, M. Göckeler, J. Najjar, R. H. Rödl, A. Schäfer, R. W. Schiel, A. Sternbeck, and W. Söldner, The moment $\langle x \rangle_{u-d}$ of the nucleon from $N_f = 2$ lattice QCD down to nearly physical quark masses, Phys. Rev. D **90**, 074510 (2014).
[1048] L. A. Harland-Lang, A. D. Martin, P. Motylinski, and R. S. Thorne, Parton distributions in the LHC era: MMHT 2014 PDFs, Eur. Phys. J. C **75**, 204 (2015).
[1049] H1, ZEUS Collaboration, Combination of measurements of inclusive deep inelastic $e^{\pm}p$ scattering cross sections and QCD analysis of HERA data, Eur. Phys. J. C **75**, 580 (2015).
[1050] S. Dulat, T.-J. Hou, J. Gao, M. Guzzi, J. Huston, P. Nadolsky, J. Pumplin, C. Schmidt, D. Stump, and C.-P. Yuan, New parton distribution functions from a global analysis of quantum chromodynamics, Phys. Rev. D **93**, 033006 (2016).
[1051] A. Accardi, L. T. Brady, W. Melnitchouk, J. F. Owens, and N. Sato, Constraints on large-x parton distributions from new weak boson production and deep-inelastic scattering data, Phys. Rev. D **93**, 114017 (2016).
[1052] S. Alekhin, J. Blümlein, S. Moch, and R. Placakyte, Parton distribution functions, α_s, and heavy-quark masses for LHC Run II, Phys. Rev. D **96**, 014011 (2017).
[1053] NNPDF Collaboration, Parton distributions from high-precision collider data, Eur. Phys. J. C **77**, 663 (2017).
[1054] JAM Collaboration, Strange quark suppression from a simultaneous Monte Carlo analysis of parton

distributions and fragmentation functions, Phys. Rev. D **101**, 074020 (2020).
[1055] T.-J. Hou *et al.*, New CTEQ global analysis of quantum chromodynamics with high-precision data from the LHC, Phys. Rev. D **103**, 014013 (2021).
[1056] D. de Florian, R. Sassot, M. Stratmann, and W. Vogelsang, Extraction of spin-dependent parton densities and their uncertainties, Phys. Rev. D **80**, 034030 (2009).
[1057] NNPDF Collaboration, A first unbiased global determination of polarized PDFs and their uncertainties, Nucl. Phys. **B887**, 276 (2014).
[1058] J. J. Ethier, N. Sato, and W. Melnitchouk, First simultaneous extraction of spin-dependent parton distributions and fragmentation functions from a global QCD analysis, Phys. Rev. Lett. **119**, 132001 (2017).
[1059] S. Li, A. Accardi, M. Cerutti, I. P. Fernando, C. E. Keppel, W. Melnitchouk, P. Monaghan, G. Niculescu, M. I. Niculescu, and J. F. Owens, Extraction of the neutron F_2 structure function from inclusive proton and deuteron deep-inelastic scattering data, Phys. Rev. D **109**, 074036 (2024).
[1060] M. Della Morte, A. Francis, V. Gülpers, G. Herdoíza, G. von Hippel, H. Horch, B. Jäger, H. B. Meyer, A. Nyffeler, and H. Wittig, The hadronic vacuum polarization contribution to the muon $g-2$ from lattice QCD, J. High Energy Phys. 10 (2017) 020.
[1061] M. Luscher, Computational strategies in lattice QCD, in *Les Houches Summer School: Session 93: Modern Perspectives in Lattice QCD: Quantum Field Theory and High Performance Computing* (2010), arXiv:1002.4232.
[1062] B. Jäger, T. D. Rae, S. Capitani, M. Della Morte, D. Djukanovic, G. von Hippel *et al.*, A high-statistics study of the nucleon EM form factors, axial charge and quark momentum fraction, Proc. Sci., LATTICE2013 (**2014**) 272 [arXiv:1311.5804].
[1063] S. Capitani, M. Della Morte, G. von Hippel, B. Knippschild, and H. Wittig, Scale setting via the Ω baryon mass, Proc. Sci., LATTICE2011 (**2011**) 145 [arXiv:1110.6365].
[1064] [ALPHA 13A] S. Lottini, Chiral behaviour of the pion decay constant in $N_f = 2$ QCD, Proc. Sci., LATTICE2013 (**2014**) 315 [arXiv:1311.3081].
[1065] M. Creutz, Monte Carlo study of quantized SU(2) gauge theory, Phys. Rev. D **21**, 2308 (1980).
[1066] R. J. Hudspith, M. F. M. Lutz, and D. Mohler, Precise Omega baryons from lattice QCD, arXiv:2404.02769.
[1067] [CLS 21] B. Strassberger *et al.*, Scale setting for CLS $2+1$ simulations, Proc. Sci., LATTICE2021 (**2022**) 135 [arXiv:2112.06696].
[1068] O. Bar, Chiral perturbation theoryand nucleon–pion-state contaminations in lattice QCD, Int. J. Mod. Phys. A **32**, 1730011 (2017).
[1069] V. Cirigliano and I. Rosell, $\pi/K \to e\bar{\nu}_e$ branching ratios to $O(e^2p^4)$ in chiral perturbation theory, J. High Energy Phys. 10 (2007) 005.
[1070] B. Ananthanarayan and B. Moussallam, Four-point correlator constraints on electromagnetic chiral parameters and resonance effective Lagrangians, J. High Energy Phys. 06 (2004) 047.
[1071] F. Niedermayer, P. Rufenacht, and U. Wenger, Fixed point gauge actions with fat links: Scaling and glueballs, Nucl. Phys. **B597**, 413 (2001).
[1072] [ALPHA 05A] M. Della Morte, A. Shindler, and R. Sommer, On lattice actions for static quarks, J. High Energy Phys. 08 (2005) 051.
[1073] M. Donnellan, F. Knechtli, B. Leder, and R. Sommer, Determination of the static potential with dynamical fermions, Nucl. Phys. **B849**, 45 (2011).
[1074] A. Hasenfratz and F. Knechtli, Flavor symmetry and the static potential with hypercubic blocking, Phys. Rev. D **64**, 034504 (2001).
[1075] A. Deuzeman and U. Wenger, Gradient flow and scale setting for twisted mass fermions, Proc. Sci., LATTICE2012 (**2012**) 162.
[1076] [ETM 15A] A. Abdel-Rehim *et al.*, First physics results at the physical pion mass from $N_f = 2$ Wilson twisted mass fermions at maximal twist, Phys. Rev. D **95**, 094515 (2017).
[1077] O. Bär and M. Golterman, Chiral perturbation theory for gradient flow observables, Phys. Rev. D **89**, 034505 (2014); Phys. Rev. D **89**, 099905(E) (2014).
[1078] S. Schaefer, Status and challenges of simulations with dynamical fermions, Proc. Sci., LATTICE2012 (**2012**) 001 [arXiv:1211.5069].
[1079] A. Ramos and S. Sint, Symanzik improvement of the gradient flow in lattice gauge theories, Eur. Phys. J. C **76**, 15 (2016).
[1080] [MILC 13B] A. Bazavov *et al.*, Symanzik flow on HISQ ensembles, Proc. Sci., LATTICE2013 (**2014**) 269 [arXiv:1311.1474].
[1081] A. Cheng, A. Hasenfratz, Y. Liu, G. Petropoulos, and D. Schaich, Improving the continuum limit of gradient flow step scaling, J. High Energy Phys. 05 (2014) 137.
[1082] Z. Fodor, K. Holland, J. Kuti, S. Mondal, D. Nogradi, and C. H. Wong, The lattice gradient flow at tree-level and its improvement, J. High Energy Phys. 09 (2014) 018.
[1083] [HPQCD 11B] R. J. Dowdall *et al.*, The upsilon spectrum and the determination of the lattice spacing from lattice QCD including charm quarks in the sea, Phys. Rev. D **85**, 054509 (2012).
[1084] [ETM 20] G. Bergner, P. Dimopoulos, J. Finkenrath, E. Fiorenza, R. Frezzotti, M. Garofalo *et al.*, Quark masses and decay constants in $N_f = 2+1+1$ isoQCD with Wilson clover twisted mass fermions, in *Proceedings of the 37th International Symposium on Lattice Field Theory (Lattice 2019) Wuhan, Hubei, China, 2019* (2020), Vol. LATTICE2019, p. 181, arXiv:2001.09116.
[1085] [QCDSF/UKQCD 15B] V. G. Bornyakov *et al.*, Wilson flow and scale setting from lattice QCD, arXiv:1508.05916.
[1086] M. F. M. Lutz, Y. Heo, and X.-Y. Guo, Low-energy constants in the chiral Lagrangian with baryon octet and decuplet fields from Lattice QCD data on CLS ensembles, Eur. Phys. J. C **83**, 440 (2023).
[1087] V. Bornyakov *et al.*, Determining the scale in lattice QCD, arXiv:1512.05745.
[1088] T. M. B. Asmussen, R. Höllwieser, F. Knechtli, and T. Korzec, The determination of r_0 and r_1 in Nf $= 2+1$

QCD, *Proc. Sci.*, LATTICE2023 (2024) 296 [arXiv:2312.14726].
[1089] [MILC 09B] A. Bazavov *et al.*, Results from the MILC Collaboration's SU(3) chiral perturbation theory analysis, Proc. Sci., LAT2009 (**2009**) 079 [arXiv:0910.3618].
[1090] [RBC/Bielefeld 07] M. Cheng *et al.*, The QCD equation of state with almost physical quark masses, Phys. Rev. D **77**, 014511 (2008).
[1091] [HPQCD 03] M. Wingate, C. T. Davies, A. Gray, G. P. Lepage, and J. Shigemitsu, The B_s and D_s decay constants in three flavor lattice QCD, Phys. Rev. Lett. **92**, 162001 (2004).
[1092] A. Duncan, E. Eichten, and H. Thacker, Electromagnetic structure of light baryons in lattice QCD, Phys. Lett. B **409**, 387 (1997).
[1093] M. Hansen, B. Lucini, A. Patella, and N. Tantalo, Gauge invariant determination of charged hadron masses, J. High Energy Phys. 05 (2018) 146.
[1094] B. Lucini, A. Patella, A. Ramos, and N. Tantalo, Charged hadrons in local finite-volume QED + QCD with C* boundary conditions, J. High Energy Phys. 02 (2016) 076.
[1095] Z. Fodor, C. Hoelbling, S. D. Katz, L. Lellouch, A. Portelli, K. K. Szabo, and B. C. Toth, Quantum electrodynamics in finite volume and nonrelativistic effective field theories, Phys. Lett. B **755**, 245 (2016).
[1096] M. Di Carlo, M. T. Hansen, A. Portelli, and N. Hermansson-Truedsson, Relativistic, model-independent determination of electromagnetic finite-size effects beyond the pointlike approximation, Phys. Rev. D **105**, 074509 (2022).
[1097] J. Bijnens, J. Harrison, N. Hermansson-Truedsson, T. Janowski, A. Jüttner, and A. Portelli, Electromagnetic finite-size effects to the hadronic vacuum polarization, Phys. Rev. D **100**, 014508 (2019).
[1098] M. Göckeler, R. Horsley, E. Laermann, P. E. L. Rakow, G. Schierholz, R. Sommer *et al.*, QED: A lattice investigation of the chiral phase transition and the nature of the continuum limit, Nucl. Phys. **B334**, 527 (1990).
[1099] M. G. Endres, A. Shindler, B. C. Tiburzi, and A. Walker-Loud, Massive photons: An infrared regularization scheme for lattice QCD + QED, Phys. Rev. Lett. **117**, 072002 (2016).
[1100] U. J. Wiese, C periodic, and G periodic QCD at finite temperature, Nucl. Phys. **B375**, 45 (1992).
[1101] L. Polley, Boundaries for $SU(3)_c x U(1)_{el}$ lattice gauge theory with a chemical potential, Z. Phys. C **59**, 105 (1993).
[1102] M. A. Clark, M. Della Morte, Z. Hall, B. Hörz, A. Nicholson, A. Shindler *et al.*, QED with massive photons for precision physics: Zero modes and first result for the hadron spectrum, Proc. Sci., LATTICE2021 (**2022**) 281 [arXiv:2201.03251].
[1103] [RCstar 22] L. Bushnaq, I. Campos, M. Catillo, A. Cotellucci, M. Dale, P. Fritzsch, J. Lücke, M. K. Marinković, A. Patella, and N. Tantalo, First results on QCD + QED with C* boundary conditions, J. High Energy Phys. 03 (2023) 012.
[1104] P. Boyle, V. Gülpers, J. Harrison, A. Jüttner, C. Lehner, A. Portelli, and C. T. Sachrajda, Isospin breaking corrections to meson masses and the hadronic vacuum polarization: A comparative study, J. High Energy Phys. 09 (2017) 153.
[1105] P. Ball and R. Zwicky, New results on $B \to \pi, K, \eta$ decay form factors from light-cone sum rules, Phys. Rev. D **71**, 014015 (2005).
[1106] D. Becirevic, A. L. Yaouanc, A. Oyanguren, P. Roudeau, and F. Sanfilippo, Insight into $D/B \to \pi\ell\nu_\ell$ decay using the pole models, arXiv:1407.1019.
[1107] G. P. Lepage and S. J. Brodsky, Exclusive processes in perturbative quantum chromodynamics, Phys. Rev. D **22**, 2157 (1980).
[1108] R. Akhoury, G. F. Sterman, and Y. Yao, Exclusive semileptonic decays of B mesons into light mesons, Phys. Rev. D **50**, 358 (1994).
[1109] L. Lellouch, Lattice constrained unitarity bounds for $\bar{B}^0 \to \pi^+ \ell \overline{\nu_l}$ decays, Nucl. Phys. **B479**, 353 (1996).
[1110] C. Bourrely, I. Caprini, and L. Lellouch, Model-independent description of $B \to \pi\ell\nu$ decays and a determination of $|V_{ub}|$, Phys. Rev. D **79**, 013008 (2009).
[1111] C. Bourrely, B. Machet, and E. de Rafael, Semileptonic decays of pseudoscalar particles (M → $M'\ell\nu_\ell$) and short distance behavior of quantum chromodynamics, Nucl. Phys. **B189**, 157 (1981).
[1112] C. G. Boyd, B. Grinstein, and R. F. Lebed, Precision corrections to dispersive bounds on form-factors, Phys. Rev. D **56**, 6895 (1997).
[1113] C. G. Boyd and M. J. Savage, Analyticity, shapes of semileptonic form-factors, and $\overline{B} \to \pi\ell\bar{\nu}$, Phys. Rev. D **56**, 303 (1997).
[1114] M. C. Arnesen, B. Grinstein, I. Z. Rothstein, and I. W. Stewart, A precision model independent determination of $|V_{ub}|$ from $B \to \pi e\nu$, Phys. Rev. Lett. **95**, 071802 (2005).
[1115] T. Becher and R. J. Hill, Comment on form-factor shape and extraction of $|V_{ub}|$ from $B \to \pi l\nu$, Phys. Lett. B **633**, 61 (2006).
[1116] R. J. Hill, The modern description of semileptonic meson form factors, eConf **C060409**, 027 (2006).
[1117] R. J. Hill and G. Paz, Model independent extraction of the proton charge radius from electron scattering, Phys. Rev. D **82**, 113005 (2010).
[1118] R. J. Hill and G. Paz, Model independent analysis of proton structure for hydrogenic bound states, Phys. Rev. Lett. **107**, 160402 (2011).
[1119] Z. Epstein, G. Paz, and J. Roy, Model independent extraction of the proton magnetic radius from electron scattering, Phys. Rev. D **90**, 074027 (2014).
[1120] A. X. El-Khadra, A. S. Kronfeld, P. B. Mackenzie, S. M. Ryan, and J. N. Simone, The semileptonic decays $B \to \pi\ell\nu$ and $D \to \pi\ell\nu$ from lattice QCD, Phys. Rev. D **64**, 014502 (2001).
[1121] B. Chakraborty, C. T. H. Davies, P. G. de Oliviera, J. Koponen, G. P. Lepage, and R. S. Van de Water, The hadronic vacuum polarization contribution to a_μ from full lattice QCD, Phys. Rev. D **96**, 034516 (2017).
[1122] M. Hoferichter, J. Ruiz de Elvira, B. Kubis, and U.-G. Meißner, Roy–Steiner-equation analysis of pion–nucleon scattering, Phys. Rep. **625**, 1 (2016).

[1123] J. Gegelia and G. Japaridze, Matching heavy particle approach to relativistic theory, Phys. Rev. D **60**, 114038 (1999).
[1124] B. C. Lehnhart, J. Gegelia, and S. Scherer, Baryon masses and nucleon sigma terms in manifestly Lorentz-invariant baryon chiral perturbation theory, J. Phys. G **31**, 89 (2005).
[1125] S. R. Beane, Nucleon masses, and magnetic moments in a finite volume, Phys. Rev. D **70**, 034507 (2004).
[1126] X. L. Ren, L. S. Geng, J. Martin Camalich, J. Meng, and H. Toki, Octet baryon masses in next-to-next-to-next-to-leading order covariant baryon chiral perturbation theory, J. High Energy Phys. 12 (2012) 073.
[1127] M. Procura, B. U. Musch, T. Wollenweber, T. R. Hemmert, and W. Weise, Nucleon mass: From lattice QCD to the chiral limit, Phys. Rev. D **73**, 114510 (2006).
[1128] [QCDSF/UKQCD 03] A. Ali Khan *et al.*, The nucleon mass in $N_f = 2$ lattice QCD: Finite size effects from chiral perturbation theory, Nucl. Phys. **B689**, 175 (2004).